Tropical Geometric Counting Problems

Dissertation

der Mathematisch-Naturwissenschaftlichen Fakultät
der Eberhard Karls Universität Tübingen
zur Erlangung des Grades eines
Doktors der Naturwissenschaften
(Dr. rer. nat.)

vorgelegt von

Alheydis Beate Maria Geiger

aus München

Tübingen

2022

2020 *Mathematics Subject Classification.*

Primary:

14N10	Enumerative problems (combinatorial problems) in algebraic geometry
14T15	Combinatorial aspects of tropical varieties
14T20	Geometric aspects of tropical varieties

Secondary:

52B20	Lattice polytopes in convex geometry (including relations with commutative algebra and algebraic geometry)
52-04	Software, source code, etc. for problems pertaining to convex and discrete geometry

Contents

List of Figures

List of Tables

List of Algorithms

Chapter 1

Introduction

This thesis applies computational approaches opened up by the use of tropical geometry to enumerative questions in algebraic geometry.

A degeneration of algebraic counting problems to tropical geometry produces new concepts and computational approaches. The challenge is to find methods to lift the results in the degeneration back to the original problem. This thesis contributes towards the fundamental research in this area by investigating two geometric counting problems via tropical geometry.

The first part of this thesis closes a research gap on the recovery of the classical count of 4, 8, 16 or 28 real bitangents to smooth quartic curves by Plücker and Zeuthen [Plü39, Zeu73] from tropical geometry. Building on [LM20, CM21], we develop methods to produce an understanding of the global lifting of tropical bitangents over $\mathbb{R}$, and further over other Henselian fields. Moreover, we establish a computational tool in `polymake` for the investigation of tropical bitangents and their lifting behavior [GP], and present results of analyses using this tool. This is joint work with Marta Panizzut [GP21a, GP21b].

The second part of this thesis explores the question of tropically counting binodal surfaces. We exploit tropical floor plans, a recent enumerative tool from tropical geometry [MMSS22]. We prove that tropical floor plans recover the algebraic counts of plane curves, while for surfaces the current technique is not sufficient to asymptotically recover the second order term. To improve the approach for surfaces, we provide a classification of the smallest examples of polytopes that can appear as Newton polytopes of a binodal surface together with instructions how to use them for tropical counting. This investigation is of computational nature and is aided by functions [Gei22] written for `OSCAR`. Furthermore, we extend the definition of tropical floor plans that contains the newly found cases. Additionally, we show that these smallest cases contribute to the third order term of the asymptotic count. This research is joint work with Madeline Brandt [BG21].
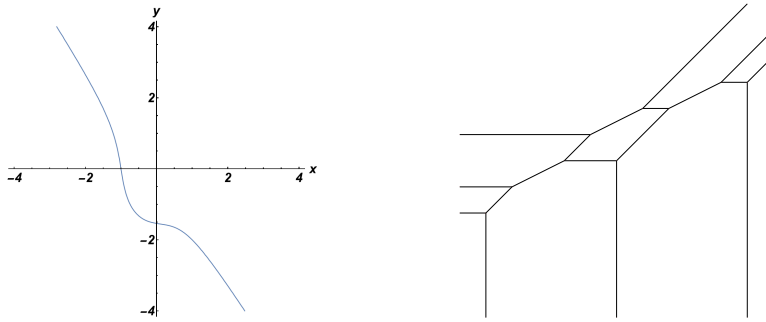
Figure 1.1: The curve $V(2^5 + x + x^2 + 2^5 x^3 + 2^3 y + xy + 2^3 x^2 y + 2^2 y^2 + 2^2 xy^2 + 2^3 y^3)$ and its tropicalization under the 2-adic valuation.

1.1 Tropical enumerative geometry

What is tropical geometry?

Tropical geometry connects and combines methods from many different areas of mathematics, such as algebraic geometry, combinatorics and polyhedral geometry. It can be viewed as a linear degeneration of algebraic geometry towards polyhedral combinatorics.

Tropical geometry is a relatively young branch of mathematics. Its beginnings can be traced back to the 1970s and 1980s where different fundamental ideas appeared: The introduction of the logarithmic limit-set of algebraic varieties by Bergman [Ber71], Viro's patchworking method [Vir84], amoebas of Laurent polynomials by Gelfand, Kapronov and Zelevinsky [GKZ94], Maslov's dequantization [KM97], as well as work by Bieri and Groves on characters induced by valuations [BG84]. The name "tropical" goes back to a suggestion by Christian Choffurt to Imre Simon who pioneered the use of the min-plus algebra for optimization theory [Sim88]. Another of the suggested names for tropical varieties was "logarithmic limit sets", which emphasizes the view of tropical geometry as a degeneration of algebraic geometry.

Algebraic geometry is concentrated on solving polynomial equations. Its main objects of study are algebraic varieties, which are zero sets of polynomials. Its challenges include the solvability of polynomials over different (not necessarily algebraically closed) fields. Tropical varieties can be regarded as degenerations of algebraic varieties. They are balanced polyhedral complexes, in particular they are piecewise linear. See Figure 1.1 for an example. In the degeneration process, called *tropicalization*, we lose some information. Still some data is preserved, like the dimension and even, using an adapted tropical notion, the degree. One advantage of the degeneration is that new methods from polyhedral geometry and combinatorics can be applied to the tropical object.

The results gained by tropical methods can be moved back to the algebraic setting

via the concept of lifting, sometimes also called realizability. The relationship
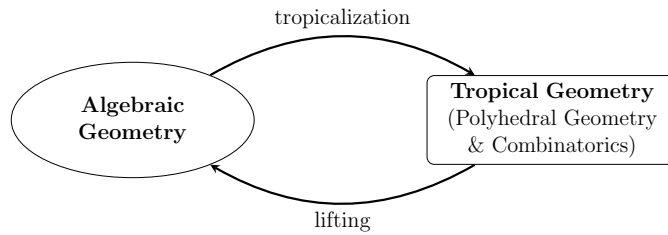
Figure 1.2: The relationship between algebraic and tropical geometry

between algebraic and tropical geometry as depicted in Figure 1.2 is a give and take: We will see many examples of how to obtain results in algebraic geometry via tropical geometry in the following. But it is also possible to gain results in combinatorics from algebraic geometry [AHK18].

Tropical geometry has established itself as a theory on its own, concerned also with abstract tropical varieties, of which not all can be realized as tropicalizations of algebraic varieties. This thesis is focused on embedded tropical geometry, where tropical varieties arise from tropicalization. The interplay between coordinate changes and tropicalization is at the core of tropical modification theory, on which the results in [LM20], which are foundational for Part I of this thesis, are based.

Tropical geometry has many applications, both in- and outside of mathematics, such as in economy [BK19, TY19] or machine learning [ZNL18, MCT21]. Inside of pure mathematics, its areas of application cover, but are not limited to, arithmetic geometry [KRZB16], topology and geometry of moduli spaces [ACP15, CGP21, RSS14], and elimination theory [ST08]. The list of references given here is by far not complete. Another area of successful application of tropical methods in mathematics is enumerative geometry.

What is enumerative geometry?
Enumerative geometry is concerned with solving counting problems, like enumerating the number of geometric objects that satisfy certain conditions. Mathematicians have been interested in these kind of problems since ancient Greece. One example are the rings of Apollonius. Apollonius of Perga (262 B.C. - 190 B.C.) stated and solved the still memorable question of how many circles are tangent to three given circles, see Figure 1.3. Though the original solution was lost, a later report passed down his result stating that there are 8 circles tangent to three given circles.

Counting problems can be stated for different areas in geometry. In algebraic geometry, the typical enumerative question focuses on the number of algebraic varieties of a fixed dimension and type (e.g. a fixed number of nodal singularities) that pass through a certain number of given points in a generic distribution.
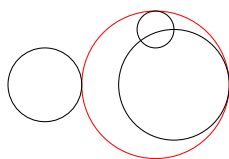
Figure 1.3: An example of Apollonius' problem: The three given circles are depicted in black, one circle tangent to all three is shown in red.

A prominent example for this are the Gromov-Witten invariants of the complex projective plane $\mathbb{P}_{\mathbb{C}}^2$, which count the number of irreducible plane curves of degree d and genus g satisfying generic point conditions. Dropping the irreducibility requirement, these numbers are sometimes called the multicomponent Gromov-Witten invariants of $\mathbb{P}_{\mathbb{C}}^2$. A simple example is the number of lines through 2 points in general position, which is one. The numbers of conics through 5 points is still relatively simple to determine; see Figure 1.4. For higher degree curves the problem quickly becomes more involved.
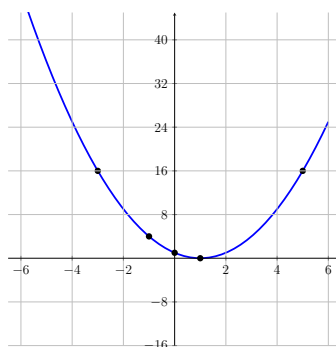
Figure 1.4: Five points in general position determine a conic curve.

Of course, there also exist other counting problems in algebraic geometry that count varieties satisfying other counting conditions.These can be inclusions of lower dimensional varieties (for curves these are always points), or tangency conditions. An interesting such problem concerns the number of lines on a smooth cubic surface [Cay49, Sal49]. This problem is connected in one of the so called "mathematical trinities" by Vladimir Arnold [Arn99] together with two other enumerative problems: the number of (real) bitangents to a quartic curve and the number of tritangents to a space sextic. A space sextic is a curve in $\mathbb{P}^3$ of genus 4 and degree 6 that arises as the complete intersection of a quadric and a cubic surface.

Why tropical enumerative geometry?
In the past, it has become apparent that tropical geometry provides powerful tools to tackle algebraic enumerative questions and that these methods open

new approaches. A remarkable example is the ground-breaking Correspondence Theorem by Mikhalkin [Mik05] stating that the Gromov-Witten invariants can be recovered via tropical techniques. Over time, various tropical tools with different advantages have been developed for counting curves [GM07, BM07], and many new results in this area have been obtained [BBLdM18, BM07, BM09, FM10, GS18, GK08, IKS03].

The fascinating thing about using tropical geometry to solve algebraic counting problems is that despite the loss of information during the degeneration, we can recover the algebraic count by applying appropriate lifting multiplicities.

As described above, we can go from an algebraic variety to a tropical variety via tropicalization. The way back is not unique. We call elements in the fiber of tropicalization *lifts* of the tropical variety over a fixed field. This fiber is in general infinite. When counting algebraic objects we always have conditions that our algebraic variety has to satisfy. We can tropicalize these conditions too and obtain a tropical translation of the counting problem. To recover the algebraic count from the tropical one, we fix a lift of the conditions (e.g. a lift of the point conditions) and intersect this with the fiber of tropicalization of the tropical variety. If our choices are generic, this gives us a finite number, the *lifting multiplicity*.

We can now define lifting multiplicities for any base field on the algebraic side and only consider one tropical situation. This is an especially noteworthy property of tropical geometry: tropical methods work independent of the starting fields on the algebraic side. This allows simultaneous results for different fields. For the Gromov-Witten invariants, the tropical methods, counted with adapted multiplicity, recover the Welschinger invariants, which are the analogue of the Gromov-Witten invariants over $\mathbb{R}$ [IKS03].

How does mathematical software come into play?
In recent years, computational methods took a more prominent role in the proof of fascinating results in tropical and algebraic geometry. Tropical geometry degenerates algebraic questions into piecewise linear problems, and allows the use of polyhedral geometry via the duality. As in polyhedral geometry problems are often discrete, it enables a computational approach in these cases.

Among the noteworthy software in the areas of commutative algebra, tropical, polyhedral and algebraic geometry there are (with different focuses) `Macaulay2` [GS], `Singular` [DGPS21], `gfan` [Jen], `polymake` [GJ00] and its database `polyDB`, [Paf17] and last but no least the relatively young but growing computer algebra software `OSCAR` [osc].

As computations in research increase, it is more and more important to make written code, software and computationally obtained data available to other researchers in order to ensure reproducibility. In this connection we want to mention the

FAIR data principle[1] which stands for four important aspects when using software for mathematical research: **F**indable, **A**ccessible, **I**nteroperable and **R**eusable. In both projects on which this thesis is based, we strove to adhere to these principles. With this in mind, we want to refer to the Mathematical Research Data Initiative MaRDI [MaR] which is the newly established consortia initiative of mathematical science. This has already lead to the building of mathematical repositories like the MathRepo[2] of the MPI MiS in Leipzig [FG22] where we consider publishing the code produced for Part II of this thesis.

This thesis considers tropical enumerative problems and applies computational methods, mainly using `polymake` and `OSCAR`, for their investigation and solution.

1.2 Topics and results

The two parts of the thesis are dedicated to two different counting problems via tropical geometry: the enumeration of bitangents to quartic curves and the enumeration of multi-nodal surfaces. Here we give an overview of the main results and their impact for further research. A detailed overview of the structure of the thesis with a summary of the content of each chapter can be found in Section 1.3.

1.2.1 Part I

One of the so called "mathematical trinities" by Vladimir Arnold [Arn99] connects three enumerative problems - 27 lines on a cubic surface, 28 bitangents to a plane quartic curve, 120 tritangents of a space sextic. These enumerative questions are also interesting from the tropical point of view. When tropicalizing algebraic enumerative questions, we often observe a superabundance phenomenon, i.e., we tropically see more objects than algebraically.

For example, a tropical smooth cubic surface can contain infinitely many lines [Vig10], while an algebraic cubic surface contains exactly 27 [Cay49]. For cubic surfaces, there has been a lot of work on understanding this situation tropically by classifying the lines into families and investigating their lifting behavior [PV22, Gei20, BS15, BK12]. Particularly to mention in this context is the work of Joswig et al. on the computational investigation of the unimodular secondary fan of cubic surfaces [JPS20], and the `polymake` extensions `a-tint` [Ham14] and `CubicSurfaces` [JPS] for computing lines in tropical cubic surfaces. However, the realizability problem of lines on cubic surfaces is not completely solved yet.

Something similar happens when we consider the question of 28 bitangents to a quartic curve tropically. A tropical smooth quartic curve can have infinitely

---

[1] https://www.go-fair.org/fair-principles/
[2] https://mathrepo.mis.mpg.de/
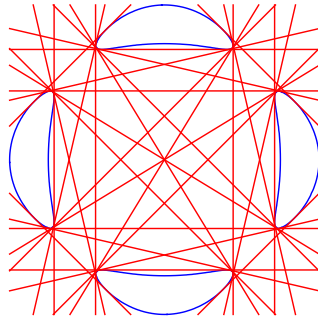
Figure 1.5: A real quartic curve with 28 real bitangents

many tropical bitangents [BLM+16] that can be grouped in 7 (possibly infinite) equivalence classes. Each of these give rise to 4 bitangent lines to a complex quartic curve [CJ17, LM20], thus recovering the count $28 = 7 \cdot 4$ by Plücker [Plü34]. One is also interested in the numbers of solutions over non-algebraically closed fields like $\mathbb{R}$. To keep to the mathematical trinity discussed above, we consider the following three examples: For real cubic surfaces it is known that they contain either 3, 9, 15 or 27 real lines [Seg42]. For real smooth quartic curves it is a result by Plücker and Zeuthen [Plü39, Zeu73] that there are either 4, 8, 16 or 28 real bitangents. For space sextics the situation is more involved: the number of real tritangents depends on the genus g and the number s of ovals, which are closed loops in the real part of the curve, and on whether the sextic curve separates the quadric surface in which it is contained into more than one component [Kra98]. Furthermore, a space sextic with 5 ovals can have between 84 and 120 totally real tritangents and any integer in this interval is possible [KRSNS18].

As described above, tropical geometry allows - by counting with different multiplicities - the investigation over different base fields. Thus, it provides the option of solving such enumerative questions (real and complex) simultaneously, additionally providing tools for other valued fields. This motivates the investigation of such enumerative questions with tropical geometry.

In the case of bitangents to quartic curves, Cueto and Markwig [CM21] determined the real lifting conditions of tropical bitangents and proved that each equivalence class lifts to either 0 or 4 bitangents to a real quartic curve. However, there was still a research gap in tropically recovering the full count of 4, 8, 16 or 28 real bitangents classically proven by Plücker and Zeuthen [Plü39, Zeu73], as the methods on the tropical side were not developed far enough to produce these numbers.

Question 1.2.1. Can the tropical counting methods be extended in such a way that we can prove that for any tropicalized quartic of the 7 tropical bitangent classes only 1, 2, 4 or 7 can lift over $\mathbb{R}$?

This question is answered by the joint work with Marta Panizzut in the preprints [GP21a, GP21b], on which Part I of this thesis is based. We develop methods to produce an understanding of the global lifting of all 7 tropical bitangent classes over ℝ. We hope that our results can be adapted in the future to count real tritangents of space sextics and bitangents of quartics over other fields.

Our work builds on the classification of all shapes of bitangent classes together with their real lifting conditions from [CM21].

A bitangent shape is the collection of all equivalent bitangent lines in the dual tropical plane; it is a connected polyhedral complex. Tropical plane curves are dual to a subdivision of its Newton polygon. Figure 1.6 shows the bitangent shapes to a tropical quartic curve and its dual subdivision. We say two curves have the same combinatorial type if they they have the same dual subdivision.

As the shapes of the bitangent classes change for different edge lengths of a fixed combinatorial type of the tropical quartic, we introduce the notion of deformation classes that collect the deforming shapes and classify them. This classification is the first main result and the cornerstone in the proofs of the following theorems in this part of the thesis.

Theorem 4.2.3. There are 24 deformation classes of tropical bitangent classes to generic smooth tropical quartic curves up to S_3-symmetry. Representatives for each class are depicted in Figure 4.39.

The deformation classes are defined by their dual deformation motifs, which are sets of triangles in the dual subdivision of the tropical quartic curve that are determined by the bitangent shapes in the deformation class and their tangencies to the quartic. For an example of a tropical quartic curve with its 7 bitangent classes and a dual deformation motif consider Figure 1.6.

As mentioned above, the shapes of the bitangent classes change for different edge lengths of a tropical quartic with fixed dual subdivision. The real lifting conditions have been determined per bitangent shape in [CM21]. Hence, a priori we could obtain different numbers of real lifts for two tropical quartics with the same combinatorial type.

Using the concept of deformation classes and dual motifs, we can prove that this is not the case. More precisely, we are able to prove an even stronger statement: that we do not need to know the appearing bitangent shapes to a tropical quartic, but that the dual subdivision is already enough to determine the real lifting behavior.

Theorem 5.1.4. The real lifting conditions of tropical bitangent classes only depend on the dual subdivision of the smooth tropical quartic curve.

This second main result has an interesting corollary which has high impact for future research as it extends the statement to Henselian fields.
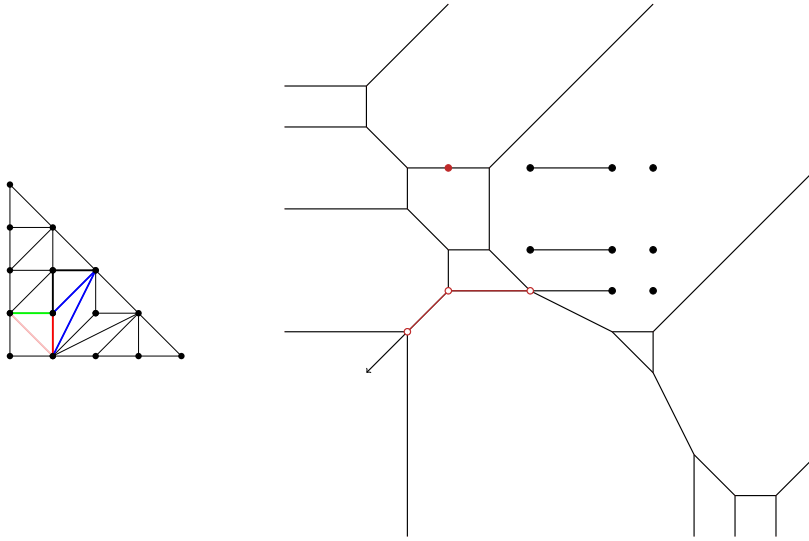
Figure 1.6: A smooth tropical quartic curve with its 7 bitangent classes and its dual subdivision. The thickly drawn edges in the subdivision form the dual deformation motif of the bitangent class at the bottom left side.

Corollary 5.1.5. *The lifting conditions of tropical bitangent classes over a Henselian field with residue characteristic $\neq 2$ and 2-divisible value group only depend on the dual subdivision of the smooth tropical quartic curve.*

It follows that the problem of tropically counting the number of real bitangents is a discrete counting problem and allows a computational proof. We reuse the data computed for a different research project in [BJMS15]. This data provides us with a list of the 1278 S_3-representatives of the unimodular subdivisions of quartic curves. To recover the count, we implement an algorithmic search for the dual deformation motifs in `polymake` (Algorithm 1). By adding the real lifting conditions from [CM21] (which are sign conditions on the coefficents) for each deformation class as data, the program can run over all possible sign vectors and evaluate the lifting conditions (Algorithm 2).

Theorem 5.2.2. Let Γ be a generic tropicalization of a smooth quartic plane curve $V(f)$ defined over a real closed complete non-Archimedean valued field. Either 1, 2, 4 or 7 of its bitangent classes admit a lift to 4 real bitangents to $V(f)$ each.

To make our results reproducible and the developed code accessible to other researchers, we implemented the extension `TropicalQuarticCurves` [GP] to the mathematical software `polymake`. The extension allows users to compute information about the associated tropical bitangents and their real lifting behavior for tropical smooth quartics. Moreover, the data of the 1278 triangulations together

with the properties with respect to the tropical bitangents are available on the `polymake` database `polyDB` [Paf17].

We are confident that our software and the stored data will be useful for future research in the area of tropical bitangents. Not only do they make the computation of examples much more accessible, but the code can be adapted to count arithmetic multiplicities of tropical bitangents [MSP22]. Moreover, the classification of the deformation motifs provides first steps to find bitangents for higher degree curves. And as the lifting conditions are stored independent of the base field, it is possible to already use the code for investigating the lifting of bitangents over other Henselian fields, using the statement of Corollary 5.1.5.

After an introduction of the extension `TropicalQuarticCurves` and the database collection in Section 6.1, Chapter 6 shows how the software can be used for further research: We analyze the distribution of orbit sizes (Theorem 6.2.1) and possible numbers of real bitangents (Theorem 6.2.3).

If we fix 28 lines as our bitangents in algebraic geometry, there is a unique quartic curve that has those lines as its bitangents [CS03]. It is therefore a natural question - which we have been asked at numerous occasions in conferences or discussions - whether the tropical seven bitangent classes uniquely determine a tropical quartic.

We obtain the following combinatorial version of the statement that bitangents determine the curve.

Theorem 6.2.5. The combinatorial type of a tropical quartic curve is determined by its 7 dual deformation motifs.

We follow up on this question by asking whether we can improve on this result by fixing more data. In Section 6.2, we consider one example in detail and find that the bitangent shapes and their positions are not enough to fix even the skeleton of the tropical curve. However, we observe that by adding the tropicalized tangency points, we can recover the skeleton of the tropical quartic curve from its bitangents. It is instinctive to ask whether this is true in general, so we pose the following open problem:

Problem 6.2.8. Is it in general possible to determine the skeleton of a smooth tropical quartic curve from its bitangent shapes and the tropical tangency points of its realizable representatives?

Another related research question is concerned with computing arithmetic multiplicities of (tropical) bitangents [LV21, MSP22]. As mentioned above, this is a possible application of the extension `TropicalQuarticCurves`. However, to determine arithmetic multiplicities of tropical bitangents, it is important to be able to know exactly which shape appears for a bitangent class and a chosen tropical coefficient vector [MSP22]. Our analysis of the deformation of the shapes for the classification in Theorem 4.2.3 already yields the following result.

Theorem 6.3.1. For a given unimodular triangulation $\mathcal{T}$ of $4\Delta_2$ we can subdivide the associated secondary cone $\Sigma(\mathcal{T})$ by hyperplanes, such that for each chamber the bitangent shapes of the corresponding quartic curves are constant.

These hyperplanes can be computed for a given deformation class using the `polymake` extension and they are stored in the database collection for the representatives.

The last subsection of this part of the thesis, Section 6.3.2, is independent work of the author that is not part of the joint project with Marta Panizzut. It investigates the areas of non-genericity in secondary cones for generic triangulations. The computations of the lifting conditions in [CM21] build on modifications of the tropical quartic. For this a genericity assumption is necessary, as the excluded cases are not yet understood. One of these conditions concerns the lattice length of certain edges of the quartic curve (Remark 3.3.2). For some triangulations there are lower-dimensional areas in the secondary cone, for which the corresponding quartic curves are non-generic. We identify these areas as half-hyperplanes in Proposition 6.3.4 and give their description in Table 6.5.

As the lifting conditions are understood for the complement of these half-hyperplanes in the interior of the secondary cone, we hope that it is possible to determine the lifting conditions from that. This in its turn might help to understand the lifting conditions for the cases where the triangulation already determines a violation of the genericity constraint.

1.2.2 Part II

We have seen in the first part of the introduction that tropical geometry offers a powerful toolkit for the enumeration of plane curves.

A natural generalization of the counting problem of plane curves is the counting of multi-nodal surfaces using tropical methods. Tropical singular surfaces were first investigated in [MMS12]. More results on tropically counting singular surfaces have been developed in the following years [MMS18, MMSS22, Sin22, BG20]. In [MMSS22], the authors developed a new counting tool for surfaces: tropical floor plans. They proved that asymptotically, i.e., for degree $d \gg \delta$ where δ is the number of nodes, tropical floor plans recover the highest order term of the polynomial

$$N_{\delta,\mathbb{C}}^{\mathbb{P}^3}(d) = \frac{4^\delta d^{3\delta}}{\delta!} - \frac{3 \cdot 4^\delta}{\delta!} d^{3\delta-1} + \mathcal{O}(d^{3\delta-2})$$

describing the count. Tropical floor plans can be viewed as a tool to break down the information encoded in the dual subdivision to lower dimensional varieties by using the combinatorics induced by point conditions in Mikhalkin position [MMSS22]. In the case of surfaces, this leads to the much better understood case of plane curves.
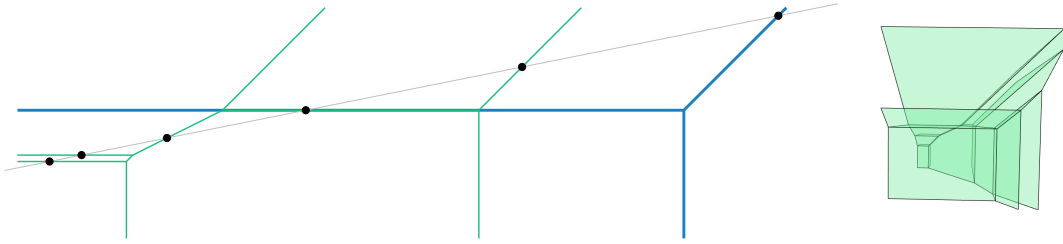
Figure 1.7: A tropical floor plan of a tropical singular surface of degree 2

Figure 1.7 depicts the tropical floor plan of a tropical surface of degree 2 with one node. Considering the additionally displayed picture of the tropical surface, one can find the curves from the floor plan in the picture of the surface. This example shows why the phrase "floor plan" is fitting.

The results in Part II are joint work with Madeline Brandt [BG21].

In Section 8.1, we show that the tropical floor plans for plane curves, also defined in [MMSS22], can be generalized to recover the multicomponent Gromov-Witten invariants of $\mathbb{P}^2_{\mathbb{C}}$.

Theorem 8.1.7. The number of tropical floor plans of degree d with δ nodes counted with complex multiplicity equals the Gromov-Witten number $N_{d,g}$ of curves with genus $g = \frac{(d-1)(d-2)}{2} - \delta$ and degree d passing through $3d-1+g$ general points:

$$N_{\text{floor}}(d,g) = N_{d,g}.$$

This motivates the use of tropical floor plans not only for the asymptotic counting of surfaces but also for recovering the count for concrete examples.

However, for tropical surfaces the situation is much more involved than for curves. Nevertheless, Part II of this thesis presents first results of an investigation on how to use tropical floor plans to count multi-nodal tropical surfaces.

When using tropical floor plans for counting, we choose the point conditions in Mikhalkin position which is algebraically and tropically generic and allows us (for one-nodal surfaces) to assume that the subdivision is *floor decomposed* [BBLdM18, BM09, MMSS22]. Tropical floor plans now break down the information encoded in the subdivision to lower dimensional varieties by use of this decomposition.

If the nodes in the tropical surface are far enough apart, it is possible to asymptotically count δ-nodal surfaces of degree d via this concept [MMSS22] as mentioned above. After generalizing the methods of floor plans to nodes closer together but still tropically separated, Madeline Brandt and I achieved the following count:

Theorem ([BG20, Theorem 1.3])**.** *Of the* 280 *complex binodal cubic surfaces,* 214 *tropicalize to tropical surfaces with separated nodes.*

This implies that tropical floor plans which only enumerate separated nodes are not sufficient for recovering the full complex count. We want to improve this count and ask the following questions.

Question 1.2.2.   1. Are separated nodes enough to recover the second order term of $N_{\delta,\mathbb{C}}^{\mathbb{P}^3}(d)$?

2. Which polytope complexes hide unseparated nodes?

3. How can we use tropical floor plans to count multi-nodal surfaces with unseparated nodes?

For the purpose of answering (1), we introduce artificial δ-nodal floor plans in Section 8.2 that simulate how many surfaces there would be if the nodes did not interact at all. We prove that the number of artificial floor plans $I_\delta(d)$ is always at least the number of tropical floor plans counting separated nodes, and use the count of artificial floor plans to produce an upper bound for the number of surfaces with separated nodes for bi- and trinodal surfaces.

Theorem 8.2.6. For $\delta = 2, 3$ the number of surfaces with separated nodes is at most:

$$I_2(d) = 8d^6 - \frac{168}{5}d^5 + \mathcal{O}(d^4), \qquad I_3(d) = \frac{32}{3}d^9 - \frac{1341}{35}d^8 + \mathcal{O}(d^7).$$

Consequently, surfaces with separated nodes are insufficient to asymptotically count binodal and trinodal surfaces up to two degrees. Hence, it is necessary to understand how two nodes on a surface give rise to non-separated nodes under tropicalization and how to count these with tropical floor plans (Question 1.2.2 (2) and (3)).

The main goal of Chapters 9 and 10 is to lay a foundation towards answering these questions.

We call polytopes that can be Newton polytopes of binodal surfaces *binodal polytopes*. Investigating small examples, we find a lower bound the for the number of lattice points of binodal polytopes.

Lemma 9.1.9. *Let Ω be a 3-dimensional binodal polytope. Then $|\Omega \cap \mathbb{Z}^3| \geq 6$.*

We use the classification of polytopes with 6 lattice points by Blanco and Santos [BS16b] to discover all those polytopes that could appear in the dual subdivision of a binodal surface. Since these are infinite polytope families, we can only check for finitely many polytopes whether they are truly the support of a binodal surface. We obtain the following conjecture.

Conjecture 9.2.8. *There are* 6 *families of binodal polytopes with* 6 *lattice points and of width* 1 *up to integral unimodular affine transformations (Definition 9.2.2). They are depicted in Figure 9.1.*

We prove that in these cases the two nodes tropicalize to the same vertex of the tropical surface.

Proposition 9.1.10. *Let* Ω *be a binodal polytope with* 6 *lattice points, and let S be a binodal surface over* $\mathbb{C}\{\{t\}\}$ *with Newton polytope* Ω. *Then trop(S) is a fan and both nodes tropicalize to the vertex of the fan.*

For each of the 6 binodal polytope families we compute all lattice paths. Building on computations with `OSCAR` code [Gei22] (see Algorithms 9 and 10 and the functions in Appendix B.2), we further state conjectures on their multiplicities. These computations are expensive, so they only yield solutions for small input.

The conjectures are written down individually for each polytope in dependence of the parameters of the polytope family and can be found here:

- Polytope family with number 8: Conjecture 9.4.4,
- Polytope family with number 10: Conjecture 9.4.9,
- Polytope family with number 13: Conjecture 9.4.13,
- Polytope family with number 14: Conjecture 9.4.17,
- Polytope family with number 20: Conjecture 9.4.21,
- Polytope family with number 21: Conjecture 9.4.24,

where the numbering of the polytope families comes from the list extracted from the classification in [BS16b].

In the next step, we investigate which of these polytopes can appear in the dual subdivision of a surface of degree d passing through $n = \binom{d+3}{3} - \delta - 1$ points where $\delta = 2$.

Theorem 10.1.6. Of the binodal polytopes with 6 lattice points of width 1 only polytopes of the families with numbers 10, 13 and 20 (see Figure 1.8) can appear in the dual subdivision of a binodal floor decomposed surface of degree d through n points in Mikhalkin position. They can only appear if $d > 4$.

To determine the contribution of these surfaces to the count, we ascertain the possible lattice paths, which encode the point conditions in the dual subdivision and compute their multiplicities via hyperplane sections of the binodal variety using the same algorithms and code as for the data foundation of the conjectures above.
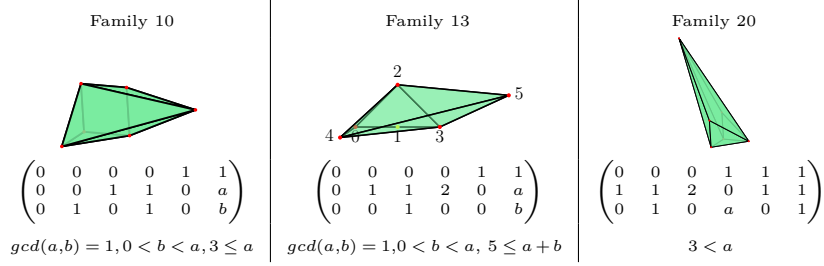
Figure 1.8: The three binodal polytope families that can appear in the dual subdivision of a degree d surface through points in Mikhalkin position.

Conjecture 10.2.2. *Let S be a floor decomposed, tropical binodal surface of degree d passing through points in Mikhalkin position such that the dual subdivision contains one of the binodal polytopes*

$$\tilde{\Omega}_I^{(10)}(a),\ \tilde{\Omega}_{II}^{(10)}(a),\ \tilde{\Omega}_{III}^{(10)}(a),\ \tilde{\Omega}_I^{(13)}(a),\ \tilde{\Omega}_{II}^{(13)}(a),\ \tilde{\Omega}^{(20)}(a),$$

and only unimodular simplices everywhere else. Then the complex lifting multiplicity of S is given by

$$mult_{\mathbb{C}}(S) = \begin{cases} a-3 & for\ \tilde{\Omega}^{(20)}(a);\ and\ for\ \tilde{\Omega}_I^{(13)}(a), \tilde{\Omega}_{II}^{(13)}(a)\ if\ a\ odd, \\ a-2 & else. \end{cases}$$

Conjecture 10.2.2 is verified using [Gei22] for polytope family 10 when $3 \leq a \leq 7$, for family 13 when $4 \leq a \leq 9$, and for family 20 when $a \leq 7$.

Building on the proof of Theorem 10.1.6, we extend the definition of tropical floor plans to contain the binodal polytopes.

As final step of this thesis, we prove that up to $d \leq 7$ the binodal polytopes contribute $\frac{1}{4}d^4 + \mathcal{O}(d^3)$ to the third-highest term of the polynomial $N_{2,\mathbb{C}}^{\mathbb{P}^3}(d)$. For $d > 7$ this result relies on conjectured multiplicities of the binodal polytopes.

Conjecture 10.2.5. *Assuming Conjecture 10.2.2 is true, it follows that floor decomposed tropical degree d surfaces with a binodal polytope with 6 vertices and width 1 in the dual subdivision contribute $\frac{1}{4}d^4 + \mathcal{O}(d^3)$ surfaces to the count of binodal degree d surfaces $N_{2,\mathbb{C}}^{\mathbb{P}^3}(d)$. So, they contribute to the third highest term of the polynomial $N_{2,\mathbb{C}}^{\mathbb{P}^3}(d)$.*

15

1.3 Structure of content

This section gives a short overview over the content and structure of the thesis to allow a specific lookup of topics.

Chapter 2 contains some background on polyhedral (Section 2.1) and tropical geometry (Section 2.2). This background adheres to both parts of the thesis. The main references for this chapter are [Tho06, GKZ94, MS15, RGST05].

Part I
This part is concerned with tropical bitangents to tropical quartic curves. Chapters 4, 5 and most of Chapter 6 are based on the preprints [GP21a, GP21b] which are joint work with Marta Panizzut.

In **Chapter 3**, we recapitulate definitions and results on tropical bitangents from [BJMS15, BLM+16, LM20, CM21]. This contains skeleta and leaves of tropical quartic curves and the action of S_3 on a tropical quartic curve (Section 3.1), tropical bitangent classes and shapes (Section 3.2) and their lifting behaviors (Section 3.3).

In **Chapter 4**, we introduce deformation classes of tropical bitangents (Section 4.1) and classify them up to S_3 equivalence (Section 4.2), thus proving Theorem 4.2.3.

In **Chapter 5**, we investigate the lifting behavior of deformation classes. In Section 5.1, we prove that the lifting conditions for bitangent shapes as determined in [CM21] are the same for all shapes collected together in the same deformation class, not only over $\mathbb{R}$, Theorem 5.1.4, but also over arbitrary Henselian fields with residue characteristic $\neq 2$ and 2-divisible value group; see Corollary 5.1.5.
We use the result for $\mathbb{R}$ in Section 5.2 to prove in Theorem 5.2.2 the count of Plücker and Zeuthen [Plü34, Plü39, Zeu73] of the possible numbers of real bitangents (4, 8, 16 and 28) for tropically smooth generic quartic curves.

In **Chapter 6**, the `polymake` extension `TropicalQuarticCurves` and database entry `Tropical:QuarticCurves` are introduced (Section 6.1).
Section 6.2 shows the results of data analyses on the distribution of orbit sizes (Theorem 6.2.1), numbers of possible real bitangents (Theorem 6.2.3), and numbers of sign vectors of decidable lifting for a non-generic bitangent shape (C) (Problem 6.2.4 and Table 6.3). It further contains an investigation of the question whether the tropical bitangents determine the tropical quartic curve: Theorem 6.2.5 proves that the combinatorial type of a tropical quartic curve is determined by its dual deformation motifs. From there, we work along an example towards Problem 6.2.8

stating whether the skeleton of a tropical quartic curve is in general determined by its bitangent shapes and their tropical tangency points.

Section 6.3 classifies the hyperplanes that determine the deformation between the bitangent shapes for each deformation class (Theorem 6.3.1) and the lower dimensional areas in generic secondary cones for which the corresponding tropical quartic curve is not generic (Proposition 6.3.4).

Part II

This part is concerned with the enumeration of multi-nodal surfaces via tropical floor plans continuing the research from the joint article [BG20] with Madeline Brandt. Chapters 8-10 are based on the preprint [BG21] which is joint work with Madeline Brandt.

In **Chapter 7**, we introduce results of the research on tropical singular surfaces (Section 7.1) and go over definitions from counting surfaces and curves, especially lattice paths (Section 7.2), and introduce tropical floor plans (Section 7.3). The main references for this chapter are [MMS12, MMS18, MMSS22, BG20].

Chapter 8 contains two independent sections on tropical floor plans. In Section 8.1, we prove Theorem 8.1.7, which states that tropical floor plans can be extended to successfully count plane curves and recover the multicomponent Gromov-Witten invariants.

In Section 8.2, we investigate how tropical floor plans for surfaces with separated nodes contribute to the asymptotic count and prove that unseparated nodes are necessary to recover the second order term of the asymptotic count of binodal and trinodal surfaces; see Theorem 8.2.6.

In **Chapter 9**, we take a first step in the search for polytopes that encode unseparated nodes. We start in Section 9.1 with the definitions of binodal varieties and first requirements for polytopes that encode two isolated singularities, like Lemma 9.1.9 and Proposition 9.1.10.

In Section 9.2, we identify all lattice polytopes with 6 lattice points of width 1 that can be binodal by using a classification of Blanco and Santos [BS16b]. We first exclude those polytopes that cannot be binodal (Propositions 9.2.4 and 9.2.5). Remaining are 6 infinite families, for which we can only verify the claim, that these indeed are binodal, for small parameter values; see Conjecture 9.2.8.

In Section 9.3, we investigate lattice paths for dual subdivisions of binodal surfaces (Section 9.3.1) and how to compute their multiplicities (Section 9.3.2).

These results are used in Section 9.4 where we identify all lattice paths for each of the binodal polytope families found in Section 9.2 (Propositions 9.4.3, 9.4.8, 9.4.12,

9.4.16, 9.4.20, 9.4.23) and pose conjectures for the lattice path multiplicities, which we verify for small values using code in `OSCAR` (Conjectures 9.4.4, 9.4.9, 9.4.13, 9.4.17, 9.4.21, 9.4.24).

Section 9.5 illustrates the application of the results of the previous sections by two counting examples.

Chapter 10 is concerned with applying the previous results to the counting of binodal degree d surfaces. Section 10.1 examines which binodal polytopes can appear for floor decomposed surfaces of degree d passing through points in Mikhalkin position (Theorem 10.1.6).

Section 10.2 describes how to count these using tropical floor plans (Conjectures 10.2.5 and 10.2.2, Definition 10.2.1).

Appendix A collects first results of the investigation which lattice polytopes with 6 lattice points and width 2 or 3, as classified in [BS16b], can be binodal.

Appendix B.1 contains additional functions not bundled in the extension `TropicalQuarticCurves` which were used for the proof of Theorem 5.2.2 and the analyses described in Section 6.2.

Appendix B.2 presents the `OSCAR` functions from [Gei22] written for the computations in Part II: computing the binodal variety and its degree, the multiplicities of lattice paths, and the dimension of the singular locus of a given surface.

1.4 Open questions

The results of this thesis and the developed methods lay the foundation for more interesting research in this area. We collect new questions arising from the contributions of this thesis, as well as some remaining open problems, for future investigation.

Part I: Tropical Bitangents to plane quartic curves

1. Which numbers do we see for the lifting of bitangents over other Henselian fields? By [CM21] and Corollary 5.1.5, we can conclude that it will be multiples of 4, but will we see the same collection of numbers as over $\mathbb{R}$?

2. What are the lifting conditions for bitangent shape (C) if the tropical quartic is not generic?

3. Is it in general possible to determine the skeleton of a smooth tropical quartic curve from its bitangent shapes and the tropical tangency points of its

realizable representatives such that the only remaining edge length changes correspond to the pulling of generalized leafs?

If yes, does every tropical quartic in such a family allow a lift with 28 real bitangents? These questions are stated in Problem 6.2.8.

4. Real lifts of bitangents on a tropically smooth quartic curve are totally real [CM21]. Since there are quartics with real but not totally real bitangents, we know that these quartics are not tropically smooth. By [LL18], non-smooth tropical quartic curves have 7 bitangent classes counted with multiplicity. We ask:

   What are the (real) lifting conditions of tropical bitangents of not smooth tropical quartic curves?

   An answer to this question could give rise to a complete tropical proof of the count by Plücker and Zeuthen.

5. After a projection, the tritangent planes of a space sextic can be considered as bidegree-(1,1) curves and the space sextic as a bidegree-(3,3) curve. Thus, classifying tropical tritangent shapes and determining their real lifting conditions is similar to the situation of bitangents to quartic curves.

   Can the techniques of tropical bitangents to quartics be adapted to the situation of tritangent planes of a space sextic?

Part II: Towards tropically counting binodal surfaces

1. We are still missing 66 surfaces from the count of binodal cubic surfaces. These surfaces must contain unseparated nodes, which are encoded via binodal polytopes with 7 or more vertices in their dual subdivisions. These polytopes could have width 1 or width greater than 1, in which case we expect them to be subdivided into width 1 polytopes. This question extends to understanding unseparated nodes in more generality.

2. At this time, we do not know how to prove Conjecture 10.2.2. This would require a technique for symbolic computation with Gröbner bases for polynomial ideals with parameters in the exponents, or other methods.

3. We did not investigate the contribution of the binodal polytopes determined in this paper with respect to a count over $\mathbb{R}$, but this could be an interesting direction of future research.

4. There are finitely many polytopes with 6 lattice points of width 2 or 3, classified by [BS16b]. They are displayed in Appendix A together with the dimension and degree of their generalized binodal varieties as far as they

could be computed. Due to the larger values of the vertices this was not possible for all of them. Which of these polytopes are binodal?

5. Do multi-nodal surfaces through points in Mikhalkin position always have floor decomposed dual subdivisions?

6. Initial computations indicate that the binodal polytopes studied in Chapter 9 are also Newton polytopes of cuspidal surfaces. For these polytopes, the cusp would tropicalize to the vertex of the tropical surface. So, these polytopes could contribute to a count of cuspidal tropical surfaces using methods similar to the ones used in this paper.

1.5 Acknowledgements

... Hannah Markwig, Michael Joswig and Angelica Cueto for interesting discussions on the topic of tropical bitangents and for their comments on earlier versions of the papers that Part I is build on;

... Hannah Markwig, Sam Payne and Kris Shaw for telling Marta and me about their current project and allowing us to mention it in our paper and in my thesis;

... Hannah Markwig and Angelica Cueto for allowing me to include figures from their paper [CM21];

... Angelica Cueto for pointing out a mistake in one of my first talks;

... Janko Böhm for suggesting interesting questions to the project of binodal surfaces;

... Eugenii Shustin for his answers on enumerative questions;

... Tommy Hofmann for his assistance with writing the `OSCAR` functions;

... Lars Kastner and Benjamin Lorenz for their help with `polymake` computations;

... Marvin Hahn for his interesting question on tropical bitangents and that he did not stop asking until we had an answer.

... Matilde Manzaroli and Victoria Schleis for their time in reading some parts of this thesis and for their helpful comments.

Last, but not least, I thank my family and friends, most of all my husband for enduring and supporting me over the critical last weeks and for his infinite patience, when I could not stop talking about my thesis.

This PhD Dissertation was typeset with LaTeX2.[3]

---

[3]LaTeX2 is an extension of LaTeX. LaTeX is a collection of macros for TeX. TeX is a trademark of the American Mathematical Society.

Chapter 2

Preliminaries

Tropical geometry is connected to many areas in mathematics. Its definitions rely partially on polyhedral geometry. In this chapter, we introduce tropical geometry with a focus on the interplay with objects from polyhedral geometry. We give a short overview of some basics of polyhedral and tropical geometry. Standard definitions of tropical and polyhedral objects that will be used in further chapters are collected. This chapter provides an introduction, but it can also be used as a reference chapter. The main references for this chapter are [Tho06, GKZ94, MS15, RGST05].

The chapter is structured as follows: Section 2.1 recalls some definitions from polyhedral geometry. In Section 2.2, a very brief introduction to tropical geometry is given, highlighting three different aspects: tropical algebraic geometry (Section 2.2.1), tropicalization of algebraic varieties and the realizability question (Section 2.2.2), and the duality connecting tropical and polyhedral geometry (Section 2.2.3).

2.1 Basics of polyhedral geometry

As the name suggests, polyhedral geometry is concerned with the study of polyhedral objects, like polytopes or polyhedral complexes, their combinatorics and geometry. In this brief summary of some of the basics of polyhedral geometry, we define, among others, (balanced) polyhedral complexes, normal fans, (regular) subdivisions and triangulations the secondary fan and dual polyhedral complexes.

The main references for this section are [Tho06, Chapters 4, 7, 8], [GKZ94, Chapter 7] and [MS15, Section 2.3, Chapter 3].

Definition 2.1.1. A *polyhedral complex* $\mathcal{C}$ in $\mathbb{R}^n$ is a finite collection of polyhedra in $\mathbb{R}^n$ satisfying the following conditions:

(a) $\emptyset \in \mathcal{C}$

(b) If $P \in \mathcal{C}$ and F a face of P, then $F \in \mathcal{C}$

(c) For $P, Q \in \mathcal{C}$ it holds that $P \cap Q$ is a face of both P and Q.

We call an element of $\mathcal{C}$ a *d-cell* if it is a polyhedron of dimension d.

The k-skeleton of $\mathcal{C}$ is the polyhedral complex consisting of all cells of $\mathcal{C}$ of dimension $\leq k$. We set

$$\dim(\mathcal{C}) := \max_{Q \in \mathcal{C}}\{\dim(Q)\}.$$

A polyhedral complex is called *pure dimensional* if all cells maximal with respect to inclusion have the same dimension. The *support* $|\mathcal{C}|$ of $\mathcal{C}$ is the set

$$|\mathcal{C}| = \{\mathbf{x} \in \mathbb{R}^n : \exists P \in \mathcal{C} \text{ such that } \mathbf{x} \in P\}.$$

A *subcomplex* $\mathcal{C}'$ of a polyhedral complex $\mathcal{C}$ is a polyhedral complex such that every cell of $\mathcal{C}'$ is a cell of $\mathcal{C}$. We write $\mathcal{C}' \subset \mathcal{C}$.

Definition 2.1.2. If all the polyhedra in a polyhedral complex are cones, the complex is called a *polyhedral fan*. Since we do not consider any other sort of fan in this thesis, a *fan* will always mean a polyhedral fan.

Definition 2.1.3 ([MS15, Definition 2.3.6])**.** Consider a cell σ of a polyhedral complex $\mathcal{C}$ in $\mathbb{R}^n$. The *star* of σ in $\mathcal{C}$ is a fan in $\mathbb{R}^n$ with its cones indexed by the cells $\tau \in \mathcal{C}$ that contain σ as a face. The star of $\sigma \in \mathcal{C}$ is denoted $\mathrm{star}_{\mathcal{C}}(\sigma)$.

More descriptively: the star at a cell σ of a polyhedral complex $\mathcal{C}$ is the fan that can be seen when looking locally at $\mathcal{C}$ around σ. We need this definition to be able to define balanced polyhedral complexes, which will resurface in Sections 2.2.1 and 2.2.3 in the context of tropical varieties.

Definition 2.1.4. Let $\mathcal{C}$ be a rational fan in $\mathbb{R}^n$, pure of dimension d. Fix weights $m(\sigma) \in \mathbb{N}$ for all cones σ of dimension d. Given a cone $\tau \in \mathcal{C}$ of dimension $d-1$, let L be the linear space parallel to τ. Thus, L is a $(d-1)$-dimensional subspace of $\mathbb{R}^n$. Since τ is a rational cone, the abelian group $L_{\mathbb{Z}} = L \cap \mathbb{Z}^n$ is free of rank $d-1$, with $N(\tau) = \mathbb{Z}^n/L_{\mathbb{Z}} \cong \mathbb{Z}^{n-d+1}$. For each $\sigma \in \mathcal{C}$ with $\tau \not\subseteq \sigma$, the set $(\sigma + L)/L$ is a one-dimensional cone in $N(\tau) \otimes_{\mathbb{Z}} \mathbb{R}$. Let $\mathbf{v}_\sigma$ be the first lattice point on this ray. The fan $\mathcal{C}$ is *balanced at τ* if

$$\sum m(\sigma)\mathbf{v}_\sigma = 0.$$

The fan $\mathcal{C}$ is *balanced* if it is balanced at all $\tau \in \mathcal{C}$ with $\dim(\tau) = d-1$.

If $\mathcal{C}$ is a pure polyhedral complex of dimension d with weights $m(\sigma) \in \mathbb{N}$ on each d-dimensional cell in $\mathcal{C}$, then for each $\tau \in \mathcal{C}$ the fan $\mathrm{star}_{\mathcal{C}}(\tau)$ inherits a weighting function m.

The polyhedral complex $\mathcal{C}$ is *balanced* if the fan $\mathrm{star}_{\mathcal{C}}(\tau)$ is balanced for all $\tau \in \mathcal{C}$ with $\dim(\tau) = d-1$.

Given a polyhedron there is a natural way to obtain an associated polyhedral fan.

Definition 2.1.5. Let $P \subset \mathbb{R}^n$ be a polyhedron. The *outer normal cone* $\mathcal{N}_P(F)$ of a face F of P is the cone consisting of the outer normal vectors to the face F. The polyhedral fan consisting of the outer normal cones of every face of P is called *outer normal fan* of P, denoted $\mathcal{N}_P$.

Remark 2.1.6. The inner normal cone is defined analogously by the inner normal vectors. We can obtain the inner normal fan from the outer normal fan, by multiplying the cones with -1.

In the following we consider polytopes, which are bounded polyhedra.

Definition 2.1.7. Let P be a polytope. A *subdivision* of P is a polyhedral complex $\mathcal{S}$ with support P. As the union of all maximal cells (with respect to inclusion) has to be P, the complex $\mathcal{S}$ is of pure dimension $\dim(P)$.

A subdivision is called a *triangulation* if all the maximal elements of $\mathcal{S}$ are simplices.

If P is a lattice polytope and $\mathcal{S}$ is a subdivision such that every element of $\mathcal{S}$ is a lattice polytope, we call the subdivision a *lattice subdivision*.

If a lattice subdivision consists only of simplices of minimal lattice volume, it is called a *unimodular triangulation*.

Since we will only consider lattice subdivisions in this thesis, subdivision and triangulation will always refer to subdivisions in which every element is a lattice polytope resp. lattice simplex.

Definition 2.1.8. Let $\mathcal{A} \subset \mathbb{R}^n$ be a finite set and $P = \operatorname{conv}(\mathcal{A})$. A *lifting function* is a function $\alpha : \mathcal{A} \to \mathbb{R}$ and the corresponding *lifted polytope* is defined as

$$\widetilde{P}_\alpha := \operatorname{conv}\{(v, \alpha(v)) \mid v \in \mathcal{A}\} \subset \mathbb{R}^{n+1}.$$

Projecting the upper faces of $\widetilde{P}_\alpha$ to $\mathbb{R}^n$ by deleting the last coordinate, we obtain a collection of subpolytopes of P. Those polytopes form a polyhedral complex with support P, i.e., the lifting function α induces a subdivision $\mathcal{S}_\alpha$ of P.

A subdivision that arises in this way is called *regular*.

Fixing an order of the elements in $\mathcal{A}$, the image of a lifting function α can be written as a vector $(\alpha_1, \ldots, \alpha_N) \in \mathbb{R}^N$, where $N = |\mathcal{A}|$. This vector will be called *weight vector*.

For a lattice polytope the regular subdivision induced by α is a lattice subdivision.

Definition 2.1.9. We say that *all points are visible* in a regular lattice subdivision of P induced by a lifting function α if for every lattice point v of the polytope P, the point $(v, \alpha(v))$ is contained in an upper face of the lifted polytope $\tilde{P}_\alpha$.

In particular for a unimodular triangulation always all points are visible.

For a given regular subdivision $\mathcal{S}$ there is an associated cone, the secondary cone, which parametrizes all lifting functions that give rise to $\mathcal{S}$.

Definition 2.1.10 ([GKZ94, Definition 1.4 & Proposition 1.5])**.** For a given regular subdivision $\mathcal{S}$ of $\mathrm{conv}(\mathcal{A})$, we define the *secondary cone* to $\mathcal{S}$ as

$$\Sigma(\mathcal{S}) = \{\alpha : \mathcal{A} \to \mathbb{R} \mid \mathcal{S}_\alpha = \mathcal{S}\} \subset \mathbb{R}^N.$$

The cone $\Sigma(\mathcal{S})$ is an open cone in $\mathbb{R}^N$. If $\mathcal{S}$ is a regular unimodular triangulation, then the secondary cone is full dimensional, i.e., $\dim(\Sigma(\mathcal{S})) = N$.

The collection of secondary cones forms a fan called the *secondary fan* of $\mathrm{conv}(\mathcal{A})$.

Sometimes we will consider secondary cones modulo $(1,\ldots,1)\mathbb{R}$, because two lifting functions $\alpha_1, \alpha_2 : \mathcal{A} \to \mathbb{R}$ that satisfy

$$\begin{aligned}
\alpha_1(\mathcal{A}) &= (\alpha_1(a_1),\ldots,\alpha_1(a_N)) \\
&= (\alpha_2(a_1),\ldots,\alpha_2(a_N)) + \mu \cdot (1,\ldots,1) = \alpha_2(\mathcal{A}) + \mu \cdot (1,\ldots,1)
\end{aligned}$$

induce the same lifted polytope up to a translation by μ in the last coordinate of every lattice point. For more, see Definition 2.1.14.

We will only consider the following definitions for lattice polytopes, even though they hold more generally.

Definition 2.1.11 ([GKZ94, Chapter 7 1.D])**.** Let Q be a lattice polytope in $\mathbb{R}^m$, $n = |Q \cap Z^m|$. The *GKZ-vector* of a triangulation $\mathcal{T}$ is the vector

$$\varphi_\mathcal{T} := (\mathrm{vol}_\mathcal{T}(p_i) \mid i \in \{0,\ldots,n\}),$$

where p_i are the lattice points of P in a fixed order and

$$\mathrm{vol}_\mathcal{T}(p_i) = \sum_{\substack{\Delta \text{ simplex in } \mathcal{T} \\ p_i \in \Delta}} \text{euclidean volume}(\Delta).$$

Definition 2.1.12 ([GKZ94, Chapter 7.D, Definition 1.6])**.** Let Q be a lattice polytope in $\mathbb{R}^m$, $n = |Q \cap Z^m|$. The *secondary polytope* $\mathcal{P}(Q)$ is the convex hull $\mathrm{conv}\{\varphi_\mathcal{T}\}$ in the space $\mathbb{R}^m$ of the GKZ-vectors for all the triangulations $\mathcal{T}$ of Q.

The secondary polytope contains much data about the regular subdivisions of a lattice polytope.

Theorem 2.1.13 ([GKZ94, Chapter 7.D, Theorem 1.7])**.** *Let Q be a lattice polytope.*

(a) *The vertices of the secondary polytope $\mathcal{P}(Q)$ are precisely the GKZ-vectors of the regular triangulations of Q.*

(b) For a regular triangulation $\mathcal{T}$ of Q we have $\varphi_{\mathcal{T}} \neq \varphi_{\mathcal{T}'}$ for any other triangulation $\mathcal{T}'$ of Q.

(c) The secondary fan of Q coincides with the (outer) normal fan of the secondary polytope $\mathcal{P}(Q)$ of Q.

There are algorithmic methods to compute all triangulations of a given point configuration and by that obtaining the GKZ-vectors, the secondary polytope and the secondary fan. They are implemented in different software, like `Gfan` [Jen], `TOPCOM` [Ram02] and `MPTOPCOM` [JJK20, JJK18].

We can assign a *dual polyhedral complex* to a polytope with a regular subdivision:

Definition 2.1.14. Let P be an n-dimensional polytope in $\mathbb{R}^n$, $\omega \in \mathbb{R}^N$ a weight vector, where $N = |P \cap \mathbb{Z}^n|$. Recall, the lifted polytope is $\widetilde{P}_\omega = \{(v_i, \omega_i) : v_i \in P \cap \mathbb{Z}^n, i = 1, \ldots, N\}$.
Let $\pi : \mathbb{R}^{n+1} \to \mathbb{R}^n$ be the projection to the first n coordinates.

By Definition 2.1.8 we know that the subdivision induced by the weights ω consists of the projection of the upper faces of $\widetilde{P}_\omega$ to $\mathbb{R}^n$. Any polytope in the subdivision of P is of the form $\pi(F)$, where F is an upper face of $\widetilde{P}_\omega$, i.e., for some $\mathbf{v} \in \mathbb{R}^{n+1}$ with last coordinate positive:

$$F = \text{face}_{\mathbf{v}}(\widetilde{P}_\omega) := \{\mathbf{x} \in \widetilde{P}_\omega \mid \mathbf{v} \cdot \mathbf{x} \geq \mathbf{v} \cdot \mathbf{y} \ \forall \mathbf{y} \in \widetilde{P}_\omega\}.$$

Let $\mathcal{N}(F)$ be the (outer) normal cone to F, i.e., $\mathcal{N}(F) = \{\mathbf{v} \in \mathbb{R}^{n+1} : \text{face}_{\mathbf{v}}(\widetilde{P}_\omega) = F\}$. By restricting the projection π to the intersection of $\mathcal{N}(F)$ with the plane $x_{n+1} = 1$ and denoting this by $\tilde{\pi}$, we obtain the set $\tilde{\pi}(\mathcal{N}(F)) := \{\mathbf{w} \in \mathbb{R}^n \mid (\mathbf{w}, 1) \in \mathcal{N}(F)\}$. As F ranges over all upper faces of $\widetilde{P}_\omega$ the sets $\tilde{\pi}(\mathcal{N}(F))$ form a polyhedral complex in $\mathbb{R}^n$. This is the *dual polyhedral complex* to the subdivision of P induced by ω.

A translation of the lifted polytope in the direction of the $(n+1)$th-coordinate will give the same dual polyhedral complex. Hence, we sometimes consider the weight vector in the quotient space $\omega \in \mathbb{R}^N / (1, \ldots, 1)\mathbb{R}$.

As we see from this definition there is a correspondence between the polytopes that are elements of the subdivision and the cells of the dual polyhedral complex.

Corollary 2.1.15. *Let $P \subset \mathbb{R}^n$ be a n-dimensional polytope with weight vector ω and lifted polytope $\widetilde{P}_\omega \subset \mathbb{R}^{n+1}$. There is a one-to-one correspondence between the elements of the subdivision of P induced by ω and the cells of the dual polyhedral complex: For a polytope F in the subdivision of P its dual cell in the dual polyhedral complex is given by $F^\vee := \tilde{\pi}(\mathcal{N}(F)) = \{\mathbf{w} \in \mathbb{R}^n \mid (\mathbf{w}, 1) \in \mathcal{N}(F)\}$. The map $F \mapsto F^\vee$ is a bijection and it is inclusion reversing. For elements Q, R of the subdivision, we know:*

(i) If Q is a face of R, then $R^\vee$ is a face of $Q^\vee$.
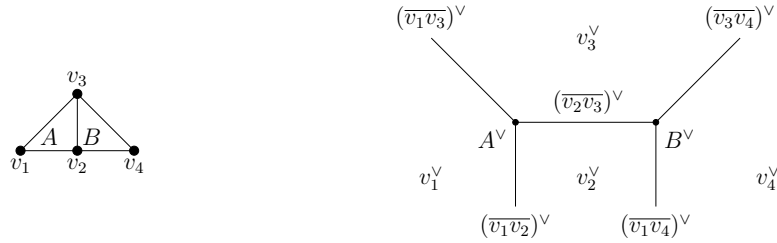
Figure 2.1: A regular subdivision and its dual polyhedral complex

(ii) *The affine linear subspaces* $\mathrm{Aff}(Q)$ *and* $\mathrm{Aff}(Q^\vee)$ *are orthogonal in* $\mathbb{R}^n$.

(iii) Q *is contained in a facet of* P *if and only if* $Q^\vee$ *is an unbounded cell.*

(iv) *If* $\dim(Q) = k$, *the dual cell* $Q^\vee$ *has dimension* $n - k$.

2.2 Brief introduction to tropical geometry

This section gives a brief overview of tropical geometry, but it can also be used as a reference section. In this introduction, we focus on the case of tropical codimension 1 varieties, i.e., tropical plane curves and hypersurfaces, since these are the main objects this thesis deals with. An extensive and detailed introduction to tropical geometry can be found in [MS15].

We present three different aspects of tropical geometry: tropical algebraic geometry (Section 2.2.1), tropical geometry as a shadow of algebraic geometry by tropicalization (Section 2.2.2), and the duality between tropical and polyhedral geometry (Section 2.2.3).

There are two conventions with different advantages in tropical geometry: *min*- and *max*-convention. See Remark 2.2.21. This thesis adheres to the *max*-convention unless explicitly stated otherwise.

2.2.1 Tropical algebraic geometry

Tropical algebraic geometry is concerned with similar questions as algebraic geometry, with the difference that instead of polynomials we consider tropical polynomials. In this section we introduce the tropical semifield, which is the base of tropical arithmetic, and tropical polynomials. The show ideas of what tropical algebraic geometry is concerned with and to give the foundations for Part I of this thesis, we present foundational results of tropical intersection of plane curves.

(a) $V(x \oplus y \oplus 0)$, a non-degenerate tropical line   (b) $V(x \oplus y)$, a degenerate tropical line
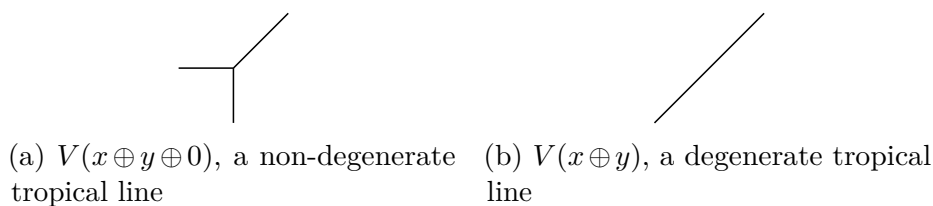
Figure 2.2: A degenerate and a non-degenerate tropical line in $\mathbb{R}^2$. In this thesis tropical lines will always be non-degenerate.

Definition 2.2.1. The *tropical semifield* $(\mathbb{R} \cup \{-\infty\}, \oplus, \odot)$ is the set $\mathbb{R} \cup \{-\infty\}$ together with the operations $x \oplus y = \max\{x, y\}$ and $x \odot y = x + y$, where $-\infty$ is the neutral element of addition, and we have $x \odot (-\infty) := -\infty \ \forall x \in \mathbb{R} \cup \{-\infty\}$.

A *tropical (Laurent) monomial* is a finite tropical product of variables x_i with integer coefficients $u_i \in \mathbb{Z}$

$$\mathbf{x}^{\odot \mathbf{u}} = x_1^{\odot u_1} \cdots x_n^{\odot u_n} = \sum_{i=1}^{n} u_i x_i = \mathbf{u} \cdot \mathbf{x}.$$

A *tropical (Laurent) polynomial* is a finite tropical linear combination of tropical monomials with coefficients $\lambda_{\mathbf{u}}$ in the tropical semiring

$$f = \bigoplus_{\mathbf{u} \in \mathbb{Z}^n} \lambda_{\mathbf{u}} \odot \mathbf{x}^{\odot \mathbf{u}}.$$

The *tropical hypersurface* $\mathrm{Trop}(V(f))$ is defined as

$$\mathrm{Trop}(V(f)) = \{\mathbf{a} \in \mathbb{R}^n \mid \text{the maximum in } f(\mathbf{a}) \text{ is achieved at least twice}\}.$$

In particular, a *tropical plane curve* is given as the tropical hypersurface of a tropical polynomial in two variables.

In this thesis, we will always assume that tropical lines in $\mathbb{R}^2$ are non-degenerate. This means that each tropical plane line consists of three rays in the directions $-e_1$, $-e_2$ and $e_1 + e_2$ given by the standard basis of $\mathbb{R}^2$ joined together in one vertex. See Figure 2.2 for a picture of a non-degenerate tropical line and a degenerate tropical line.

By [MS15, Structure Theorem for Tropical Varieties, Theorem 3.3.5], tropical varieties are *balanced weighted polyhedral complexes* (Definition 2.1.4). For plane tropical curves this means, that for each edge e there is an associated weight $m(e)$, also called *multiplicity*, such that each vertex t of the curve satisfies the following *balancing condition*:

$$\sum_{e \text{ incident edge to } t} m(e)v(e) = 0,$$

where $v(e) \in \mathbb{Z}^2$ is the *primitive direction vector* of e, i.e., the integer direction vector of the edge e with smallest absolute value of the coordinates. The information on the correct multiplicity for the tropical plane curve is stored in its tropical polynomial and can be extracted by using the duality explained in Section 2.2.3. See Lemma 2.2.15 and Example 2.2.16.

Definition 2.2.2 ([RGST05]). Two tropical plane curves C, D intersect *transversally* if their intersection consists only of finitely many points that are not vertices of C or D. Otherwise they intersect *non-transversally*.

Definition 2.2.3 ([RGST05], intersection multiplicity). For two tropical plane curves C, D intersecting transversally, the intersection multiplicity in a point $p \in C \cap D$ is defined as follows: Since p is not a vertex of C or D it is contained in exactly one edge in C and D each. Let $u_1 \in \mathbb{Z}^2$ be the primitive direction vector of the edge in C that contains p, and $u_2 \in \mathbb{Z}^2$ the primitive direction vector of the edge in D that contains p. The *intersection multiplicity* of C and D in p is:

$$(C \cdot D)_p = |\det(u_1, u_2)| \cdot m_1 \cdot m_2,$$

where m_1 resp. m_2 is the multiplicity of the edge of C resp. D that contains p.

The *intersection multiplicity* of the two curves is computed via:

$$C \cdot D = \sum_{p \in C \cap D} (C \cdot D)_p.$$

If two curves intersect non-transversally, the intersection multiplicity cannot be computed as above. For this we need the stable intersection principle. Let $C_{\epsilon v}$ denote the tropical curve $C + \epsilon v$ where $v \in \mathbb{R}^2$ is an arbitrary vector and $\epsilon \in \mathbb{R}$ is small. Thus, $C_{\epsilon v}$ is a tropical plane curve nearby the original curve C.

Theorem 2.2.4 ([MS15, Theorem 1.3.3]). *The limit of the point configuration* $C_{\epsilon v} \cap D_{\epsilon w}$ *is independent of the choice of perturbations* $v, w \in \mathbb{R}^2$. *It is a well-defined multiset of* $c \cdot d$ *points contained in the intersection* $C \cap D$ *with* $c = \deg(C)$, $d = \deg(D)$.

Definition 2.2.5 ([RGST05], stable intersection). Let C, D be two tropical plane curves. The *stable intersection* of C and D is the multiset of points

$$C \cap_{st} D = \lim_{\epsilon \to 0} (C_{\epsilon v} \cap D_{\epsilon w}),$$

where $v, w \in \mathbb{R}^2$ are generic vectors.

2.2.2 Tropicalization of algebraic varieties

Tropical geometry can be considered as a combinatorial shadow or a linear degeneration of algebraic variety. In this section we formalize these notions. The main reference is [MS15].

Definition 2.2.6. Let K be a field and let K^* denote the non-zero elements of K. A *non-Archimedean valuation* on K is a function $\mathrm{val} \colon K \to \mathbb{R} \cup \infty$ that satisfies the following conditions:

  (a) $\mathrm{val}(a) = \infty$ if and only if $a = 0$.

  (b) $\mathrm{val}(ab) = \mathrm{val}(a) + \mathrm{val}(b)$ for all $a, b \in K$.

  (c) $\mathrm{val}(a + b) \geq \min\{\mathrm{val}(a), \mathrm{val}(b)\}$ for all $a, b \in K$.

As we will not consider any other type of valuation in this thesis, a valuation will always be a non-Archimedean valuation.

Since only 0 maps to ∞, we can identify a valuation with its restriction $K^* \to \mathbb{R}$. Thus the image of a valuation is an additive subgroup of $\mathbb{R}$.

A valuation is called *trivial* if $\mathrm{val}(a) = 0$ for all $a \in K^*$. Every field can be equipped with a trivial valuation.

We call (K, val) a *valued field* if K is a field and val a valuation on K.

Remark 2.2.7. Throughout this work, we will assume that $1 \in \mathrm{im}(\mathrm{val})$ for any given non-trivial valuation val on K. This is no severe restriction, since for any $\lambda \in \mathbb{R}_{>0}$ the map $(\lambda \cdot \mathrm{val}) \colon K^* \to \mathbb{R}$ is also a valuation. Thus, we can always assume that $\mathbb{Z} \subset \mathrm{im}(\mathrm{val})$ for a non-trivial valuation. If the field K is algebraically closed, the image of a non-trivial valuation on K contains $\mathbb{Q}$ and is thus dense in $\mathbb{R}$.

Definition 2.2.8. Let (K, val) be a valued field K and let $R := \{a \in K \,|\, \mathrm{val}(a) \geq 0\}$ be the associated valuation ring with maximal ideal $\mathfrak{m} = \{a \in K \,|\, \mathrm{val}(a) > 0\}$. The quotient $\Bbbk := R/\mathfrak{m}$ is called the *residue field*.

The map $\mathrm{res} \colon R \to \Bbbk$, $a \mapsto a + \mathfrak{m}$ is called the *residue map*. It can be extended to $R[x] \to \Bbbk[x]$ by $f(x) = \sum_{i=0}^{n} a_i x^i \in R[x] \mapsto \mathrm{res}(f)(x) = \sum_{i=0}^{n} \mathrm{res}(a_i) x^i \in \Bbbk[x]$.

A valued field is called *Henselian* if it satisfies the following property: For every $f(x) \in R[x]$ such that $\mathrm{res}(f)(x)$ has a simple root $a \in \Bbbk$, there exists an element $r \in R$ such that $\mathrm{res}(r) = a$ and $f(r) = 0$.

In this work, we will only consider Henselian fields with a 2-divisible value group. An example of a Henselian valued field for which the image of the valuation is dense in $\mathbb{R}$ is the field of Puiseux series over $\mathbb{C}$ or $\mathbb{R}$.

Example 2.2.9. The field of *Puiseux series* $\mathbb{K}\{\{t\}\}$ with coefficients in $\mathbb{K} \in \{\mathbb{R}, \mathbb{C}\}$ is defined as the set of all formal power series

$$c(t) = c_1 t^{a_1} + c_2 t^{a_2} + c_3 t^{a_3} + \cdots,$$

where $a_1 < a_2 < a_3 < \cdots$ are elements in $\mathbb{Q}$ with a common denominator and $c_j \in \mathbb{K} \setminus \{0\}$ for all indices j.

It has a natural non-trivial valuation given by

$$\mathrm{val} : \mathbb{K}\{\{t\}\}^* \to \mathbb{R}, \ c(t) \mapsto a_1,$$

where a_1 is the lowest exponent of t appearing in the series $c(t)$.

The residue map is given by $\mathrm{res} : \mathbb{K}\{\{t\}\} \to \mathbb{K}, \ c(t) \mapsto c_1$, where c_1 is the coefficient of the term with the smallest exponent of t appearing in the series $c(t)$. It can be shown that $\mathbb{K}\{\{t\}\}$ is Henselian.

Furthermore, it can be proven that the field of Puiseux series over $\mathbb{C}$ is algebraically closed.

Definition 2.2.10. Let (K, val) be a valued field and $F = \sum_{\mathbf{u} \in \mathbb{N}^n} a_{\mathbf{u}} \mathbf{x}^{\mathbf{u}} \in K[\mathbf{x}]$ a polynomial in n variables $\mathbf{x} = (x_1, \ldots, x_n)$. There is a canonical way, called *tropicalization*, to degenerate F to a tropical polynomial:

$$\begin{aligned} \mathrm{Trop}(F) &= \bigoplus_{\mathbf{u} \in \mathbb{N}^n} - \mathrm{val}(a_{\mathbf{u}}) \odot \mathbf{x}^{\odot \mathbf{u}} \\ &= \max_{\mathbf{u} \in \mathbb{N}^n} \{- \mathrm{val}(a_{\mathbf{u}}) + \mathbf{u} \cdot \mathbf{x}\}. \end{aligned}$$

The following theorem shows that there are different ways how to view or compute the tropicalization of an algebraic variety.

Theorem 2.2.11 ([MS15, Theorem 3.2.3], Fundamental Theorem of Tropical Algebraic Geometry)**.** *Let K be an algebraically closed field with a nontrivial valuation, let I be an ideal in $K[x_1^{\pm}, \ldots, x_n^{\pm}]$ and length $X = V(I)$ be its variety in the algebraic torus $T^n \cong (K^*)^n$. Then the following three subsets of $\mathbb{R}^n$ coincide*

1. the tropical variety $\mathrm{Trop}(X) := \bigcap_{F \in I} \mathrm{Trop}(V(F))$,

2. the closure of the set of coordinatewise valuations of points in X

$$\mathrm{val}(X) = \overline{\{(\mathrm{val}(y_1), \ldots, \mathrm{val}(y_n)) : (y_1, \ldots, y_n) \in X\}}.$$

Furthermore, if X is irreducible and $\mathbf{w} \in (\mathrm{im}(\mathrm{val}))^n \cap \mathrm{Trop}(X)$, then the set

$$\{\mathbf{y} \in X : \mathrm{val}(\mathbf{y}) = \mathbf{w}\}$$

is Zariski dense in the classical variety X.

Note that for the tropicalization of a hypersurface $V(I)$ with $I = \langle F \rangle$, we do not need to take the intersection over the tropicalization of all polynomials in I to obtain the tropical hypersurface, but that $\text{Trop}(V(I)) = \text{Trop}(V(F))$.

Definition 2.2.12. An algebraic variety $X = V(I)$ is called a *lift* of a tropical variety Y, if $\text{Trop}(X) = Y$.

For two tropical varieties Y, Y' satisfying some relative relation, e.g. $Y' \subset Y$, with a fixed lift X for one of them, we are interested in the *relative realizability*, i.e. the answer to the question of whether there exists an algebraic variety X' a lift of Y' such that the pair X, X' satisfies the same relative relation as the tropical varieties, and if yes, how many there are. This number is then called the *lifting multiplicity*.

One example for this is the lifting multiplicity of tropical bitangents as explained in Definition 3.3.1.

Another example is a tropical hypersurface X satisfying point conditions in $\mathbb{R}^n$. For a fixed set of lifts of these points in $\mathbb{K}^n$, we can ask for the number of lifts of X that satisfy these point conditions, the lifting multiplicity. This is the foundation for the work in Part II. See Section 7.2 for point conditions on tropical surfaces.

2.2.3 Duality between tropical and polyhedral geometry

The duality between cells of tropical hypersurfaces and subdivisions of polytopes is an important concept in tropical geometry. We introduce the Newton polytope and see that tropical hypersurfaces are balanced polyhedral complexes. This section further provides examples how the duality can be used to determine curves or surfaces. We conclude with an explanation of how to switch between the two different conventions (*min*- and *max*-convention) in tropical geometry. The definitions in this chapter and in the following are using *max*-convention unless explicitly stated otherwise.

Definition 2.2.13. For a tropical polynomial $f = \bigoplus_{\mathbf{u}} \lambda_{\mathbf{u}} \odot \mathbf{x}^{\odot \mathbf{u}}$, the *Newton polytope* N_f is defined as the lattice polytope

$$N_f = \text{conv}\{\mathbf{u} | \lambda_{\mathbf{u}} \neq \infty\}.$$

Let n be the number of variables in f. The tropical coefficients $\lambda_{\mathbf{u}}$ of f induce a lifting function of $N_f \cap Z^n$ to $\mathbb{R}$ and thus induce a regular subdivision of N_f as described in Definition 2.1.8. The subdivision induced by the coefficients $\lambda_{\mathbf{u}}$ will be denoted by $\mathcal{S}_{\lambda_{\mathbf{u}}}$. In this setting we can write the secondary cone of $\mathcal{S}$ as

$$\Sigma(\mathcal{S}) = \{\lambda \in \mathbb{R}^{|N_f \cap \mathbb{Z}^n|} | \mathcal{S}_\lambda = \mathcal{S}\}.$$

Figure 2.3: A tropical curve with its multiplicities and primitive direction vectors. It is a balanced polyhedral complex.

Proposition 2.2.14 ([MS15, Proposition 3.1.6]). *Let $f \in K[x_1^\pm, \ldots, x_n^\pm]$ be a Laurent polynomial. The tropical hypersurface $\mathrm{Trop}(V(f))$ is the support of a polyhedral complex of pure dimension $n-1$ in $\mathbb{R}^n$.*
It is the $(n-1)$-skeleton of the polyhedral complex dual to the subdivision of the Newton polytope of $f = \sum_{\mathbf{u} \in \mathbb{Z}^n} c_\mathbf{u} \mathbf{x}^\mathbf{u}$ given by the weights $\mathrm{val}(c_\mathbf{u})$ on the lattice points in $\mathrm{Newt}(f)$.

As already mentioned in Section 2.2.1 tropical varieties are balanced weighted polyhedral complexes. In the proposition above, we see how a tropical hypersurface arises as a polyhedral complex. The following lemma explains how to get the multiplicities for the balancing condition (Definition 2.1.4) from the tropical polynomial.

Lemma 2.2.15 ([MS15, Proposition 3.3.2 and Lemma 3.4.6]). *Let $F = \sum a_\mathbf{u} x^\mathbf{u} \in K[x_1^\pm, \ldots, x_n^\pm]$, let $\mathcal{S}$ be the regular subdivision of the Newton polytopes N_f induced by $(-\mathrm{val}(c_\mathbf{u}))$. Let $\mathcal{C}$ be the polyhedral complex supported on $\mathrm{Trop}(V(F))$ dual to $\mathcal{S}$.*
The multiplicity of a maximal cell σ of $\mathcal{C}$ is the lattice length of the edge $e(\sigma)$ of $\mathcal{S}$ dual to σ and with these multiplicities $\mathrm{Trop}(V(F))$ is a balanced polyhedral complex.

We illustrate this for a plane curve in the following example.

Example 2.2.16. Consider the polynomial $f = 0 \oplus (-2) \odot x \oplus x \odot y \oplus x^2$. It's Newton polytope N_f is the triangle with lattice points $(0,0)$, $(1,0)$, $(1,1)$ and $(2,0)$. The dual subdivision is the trivial subdivision. Therefore, we have two edges of lattice length 1 and one edge of lattice length 2.

The maximal cells of the polyhedral complex supporting $V(f)$ are the three rays dual to the edges of N_f. Figure 2.3 shows N_f, the tropical curve $V(f)$, the primitive direction vectors and the multiplicities.

Definition 2.2.17. A tropical hypersurface $\mathrm{Trop}(V(f)) \subset \mathbb{R}^n$ has *degree d* if its Newton polytope is

$$d\Delta_n := \mathrm{conv}\{\mathbf{0}, d \cdot e_i \mid i = 1, \ldots, n\} \subset \mathbb{R}^n.$$

Definition 2.2.18. A tropical hypersurface $\mathrm{Trop}(V(f))$ is *smooth* if the regular subdivision of N_f induced by the coefficients of $\mathrm{Trop}(f)$ is a unimodular triangulation.

In the case of a smooth hypersurface all multiplicities of the maximal cells in the polyhedral complex are one. For a tropical plane curve this means that all edges have weight one.

The name smooth for tropical surfaces dual to unimodular triangulations is justified by [MS15, Proposition 4.5.1] proving that for a Laurent polynomial f inducing a regular unimodular triangulation of its Newton polytope the hypersurface $V(f) \subset (K^*)^n$ is smooth.

For a tropical polynomial f with coefficients $\lambda_{\mathbf{u}}$, the subdivision $\mathcal{S}_{\lambda_{\mathbf{u}}}$ of N_f is dual to the tropical hypersurface $\mathrm{Trop}(V(f))$ via an inclusion reversing bijection. This duality comes from the duality described in Corollary 2.1.15. The notation $\cdot^\vee$ as used in Corollary 2.1.15 will from now on not only refer to the dual element in the polyhedral complex, but also the other way round.

Example 2.2.19. For a tropical plane curve the duality means especially:

$$
\begin{aligned}
\text{subdivision} &\longleftrightarrow \text{tropical curve } C, \\
2-\text{dimensional cell } Q &\longleftrightarrow \text{Vertex } v, \\
\text{Edge } E &\longleftrightarrow \text{Edge } e, \\
\text{Vertex } V &\longleftrightarrow \text{connected region } V^\vee \text{ of } \mathbb{R}^2 \setminus C.
\end{aligned}
$$

The duality can be used to compute the tropical curve from the subdivision and vice versa. Starting with the subdivision and the weight vector $(\lambda_{\mathbf{u}})$ that induces the subdivision, we construct the tropical curve as follows: The edges of the tropical curve are outward orthogonal to the edges in the subdivision. A vertex of the curve is dual to a 2-dimensional cells $\mathrm{conv}\{(i_0,j_0),\ldots,(i_k,j_k)\}$ in the subdivision and the coordinates of the vertex in the plane can be computed by solving

$$
\lambda_{i_0,j_0} + i_0 x + j_0 y = \ldots = \lambda_{i_k,j_k} + i_k x + j_k y.
$$

Example 2.2.20. For a tropical surface S, we can also use the duality to describe the vertices and edges of the surface, or equivalently the 3-dimensional regions of $\mathbb{R}^3 \setminus S$. Let Ω be the Newton polytope of S. The computation of the vertices of S from the subdivision of Ω induced by the weight vector to S is analogous to the 2-dimensional case described above. As the computation of the 3-dimensional regions $\mathbb{R}^3 \setminus S$ for a non-trivial subdivision is a collection of the computations for smaller polytopes with the trivial subdivision, we will only illustrate the case of the trivial subdivision here. Also, this is the case used in the investigations in the Chapters 9 and 10.

Since we are in the trivial valuation case, we can assume all weights to be zero. Thus, the unique vertex of S is at $(0,0,0)$. Let $\omega_{i_0}, \ldots, \omega_{i_n}$ denote the vertices of Ω. Each vertex is dual to a 3-dimensional region of $\mathbb{R}^3 \setminus S$. Note that in the trivial valuation case the regions of $\mathbb{R}^3 \setminus S$ are open 3-dimensional cones. The cone dual to a vertex is generated by the outer normal vectors of the facets of Ω that contain the vertex. We use this to compute the rays that span the region $\omega_{i_j}^{\vee}$. The cone spanned by these rays added to the vertex dual to the polytope (here $(0,0,0)$) defines the region. With a non-trivial valuation, we might obtain a polyhedron which is not a cone if some of the rays meet other vertices of the surface.

We illustrate the computation for one example. Let

$$\Omega = \text{conv}\left\{ \begin{pmatrix} 0 \\ 0 \\ 0 \end{pmatrix}, \begin{pmatrix} 0 \\ 1 \\ 1 \end{pmatrix}, \begin{pmatrix} 0 \\ 1 \\ 2 \end{pmatrix}, \begin{pmatrix} 0 \\ 2 \\ 1 \end{pmatrix}, \begin{pmatrix} 1 \\ 0 \\ 0 \end{pmatrix}, \begin{pmatrix} 1 \\ 3 \\ 1 \end{pmatrix} \right\}.$$

The vertices of this polytope are

$$\omega_0 = \begin{pmatrix} 0 \\ 0 \\ 0 \end{pmatrix}, \ \omega_2 = \begin{pmatrix} 0 \\ 1 \\ 2 \end{pmatrix}, \ \omega_3 = \begin{pmatrix} 0 \\ 2 \\ 1 \end{pmatrix}, \ \omega_4 = \begin{pmatrix} 1 \\ 0 \\ 0 \end{pmatrix}, \ \omega_5 = \begin{pmatrix} 1 \\ 3 \\ 1 \end{pmatrix}.$$

We compute the region dual to the first vertex $\omega_0 = (0,0,0)$. First we need to determine to which facets ω_0 belongs: These are $\overline{\omega_0, \omega_2, \omega_3}$, $\overline{\omega_0, \omega_2, \omega_4}$, $\overline{\omega_0, \omega_3, \omega_5}$ and $\overline{\omega_0, \omega_4, \omega_5}$. Since ω_0 is the origin, we can compute the outer normal vector of one of these facets by computing the cross product of the other two vertices spanning the facet and taking care to have the correct signs such that the resulting vector is pointing outwards. Hence, the cone $\omega_0^{\vee}$ is given by the positive hull of the rays:

$$\omega_2 \times \omega_3 = \begin{pmatrix} 0 \\ 1 \\ 2 \end{pmatrix} \times \begin{pmatrix} 0 \\ 2 \\ 1 \end{pmatrix} = \begin{pmatrix} -3 \\ 0 \\ 0 \end{pmatrix},$$

$$\omega_4 \times \omega_2 = \begin{pmatrix} 1 \\ 0 \\ 0 \end{pmatrix} \times \begin{pmatrix} 0 \\ 1 \\ 2 \end{pmatrix} = \begin{pmatrix} 0 \\ -2 \\ 1 \end{pmatrix},$$

$$\omega_3 \times \omega_5 = \begin{pmatrix} 0 \\ 2 \\ 1 \end{pmatrix} \times \begin{pmatrix} 1 \\ 3 \\ 1 \end{pmatrix} = \begin{pmatrix} -1 \\ 1 \\ -2 \end{pmatrix},$$

$$\omega_5 \times \omega_4 = \begin{pmatrix} 1 \\ 3 \\ 1 \end{pmatrix} \times \begin{pmatrix} 1 \\ 0 \\ 0 \end{pmatrix} = \begin{pmatrix} 0 \\ 1 \\ -3 \end{pmatrix}.$$

For a proof of the duality as described in Examples 2.2.19 and 2.2.20, and for further details, see [MS15].

Remark 2.2.21. There exist two parallel conventions with regard to tropical arithmetic: The tropical semifield can also be defined as $(\mathbb{R} \cup \{\infty\}, \oplus, \odot)$ with $\oplus = \min$ and $\odot = +$. This *min*-convention is used in [MS15].

The two conventions have different advantages. The difference in working with the *min*- and *max*-convention lies particularly in the tropicalization of a polynomial and the duality. The tropicalization of a polynomial $f = \sum_{\mathbf{u}} c_{\mathbf{u}} \mathbf{x}^{\mathbf{u}}$ in the *min*-convention is given by substituting $+ \mapsto \min$, $\cdot \mapsto +$ and $c_{\mathbf{u}} \mapsto \mathrm{val}(c_{\mathbf{u}})$. With respect to the duality the difference to the *max*-convention are:

1. To obtain the dual subdivision of the Newton Polytope in the *min*-convention we use the lower faces instead of the upper faces. See Definition 2.1.8. Since the *max*-convention uses $c_{\mathbf{u}} \mapsto -\mathrm{val}(c_{\mathbf{u}})$, this yields the same subdivision for the tropicalization of a fixed polynomial for both conventions; see next item.

2. The secondary fan to the subdivisions coming from projecting the lower faces is the inner normal fan of the secondary polytope. To switch from the projection of the lower faces to the projection of the upper faces, we have to multiply with (-1): If a weight vector w induces a subdivision $\mathcal{S}$ via the lower faces, then $-w$ induces the same subdivision via the projection of the upper faces. See Remark 2.1.6.

3. When constructing the dual polyhedral complex to the subdivision as in Definition 2.1.14, the inner normal fan is used. This means that for example for plane curves the direction of the edges is inwards orthogonal to the edges in the dual subdivision.

In this thesis we will use the *max*-convention unless explicitly stated otherwise.

Part I

Tropical bitangents to plane quartic curves

Chapter 3

Preliminaries

In this chapter, we present the state of the art on tropical bitangents of plane quartics. We first introduce tropical plane quartic curves and their triangulations in Section 3.1, [BLM$^+$16, BJMS15]. Then, in Section 3.2 we define tropical bitangents, their equivalence classes and shapes according to [LM20, CM21]. In Section 3.3, the results of [LM20, CM21] with respect to the complex and real lifting behavior of tropical bitangent classes are given.

Notation 3.0.1. In Part I of this thesis let $\mathbb{K}_{\mathbb{R}}$ be a real closed complete non-archimedean valued field, and let $\mathbb{K}$ be its algebraic closure. As an example keep the fields of Puiseux series $\mathbb{R}\{\{t\}\}$ and $\mathbb{C}\{\{t\}\}$ in mind (Example 2.2.9).

3.1 Tropical quartic curves

In this section, we introduce tropical quartic curves, the action of the permutation group S_3 on the dual subdivision, and recall the definition of the skeleton and of generalized leaves. Main references for this section are [BLM$^+$16, BJMS15].

Definition 3.1.1. A *plane quartic curve $V(f)$* is the zero set of a polynomial of degree four

$$f(x,y) = a_{00} + a_{10}x + a_{01}y + a_{20}x^2 + a_{11}xy + a_{02}y^2 + a_{30}x^3 + a_{21}x^2y \quad (3.1)$$
$$+ a_{12}xy^2 + a_{03}y^3 + a_{40}x^4 + a_{31}x^3y + a_{22}x^2y^2 + a_{13}xy^3 + a_{04}y^4.$$

We say a tropical plane curve is a *tropical quartic curve* if its Newton polygon is the 4-dilated 2-dimensional simplex $4\Delta_2$.

For a smooth tropical quartic curve the dual subdivision is a unimodular triangulation of $4\Delta_2$ in which every lattice point is a vertex of the subdivision; see Definition 2.2.18. Since the $|4\Delta_2 \cap \mathbb{Z}^2| = 15$ lattice points p_{ij} correspond to the monomials $x^i y^i$ of a polynomial f defining a lift of the tropical quartic, this implies in particular that for any lift the coefficients a_{ij} are all non-zero.

Notation 3.1.2. We write p_{ij} for the lattice point (i,j) in $4\Delta_2$. The valuations of the coefficients of the polynomial f will be denoted $\lambda_{ij} = \text{val}(a_{ij})$. Thus, the tropicalization of $V(f)$ is given by the tropical polynomial with coefficients $-\lambda_{ij}$. The subdivision induced by $(-\lambda_{ij})$ will be denoted $\mathcal{T}_{(-\lambda_{ij})}$ or $\mathcal{T}$ if there is no danger of confusion. The notation $\cdot^{\vee}$ is used to refer to the dual of an edge or triangles of the subdivision $\mathcal{T}$ in the tropical curve Γ, and vice versa. We direct the reader to Corollary 2.1.15, Proposition 2.2.14 and Example 2.2.19 for some background on this duality. The secondary cone (Definition 2.1.10) of a subdivision $\mathcal{T}$ of $4\Delta_2$ is a relative open cone in $\mathbb{R}^{15}$ denoted by $\Sigma(\mathcal{T})$. The tropical quartic curve defined by a point $c \in \Sigma(\mathcal{T})$ as its coefficients will be written as Γ_c. The order of coordinates in $\Sigma(\mathcal{T}) \subset \mathbb{R}^{15}$ is given by the order of the monomials in Equation (3.1).

Let S_3 denote the permutation group on 3 elements. Consider a homogenized quartic polynomial

$$
\begin{aligned}
f^{\text{hom}}(x,y,z) = {} & a_{004}z^4 + a_{103}xz^3 + a_{013}yz^3 + a_{202}x^2z^2 + a_{112}xyz^2 + a_{022}y^2z^2 \\
& + a_{301}x^3z + a_{211}x^2yz + a_{121}xy^2z + a_{031}y^3z + a_{400}x^4 + a_{310}x^3y \\
& + a_{220}x^2y^2 + a_{130}xy^3 + a_{040}y^4,
\end{aligned}
$$

where $a_{ijk} = a_{ij}$ and $k = 4 - i - j$. An element $\sigma \in S_3$ acts on the indices of the coefficients a_{ijk} by permuting their order. For example $\sigma = (x\,y) \in S_3$ acts via $\sigma(a_{ijk}) = a_{jik}$ by switching the index entry belonging to the x-exponent with the second index that corresponds to the y-exponent. Thus, the image of f^{hom} under $\sigma = (x\,y)$ is

$$
\begin{aligned}
\sigma(f^{\text{hom}}(x,y,z)) = {} & a_{004}z^4 + a_{013}xz^3 + a_{103}yz^3 + a_{022}x^2z^2 + a_{112}xyz^2 + a_{202}y^2z^2 \\
& + a_{031}x^3z + a_{121}x^2yz + a_{211}xy^2z + a_{301}y^3z + a_{040}x^4 + a_{130}x^3y \\
& + a_{220}x^2y^2 + a_{310}xy^3 + a_{400}y^4.
\end{aligned}
$$

In the same way does S_3 act on $\text{Trop}(f)$. As the dual subdivision of the Newton polytope is induced by the coefficients $-\lambda_{ij} = -\text{val}(a_{ij})$, this means that S_3 also acts on the subdivision. The action of S_3 on the subdivisions of the Newton polytope corresponds to the group of rotations and reflections along axes through a vertex of $4\Delta_2$ and the midpoint of the opposite boundary edge. This is visualized in Figure 3.1. An example of the action of S_3 on a unimodular triangulation of $4\Delta_2$ is depicted in Figure 3.2.

Definition 3.1.3. We say that two tropical quartic curves have the same *combinatorial type*, if the they have the same dual subdivision, i.e. their coefficient vectors are in the same secondary cone.

$$(x\,y): \lambda_{ij} \mapsto \lambda_{ji} \qquad (x\,z): \lambda_{ij} \mapsto \lambda_{4-i-j,j}$$
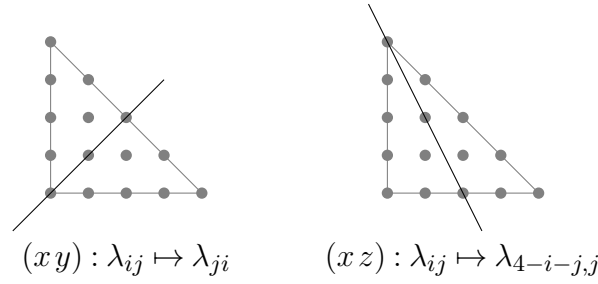
Figure 3.1: Actions of generators of S_3 on the dual subdivision induced by (λ_{ij}).
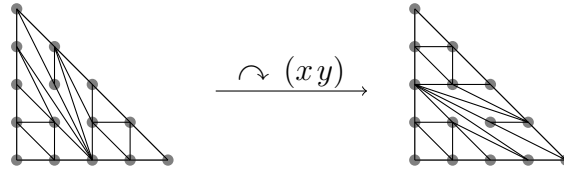
Figure 3.2: Action of $\sigma = (x\,y) \in S_3$ on a unimodular subdivision of $4\Delta_2$. The subdivision on the left side is symmetric with respect to $(x\,z)$.

Two subdivisions $\mathcal{T}, \mathcal{T}'$ of (the lattice point of) $4\Delta_2$ are *symmetric or equivalent up to S_3* if there exists $\sigma \in S_3$ such that $\mathcal{T} = \sigma(\mathcal{T}')$.

Recall that a subdivision is regular, if it can be induced by a lifting function; see Definition 2.1.8.

Theorem 3.1.4 ([BJMS15])**.** *There exist exactly* 1279 *unimodular triangulations of $4\Delta_2$ up to S_3 symmetry, of these exactly* 1278 *are regular.*

This means, that there are 1278 different combinatorial types of tropical smooth quartic curves. We can sort these into four different classes: honeycomb, Mickey Mouse, one-bridge and two-bridge by the shape of their skeleta [BJMS15], [BLM$^+$16, Remark 2.4]. The four types are depicted in Figure 3.3.

Definition 3.1.5 ([BJMS15, BLM$^+$16])**.** Considering a tropical plane curve as a graph. We call an edge a *generalized leaf* if the edge is not part of a loop and one of the two graphs obtained from cutting the edge is a tree.

The *skeleton* of a smooth plane tropical curve is the subgraph obtained by contracting all the leaf edges.

Figure 3.4 shows the skeleton and the leaves of an exemplary quartic curve.

(a) Honeycomb   (b) Mickey Mouse   (c) One-Bridge   (d) Two-Bridge
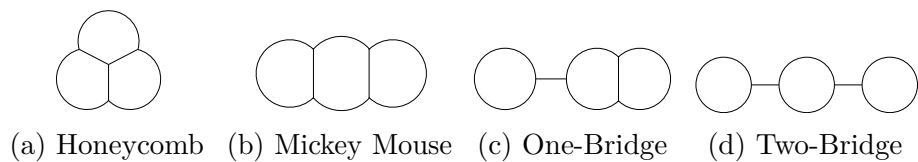
Figure 3.3: The four types of skeleta of tropical quartic curves
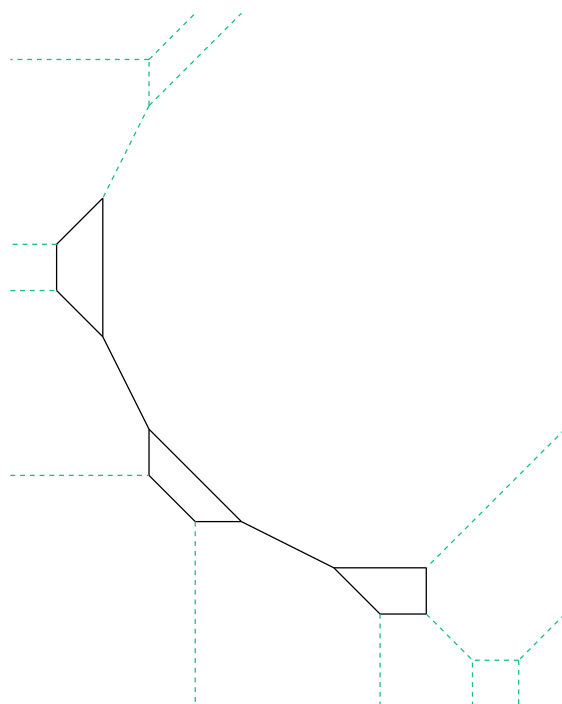
Figure 3.4: Skeleton and generalized leaves of a tropical quartic curve. The generalized leaves are depicted green and dashed. The skeleton, in black solid edges, is of type two-bridge.

3.2 Tropical bitangent lines

We recall the definition of tropical bitangents and collect what is known about them following [BLM$^+$16, LM20, CM21]. After introducing tropical bitangent classes, we review the classification of bitangent shapes and their dual subcomplexes in the subdivision up to S_3-action. In Chapter 4, we will refine this classification by introducing deformation classes.

Definition 3.2.1 ([BLM$^+$16, Definition 3.1]). A tropical line Λ is *bitangent* to a smooth tropical plane quartic curve Γ if their intersection $\Lambda \cap \Gamma$ has two components with stable intersection multiplicity 2, or one component with stable intersection multiplicity 4.

Recall that the stable intersection of plane curves was introduced in Definition 2.2.5. The definition of intersection multiplicity can be found in Definition 2.2.3.

In this thesis we will only consider non-degenerate lines as tropical bitangents. A superabundance phenomenon appears for tropical quartic curves and their bitangents: contrary to the classical algebraic situation a smooth tropical quartic curve can have infinitely many bitangent lines. Figure 3.5 shows a smooth tropical quartic curve with infinitely many tropical bitangent lines: The horizontal ray of every tropical line with vertex in the gray square meets the tropical quartic in the same edge with direction $(-1, 2)$ thus giving intersection multiplicity 2. Similarly the vertical ray of every tropical line with vertex in the gray square meets the tropical quartic in the same edge with direction $(2, -1)$ providing intersection multiplicity 2. Thus every tropical line with vertex in the gray square is bitangent to the quartic.

Theorem 3.2.2 ([BLM$^+$16, Theorem 3.9]). *Every smooth tropical plane quartic curve Γ admits precisely 7 bitangent lines up to equivalence.*

By [BLM$^+$16, Definition 3.8] two bitangents are equivalent if they correspond to linearly equivalent theta characteristics. Descriptively, this means that two bitangents are equivalent if they can be continuously translated into each other while preserving the bitangency [BLM$^+$16].

Definition 3.2.3 ([CM21, Definition 3.1]). Given a tropical bitangent line Λ to a generic tropical smooth plane quartic Γ, its *tropical bitangent class* is the connected components of the subset of $\mathbb{R}^2$ containing the vertices of all tropical bitangent lines linearly equivalent to Λ. The shape of a tropical bitangent class refines each class by coloring those points belonging to the tropical quartic Γ.

The bitangent classes are connected polyhedral complexes [CM21, Corollary 3.3]. Formally they live in the dual plane $\mathbb{R}^\vee$. Standard duality identifies a non-degenerate
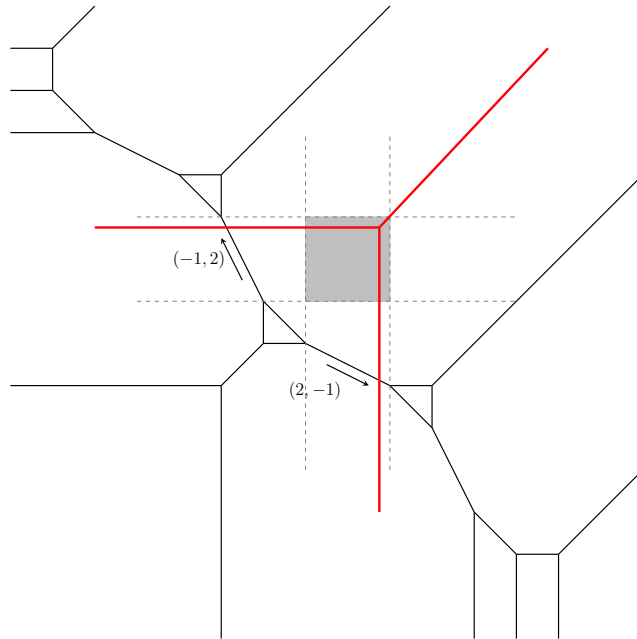
Figure 3.5: Example of a tropical smooth quartic curve with infinitely many bitangent lines: Every tropical line with vertex in the gray square is bitangent to the curve.

tropical line in $\mathbb{R}^2$ with the negative of its vertex as point in the dual plane $\mathbb{R}^\vee$. However, for improved visualization the tropical quartic curve and its bitangent classes will be drawn on the same plane, i.e., we abandon the minus sign in front of the coordinates in the identification with the dual plane. Thus, the bitangent classes are min-tropical sets [CM21, Theorem 1.1]

The classification up to S_3-symmetry of the bitangent shapes by [CM21] is depicted in Figure 3.6.

By [CM21, Corollary 4.12], the existence of a bitangent shape representative for a tropical quartic curve partially determines its dual subdivision. Figure 3.7 shows the summary of the determined parts of the subdivision for S_3-representatives of each shape as in [CM21, Figure 8].

In Figure 3.7, the same color coding as in [CM21] is used: Solid edges have to appear in the triangulations. Dotted edges represent possible edges of which one has to occur in the triangulation. Vertices colored in black are vertices that always must be present, while the colored vertices either have to form a triangle with an edge of the same color or are endpoints of dotted edges of the same color. The colors encode different types of tangencies, see [CM21, Remark 4.13].

Definition 3.2.4. A bitangent shape and its corresponding subcomplex in the triangulation are in *identity position* if they are in position as in Figures 3.6 and 3.7.
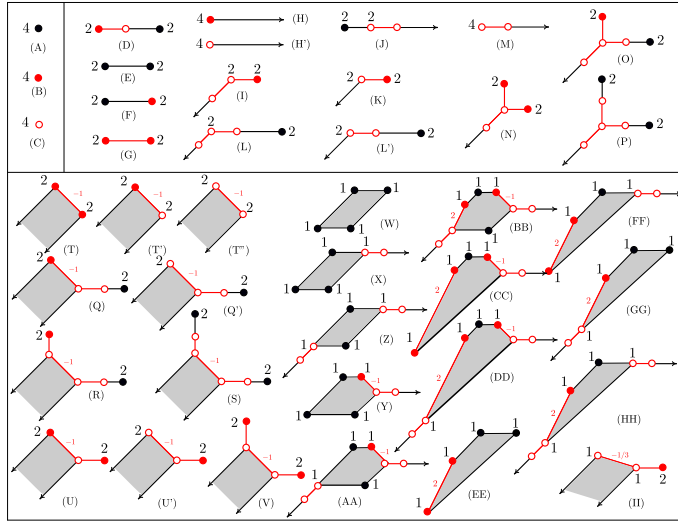
Figure 3.6: Shapes of bitangent classes to tropical smooth quartics. The black numbers above the vertices indicate the lifting representatives in each class and their lifting multiplicities. Red vertices or line segments are contained in the quartic curve, a red vertex filled with white coincides with a vertex of the quartic curve. Figure taken from [CM21, Figure 6].
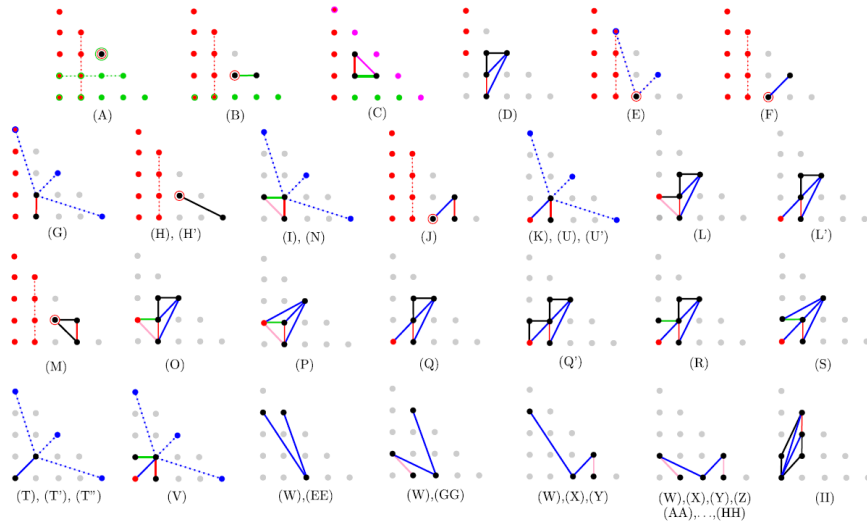
Figure 3.7: The dual subcomplexes of all the bitangent classes. The color coding is explained in [CM21, Remark 4.13]. Figure taken from [CM21, Figure 8].

Notation 3.2.5. For a given tropical quartic curve, not all bitangent shapes might be in identity position. We indicate the element in S_3 that acted on the shape in identity position to bring it in the form in which it appears for the quartic by adding the permutation to the index of the shape. An example is illustrated in Figure 3.8. Figure 3.8c shows a tropical smooth quartic curve with two bitangent classes of shape (B). The dual parts in the subdivision are depicted in Figure 3.8a and 3.8b. We see that the dual part in Figure 3.8a is identity position, so we label the bitangent class in Figure 3.8c with (B). However, the dual subdivision in Figure 3.8b is not in identity position. Letting $\sigma = (x\,z\,y) = (x\,y\,z)^{-1}$ act on the three triangles determined by the bitangent class, we observe that it is moved to identity position. So this bitangent class is labeled $(B)_{(xyz)}$ as its subcomplex is the image of the identity position under $(x\,y\,z)$.

(a) Triangles to (B) in identity position.

(b) Triangles to (B) after action of $(x\,y\,z)$.

(c) Bitangent classes to the curve
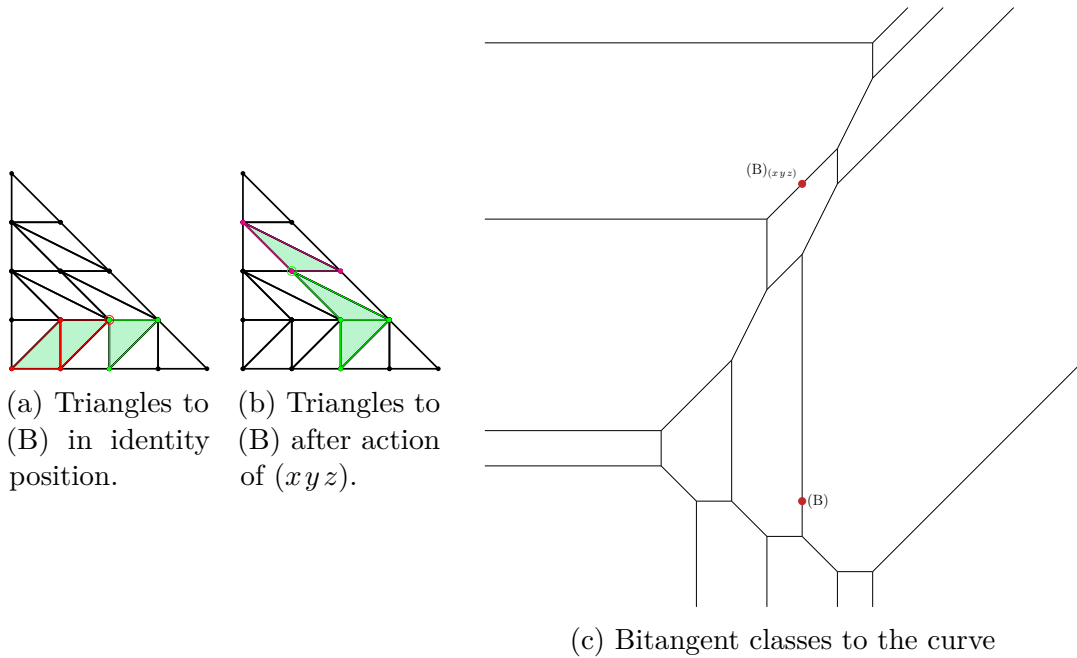
Figure 3.8: Tropical smooth quartic curve with two bitangent classes of shape (B), one in identity position, one the image of $(x\,y\,z) \in S_3$.

3.3 Lifting tropical bitangent lines

The question of relative realizability was introduced in Definition 2.2.12. It is at the core of applying tropical geometry to algebraic problems. In this section we go over the results from [LM20, CM21] on lifting smooth tropical quartics and their tropical bitangents. After introducing the lifting multiplicity, we recall important genericity constraints for the tropical quartic curve from [LM20, CM21] to which we will adhere for the rest of Part I. Finally, we review the real lifting conditions determined in [CM21], on which the main results of Chapter 5 rely, and the position of the tropicalization of tangency points.

Definition 3.3.1 ([CM21, Definition 2.8]). Let $\mathbb{K}$ be the algebraic closure of a real closed, complete non-Archimedean valued field. Let Λ be a tropical bitangent to a tropical smooth quartic curve Γ with tangency points P and P'. We say Λ lifts over $\mathbb{K}$ if there exists a bitangent L to $V(f)$ defined over $\mathbb{K}$ with tangency points p and p' such that

$$\mathrm{Trop}(V(f)) = \Gamma, \quad \mathrm{Trop}(L) = \Lambda, \quad \mathrm{Trop}(p) = P, \quad \text{and} \quad \mathrm{Trop}(p') = P'.$$

Such a tropical bitangent Λ will also be called *realizable.*
  The *lifting multiplicity* of Λ is the number of such bitangent triples (L, p, p').

Remark 3.3.2 (Genericity constraints, [CM21, Remark 2.1]). The work in the following chapters of this thesis builds on the results in [LM20, CM21]. Their computations of the lifting conditions make certain genericity constraints on the tropical quartic Γ necessary.
  As remarked earlier, we assume the tropical quartic curve Γ to be smooth and the tropical bitangent lines to be non-degenerate. Further we assume the following conditions:

  (i) if Γ contains a vertex v adjacent to three bounded edges with directions $-e_1$, $-e_2$ and $e_1 + e_2$, then the shortest of these edges is unique;

 (ii) A lift $V(f)$ of Γ has no hyperflexes, i.e., no bitangent for which the two tangency points coincide;

(iii) the coefficients of f, with $V(f)$ a lift of Γ, are generic enough to guarantee that if the tangencies occur in the relative interior of the same end of Λ, then the local systems defined by these two points are inconsistent.

These conditions are necessary to ensure that the computational lifting techniques in [LM20] are valid. Condition (i) will be particularly relevant in our analysis of the lifting conditions of shape (C).

In the remainder of this thesis, we will only consider tropical smooth quartic curves that are generic by this conditions.

Theorem 3.3.3 ([LM20, Theorem 4.1]). *Let Γ be a generic tropical smooth quartic curve. The sum of the complex lifting multiplicities over the bitangents in the same equivalence class is always 4, and every partition of 4 except $3+1$ appears for some bitangent shape as the sum of the complex lifting multiplicities of its representatives.*

The small numbers in Figure 3.6 for each bitangent shape indicate the representatives that lift and its corresponding complex lifting multiplicity.

The local complex lifting multiplicity at each tangency point as computed by [LM20] can be 1 or 2. As not every polynomial equation of degree 2 has real solutions, we are interested in the number of *real* lifts, that is, the lifting multiplicity when $V(f)$ and ℓ are defined over $\mathbb{K}_{\mathbb{R}}$.

Theorem 3.3.4 ([CM21, Theorem 1.2]). *Let Γ be a generic tropicalization of a smooth plane quartic $V(f)$ defined over a real closed complete non-Archimedean valued field $\mathbb{K}_{\mathbb{R}}$. Then a bitangent class of a given shape has either zero or exactly four lifts to real bitangents to $V(f)$.*

Furthermore, for an S_3-representative of each bitangent shape, Cueto and Markwig determined the conditions for the bitangent class to have four lifts to real bitangents, [CM21, Table 1]. These are conditions on the signs s_{ij} of the coefficients a_{ij} of a real lift f of the tropical quartic curve. They are summarized in Table 3.1.

Notation 3.3.5. The parameters i, j, k, v, u used in the real lifting conditions in Table 3.1 are used to parametrize the position of certain vertices in the dual bitangent motif.

Consider for example shape (A): the signs s_{1v}, $s_{1,v+1}$ belong to the coefficients corresponding to the vertices p_{1v}, $p_{1,v+1}$, which form the red edge in the dual bitangent motif, while the signs $s_{u1}, s_{u+1,1}$ belong to the coefficients corresponding to the vertices p_{u1}, $p_{u+1,1}$, which form the green edge in the dual bitangent motif of shape (A). The sign s_{0i} the corresponds to the lattice point p_{0i}, which forms a triangle with the red edge $\overline{p_{1v}p_{1,v+1}}$. Analogously the sign s_{j0} is associated to the lattice point p_{j0} which forms a triangle with the green edge $\overline{p_{u1}p_{u+1,1}}$.

For some bitangent shapes like shape (B) the green edge is fixed, however, the vertex on the boundary forming a vertex with the edge is still free to be chosen. Thus, for some shapes there is only a parameter i or j but no v or u.

The parameter k only appears for shapes for which the dual bitangent motif in identity position offers a choice between vertices on the diagonal boundary edge of $4\Delta_2$. The sign $s_{k,4-k}$ corresponds to the lattice point $p_{k,4-k}$ which forms a blue edge in the dual bitangent motif with p_{11}. Note that $k \in \{0,2,4\}$.

Shape	Lifting conditions
(A)	$(-s_{1v}s_{1,v+1})^i s_{0i}s_{22} > 0$ and $(-s_{u1}s_{u+1,1})^j s_{j0}s_{22} > 0$
(B)	$(-s_{1v}s_{1,v+1})^{i+1} s_{0i}s_{21} > 0$ and $(-s_{21})^{j+1} s_{31}^j s_{1v}s_{1,v+1}s_{j0} > 0$
(C)	$(-s_{11}s_{12})^i s_{0i}s_{20} > 0$ and $(-s_{21}s_{12})^k s_{k,4-k}s_{20} > 0$ if $j = 2$ $(-s_{11})^{i+1}s_{12}^i s_{21}s_{0i}s_{j0} > 0$ and $(-s_{21})^{k+1}s_{12}^k s_{11}s_{k,4-k}s_{j0} > 0$ if $j = 1,3$
(H),(H')	$(-s_{1v}s_{1,v+1})^{i+1} s_{0i}s_{21} > 0$ and $-s_{21}s_{1v}s_{1,v+1}s_{40} > 0$
(M)	$(-s_{1v}s_{1,v+1})^{i+1} s_{0i}s_{21} > 0$ and $s_{31}s_{1v}s_{1,v+1}s_{30} > 0$
(D)	$(-s_{10}s_{11})^i s_{0i}s_{22} > 0$
(E),(F),(J)	$(-s_{1v}s_{1,v+1})^i s_{0i}s_{20} > 0$
(G)	$(-s_{10}s_{11})^i s_{0i}s_{k,4-k} > 0$
(I),(N)	$-s_{10}s_{11}s_{01}s_{k,4-k} > 0$
(K),(T),(T'), (T"), (U), (U'),(V)	$s_{00}s_{k,4-k} > 0$
(L),(O),(P)	$-s_{10}s_{11}s_{01}s_{22} > 0$
(L'),(Q),(Q'), (R),(S)	$s_{00}s_{22} > 0$
rest	no conditions

Table 3.1: The real lifting conditions of the bitangent shapes in their identity positions as determined in [CM21, Table 11].

The following example illustrates how the real lifting conditions can be computed.

Example 3.3.6. Consider the quartic polynomial

$$f(x,y) = t^{14} + x + t^{13}y + t^4x^2 + xy + t^{14}y^2 + t^9x^3 + tx^2y \qquad (3.2)$$
$$+ t^4xy^2 + t^{16}y^3 + t^{15}x^4 + t^4x^3y + x^2y^2 + t^9xy^3 + t^{19}y^4 \in \mathbb{R}\{\{t\}\}.$$

Its tropicalization and the dual triangulation are depicted in Figure 3.9.

(a) Dual subdivision

(b) The tropicalized curve Trop(f) and its 7 bitangent classes.
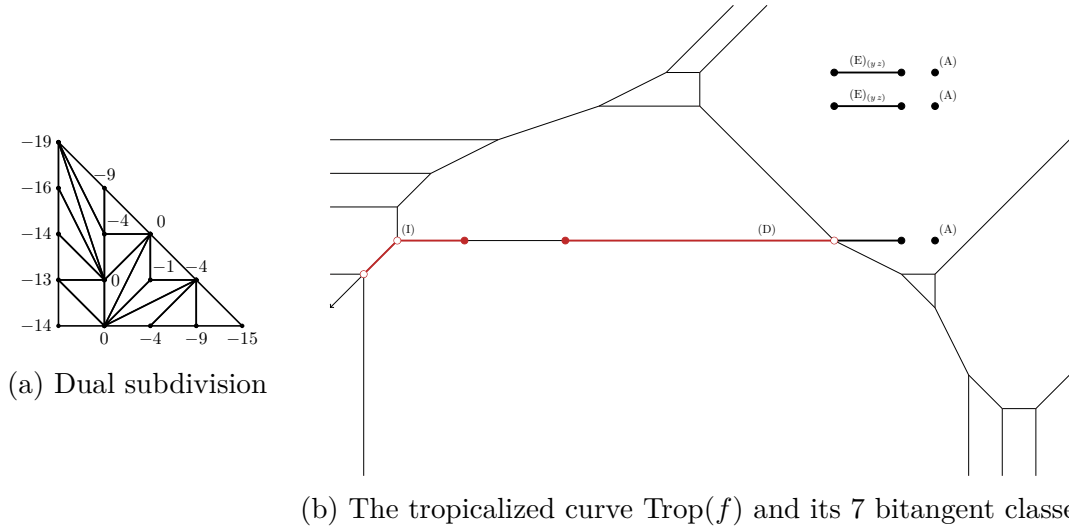
Figure 3.9: The tropicalization of the quartic curve $V(f)$ in Equation (3.2), with its 7 tropical bitangent classes and its dual subdivision.

The 7 bitangent shapes are illustrated in Figure 3.9b. The bitangent classes of shape (A), (D) and (I) are in identity position, the two bitangent classes of shape (E) are in the image of (yz). The sign conditions for the bitangent shapes in identity position can be read off of Table 3.1.

For this we need to find the correct values for the parameters i, j, u, v, k according to Notation 3.3.5, we will do this exemplary with the lowest bitangent class of shape (A) in Figure 3.9b. The dual bitangent motif contains the two triangles $(\overline{p_{10}p_{11}p_{01}})$, $(\overline{p_{10}p_{11}p_{22}})$ corresponding to the bounded horizontal edge the bitangent intersects. From this we see $(\overline{p_{10}p_{11}p_{01}}) = (\overline{p_{1v}p_{1,v+1}p_{0i}})$, so $v = 0$, $i = 1$. The two triangles corresponding to the vertical bounded edge intersected by the bitangent are $(\overline{p_{21}p_{31}p_{10}})$, $(\overline{p_{21}p_{31}p_{22}})$, so we conclude $u = 2$, $j = 1$.

For the sign conditions of the two bitangent classes of shape $(E)_{(yz)}$, we need to apply $(yz)^{-1} = (yz)$ to the triangulation, read the sign conditions off Table 3.1 and then apply (yz) back on the indices. We demonstrate this for the higher bitangent shape of shape $(E)_{(yz)}$. The dual bitangent motif to the shape as given consists

shape	lifting conditions	cond. satisfied	number of lifts
(A)	$s_{04}s_{22} > 0$ $(-s_{21}s_{31})s_{10}s_{22} > 0$	no	0
(A)	$s_{04}s_{22} > 0$ $(-s_{21}s_{31})s_{10}s_{22} > 0$	no	0
(A)	$(-s_{10}s_{11})s_{01}s_{22} > 0$ $(-s_{21}s_{31})s_{10}s_{22} > 0$	no	0
(D)	$(-s_{10}s_{11})s_{01}s_{22} > 0$	no	0
(E)$_{(yz)}$	$s_{04}s_{22} > 0$	yes	4
(E)$_{(yz)}$	$s_{04}s_{22} > 0$	yes	4
(I)	$-s_{10}s_{11}s_{01}s_{04} > 0$	no	0

Table 3.2: Real lifting conditions of the bitangent classes of $\mathrm{Trop}(f)$ and the corresponding numbers of real bitangents to $V(f)$.

of the triangles $(\overline{p_{04}p_{12}p_{13}})$, $(\overline{p_{12}p_{13}p_{22}})$ and the edge $(\overline{p_{10}p_{22}})$. After applying $(yz)^{-1} = (yz)$, the dual bitangent motif consists of the triangles: $(\overline{p_{00}p_{11}p_{10}})$, $(\overline{p_{11}p_{10}p_{20}})$ and the edge $(\overline{p_{13}p_{20}})$. Thus, we are in the case that $p_{1v} = p_{10}$, $p_{1,v+1} = p_{11}$ and $p_{0i} = p_{00}$. Hence, the lifting condition is

$$(-s_{10}s_{11})^0 s_{00}s_{20} > 0.$$

Applying (yz) back on the indices of the real lifting condition we obtain:

$$(-s_{13}s_{12})^0 s_{04}s_{22} = s_{04}s_{22} > 0.$$

Table 3.2 shows the real lifting conditions for the 7 bitangent classes by their shapes (classes with the same shape are ordered by their appearance in Figure 3.9b top to bottom). We see that the quartic polynomial f from above has exactly 8 real bitangent lines.

For two algebraic curves C_1 and C_2 that do not share a component, we know that $\mathrm{Trop}(C_1 \cap C_2) \subset \mathrm{Trop}(C_1) \cap \mathrm{Trop}(C_2)$. If the intersection of the tropical curves is not transversal, we know this inclusion to be strict.

Definition 3.3.7. Let $\Gamma = \mathrm{Trop}(V(F))$ be a tropical quartic curve and $\Lambda = \mathrm{Trop}(L)$ a realizable bitangent line to Γ, i.e., L is a bitangent to $V(f)$. The tropicalization of a tangency point of L to $V(f)$ will be called *tropical tangency point*.

Proposition 3.3.8 ([LM20, Section 2.2]). *Let Γ be a tropical quartic curve and Λ a realizable tropical line intersecting Γ non-transversally. The following describes the position of the tropical tangency points.*

1. *If Λ meets Γ in a line segment with stable intersection of multiplicity 2, the tropicalization of a tangency point has to be the midpoint of the line segment.*

2. *If a connected component of $\Lambda \cap \Gamma$ consists of a vertex and 3 edges in the standard directions, the total intersection multiplicity equals 4 and we can have two points of tangency. If the minimal lattice lengths of the three adjacent edges is μ_1, the two points of tangency appear on the other two edges at distance $(\mu - \mu_1)/2$ from the vertex, where μ is the lattice length of the corresponding edge.*

(a)   (b)   (c)   (d)
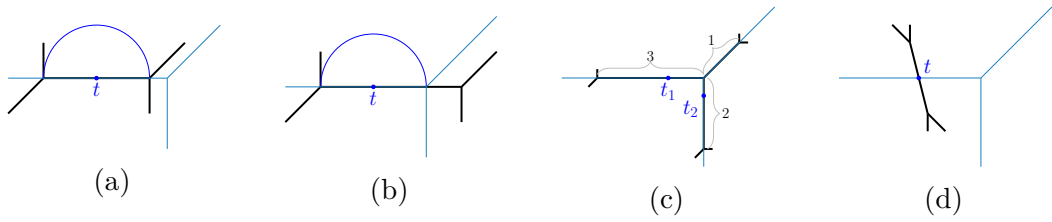
Figure 3.10: The different positions of tropical tangency points depending on the intersection. Figures 3.10a and 3.10b illustrate case (1) in Proposition 3.3.8, Figure 3.10c illustrates case (2) in Proposition 3.3.8, and Figure 3.10d illustrates a transversal intersection.

Chapter 4

Deformation classes of tropical bitangents

Tropical quartic curves can be described via the secondary fan (Definition 2.1.10). Each combinatorial type $\mathcal{T}$ corresponds to a secondary cone and the choice of edge lengths for the tropical curve together with its position in the plane corresponds to the choice of a weight vector in the cone $\Sigma(\mathcal{T})/(1,\ldots,1)\mathbb{R}$; recall Definition 2.1.14. However, the shapes of the 7 bitangent classes do not always remain constant within a secondary cone. In other words, when choosing different weight vectors that induce the same unimodular triangulation, we can observe different bitangent shapes for the tropical quartic curves induced by the weight vectors.

The aim of this chapter is to understand how the bitangent shapes deform when we fix a combinatorial type of the quartic curve. To this purpose we first define deformation classes of tropical bitangents to quartic curves and their dual deformation motifs. This terminology is inspired by [PV22].

In Section 4.2, we present the first main theorem of this thesis: A full classification of the deformation classes of tropical bitangents, Theorem 4.2.3, and give an extensive proof of the classification. All dual deformation motifs up to S_3-equivalence can be found in Figure 4.39.

This classification is a preparation for the second main result, which is presented in Chapter 5. There we investigate the lifting conditions of deformation classes and obtain that the lifting conditions are constant on the cones of the secondary fan corresponding to generic, smooth tropical quartic curves; see Theorem 5.1.4.

The results are joint work with Marta Panizzut [GP21b].

4.1 Deformations of bitangent shapes

When considering different examples of tropical quartic curves and their bitangent classes, one observes that different shapes appear for different choices of edge lengths for the same combinatorial type of the quartic; see Example 4.1.1. This motivated the introduction of deformation classes.

The terminology of *bitangent motifs* and *deformation motifs* is inspired by the one used in [PV22, JPS20] for the classification of families of tropical lines on

tropical smooth cubic surfaces.

This section is based on joint work with Marta Panizzut [GP21b].

For a subdivision $\mathcal{T}$ that contains a subcomplex as in Figure 3.7, i.e., a subcomplex determined by a bitangent shape, it is not necessary that for every curve with coefficient vector $c \in \Sigma(\mathcal{T})$ the bitangent shape will appear. These subcomplexes are only a necessary condition for the appearance of the bitangent shape. The bitangent shapes depend additionally on the edge lengths of the tropical curve, that are determined by $c \in \Sigma(\mathcal{T})$. This is illustrated in Example 4.1.1. However, it is always possible to find a coefficient vector in $\Sigma(\mathcal{T})$ such that the bitangent shape will appear for the induced curve if its determined part is contained in the subdivision. This is not trivial and will be explained in Chapter 4, while Section 6.3.1 shows how to find a fitting coefficient vector.

Example 4.1.1. Figure 4.1 shows a unimodular triangulation and three tropical curves of this combinatorial type with different edge lengths. We observe, that the bitangent classes deform their shape with the change of the edge lengths of the quartic. The colored edges in the triangulation $\mathcal{T}$ in Figure 4.1a correspond to the shapes (B), (M) and $(B)_{(yz)}$ from the classification in Figure 3.6. Let **a** denote the coefficient vector of an algebraic curve of degree 4 with entries ordered as in Equation (3.1). Then we conclude from Figure 4.1 that for each of the three shapes (B), (M) and $(B)_{(yz)}$ there exist coefficient vectors in $\Sigma(\mathcal{T})$ that induce the shape. Examples are given in the table below. These coefficient vectors correspond to the curves in Figure 4.1.

(a) Triangulation $\mathcal{T}$ (b) Shape (B)   (c) Shape (M)   (d) Shape $(B)_{(yz)}$
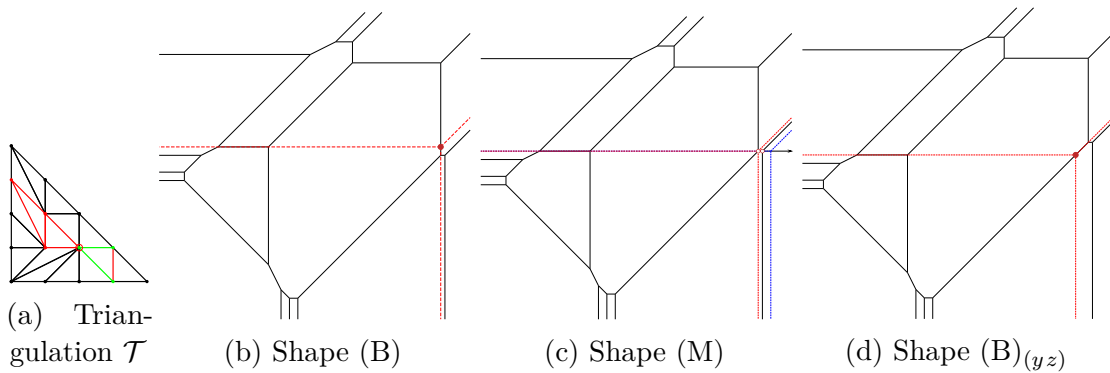
Figure 4.1: The dual triangulation does not fix the shapes of the bitangent classes, since they can change when choosing different edge lengths for the curve.

Shape	coefficient in $\Sigma(\mathcal{T})$
(B)	$\lambda_1 = (13, 0, 0, -15, 10, -15, -32, 0, -11, -34, -84, -51, -41, -57, -77)$
(M)	$\lambda_2 = (12, 0, 0, -14, 10, -14, -30, 0, -10, -32, -81, -50, -40, -55, -74)$
$(B)_{(yz)}$	$\lambda_3 = (11, 0, 0, -13, 11, -13, -28, 2, -8, -30, -81, -50, -40, -55, -74)$

The change of bitangent shapes for different choices of coefficients in the secondary cone motivates the definition of deformation classes, which roughly group together all those shapes that can deform into each other.

Note, that it is not obvious that the three bitangent classes for each choice of edge lengths have the same real lifting behavior. The lifting conditions were computed per shape in identity position. Here we observe a change from shape (B) over shape (M) to shape (B)$_{(yz)}$. Theorem 5.1.4 states that these changes actually have no impact on the real lifting behavior of the bitangent class. This is the main result of Section 5.1.

Definition 4.1.2. Let Γ be a tropical smooth quartic curve with dual triangulation $\mathcal{T}$, and let B be a bitangent class of Γ of a fixed shape. The *dual bitangent motif* of (Γ, B) is the subcomplex of $\mathcal{T}$ that is fully determined by the shape of B. Dual bitangent motifs are classified in [CM21, Figure 8].

Definition 4.1.3. Given a tropical quartic Γ_c with dual triangulation $\mathcal{T}$, $c \in \Sigma(\mathcal{T})$, and a tropical bitangent class B, we say that a tropical bitangent class B' is in the same *deformation class* as B if the following conditions are satisfied:

▷ There exists $\Gamma_{c'}$ with $c' \in \Sigma(\mathcal{T})$ having B' as one of its bitangent classes.

▷ There is a continuous deformation from Γ_c to $\Gamma_{c'}$ given by a path in the secondary cone $\Sigma(\mathcal{T})$ from c to c' that induces B to change to B'.

We use the notation B_ω to indicate the deformation of B in Γ_ω for ω in the path. Given a unimodular triangulation $\mathcal{T}$ of $4\Delta_2$ and a dual quartic curve Γ, let $\mathcal{D}$ be the deformation class of one of its seven bitangent classes. The *dual deformation motif of $(\mathcal{T}, \mathcal{D})$* is the union of the dual bitangent motifs of all shapes belonging to bitangent classes in $\mathcal{D}$.

We label deformation classes using the letters of the shapes of tropical bitangents. If the class contains the image of shapes under the action of an element $\sigma \in S_3$, we use the notation $+\sigma$. For instance, in Example 4.1.1 we have seen a deformation between the shapes (B), (M) and (B)$_{(yz)}$. This indeed forms a deformation class and since shape (M) is symmetric with respect to $(yz) \in S_3$ this class will be denoted (B M)$+(yz)$.

Corollary 4.1.4. *Each smooth tropical quartic Γ has 7 distinct deformation classes which only depend on the dual triangulation $\mathcal{T}$ of Γ.*

This follows directly from the definition. Changing the coefficients defining Γ in the secondary cone $\Sigma(\mathcal{T})$ induces a variation in the shapes of the tropical bitangents within the deformation class.

(a) no (A)   (b) no (E)   (c) no (G)   (d) no (G), (I), (N), (K),
(U), (U'), (T), (T'), (T"), (V)

(e) no (G), (I), (N)   (f) no (G), (K), (U), (U'),   (g) no (T")
(T), (T'), (T"), (V)
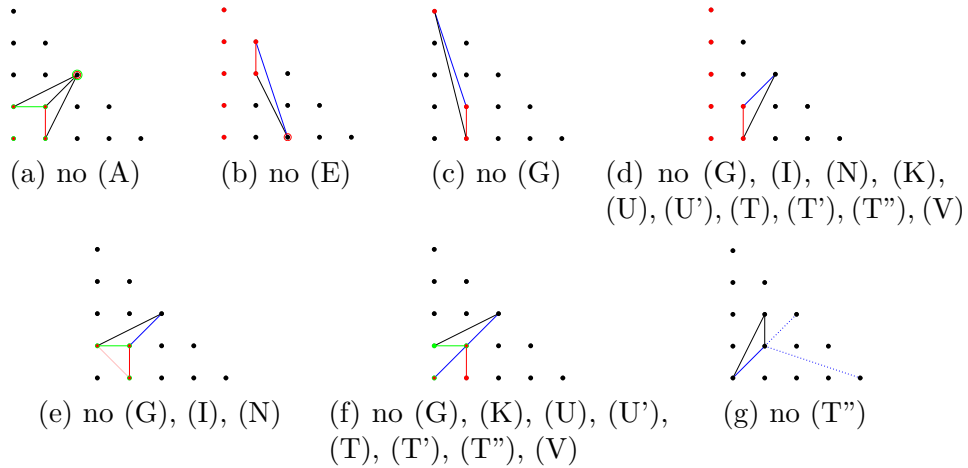
Figure 4.2: These bitangent motifs appear in the condensed classification in Figure 3.7 of the bitangent shapes but they do not lead to the shapes under which they are listed.

4.2 Classification

This section contains a full classification of the deformation classes of tropical bitangents, which is the first main result of Part I. The proof of the classification takes place in three steps: first we sort through the set of bitangent motifs from [CM21], then we classify all deformation classes that contain only one shape and can thus be viewed as constant, before we classify all remaining deformations of bitangent shapes. The section is based on joint work with Marta Panizzut [GP21b].

Proposition 4.2.1. *The bitangent motifs depicted in Figure 4.2 are each part of a different bitangent motif such that they do not lead to the bitangent shape under which they can be found in Figure 3.7.*

The summary of the dual bitangent motifs by [CM21] as shown in Figure 3.7 is very condensed, and, as a consequence, for some figures with dotted edges not all combinations lead to the assigned bitangent shape.

Proof. We prove the claim by going through the different bitangent motifs from Figure 4.2.

(4.2a) This bitangent motifs appears when in the picture to (A) in Figure 3.7 the red and green edges $\overline{p_{10}p_{11}}$ and $\overline{p_{01}p_{11}}$ are chosen. Shape (A) appears in identity position when the tropical line intersects the quartic non-transversally in a bounded edge (dual to the red resp. green edge) with its horizontal and vertical ray. However, we observe that in the configuration in Figure 4.2a
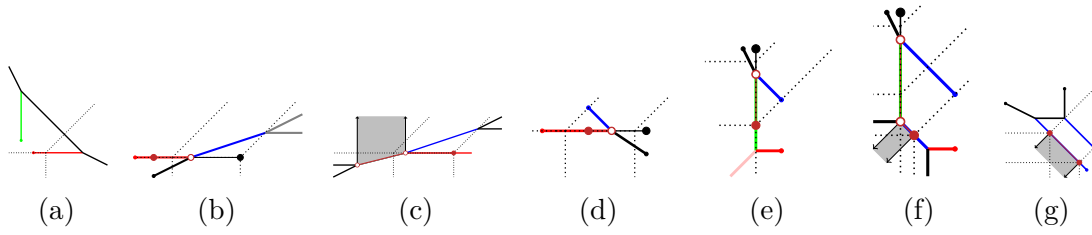
Figure 4.3: The parts of the quartic curve dual to the bitangent motifs from Figure 4.2

the horizontal bounded edge dual to the red edge in the motif will always be right of the vertical bounded edge dual to the green edge in the triangulation. Therefore, an intersection with a tropical line as described above is not possible. This is illustrated in Figure 4.3a. Instead this bitangent motif will give rise to a bitangent class of shape (P) or (S) depending on its completion in the lower left corner.

(4.2b) When we choose the red edge $\overline{p_{12}p_{13}}$ together with the blue edge $\overline{p_{20}p_{13}}$ in Figure 3.7 for (E), we obtain the picture from Figure 4.2b. The edge $\overline{p_{20}p_{12}}$ exists because of the unimodularity of the triangulation. Thus, we see a dual picture as in Figure 4.3b. We observe, that the bitangent class will intersect the quartic in every possible completion of the triangulation. Therefore, shape (E) will never appear for this bitangent motif. Depending on the completion in the leftmost column and the edge lengths of the dual curve, the dual subdivision leads to bitangent shapes (D), (L), (L'), (O), (Q), (Q') or (R).

(4.2c) The smoothness of the quartic curve leads to a unique completion of the triangulation around the triangle $\overline{p_{01}p_{11}p_{04}}$. The dual picture, i.e., the dual part of the quaric curve, is depicted in Figure 4.3c. As we see in the dual picture, the dual motif induces a bitangent shape (II). This is independent of edge lengths and the remaining not fixed triangulation.

(4.2d) The constellation depicted in Figure 4.2d is a possible completion of dual motif of shape (G) or, depending on the choice of the red lattice point with x-coordinate zero, of the shapes (I), (N), (K), (U), (U'), (T), (T'), (T") or (V). However, the existence of this triangle in the subdivision leads instead to bitangent shapes (D), (L), (L'), (O), (Q), (Q'), (R), (S) or (P) depending on the completion of the triangulation and the edge lengths of the quartic. This is due to the fact, that the triangle $\overline{p_{10}p_{11}p_{22}}$ is dual to a part of the curve as shown in Figure 4.3d. We see, that there is always, independent of edge lengths or the surrounding curve, a bounded line segment of the bitangent

class that does not lie on the curve. This excludes the shapes (G), (I), (N), (K), (U), (U'), (T), (T'), (T") and (V).

(4.2e) The bitangent motif shown in Figure 4.2e is a possible completion of the bitangent motifs of shapes (G), (I) and (N). Similar to the case before, an observation of the curve in Figure 4.3e dual to the bitangent motif yields that the bitangent class in question always contains a bounded line segment not contained in the quartic curve. Hence, the bitangent motif does not induce shapes (G), (I) or (N). Depending on the completion of the unimodular triangulation and the edge lengths of the quartic, we instead observe bitangent shapes (D), (L), (O) or (P).

(4.2f) The triangles shown in Figure 4.2f is a possible completion of the bitangent motifs of shapes (G), (K), (U), (U'), (T), (T'), (T") and (V). The part of the quartic curve dual to the triangles is illustrated in Figure 4.3f. As before, we see that independent of the edge lengths of the quartic curve the bitangent class will contain a line segment that does not lie on the curve. Thus, it follows that the bitangent motif does not induce the shapes (G), (K), (U), (U'), (T), (T'), (T") and (V). Instead, depending on the completion of the unimodular triangulation and the edge lengths, the triangles lead to bitangent shapes (D), (L'), (Q), (Q'), (R) or (S).

(4.2g) When the triangle neighboring the edge $(\overline{p_{00}p_{11}})$ in the triangulation is given by $(\overline{p_{00}p_{11}p_{12}})$ (up to S_3-symmetry) as shown in Figure 4.2g, the bitangent shape (T") cannot appear for the dual quartic curve. The reason is, that for shape (T") the two vertices bounding the line segment of the bitangent class contained in $(\overline{p_{00}p_{11}})^\vee$ have to coincide with vertices of the quartic. However, as Figure 4.3g illustrates for the case of $(\overline{p_{11}p_{22}})$ as blue edge in the triangulation, shape (T") is not possible. For the case of $(\overline{p_{11}p_{40}})$ as blue edge in the triangulation, a similar picture can be drawn. The summarizing argument for this case is, that the y-coordinate of $(\overline{p_{00}p_{11}p_{12}})^\vee$ by the triangulation always has to be at least as large as the y-coordinate of the upper vertex of the edge $(\overline{p_{11}p_{22}})^\vee$ resp. $(\overline{p_{11}p_{40}})^\vee$. So the the vertex $(\overline{p_{00}p_{11}p_{12}})^\vee$ can never be part of the bitangent class. Thus, shape (T") cannot occur for this possible completion of its dual bitangent motif.

$\square$

To exclude these cases and avoid confusion, we will adapt a less condensed way of notating the dual bitangent motifs.

We will now classify all deformation classes that consist of only one bitangent shape.
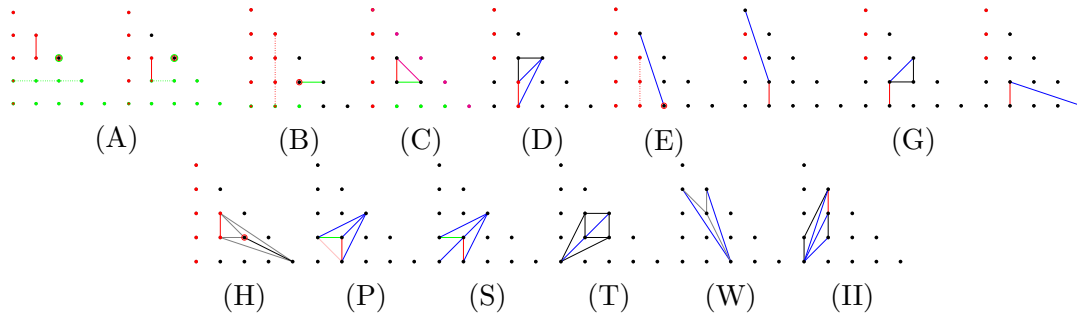
Figure 4.4: Dual bitangent motifs of bitangent classes with constant shape in their deformation class.

Proposition 4.2.2. *Let Γ be a tropical smooth quartic curve dual to a triangulation $\mathcal{T}$ of $4\Delta_2$. Let B be a bitangent class of Γ with dual bitangent motif belonging to the collection in Figure 4.4, modulo S_3-symmetry. Then the shape of B is constant in its deformation class, in other words, the deformation class of B is constant.*

Proof. The proof is structured by a case distinction. For each case the combinatorial structure induced on the curve by the dual bitangent motif makes a change of the two tangencies by different edge lengths impossible. Thus, the shape of the bitangent class is fully determined by its dual deformation motif. The argumentation for each case contains a picture of the dual deformation motif and the relevant dual part of the tropical quartic curve. If the dual bitangent motif offers different choices of triangles, the tropical curve is illustrated only for one of them.

Deformation class (A)

(a) Dual deformation motif (A)   (b) Example of bitangent shape (A) with the relevant parts of the curve
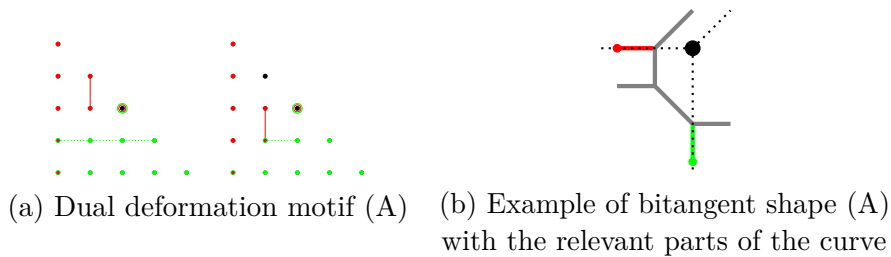
Figure 4.5: Deformation class (A)

When applying duality, we observe from the dual bitangent motifs that the horizontal bounded edge dual to the red edge in the triangulation will always be completely contained in the area with x-coordinate smaller, and y-coordinate larger than appears in the vertical bounded edge dual to the green edge in the

61

triangulation. This relative behavior of the two line segments is determined by the combinatorics of the triangulation and cannot be changed by the edge lengths of the quartic. Therefore, both line segments uniquely define a tropical bitangent line of shape (A).

Deformation class (B)

(a) Dual deformation motif (B)   (b) Example of bitangent shape (B)
                                  with the relevant parts of the curve
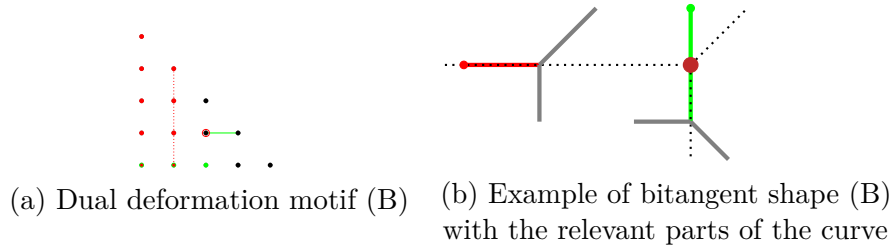
Figure 4.6: Deformation class (B)

A bitangent class of shape (B) intersects the quartic non transversally with its horizontal and vertical ray. The edge of the quartic intersecting with the horizontal ray is contained in the bitangent and it is dual to a red edge in the dual bitangent motif. This tangency has to be persevered by any deformation of the shape. The intersection of the vertical ray with the bounded edge of Γ dual to the green edge in the dual bitangent motif in Figure 4.6 is such that the vertex of the bitangent line is contained in the interior of the edge of Γ. By changing the edge lengths of the quartic, this vertex could move onto another adjacent edge of Γ, thus changing the shape of the bitangent class. We claim that this cannot happen when the green edge forms a triangle with p_{00}, p_{10}, or p_{20}, which are the only allowed lattice points by the bitangent motif.

Denote the two vertices of the green vertical bounded edge in the quartic curve by (a,b_1) and (a,b_2), with $b_1 < b_2$. Let c be the y-coordinate of the red horizontal bounded edge of the quartic. For all the possible choices of vertices for the green and red triangle in the subdivision, we observe that the vertices (a,b_1) and (a,b_2) always satisfy $b_1 < c < b_2$. Therefore, the bitangent shape cannot deform.

Deformation class (C)

Let Γ be a tropical quartic curve with a bitangent class of shape (C). This implies that the quartic contains a vertex v which is incident to three bounded edges of direction $-e_1$, $-e_2$ and $e_1 + e_2$. The bitangent class consists of one single tropical line with vertex v. Changes in the edge lengths of the quartic have no influence on the existence of v and thus do not interfere with the actual shape of the bitangent class.

(a) Dual deformation motif (C)

(b) Example of bitangent shape (C) with the relevant parts of the curve
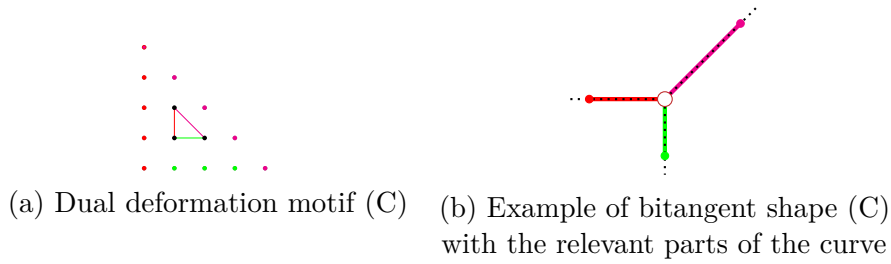
Figure 4.7: Deformation class (C)

Deformation class (D)

(a) Dual deformation motif (D)

(b) Example of bitangent shape (D) with the relevant parts of the curve
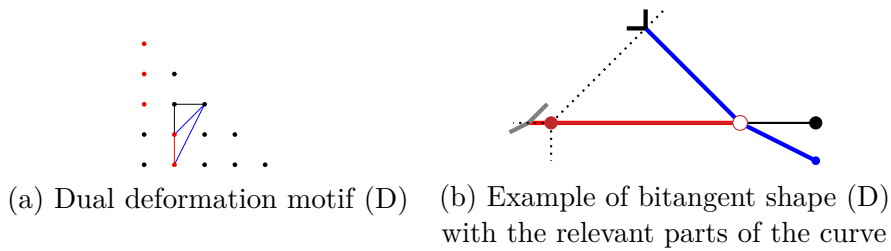
Figure 4.8: Deformation class (D)

We consider the dual bitangent motif depicted in Figure 4.8 where the red edge forms a triangle with p_{02}, p_{03} or p_{04}. In each case, changing the edge lengths of Γ cannot deform the shape of the bitangent class because the slopes of the edges adjacent to the bounded horizontal edge $\overline{p_{10}p_{11}}^{\vee}$ have to be lower than 1 by the triangulation. Thus, the vertex of Γ dual to the triangle formed by the red edge $\overline{p_{10}p_{11}}$ with one of the red vertices must have a y-coordinate such that a diagonal line through $(\overline{p_{12}p_{11}p_{22}})^{\vee}$ cannot meet the vertex bounding $\overline{p_{10}p_{11}}^{\vee}$ at the left side.

Deformation class (E)

(a) Dual deformation motif (E)

(b) Example of bitangent shape (E) with the relevant parts of the curve
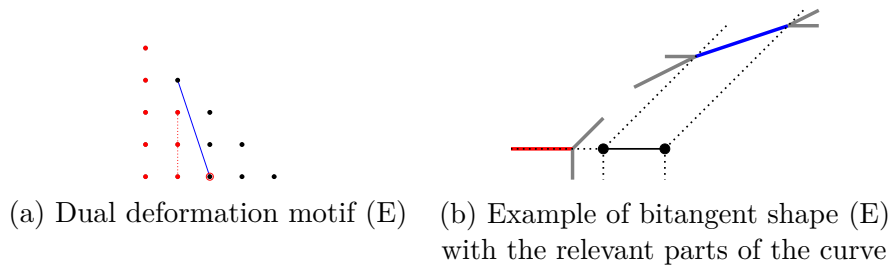
Figure 4.9: Deformation class (E)

We consider the dual bitangent motif shown in Figure 4.9. We observe that by the unimodularity of the triangulation we know the two triangles with edge $\overline{p_{20}p_{13}}$. By Proposition 4.2.1 we know that the edge $(\overline{p_{12}p_{13}})^\vee$ cannot be responsible for the non-transversal intersection of multiplicity 2 of the bitangent lines with the quartic. The bitangent class is determined by the intersection of a vertical ray passing through the edge $(\overline{p_{10}p_{11}})^\vee$, resp. $(\overline{p_{11}p_{12}})^\vee$, with diagonal rays passing through the vertices of $(\overline{p_{20}p_{13}})^\vee$. It follows, that independent of the edge lengths of the quartic, the bitangent class can never intersect with the quartic curve. Moreover, it will always consist of a bounded line segment.

Deformation class (G)

(a) Dual deformation motif (G)

(b) Example of bitangent shape (G) with the relevant parts of the curve
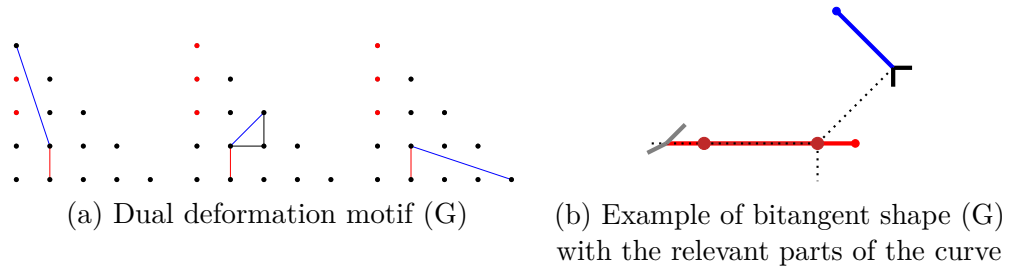
Figure 4.10: Deformation class (G)

Considering the dual bitangent motifs shown in Figure 4.10, we see that there are three possible options for the red edge to form a triangle except for the case that the blue edge is $\overline{p_{11}p_{04}}$, see Proposition 4.2.2. For each case, varying the edge lengths of the quartic only changes the position of the bitangent class on the horizontal bounded edge $(\overline{p_{10}p_{11}})^\vee$ of Γ. The bitangent class cannot extend because of the slopes of the adjacent edges to the vertices of $(\overline{p_{10}p_{11}})^\vee$ and $(\overline{p_{11}p_{22}})^\vee$. For an illustration see Figure 4.10. This figure only shows the situation for one of the choices for the blue edge. The other cases are analogous.

Deformation class (H)

Figure 4.11 shows the dual bitangent motif and the part of the quartic curve determined by it. The two tangencies are given by a non transversal intersection of the horizontal ray of the tropical line with the bounded edge $(\overline{p_{11}p_{12}})^\vee$, and a transversal intersection of the horizontal ray of the line with $\overline{(p_{21}p_{40})}^\vee$. We observe that edge length changes have no impact on this bitangent shape independently of the choice of completion for the unimodular triangulation.

(a) Dual deformation motif (H)

(b) Example of bitangent shape (H) with the relevant parts of the curve
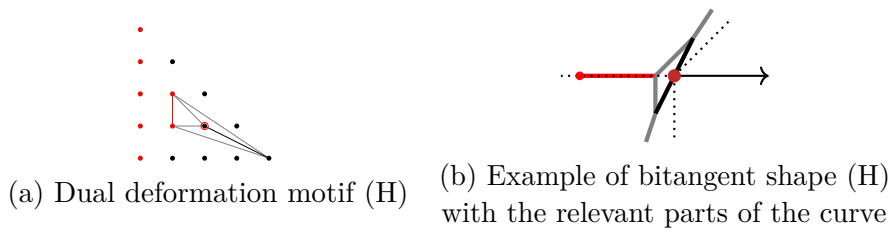
Figure 4.11: Deformation class (H)

Deformation class (P)

(a) Dual deformation motif (P)

(b) Example of bitangent shape (P) with the relevant parts of the curve
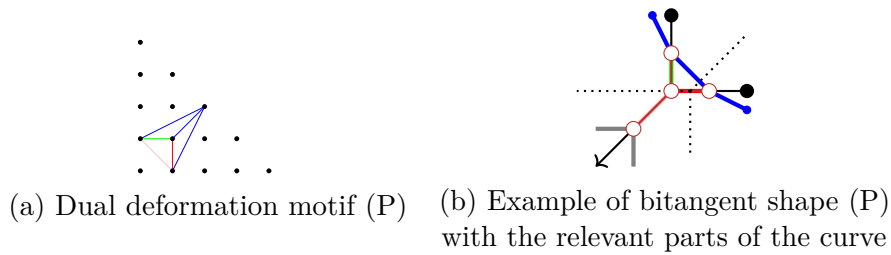
Figure 4.12: Deformation class (P)

Let Γ be a tropical quartic curve containing in its subdivision the triangles as in Figure 4.12. Then the dual edges in Γ lead to a bitangent class of shape (P). Any change in the edge lengths of Γ does not interfere with the relative position of the edges determined by the dual bitangent motif, since the edges are all connected and form a cycle. Hence, the bitangent shape (P) is itself independent of edge length changes.

Deformation class (S)

(a) Dual deformation motif (S)

(b) Example of bitangent shape (S) with the relevant parts of the curve
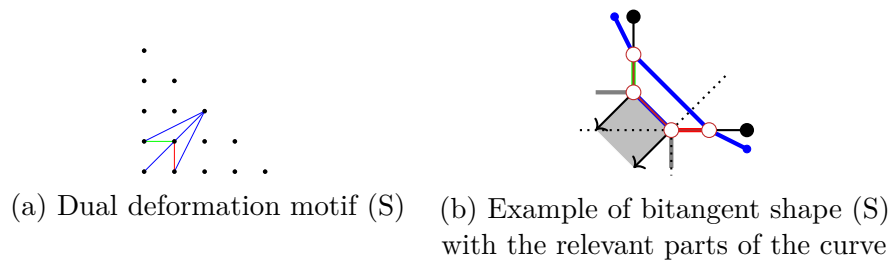
Figure 4.13: Deformation class (S)

Consider the bitangent motif in Figure 4.13 and the part of the tropical quartic curve Γ dual to the depicted triangles. Any change in the edge lengths of Γ does

not interfere with the relative position of those edges, since they are connected and form a cycle. As the bitangent motif induces the bitangent shape (S), it follows that its deformation class is constant and consists only of the shape (S).

Deformation class (T)

(a) Dual deformation motif (T) (b) Example of bitangent shape (T) with the relevant parts of the curve
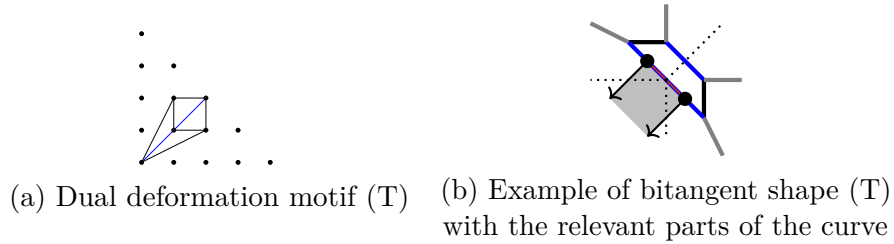
Figure 4.14: Deformation class (T)

The dual bitangent motif in Figure 4.14 fixes connected edges of the quartic curve that form a cycle. Due to the fixed directions of the edges, the relative positions of the two blue edges $(\overline{p_{00}p_{11}})^\vee$ and $(\overline{p_{11}p_{22}})^\vee$ cannot be changed by edge length changes. It follows that bitangent shape (T) cannot deform and thus forms a constant deformation class. This is independent of the choice on how to unimodularly complete the subdivision in Figure 4.14.

Deformation class (W)

(a) Dual deformation motif (W) (b) Example of bitangent shape (W) with the relevant parts of the curve
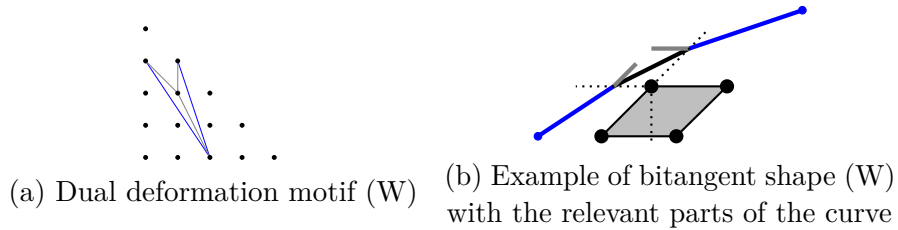
Figure 4.15: Deformation class (W)

Figure 4.15 shows a dual bitangent motif of shape (W). The difference to the other dual bitangent motifs to shape (W) is that no deformations of the shape are possible. In Figure 4.15 we also see the part of the quartic curve that is dual to the bitangent motif. We observe that the area for which the diagonal ray of the tropical line intersects $(\overline{p_{20}p_{13}})^\vee$ and the horizontal ray of the tropical line at the same time intersects $(\overline{p_{20}p_{03}})^\vee$ will always be a parallelogram that does not intersect the quartic. As this is independent of the edge lengths of the quartic curve, the dual bitangent motif defines the constant deformation class (W).

Deformation class (II)

(a) Dual deformation motif (II)

(b) Example of bitangent shape (II) with the relevant parts of the curve
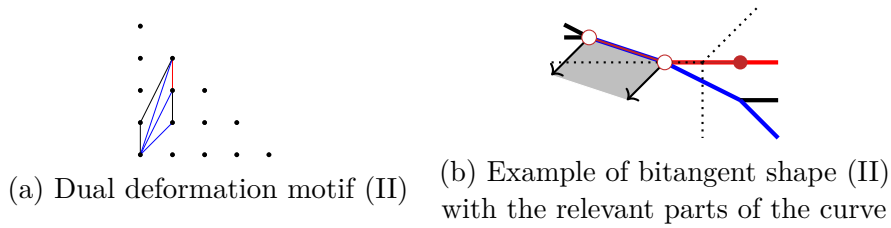
Figure 4.16: Deformation class (II)

In Figure 4.16 we see the dual bitangent motif of shape (II) and the part of the quartic curve it determines. We observe that the bitangents in the unbounded 2-dimensional cell have only one intersection point with the quartic curve of multiplicity 4. This intersection behavior is independent of the edge lengths of Γ. The bounded line segment of the bitangent class is contained in the quartic curve and its existence is independent of the edge lengths. Moreover, we observe that by the triangulation the vertex $(\overline{p_{00}p_{11}p_{12}})^{\vee}$ of the quartic curve will always have smaller x-coordinate than the right vertex of $(\overline{p_{12}p_{13}})^{\vee}$. Therefore, shape (II) cannot be deformed. $\qquad\square$

The following theorem states the full classification of the deformation classes. This is the first main result of Part I.

Theorem 4.2.3. *There are* 24 *deformation classes of tropical bitangent classes to generic smooth tropical quartic curves modulo S_3-symmetry. Orbit representatives of their dual deformation motifs are summarized in Figure 4.39.*

Proof. Proposition 4.2.2 covered the cases of the constant deformation classes. To prove the statement we need a classification of the remaining cases of deformation classes. This will be done by a comprehensive case distinction of the remaining dual bitangent motifs and an investigation of the deformation possibilities of the corresponding shapes. By transitiveness of the deformation of bitangent shapes it is sufficient to structure the case distinction by going through the dual bitangent motifs in alphabetical order. The proof is organized in sections that cover the different cases. Each part is titled by the deformation class it classifies.

Deformation class (B H' H)

Figure 4.17 shows a possible completion of the dual bitangent motif of shape (B) from Figure 3.7, which is not covered by Proposition 4.2.2. We observe that the dual bitangent motifs to shapes (H') and (H) from Figure 3.7 are contained in Figure 4.17.
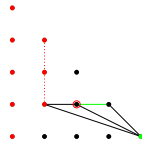
Figure 4.17: Dual deformation motif (B H' H)

The two tangencies are given as follows: The first tangency is a non-transversal intersection with $(\overline{p_{11}p_{12}})^\vee$ resp. $(\overline{p_{12}p_{13}})^\vee$. The second tangency depends on the relative position of the edges $(\overline{p_{1v}p_{1,v+1}})^\vee$ with $v \in \{1,2\}$ and $(\overline{p_{21}p_{31}})^\vee$ determined by the edge lengths of the quartic curve.

Let $a := (a_x, a_y) := (\overline{p_{1v}p_{1,v+1}p_{21}})^\vee$, and let $b := (b_x, b_y) := (\overline{p_{21}p_{31}p_{40}})^\vee$. In the following we investigate how the different relative positions, illustrated in Figure 4.18, give rise to different shapes. We distinguish three cases:

- $a_y > b_y$: Due to the remaining options in the triangulation, the upper vertex of $(\overline{p_{21}p_{31}})^\vee$ has always y coordinate larger than a. Thus, in this case the vertex of the bitangent must lie on the relative interior of the edge $(\overline{p_{21}p_{31}})^\vee$. We see shape (B) and the second tangency is given by a non-transversal intersection of the vertical ray with $(\overline{p_{21}p_{31}})^\vee$.

- $a_y = b_y$: The vertex of the bitangent coincides with the vertex $(\overline{p_{21}p_{31}p_{40}})^\vee$. We see shape (H') and the second tangency is given by the stable intersection of the vertical ray with the the curve.

- $a_y < b_y$: A horizontal line passing through $(\overline{p_{11}p_{12}})^\vee$ resp. $(\overline{p_{12}p_{13}})^\vee$ will have to intersect $(\overline{p_{21}p_{40}})^\vee$. Thus, we see shape (H) and the second tangency is given by the intersection of the vertical ray with $(\overline{p_{21}p_{40}})^\vee$.

| (B) | (H') | (H) |
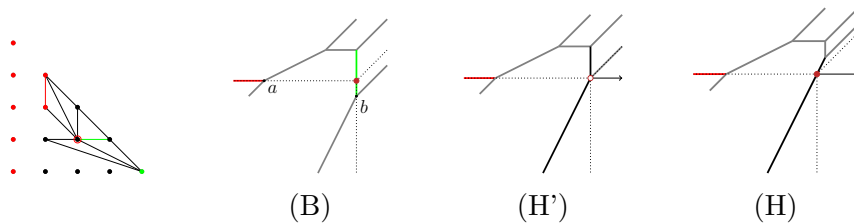
Figure 4.18: Example of deformation of shapes in deformation class (B H' H).

Figure 4.18 illustrates the deformation of the shapes for $\overline{p_{12}p_{13}}$ as red edge in the dual deformation motif. Similar pictures can be drawn for $\overline{p_{11}p_{12}}$.
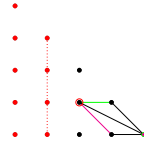
Figure 4.19: Dual deformation motif (B H' H)+$(y\,z)$

Deformation class (B H' H)+$(y\,z)$

Figure 4.19 depicts the remaining unimodular completion for the choice of the triangle formed with the green edge $(\overline{p_{21}p_{31}})$. Note that the triangles in Figure 4.19 contain the dual bitangent motifs of shapes (H') and (H) as well as (H)$_{(y\,z)}$ and (B)$_{(y\,z)}$. The tangencies appear in a similar way to the case (B H' H). The first (and by changes of edge lengths fixed) tangency is the non-transversal intersection on $(\overline{p_{1v}p_{1,v+1}})^\vee$ with $v \in \{0,1,2\}$. The second tangency depends on the relative position of the edge $(\overline{p_{1v}p_{1,v+1}})^\vee$ to the edges $(\overline{p_{21}p_{31}})^\vee$, $(\overline{p_{21}p_{40}})^\vee$ and $(\overline{p_{21}p_{30}})^\vee$. Let $a := (a_x, a_y) := (\overline{p_{1v}p_{1,v+1}p_{21}})^\vee$, $b_1 := (b_{1x}, b_{1y}) := (\overline{p_{21}p_{31}p_{40}})^\vee$, and $b_2 := (b_{2x}, b_{2y}) := (\overline{p_{21}p_{30}p_{40}})^\vee$; see Figure 4.20. By the slope of the edge $(\overline{p_{21}p_{40}})^\vee$ we have $b_{1y} > b_{2y}$. Differently to (B H' H), the case $b_{2y} \geq a_y$ is possible.

- $a_y > b_{1y}$: Analogous to the case of deformation class (B H' H), the vertex of the bitangent line has to be lying on the edge $(\overline{p_{21}p_{31}})^\vee$. We observe shape (B).

- $a_y = b_{1y}$: This is the same situation as in the case of deformation class (B H' H). The vertex of the bitangent coincides with $(\overline{p_{21}p_{31}p_{40}})^\vee$, we see shape (H').

- $b_{1y} < a_y < b_{2y}$: As for (B H' H), the horizontal ray passing through $(\overline{p_{1v}p_{1,v+1}})^\vee$ has to intersect the edge $(\overline{p_{21}p_{40}})^\vee$. This leads to a bitangent shape (H).

- $a_y = b_{2y}$: Different from the case for (B H' H), the combinatorics of the curve allows to move the vertex $(\overline{p_{21}p_{30}p_{40}})^\vee$ above the edge $(\overline{p_{1v}p_{1,v+1}})^\vee$. When they align horizontally, we observe a picture symmetric to the case $a_y = b_{1y}$ by $(y\,z)$. We see shape (H')$_{(y\,z)}$.

- $a_y < b_{2y}$: When the vertex $(\overline{p_{21}p_{30}p_{40}})^\vee$ is above the edge $(\overline{p_{1v}p_{1,v+1}})^\vee$, a horizontal ray through $(\overline{p_{1v}p_{1,v+1}})^\vee$ has to intersect the edge $(\overline{p_{21}p_{30}})^\vee$. The lower vertex of this edge must have y-coordinate smaller than a_y due to the triangulation. As the edge $(\overline{p_{21}p_{30}})^\vee$ is of the same direction as the diagonal ray of a bitangent line, we get a second non-transversal intersection and the bitangent shape (B)$_{(y\,z)}$.

<div align="center">(B)   (H')   (H)   (H')$_{(yz)}$ (B)$_{(yz)}$</div>
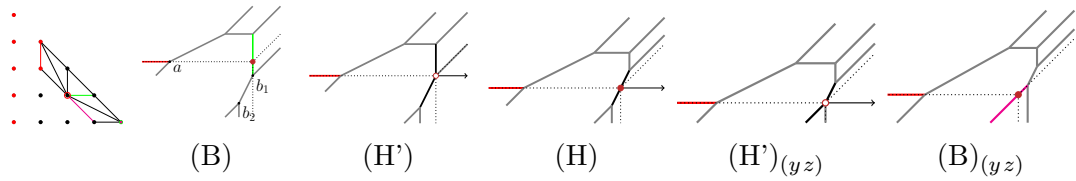
Figure 4.20: Example of deformation of shapes in deformation class (B H' H)+(yz)

Figure 4.20 illustrates the deformation behavior for an exemplary subdivision with the red edge chosen as $\overline{p_{12}p_{13}}$. Analogous pictures can be drawn for the options $\overline{p_{10}p_{11}}$ and $\overline{p_{11}p_{12}}$.

Deformation class (B M)+(yz)
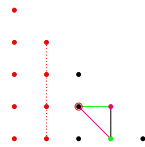
Figure 4.21: Dual deformation motif (B M)+(yz)

Figure 4.21 shows the last choice of the dual bitangent motif of shape (B). We notice, that the dual bitangent motif of shapes (M) and (B)$_{(yz)}$ are contained. The first tangency is as in the cases before given by the non-transversal intersection of the horizontal ray with $(\overline{p_{1v}p_{1,v+1}})^\vee$ for $v \in \{0,1,2\}$. The second tangency is again dependent on the relative position of $(\overline{p_{1v}p_{1,v+1}})^\vee$ to $(\overline{p_{21}p_{31}})^\vee$ and $(\overline{p_{21}p_{30}})^\vee$ which is determined by the edge lengths of the quartic. Let $a := (a_x, a_y) := (\overline{p_{1v}p_{1,v+1}p_{21}})^\vee$, and let $b := (b_x, b_y) := (\overline{p_{21}p_{31}p_{30}})^\vee$. An illustration can be found in Figure 4.22.

- $a_y > b_y$: An investigation of the options for completing the subdivision unimodularly yields that a will always be smaller than the y-coordinate of the upper vertex of $(\overline{p_{21}p_{31}})^\vee$. Hence, the vertex of the bitangent is contained in the interior of the edge $(\overline{p_{21}p_{31}})^\vee$. We see shape (B).

- $a_y = b_y$: In this case the edges $(\overline{p_{1v}p_{1,v+1}})^\vee$ and $(\overline{p_{30}p_{31}})^\vee$ align horizontally. Therefore, we obtain an infinite family of bitangent lines with vertex on the ray of direction e_1 starting at $(\overline{p_{21}p_{30}p_{31}})^\vee$. This is shape (M).

- $a_y < b_y$: This case is symmetric to $a_y > b_y$ by (yz). The lower vertex of $(\overline{p_{21}p_{30}})^\vee$ has always y-coordinate smaller than a_y. Therefore, the vertex of the bitangent line is contained in the relative interior of $(\overline{p_{21}p_{30}})^\vee$ and the second tangency is given as the non-transversal intersection of the diagonal ray with $(\overline{p_{21}p_{30}})^\vee$. This is shape (B)$_{(yz)}$.
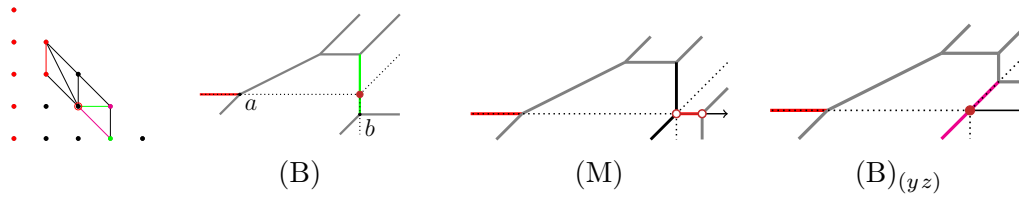
Figure 4.22: Example of deformation of shapes in deformation class (B M)+($y\,z$)

In Figure 4.22 we see an illustration of the deformation between the shapes or the choice of $\overline{p_{12}p_{13}}$ as the red edge. Analogous examples can be made for $\overline{p_{10}p_{11}}$ and $\overline{p_{11}p_{12}}$.

Deformation class (D L' Q)

Figure 4.23 shows in the leftmost picture a first case of a possible completion of the dual bitangent motif (D) that is not covered by Proposition 4.2.2. Note, that the dual bitangent motifs of the shapes (L') and (Q) are contained.
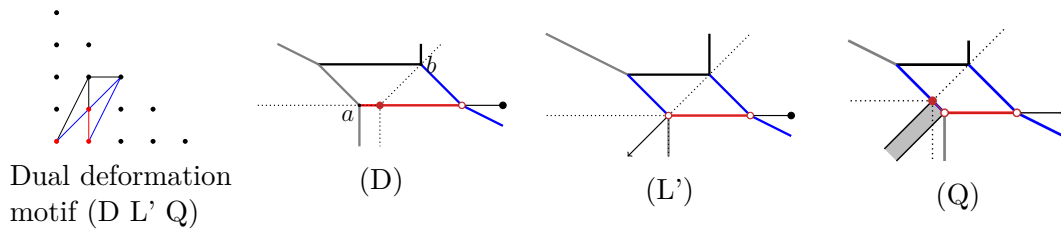
Figure 4.23: Example of deformation of shapes in deformation class (D L' Q)

The intersection of the diagonal ray of a tropical line with edge $(\overline{p_{11}p_{22}})^\vee$ resp. of the vertical ray with the edge $(\overline{p_{22}p_{10}})^\vee$ provides the first tangency. Due to the combinatorics, they can not occur together for one tropical line. For the bitangents in the class whose vertical ray intersects with the edge $(\overline{p_{22}p_{10}})^\vee$, the second tangency is given by a non-transversal intersection of the horizontal ray with $(\overline{p_{10}p_{11}})^\vee$. This part of the bitangent shape is independent of any edge length changes. If the first tangency is given by the transversal intersection of the diagonal ray with edge $(\overline{p_{11}p_{22}})^\vee$, the second tangency depends on the relative position of the vertices $a := (a_x, a_y) := (\overline{p_{00}p_{10}p_{11}})^\vee$ and $b := (b_x, b_y) := (\overline{p_{11}p_{12}p_{22}})^\vee$ as depicted in Figure 4.23.

- $a_x - a_y < b_x - b_y$: In this case the diagonal ray of the tropical line through the vertex $(\overline{p_{11}p_{12}p_{22}})^\vee$ meets the horizontal edge $(\overline{p_{10}p_{11}})^\vee$ in its relative interior. Thus, the bitangent shape is (D).

- $a_x - a_y = b_x - b_y$: In this case the two vertices $(\overline{p_{00}p_{10}p_{11}})^\vee$ and $(\overline{p_{11}p_{12}p_{22}})^\vee$ lie on a diagonal ray. Hence, in addition to the bounded edge of the bitangent shape, we obtain an infinite diagonal ray. This is shape (L').

- $a_x - a_y > b_x - b_y$: In this case a diagonal ray can intersect both edges $(\overline{p_{00}p_{11}})^\vee$ and $(\overline{p_{11}p_{22}})^\vee$. This gives shape (Q). By the slopes of the edges determined by the dual motif, the bitangent class can never reach the vertex $(\overline{p_{00}p_{11}p_{12}})^\vee$.

Deformation class (D L' Q Q' R)

The situation induced by the dual bitangent motif in Figure 4.24 is very similar to the situation for deformation clas (D L' Q). We observe again, that the triangulation contains the dual bitangent motifs of the shapes (D), (L'), (Q), (Q') and (R).
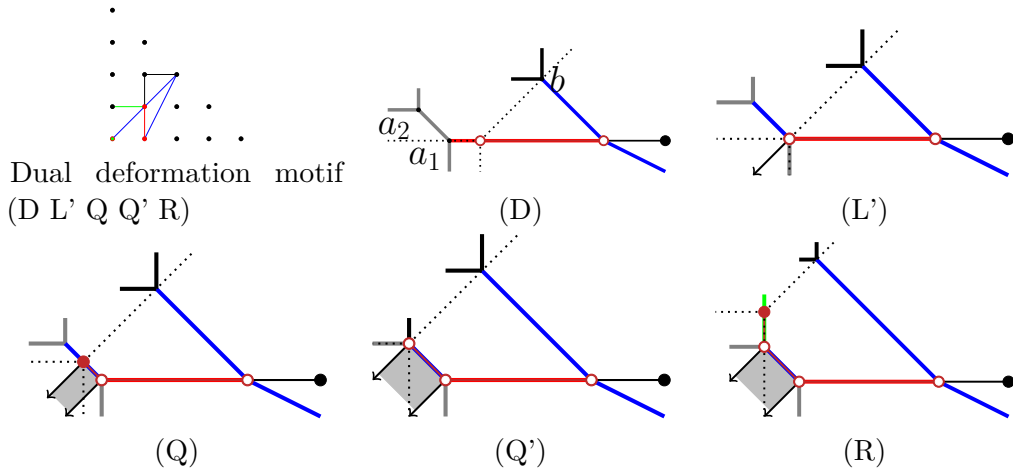
Figure 4.24: Example of deformation of shapes in deformation class (D L' Q Q' R)

We see the same two options for the first tangency as for deformation class (D L' Q). Also as before the second tangency depends on the edge lengths of the quartic, i.e., on the relative position of the vertices $a_1 := (a_{1x}, a_{1y}) := (\overline{p_{00}p_{10}p_{11}})^\vee$ resp. $a_2 := (a_{2x}, a_{2y}) := (\overline{p_{00}p_{01}p_{11}})^\vee$ to $b := (b_x, b_y) := (\overline{p_{11}p_{12}p_{22}})^\vee$ as depicted in Figure 4.24.

- $a_{2x} - a_{2y} < b_x - b_y$: Shape (D)

- $a_{2x} - a_{2y} = b_x - b_y$: Shape (L')

- $a_{2x} - a_{2y} > b_x - b_y > a_{1x} - a_{1y}$: Shape (Q)

  } as for (D L' Q)

- $b_x - b_y = a_{1x} - a_{1y}$: In contrast to the case for deformation class (D L' Q) the different combinatorial type allows a diagonal alignment of the $(\overline{p_{11}p_{12}p_{22}})^\vee$ with the right vertex of $(\overline{p_{00}p_{11}})\vee$. This is shape (Q').

- $a_{1x} - a_{1y} > b_x - b_y$: By the dual subdivision, the upper vertex of $(\overline{p_{01}p_{11}})^{\vee}$ has to have larger y-coordinate than the diagonal ray through vertex $(\overline{p_{11}p_{12}p_{22}})$ at x-coordinate a_{1x}. Thus the diagonal ray through vertex $(\overline{p_{11}p_{12}p_{22}})$ meets the vertical edge $(\overline{p_{01}p_{11}})^{\vee}$. This is shape (R).

Figure 4.24 illustrates this deformation between the shapes.

Deformation class (D L O)

Figure 4.25 shows the last remaining option for the completion of the bitangent motif of shape (D). We observe that this coincides with the dual bitangent motifs of shape (L) and (O). There are many similarities with the dual deformation motif of deformation classes (D L' Q) and (D L' Q Q' R), e.g. the first tangency is given either by an intersection of the diagonal ray with $(\overline{p_{11}p_{22}})^{\vee}$, or of the vertical ray with $(\overline{p_{10}p_{22}})^{\vee}$. The second intersection depends on the relative position of the

Dual deformation motif (D L O)   (D)   (L)   (O)
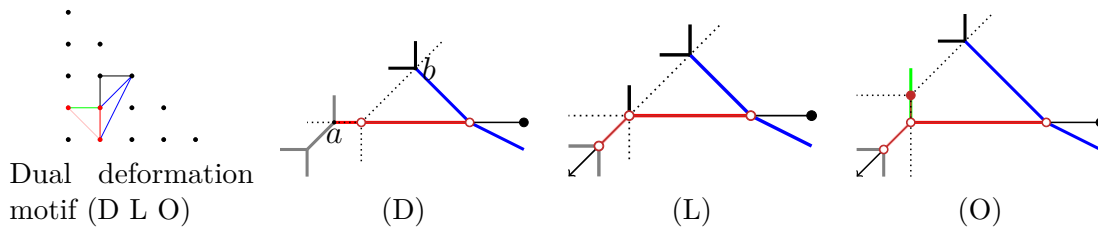
Figure 4.25: Example of deformation of shapes in deformation class (D L O)

vertex $a := (a_x, a_y) := (\overline{p_{10}p_{01}p_{11}})^{\vee}$ to the vertex $b := (b_x, b_y) := (\overline{p_{11}p_{22}p_{12}})^{\vee}$; see Figure 4.25.

- $b_x - b_y > a_x - a_y$: Analogous to (D L' Q) and (D L' Q Q' R). We see shape (D).

- $b_x - b_y = a_x - a_y$: In this case the vertices $(\overline{p_{11}p_{22}p_{12}})^{\vee}$ and $(\overline{p_{10}p_{01}p_{11}})^{\vee}$ lie on a diagonal ray. Hence, in addition to the bounded edge of the bitangent shape, we obtain an infinite diagonal ray containing the bounded edge $(\overline{p_{10}p_{01}})^{\vee}$ of the quartic. This is shape (L).

- $b_x - b_y < a_x - a_y$: By the dual subdivision, the upper vertex of $(\overline{p_{01}p_{11}})^{\vee}$ must have larger y-coordinate than the diagonal ray through vertex $(\overline{p_{11}p_{12}p_{22}})$ at x-coordinate a_x. This is analogous to the argument for (R) in the case of deformation class (D L' Q Q' R). Thus, the diagonal ray through vertex $(\overline{p_{11}p_{12}p_{22}})$ meets the vertical edge $(\overline{p_{01}p_{11}})^{\vee}$. This is shape (O).

Deformation class (E F J)

In Figure 3.7 the dual bitangent motif of shape (E) had two different choices for the blue edge. The first case lead to a constant deformation class, see Proposition 4.2.2. Here, we investigate the second case. We notice that the dual bitangent motif coincides with the dual bitangent motif of shape (F) and that by unimodularity it extends to the dual bitangent motif of shape (J), both in identity position. The horizontal bounded edge $(\overline{p_{1v}p_{1,v+1}})^\vee$ provides the first tangency via a non-transversal intersection with the horizontal ray of the tropical bitangent.

Dual deformation motif (E F J)   (E)   (J)   (F)
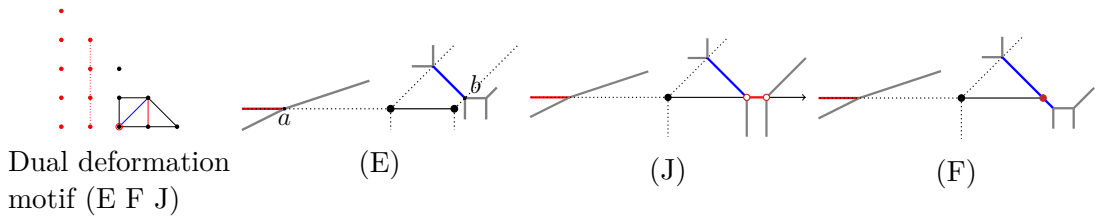
Figure 4.26: Example of deformation of shapes in deformation class (E F J)

Let $a := (a_x,a_y) := (\overline{p_{1v}p_{1,v+1}p_{20}})^\vee$ and $b := (b_x,b_y) := (\overline{p_{20}p_{30}p_{31}})^\vee$; see Figure 4.26. By the triangulation we can conclude, that a_y has to be smaller than the y-coordinate of $(\overline{p_{20}p_{21}p_{31}})^\vee$. Therefore, independent of the edge lengths of the quartic a tropical line can always non-transversally intersect its horizontal ray with $(\overline{p_{1v}p_{1,v+1}})^\vee$ and transversally intersect its diagonal ray with $(\overline{p_{20}p_{31}})^\vee$. Other options depend on the relative position of $(\overline{p_{1v}p_{1,v+1}p_{20}})^\vee = a$ and $(\overline{p_{20}p_{31}p_{30}})^\vee = b$.

- $a_y < b_y$: In this case the horizontal ray through $(\overline{p_{1v}p_{1,v+1}})^\vee$ and the diagonal rays through $(\overline{p_{20}p_{21}p_{31}})^\vee$ and $(\overline{p_{20}-p_{30}p_{31}})^\vee$ intersect outside of the quartic curve and form a bounded line segment. This is shape (E).

- $a_y = b_y$: In this case the two horizontally bounded edges are aligned. As the non-transversal intersection with $(\overline{p_{20}p_{31}})^\vee$ also give a tangency, the bitangent class is an infinite ray containing $(\overline{p_{20}p_{31}})^\vee$. This is shape (J).

- $a_y > b_y$: In this case, the bitangent class is bounded by the edge $(\overline{p_{20}p_{31}})^\vee$. This is shape (F).

We cannot obtain another shape because different x-coordinates of the edge $(\overline{p_{1v}p_{1,v+1}})^\vee$ and of $(\overline{p_{20}p_{31}p_{21}})^\vee$ do not influence the shape. Figure 4.26 illustrates the deformation in the case of $\overline{p_{12}p_{13}}$ as vertical red edge. The other two cases are analogous.
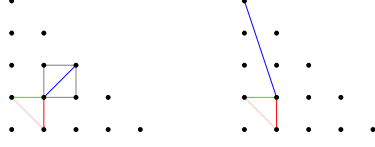
Figure 4.27: Dual deformation motifs of (G I N)+(xy)

Deformation class (G I N)+(xy)

Figure 4.27 shows a completion of the dual bitangent motif of shape (G) from Figure 3.7 that is not covered by Proposition 4.2.2. We observe that it coincides with the dual bitangent motifs of shapes (I), (N), (I)$_{(xy)}$ and (G)$_{(xy)}$. For this deformation class we have two options. As the argument is analogous for the two cases, we will only consider the case with blue edge $(\overline{p_{11}p_{22}})$ in the motif. It is portrayed in Figure 4.28. The case with with blue edge $(\overline{p_{11}p_{04}})$ is illustrated in Figure 4.29.

Independent of the edge lengths of the quartic curve, the transversal intersection of the diagonal ray of a tropical line with the blue edge $(\overline{p_{11}p_{22}})^\vee$ (resp. $(\overline{p_{11}p_{04}})^\vee$) yields a tangency. Moreover, the x-coordinate of $(\overline{p_{11}p_{22}p_{21}})^\vee$ is at least as large as the x-coordinate of the right vertex of $(\overline{p_{10}p_{11}})^\vee$, and the y-coordinate of o $(\overline{p_{11}p_{22}p_{21}})^\vee$ is always smaller than the y-coordinate of the upper vertex of $(\overline{p_{01}p_{11}})^\vee$. Therefore, the diagonal ray through $(\overline{p_{11}p_{22}p_{21}})^\vee$ will always intersect with $(\overline{p_{10}p_{11}})^\vee$ or with $(\overline{p_{01}p_{11}})^\vee$. This second tangency depends on the relative position of $(\overline{p_{11}p_{22}})^\vee$ (resp. $(\overline{p_{11}p_{04}})^\vee$) to the vertex $(p_{10}p_{01}p_{11})^\vee$.

Let $a := (a_x, a_y) := (\overline{p_{10}p_{01}p_{11}})^\vee$ and let $b_1 := (b_{1x}, b_{1y}) := (\overline{p_{11}p_{21}p_{22}})^\vee$, $b_2 := (b_{2x}, b_{2y}) := (\overline{p_{11}p_{12}p_{22}})^\vee$; see Figure 4.28. The following argument works exactly the same when choosing the other triangulation, that is when $b_1 := (\overline{p_{11}p_{12}p_{04}})^\vee$ and $b_2 := (\overline{p_{11}p_{03}p_{04}})^\vee$. By the direction of $(\overline{p_{11}p_{22}})^\vee$ (resp. $(\overline{p_{11}p_{04}})^\vee$) we always have $b_{2x} - b_{2y} < b_{1x} - b_{1y}$.

- $a_x - a_y < b_{2x} - b_{2y}$: In this case, the diagonal ray through $(\overline{11 p_{12}p_{22}})^\vee$ intersects with $(\overline{p_{10}p_{11}})^\vee$. Thus, the second tangency is given by the non-transversal intersection of the horizontal ray with $(\overline{p_{10}p_{11}})^\vee$. This is shape (G).

- $a_x - a_y = b_{2x} - b_{2y}$: In this case, the diagonal ray through $(\overline{p_{11}p_{12}p_{22}})^\vee$ aligns with $(\overline{p_{10}p_{01}p_{11}})^\vee$. Thus, in addition to the bounded line segment contained in $(\overline{p_{10}p_{11}})^\vee$ the bitangent class consists of an infinite ray passing through $(\overline{p_{10}p_{01}})^\vee$. This is shape (I).

- $b_{1x} - b_{1y} > a_x - a_y > b_{2x} - b_{2y}$: In this case, the diagonal ray through $(\overline{p_{11}p_{12}p_{22}})^\vee$ intersects with $(\overline{p_{01}p_{11}})^\vee$. Thus, in addition to the part of the bitangent class defined in case (I) we get a second bounded line segment contained in $(\overline{p_{01}p_{11}})^\vee$. This is shape (N).

- $a_x - a_y = b_{1x} - b_{1y}$: Now, the diagonal ray through the right vertex of $(\overline{p_{11}p_{22}})^\vee$ no longer intersects the relative interior of $(\overline{p_{10}p_{11}})^\vee$. Instead, the diagonal ray through $(\overline{p_{11}p_{22}p_{21}})^\vee$ aligns with $(\overline{p_{10}p_{01}p_{11}})^\vee$. Since the diagonal ray through $(\overline{11p_{12}p_{22}})^\vee$ still intersects with $(\overline{p_{01}p_{11}})^\vee$, we see shape $(I)_{(xy)}$.

- $a_x - a_y > b_{1x} - b_{1y}$: In this situation, the diagonal ray through $(\overline{p_{11}p_{22}p_{21}})^\vee$ intersects the relative interior of $(\overline{p_{01}p_{11}})^\vee$. So the bitangent class consists of a bounded line segment contained in the relative interior of $(\overline{p_{01}p_{11}})^\vee$. This is shape $(G)_{(xy)}$.

Figure 4.28 depicts the case given by choosing the blue edge $\overline{p_{11}p_{22}}$. The situation is similar if we choose the other blue edge $\overline{p_{11}p_{04}}$, as illustrated in Figure 4.29.

$\quad$ (G) $\qquad$ (I) $\qquad$ (N) $\qquad$ $(I)_{(xy)}$ $\qquad$ $(G)_{(xy)}$
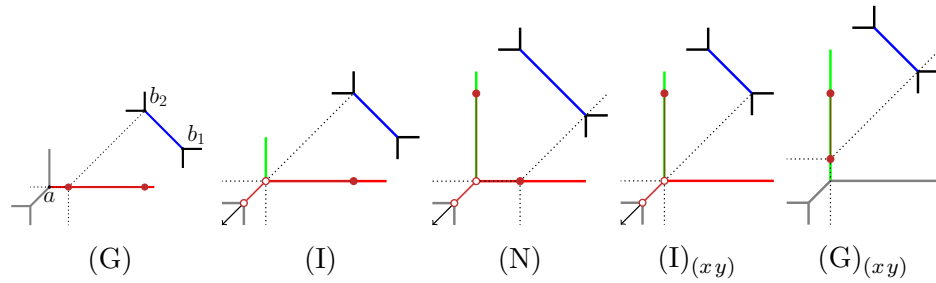
Figure 4.28: Example of deformation of shapes in deformation class (G I N)+(xy) with one tangency given by $\overline{p_{11}p_{22}}$.

$\quad$ (G) $\qquad$ (I) $\qquad$ (N) $\qquad$ $(I)_{(xy)}$ $\qquad$ $(G)_{(xy)}$
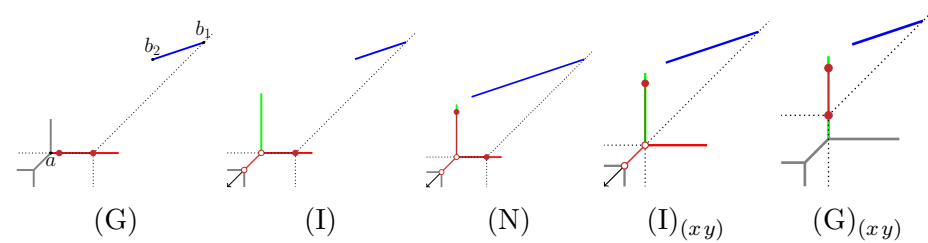
Figure 4.29: Example of deformation of shapes in deformation class (G I N)+(xy) with one tangency given by $\overline{p_{11}p_{04}}$.

Deformation class (G K U T T')

Figure 4.30 shows another choice of the dual bitangent motif of shape (G) not covered by the previous investigations. This contains the dual bitangent motifs of the shapes (K), (U), (T) and (T'). It also contains the dual bitangent motif of shape (T''), but it follows from Proposition 4.2.1 that (T'') cannot appear. Similarly to
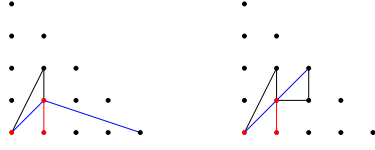
Figure 4.30: Dual deformation motifs of (G K U T T')

deformation class (G I N)+$(x\,y)$, we have to distinguish two cases. As the argument for both cases is analogous, we only consider the case with blue edge $(\overline{p_{11}p_{22}})^\vee$ in detail. Similar to the deformation class (G I N)+$(x\,y)$ the transversal intersection of the diagonal ray of a tropical line with $(\overline{p_{11}p_{22}})^\vee$ (resp. $(\overline{p_{11}p_{40}})^\vee$) provides the first tangency. The second tangency depends on the relative position of $(\overline{p_{11}p_{22}})^\vee$ to the vertex $(\overline{p_{00}p_{10}p_{11}})^\vee$.

Let $a := (a_x, a_y) := (\overline{p_{00}p_{10}p_{11}})^\vee$, $b_1 := (b_{1x}, b_{1y}) := (\overline{p_{11}p_{12}p_{22}})^\vee$ and $b_2 := (b_{2x}, b_{2y}) := (\overline{p_{11}p_{21}p_{22}})^\vee$ as illustrated in Figure 4.32. By the triangulation we know: $b_{1x} - b_{1y} > b_{2x} - b_{2y}$.

- $a_x - a_y < b_{2x} - b_{2y}$: The diagonal rays through $(\overline{p_{11}p_{12}p_{22}})^\vee$ and $(\overline{p_{11}p_{21}p_{22}})^\vee$ both intersect the relative interior of $(\overline{p_{10}p_{11}})^\vee$. We observe shape (G).

- $a_x - a_y = b_{2x} - b_{2y}$: The diagonal ray through $(\overline{p_{11}p_{12}p_{22}})^\vee$ passes through $(\overline{p_{00}p_{10}p_{11}})^\vee$ while the diagonal ray through $(\overline{p_{11}p_{21}p_{22}})^\vee$ still intersects the relative interior of $(\overline{p_{10}p_{11}})^\vee$. Since the adjacent edge to $(\overline{p_{00}p_{10}p_{11}})^\vee$ is of direction $(1, -1)$ the bitangent class contains in addition to the bounded line segment contained in $(\overline{p_{10}p_{11}})^\vee$ an infinite ray starting from $(\overline{p_{00}p_{10}p_{11}})^\vee$ in direction $(-1, -1)$. This is shape (K).

- $b_{1x} - b_{1y} > a_x - a_y > b_{2x} - b_{2y}$: The diagonal ray through $(\overline{p_{11}p_{21}p_{22}})^\vee$ still intersects the relative interior of $(\overline{p_{10}p_{11}})^\vee$. However, the diagonal ray through $(\overline{p_{11}p_{12}p_{22}})^\vee$ passes now through the relative interior of the edge $(\overline{p_{00}p_{11}})^\vee$ at (s_1, s_2). Thus, there exists an unbounded 2-cell in the bitangent class defined by $(\overline{p_{10}p_{11}})^\vee$ and the diagonal rays through $(\overline{p_{00}p_{10}p_{11}})^\vee$ and (s_1, s_2). This is shape (U).

- $a_x - a_y = b_{1x} - b_{1y}$: In this situation, the diagonal ray through $(\overline{p_{11}p_{21}p_{22}})^\vee$ aligns with the vertex $(\overline{p_{00}p_{10}p_{11}})^\vee$, while the diagonal ray through $(\overline{p_{11}p_{12}p_{22}})^\vee$ passes through the relative interior of the edge $(\overline{p_{00}p_{11}})^\vee$ at (s_1, s_2). Thus, the bounded line segment of the bitangent class vanishes, leaving the 2-dimensional cell bounded in 3 directions by by $(\overline{p_{10}p_{11}})^\vee$ and the diagonal rays through $(\overline{p_{00}p_{10}p_{11}})^\vee$ and (s_1, s_2). This is shape (T').

- $a_x - a_y > b_{1x} - b_{1y}$: Both diagonal rays through $(\overline{p_{11}p_{21}p_{22}})^\vee$ and $(\overline{p_{11}p_{12}p_{22}})^\vee$ intersect the relative interior of the edge $(\overline{p_{00}p_{11}})^\vee$. This is shape (T).

We can deduce from the triangulation, that the y-coordinate of vertex $(\overline{p_{00}p_{11}p_{12}})^\vee$ will always be at least as large as the y-coordinate of the upper vertex of $(\overline{p_{11}p_{22}})^\vee$ (resp. $(\overline{p_{11}p_{40}})^\vee$). Hence, the list of deformations above is complete.

Figure 4.31 depicts the described deformation of the bitangent shapes for the case $\overline{p_{11}p_{22}}$ as blue edge in the dual motif. The analogous situation for the blue edge $\overline{p_{11}p_{40}}$ in the dual motif is depicted in Figure 4.32.
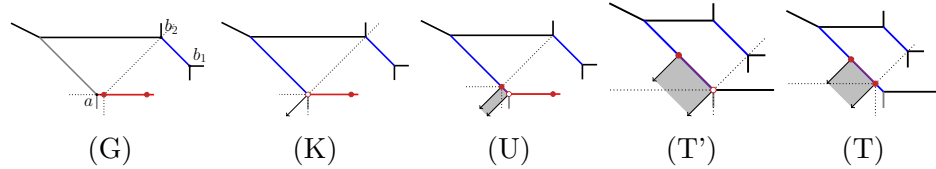
Figure 4.31: Example of deformation of shapes in deformation class (G K U T T') with one tangency given by $\overline{p_{11}p_{40}}$.
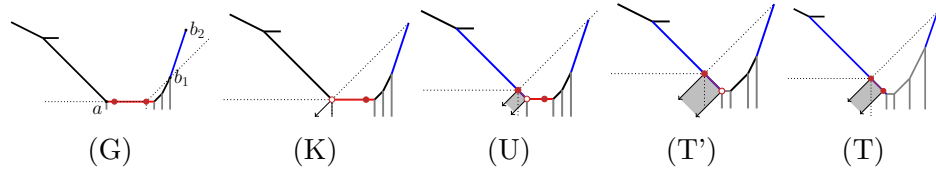
Figure 4.32: Example of deformation of shapes in deformation class (G K U T T') with one tangency given by $\overline{p_{11}p_{22}}$.

Deformation class (G K U U' T T' T" V)$+(x\,y)$
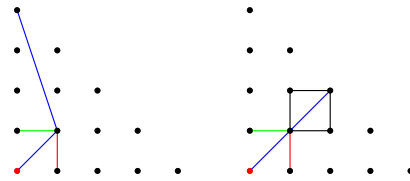
Figure 4.33: Dual deformation motifs of (G K U U' T T' T" V)$+(x\,y)$

Figure 4.33 shows the remaining possible completion of the dual bitangent motif of shape (G). Please note, that it contains the dual bitangent motifs of shapes (K), (U), (U'), (T), (T'), (T") and (V) and their images under $(x\,y) \in S_3$. We have to distinguish two cases depending on whether the edge $\overline{p_{11}p_{22}}$ or the edge $\overline{p_{11}p_{04}}$ is contained. The argument for both cases is similar which is why we only consider the case for $\overline{p_{11}p_{22}}$ in detail.

Let $a_1 := (a_{1x}, a_{1y}) := (\overline{p_{00}p_{10}p_{11}})^\vee$, $a_2 := (a_{2x}, a_{2y}) := (\overline{p_{00}p_{01}p_{11}})^\vee$, $b_1 := (b_{1x}, b_{1y}) := (\overline{p_{11}p_{21}p_{22}})^\vee$, and $b_2 := (b_{2x}, b_{2y}) := (\overline{p_{11}p_{12}p_{22}})^\vee$ as depicted in Figure 4.34. By the triangulation we know

$$b_{1x} - b_{1y} > b_{2x} - b_{2y} \text{ and } a_{1x} - a_{1y} > a_{2x} - a_{2y}.$$

- $a_{1x} - a_{1y} < b_{2x} - b_{2y}$: Shape (G)

- $a_{1x} - a_{1y} = b_{2x} - b_{2y}$: Shape (K)

- $b_{1x} - b_{1y} > a_{1x} - a_{1y} > b_{2x} - b_{2y} > a_{2x} - a_{2y}$: Shape (U)

- $b_{1x} - b_{1y} = a_{1x} - a_{1y} > b_{2x} - b_{2y} > a_{2x} - a_{2y}$: Shape (T')

- $a_{1x} - a_{1y} > b_{1x} - b_{1y} > b_{2x} - b_{2y} > a_{2x} - a_{2y}$: Shape (T)

  $\left.\right\}$ as for (G K U T T')

- $b_{1x} - b_{1y} > a_{1x} - a_{1y} > b_{2x} - b_{2y} = a_{2x} - a_{2y}$: In this case the diagonal ray through $b_2 = (\overline{p_{11}p_{12}p_{22}})^\vee$ aligns with the vertex $a_2 = (\overline{p_{00}p_{01}p_{11}})^\vee$. The remaining inequalities are as before for shape (U), such that the difference is only that here the edge $(\overline{p_{00}p_{11}})^\vee$ including its vertices is completely contained in the bitangent class. This is shape (U').

- $b_{1x} - b_{1y} = a_{1x} - a_{1y} > b_{2x} - b_{2y} = a_{2x} - a_{2y}$: As for shape (U') we have that the diagonal ray through $b_2 = (\overline{p_{11}p_{12}p_{22}})^\vee$ aligns with the vertex $a_2 = (\overline{p_{00}p_{01}p_{11}})^\vee$. However, the diagonal ray through $b_1 = (\overline{p_{11}p_{21}p_{22}})^\vee$ no longer intersects the relative interior of the edge $(\overline{p_{10}p_{11}})^\vee$ but aligns with the vertex $a_1 = (\overline{p_{00}p_{10}p_{11}})^\vee$. We see shape (T").

- $b_{1x} - b_{1y} > a_{1x} - a_{1y} > a_{2x} - a_{2y} > b_{2x} - b_{2y}$: In this case the diagonal through vertex $b_1 := (\overline{p_{11}p_{21}p_{22}})^\vee$ intersects the relative interior of $(\overline{p_{10}p_{11}})^\vee$ and the diagonal ray through $b_2 = (\overline{p_{11}p_{12}p_{22}})^\vee$ intersects the relative interior of $(\overline{p_{01}p_{11}})^\vee$. The intersection in both cases has to be in the relative interior, as diagonal rays passing through $b_1 = (\overline{p_{11}p_{21}p_{22}})^\vee$ and $b_2 = (\overline{p_{11}p_{12}p_{22}})^\vee$ can never meet the upper vertex of $(\overline{p_{01}p_{11}})^\vee$ or the right vertex of $(\overline{p_{10}p_{11}})^\vee$. This is shape (V).

- $a_{1x} - a_{1y} > b_{1x} - b_{1y} > b_{2x} - b_{2y} = a_{2x} - a_{2y}$: Shape $(T')_{(x\,y)}$.

- $a_{1x} - a_{1y} = b_{1x} - b_{1y} > a_{2x} - a_{2y} > b_{2x} - b_{2y}$: Shape $(U')_{(x\,y)}$.

- $a_{1x} - a_{1y} > b_{1x} - b_{1y} > a_{2x} - a_{2y} > b_{2x} - b_{2y}$: Shape $(U)_{(x\,y)}$.

- $b_{1x} - b_{1y} = a_{2x} - a_{2y}$: Shape $(K)_{(x\,y)}$.

- $a_{2x} - a_{2y} > b_{1x} - b_{1y}$: Shape $(G)_{(x\,y)}$.

  $\left.\right\}$ symmetric by $(x\,y) \in S_3$ to the first five cases

As diagonal rays passing through $b_1 = (\overline{p_{11}p_{21}p_{22}})^\vee$ and $b_2 = (\overline{p_{11}p_{12}p_{22}})^\vee$ can never meet the upper vertex of $(\overline{p_{01}p_{11}})^\vee$ or the right vertex of $(\overline{p_{10}p_{11}})^\vee$, the above list describes all possible deformations. Figure 4.34 shows the deformation of the shapes. As done for the deformation classes (G I N)+$(x\,y)$ and (G K U T T'), an analogous picture can be drawn for $\overline{p_{11}p_{04}}$.
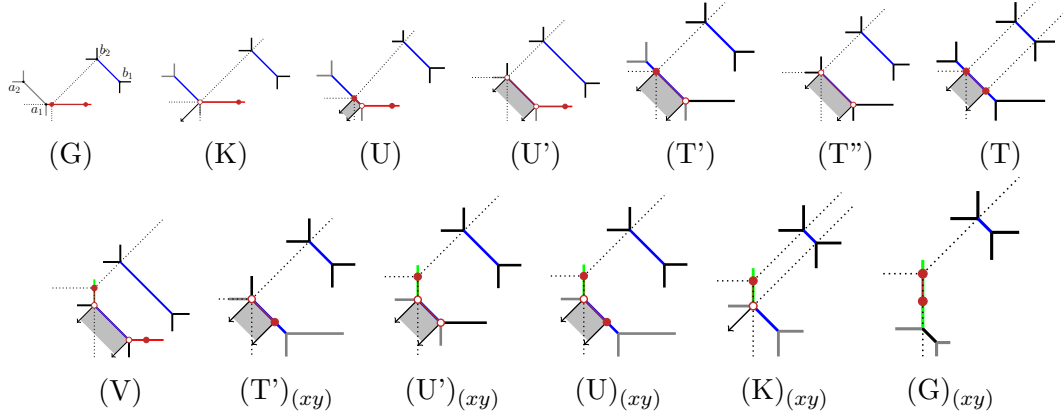
Figure 4.34: Example of the deformations of shapes in deformation class (G K U U' T T' T" V)+$(x\,y)$

Deformation class (W X Y EE GG)
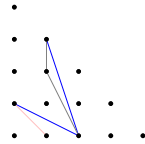
Figure 4.35: Dual deformation motif of (W X Y EE GG)

Figure 4.35 shows the dual bitangent motifs of shapes (W), $(X)_{(x\,z)}$, $(Y)_{(x\,z)}$, (EE) and (GG). We will prove that these shapes form a deformation class, see Figure 4.36, and that there are no further deformation possible.

Consider the vertices $a_1 := (a_{1x}, a_{1y}) := (\overline{p_{10}p_{01}p_{11}})^\vee$, $a_2 := (a_{2x}, a_{2y}) := (\overline{p_{01}p_{20}p_{11}})^\vee$, $b_1 := (b_{1x}, b_{1y}) := (\overline{p_{20}p_{13}p_{21}})^\vee$, and $b_2 := (b_{2x}, b_{2y}) := (\overline{p_{20}p_{13}p_{12}})^\vee$. We know from the triangulation that

$$b_{1x} - b_{1y} > b_{2x} - b_{2y},$$
$$a_{1x} - a_{1y} > a_{2x} - a_{2y},$$
$$b_{2x} - b_{2y} > a_{2x} - a_{2y},$$

$$b_{1y} > b_{2y} > a_{2y} > a_{1y}.$$

Therefore, in every case one of the tangencies is given by the transversal intersection of the diagonal ray of the tropical line with the edge $(\overline{p_{20}p_{13}})^\vee$. We note that due to its position and slope, $(\overline{p_{20}p_{13}})^\vee$ never intersects the the bitangent class. The second tangency can always be given by the transversal intersection of the horizontal ray with $(\overline{p_{01}p_{20}})^\vee$. As the intersection of the diagonal rays from the vertices of $(\overline{p_{20}p_{13}})^\vee$ with the horizontal rays from the vertices of $(\overline{p_{01}p_{20}})^\vee$ always lead to a 2-dimensional bounded cell, we conclude that any bitangent shape in this deformation class will always contain a 2-dimensional bounded cell. Depending on the relative positions of the vertex $(\overline{p_{10}p_{01}p_{20}})^\vee = a$ to the edge $(\overline{p_{20}p_{13}})^\vee$, other tangency intersections are possible for elements in the bitangent class. It is recommended to consider Figure 4.38 when reading the remaining part of the proof.

- $a_{1x} - a_{1y} < b_{2x} - b_{2y}$: In this case, the area bounded by the diagonal rays through the vertices $(\overline{p_{20}p_{13}p_{12}})^\vee$ and $(\overline{p_{20}p_{13}p_{21}})^\vee$ and the horizontal rays through the vertices $(\overline{p_{10}p_{01}p_{20}})^\vee$ and $(\overline{p_{01}p_{20}p_{11}})^\vee$ forms a parallelogram that does not intersect the quartic curve. This is shape (W).

- $a_{1x} - a_{1y} = b_{2x} - b_{2y}$: Here the diagonal ray through $b_2 = (\overline{p_{20}p_{13}p_{12}})^\vee$ aligns with $a_1 = (\overline{p_{10}p_{01}p_{20}})^\vee$. Thus, the bitangent class extends from the parallelogram to a parallelogram together with the infinite diagonal ray starting at $a_1 = (\overline{p_{10}p_{01}p_{20}})^\vee$ in direction $(-1, -1)$ containing the edge $(\overline{p_{10}p_{01}})^\vee$ completely. This is shape $(X)_{xz}$.

- $b_{2x} - b_{2y} < a_{1x} - a_{1y} < b_{1x} - b_{1y}$: In this case, the diagonal ray through $b_2 = (\overline{p_{20}p_{13}p_{12}})^\vee$ intersects the relative interior of the egde $(\overline{p_{01}p_{20}})^\vee$. Since the diagonal ray through $b_1 = (\overline{p_{20}p_{13}p_{21}})^\vee$ still passes right of $a_1 = (\overline{p_{10}p_{01}p_{20}})^\vee$, we keep the three vertices of the bitangent class outside of the quartic curve and the infinite diagonal ray starting at $a_1 = (\overline{p_{10}p_{01}p_{20}})^\vee$ in direction $(-1, -1)$ containing the edge $(\overline{p_{10}p_{01}})^\vee$ completely. The bitangent class additionally contains the part of the edge $(\overline{p_{01}p_{20}})^\vee$ from the vertex $a_1 = (\overline{p_{10}p_{01}p_{20}})^\vee$ till the intersection of the edge with the diagonal ray through $b_2 = (\overline{p_{20}p_{13}p_{12}})^\vee$. This is shape $(Y)_{xz}$.

- $a_{1x} - a_{1y} = b_{1x} - b_{1y}$: In this case, the diagonal ray through $b_1 = (\overline{p_{20}p_{13}p_{21}})^\vee$ aligns with $a_1 = (\overline{p_{10}p_{01}p_{20}})^\vee$. We obtain a trapezoid with one edge part of the edge $(\overline{p_{01}p_{20}})^\vee$ from the quartic curve, together with the infinite diagonal ray starting at $a_1 = (\overline{p_{10}p_{01}p_{20}})^\vee$ in direction $(-1, -1)$ containing the edge $(\overline{p_{10}p_{01}})^\vee$ completely. This is shape (EE).

- $a_{1x} - a_{1y} > b_{1x} - b_{1y}$: In this case, the diagonal ray through $b_1 = (\overline{p_{20}p_{13}p_{21}})^\vee$ intersects the relative interior of the edge $(\overline{p_{01}p_{20}})^\vee$. Thus, the infinite ray is no longer part of the bitangent class, and we obtain a trapezoid with one edge contained in the edge $(\overline{p_{01}p_{20}})^\vee$ from the quartic curve. This is shape (GG).

As the argument above covers all possible cases for the given dual motif, we conclude that the list of deformations is complete. Figure 4.36 shows the deformation of the shapes.
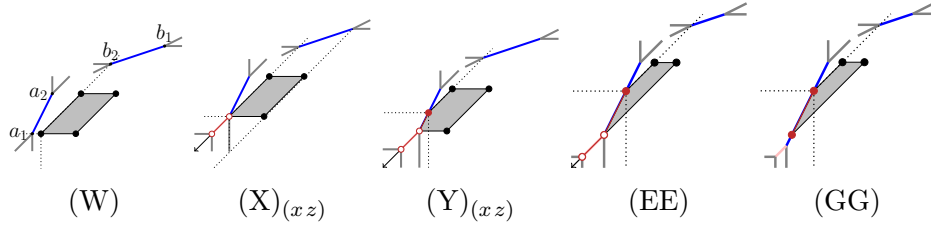
Figure 4.36: Example of the deformations of shapes in deformation class (W X Y EE GG).

Deformation class (W ... HH)$+(x\,z)$
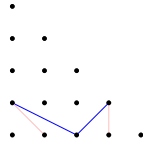
Figure 4.37: Dual deformation motif of (W ... HH)

Figure 4.37 shows the dual bitangent motif of the shapes (W), (X), (Y), (Z) and (AA) to (HH) and their images under $(x\,z) \in S_3$. The tangencies are given by transversal intersections with the edges $(\overline{p_{20}p_{31}})^\vee$ and $(\overline{p_{20}p_{01}})^\vee$. However, depending on their relative positions given by the edge lengths of the quartic there are different additional options for tangencies given by non-transversal intersections of the horizontal resp. diagonal ray of the tropical line with the edge $(\overline{p_{30}p_{31}})^\vee$ resp. $(\overline{p_{10}p_{01}})^\vee$. Let $a_1 := (a_{1x},a_{1y}) := (\overline{p_{10}p_{01}p_{20}})^\vee$, $a_2 := (a_{2x},a_{2y}) := (\overline{p_{20}p_{01}p_{11}})^\vee$, $b_1 := (b_{1x},b_{1y}) := (\overline{p_{20}p_{31}p_{30}})^\vee$, and $b_2 := (b_{2x},b_{2y}) := (\overline{p_{20}p_{31}p_{21}})^\vee$.

By the triangulation we know that the following inequalities always have to be satisfied:

$$\left.\begin{aligned}
b_{1x} - b_{1y} > b_{2x} - b_{2y} > a_{2x} - a_{2y}, \\
a_{1x} - a_{1y} > a_{2x} - a_{2y},
\end{aligned}\right\} \tag{4.1}$$

$$b_{2y} > b_{1y}, \qquad\qquad\qquad\qquad\qquad\left.\begin{array}{c}\\\\\end{array}\right\} \tag{4.2}$$

$$b_{2y} > a_{2y} > a_{1y},$$

$$b_{1x} > b_{2x} > a_{2x} > a_{1x}. \tag{4.3}$$

These data imply, that the the edges $(\overline{p_{20}p_{13}})^{\vee}$ and $(\overline{p_{01}p_{20}})^{\vee}$ are, for any choice of edge lengths of the quartic curve, positioned in a way that ensures that the intersection of diagonal rays through b_1 and b_2 with horizontal auxiliary lines through a_1 and a_2 will always form a bounded 2-dimensional cell that might additionally be bounded by some edges of the quartic curve. Hence, any shapes appearing in this deformation class must contain a bounded 2-dimensional cell. Since (W), (X), (Y), (Z) and (AA) to (HH) and their images under $(x\,z)$ are the only shapes that satisfy this condition and have dual bitangent motif contained in Figure 4.37, it only remains to prove that they and their images under $(x\,z)$ indeed do appear.

We prove this by considering all the possible relative positions of the diagonal rays through the relevant vertices a_1, a_2, b_1, b_2 given by the inequalities $\boldsymbol{\alpha}, \boldsymbol{\beta}, \boldsymbol{\gamma}, \boldsymbol{\delta}$, and $\boldsymbol{\epsilon}$:

$$\boldsymbol{\alpha} \; : \; b_{1x} - b_{1y} > b_{2x} - b_{2y} > a_{1x} - a_{1y} > a_{2x} - a_{2y},$$

$$\boldsymbol{\beta} \; : \; b_{1x} - b_{1y} > b_{2x} - b_{2y} = a_{1x} - a_{1y} > a_{2x} - a_{2y},$$

$$\boldsymbol{\gamma} \; : \; b_{1x} - b_{1y} > a_{1x} - a_{1y} > b_{2x} - b_{2y} > a_{2x} - a_{2y},$$

$$\boldsymbol{\delta} \; : \; b_{1x} - b_{1y} = a_{1x} - a_{1y} > b_{2x} - b_{2y} > a_{2x} - a_{2y},$$

$$\boldsymbol{\epsilon} \; : \; a_{1x} - a_{1y} > b_{1x} - b_{1y} > b_{2x} - b_{2y} > a_{2x} - a_{2y},$$

together with the possible relative positions of the horizontal rays through the vertices a_1, a_2, b_1, b_2 given by the inequalities **I**, **II**, **III**, **IV**, and **V**:

$$\mathbf{I} \; : \; b_{2y} > b_{1y} > a_{2y} > a_{1y},$$

$$\mathbf{II} \; : \; b_{2y} > b_{1y} = a_{2y} > a_{1y},$$

$$\mathbf{III} \; : \; b_{2y} > a_{2y} > b_{1y} > a_{1y},$$

$$\mathbf{IV} \; : \; b_{2y} > a_{2y} > b_{1y} = a_{1y},$$

$$\mathbf{V} \; : \; b_{2y} > a_{2y} > a_{1y} > b_{1y}.$$

The Equations (4.1) and (4.2) show that the above lists are all the possible inequalities that can appear. We now consider all possible combinations of these, which provides a full list of all possible relative positions of the edges $(\overline{p_{20}p_{13}})^{\vee}$ and $(\overline{p_{01}p_{20}})^{\vee}$ that are relevant for the bitangent shapes. Table 4.1 summarizes which shapes appear for which combinations of the inequalities out of $\{\boldsymbol{\alpha}, \boldsymbol{\beta}, \boldsymbol{\gamma}, \boldsymbol{\delta}, \boldsymbol{\epsilon}\}$ and $\{\mathbf{I}, \mathbf{II}, \mathbf{III}, \mathbf{IV}, \mathbf{V}\}$.

	$\boldsymbol{\alpha}$	$\boldsymbol{\beta}$	$\boldsymbol{\gamma}$	$\boldsymbol{\delta}$	$\boldsymbol{\epsilon}$
I	(W)	(X)$_{(xz)}$	(Y)$_{(xz)}$	(GG)	(EE)
II	(X)	(Z)	(AA)$_{(xz)}$	(HH)	(FF)
III	(Y)	(AA)	(BB)	(DD)	(CC)
IV	(GG)$_{(xz)}$	(HH)$_{(xz)}$	(DD)$_{(xz)}$	x	x
V	(EE)$_{(xz)}$	(FF)$_{(xz)}$	(CC)$_{(xz)}$	x	x

Table 4.1: The bitangent shapes induced by the different relative positions of the edges $(\overline{p_{20}p_{13}})^\vee$ and $(\overline{p_{01}p_{20}})^\vee$ given by the inequalities $\{\boldsymbol{\alpha},\boldsymbol{\beta},\boldsymbol{\gamma},\boldsymbol{\delta},\boldsymbol{\epsilon}\}$ and $\{\mathbf{I},\mathbf{II},\mathbf{III},\mathbf{IV},\mathbf{V}\}$.

Table 4.1 contains no shapes for the combinations $(\mathbf{IV},\boldsymbol{\delta})$, $(\mathbf{IV},\boldsymbol{\epsilon})$, $(\mathbf{V},\boldsymbol{\delta})$ and $(\mathbf{V},\boldsymbol{\epsilon})$, because these can never appear:

$(\mathbf{IV},\boldsymbol{\delta})$ By $\mathbf{IV}$ we have $b_{1y} = a_{1y}$ and by $\boldsymbol{\delta}$ we have $b_{1x} - b_{1y} = a_{1x} - a_{1y}$. This implies $a_{1x} = b_{1x}$ which contradicts Equation (4.3).

$(\mathbf{IV},\boldsymbol{\epsilon})$ By $\mathbf{IV}$ we have $b_{1y} = a_{1y}$ and by $\boldsymbol{\epsilon}$ we have $a_{1x} - a_{1y} > b_{1x} - b_{1y}$. This implies $a_{1x} > b_{1x}$ which contradicts Equation (4.3).

$(\mathbf{V},\boldsymbol{\delta})$ By $\mathbf{V}$ we have $a_{1y} > b_{1y}$ and by $\boldsymbol{\delta}$ we have $b_{1x} - b_{1y} = a_{1x} - a_{1y}$. This implies $a_{1x} > b_{1x}$ which contradicts Equation (4.3).

$(\mathbf{V},\boldsymbol{\epsilon})$ By $\mathbf{V}$ we have $a_{1y} > b_{1y}$ and by $\boldsymbol{\epsilon}$ we have $a_{1x} - a_{1y} > b_{1x} - b_{1y}$. This implies $a_{1x} > b_{1x}$ which contradicts Equation (4.3).

Figure 4.38 confirms the statement from the Table 4.1 by illustrating all the deformations of the shapes. Since we checked all dual bitangent motifs and their possible completions, the classification is complete. $\qquad\square$

Remark 4.2.4. Note that in the proof the conditions for the deformation of the shapes are determined for every deformation class and that the areas of deformation are described via linear inequalities. These facts will be used for the proof of Theorem 6.3.1 in Section 6.3.1.
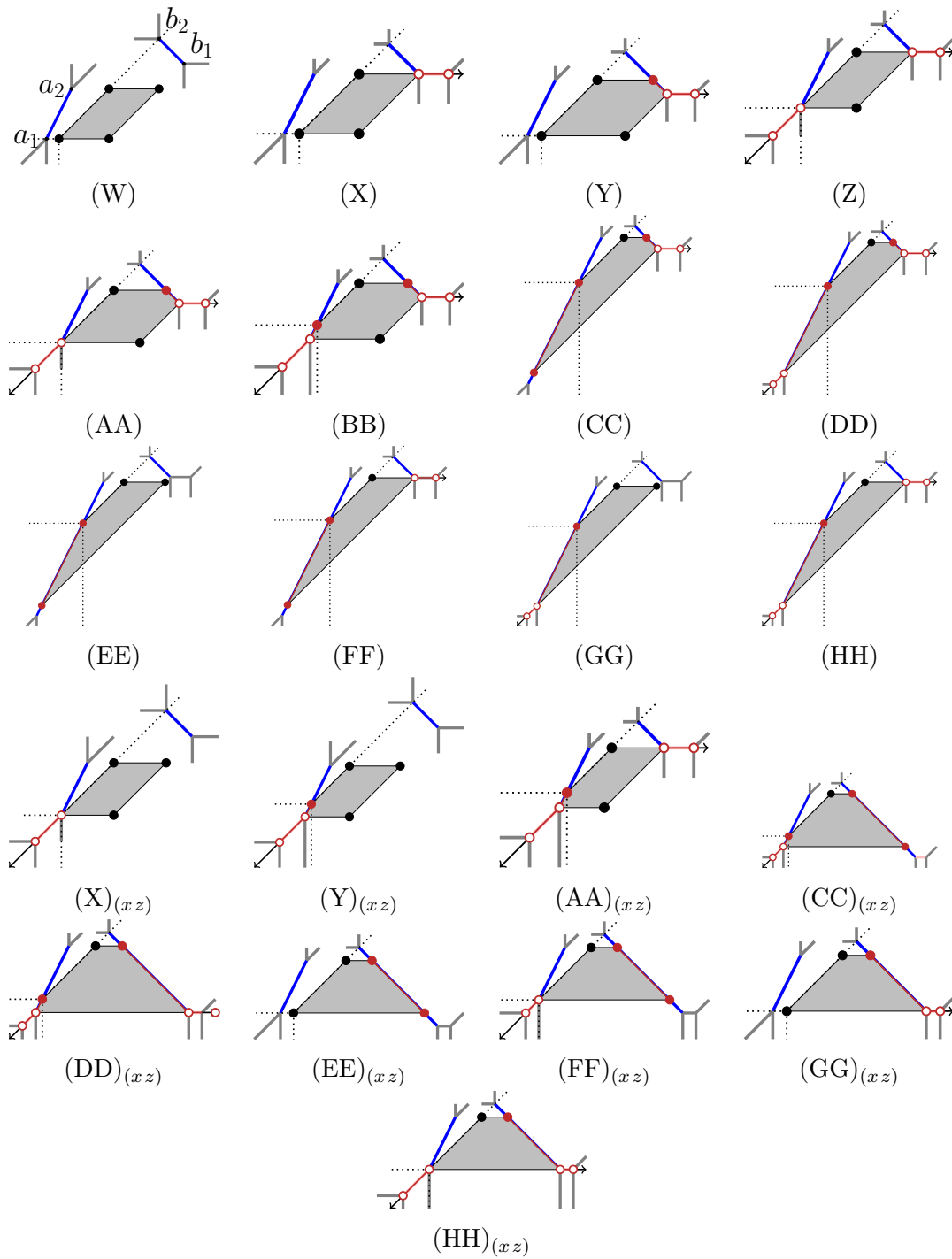
Figure 4.38: Example of deformation of shapes in deformation class (W ... HH)+$(x\,z)$
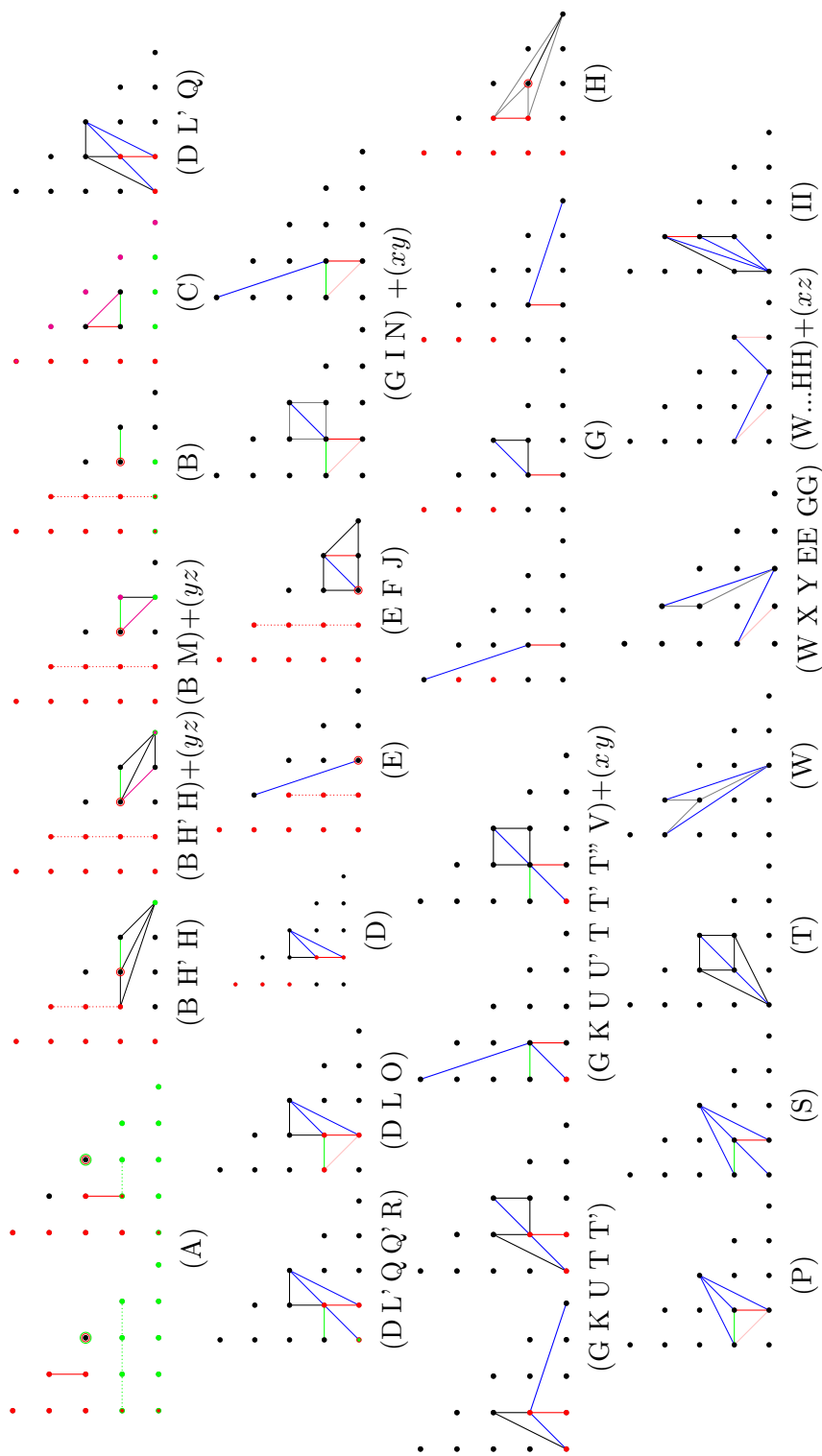
Figure 4.39: A list of the dual deformation motifs of all 24 deformation classes

Chapter 5

Tropical count of real bitangents to tropically smooth quartics

The definition and classification of deformation classes of tropical bitangents in Chapter 4 raise the question how the real lifting conditions of different bitangent shapes inside a deformation class behave. This chapter answers this question in Theorem 5.1.4 and uses the result to provide a tropical count of the numbers of real bitangents to real quartic curves in Theorem 5.2.2.

The identification of the real lifting behavior of deformation classes in Theorem 5.1.4 is the second main result of Part I. It turns out that the lifting conditions are the same for every bitangent shape in a deformation class, not only over $\mathbb{R}$ but also over arbitrary Henselian fields with residue field $\Bbbk$ of $\operatorname{char}(\Bbbk) \neq 2$ and 2-divisible value group, Corollary 5.1.5.

Since the lifting conditions can be computed directly from the dual triangulation, this enables a computational count of the number of real bitangents to tropically smooth algebraic quartic curves. In joint work with Marta Panizzut, we developed the `polymake` extension `TropicalQuarticCurves` motivated by the computational proof of Theorem 5.2.2. The extension is introduced in detail in Section 6.1: The properties which the extension allows to compute are illustrated with code snippets and examples in Section 6.1. Section 6.2 shows applications of the code that exceed the proof of Theorem 5.2.2. Moreover, the developed software will be useful for future research in the area, for example to investigate the lifting conditions over Henselian fields or to study arithmetic multiplicities of tropical bitangents [MSP22].

The results in this chapter build on the preprints [GP21b, GP21a] which are joint work with Marta Panizzut.

5.1 Real lifting conditions of deformation classes

The aim of this section is to prove that the real lifting conditions as determined for the bitangent shapes in [CM21] are constant for each deformation class. This is shown in Theorem 5.1.4. For this we consider deformation class (C) separately,

and then go through every deformation class one by one and check the real lifting conditions of the bitangent shapes in the deformation class.

By Theorem 5.1.4, the different shapes collected in one deformation class have the same real lifting conditions, so we can speak of the real lifting conditions of deformation classes. Moreover, this imprints the fact that the real lifting conditions of the bitangent classes of a tropical quartic curve only depend on its dual subdivision.

In Corollary 5.1.5, we obtain that not only the lifting conditions over $\mathbb{R}$ depend only on the deformation classes, but that this result holds more generally for arbitrary Henselian fields with non-Archimedean valuation and residue field $\mathbb{k}$ of $\mathrm{char}(\mathbb{k}) \neq 2$ and 2-divisible value group (Definition 2.2.8).

The results in this section make it possible to recover a tropical count of the number of real bitangents in Section 5.2. This section is based on [GP21b] which is joint work with Marta Panizzut.

Remark 5.1.1. For constant deformation classes it seems at first glance clear that the real lifting conditions do not change. However, for deformation class (C) we observe a special situation, which is impossible for the other constant deformation classes: For shape (C) the identity position depends on the edge lengths of the quartic. We recall the specific genericity constraint from (i) in Remark 3.3.2 that is of relevance in this situation: If the tropical quartic curve contains a vertex v adjacent to three bounded edges with directions $-e_1$, $-e_2$ and $e_1 + e_2$, then there exists a unique shortest edge. Bitangent shape (C) consists of one point that coincides with a vertex v as described above. Cueto and Marking chose the edge with direction $-e_2$ as shortest edge. We denote this as the *identity position* for shape (C), since the real lifting conditions for shape (C) were computed in [CM21] under this assumption.

Any generic tropical quartic having a bitangent class of shape (C) at a vertex v, but with different edge lengths, can be brought into this position by applying an action of S_3. This changes the dual subdivision accordingly. As consequence, it also changes the formula for the real lifting conditions of (C).

We take a close look at this situation in the following example.

Example 5.1.2. We consider the two smooth tropical quartic curves shown in Figures 5.1b and 5.1c dual to the triangulation $\mathcal{T}$ in Figure 5.1a. These quartic curves have a bitangent class of shape (C). We denote with λ_1, λ_2 and λ_3 the lattice lengths of the edges adjacent to the vertex that forms the bitangent class of shape (C) with direction $-e_2$, $-e_1$ and $e_1 + e_2$, respectively. For the tropical curve in Figure 5.1b, these lengths satisfy what we call the *identity case* of the genericity condition: $\lambda_1 < \lambda_2 \leq \lambda_3$. We substitute $i = 2, j = 1, k = 2$ in the real

lifting condition for (C) in Table 3.1 obtaining

$$- s_{11}s_{21}s_{02}s_{10} > 0 \text{ and } - s_{21}s_{11}s_{22}s_{10} > 0. \tag{5.1}$$

(a) Triangulation $\mathcal{T}$

(b) Generic curve in identity position.

(c) Generic curve not in identity position.
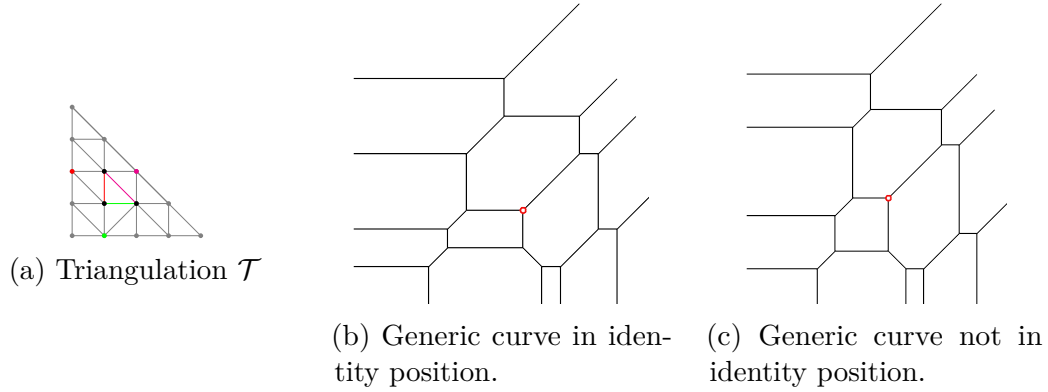
Figure 5.1: Smooth tropical quartic with bitangent class of shape (C)

By choosing a different weight vector in $\Sigma(\mathcal{T})$, we can deform the edge lengths such that they satisfy $\lambda_2 < \lambda_1 \le \lambda_3$. This is the case for the quartic curve in Figure 5.1c. For this tropical quartic curve the bitangent class of shape (C) is no longer in identity position. In order to apply the lifting formula, we need to apply the action of $(x\,y)$ to switch the lengths λ_1 and λ_2, inducing also an action on the triangulation $\mathcal{T}$. The image of the curve and of $\mathcal{T}$ under $(x\,y)$ is depicted in Figure 5.2. Now, we have to substitute $i = 1, j = 2, k = 2$ in the lifting conditions for shape (C) obtaining

$$-s_{11}s_{12}s_{01}s_{20} > 0 \text{ and } s_{22}s_{20} > 0.$$

(a) Image of the triangulation in Figure 5.1a under $(x\,y)$.

(b) Image of the quartic curve in Figure 5.1c under $(x\,y)$.
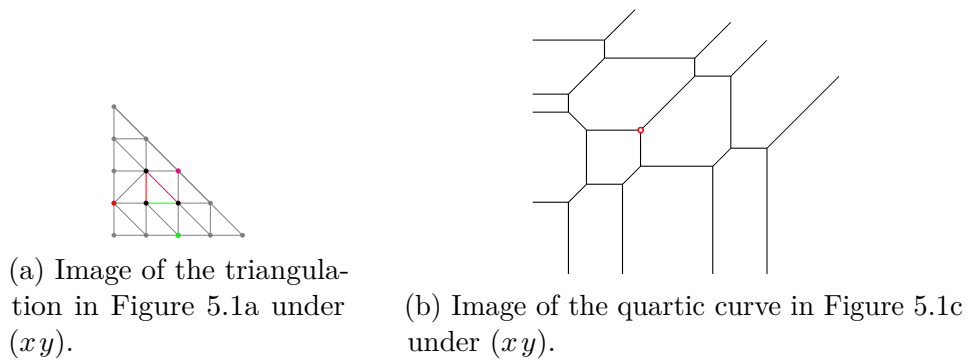
Figure 5.2: The $(x\,y)$-transformation of the tropical curve in Figure 5.1c and its dual triangulation.

We then deduce the lifting conditions for the original quartic with $\lambda_2 < \lambda_1 \leq \lambda_3$ by applying $(x\,y)^{-1} = (x\,y)$:

$$-s_{11}s_{21}s_{10}s_{02} > 0 \text{ and } s_{22}s_{02} > 0. \tag{5.2}$$

The second inequalities in (5.1) and (5.2) are different. However, we observe that the first inequality $-s_{11}s_{21}s_{10}s_{02} > 0$ is true if and only if $s_{02} = -s_{11}s_{21}s_{10}$. Substituting this equation into the second inequality, we see that the real lifting conditions are equivalent.

Proposition 5.1.3. *Let Γ be a smooth tropical plane quartic curve with dual triangulation $\mathcal{T}$ generic and a bitangent class B of shape (C). For every $c \in \Sigma(\mathcal{T})$ inducing a generic quartic curve the real lifting conditions of B_c in Γ_c are equivalent.*

Proof. We fix the following notation, see also Figure 5.3:

- i is the y-coordinate of the vertex p_{0i}, which forms a triangle with the (red) edge $\overline{p_{11}p_{12}}$,

- j is the x-coordinate of the vertex p_{j0}, which forms a triangle with the (green) edge $\overline{p_{11}p_{21}}$,

- k is the x-coordinate of the vertex $p_{k,4-k}$, which forms a triangle with the (pink) edge $\overline{p_{12}p_{21}}$.
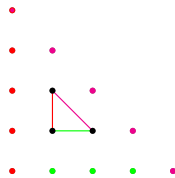
Figure 5.3: The dual deformation motif to shape (C) in identity position

We compute the real lifting conditions of shape (C) for a bitangent class not in identity position. Suppose that Γ_c has a unique shortest edge among λ_1, λ_2, λ_3. Then there exists $\sigma \in S_3$ such that for $\sigma(\Gamma)$ the lattice lengths of the edges adjacent to $\sigma(B)$ satisfy $\lambda_1 < \lambda_2 \leq \lambda_3$. This corresponds to $\sigma(B)$ being in identity position. We can then determine the real lifting condition for $\sigma(B)$ using Table 3.1 and the parameters from $\sigma(\mathcal{T})$. In order to do this, we first need to look at the images of the three lattice points p_{0i}, p_{j0} and $p_{k,4-k}$ under σ. Their images will lie in the boundary of $4\Delta_2$: $\sigma(p_{0i}), \sigma(p_{j0}), \sigma(p_{k,4-k}) \in \{p_{0\tilde{i}}, p_{\tilde{j}0}, p_{\tilde{k},4-\tilde{k}}\}$. Secondly, we substitute the values of the tilde indices into the lifting conditions, and then apply σ^{-1} to obtain the real lifting conditions of $B = \sigma^{-1}(\sigma(B))$ in $\Gamma = \sigma^{-1}(\sigma(\Gamma))$. Finally,

we have to compare the lifting conditions of the bitangent class B of shape (C) in Γ with the ones of B_c of shape (C) in Γ_c where $c \in \Sigma(\mathcal{T})$ such that the dual deformation motif of (Γ_c, B_c) is in identity position and Γ_c satisfies $\lambda_1 < \lambda_2 \leq \lambda_3$. If the conditions are equivalent, we have proven that the real lifting conditions do not change. Since S_3 is generated by $(x\,y)$ and $(x\,z)$, it suffices to check the cases $\lambda_2 < \lambda_1 \leq \lambda_3$ and $\lambda_3 < \lambda_2 \leq \lambda_1$.

If the tropical quartic satisfies $\lambda_2 < \lambda_1 \leq \lambda_3$, we apply $\sigma = (x\,y)$ to obtain a generic representative of the identity position. Now, $\sigma(p_{0i}) = p_{i0}$ and $\sigma(p_{j0}) = p_{0j}$ and $\sigma(p_{k,4-k}) = p_{4-k,k}$, so we have to substitute

$$i \mapsto j,$$
$$j \mapsto i,$$
$$k \mapsto 4 - k$$

in the real lifting conditions in Table 3.1. Here the values of i, j, k are as in the quartic we started with. Thus, the real lifting conditions for $\sigma(B)$ are

$$\begin{aligned}
&\text{if } i = 1,3 &&(-s_{11})^{j+1}s_{12}^j s_{21}s_{0j}s_{i0} > 0 &&(-s_{21})^{4-k+1}s_{12}^{4-k}s_{11}s_{4-k,k}s_{i0} > 0,\\
&\text{if } i = 2 &&(-s_{11}s_{12})^j s_{0j}s_{20} > 0 &&(-s_{12}s_{21})^{4-k}s_{4-k,k}s_{20} > 0.
\end{aligned}$$

We now apply $(x\,y)^{-1} = (x\,y)$. Note that this acts on the indices of the signs but not on the exponents. We obtain the conditions

$$\begin{aligned}
&\text{if } i = 1,3 &&(-s_{11})^{j+1}s_{21}^j s_{12}s_{j0}s_{0i} > 0 &&(-s_{12})^{4-k+1}s_{21}^{4-k}s_{11}s_{k,4-k}s_{0i} > 0,\\
&\text{if } i = 2 &&(-s_{11}s_{21})^j s_{j0}s_{02} > 0 &&(-s_{21}s_{12})^{4-k}s_{k,4-k}s_{02} > 0.
\end{aligned}$$

Now, we suppose that we have a quartic for which we can, by edge length changes, switch between the cases $\lambda_1 < \lambda_2 \leq \lambda_3$ and $\lambda_2 < \lambda_1 \leq \lambda_3$. For such a quartic the dual triangulation must satisfy $i, j \in \{1, 2, 3\}$, otherwise the genericity condition is not satisfied. We compare the real lifting conditions for the different cases after simplifying some exponents:

	$\lambda_1 < \lambda_2 \leq \lambda_3$	$\lambda_2 < \lambda_1 \leq \lambda_3$
$i, j \in 1, 3$	$s_{12}s_{21}s_{0i}s_{j0} > 0$	$s_{21}s_{12}s_{j0}s_{0i} > 0$
	$(-s_{21})^{k+1}s_{12}^k s_{11}s_{k,4-k}s_{j0} > 0$	$(-s_{12})^{k+1}s_{21}^k s_{11}s_{k,4-k}s_{0i} > 0$
$i = j = 2$	$s_{02}s_{20} > 0$	$s_{20}s_{02} > 0$
	$(-s_{12}s_{21})^k s_{k,4-k}s_{20} > 0$	$(-s_{21}s_{12})^k s_{k,4-k}s_{02} > 0$
$j = 2, i \in \{1, 3\}$	$-s_{11}s_{12}s_{0i}s_{20} > 0$	$-s_{11}s_{12}s_{20}s_{0i} > 0$
	$(-s_{12}s_{21})^k s_{k,4-k}s_{20} > 0$	$(-s_{12})^{k+1}s_{21}^k s_{11}s_{k,4-k}s_{0i} > 0$
$j \in \{1, 3\}, i = 2$	$-s_{11}s_{21}s_{02}s_{j0} > 0$	$-s_{11}s_{21}s_{j0}s_{02} > 0$
	$(-s_{21})^{k+1}s_{12}^k s_{11}s_{k,4-k}s_{j0} > 0$	$(-s_{21}s_{12})^k s_{k,4-k}s_{02} > 0$

We see that in each case the first inequalities are the same. The second inequalities differ, but it can be shown that they are equivalent by taking the first inequalities into account. We go through the four cases:

- $i, j \in \{1, 3\}$: From the first inequality $s_{12}s_{21}s_{0i}s_{j0} > 0$, which coincides for the two different edge lengths, we can conclude that $s_{j0} = s_{12}s_{21}s_{0i}$. We substitute this in the second inequality of the case $\lambda_1 < \lambda_2 \leq \lambda_3$ and obtain

$$
\begin{aligned}
0 < (-s_{21})^{k+1}s_{12}^k s_{11}s_{k,4-k}s_{j0} &= (-s_{21})^{k+1}s_{12}^k s_{11}s_{k,4-k}s_{12}s_{21}s_{0i} \\
&= (-s_{21})^{k+2}s_{12}^{k+1}s_{11}s_{k,4-k}s_{0i}
\end{aligned}
$$

which coincides with the second inequality of $\lambda_2 < \lambda_1 \leq \lambda_3$ since the parity of k and $k+2$ are the same.

- $i = j = 2$: From the first inequality $s_{02}s_{20} > 0$, which coincides for the two different edge lengths, it follows that $s_{02} = s_{20}$. We substitute this in the second inequality of the case $\lambda_1 < \lambda_2 \leq \lambda_3$ and obtain

$$
0 < (-s_{12}s_{21})^k s_{k,4-k}s_{20} = (-s_{12}s_{21})^k s_{k,4-k}s_{02},
$$

which coincides with the second inequality of $\lambda_2 < \lambda_1 \leq \lambda_3$.

- $j = 2, i \in \{1, 3\}$: From the first inequality $-s_{11}s_{12}s_{0i}s_{20} > 0$, which coincides for the two different edge lengths, it follows $s_{20} = -s_{11}s_{12}s_{0i}$. We substitute this in the second inequality of the case $\lambda_1 < \lambda_2 \leq \lambda_3$ and obtain

$$
\begin{aligned}
0 < (-s_{12}s_{21})^k s_{k,4-k}s_{20} &= (-s_{12}s_{21})^k s_{k,4-k} \cdot (-1)s_{11}s_{12}s_{0i} \\
&= (-s_{12})^{k+1}(s_{21})^k s_{k,4-k}s_{11}s_{0i}.
\end{aligned}
$$

This is the second inequality of $\lambda_2 < \lambda_1 \leq \lambda_3$.

- $j \in \{1, 3\}, i = 2$: From the first inequality $-s_{11}s_{21}s_{02}s_{j0} > 0$, which coincides for the two different edge lengths, it follows that $s_{j0} = -s_{11}s_{21}s_{02}$. We substitute this in the second inequality of the case $\lambda_1 < \lambda_2 \leq \lambda_3$ and obtain

$$
\begin{aligned}
0 < (-s_{21})^{k+1}s_{12}^k s_{11}s_{k,4-k}s_{j0} &= (-s_{21})^{k+1}s_{12}^k s_{11}s_{k,4-k} \cdot (-1)s_{11}s_{21}s_{02} \\
&= (-s_{21})^{k+2}s_{12}^k s_{11}s_{k,4-k}s_{11}s_{02},
\end{aligned}
$$

which coincides with the second inequality of $\lambda_2 < \lambda_1 \leq \lambda_3$.

It follows that for the edge length change between $\lambda_1 < \lambda_2 \leq \lambda_3$ and $\lambda_2 < \lambda_1 \leq \lambda_3$ the real lifting conditions for shape (C) do not change.

The last step to complete the proof is to consider Γ such that $\lambda_1 < \lambda_3 \le \lambda_2$. To obtain the real lifting conditions for (C), we have to apply $\sigma = (x\,z)$ to the subdivision and the curve to obtain a generic representative of the identity position. We apply σ to the lattice points p_{0i}, p_{j0} and $p_{k,4-k}$ to obtain the values that we have to substitute in the real lifting conditions for $\sigma(B)$ and we obtain

$$i \mapsto 4 - k,$$
$$j \mapsto 4 - j,$$
$$k \mapsto 4 - i.$$

So the lifting conditions for $\sigma(B)$ are given as:

$$\text{if } 4 - j = 1,3 : (-s_{11})^{4-k+1} s_{12}^{4-k} s_{21} s_{0,4-k} s_{4-j,0} > 0$$
$$(-s_{21})^{4-i+1} s_{12}^{4-i} s_{11} s_{4-i,i} s_{4-j,0} > 0,$$

$$\text{if } 4 - j = 2 : (-s_{11} s_{12})^{4-k} s_{0,4-k} s_{20} > 0$$
$$(-s_{12} s_{21})^{4-i} s_{4-i,i} s_{20} > 0.$$

Applying $(x\,z)^{-1} = (x\,z)$ to the indices in these inequalities gives the real lifting conditions of B when $\lambda_1 < \lambda_3 \le \lambda_2$:

$$\begin{array}{lll}
\text{if } j = 1,3 & (-s_{21})^{k+1} s_{12}^{k} s_{11} s_{k,4-k} s_{j0} > 0 & (-s_{11})^{i+1} s_{12}^{i} s_{21} s_{0i} s_{j0} > 0, \\
\text{if } j = 2 & (-s_{21} s_{12})^{k} s_{k,4-k} s_{20} > 0 & (-s_{12} s_{11})^{i} s_{0i} s_{20} > 0.
\end{array}$$

Now we have to prove that changing the edge lengths between the two cases $\lambda_1 < \lambda_2 \le \lambda_3$ and $\lambda_1 < \lambda_3 \le \lambda_2$ does not change the lifting conditions:

	$\lambda_1 < \lambda_2 \le \lambda_3$	$\lambda_1 < \lambda_3 \le \lambda_2$
$j \in \{1,3\}$	$(-s_{11})^{i+1} s_{12}^{i} s_{21} s_{0i} s_{j0} > 0$	$(-s_{21})^{k+1} s_{12}^{k} s_{11} s_{k,4-k} s_{j0} > 0$
	$(-s_{21})^{k+1} s_{12}^{k} s_{11} s_{k,4-k} s_{j0} > 0$	$(-s_{11})^{i+1} s_{12}^{i} s_{21} s_{0i} s_{j0} > 0$
$j = 2$	$(-s_{11} s_{12})^{i} s_{0i} s_{20} > 0$	$(-s_{21} s_{12})^{k} s_{k,4-k} s_{20} > 0$
	$(-s_{12} s_{21})^{k} s_{k,4-k} s_{20} > 0$	$(-s_{12} s_{11})^{i} s_{0i} s_{20} > 0$

We observe that for any choice of j the first lifting condition for $\lambda_1 < \lambda_2 \le \lambda_3$ coincides with the second lifting condition for $\lambda_1 < \lambda_3 \le \lambda_2$, while the second lifting condition for $\lambda_1 < \lambda_2 \le \lambda_3$ coincides with the first lifting condition for $\lambda_1 < \lambda_3 \le \lambda_2$. Since $(x\,y)$ and $(x\,z)$ generates S_3, it follows that for any generic quartic curve with shape (C) the real lifting conditions are independent of the edge lengths as long as there exists a unique shortest edge adjacent to the vertex contained in shape (C). $\qquad\square$

Now we can prove the second main result of Part I:

Theorem 5.1.4. *Let* Γ *be a generic tropical smooth quartic curve with dual triangulation* $\mathcal{T}$*, and let B be a tropical bitangent class. For every* $c \in \Sigma(\mathcal{T})$*, the real lifting conditions of* B_c *in* Γ_c *are independent on the shape of the bitangent class.*

In other words: real lifting conditions of tropical bitangent classes to Γ *only depend on the dual subdivision* $\mathcal{T}$ *of* Γ*.*

The real lifting conditions for each deformation class are summarized in Table 5.1.

Proof. For deformation class (C) the claim is proven in Propostion 5.1.3. The remaining constant deformation classes are not bound on the genericity constraint connected to the edge lengths of the quartic and thus only contain one shape of one fixed position with respect to S_3. It follows directly that their real lifting conditions are fixed for the whole deformation class.

The shapes in the deformation classes (W X Y EE GG) and (W ... HH)+$(x\,z)$ all have trivial real lifting conditions, meaning they always lift, so we do not need to consider these two deformation classes. We go through the remaining ones and for each compare the lifting conditions of the different shapes.

Deformation class (B H' H)

First, remark that the shapes in this deformation class are all in the image of the same permutation $\sigma \in S_3$ which we here assume to be $\sigma = id$.

We recall the notation used in [CM21] to connect the real lifting conditions to the dual bitangent motifs: the sign s_{0i} corresponds to the monomial given by the lattice point p_{0i} forming a triangle with the red edge ($\overline{p_{1v}p_{1,v+1}}$) in the dual bitangent motif, which is the same for all three shapes. The sign s_{j0} corresponds to the monomial given by the lattice point p_{j0} that forms a triangle with the green edge ($\overline{p_{21}p_{31}}$) in the dual bitangent motif of shape (B).

Shape	real lifting condition
(B)	$(-s_{1v}s_{1,v+1})^{i+1}s_{0i}s_{21} > 0$ and $(-s_{21})^{j+1}s_{31}^{j}s_{1v}s_{1,v+1}s_{j0} > 0$
(H),(H')	$(-s_{1v}s_{1,v+1})^{i+1}s_{0i}s_{21} > 0$ and $-s_{21}s_{1v}s_{1,v+1}s_{40} > 0$
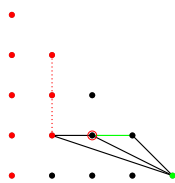
 From the dual bitangent motif we conclude that $p_{j0} = p_{40}$. Substituting $j = 4$ in the real lifting conditions for (B), we obtain the same lifting conditions as for shapes (H) and (H'). The remaining parameters v and i are determined by the triangulation and are therefore the same for all three shapes.

Deformation class (B H' H)$+(y\,z)$

For the explanation of the parameters i, j and v, we refer to the paragraph on deformation class (B H' H).

Shape	real lifting condition
(B)	$(-s_{1v}s_{1,v+1})^{i+1}s_{0i}s_{21} > 0$ and $(-s_{21})^{j+1}s_{31}^{j}s_{1v}s_{1,v+1}s_{j0} > 0$
(H),(H')	$(-s_{1v}s_{1,v+1})^{i+1}s_{0i}s_{21} > 0$ and $-s_{21}s_{1v}s_{1,v+1}s_{40} > 0$

We note that in this deformation class the shape $(H)_{(y\,z)}$ is (in general) not equal to the bitangent shape (H) after permutation with $(y\,z)$. Instead, the dual bitangent motifs to both the shapes (H) and $(H)_{(y\,z)}$ are equal. So the dual bitangent motif to $(y\,z)^{-1}(H)_{(y\,z)}$ has real lifting conditions

$$(-s_{1,3-v}s_{1,2-v})^{4-i+1}s_{0,4-i}s_{21} > 0 \text{ and } -s_{21}s_{1,3-v}s_{1,2-v}s_{40} > 0.$$

Applying $(y\,z)$ onto these conditions, we obtain the same real lifting conditions as we see for shape (H) in this deformation class. The exact same holds for shapes (H') and $(H')_{(y\,z)}$.
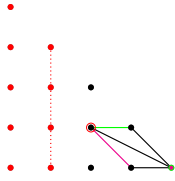
 From the argument above we know that the real lifting conditions for the bitangent shapes (H) and $(H)_{(y\,z)}$ that appear in this deformation class are the same. Thus, the equality of the real lifting conditions for all shapes in this deformation class follows from the statement for deformation class (B H' H).

Deformation class (B M)$+(y\,z)$

We refer to the paragraph on deformation class (B H' H) for the explanation of the parameters i, j and v.

Similar to the case of deformation class (B H' H)$+(y\,z)$, we note that the dual bitangent motifs of shape (M) and $(M)_{(y\,z)}$ coincide. This implies that the bitangent shapes coincide since the triangle $(\overline{p_{30}p_{31}p_{21}})$ is symmetric under $(y\,z)$. It follows that the real lifting conditions have to be equal.

Without this geometric argument, we can demonstrate the equality of the lifting conditions analogously to the case of deformation class (B H' H)$+(y\,z)$: we consider the real lifting conditions of $(y\,z)((M)_{(y\,z)})$, apply $(y\,z)$ to them and compare them with the real lifting conditions of (M).

Shape	real lifting condition
(B)	$(-s_{1v}s_{1,v+1})^{i+1}s_{0i}s_{21} > 0$ and $(-s_{21})^{j+1}s_{31}^{j}s_{1v}s_{1,v+1}s_{j0} > 0$
(M)	$(-s_{1v}s_{1,v+1})^{i+1}s_{0i}s_{21} > 0$ and $s_{31}s_{1v}s_{1,v+1}s_{30} > 0$
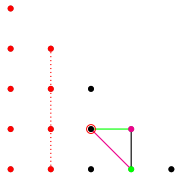
We conclude from the dual bitangent motif of shape (B) that we have to substitute $j = 3$ in the real lifting conditions. In this case te real lifting conditions for shape (B) and (M) coincide.

Since we argued above that the real lifting conditions for (M) and $(M)_{(yz)}$ are the same, we conclude that the real lifting conditions of shape $(B)_{(yz)}$ coincide with the other shapes in this deformation class.

Deformation class (D L' Q)

We recall, that the parameter i in the real lifting condition of shape (D) is determined by the lattice point p_{0i} which forms a triangle with the red edge $(\overline{p_{10}p_{11}})$ in the dual bitangent motif.

We note that all shapes in this deformation class are in the image of the same $\sigma \in S_3$. Without loss of generality, we can assume the shapes to be in identity position.

Shape	real lifting condition
(D)	$(-s_{10}s_{11})^i s_{0i} s_{22} > 0$
(L'),(Q)	$s_{00} s_{22} > 0$
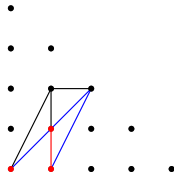
From the dual deformation motif we see that p_{00} forms a triangle with $(\overline{p_{10}p_{11}})$. Thus, we have to substitute $i = 0$ in the real lifting condition. In this case, shape (D) has the same real lifting conditions as shapes (L') and (Q).

Deformation class (D L' Q Q' R)

We refer to the case of deformation class (D L' Q) for an explanation of the parameter i.

Notice that again all shapes in this deformation class are in the image of the same $\sigma \in S_3$. Therefore, we can assume, without loss of generality, that the shapes are in identity position.

Shape	real lifting condition
(D)	$(-s_{10}s_{11})^i s_{0i} s_{22} > 0$
(L'),(Q),(Q'),(R)	$s_{00} s_{22} > 0$
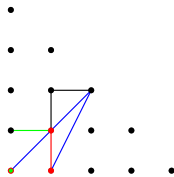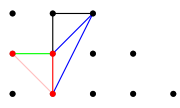
We see the triangle $(\overline{p_{00}p_{10}p_{11}})$ in the dual deformation motif. As for (D L' Q) this means we have to substitute $i = 0$ in the real lifting condition. Thus, the real lifting conditions for all shapes in this deformation class coincide.

Deformation class (D L O)

As for the previous cases all shapes in this deformation class are in the image of the same $\sigma \in S_3$, such that without loss of generality we can assume the shapes to be in identity position.

Shape	real lifting condition
(D)	$(-s_{10}s_{11})^i s_{0i}s_{22} > 0$
(L),(O)	$-s_{10}s_{11}s_{01}s_{22} > 0$

Explanation to the parameter i in the real lifting condition can be found in the case to deformation class (D L' Q).
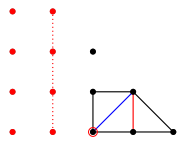
We see in the dual deformation motif that the lattice point p_{01} forms a triangle with the red edge $(\overline{p_{10}p_{11}})$. Hence, we have to substitute $i = 1$ in the real lifting conditions of shape (D). We observe that we obtain the same real lifting conditions as for shapes (L) and (O).

Deformation class (E F J)

We conclude from the proof of Theorem 4.2.3 that all shapes in this deformation class are in the image of the same $\sigma \in S_3$, such that without loss of generality we can assume the shapes to be in identity position.

Recall that the parameters v and i in the real lifting condition are given by the dual bitangent motif in the following way: the edge $(\overline{p_{1v}p_{1,v+1}})$ forms a triangle with p_{20} and one with p_{0i}.

Shape	real lifting condition
(E), (F), (J)	$(-s_{1v}s_{1,v+1})^i s_{0i}s_{20} > 0$

We note that as the three shapes (E), (F) and (J) are in the same position with respect to the action of S_3, and that all three shapes correspond to the same two triangles formed with the edge $(\overline{p_{1v}p_{1,v+1}})$. Thus, we see that the real lifting condition as determined in Table 3.1 and depicted above is constant for this deformation class.

Deformation class (G I N)+(xy)

This deformation class, similar to deformation classes (B H' H)+(yz) and (B M)+(yz), contains (G) and (G)$_{(xy)}$. In general, we don't have (xy)(G)=(G)$_{(xy)}$.

We recall that the parameter i is determined by the lattice point p_{0i} forming a triangle with $(\overline{p_{10}p_{11}})$ and that k is determined by the blue edge $(\overline{p_{11}p_{k,4-k}})$.

Shape	real lifting condition
(G)	$(-s_{10}s_{11})^i s_{0i}s_{k,4-k} > 0$
(I),(N)	$-s_{10}s_{11}s_{01}s_{k,4-k} > 0$
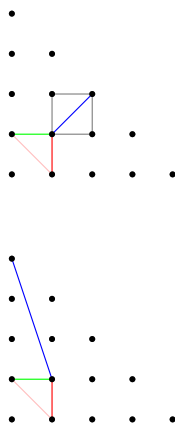
We see in the dual bitangent motif of shape (G) in identity position that p_{01} forms a triangle with $(\overline{p_{10}p_{11}})$. This implies that we have to substitute $i = 1$ in the real lifting condition of shape (G). We observe that in this case the real lifting conditions of the shapes in identity position (G), (I) and (N) coincide.

Similar to the case of (M) and $(M)_{(yz)}$ in deformation classes (B M)+(yz) we can argue that (N) and $(N)_{(xy)}$ have the same real lifting conditions.

By the same argument as above for (G), (I) and (N) in identity position, we conclude that $(N)_{(xy)}$, $(I)_{(xy)}$ and $(G)_{(xy)}$ have the same real lifting conditions. It follows that the real lifting conditions are constant for all shapes in this deformation class.

Deformation class (G K U T T')

All shapes in this deformation class are in the image of the same $\sigma \in S_3$. Hence, without loss of generality, we can assume the shapes to be in identity position. We refer to the case of deformation class (G I N)+(xy) to an explanation of the parameters i and k in the real lifting conditions below.

Shape	real lifting condition
(G)	$(-s_{10}s_{11})^i s_{0i}s_{k,4-k} > 0$
(K), (T), (T'), (U)	$s_{00}s_{k,4-k} > 0$
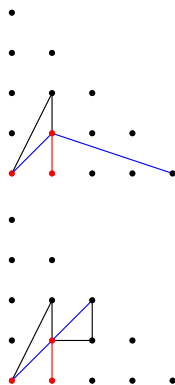
In the dual bitangent motif of shape (G) contained in the dual deformation motif we see that p_{00} forms a triangle with the edge $(\overline{p_{10}p_{11}})$. Hence, we have to substitute $i = 0$ in the real lifting condition of shape (G). The edge $(\overline{p_{11}p_{k,4-k}})$ is determined by the dual deformation motif, and it is therefore the same for all bitangent shapes in this deformation class. We obtain that the real lifting conditions are the same for each shape in this deformation class.

Deformation class (G K U U' T T' T'' V)+$(x\,y)$

Similar to deformation classes (G I N)+$(x\,y)$, this deformation class contains for the shapes (G), (K), (U), (U') (T), (T'), (T'') and (V) their images under $(x\,y)$. Depending on the edge $(\overline{p_{11}p_{k,4-k}})$ we don't have have $(x\,y)$(G)=(G)$_{(x\,y)}$ (resp. for the other shapes), since $(x\,y)((G)_{(x\,y)})$ would have a different dual bitangent motif if $(\overline{p_{11}p_{k,4-k}})$ is not symmetric with respect to $(x\,y)$.

Shape	real lifting condition
(G)	$(-s_{10}s_{11})^i s_{0i}s_{k,4-k} > 0$
(K), (T), (T'), (T''), (U), (U'), (V)	$s_{00}s_{k,4-k} > 0$

We recall that the parameter i is determined by the lattice point p_{0i} forming a triangle with $(\overline{p_{10}p_{11}})$ and that k is determined by the blue edge $(\overline{p_{11}p_{k,4-k}})$.
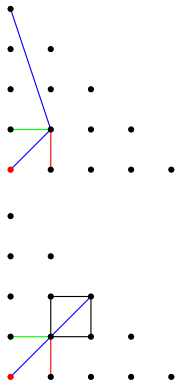
We observe that in both dual deformation motifs the lattice point p_{00} forms a triangle with the edge $(\overline{p_{10}p_{11}})$, so we have to substitute $i = 0$ in the real lifting conditions of shape (G) in identity position. It follows that all the shapes in identity position in this deformation class have the same real lifting conditions.

We remark that shape (V) and shape (V)$_{(x\,y)}$ are the same sets of vertices, since the triangles $(\overline{p_{00}p_{10}p_{11}})$, $(\overline{p_{00}p_{01}p_{11}})$ determining the vertices of the tropical quartic curve contained in the bitangent class are symmetric under $(x\,y)$. As the triangulation stays constant during the deformations, it follows that they also both correspond to the same edge $(\overline{p_{11}p_{k,4-k}})$ and are thus equal. Hence, the lifting conditions are the same.

This case is similar to shape (N) in deformation class (G I N)+$(x\,y)$ or shape (M) in deformation class (B M)+$(y\,z)$. With an analogous argument as for the shapes in identity position of this deformation class, the shapes in position $(x\,y)$ in this deformation class have the same real lifting conditions.

Since the case $(\overline{p_{11}p_{22}})$ is fully symmetric with respect to $(x\,y)$, the argument above is corroborated by the following table computing the lifting conditions for each shape and position thus showing that they are equal.

shape	permutation	lifting condition	parameters
(G)	identity	$(-s_{10}s_{11})^i s_{0i}s_{04} > 0$	$i = y$-coor. of vertex at $x=0$ forming a triangle with $\overline{p_{10}p_{11}}$ p_{04} vertex of edge $\overline{p_{11}p_{k,4-k}}$
(K),(T), (U),(V)	identity	$s_{00}s_{04} > 0$	p_{04} vertex of edge $\overline{p_{11}p_{k,4-k}}$
(K),(T), (U),(V)	$(x\,y)$	$s_{00}s_{04} > 0$	p_{04} vertex of edge $\overline{p_{11}p_{4-k,k}}$
(G)	$(x\,y)$	$(-s_{01}s_{11})^i s_{i0}s_{04} > 0$	$i = x$-coor. of vertex at $y=0$ forming a triangle with $\overline{p_{01}p_{11}}$, p_{04} vertex of $\overline{p_{11}p_{4-k,k}}$

The value of k changes when we consider the $(x\,y)$ permutation. However, the (blue) edge $\overline{p_{11}p_{04}}$ in the subdivision stays the same in all cases. Since the vertex relevant to the value of i is p_{00} in both cases, we substitute $i=0$ and obtain the real lifting condition $s_{00}s_{04} > 0$ for all shapes in this deformation class. $\qquad\square$

deformation class	Lifting conditions
(A)	$(-s_{1v}s_{1,v+1})^i s_{0i}s_{22} > 0$ and $(-s_{u1}s_{u+1,1})^j s_{j0}s_{22} > 0$
(B H' H), (B H' H)+(yz), (H)	$(-s_{1v}s_{1,v+1})^{i+1} s_{0i}s_{21} > 0$ and $-s_{21}s_{1v}s_{1,v+1}s_{40} > 0$
(B M)+(yz)	$(-s_{1v}s_{1,v+1})^{i+1} s_{0i}s_{21} > 0$ and $s_{31}s_{1v}s_{1,v+1}s_{30} > 0$
(B)	$(-s_{1v}s_{1,v+1})^{i+1} s_{0i}s_{21} > 0$ and $(-s_{21})^{j+1}s_{31}^{j} s_{1v}s_{1,v+1}s_{j0} > 0$ with $j \in \{0,1,2\}$
(C)	if j=2: $(-s_{11}s_{12})^i s_{0i}s_{20} > 0$ and $(-s_{21}s_{12})^k s_{k,4-k}s_{20} > 0$ if j=1,3 $(-s_{11})^{i+1}s_{12}^i s_{21}s_{0i}s_{j0} > 0$ and $(-s_{21})^{k+1}s_{12}^k s_{11}s_{k,4-k}s_{j0} > 0$
(D)	$(-s_{10}s_{11})^i s_{0i}s_{22} > 0$ with $i \in \{2,3,4\}$
(D L O), (P)	$-s_{10}s_{11}s_{01}s_{22} > 0$
(D L' Q), (D L' Q Q' R), (S), (T)	$s_{00}s_{22} > 0$
(E), (E F J)	$(-s_{1v}s_{1,v+1})^{i+1} s_{0i}s_{20} > 0$
(G)	$(-s_{10}s_{11})^i s_{0i}s_{k,4-k} > 0$ with $i \in \{2,3,4\}$
(G I N)+(xy)	$-s_{10}s_{11}s_{01}s_{k,4-k} > 0$

deformation class	Lifting conditions
(G K U U' T T'), (G K U U' T T' T'' V)+(xy)	$s_{00}s_{k,4-k} > 0$
rest	no conditions

Table 5.1: Real lifting conditions of the deformation classes in their positions as in Figure 4.39.

Markwig, Payne and Shaw characterize the lifting conditions of bitangent shapes over arbitrary Henselian fields (Definition 2.2.8) with residue field $\Bbbk$ of char$(\Bbbk) \neq 2$ and 2-divisible value group in their work [MSP22]. The lifting conditions originate in the solvability of quadratic equations that come from tropical modifications. For real lifts the conditions are on the signs of the coefficients since over $\mathbb{R}$ the square root can only be applied to positive numbers. Over arbitrary Henselian fields, the conditions transform to products or quotients of the coefficients being squares over the chosen field. This is why we need the value group to be 2-divisible. The sets of coefficients of the lift of the quartic curve that have to satisfy the conditions for any given shape does not change when we move from $\mathbb{R}$ to a Henselian field with odd or zero residue characteristic. We thus obtain the following Corollary of Theorem 5.1.4.

Corollary 5.1.5. *Let Γ be a generic tropical smooth quartic curve with dual triangulation $\mathcal{T}$ and let K be a non-Archimedean valued Henselian field with 2-divisible value group such that the residue field $\Bbbk$ satisfies char$(\Bbbk) \neq 2$.*

The lifting conditions of the tropical bitangent classes to Γ over K only depend on the dual subdivision $\mathcal{T}$.

Therefore, deformation classes are relevant for the lifting behavior of tropical bitangents over other Henselian fields, not only over real closed fields.

Proof. Let K be a non-Archimedean valued Henselian field with 2-divisible value group and residue field $\Bbbk$ such that char$(\Bbbk) \neq 2$, see Definition 2.2.8.

An analogous investigation to the proof of Theorem 5.1.4 shows that the lifting conditions again are constant in every deformation class. The local lifting conditions arise from the existence of a solution to a certain polynomial equation of degree 2 over the residue field, that over the Henselian property can then be moved to the base field. Here we need the value group to be 2-divisible. For every bitangent shape, the radicands can be computed from the data in [CM21]. In [CM21] only the signs of the radicands are needed. Thus, the real lifting conditions correspond to the signs of the radicands up to factors of even exponent. For lifting over a Henselian field K, we are interested in whether or not the radicands are squares in K. Factors of even exponent are here again not important. Also, in [CM21] the

product of the signs of the nominator and denominator is considered if a factor is a fraction. However, the product of two non-zero elements in a field is a square if and only if their quotient is a field, so again this change from the radicand to the sign conditions does not matter when we consider lifting over K.

Because the solutions for the lifting equations in the residue field have coefficients which are powers of 2, we require $\text{char}(\Bbbk) \neq 2$.

We provide details for deformation class (B H' H). The local lifting condition at each tangency intersection is the existence of a solution to a certain polynomial equation of degree 2, achieved by tropical modifications [LM20, CM21]. Therefore, the lifting conditions over K are that the radicands of the solutions of the polynomial equations are squares over K. By the Henselian property this condition can be formulated in working over the residue field $\Bbbk$. For $K = \mathbb{R}\{\{t\}\}$ the a_{ij} below are the initial terms of the coefficients of the quartic curve.

For bitangents of shape (B) belonging to deformation class (B H' H), the two radicands in $\Bbbk$ can be computed from the formulas in [CM21, Propositions 5.2 & 6.3, Table 10]. They are R_1, R_2 as below:

$$R_1 := (\frac{a_{1v}}{a_{1,v+1}})^{i+1} a_{0i} a_{21} (-1)^{i+1},$$

$$R_2 := (\frac{a_{21}}{a_{31}})^{4+2} a_{40} a_{31} (-1)^{4+2+1} \frac{a_{1,v+1}}{a_{1v}} \frac{a_{21}}{a_{31}}$$

$$\tilde{R}_2 := - a_{40} \frac{a_{1,v+1}}{a_{1v}} a_{21},$$

where $\tilde{R}_2$ is simplified by deleting the factor $(\frac{a_{21}}{a_{31}})^{4+2}$ which is always a square and by using the equation $(-1)^{4+2+1} = -1$. Thus, R_2 is a square if and only if $\tilde{R}_2$ is a square.

For (H'), (H) the radicands are by [CM21, Propositions 5.3 & 6.3, Table 10] given as

$$R_1 := (\frac{a_{1v}}{a_{1,v+1}})^{i+1} a_{0i} a_{21} (-1)^{i+1},$$

$$R_2 := - a_{40} a_{21} \frac{a_{1v}}{a_{1,v+1}}.$$

We recognise the same coefficients whose signs are relevant for the real lifting conditions as in Table 5.1 for deformation class (B H' H), only that now we have quotients when before we had only products. However, both for signs as for squares the condition to be positive resp. a square is equivalent for products and quotients:

$$a \cdot b = c^2 \iff \frac{a}{b} = \tilde{c}^2, \text{ with } \tilde{c} = \frac{c}{b}.$$

To conclude, we see that the two relevant radicands for the shapes (B), (H') and (H) in the deformation class (B H' H) are the same. Therefore, the lifting conditions over the Henselian field K are the same for all bitangent shapes in this deformation class.

Moreover, we observe that the lifting conditions are satisfied if and only if

$$(-1)^{i+1}(a_{1v}a_{1,v+1})^{i+1}a_{0i}a_{21} = A^2 \text{ and}$$
$$-a_{40}a_{21}a_{1v}a_{1,v+1} = B^2,$$

for some $A, B \in K$. Note, that substituting s for a and "equals a square" with "is positive" this is gives the real lifting condition for deformation class (B H' H) as in Table 5.1.

For the other deformation classes we make similar observations and come to the same conclusion. Only for shape (C) the situation is more interesting, so we consider the case here.

We recall that for shape (C) we have to consider different edge length cases because the lifting conditions were computed for the case that the bounded edge of direction $-e_2$ adjacent to the vertex of bitangent shape (C) is the shortest. We also recall form the proof of Proposition 5.1.3 that we needed to consider only the two cases $\lambda_2 < \lambda_1 \leq \lambda_3$ and $\lambda_1 < \lambda_3 \leq \lambda_2$, where λ_1, λ_2 and λ_3 denote the lattice lengths of the edges adjacent to the vertex that forms the bitangent class of shape (C) with direction $-e_2$, $-e_1$ and $e_1 + e_2$, respectively.

We first check the case $\lambda_2 < \lambda_1 \leq \lambda_3$. The following table shows the square conditions for the radicands [CM21, Proposition 6.4, Lemma 6.5] for the identity position $\lambda_1 < \lambda_2 \leq \lambda_3$, and for the changed position with $\lambda_2 < \lambda_1 \leq \lambda_3$. The radicands are already partially simplified by eliminating square factors.

	$\lambda_1 < \lambda_2 \leq \lambda_3$	$\lambda_2 < \lambda_1 \leq \lambda_3$
$j \in \{1,3\}$	$a_{12}^i a_{21}^{-j} a_{0i} a_{j0} = A^2$	$a_{21}^j a_{12}^{-i} a_{0i} a_{j0} = C^2$
$i \in \{1,3\}$	$(-1)^{k+1} a_{21}^{k-j} a_{12}^k a_{11}^j a_{k,4-k} a_{j0} = B^2$	$(-1)^{k+1} a_{12}^{k-i} a_{21}^k a_{11}^i a_{k,4-k} a_{0i} = D^2$
$j = 2$	$a_{02} a_{20} = A^2$	$a_{02} a_{20} = C^2$
$i = 2$	$(-1)^k a_{21}^k a_{12}^k a_{k,4-k} a_{20} = B^2$	$(-1)^k a_{12}^k a_{21}^k a_{k,4-k} a_{02} = D^2$
$j = 2$	$(-a_{11})^i a_{12}^i a_{0i} a_{20} = A^2$	$-a_{11}^i a_{12}^{-i} a_{20} a_{0i} = C^2$
$i \in \{1,3\}$	$(-1)^k a_{12}^k a_{21}^k a_{k,4-k} a_{20} = B^2$	$(-1)^{k+1} a_{12}^{k-i} a_{21}^k a_{11}^i a_{k,4-k} a_{0i} = D^2$
$j \in \{1,3\}$	$-a_{11}^j a_{21}^{-j} a_{02} a_{j0} = A^2$	$(-a_{11})^j a_{21}^j a_{j0} a_{02} = C^2$
$i = 2$	$(-1)^{k+1} a_{21}^{k-j} a_{12}^k a_{11}^j a_{k,4-k} a_{j0} = B^2$	$(-1)^k a_{21}^k a_{12}^k a_{k,4-k} a_{02} = D^2$

Similar to the proof of Proposition 5.1.3 we go through the four cases:

- $i, j \in \{1,3\}$: From the first condition of $\lambda_1 < \lambda_2 \leq \lambda_3$ we know that $a_{12}^i a_{21}^{-j} a_{0i} a_{j0}$

is a square, say A^2. By multiplying with $\frac{a_{21}^{2j}}{a_{12}^{2i}}$, we obtain the first condition for $\lambda_2 < \lambda_1 \leq \lambda_3$. Further, we can multiply the second condition of $\lambda_1 < \lambda_2 \leq \lambda_3$ with $A^2 \cdot a_{11}^{i+j}$ which is a square since $i,j \in \{1,3\}$. We obtain

$$(-1)^{k+1} a_{21}^{k-j} a_{12}^k a_{11}^j a_{k,4-k} a_{j0} \cdot (a_{12}^i a_{21}^{-j} a_{0i} a_{j0} a_{11}^{i+j})$$
$$= (-1)^{k+1} a_{21}^k a_{12}^{k+i} a_{11}^i a_{k,4-k} a_{0i} \cdot (a_{21}^{-2j} a_{j0}^2 a_{11}^{2j}).$$

This is a square if and only if $(-1)^{k+1} a_{21}^k a_{12}^{k-i} a_{11}^i a_{k,4-k} a_{0i}$ is a square, which is exactly the second condition of $\lambda_2 < \lambda_1 \leq \lambda_3$.

- $i = j = 2$: We observe that the first conditions for both cases are the same. By substitute $a_{20} = \frac{A^2}{a_{02}}$ in the second equation of the case $\lambda_1 < \lambda_2 \leq \lambda_3$ we obtain

$$(-1)^k a_{21}^k a_{12}^k a_{k,4-k} a_{20} = (-1)^k a_{21}^k a_{12}^k a_{k,4-k} \frac{A^2}{a_{02}}.$$

This is a square if and only if $(-1)^k a_{21}^k a_{12}^k a_{k,4-k} a_{02}$ is a square, which is exactly the second condition of $\lambda_2 < \lambda_1 \leq \lambda_3$.

- $j = 2, i \in \{1,3\}$: By multiplying the first condition of $\lambda_1 < \lambda_2 \leq \lambda_3$ with a_{12}^{2i} and recalling that $i \in \{1,3\}$, we observe that the first two conditions are equivalent. To prove the equivalence of the second conditions we multiply the second condition of $\lambda_1 < \lambda_2 \leq \lambda_3$ with the first condition $(-a_{11})^i a_{12}^i a_{0i} a_{20} = A^2$ and obtain

$$(-1)^k a_{12}^k a_{21}^k a_{k,4-k} a_{20} \cdot ((-a_{11})^i a_{12}^i a_{0i} a_{20})$$
$$= (-1)^{k+i} a_{12}^{k+i} a_{21}^k a_{11}^i a_{k,4-k} a_{0i} \cdot (a_{20}^2).$$

This term is a square if and only if $(-1)^{k+1} a_{12}^{k-i} a_{21}^k a_{11}^i a_{k,4-k} a_{0i}$ is a square, since $i \in \{1,3\}$. This is the second condition of $\lambda_2 < \lambda_1 \leq \lambda_3$.

- $j \in \{1,3\}, i = 2$: Similarly to the case before we see that the first two conditions are equivalent by multiplying the the first condition of $\lambda_1 < \lambda_2 \leq \lambda_3$ with a_{21}^{2j} and recalling that $j \in \{1,3\}$. To prove the equivalence of the second conditions, we multiply the second condition of $\lambda_1 < \lambda_2 \leq \lambda_3$ with the first condition $-a_{11}^j a_{21}^{-j} a_{02} a_{j0} = A^2$ and obtain

$$(-1)^{k+1} a_{21}^{k-j} a_{12}^k a_{11}^j a_{k,4-k} a_{j0} \cdot (-a_{11}^j a_{21}^{-j} a_{02} a_{j0})$$
$$= (-1)^k a_{21}^k a_{12}^k a_{k,4-k} a_{02} \cdot (a_{11}^{2j} a_{21}^{-2j} a_{j0}^2).$$

This term is a square if and only if $(-1)^k a_{21}^k a_{12}^k a_{k,4-k} a_{02}$ is a square. This is the second condition of $\lambda_2 < \lambda_1 \leq \lambda_3$.

This proves the claim for the transformation between the edge lengths $\lambda_1 < \lambda_2 \leq \lambda_3$ and $\lambda_2 < \lambda_1 \leq \lambda_3$. To finish the proof we have to consider the change of edge lengths from $\lambda_1 < \lambda_2 \leq \lambda_3$ to $\lambda_1 < \lambda_3 \leq \lambda_2$. The radicands for these cases, again simplified by eliminating square factors can be found in the tables below.

For $j \in \{1,3\}$ we have

$\lambda_1 < \lambda_2 \leq \lambda_3$	$\lambda_1 < \lambda_3 \leq \lambda_2$
$(-1)^{i+1} a_{12}^i a_{21}^{-j} a_{11}^{i+j} a_{0i} a_{j0} = A^2$	$(-1)^{-k+1} a_{12}^{-k} a_{11}^j a_{k,4-k} a_{j0} a_{21}^{-k-j} = C^2$
$(-1)^{k+1} a_{21}^{k-j} a_{12}^k a_{11}^j a_{k,4-k} a_{j0} = B^2$	$(-1)^{-i+1} a_{11}^{-i+j} a_{12}^{-i} a_{21}^{-j} a_{0i} a_{j0} = D^2$

while for $j = 2$ we have

$\lambda_1 < \lambda_2 \leq \lambda_3$	$\lambda_1 < \lambda_3 \leq \lambda_2$
$(-1)^i a_{12}^i a_{11}^i a_{0i} a_{20} = A^2$	$(-1)^k a_{12}^{-k} a_{21}^{-k} a_{k,4-k} a_{20} = C^2$
$(-1)^k a_{12}^k a_{21}^k a_{k,4-k} a_{20} = B^2$	$(-1)^i a_{12}^{-i} a_{11}^{-i} a_{0i} a_{20} = D^2$

We observe that for both cases the first conditions of $\lambda_1 < \lambda_2 \leq \lambda_3$ are equivalent to the second conditions of $\lambda_1 < \lambda_3 \leq \lambda_2$ and the other way round. It follows that in each case the conditions are equivalent, which proves the claim. □

5.2 A tropical count of real bitangents

This section contains a tropical count of Plücker and Zeuthen's number of real bitangents [Plü34, Plü39, Zeu73] to tropically smooth algebraic quartic curves stated in Theorem 5.2.2. The tropical count is achieved by computational methods. In joint work with Marta Panizzut, we developed an extension of `polymake`; see Section 6.1. In this environment, we implemented an algorithm to provide the tropical count of the Plücker-Zeuthen numbers; see Algorithm 2.

This section builds on the preprints [GP21a, GP21b], which are joint work with Marta Panizzut. Appendix B.1.1 contains functions used for the proof of Theorem 5.2.2, which are not part of the extension `TropicalQuarticCurves` introduced in Section 6.1.

First recall the notion of genericity, see Remark 3.3.2. The assumption that if the tropical curve Γ contains a vertex adjacent to three bounded edges with directions $-e_1$, $-e_2$ and $e_1 + e_2$, the shortest edge is unique mainly targets the coefficients, i.e., the weight vector in the secondary cone which induces the edge lengths of the quartic. We point out that not for every tropical smooth quartic curve with triangulation $\mathcal{T}$ the secondary cone $\Sigma(\mathcal{T})$ contains weight vectors that induce a generic representative of the combinatorial type.

Remark 5.2.1. Up to S_3-symmetry there are 8 regular unimodular triangulations of $4\Delta_2$ that can never satisfy the above mentioned genericity condition. They are different completions of the subdivision shown in Figure 5.4. Even for a
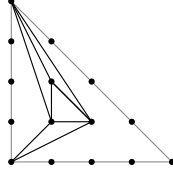
Figure 5.4: All tropical quartics whose combinatorial type is up to S_3 one of the 8 refinements to a unimodular triangulation of this subdivision can never satisfy the genericity condition.

generic triangulation there might be points in the secondary cone, such that the corresponding quartic curve is not generic. This set of non-generic points inside a generic secondary cone is always lower dimensional. The areas of non-genericity are determined in Proposition 6.3.4 in Section 6.3.2.

Now we can state and prove the third main result of Part I of this thesis.

Theorem 5.2.2. *Let* Γ *be a generic tropicalization of a smooth quartic plane curve* $V(f)$ *defined over a real closed complete non-Archimedean valued field. Either* 1*,* 2*,* 4 *or* 7 *of its bitangent classes admit a lift to* 4 *real bitangents each to* $V(f)$*.*

In other words, every smooth quartic curve over a real closed complete non-Archimedean valued field whose tropicalization is smooth and generic has either 4*,* 8*,* 16 *or* 28 *totally real bitangents.*

Proof. Let Γ be a generic tropicalization of a smooth quartic plane curve $V(f)$ defined over a real closed complete non-Archimedean valued field. Due to Tarski-Seidenberg Transfer Principle [BPR06, Theorem 1.4.2], we can assume, that $V(f)$ is defined over $\mathbb{K}_\mathbb{R}$. Let $\mathcal{T}$ denote the dual subdivision of Γ. Since Γ is tropically smooth and generic, we know that $\mathcal{T}$ is a unimodular triangulation of $4\Delta_2$ satisfying the condition (i) of Remark 3.3.2.

By Theorem 5.1.4, the real lifting conditions of the 7 bitangent classes of Γ only depend on the corresponding 7 dual deformation motifs contained in $\mathcal{T}$.

The authors of [BJMS15] computed a list of the 1278 representatives of the unimodular regular triangulations of $4\Delta_2$ modulo S_3-symmetry. We will denote this list by $\mathcal{L}$. Thus, we know that there exists $\sigma \in S_3$ such that $\sigma(\mathcal{T})$ is equal to one representative in $\mathcal{L}$. Therefore, the prove the statement for arbitrary generic tropical smooth quartic curves, we prove the statement for every generic triangulation in the list $\mathcal{L}$. This is possible, because, as we have seen in Section 5.1, the lifting conditions computed for $\sigma(\mathcal{T})$ can be transformed via application of σ^{-1} to the the lifting conditions corresponding to $\mathcal{T}$.

This approach makes a computational proof possible. The procedure is to let an algorithm run through all elements of $\mathcal{L}$ and for each compute the real lifting conditions and the number of possible lifts.

In joint work with Marta Panizzut, we implemented code in `polymake` [GJ00] to perform these computations. The functions that is not contained in the extension `TropicalQaurticCurves` can be found in Appendix B.1.1.

Note that, as explained in Remark 5.2.1, 1270 of the 1278 S_3-representatives in the list $\mathcal{L}$ are generic in the sense of condition (i) in Remark 3.3.2. Nevertheless, we ran the computations over all 1278 triangulations, with the exception that for the 8 non-generic triangulations did not compute the lifting behavior of the bitangent class of shape (C) since that is not yet understood.

The computational prof consists of three steps. The first step is to determine the set of dual deformation motifs for each triangulation in our list $\mathcal{L}$. Algorithm 1 describes this procedure.

Algorithm 1 Finding all dual deformation motifs

Input: Unimodular regular triangulation $\mathcal{T}$ of $4\Delta_2$ from the list $\mathcal{L}$.
Output: The list of all dual deformation motifs in $\mathcal{T}$.
 1: **for each** dual deformation motif M in Figure 4.39 **do**
 2:      **for each** $\sigma \in S_3$ **do**
 3:          **if** the triangles of $\sigma(M)$ are contained in $\mathcal{T}$ **then**
 4:              output $(\sigma(M),\sigma)$.
 5:          **end if**
 6:      **end for**
 7: **end for**

The output of this algorithm also confirms the implication of the classification from Theorem 4.2.3 that every unimodular triangulation as exactly 7 different associated deformation classes.

The ground work for the second step is contained in the set up of the `polymake` extension `TropicalQuarticCurves` that we developed: For every dual deformation motif in identity position we have by Table 5.1 up to two inequalities on the signs of the coefficients of f as the real lifting conditions. We associate a matrix of two sets to each dual deformation motif. Each set encodes one of the up to two inequalities. This is more closely described in Section 6.1.1.

Now in the second step we collect all real lifting conditions for each generic triangulation in our list $\mathcal{L}$ of S_3-representatives.

The function detecting the dual deformation motifs inside a given triangulation remembers the element $\sigma \in S_3$ that transforms the corresponding identity position into the position occurring in the triangulation. Hence, we can let σ act on the

sets of sign conditions and compute the set of real lifting conditions for any given tropical smooth quartic curve.

In the third step, the actual counting of the real bitangents takes place. For this, we need to determine for each sign vector with $15 = |4\Delta_2 \cap \mathbb{Z}^2|$ entries how many of the real lifting conditions are satisfied. By standardizing the sign vectors to start with $+1$, we can limit the algorithm to 2^{14} sign vectors to check. By [CM21, Theorem 1.2 and Corollary 7.3], each bitangent class has either zero or exactly four lifts to totally real bitangents. That means that we have to count each satisfied real lifting condition with a multiplicity of four to achieve the correct number of real bitangents. This routine is described in Algorithm 2.

Algorithm 2 Computing the possible numbers of real bitangents

---

Input: Unimodular regular triangulation $\mathcal{T}$ of $4\Delta_2$ from the list $\mathcal{L}$.
Output: The list of all possible numbers of real bitangents of an algebraic quartic
     curve with dual subdivision $\mathcal{T}$.
 1: **for each** $v \in \{\pm 1\}^{15}$ starting with 1 **do**
 2:     $n = 0$
 3:     **for each** real lifting condition c of $\mathcal{T}$ **do**
 4:         **if** $c(v)$ is true **then**
 5:             $n + 4$.
 6:         **end if**
 7:     **end for**
 8:     **if** the value of n did not appear before **then**
 9:         output n
10:     **end if**
11: **end for**

The computation yields that any smooth quartic curve $V(f)$ for which $\mathrm{Trop}(V(f)) = \Gamma$ is smooth and generic has either 4, 8, 16 or 28 totally real bitangents. We conclude that each sign vector satisfies the real lifting conditions of 1, 2, 4 or 7 deformation classes of a generic unimodular triangulation. $\qquad\qquad\square$

The implementation of Algorithm 1 and 2 in `polymake` to prove Theorem 5.2.2 resulted in the `polymake` extension `TropicalQuarticCurves` and the database collection `Tropical:QuarticCurves` in the `polymake` database `polyDB` [Paf17]. Both are joint work with Marta Panizzut and are introduced in detail in Chapter 6.

Chapter 6

More on tropical bitangents

This chapter collects sections on different aspects of tropical bitangents, with focus on the computational feature.

Section 6.1 introduces the software extension `TropicalQuarticCurves` [GP], of `polymake` [GJ00], and the new collection `Tropical:QuarticCurves` in the database `polyDB` [Paf17] for objects in discrete geometry and related areas. This section gives an insight in the thoughts behind the code to explain which data was stored, and to communicate the handling of the code and the database.

In Section 6.2, we present results of analytical, computational investigations of the data provided by the collection `Tropical:QuarticCurves`. This includes distribution of orbit sizes or possible numbers of real bitangents (Theorems 6.2.1 & 6.2.3), as well as an investigation of the question whether the tropical bitangents determine the tropical quartic curve (Theorem 6.2.5, Problem 6.2.8). The `polymake` functions used for the computational aspects of these proofs can be found in Appendix B.1.2.

In Section 6.3, special areas of the secondary cone are determined: Those areas for which the bitangent shapes are constant, and the lower dimensional areas for which non-generic quartics appear in a secondary cone corresponding to a generic triangulation.

The sections 6.1, 6.2 and 6.3.1 are based on work for the preprint [GP21a], which is joint work with Marta Panizzut.

6.1 `polymake` extension and database

As bitangents or more generally intersections are intensely studied by the tropical community, we expect the extension `TropicalQuarticCurves` and the entry in the `polymake` database `polyDB` to be useful for further research as they make computing examples on the topic easier and more accessible.

Furthermore, other researchers can now use this software and even further develop the code, for example to study arithmetic multiplicities of tropical bitangent or the lifting conditions over other fields (Corollary 5.1.5).

In recent years, computational methods are having a more prominent role in the proof of interesting results in tropical and algebraic geometry. We believe that our approach to this project rightly fits and addresses the paramount questions and challenges on how to make these methods and data available and confirmable by the research community, following the FAIR data principles. We refer to the description of newly established consortium MaRDI [MaR] for further details.

In Section 6.1.1, we present the `polymake` extension `TropicalQuarticCurves` [GP] whose structure was inspired by the extension `TropicalCubics` [JPS], while Section 6.1.2 introduces the collection `Tropical:QuarticCurves` in the database `polyDB` [Paf17]. The collection was build out the expansion of data of [BJMS15].

The extension was used for the the computations in the proof of Theorem 5.2.2, as Algorithms 1 and 2 where implemented in `polymake` using the objects and code provided by the extension. Both the development of the extension as well as the collection of data for the database entry is joint work with Marta Panizzut and the content of this section builds on the joint paper [GP21a].

6.1.1 Smooth tropical quartic curves in `polymake`

We present the `polymake` extension `TropicalQuarticCurves` [GP] which is joint work with Marta Panizzut. In the extension `TropicalQuarticCurves`, we introduce the objects `DualSubdivisionOfQuartic` and `DeformationMotif` in the application fan, and the object `QuarticCurve<Addition>` in the application tropical. This procedure was inspired by the extension `TropicalCubics` [JPS20] for the analysis of tropical cubic surfaces.

The extension is available for `polymake` version 4.5 at

> `https://polymake.org/doku.php/extensions/tropicalquarticcurves`

Remark 6.1.1. We recall that in Chapter 2 the tropical semifield was defined via the *max*-convention (see Definition 2.2.1), and that the Chapters 3, 4 and 5 adhere to this convention. However, in `polymake` the implementation of subdivisions of point configurations used for computing regular subdivisions of polytopes, as well as the computation of their secondary cones, fits with the *min*-convention. See Remark 2.2.21 (1) and (2).

When working with tropical hypersurfaces in `polymake`, users can specify their preferred convention. As the extension `TropicalQuarticCurves` builds on these areas, the user needs to take care when a change of conventions in the computation is necessary.

The extension `TropicalQuarticCurves` contains new objects in the applications `fan` and `tropical`. We begin by introducing the additions to applications `fan`.

(a) Order of lattice points of $4\Delta_2$ in the extension `TropicalQuarticCurves`.

(b) The dual subdivision `$S`, with triangles of the dual deformation motif `$DLO` filled.
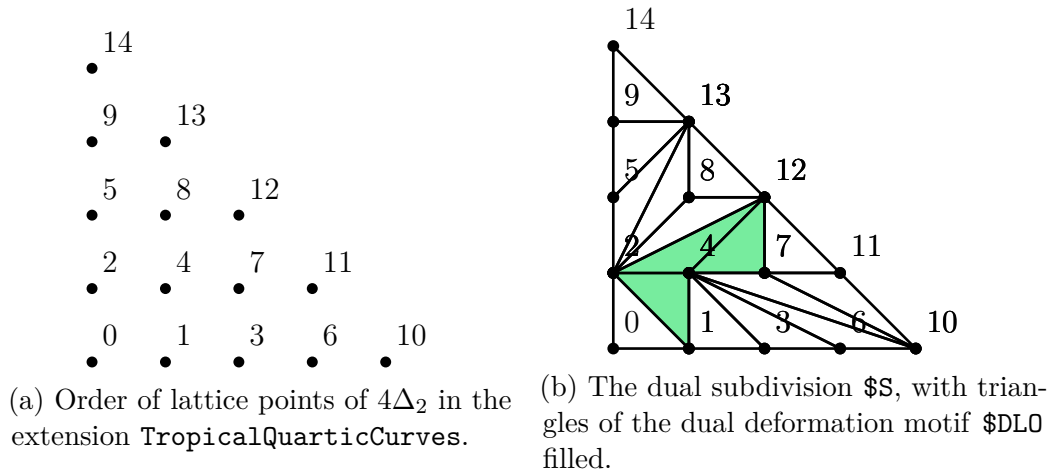
Figure 6.1: Illustrations on the order or lattice points as used in the extension

Application fan. In this application, we can work with the objects and theory on the dual side of quartic curves. This means regular subdivisions, dual deformation motifs, etc. A regular subdivision in `polymake` is usually given as a `SubdivisionOfPoints`, specified by the lattice points and either the weights or the maximal cells of the subdivision. The order of the lattice points of $4\Delta_2$ is predefined in the extension as illustrated in Figure 6.1a. Hence, a regular subdivision of $4\Delta_2$ can be given to `polymake` as a `DualSubdivisionOfQuartic` by specifying only either the weights or the maximal cells. The object `DualSubdivisionOfQuartic` is derived of the object `SubdivisionOfPoints` and therefore possesses the same properties, in addition to the ones defined by the extension.

```
fan > $S = new DualSubdivisionOfQuartic(MAXIMAL_CELLS=>[[0,1,2],
   [1,2,4],[2,4,12],[4,7,12],[2,8,12],[2,8,13],[8,12,13],[2,5,13],
    [5,9,13],[9,13,14],[7,11,12],[7,10,11],[4,7,10],[4,6,10],
   [3,4,6],[1,3,4]]);
fan > $T = new DualSubdivisionOfQuartic(WEIGHTS=>[14,9,4,6,
   0,12,4,0,5,21,3,1,0,12,31]);
fan > $M = $T->MAXIMAL_CELLS;
fan > print "[".join("],[",map(join(",",@$_),@$M))."]\n"; #for
   improved print layout
[7,11,12],[4,7,12],[8,12,13],[2,8,12],[2,4,12],[1,3,4],[0,1,2],
   [1,2,4],[2,5,13],[5,9,13],[9,13,14],[2,8,13],[3,4,6],[4,7,10],
[4,6,10],[7,10,11]
```

We observe that `$S` and `$T` have the same maximal cells and thus present the same regular subdivision. Further, we observe that the subdivision consists of 16 triangles. Therefore, it is a unimodular triangulation of $4\Delta_2$, since the volume of $4\Delta_2$ is 8 and the minimal volume of a lattice triangle is $\frac{1}{2}$. To account for the

action of S_3 on $4\Delta_2$ as described in Chapter 3, the permutation group is predefined under the property `ACTION` of `DualSubdivisionOfQuartic`.

```
fan > print $S->ACTION->ALL_GROUP_ELEMENTS;
0 1 2 3 4 5 6 7 8 9 10 11 12 13 14
0 2 1 5 4 3 9 8 7 6 14 13 12 11 10
10 6 11 3 7 12 1 4 8 13 0 2 5 9 14
10 11 6 12 7 3 13 8 4 1 14 9 5 2 0
14 9 13 5 8 12 2 4 7 11 0 1 3 6 10
14 13 9 12 8 5 11 7 4 2 10 6 3 1 0
```

To investigate the tropical bitangents we need the dual deformation motifs. For these we use the object `DeformationMotif`, which is defined from its three properties `TRIANGLES`, `TYPE` and `SYMMETRY`. The property `TRIANGLES` consists of the maximal cells of the triangulation that form the dual deformation motif. The `TYPE` is the name associated in the classification depicted in Figure 4.39. And `SYMMETRY` specifies which element of the permutation group S_3 acts on the identity position of the deformation motif to transform it to the position of the given triangles.

```
fan > $Motif1 = new DeformationMotif(TRIANGLES=>[[1,2,4],[2,4,12],
    [4,7,12]], TYPE=>"DLO",SYMMETRY=>1);
```

This dual deformation motif is depicted in Figure 6.1b. In the same way as described above for `DualSubdivisionOfQuartic`, the permutation group is encoded as property `ACTION` of `DeformationMotif`.

When defining a `DeformationMotif` from its properties, it is left to the user to ensure that the input properties are consistent with the classification from Theorem 4.2.3.

There are additional properties of `DeformationMotif` that can be computed from the three defining ones. By Theorem 5.1.4 the real lifting conditions only depend on the deformation class. They are stored for each deformation motif. Additionally, the hyperplanes that describe the deformation of the shapes within the secondary cone are computable. More details on the hyperplanes can be found in Section 6.3.

```
fan > print $Motif1->SIGN_CONDITIONS;
{-1 1 2 4 12}
{}
fan > print $Motif1->HYPERPLANES;
0 1 -1 0 1 0 0 -2 0 0 0 0 1 0 0
```

The property `SIGN_CONDITIONS` returns two possibly empty sets. The following explanation describes how to read this output. As `$Motif1` is deformation class $(D\,L\,O)_{(xz)}$ we can read off its real lifting condition from Table 5.1 and apply $(x\,y)$. We obtain

$$-s_{01}s_{11}s_{10}s_{22} > 0.$$

Since some deformation classes have two of these inequalities for their real lifting conditions, `SIGN_CONDITIONS` is always a vector with two entries. In our example the second entry is empty, since we only have one inequality. The real lifting condition $-s_{01}s_{11}s_{10}s_{22} > 0$ now translates to the set `{-1 1 2 4 12}` as follows. We remember the initial minus sign by the `-1` in the set. The remaining signs come from coefficients of the quartic curve. The ordering of the monomials of the quartic curve corresponds to the ordering of the lattice points in $4\Delta_2$ as depicted in Figure 6.1a. Thus, we have the following allocation from the inequality to the set given by `SIGN_CONDITIONS`:

$$\begin{aligned} -1 &\mapsto \texttt{-1} \\ s_{01} &\mapsto \texttt{2} \\ s_{11} &\mapsto \texttt{4} \\ s_{10} &\mapsto \texttt{1} \\ s_{22} &\mapsto \texttt{12} \end{aligned}$$

Especially for investigation of the lifting conditions, it is important to know whether the unimodular triangulation considered is generic: For non generic triangulations no sign conditions are assigned to deformation class (C), since these are not yet understood. See Remarks 3.3.2 and 5.2.1. For any generic triangulation, we can compute the collected sets of real lifting conditions.

```
fan > print $S->IS_GENERIC;
true
fan > $Signs = $S->ALL_SIGN_CONDITIONS;
fan > print "[".join("],[",map(join(",",@$_),@$Signs))."]\n"; #
   Improve output layout
[{-1 2 8 12 13},{-1 1 2 4 12}], [{-1 2 8 12 13},{10 12}], [{-1 2 8
   12 13},{10 12}], [{-1 1 2 4 12},{}], [{10 12},{}], [{10
   12},{}], [{-1 1 2 4 10},{}]
```

At this point we want to recommend to use all the functions with caution, whenever you are working with a non-generic triangulation. Also keep in mind that there are tropical quartic curves with generic dual subdivision that do not satisfy the genericity condition on their edge lengths, as mentioned in Remark 5.2.1. Section 6.3.2 provides a description of these lower dimensional areas for which we can observe non-generic points inside a generic secondary cone.

It is also possible to access the deformation motifs and their properties from `$S` via the property `ALL_DEFORMATION_MOTIFS`. This provides an array of the deformation motifs associated to the triangulation.

```
fan > $Motifs = $S->ALL_DEFORMATION_MOTIFS;
fan > $Hyperplanes = $Motifs->[3]->HYPERPLANES;
fan > $Signconditions = $Motifs->[3]->SIGN_CONDITIONS;
```

```
fan > print $Motifs->[3]->properties;
type: DeformationMotif

ACTION
type: PermutationAction<Int, Rational>

HYPERPLANES
0 1 -1 0 1 0 0 -2 0 0 0 0 1 0 0

SIGN_CONDITIONS
{-1 1 2 4 12}
{}

SYMMETRY
1

TRIANGLES
{2 4 12}
{4 7 12}
{1 2 4}

TYPE
DLO
```

Further, we can access some information on the subdivision via the properties `DENSE_UNIMODULAR`, `ORBIT_SIZE` and `DEFORMATION_MOTIFS_TYPES`.

```
fan > print $S->DENSE_UNIMODULAR; #checks whether the subdivision
    has of 16 maximal cells
true
fan > print $S->ORBIT_SIZE; #number of different subdivisions in
    the orbit of $S
6
fan > print $S->DEFORMATION_MOTIFS_TYPES; #prints the names of the
    7 deformation classes
A A A DLO E E GIN+(xy)
```

Moreover, the extension provides a function to compute the number of real bitangents for a given `DualSubdivisionOfQuartic` and a given sign vector, i.e., a vector with entries ± 1. To illustrate this, we revisit Example 3.3.6. We consider the triangulation `$S1` from Figure 3.9 and define it from its weights. Note, that the weights in Figure 3.9 are given according to the *max*-convention, so that we have to use their negative. The sign vector in Example 3.3.6 was the all positive vector, described by a vector of dimension 15 will all ones. We observe the same result as computed by hand in Example 3.3.6.

```
fan > $S1 = new DualSubdivisionOfQuartic(WEIGHTS
    =>[14,0,13,4,0,14,9,1,4,16,15,4,0,9,19]);
fan > $v = new Vector<Int>([1,1,1,1,1,1,1,1,1,1,1,1,1,1,1]);
```

```
fan > print give_pluecker($S1,$v);
8
```

Further, we can access the properties of that are defined in `polymake` for the object `SubdivisionOfPoints`. This includes the secondary cone, and minimial integer weights inducing the given subdivision.

```
fan > $SC = $S->SECONDARY_CONE;
fan > print $SC->DIM;
15
fan > $w = $S->MIN_WEIGHTS;
fan > print $w;
14 9 4 6 0 12 4 0 5 21 3 1 0 12 31
```

Application tropical. In this application, we want to work with a tropical quartic curve. For this we introduce the object `QuarticCurve<Addition>` which is derived from the object `Hypersurface<Addition>`. To define a `Hypersurface<Addition>` the user has to specify first the preferred convention (`Min` or `Max`) and then the monomials and their coefficients. Since we want to have the duality between `DualSubdivisionOfQuartic` and `QuarticCurve<Addition>` working nicely, the monomials of the tropical quartic curve are already predefined in the extension in the same fixed order as the lattice points of $4\Delta_2$. See Figure 6.1a. Hence, to define a tropical quartic curve, the user only needs to specify the convention of the tropical addition that should be used together with the coefficients.

```
fan > application "tropical";
tropical > $V = new Vector<Int>([-14,-9,-4,-6,0,-12,-4,
   0,-5,-21,-3,-1,0,-12,-31]);
tropical > $C = new QuarticCurve<Max>(COEFFICIENTS=>$V);
```

Recall from Remark 4.2.4 that the deformation of the the shapes is described by linear inequalities. Theorem 6.3.1 shows that the deformations are induced by hyperplanes intersecting the secondary cone. By using the hyperplanes describing the shape deformations inside a deformation class we can compute the 7 bitangent shapes of the tropical quartic curve from its coefficients.

```
tropical > print $C->BITANGENT_SHAPES;
A A A D E E I
```

The new objects in application `fan` and `tropical` can be used in a connected way. For example, for a given quartic curve we can recover the dual subdivision and work with its properties as described above.

```
tropical > $Sub = $Curve1->DUAL_SUBDIVISION;
tropical > print $Sub->tpe->full_name;
DualSubdivisionOfQuartic
```

However, we have

```
fan > print $Sub ->POINTS;
1 4 0 0
1 3 1 0
1 3 0 1
1 2 2 0
1 2 1 1
1 2 0 2
1 1 3 0
1 1 2 1
1 1 1 2
1 1 0 3
1 0 4 0
1 0 3 1
1 0 2 2
1 0 1 3
1 0 0 4
```

This is the homogenized 2-simplex in 3-space, an equilateral triangle. We can
still perform all the computations as before. Nevertheless, for the purposes of
visualization it might be advisable to use the following code instead in order to see
$4\Delta_2$ as in Figure 6.1a and as defined Definition 2.2.17.

```
tropical > $M = $Sub ->MAXIMAL_CELLS;
tropical > $Subdiv= new fan::DualSubdivisionOfQuartic(
   MAXIMAL_CELLS=>$M);
```

The object `$Subdiv` has as lattice points exactly the 2-dimensional lattice points
as in Figure 6.1a.

Moreover, as explained above, we can access the secondary cone of the regular
subdivision, find an interior point and define the tropical quartic corresponding to
that point.

```
tropical > use application "fan";
fan > $SC = $Sub ->SECONDARY_CONE;
fan > $v = $SC ->REL_INT_POINT;
fan > print $v;
1 5/4 7/72 5/3 31/72 1/36 17/8 15/16 11/72 0 47/18 107/72 4/9 0 0
fan > $Curve1 = new tropical::QuarticCurve<Min>(COEFFICIENTS=>$v);
fan > print $Curve1 ->BITANGENT_SHAPES;
A A A D E E G
```

If we would rather work with an integer vector of small values, we can use the
property `MIN_WEIGHTS` of the subdivision.

```
fan > $w = $Sub ->MIN_WEIGHTS;
fan > print $w;
14 9 4 6 0 12 4 0 5 21 3 1 0 12 31
fan > $Curve2 = new tropical::QuarticCurve<Min>(COEFFICIENTS=>$w);
fan > print $Curve2 ->BITANGENT_SHAPES;
A A A D E E I
```

Remark 6.1.2. Recall, that the two new objects `DualSubdivisionOfQuartic` and `QuarticCurve<Addition>`, are derived of existing `polymake` objects. This means we can use the properties of these objects. This includes the option of visualization.

```
tropical > $C->VISUAL;
```

or equivalently

```
fan > $Sub->VISUAL;
```

will provide a picture of the tropical quartic curve or respectively the unimodular triangulation.

6.1.2 The database collection `QuarticCurves`

The 1278 unimodular regular triangulations of $4\Delta_2$ computed by Brodsky et al. [BJMS15] were first available at the git repository

<p align="center">https://github.com/micjoswig/TropicalModuliData.</p>

Since our analysis of tropical quartic curves and their tropical bitangents, created additional information for each such unimodular regular triangulation, we decided to make this data available as a collection in `polyDB` [Paf17], a general database for discrete geometric objects with an interface in `polymake`. The database entries are available in the collection `QuarticCurves` within the database `Tropical` of `polyDB` at

<p align="center">https://db.polymake.org/.</p>

The database can be accessed via the web interface as well as directly from `polymake`. Each triangulation has a unique identifier, an integer between 1 and 1278 that can be used to retrieve it from the database. For each triangulation given by its maximal cells, the database entry contains:

- the GKZ-vector (see Definition 2.1.11): `GKZ_VECTOR`,

- a minimal representative as explained below: `MINIMAL_REPRESENTATIVE`,

- a boolean stating whether the triangutlation is generic: `IS_GENERIC`,

- all dual deformation motifs: `ALL_DEFORMATION_MOTIFS` and for each of these

  - their sign conditions: `SIGN_CONDITIONS`,

  - their associated hyperplanes: `HYPERPLANES`,

- the Plücker numbers of their possible real bitangents: `PLUECKER_NUMBERS`,

- an exemplary sign vector for each Plücker number: `SIGN_REPRESENTATIVES`.

We call the numbers of real bitangent lifts of a tropical quartic curve *Plücker numbers*.

The `MINIMAL_REPRESENTATIVE` to a given triangulation $\mathcal{T}$ is the minimal triangulation in the S_3 orbit of $\mathcal{T}$ with respect to the lexicographical order on the vertex labels in the maximal cells. An example is provided below. Given a triangulation $\mathcal{T}$, the property `MINIMAL_REPRESENTATIVE` is used to find the associated S_3-representative in the database. This is done via the function `find_in_database()` which computes the minimal representative of $\mathcal{T}$ and compares it with the ones stored in the database returning the identifier.

```
fan > $S = new DualSubdivisionOfQuartic(MAXIMAL_CELLS=>[[6,10,11],
    [3,6,11],[3,7,11],[7,11,12],[1,3,7],[4,8,12],[8,12,13],
    [0,4,8],[5,9,13],[9,13,14],[5,8,13],[2,5,8],[4,7,12],[0,4,7],
    [0,2,8],[0,1,7]]);
fan > print find_in_database($S);
100
```

Note that not all the properties from the above list are displayed for a chosen identifier on the web interface. However, after downloading the JSON source file for a chosen triangulation from the database, the data can be loaded into polymake and investigated within the extension.

```
polytope > application "fan";
fan > $T = load_data("YOUR/PATH/100.json");
fan > print $T->DEFORMATION_MOTIFS_TYPES;
A A A A G G T
fan > print $T->PLUECKER_NUMBERS;
{4 8 16 28}
fan > print $T->SIGN_REPRESENTATIVES;
{<1 1 1 1 1 1 1 1 1 1 1 1 1 1 1> <4>}
{<1 1 1 -1 1 1 1 1 1 1 1 1 1 1 1> <8>}
{<1 1 1 1 1 -1 1 1 1 1 1 1 1 1 1> <16>}
{<1 1 1 1 1 1 1 1 1 1 1 -1 1 1 1 1> <28>}
```

Remark 6.1.3. To compute all the possible numbers of real bitangents possible for quartic curves with the given dual unimodular triangulation, we have to evaluate the real lifting conditions for all possibilities of sign vectors $\{\pm 1\}^{15}$. The same is true for the code behind the computation of the property `SIGN_REPRESENTATIVES`, which provides for each possible number of real bitangents a sign vector with which the quartic curve would attain the given number of real bitangents. The evaluation of the real lifting conditions over all possible sign vectors is the reason, why these properties are only available for the database entries.

The function to compute the property `SIGN_REPRESENTATIVES` is documented in Appendix B.1.2 for reasons of completeness.

It is possible to obtain the values for a unimodular triangulation that does not coincide with its representative stored in the database via S_3 transformation.

The following gives an example of the property `MINIMAL_REPRESENTATIVE`.

```
fan > print "{".join("},␣{",map(join(",",@$_),@{$T->MAXIMAL_CELLS
    }))."}\n"; #for improved print layout
{0,1,2}, {1,2,3}, {2,3,4}, {2,4,5}, {3,4,6}, {5,7,8}, {5,8,9},
    {7,8,10}, {9,12,13}, {9,13,14}, {8,9,12}, {8,11,12}, {4,5,7},
    {4,7,10}, {8,10,11}, {4,6,10}

print "{".join("},␣{",map(join(",",@$_),@{$T->
    MINIMAL_REPRESENTATIVE}))."}\n"; #for improved print layout
{0,1,2}, {1,2,3}, {2,3,4}, {2,4,5}, {3,4,6}, {4,5,7}, {4,6,10},
    {4,7,10}, {5,7,8}, {5,8,9}, {7,8,10}, {8,9,12}, {8,10,11},
    {8,11,12}, {9,12,13}, {9,13,14}
```

We recall from Remark 5.2.1 that up to S_3 there are 8 regular unimodular triangulations that are non-generic. Representatives of these non-generic triangulations can be accessed under the identifiers #511, #719, #842, #905, #1095, #1114, #1191 and #1263 in the database.

Instructions on how to access the database from `polymake` can be found in the `polymake` wiki[1]. The following illustrates how a specific triangulation can be accessed via its identifier.

```
polytope > application "fan";
fan > $polydb = polyDB(); #calls the main instance of polyDB
fan > $collection = $polydb->get_collection("Tropical.
    QuarticCurves"); #to access the correct collection
fan > $cur = $collection->find_one({"_id"=>"511"});
fan > print $cur->name; #prints the identifier
511
fan >  print $cur->IS_GENERIC;
false
```

The command `->find_one` selects one database entry that satisfies the given property. In the above example this property was that the identifier `"_id"` was equal to `"511"` for which we know that there exists only one entry. (Note that the identifiers are stored as strings.) The interface to `polymake` makes other queries to the collection possible. For example, we can count all entries that satisfy a specific property. This is helpful to conduct analyses of the data as presented in the following section.

6.2 Data on tropical quartic curves

This section presents results from analytical investigations of the collected data on smooth tropical quartic curves and their bitangents, like the distribution of orbit

---

[1]`https://polymake.org/doku.php/user_guide/howto/polydb_tutorial`

sizes in Theorem 6.2.1 or the distribution of possible numbers of real bitangent lifts in Theorem 6.2.3. The latter shows that every generic tropical smooth quartic curve admits a lift to a quartic curve with 28 real bitangents.

Further, we use the computational data to investigate the question whether tropical bitangents determine the quartic curve similarly to the algebraic case [CS03]. We prove that the deformation classes determine the combinatorial type of the quartic curve using the extension `TropicalQuarticCurves` (Theorem 6.2.5). Moreover, we look at an example of a quartic curve with bitangents more closely and formulate in Problem 6.2.8 an open research question for future exploration.

The results presented in Theorems 6.2.1, 6.2.3 and 6.2.5 are joint work with Marta Panizzut for a second version of [GP21a].

Additionally, this section contains an analysis of the real lifting of shape (C) for non-generic triangulations as formulated in Problem 6.2.4 together with the explanatory paragraph and computational data in Table 6.3. This is independent work, and not part of the joint work.

The `polymake` functions used for the computational aspects in this section can be found in Appendix B.1.2.

Theorem 6.2.1. *The fourth dilation of the standard* 2*-dimensional simplex* $4\Delta_2$ *has* 7422 *regular unimodular triangulations. These are grouped into* 1278 *orbits with respect to the action of* S_3*. The distribution of the orbit sizes is shown in Table 6.1.*

1	2	3	6
2	5	72	1199

Table 6.1: Distribution of orbit sizes among smooth tropical quartic curves.

Proof. The number of regular unimodular triangulations of $4\Delta_2$ was determined by Brodsky et al. in [BJMS15]. The statement on the orbit distribution can be proven by a query over the entries of the database collection introduced in Section 6.1.2. Algorithm 3 describes the procedure. Here e_i denotes the i-th standard basis vector in $\mathbb{R}^6$ and $\mathcal{L}$ means the collection of S_3-representatives of the unimodular triangulations as saved in the database. Naturally, the entries 4 and 5 of the vector v will stay zero. The output vector is $v = (2, 5, 72, 0, 0, 1199)$. The `polymake` function for this computation can be found in Appendix B.1.2. $\square$

When considering the interplay between algebraic and tropical geometry, a naturally arising question is:

Algorithm 3 Computing the possible numbers of real bitangents

---

Input: Unimodular regular triangulation $\mathcal{T}$ of $4\Delta_2$ in $\mathcal{L}$.
Output: Distribution of the orbit sizes
 1: $v = (0,0,0,0,0,0)$
 2: **for each** $\mathcal{T}$ in $\mathcal{L}$ **do**
 3:     $\mathcal{O} = $ orbit of $\mathcal{T}$ under S_3
 4:     $i = \text{size}(\mathcal{O})$
 5:     $v = v + e_i$
 6: **end for**
 7: return v

Question 6.2.2. Does every generic smooth tropical quartic have a real lift to a smooth real quartic curve with exactly 28 bitangents?

The answer lies within the collected data.

Theorem 6.2.3. *The distribution of Plücker numbers among the* 1270 *generic smooth unimodular triangulations of* $4\Delta_2$ *is reported in Table 6.2. Every generic combinatorial type of smooth tropical quartic curve admits a lift to a plane curve with* 28 *real bitangents.*

$\{4,8,16,28\}$	$\{4,8,28\}$	$\{4,16,28\}$	$\{8,16,28\}$	$\{4,28\}$	$\{8,28\}$	$\{16,28\}$
1200	15	26	18	6	3	2

Table 6.2: Distribution of Plücker numbers among the combinatorial types of generic smooth tropical quartic curves.

Proof. Since for every unimodular triangulation in the database collection the possible numbers of real bitangents are stored as property PLUECKER_NUMBERS, the setup of the database allows a simple count of all the triangulations with the same set of possible numbers of real bitangents.

```
polytope > application "fan";
fan > $polydb = polyDB();
fan > $collection = $polydb->get_collection("Tropical.
   QuarticCurves");
fan > $n = $collection->count({"PLUECKER_NUMBERS"=>[4,8,16,28]});
fan > print $n;
1200
```

These will only count the generic triangulations. It can be checked in the database that the non-generic triangulations always contain a number outside of the allowed set $\{4, 8, 16, 28\}$ from the missing lifting behaviour of the bitangent class of shape (C).

All sets of possible Plücker numbers with non-zero output for the database query are collected together with their occurrence in the set of regular generic unimodular triangulations in Table 6.2. We observe that each such set contains the number 28, thus answering Question 6.2.2 positively. □

Recall that for non-generic triangulations the real lifting conditions of shape (C) are unknown. Therefore, we have the following open problem:

Problem 6.2.4. What is the real lifting behavior of shape (C) for an non-generic triangulation?

Since the numbers of real bitangents to smooth quartic curves were determined by Plücker and Zeuthen [Plü34, Plü39, Zeu73], it is possible for some sign vectors to conclude whether or not the shape (C) will lift. If we obtain as numbers of real bitangents 0, 12 or 24 for a non-generic triangulation, we know (since shape (C) is not counted) that in these cases the bitangent class of shape (C) has to lift. If we obtain the numbers 8 or 16, we know that shape (C) cannot lift, as this would contradict the results by Plücker and Zeuthen. Only in the case that we obtain exactly 4 real lifts we cannot decide on the realizability of shape (C) over $\mathbb{R}$. Table 6.3 shows the distribution of the sign vectors to the three cases described above.

	#511	#719	#842	#905	#1095	#1114	#1191	#1263
(C) lifts	8192	6144	8192	6144	6144	6144	6144	6144
(C) cannot lift	4096	2048	0	2048	2048	2048	2048	2048
unclear	4096	8192	8192	8192	8192	8192	8192	8192

Table 6.3: The distribution of the 2^{14} sign vectors on the three different cases of realizability of shape (C) over $\mathbb{R}$ for each of the eight non-generic triangulations by their database identifiers.

In algebraic geometry, a smooth quartic curve is uniquely determined by its 28 bitangent lines [CS03]. Theorem 6.2.5 shows that we can replicate this result on the combinatorial side of the tropical world with respect to the dual deformation classes and the combinatorial type of the quartic curve. In other words, for an allowed choice of 7 dual deformation motifs in $4\Delta_2$ there exists a unique completion

to a regular unimodular triangulation. A choice of dual deformation motifs is *allowed*, if they fit together into a regular subdivision of $4\Delta_2$.

Theorem 6.2.5. *The combinatorial type of a tropical quartic curve is determined by its 7 dual deformation motifs.*

Proof. The proof is of computational nature. For every triangulation in the set of 1278 representatives stored in the database, we collected the triangles that belonged to the seven dual deformation motif of the triangulation. Hence, each such set is the part of the triangulation fixed by the deformation classes of bitangents of its dual quartic curves. Collecting the orbits of these subcomplexes of the triangulations in a set, we counted 7422 different subcomplexes. The procedure is illustrated in Algorithm 4. The code can be found in Appendix B.1.2.

Algorithm 4 Computing the number of allowed sets of dual deformation motifs

---

Input: Unimodular regular triangulation $\mathcal{T}$ of $4\Delta_2$ in $\mathcal{L}$.
Output: Number of different sets of dual deformation motifs
 1: $S = \{\}$
 2: **for each** $\mathcal{T}$ in $\mathcal{L}$ **do**
 3:      T = set of all triangles determined by the dual deformations motifs of $\mathcal{T}$
 4:      **for each** $\sigma \in S_3$ **do**
 5:          add $\sigma(T)$ to the set S
 6:      **end for**
 7: **end for**
 8: return $|S|$

As there only exist 7422 regular unimodular triangulations of $4\Delta_2$ [BJMS15], we conclude that every triangulation has its unique set of dual deformation motifs. In other words, the 7 dual deformation motifs uniquely determine the unimodular triangulation, i.e., the combinatorial type of the quartic curve. $\qquad\square$

The question remains whether we observe a similar situation to the algebraic setting [CS03] for tropical quartic curves and their bitangent classes.

Question 6.2.6. Is a smooth tropical quartic curve determined by the positions and shapes of its 7 bitangent classes?

Here we consciously avoid the mention of deformation classes or bitangent motifs, since we now only consider the situation in the plane, i.e., we know about the positions of the bitangent classes in $\mathbb{R}^2$ and we know their shape out of the collection in Figure 3.6.
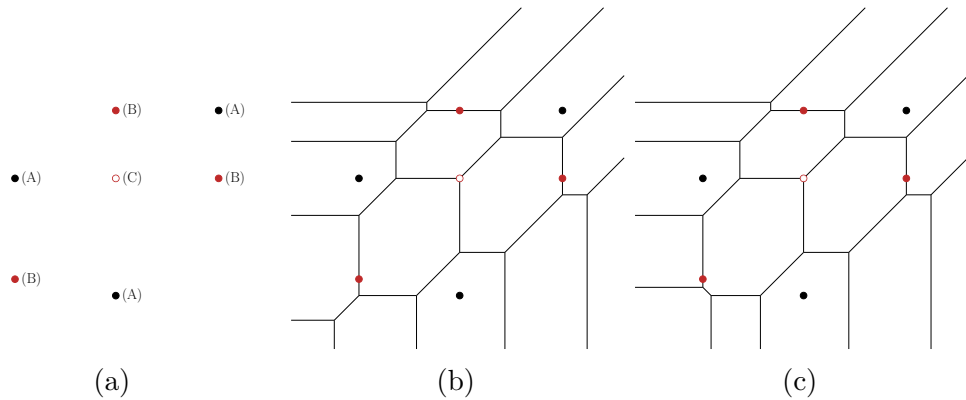
Figure 6.2: In Figure 6.2a we see the given bitangent shapes in their determined positions. Figures 6.2b and 6.2c show two smooth tropical quartic curves of different combinatorial type satisfying the conditions from Figure 6.2a.

An example is shown in Figure 6.2. This example also already answers Question 6.2.6 since we observe two tropical quartic curves of different combinatorial type with the given bitangent shapes in the predefined positions.

By Theorem 6.2.5 we know that combinatorial type is determined by the dual deformation motifs of the bitangent classes, and we observe that the deformation classes of the leftmost bitangent class of shape (B) differs for the two quartic curves in Figure 6.2. Therefore, we ask:

Question 6.2.7. Is a smooth tropical quartic curve determined by the positions and dual deformation motifs of its 7 bitangent classes?

In Figure 6.3 we see two different options on how the tropical quartic curve can change without affecting either its combinatorial type or the shapes and positions of its bitangent classes. Accordingly, the answer to Question 6.2.7 is again negative.

If we additionally fix the tropical tangency points for each bitangent class for the quartic curve in Figure 6.3, it is possible to reconstruct the coefficients of the quartic curve except for the coefficients to the monomials x^0y^0, x^4y^0 and x^0y^4. Recalling the notions of Definition 3.1.5, this means that the skeleton of the tropical quartic curve is fixed by the position of the tangencies and the shapes of the bitangent classes, and only the generalized leaves can still be pulled. To prove this for the curve in Figure 6.3, recall the position of the tropical tangency points as described in Proposition 3.3.8. A few steps of this process are illustrated in Figure 6.4. In Figure 6.4a and 6.4b the first tangency points of bitangent classes (3) and (6) are used to determine the first edge of the quartic. In Figure 6.4c, the first tropical tangency point of bitangent class (4) together with the position of the vertex of the quartic coinciding with the bitangent class of shape (C) determines another edge

(a) Change of edge lengths in the skeleton of the curve.

(b) Pulling the leaves of the curve.
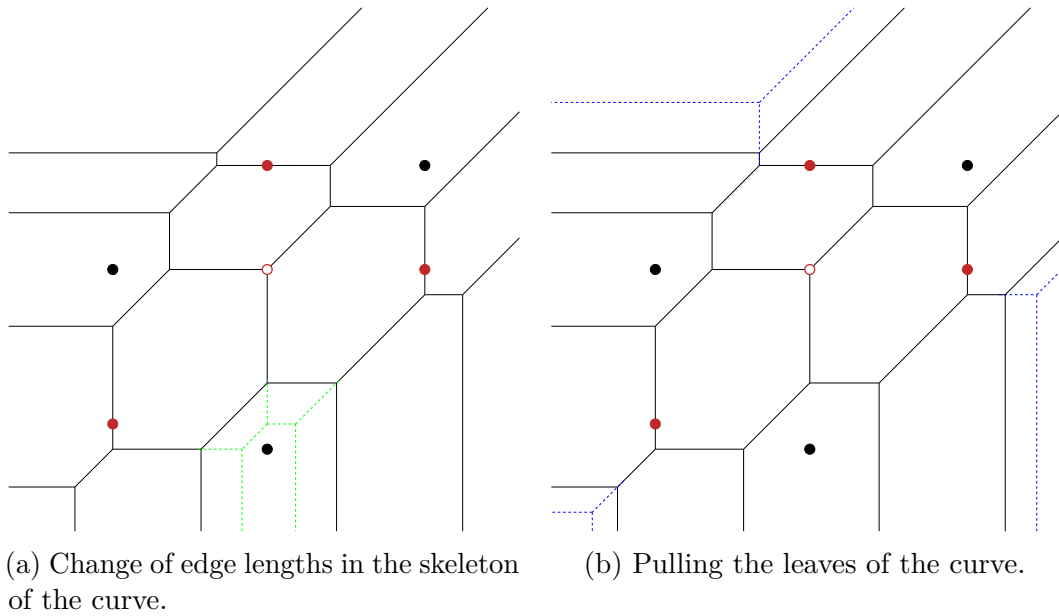
Figure 6.3: A smooth tropical quartic curve dual to the honeycomb triangulation with its 7 bitangent shapes. We see two possible changes of the edges of the quartic that do not interfere with the given bitangent shapes.

of the quartic. In Figure 6.4d, all tropical tangency points are drawn, where the notation $t_j^{(i)}$ denotes the j-th tangency point $j \in \{1,2\}$ of the (i)-th bitangent class, $i \in \{1,...,7\}$. The dotted edges in the skeleton do not contain tropical tangency points. They are fixed by the balancing condition and the fact that we have a tropical smooth curve of degree 4.

So the edge length changes depicted in Figure 6.3a are no longer possible when we fix the tropical tangency points. The only possible changes left are the pulling of leaves as illustrated in Figure 6.3b. Please note that we did not need the dual deformation motifs of the bitangent classes to fix the skeleton.

This indicates the following interesting question, which we leave for further research.

Problem 6.2.8. Is it in general possible to determine the skeleton of a smooth tropical quartic curve from its bitangent shapes and the tropical tangency points of its realizable representatives such that the only remaining edge length changes correspond to varying the edge lengths of generalized leaves?

If yes, does every tropical quartic in such a family allow a lift with 28 real bitangents?
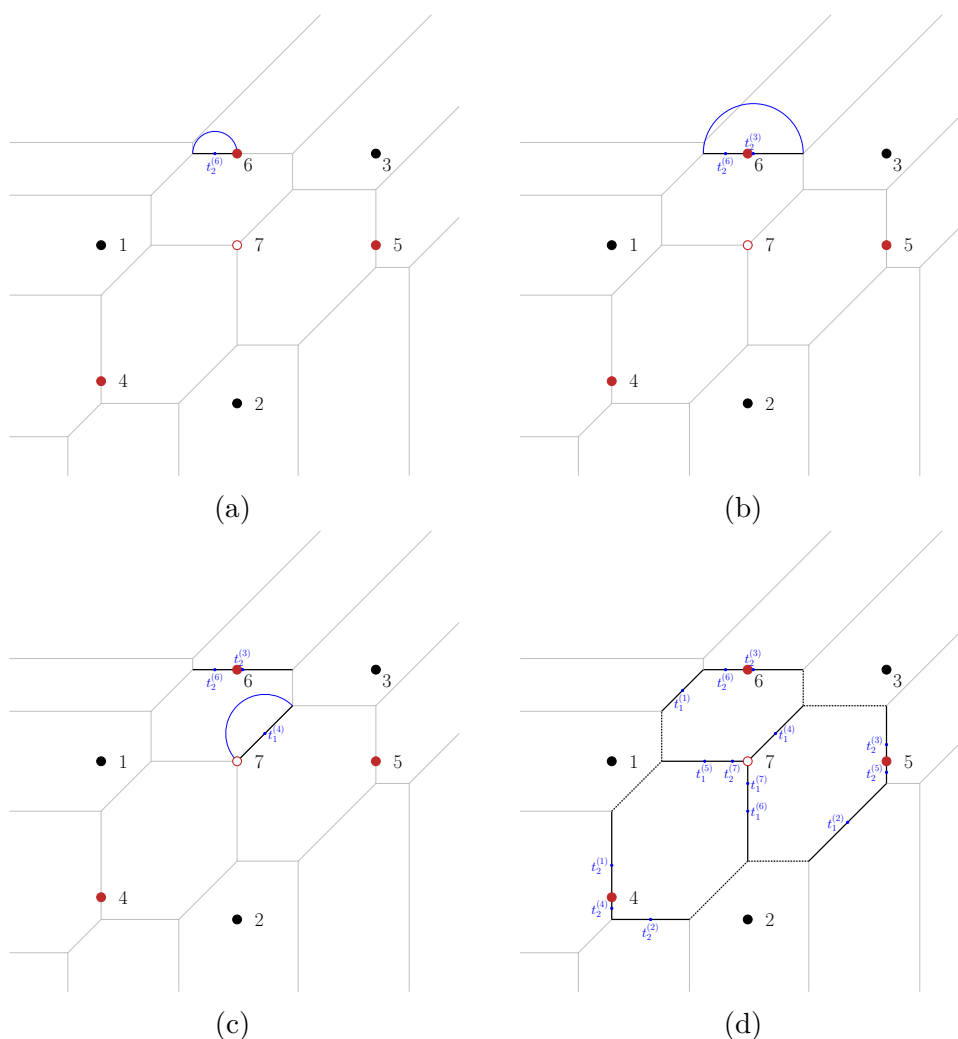
Figure 6.4: The bitangent shapes and their tropical tangency points fix the skeleton of the quartic curve.

6.3 Hyperplane arrangements

We have seen in Chapter 4 that changes between bitangent shapes, which belong to the same deformation class, for a given combinatorial type of the quartic curve corresponds to choosing a different coefficient vector from the associated secondary cone. This section focuses on special areas in the secondary cone.

Section 6.3.1 is concerned with the areas of a given secondary cone for which every tropical quartic has the same set of bitangent shapes, which turn out to be chambers of a hyperplane arrangement (Theorem 6.3.1).

The chambers of constant bitangent shapes are interesting not only for computations of the exact shape visible for a given quartic curve, but also for further research in the area of tropical bitangents [MSP22]. Theorem 6.3.1 additionally provides a full list up to S_3-action. This first subsection builds on joint work with Marta Panizzut [GP21a].

Section 6.3.2 investigates the lower dimensional areas in secondary cones of generic triangulations for which the tropical curve does not satisfy the genericity condition. These areas are determined in Proposition 6.3.4.

6.3.1 Hyperplanes of deformation classes

This subsection, which builds on joint work with Marta Panizzut [GP21a], investigates the areas of the secondary cones of unimodular triangulations, in which for every tropical quartic curve the bitangent shapes are constant. There are 128 secondary cones up to S_3-equivalence, for which the whole interior of the cone satisfies this condition. The remaining 1150 secondary cones up to S_3-equivalence are refined by the condition of constant bitangent shapes as determined in Theorem 6.3.1.

The results in this section are important for further research, when there are properties of bitangent shapes that are not constant within a deformation class. One example are arithmetic multiplicities of tropical bitangents as explained below.

By Corollary 5.1.5 the lifting conditions, not only over $\mathbb{R}$ but also over arbitrary Henselian fields K with residue characteristic $\neq 2$, depend solely on the deformation classes. Consequently one might wonder, whether the exact knowledge of which shape a bitangent class attains has any use exceeding the creation of examples. But there is at least one property of bitangent classes that indeed depend on the shape and can vary within a deformation class. When studying bitangent lines to quartic curves in arithmetic geometry, one is interested in the arithmetic multiplicity [LV21, Definition 1.2]. The arithmetic multiplicity of tropical bitangent classes of quartic curves over any field, as investigated in [MSP22], can vary between different shapes in the same deformation class. More precisely, [MSP22] provides examples of shapes with different arithmetic multiplicities that belong to the same deformation class. One of these is given by the shapes (W) and (BB) of deformation class (W...HH)+(xz), which have different arithmetic multiplicities.

As noted in Remark 4.2.4, the proof of Theorem 4.2.3 implies that the deformations of the shapes inside a dual deformation class are described by linear equations. This means that for their investigation we consider hyperplane arrangements secondary cones.

Theorem 6.3.1. *For a given unimodular triangulation $\mathcal{T}$ of $4\Delta_2$ we can subdivide the associated secondary cone $\Sigma(\mathcal{T})$ by hyperplanes, such that for each chamber*

in the hyperplane arrangement the bitangent shapes of the corresponding quartic curves are constant.

The hyperplanes depend on the deformation motifs and are classified for the identity position of the dual deformation motifs in Table 6.4.

Proof. The main argument of the proof is that the deformations between shapes inside a deformation class are described by linear inequalities that provide hyperplanes refining the secondary cone.

We recall that the changes of shapes inside a deformation class arise from the change of relative positions of relevant edges or vertices. In the proof of Theorem 4.2.3, the relevant edges and vertices were identified for every deformation class together with their relative positions by inequalities and which shape these induce.

We give the details of the computation for the hyperplane of deformation class (E F J). For the other cases the method is the same.

We use the notation (λ_{ij}) for a coefficient vector in $\Sigma(\mathcal{T})$ whose coordinates correspond to the lattice points p_{ij} of $4\Delta_2$.

Recall from the proof of Theorem 4.2.3 the following notations:

$$a = (a_x, a_y) := (\overline{p_{1v}p_{1,v+1}p_{20}})^\vee,$$
$$b = (b_x, b_y) := (\overline{p_{20}p_{30}p_{31}})^\vee.$$

The classification then states, that we observe the shapes (E), (F) or (J) depending on the relation between a_y and b_y:

$$a_y < b_y \to \text{Shape (E)},$$
$$a_y = b_y \to \text{Shape (J)},$$
$$a_y > b_y \to \text{Shape (F)}.$$

To determine the hyperplane that separates shape (E) from shape (F) we have to compute the values of a_y and b_y in dependence of the coefficient vector $(\lambda_{ij}) \in \Sigma(\mathcal{T})$.

Note that in order to adhere to the `polymake` convention in which the points in the secondary cone induce subdivisions via the *min*-convention (Remark 6.1.1), the coefficient vector (λ_{ij}) is the vector of valuations of coefficients of a lift. In other words: if (a_{ij}) are the coefficients of a lift of the tropical quartic curve we have $\lambda_{ij} = \text{val}(a_{ij})$. As we draw our quartic curves and tropical bitangents in the *max*-convention, this implies that for the following computation of the coordinates of a and b we have to use $-\lambda_{ij}$. We refer to Remark 2.2.21 for the details of the *min/max*-conventions.

To compute the coordinates of a and b, we recall from Example 2.2.19 how to compute vertices of the tropical curve from the duality. We have to solve the

following equations:

For a :
$$-\lambda_{1v} + a_x + v \cdot a_y = -\lambda_{1,v+1} + a_x + (v+1) \cdot a_y = -\lambda_{20} + 2 \cdot a_x.$$
For b :
$$-\lambda_{20} + 2 \cdot b_x = -\lambda_{30} + 3 \cdot b_x = -\lambda_{31} + 3 \cdot b_x + b_y.$$

This yields:

$$a_y = \lambda_{1,v+1} - \lambda_{1v},$$
$$b_y = \lambda_{31} - \lambda_{30}.$$

Therefore, the hyperplane separating the shapes in deformation class (E F J) is given by $H := \{\lambda_{1,v+1} - \lambda_{1v} - \lambda_{31} + \lambda_{30} = 0\}$, with the negative halfspace $H_{<0}$ corresponding to shape (E), the positive halfspace $H_{>0}$ corresponding to shape (F), and the hyperplane H itself correspond to shape (J). See Figure 6.5 for an example. Table 6.4 states all the linear inequalities describing the different shapes for every deformation class in identity position. $\qquad\square$

The hyperplanes that determine the changes of the shapes for a deformation class are stored in the database as a property of the deformation motif. If a triangulation contains only deformation motifs without hyperplanes, then each of its dual tropical quartic curves has the same collection of shapes of bitangent classes.

Proposition 6.3.2. *There are* 128 *unimodular triangulations modulo S_3 action with dual smooth tropical curves having constant shapes of bitangent classes.*

Proof. This statement can be proven similarly to the Theorems in Section 6.2 by going over the entries of the database collection `Tropical:QuarticCurves` in `polyDB`. For every deformation class that contains only one shape, i.e., for every constant deformation class, we have not assigned a hyperplane. On the other hand, every not constant deformation class has hyperplanes assigned that describe the deformations of the shapes. See Theorem 6.3.1. Thus, we can identify all those unimodular triangulations for which the quartic curves have only constant deformation classes by checking the existence of assigned hyperplanes for each of their seven deformation motifs. If none have assigned hyperplanes, we add the triangulation to our count. The computation yields 128 unimodular triangulations for which we only have constant deformation classes. The `polymake` code and the database identifiers of the cones with constant shapes are available in Appendix B.1.2. $\qquad\square$
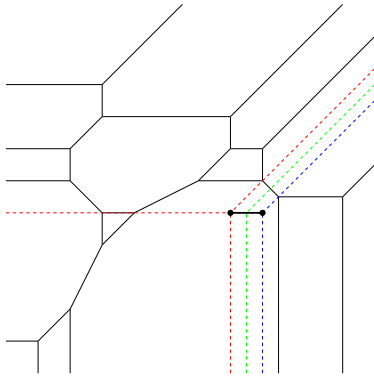
For $-\lambda_1 = (0,5,5,9,8,5,6.5,9,9,4,2,7,8,7,1)$ we have

$$
\begin{aligned}
(\lambda_1)_8 - (\lambda_1)_4 &= -9 + 8 \\
&= -1 \\
&< -0.5 = -7 + 6.5 \\
&= (\lambda_1)_{11} - (\lambda_1)_6,
\end{aligned}
$$

so we see Shape (E).
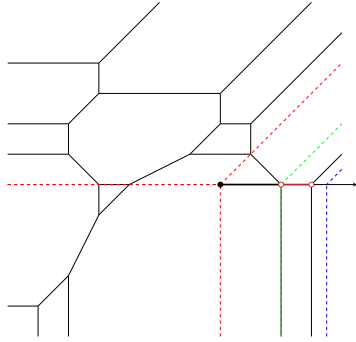
For $-\lambda_2 = (0,5,5,9,8,5,6,9,9,4,2,7,8,7,1)$ we have

$$
\begin{aligned}
(\lambda_2)_8 - (\lambda_2)_4 &= -9 + 8 \\
&= -1 \\
&= -7 + 6 = (\lambda_2)_{11} - (\lambda_2)_6,
\end{aligned}
$$

so we see Shape (J).
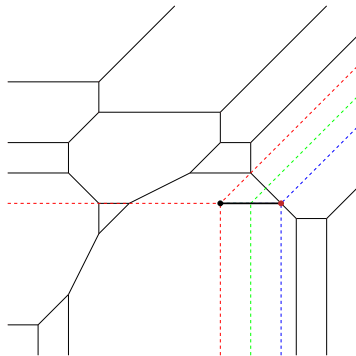
For $-\lambda_3 = (0,5,5,9,8,5,5.5,9,9,4,1,7,8,7,1)$ we have

$$
\begin{aligned}
(\lambda_3)_8 - (\lambda_3)_4 &= -9 + 8 \\
&= -1 \\
&> -1.5 = -7 + 5.5 \\
&= (\lambda_3)_{11} - (\lambda_3)_6,
\end{aligned}
$$

so we see Shape (F).

Figure 6.5: The different shapes that appear for one bitangent class when choosing different edge lengths are given by linear inequalities. Note that here the edge $(\overline{p_{1v}p_{1,v+1}}) = (\overline{p_{11}p_{12}})$, so for a coefficient vector $\lambda \in \Sigma$ we have the hyperplane given by $\lambda_8 - \lambda_4 - \lambda_{11} + \lambda_6 = 0$, since these indices give the position of the corresponding lattice points starting at 0 in the order as fixed in Figure 6.1a.

We can use the `polymake` function `HyperplaneArrangements` [KP20] for the other triangulations, to analyze the chamber decomposition induced by the hyperplanes on their secondary cones as the following example illustrates.

```
fan > $DS = new DualSubdivisionOfQuartic(MAXIMAL_CELLS=>
    [[0,1,2],[1,2,3],[2,3,4],[5,8,9],[9,13,14],[8,11,12],[3,7,8],
    [6,10,11],[3,6,11],[3,7,11],[8,12,13],[3,4,8],[2,5,8],[8,9,13],
[7,8,11],[2,4,8]]);
fan > $DM = $DS->ALL_DEFORMATION_MOTIFS;
fan > print $DM->[6]->TYPE;
W...HH+(xz)
```

The triangulation has a dual deformation motif of type (W...HH)+(xz). We now look at the chamber decomposition of the secondary cone defined by the hyperplane arrangement given by the hyperplanes associated to the deformation class.

```
fan > $Hyps = $DM->[6]->HYPERPLANES;
fan > $SC = $DS->SECONDARY_CONE;
fan > $HA = new HyperplaneArrangement(HYPERPLANES=>$Hyps);
fan > $CD = $HA->CHAMBER_DECOMPOSITION;
```

Consider the first chamber in the arrangement. We extract the corresponding cone and pick a point in its relative interior.

```
fan > $R = $CD->RAYS;
fan > $NR = $R->minor($CD->MAXIMAL_CONES->[0], All);
fan > $C = new Cone(INPUT_RAYS=>$NR, INPUT_LINEALITY=>$HA->
    LINEALITY_SPACE);
fan > $Cone = intersection($C, $SC); #intersect with the secondary
     cone
fan > print $Cone->DIM;
15
fan > $NP = $Cone->REL_INT_POINT;
```

We compute the tropical quartic curve defined by the coordinates of that point and check its bitangent shapes.

```
fan > application 'tropical';
tropical > $H = new QuarticCurve<Min>(COEFFICIENTS=>$NP);
tropical > print $H->BITANGENT_SHAPES;
A B B E F N EE
```

In this example, we see that tropical quartic curves with coefficients in the cone corresponding to the first chamber in the hyperplane arrangement have a bitangent class of shape (EE) within the deformation class (W...HH)+(xz).

deformation class	shape	condition
(B H' H)	(B)	$\lambda_{1,v+1} - \lambda_{1v} > 2\lambda_{31} - \lambda_{40} - \lambda_{21}$
	(H')	$\lambda_{1,v+1} - \lambda_{1v} = 2\lambda_{31} - \lambda_{40} - \lambda_{21}$
	(H)	$\lambda_{1,v+1} - \lambda_{1v} < 2\lambda_{31} - \lambda_{40} - \lambda_{21}$
(B H' H)+(yz)	(B)	$\lambda_{1,v+1} - \lambda_{1v} > 2\lambda_{31} - \lambda_{40} - \lambda_{21}$
	(H')	$\lambda_{1,v+1} - \lambda_{1v} = 2\lambda_{31} - \lambda_{40} - \lambda_{21}$
	(H)	$\lambda_{1,v+1} - \lambda_{1v} < 2\lambda_{31} - \lambda_{40} - \lambda_{21}$
	(H')$_{(yz)}$	$\lambda_{1,v+1} - \lambda_{1v} = -2\lambda_{30} - \lambda_{40} - \lambda_{21}$
	(B)$_{(yz)}$	$\lambda_{1,v+1} - \lambda_{1v} < -2\lambda_{30} - \lambda_{40} - \lambda_{21}$
(B M)+(yz)	(B)	$\lambda_{1,v+1} - \lambda_{1v} > \lambda_{31} - \lambda_{30}$
	(M)	$\lambda_{1,v+1} - \lambda_{1v} = \lambda_{31} - \lambda_{30}$
	(B)$_{(yz)}$	$\lambda_{1,v+1} - \lambda_{1v} < \lambda_{31} - \lambda_{30}$
(D L' Q)	(D)	$-2\lambda_{12} + \lambda_{11} + \lambda_{22} > 2\lambda_{10} - \lambda_{00} - \lambda_{11}$
	(L')	$-2\lambda_{12} + \lambda_{11} + \lambda_{22} = 2\lambda_{10} - \lambda_{00} - \lambda_{11}$
	(Q)	$3\lambda_{11} - 2\lambda_{12} + \lambda_{00} < -2\lambda_{12} + \lambda_{11} + \lambda_{22} < 2\lambda_{10} - \lambda_{00} - \lambda_{11}$
(D L' Q Q' R)	(D)	$-2\lambda_{12} + \lambda_{11} + \lambda_{22} > 2\lambda_{10} - \lambda_{00} - \lambda_{11}$
	(L')	$-2\lambda_{12} + \lambda_{11} + \lambda_{22} = 2\lambda_{10} - \lambda_{00} - \lambda_{11}$
	(Q)	$2\lambda_{01} - \lambda_{00} + \lambda_{11} < -2\lambda_{12} + \lambda_{11} + \lambda_{22} < 2\lambda_{10} - \lambda_{00} - \lambda_{11}$
	(Q')	$2\lambda_{01} - \lambda_{00} + \lambda_{11} = -2\lambda_{12} + \lambda_{11} + \lambda_{22} < 2\lambda_{10} - \lambda_{00} - \lambda_{11}$
	(R)	$-2\lambda_{12} + \lambda_{11} + \lambda_{22} < 2\lambda_{01} - \lambda_{00} - \lambda_{11} < 2\lambda_{10} - \lambda_{00} - \lambda_{11}$
(D L O)	(D)	$-2\lambda_{12} + \lambda_{11} + \lambda_{22} > \lambda_{10} - \lambda_{01}$
	(L)	$-2\lambda_{12} + \lambda_{11} + \lambda_{22} = \lambda_{10} - \lambda_{01}$
	(O)	$-2\lambda_{12} + \lambda_{11} + \lambda_{22} < \lambda_{10} - \lambda_{01}$
(E F J)	(E)	$\lambda_{1,v+1} - \lambda_{1v} < \lambda_{31} - \lambda_{30}$
	(J)	$\lambda_{1,v+1} - \lambda_{1v} = \lambda_{31} - \lambda_{30}$
	(F)	$\lambda_{1,v+1} - \lambda_{1v} > \lambda_{31} - \lambda_{30}$
(G I N)+(xy)	(G)	$\lambda_{10} - \lambda_{01} < -2\lambda_{03} + \lambda_{11} + \lambda_{04} < 2\lambda_{12} - \lambda_{11} - \lambda_{04}$
blue edge $\overline{p_{11}p_{04}}$	(I)	$\lambda_{10} - \lambda_{01} = -2\lambda_{03} + \lambda_{11} + \lambda_{04} < 2\lambda_{12} - \lambda_{11} - \lambda_{04}$

deformation class	shape	condition
	(N)	$-2\lambda_{03} + \lambda_{11} + \lambda_{04} < \lambda_{10} - \lambda_{01} < 2\lambda_{12} - \lambda_{11} - \lambda_{04}$
	(I)$_{(xy)}$	$-2\lambda_{03} + \lambda_{11} + \lambda_{04} < \lambda_{10} - \lambda_{01} = 2\lambda_{12} - \lambda_{11} - \lambda_{04}$
	(G)$_{(xy)}$	$-2\lambda_{03} + \lambda_{11} + \lambda_{04} < 2\lambda_{12} - \lambda_{11} - \lambda_{04} < \lambda_{10} - \lambda_{01}$
(G I N)+(xy) blue edge $\overline{p_{11}p_{22}}$	(G)	$\lambda_{10} - \lambda_{01} < -2\lambda_{12} + \lambda_{11} + \lambda_{22} < 2\lambda_{21} - \lambda_{11} - \lambda_{22}$
	(I)	$\lambda_{10} - \lambda_{01} = -2\lambda_{12} + \lambda_{11} + \lambda_{22} < 2\lambda_{21} - \lambda_{11} - \lambda_{22}$
	(N)	$-2\lambda_{12} + \lambda_{11} + \lambda_{22} < \lambda_{10} - \lambda_{01} < 2\lambda_{21} - \lambda_{11} - \lambda_{22}$
	(I)$_{(xy)}$	$-2\lambda_{12} + \lambda_{11} + \lambda_{22} < \lambda_{10} - \lambda_{01} = 2\lambda_{21} - \lambda_{11} - \lambda_{22}$
	(G)$_{(xy)}$	$-2\lambda_{12} + \lambda_{11} + \lambda_{22} < 2\lambda_{21} - \lambda_{11} - \lambda_{22} < \lambda_{10} - \lambda_{01}$
(G K U T T') blue edge $\overline{p_{11}p_{40}}$	(G)	$2\lambda_{10} - \lambda_{00} - \lambda_{11} < -2\lambda_{21} + \lambda_{11} + \lambda_{40} < 2\lambda_{30} - \lambda_{11} - \lambda_{40}$
	(K)	$2\lambda_{10} - \lambda_{00} - \lambda_{11} = -2\lambda_{21} + \lambda_{11} + \lambda_{40} < 2\lambda_{30} - \lambda_{11} - \lambda_{40}$
	(U)	$-2\lambda_{21} + \lambda_{11} + \lambda_{40} < 2\lambda_{10} - \lambda_{00} - \lambda_{11} < 2\lambda_{30} - \lambda_{11} - \lambda_{40}$
	(T')	$-2\lambda_{21} + \lambda_{11} + \lambda_{40} < 2\lambda_{10} - \lambda_{00} - \lambda_{11} = 2\lambda_{30} - \lambda_{11} - \lambda_{40}$
	(T)	$-2\lambda_{21} + \lambda_{11} + \lambda_{40} < 2\lambda_{30} - \lambda_{11} - \lambda_{40} < 2\lambda_{10} - \lambda_{00} - \lambda_{11}$
(G K U T T') blue edge $\overline{p_{11}p_{22}}$	(G)	$2\lambda_{10} - \lambda_{00} - \lambda_{11} < -2\lambda_{12} + \lambda_{11} + \lambda_{22} < 2\lambda_{21} - \lambda_{11} - \lambda_{22}$
	(K)	$2\lambda_{10} - \lambda_{00} - \lambda_{11} = -2\lambda_{12} + \lambda_{11} + \lambda_{22} < 2\lambda_{21} - \lambda_{11} - \lambda_{22}$
	(U)	$-2\lambda_{12} + \lambda_{11} + \lambda_{22} < 2\lambda_{10} - \lambda_{00} - \lambda_{11} < 2\lambda_{21} - \lambda_{11} - \lambda_{22}$
	(T')	$-2\lambda_{12} + \lambda_{11} + \lambda_{22} < 2\lambda_{10} - \lambda_{00} - \lambda_{11} = 2\lambda_{21} - \lambda_{11} - \lambda_{22}$
	(T)	$-2\lambda_{12} + \lambda_{11} + \lambda_{22} < 2\lambda_{21} - \lambda_{11} - \lambda_{22} < 2\lambda_{10} - \lambda_{00} - \lambda_{11}$
(G K U U' T T' T'' V)+(xy) blue edge $\overline{p_{11}p_{04}}$	(G)	$-2\lambda_{01} + \lambda_{00} + \lambda_{11} < 2\lambda_{10} - \lambda_{00} - \lambda_{11} < -2\lambda_{03} + \lambda_{11} + \lambda_{04} < 2\lambda_{12} - \lambda_{11} - \lambda_{04}$
	(K)	$-2\lambda_{01} + \lambda_{00} + \lambda_{11} < 2\lambda_{10} - \lambda_{00} - \lambda_{11} = -2\lambda_{03} + \lambda_{11} + \lambda_{04} < 2\lambda_{12} - \lambda_{11} - \lambda_{04}$
	(U)	$-2\lambda_{01} + \lambda_{00} + \lambda_{11} < -2\lambda_{03} + \lambda_{11} + \lambda_{04} < 2\lambda_{10} - \lambda_{00} - \lambda_{11} < 2\lambda_{12} - \lambda_{11} - \lambda_{04}$
	(U')	$-2\lambda_{01} + \lambda_{00} + \lambda_{11} = -2\lambda_{03} + \lambda_{11} + \lambda_{04} < 2\lambda_{10} - \lambda_{00} - \lambda_{11} < 2\lambda_{12} - \lambda_{11} - \lambda_{04}$
	(T')	$-2\lambda_{01} + \lambda_{00} + \lambda_{11} < -2\lambda_{03} + \lambda_{11} + \lambda_{04} < 2\lambda_{10} - \lambda_{00} - \lambda_{11} = 2\lambda_{12} - \lambda_{11} - \lambda_{04}$
	(T)	$-2\lambda_{01} + \lambda_{00} + \lambda_{11} < -2\lambda_{03} + \lambda_{11} + \lambda_{04} < 2\lambda_{12} - \lambda_{11} - \lambda_{04} < 2\lambda_{10} - \lambda_{00} - \lambda_{11}$
	(T')$_{(xy)}$	$-2\lambda_{01} + \lambda_{00} + \lambda_{11} = -2\lambda_{03} + \lambda_{11} + \lambda_{04} < 2\lambda_{12} - \lambda_{11} - \lambda_{04} < 2\lambda_{10} - \lambda_{00} - \lambda_{11}$
	(T'')$_{(xy)}$	$-2\lambda_{01} + \lambda_{00} + \lambda_{11} = -2\lambda_{03} + \lambda_{11} + \lambda_{04} = 2\lambda_{12} - \lambda_{11} - \lambda_{04} < 2\lambda_{10} - \lambda_{00} - \lambda_{11}$
	(V)	$-2\lambda_{03} + \lambda_{11} + \lambda_{04} < -2\lambda_{01} + \lambda_{00} + \lambda_{11} < 2\lambda_{10} - \lambda_{00} - \lambda_{11} < 2\lambda_{12} - \lambda_{11} - \lambda_{04}$

deformation class	shape	condition
	$(U')_{(xy)}$	$-2\lambda_{03}+\lambda_{11}+\lambda_{04} < -2\lambda_{01}+\lambda_{00}+\lambda_{11} < 2\lambda_{10}-\lambda_{00}-\lambda_{11} = 2\lambda_{12}-\lambda_{11}-\lambda_{04}$
	$(U)_{(xy)}$	$-2\lambda_{03}+\lambda_{11}+\lambda_{04} < -2\lambda_{01}+\lambda_{00}+\lambda_{11} < 2\lambda_{12}-\lambda_{11}-\lambda_{04} < 2\lambda_{10}-\lambda_{00}-\lambda_{11}$
	$(K)_{(xy)}$	$-2\lambda_{03}+\lambda_{11}+\lambda_{04} < -2\lambda_{01}+\lambda_{00}+\lambda_{11} = 2\lambda_{12}-\lambda_{11}-\lambda_{04} < 2\lambda_{10}-\lambda_{00}-\lambda_{11}$
	$(G)_{(xy)}$	$-2\lambda_{03}+\lambda_{11}+\lambda_{04} < 2\lambda_{12}-\lambda_{11}-\lambda_{04} < -2\lambda_{01}+\lambda_{00}+\lambda_{11} < 2\lambda_{10}-\lambda_{00}-\lambda_{11}$
(G K U U' T T' T'' V)+(xy) blue edge $\overline{p_{11}p_{22}}$	(G)	$-2\lambda_{01}+\lambda_{00}+\lambda_{11} < 2\lambda_{10}-\lambda_{00}-\lambda_{11} < -2\lambda_{12}+\lambda_{11}+\lambda_{22} < 2\lambda_{21}-\lambda_{11}-\lambda_{22}$
	(K)	$-2\lambda_{01}+\lambda_{00}+\lambda_{11} < 2\lambda_{10}-\lambda_{00}-\lambda_{11} = -2\lambda_{12}+\lambda_{11}+\lambda_{22} < 2\lambda_{21}-\lambda_{11}-\lambda_{22}$
	(U)	$-2\lambda_{01}+\lambda_{00}+\lambda_{11} < -2\lambda_{12}+\lambda_{11}+\lambda_{22} < 2\lambda_{10}-\lambda_{00}-\lambda_{11} < 2\lambda_{21}-\lambda_{11}-\lambda_{22}$
	(U')	$-2\lambda_{01}+\lambda_{00}+\lambda_{11} = -2\lambda_{12}+\lambda_{11}+\lambda_{22} < 2\lambda_{10}-\lambda_{00}-\lambda_{11} < 2\lambda_{21}-\lambda_{11}-\lambda_{22}$
	(T')	$-2\lambda_{01}+\lambda_{00}+\lambda_{11} < -2\lambda_{12}+\lambda_{11}+\lambda_{22} < 2\lambda_{21}-\lambda_{11}-\lambda_{22} < 2\lambda_{10}-\lambda_{00}-\lambda_{11}$
	(T)	$-2\lambda_{01}+\lambda_{00}+\lambda_{11} < -2\lambda_{12}+\lambda_{11}+\lambda_{22} < 2\lambda_{21}-\lambda_{11}-\lambda_{22} = 2\lambda_{10}-\lambda_{00}-\lambda_{11}$
	$(T')_{(xy)}$	$-2\lambda_{01}+\lambda_{00}+\lambda_{11} = -2\lambda_{12}+\lambda_{11}+\lambda_{22} < 2\lambda_{21}-\lambda_{11}-\lambda_{22} < 2\lambda_{10}-\lambda_{00}-\lambda_{11}$
	$(T'')_{(xy)}$	$-2\lambda_{01}+\lambda_{00}+\lambda_{11} = -2\lambda_{12}+\lambda_{11}+\lambda_{22} < 2\lambda_{21}-\lambda_{11}-\lambda_{22} = 2\lambda_{10}-\lambda_{00}-\lambda_{11}$
	(V)	$-2\lambda_{12}+\lambda_{11}+\lambda_{22} < -2\lambda_{01}+\lambda_{00}+\lambda_{11} < 2\lambda_{10}-\lambda_{00}-\lambda_{11} < 2\lambda_{21}-\lambda_{11}-\lambda_{22}$
	$(U')_{(xy)}$	$-2\lambda_{12}+\lambda_{11}+\lambda_{22} < -2\lambda_{01}+\lambda_{00}+\lambda_{11} < 2\lambda_{21}-\lambda_{11}-\lambda_{22} < 2\lambda_{10}-\lambda_{00}-\lambda_{11}$
	$(U)_{(xy)}$	$-2\lambda_{12}+\lambda_{11}+\lambda_{22} < -2\lambda_{01}+\lambda_{00}+\lambda_{11} < 2\lambda_{10}-\lambda_{00}-\lambda_{11} < 2\lambda_{21}-\lambda_{11}-\lambda_{22}$
	$(K)_{(xy)}$	$-2\lambda_{12}+\lambda_{11}+\lambda_{22} < -2\lambda_{01}+\lambda_{00}+\lambda_{11} = 2\lambda_{10}-\lambda_{00}-\lambda_{11} < 2\lambda_{21}-\lambda_{11}-\lambda_{22}$
	$(G)_{(xy)}$	$-2\lambda_{12}+\lambda_{11}+\lambda_{22} < -2\lambda_{01}+\lambda_{00}+\lambda_{11} < 2\lambda_{21}-\lambda_{11}-\lambda_{22} < 2\lambda_{10}-\lambda_{00}-\lambda_{11}$
(W X Y EE GG)	(W)	$\lambda_{20}-\lambda_{11} < \lambda_{10}-\lambda_{01} < -2\lambda_{12}+\lambda_{13}+\lambda_{20} < 2\lambda_{21}-\lambda_{20}-\lambda_{13}$
	(X)	$\lambda_{20}-\lambda_{11} < \lambda_{10}-\lambda_{01} = -2\lambda_{12}+\lambda_{13}+\lambda_{20} < 2\lambda_{21}-\lambda_{20}-\lambda_{13}$
	(Y)	$\lambda_{20}-\lambda_{11} < -2\lambda_{12}+\lambda_{13}+\lambda_{20} < \lambda_{10}-\lambda_{01} < 2\lambda_{21}-\lambda_{20}-\lambda_{13}$
	(EE)	$\lambda_{20}-\lambda_{11} < -2\lambda_{12}+\lambda_{13}+\lambda_{20} < 2\lambda_{21}-\lambda_{20}-\lambda_{13} < \lambda_{10}-\lambda_{01}$
	(GG)	$\lambda_{20}-\lambda_{11} < -2\lambda_{12}+\lambda_{13}+\lambda_{20} < 2\lambda_{21}-\lambda_{20}-\lambda_{13} = \lambda_{10}-\lambda_{01}$
(W...HH)+(xz)	(W)	$\lambda_{20}-\lambda_{11} < \lambda_{10}-\lambda_{01} < -2\lambda_{21}+\lambda_{31}+\lambda_{20} < 2\lambda_{30}-\lambda_{20}-\lambda_{31}$ $-2\lambda_{10}+\lambda_{01}+\lambda_{20} < 2\lambda_{11}-\lambda_{20}-\lambda_{01} < \lambda_{31}-\lambda_{30} < \lambda_{21}-\lambda_{20}$
	(X)	$\lambda_{20}-\lambda_{11} < \lambda_{10}-\lambda_{01} < -2\lambda_{21}+\lambda_{31}+\lambda_{20} < 2\lambda_{30}-\lambda_{20}-\lambda_{31}$ $-2\lambda_{10}+\lambda_{01}+\lambda_{20} < 2\lambda_{11}-\lambda_{20}-\lambda_{01} = \lambda_{31}-\lambda_{30} < \lambda_{21}-\lambda_{20}$
	(Y)	$\lambda_{20}-\lambda_{11} < \lambda_{10}-\lambda_{01} < -2\lambda_{21}+\lambda_{31}+\lambda_{20} < 2\lambda_{30}-\lambda_{20}-\lambda_{31}$

deformation class	shape	condition
	(Z)	$-2\lambda_{10}+\lambda_{01}+\lambda_{20} < \lambda_{31}-\lambda_{30} < 2\lambda_{11}-\lambda_{20}-\lambda_{01} < \lambda_{21}-\lambda_{20}$
		$\lambda_{20}-\lambda_{11} < \lambda_{10}-\lambda_{01} = -2\lambda_{21}+\lambda_{31}+\lambda_{20} < 2\lambda_{30}-\lambda_{20}-\lambda_{31}$
	(AA)	$-2\lambda_{10}+\lambda_{01}+\lambda_{20} < 2\lambda_{11}-\lambda_{20}-\lambda_{01} = \lambda_{31}-\lambda_{30} < \lambda_{21}-\lambda_{20}$
		$\lambda_{20}-\lambda_{11} < \lambda_{10}-\lambda_{01} = -2\lambda_{21}+\lambda_{31}+\lambda_{20} < 2\lambda_{30}-\lambda_{20}-\lambda_{31}$
	(BB)	$\lambda_{20}-\lambda_{11} < -2\lambda_{21}+\lambda_{31}+\lambda_{20} < \lambda_{10}-\lambda_{01} < 2\lambda_{11}-\lambda_{20}-\lambda_{01} < \lambda_{21}-\lambda_{20}$
		$-2\lambda_{10}+\lambda_{01}+\lambda_{20} < \lambda_{31}-\lambda_{30} < 2\lambda_{11}-\lambda_{20}-\lambda_{01} < \lambda_{21}-\lambda_{20}$
	(CC)	$\lambda_{20}-\lambda_{11} < -2\lambda_{21}+\lambda_{31}+\lambda_{20} < 2\lambda_{30}-\lambda_{20}-\lambda_{31} < \lambda_{10}-\lambda_{01}$
		$-2\lambda_{10}+\lambda_{01}+\lambda_{20} < \lambda_{31}-\lambda_{30} < 2\lambda_{11}-\lambda_{20}-\lambda_{01} < \lambda_{21}-\lambda_{20}$
	(DD)	$\lambda_{20}-\lambda_{11} < -2\lambda_{21}+\lambda_{31}+\lambda_{20} < \lambda_{10}-\lambda_{01} = 2\lambda_{30}-\lambda_{20}-\lambda_{31}$
		$-2\lambda_{10}+\lambda_{01}+\lambda_{20} < \lambda_{31}-\lambda_{30} < 2\lambda_{11}-\lambda_{20}-\lambda_{01} < \lambda_{21}-\lambda_{20}$
	(EE)	$\lambda_{20}-\lambda_{11} < -2\lambda_{21}+\lambda_{31}+\lambda_{20} < 2\lambda_{30}-\lambda_{20}-\lambda_{31} < \lambda_{10}-\lambda_{01}$
		$-2\lambda_{10}+\lambda_{01}+\lambda_{20} < 2\lambda_{11}-\lambda_{20}-\lambda_{01} < \lambda_{31}-\lambda_{30} < \lambda_{21}-\lambda_{20}$
	(FF)	$\lambda_{20}-\lambda_{11} < -2\lambda_{21}+\lambda_{31}+\lambda_{20} < 2\lambda_{30}-\lambda_{20}-\lambda_{31} < \lambda_{10}-\lambda_{01}$
		$-2\lambda_{10}+\lambda_{01}+\lambda_{20} < 2\lambda_{11}-\lambda_{20}-\lambda_{01} < \lambda_{31}-\lambda_{30} < \lambda_{21}-\lambda_{20}$
	(GG)	$\lambda_{20}-\lambda_{11} < -2\lambda_{21}+\lambda_{31}+\lambda_{20} < \lambda_{10}-\lambda_{01} = 2\lambda_{30}-\lambda_{20}-\lambda_{31}$
		$-2\lambda_{10}+\lambda_{01}+\lambda_{20} < 2\lambda_{11}-\lambda_{20}-\lambda_{01} < \lambda_{31}-\lambda_{30} < \lambda_{21}-\lambda_{20}$
	(HH)	$\lambda_{20}-\lambda_{11} < -2\lambda_{21}+\lambda_{31}+\lambda_{20} < \lambda_{10}-\lambda_{01} = 2\lambda_{30}-\lambda_{20}-\lambda_{31}$
		$-2\lambda_{10}+\lambda_{01}+\lambda_{20} < 2\lambda_{11}-\lambda_{20}-\lambda_{01} < \lambda_{31}-\lambda_{30} < \lambda_{21}-\lambda_{20}$
	$+(x\,z)$	to get all the $(x\,z)$ transposes, apply $(x\,z)$ to the conditions.

Table 6.4: The coefficient conditions for the shape changes of the bitangents for the identity representative to each deformation class with more than one shape. Note that $\lambda_{ij} = \mathrm{val}(a_{ij})$.
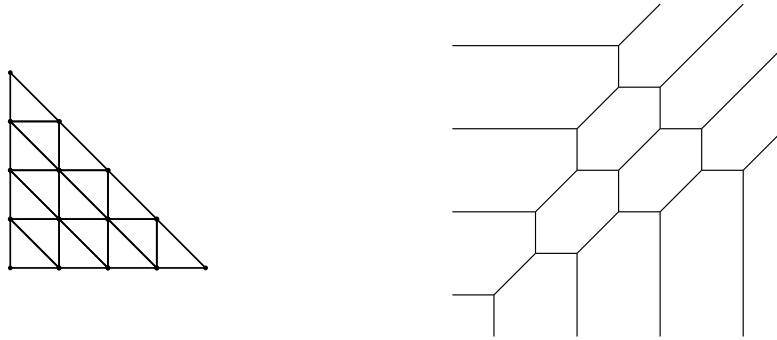
Figure 6.6: A tropical quartic curve not satisfying the genericity conditions from Remark 3.3.2 together with its generic unimodular triangulation.

6.3.2 Hyperplanes for (C) non-generic

This section focuses on the areas in secondary cones corresponding to generic unimodular triangulations for which a point in the area induces a tropical curve that does not satisfy the genericity constraint (i) from Remark 5.2.1. When applying the results of Chapter 5 on a tropical quartic curve, or more generally on a combinatorial type, it is important to be able to check the genericity for a chosen tropical coefficient vector.

Further, an understanding of these areas might help to understand the full dimensional secondary cones for which every point induces a non-generic tropical quartic curve (Remark 5.2.1).

Definition 6.3.3. We call a full-dimensional secondary cone *generic* if the corresponding unimodular triangulation is not equivalent via S_3 to one of the eight non-generic triangulations as mentioned in Remark 5.2.1.

Recall that a generic triangulation does not necessarily imply that every dual tropical quartic curve satisfies the genericity conditions. As an example consider the quartic curve in Figure 6.6 which has as dual subdivision the honeycomb triangulation which is generic.

In Remark 5.2.1, we claimed that these areas in generic secondary cones for which the tropical curves are non-generic, because they violate condition (i) in Remark 3.3.2, are lower dimensional. Note, that this situation can only occur if the triangulation corresponding to the secondary cone contains the triangle $(\overline{p_{11}p_{12}p_{21}})$. In this case, we say the secondary cone *allows bitangent shape (C)*. The following proposition contains a full description of these non-genericity areas.

Proposition 6.3.4. *The areas of non-generic curves in a generic secondary cone that allows bitangent shape (C) are intersections of the cone with at most three half-hyperplanes. They are described in Table 6.5.*
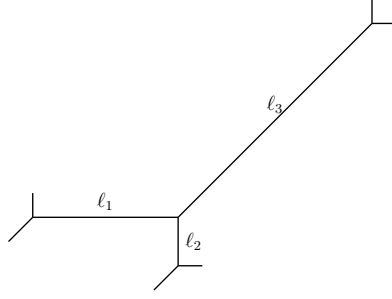
Figure 6.7: Illustration of the part of the tropical quartic curve relevant for a bitangent class of shape (C) together with the euclidean edge lengths.

$\{\boldsymbol{\mu_3} > \boldsymbol{\mu_2} = \boldsymbol{\mu_1}\}$
$\lambda_{21} - 2\lambda_{11} + \lambda_{0i} - (i-1)(\lambda_{12} - \lambda_{11}) = \lambda_{12} - 2\lambda_{11} + \lambda_{j0} - (j-1)(\lambda_{21} - \lambda_{11})$
$(k-3)\lambda_{12} - (k-1)\lambda_{21} + \lambda_{k,4-k} + \lambda_{11} > \lambda_{12} - 2\lambda_{11} + \lambda_{j0} - (j-1)(\lambda_{21} - \lambda_{11})$
$\{\boldsymbol{\mu_2} > \boldsymbol{\mu_1} = \boldsymbol{\mu_3}\}$
$\lambda_{21} - 2\lambda_{11} + \lambda_{0i} - (i-1)(\lambda_{12} - \lambda_{11}) = (k-3)\lambda_{12} - (k-1)\lambda_{21} + \lambda_{k,4-k} + \lambda_{11}$
$\lambda_{12} - 2\lambda_{11} + \lambda_{j0} - (j-1)(\lambda_{21} - \lambda_{11}) > \lambda_{21} - 2\lambda_{11} + \lambda_{0i} - (i-1)(\lambda_{12} - \lambda_{11})$
$\{\boldsymbol{\mu_1} > \boldsymbol{\mu_3} = \boldsymbol{\mu_2}\}$
$\lambda_{12} - 2\lambda_{11} + \lambda_{j0} - (j-1)(\lambda_{21} - \lambda_{11}) = (k-3)\lambda_{12} - (k-1)\lambda_{21} + \lambda_{k,4-k} + \lambda_{11}$
$\lambda_{21} - 2\lambda_{11} + \lambda_{0i} - (i-1)(\lambda_{12} - \lambda_{11}) > (k-3)\lambda_{12} - (k-1)\lambda_{21} + \lambda_{k,4-k} + \lambda_{11}$

Table 6.5: The non-generic areas are given by intersecting the three half-hyperplanes as given above with the secondary cone that allows shape (C). Here, $\lambda_{ij} = \mathrm{val}(a_{ij})$.

Proof. Let $\mathcal{T}$ be a generic triangulation that contains the triangle $(\overline{p_{11}p_{12}p_{21}})$. The areas in the secondary cone of $\mathcal{T}$ for which the elements induce a non-generic tropical quartic curve can be computed by computing the hyperplanes that determine whether two of the edges adjacent to the vertex v have the same lattice length.

Let ℓ_1, ℓ_2, ℓ_3 denote the euclidean lengths of the edges of direction $-e_1, -e_2$ and $e_1 + e_2$. See Figure 6.7. Let μ_1, μ_2 and μ_3 denote the lattice lengths. Then we know:

$$\begin{aligned} \mu_1 &= \ell_1, \\ \mu_2 &= \ell_2, \\ \mu_3 &= \frac{1}{\sqrt{2}}\ell_3. \end{aligned}$$

Now we have to compute the hyperplanes for which two of the lengths are equal:

$$H_1 := \{\mu_1 = \mu_2\}, \ H_2 := \{\mu_1 = \mu_3\}, \ H_3 := \{\mu_2 = \mu_3\}.$$

Thus, the areas of non-generic curves will be intersections of the relevant secondary cone with the three half-hyperplanes:

$$H_1 \cap \{\mu_3 > \mu_2\},$$
$$H_2 \cap \{\mu_2 > \mu_1\},$$
$$H_3 \cap \{\mu_1 > \mu_3\}.$$

In order to obtain equations for the three half-hyperplanes that we can apply to the secondary cone $\Sigma(\mathcal{T})$, we have to compute μ_1, μ_2 and μ_3 from in dependence of the *min*-convention coefficients $(\lambda_{ij}) \in \Sigma(\mathcal{T})$. This works via the same strategy as the computation of the hyperplanes in the proof of Theorem 6.3.1. We note:

$$\mu_1 := \overline{(p_{11}p_{12}p_{21})}_x^{\vee} - \overline{(p_{0i}p_{11}p_{12})}_x^{\vee},$$
$$\mu_2 := \overline{(p_{11}p_{12}p_{21})}_y^{\vee} - \overline{(p_{j0}p_{11}p_{21})}_y^{\vee},$$
$$\mu_3 := \frac{1}{\sqrt{2}}\sqrt{(\overline{(p_{11}p_{12}p_{21})}_x^{\vee} - \overline{(p_{k,4-k}p_{21}p_{12})}_x^{\vee})^2 + (\overline{(p_{11}p_{12}p_{21})}_y^{\vee} - \overline{(p_{k,4-k}p_{21}p_{12})}_y^{\vee})^2}.$$

Here i, j, k are used as in the proof of Proposition 5.1.3, only that we allow $i, j, k \in \{0,1,2,3,4\}$, that means this computations works independently of the identity position of the dual deformation motif of shape (C). Computing the vertices $\overline{(p_{0i}p_{11}p_{12})}^{\vee}$, $\overline{(p_{j0}p_{11}p_{21})}^{\vee}$, $\overline{(p_{k,4-k}p_{21}p_{12})}^{\vee}$ and $\overline{(p_{11}p_{12}p_{21})}^{\vee}$ as described in Example 2.2.19, we obtain:

$$\mu_1 := \lambda_{21} - 2\lambda_{11} + \lambda_{0i} - (i-1)(\lambda_{12} - \lambda_{11}),$$
$$\mu_2 := \lambda_{12} - 2\lambda_{11} + \lambda_{j0} - (j-1)(\lambda_{21} - \lambda_{11}),$$
$$\mu_3 := (k-3)\lambda_{12} - (k-1)\lambda_{21} + \lambda_{k,4-k} + \lambda_{11},$$

where $\lambda_{ij} = \mathrm{val}(a_{ij})$. Hence, the areas in the secondary cone that do not give generic curves are as described in Table 6.5. $\qquad \square$

Example 6.3.5. The *min*-convention coefficients for the tropical quartic curve depicted in Figure 6.6 are $w = (5,2,2,1,0,1,2,0,0,2,5,2,1,2,5)$, ordered as in Figure 6.1a. From the subdivision we read off that $i = j = k = 2$ and we thus have the following formula for the lattice lengths μ_1, μ_2, μ_3:

$$\mu_1 := \lambda_{21} - 2\lambda_{11} + \lambda_{02} - (\lambda_{12} - \lambda_{11}),$$
$$\mu_2 := \lambda_{12} - 2\lambda_{11} + \lambda_{20} - (\lambda_{21} - \lambda_{11}),$$
$$\mu_3 := -\lambda_{12} - \lambda_{21} + \lambda_{22} + \lambda_{11}.$$

We substitute the entries of w into the formula according to the ordering and obtain

$$\mu_1 = 0 - 2 \cdot 0 + 1 - (1 \cdot (0 - 0)) = 1,$$
$$\mu_2 = 0 - 2 \cdot 0 + 1 - 1 \cdot (0 - 0) = 1,$$
$$\mu_3 = -1 \cdot 0 - 1 \cdot 0 + 1 + 0 = 1.$$

So w is indeed contained in all three half-hyperplanes.

We know the lifting conditions for the bitangent class of shape (C) outside of these half-hyperplanes in the secondary cone. Moreover, the lifting conditions are constant in the secondary cone apart for the non-genericity areas. Since these areas are of codimension 1, we state the following open problem:

Problem 6.3.6. Do the lifting conditions of shape (C) in generic position extend to the half-hyperplanes describing the non-generic areas?

An answer to this problem might open new ways to tackle Problem 6.2.4 of the lifting conditions of shape (C) for non-generic full-dimensional secondary cones.

Part II

Towards tropically counting binodal surfaces

141

Chapter 7

Preliminaries

In this chapter, we provide background on tropical singular surfaces and the theory of their enumeration. First, we define tropical singular surfaces and recall what is known about them in Section 7.1. Then, lattice paths and points in Mikhalkin position are defined in Section 7.2. They form one of the key tools for the enumeration of tropical surfaces. In Section 7.3, we introduce another key tool: the concept of tropical floor plans for counting singular surfaces.

The main references for this chapter are [MMS12, MMS18, MMSS22, BG20]. The results and proofs in the following chapters build on the results, notation and definitions introduced here.

Notation 7.0.1. In Part II of this thesis, we fix $\mathbb{K} = \mathbb{C}\{\{t\}\}$ the field of complex Puiseux-series with its natural non-trivial valuation; see Example 2.2.9.

7.1 Tropical singular surfaces

This section introduces the notions of tropical singular surfaces, of their support and of the tropical discriminant. We recall from Section 2.2.3 that, by definition, a tropical surface is smooth if its dual subdivision is a unimodular triangulation. This section further recalls the results from [MMS12] on the classification of isolated nodes in tropical singular surfaces via circuits.

Definition 7.1.1. Let S be a tropical surface in $\mathbb{R}^3$. We say that S is a *tropical singular surface*, if there exists an algebraic variety X in $\mathbb{K}^3$ such that $S = \mathrm{Trop}(X)$ and X is a singular surface. A point on S is a *tropical singularity* or *tropical node* if it is the tropicalization of a singularity/node of a lift of S.

Note that for tropical smooth hypersurfaces we know that every lift has to be algebraically smooth. The same is not true for tropical singular surfaces: There can be both smooth and singular lifts. For the definition of a lift, see Definition 2.2.12.

Definition 7.1.2. For a hypersurface $V(f) \subset \mathbb{K}^3$ with $f = \sum_{(i,j,k) \in \mathbb{N}^3} a_{ijk} x^i y^j z^k$ we call the set $\{(i,j,k) \in \mathbb{N}^3 | a_{ijk} \neq 0\}$ the *support of the hypersurface* or the *support of the polynomial f*.

The Newton polytope Ω of $V(f)$ is the convex hull of the support of f, as can be seen by comparing the above with Definition 2.2.13. By abuse of notation we will sometimes use the expression Ω *is the support of f*.

Definition 7.1.3. Let Ω be a lattice polytope with $\Omega \cap \mathbb{Z}^3 = \{\omega_0, \dots, \omega_{N+1}\}$. Consider the set of singular surfaces with support $\Omega \cap \mathbb{Z}^3$ that have a singularity in the torus $(\mathbb{K}^*)^3$, where $\mathbb{K}^* := \mathbb{K} \setminus \{0\}$:

$$
\begin{aligned}
\operatorname{Sing}_{\text{aff}}(\Omega) = & \{(a_{\omega_0}, \dots, a_{\omega_{N+1}}) \in (\mathbb{K}^*)^{N+2} \mid V(f) \text{ with } f = \sum_{i=0}^{N+1} a_{\omega_i} \underline{x}^{\omega_i} \text{ is singular} \\
& \text{at a point } (x\,y\,z) \in (\mathbb{K}^*)^3\} \\
= & V(f, \frac{\partial f}{\partial x}, \frac{\partial f}{\partial y}, \frac{\partial f}{\partial z}, 1 - txyz) \cap \mathbb{K}[a_{\omega_0}, \dots, a_{\omega_{N+1}}].
\end{aligned}
$$

This is a variety. Multiplying all the coordinates a_{ω_i} with a non-zero scalar does not change the support of the surface or the existence of the singularity. Therefore, we can consider this as a projective variety:

$$
\begin{aligned}
\operatorname{Sing}(\Omega) = & \{(a_{\omega_0} : \dots : a_{\omega_{N+1}}) \in \mathbb{P}^{N+1} \mid \text{ all } a_{\omega_i} \neq 0, \text{ and } V(f) \text{ with } f = \sum_{i=0}^{N+1} a_{\omega_i} \underline{x}^{\omega_i} \\
& \text{is singular at a point } (x\,y\,z) \in (\mathbb{K}^*)^3\} \\
= & (\operatorname{Sing}_{\text{aff}}(\Omega)/\sim) \setminus V(a_{\omega_0} \cdots a_{\omega_{N+1}}).
\end{aligned}
$$

We call $\operatorname{Sing}(\Omega)$ the *discriminant of hypersurfaces of support $\Omega \cap \mathbb{Z}^3$*.

The *tropical discriminant* is its tropicalization:

$$
\operatorname{Trop}(\operatorname{Sing}(\Omega)) \subset \mathbb{R}^{N+2}/(1,\dots,1)\mathbb{R}.
$$

Since $\operatorname{Sing}(\Omega) \subset \mathbb{P}^{N+1} \setminus V(X_0 \cdot \dots \cdot X_{N+1})$, its tropicalization lives in $\mathbb{R}^{N+2}$.

We know from Section 2.2.2 that multiplication becomes addition under tropicalization. Hence, taking the quotient with respect to multiplication with a non-zero scalar is tropically mirrored by taking the quotient with the space generated by the all one vector $(1,\dots,1)\mathbb{R}$. The arising space $\mathbb{R}^{N+2}/(1,\dots,1)\mathbb{R}$ is consequently called the *tropical projective torus*.

Moreover, for a point in $\operatorname{Sing}(\Omega)$ the tropicalization of the corresponding surface has a tropical singularity in $\mathbb{R}^3$, since every surface with coefficient vector in $\operatorname{Sing}(\Omega)$

has a singularity in the torus $(\mathbb{K}^*)^3$ which tropicalizes to a dense subset of $\mathbb{R}^3$ (Section 2.2.2).

Remark 7.1.4. It follows from [GKZ94, 10.1.2] that $\mathrm{Trop}(\mathrm{Sing}(\Omega))$ is a subfan of the codimension 1 skeleton of the secondary fan of Ω.

Remark 7.1.5. If a tropical singular surface satisfies point conditions in general position, all lattice points in the dual subdivision of S are visible (Definition 2.1.9), and the corresponding secondary cone is of codimension 1. In particular, the dual subdivision of S contains exactly one of the 5 circuits depicted in Figure 7.1 and all polytopes in the subdivision that do not contain the circuit are unimodular simplices.

Circuit (A)   Circuit (B)   Circuit (C)   Circuit (D)   Circuit (E)
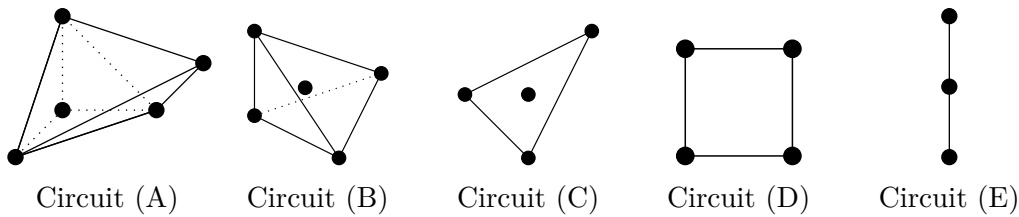
Figure 7.1: Circuits that encode a single node inside a dual subdivision

Theorem 7.1.6 ([MMS12, Theorem 2 and 4])**.** *Let S be a tropical surface with Newton polytope Ω satisfying $|\Omega \cap \mathbb{Z}^3| - 2$ point conditions in general position. Then S is a tropical singular surface if and only if it contains one of the circuits from Figure 7.1 as described below:*

1. *Circuit (A) or (B) have to satisfy no additional conditions.*

2. *Circuit (C) lies*

   a) *not on the boundary of Ω, then it does not have to satisfy additional conditions.*

   b) *on the boundary of Ω, and appears in the subdivision as the base triangle of a tetrahedron $P \subsetneq \Omega$ of normalized volume $\mathrm{vol}(P) = 9$.*

3. *Circuit (D) does not lie on the boundary of Ω.*

4. *Circuit (E) is contained in the subdivision*

   a) *together with either 3 lattice points such that any two of these together with the circuit span $\mathbb{R}^3$.*

   b) *together with 4 lattice points of which exactly 2 lie on a plane with the circuit and the other 2 lie outside of this plane.*

The circuits in their perspective positions encode a tropical singularity. The following theorem describes the position of the tropical singularity in the surface depending on the circuit and its position.

Theorem 7.1.7 ([MMS12, Theorem 2])**.** *Let S be a singular tropical surface satisfying point conditions in general position. Then S contains only finitely many singular points. Their possible locations depend on the circuit and how it is contained in the subdivision:*

1. *Circuit (A) or (B) is contained in the subdivision. The dual cell of the circuit is a vertex V of the tropical surface S and this vertex is the only singular point.*

2. *Circuit (C) is contained in the subdivision*

   a) *as in Theorem 7.1.6 (2a), i.e., as the base triangle of a tetrahedron in the subdivision. Then there is a singularity on the edge E dual to the circuit whose distance from the vertex of E depends on six coefficients of the tropical polynomial.*

   b) *as in Theorem 7.1.6 (2b), i.e., as the base triangle of two tetrahedra in the subdivision. Let E be the edge dual to the circuit. Either there is a singularity at the midpoint of E or at points which divide E with the ration $3:1$ or the edge E admits finitely many (bounded or unbounded) extensions to a virtual edge with a singularity at the positions described for (2a).*

3. *Circuit (D) is contained in the subdivision as in Theorem 7.1.6 (3), i.e., as the base parallelogram for two pyramids. Then S contains a unique singular point which is the midpoint of the edge E dual the circuit.*

4. *Circuit (E) is contained in the subdivision as in Theorem 7.1.6 (4). The dual cell to circuit (E) is a 2-dimensional cell of S. If this cell is a triangle or trapeze, there is a singular point at the weighted barycenter resp. generalized midpoint (see explanation below).*

   An arbitrary 2-dimensional cell dual to circuit (E) admits finitely many extensions to a triangle or a trapeze, with a singularity at the position described above.

   The generalized midpoint *of a trapeze is the midpoint of the line segment parallel to the two parallel edges on the same distance to the two parallel edges of the trapeze. The* weighted barycenter *of a triangle is the weighted sum of the vertices, where each vertex is weighted with the area of the projection (along circuit (E)) of the polytope dual to the vertex in the dual subdivision.*

7.2 Lattice paths

This section introduces a special point configuration called Mikhalkin position. In this position, the points are situated such that they are algebraically in general position and their tropicalization is tropically in general position. This allows us to draw conclusions from the counting results in tropical geometry towards the answer of the enumeration problem in algebraic geometry.

Further, we see how points in Mikhalkin position induce lattice paths for the dual subdivisions of tropical surfaces and how this can determine the subdivision.

Definition 7.2.1 ([MMS18, Section 3.1], points in Mikhalkin position). For a point configuration $\mathbf{p} = (p_1,...,p_n)$ of n points in $\mathbb{K}^3$, we denote by $q_i = \text{Trop}(p_i) \in \mathbb{R}^3$ for $i = 1,...,n$ the tropicalized points. We say $\mathbf{p}$ is in *Mikhalkin position* if the p_i are in general position in $\mathbb{K}^3$ and the q_i are distributed with growing distances along a line $\{\lambda \cdot (1,\eta,\eta^2)|\lambda \in \mathbb{R}\} \subset \mathbb{R}^3$, where $0 < \eta \ll 1$.

We say a tropical surface *passes through points in Mikhalkin position* if it passes through the q_i.

By abuse of notation we will also use the expression *in Mikhalkin position* with respect to the tropicalized points q_i.

To find such a point configuration is possible by [Mik05, Theorem 1, Section 7.1].

Remark 7.2.2. For a surface $S \subset \mathbb{K}^3$ with δ nodes and with Newton polytope Ω, we have to fix $|\Omega \cap \mathbb{Z}^3| - \delta - 1$ many points in general position to obtain a finite counting problem [CC99].

For surfaces of degree d, this is $\binom{d+3}{3} - \delta - 1$ since the Newton polytope $\Omega = d\Delta_3$ has $\binom{d+3}{3}$ lattice points.

Definition 7.2.3 ([MMS18, Section 3.2], Lattice path). Let $v \in \mathbb{R}^3$ be a fixed vector. Consider the partial order $\succ$ in $\mathbb{R}^3$ where $u \succ u' \Leftrightarrow \langle u - u', v \rangle > 0$. Order the points of $\Omega \cap \mathbb{Z}^3$ according to $\succ$:

$$\Omega \cap \mathbb{Z}^3 = \{w_0,...,w_{N+1}\}, w_i \prec w_{i+1} \text{ for all } i = 0,...,N.$$

Given a subset $A \subset \Omega \cap \mathbb{Z}^3$ consisting of $m \geq 2$ points $a_1 \prec a_2 \prec \cdots \prec a_m$, we call an ordered subset of the set of segments $P(A) := \{[a_i, a_{i+1}] : i = 1,...,m-1\}$ a *lattice path* supported on A if it covers the whole set A. The set $P(A)$ is called the *complete lattice path* supported on A.

We call a lattice path *connected* if the union of its segments is connected and starts at ω_0 and ends at ω_{N+1}.

We call a lattice path *connected from k to l* if the union of its segments is connected and starts at ω_k and ends at ω_l, $0 < k, l < N+1$.

A lattice path is called *disconnected* if the union of its segments is disconnected.

For a tropical surface passing through points in Mikhalkin position, we know that the points are contained in the interior of 2-dimensional cells of the surface [MMS18]. As 2-dimensional cells correspond to edges in the dual subdivision of the Newton polytope Δ, these point conditions lead to a path of the lattice points of Δ as follows.

Let $v = (1,\eta,\eta^2)$ with $0 < \eta \ll 1$. Given a smooth or nodal tropical surface with Newton polytope Δ passing through points in Mikhalkin position, the set of edges in the dual subdivision of Δ corresponding to 2-dimensional cells containing one of the points forms a lattice path as above. In the smooth case, we can use the lattice path to construct the dual subdivision of the Newton polytope by the smooth extension algorithm [MMS18, Section 3.3].

Remark 7.2.4 ([MMS18, Remark 3.1. (2)]). The set of singular tropical surfaces with a fixed Newton polytope passing through points in Mikhalkin position is finite. All its elements are singular tropical surfaces for which all points are visible in the dual subdivision (Definition 2.1.9) and the corresponding secondary cone is of codimension 1. Furthermore, each marked point q_i, $1 \le i \le n$, is in the interior of a different 2-cell of the tropical surface.

Since 2-cells of a tropical surface S correspond to edges in the dual subdivision, we can construct a lattice path from the marked points q_i as follows: Let E_i denote the edge in the dual subdivision corresponding to the 2-cell of S containing q_i. Then $P(S,\mathbf{q})$ denotes the lattice path given by the segments of lattice points of S associated to the edges E_i.

Lemma 7.2.5 ([MMS18, Lemma 3.2]). *We fix a point configuration $\mathbf{p}$ in Mikhalkin position. Let S be a tropical surface with one node passing through $\mathbf{q} = \mathrm{Trop}(\mathbf{p})$. The lattice path $P(S,\mathbf{q})$ satisfies exactly one of the following conditions:*

(i) *$P(S,\mathbf{q}) = P(A)$, where $A = \Omega \cap \mathbb{Z}^3 \setminus \{w_k\}$ for some $1 \le k \le N$. In this case the lattice path is connected and we call this path Γ_k.*

(ii) *$P(S,\mathbf{q}) = P(A') \cup P(A'')$, where A is partitioned in $A' = \{\omega_0,\ldots,\omega_k\}$, and $A'' = \{\omega_{k+1},\ldots,\omega_{N+1}\}$ for some $1 \le k \le N-1$. In this case the lattice path is disconnected and we call this path $\Gamma_{[k,k+1]}$.*

(iii) *$P(S,\mathbf{q}) = P(A)$, where $A = \Omega \cap \mathbb{Z}^3 \setminus \{\omega_k\}$ for $k = 0, N+1$. In this case the lattice path is connected from 1 to $N+1$, resp. 0 to N, and we denote this path Γ_0 resp. Γ_{N+1}.*

Remark 7.2.6. Let L be a line of direction $(1,\eta,\eta^2)$ on which the tropicalized points $\mathbf{q} = (q_1,\ldots,q_n)$ of point conditions in Mikhalkin position are distributed. Let S be a tropical surface with one node that satisfies the point conditions and has Newton polytope Ω. It follows that $N+1 = |\Omega \cap \mathbb{Z}^3| - 1$ and $n = N$. Then $L \setminus \mathbf{q}$ has $N+1$

line segments. These pass through 3-dimensional regions of $\mathbb{R}^3 \setminus S$, which are dual to some vertices of the subdivision of Ω. Since $|\Omega \cap \mathbb{Z}^3| = N + 2$, and all N points are contained in different 2 cells of S, $\mathbb{R}^3 \setminus S$ can consist of $N + 2$ or $N + 1$ regions.

If both $L \setminus \mathbf{q}$ and $\mathbb{R}^3 \setminus S$ consist of $N + 1$ components, the lattice path is connected of type Γ_k with $k \in \{1, \ldots, N\}$.

If $\mathbb{R}^3 \setminus S$ has $N + 2$ components, there is an additional intersection point y of L with S that is not part of the point conditions. If $y \succ q_1$, the arising lattice path is connected from 1 to $N + 1$. If $y \prec q_n$, the arising lattice path is connected from 0 to N. Otherwise, $q_k \succ y \succ q_{k+1}$ with $k \notin \{0, N + 1\}$, and the lattice path is disconnected of type $\Gamma_{[k, k+1]}$.

The following lemma explains how a given subdivision can be extended when the Newton polytope is enlarged. It is called the smooth extension algorithm. This is applied, for example, when we start with a subdivision containing a circuit in one of the positions as in Theorem 7.1.7 and we want to extend to a subdivision of $d\Delta_3$ dual to a singular degree d surface satisfying point conditions.

Lemma 7.2.7 ([MMS18, Lemma 3.4], smooth extension algorithm)**.** *The following data is given:*

- *a convex lattice polytope $\rho' \subset \mathbb{R}^n$ and a convex piecewise linear function $\nu' : \rho' \to \mathbb{R}$, whose linearity domains define a subdivision $\mathcal{T}'$ of ρ' into convex lattice subpolytopes;*

- *a convex lattice polytope $\rho'' \subset \mathbb{R}^n$ such that $\rho_0 = \rho' \cap \rho''$ is a cell of the subdivision $\mathcal{T}'$ and a face of ρ'' of codimension 1.*

Pick a point $\omega \in (\rho'' \cap \mathbb{Z}^n) \setminus \rho'$. Then there exists a unique extension of $\mathcal{T}'$ to a convex subdivision $\mathcal{T}$ of $\rho = \mathrm{conv}(\rho' \cup \rho'')$ such that

- *the vertices of $\mathcal{T}$ are the vertices of $\mathcal{T}'$ and of ρ'',*

- *ρ'' is a cell of $\mathcal{T}$,*

- *the cells of $\mathcal{T}$ are linearity domains of a convex piecewise linear function $\nu : \rho \to \mathbb{R}$ such that $\nu|_{\rho'} = \nu'$ and $\nu(\omega) \gg \max \nu'$.*

The algorithm is called smooth extension algorithm, because if we start the algorithm with a subdivision of ρ' containing a circuit, the emerging tropical surface has no singular points on the 2-cells dual to cells of the subdivision outside of ρ'. Figure 7.2 illustrates the steps of the smooth extension algorithm on an example.

Remark 7.2.8. The smooth extension algorithm is a generalization to dimension 3 of the lattice path algorithm by Mikhalkin for counting plane curves through generic points [Mik05]. This algorithm is described roughly in the proof of Theorem 8.1.7 in Section 8.1, where we additionally point out some parallels between point conditions and lattice paths for dimensions 2 and 3.
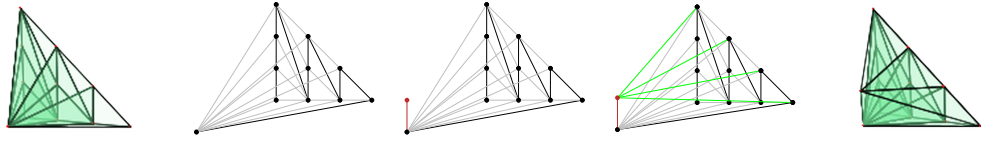
Figure 7.2: Example of smooth extension algorithm

The smooth extension algorithm is used to prove the following statement.

Lemma 7.2.9 ([MMS18, Lemma 3.6])**.** *Let* $\Omega = \mathrm{conv}(A)$, *where* $A \subset \Omega \cap \mathbb{Z}^3$, $|A| = N + 1$, *and* $A = \{a_0, ..., a_N\}$, *where the order* $a_0 \prec a_1 \prec ... \prec a_N$ *is induced by* $v = (1, \eta, \eta^2)$; *let* **q** *be a sequence of* N *points in* $v\mathbb{R} \subset \mathbb{R}^3$, *coming from the tropicalization of points in Mikhalkin position. Then:*

- *In the space of tropical surfaces defined by tropical polynomials of the form* $F : \mathbb{R}^3 \to \mathbb{R}$, $F(X) = \min_{a_i \in A}(c_i + \langle a_i, X \rangle)$, $c_i \in \mathbb{R}$, $i = 0, ..., N$, *there exists a unique surface* $S = S(A, \mathbf{q})$, *that passes through* **q**.

- *Each point of* **q** *belongs to the interior of some 2-cell of* S, *and distinct points belong to distinct cells.*

- *The dual subdivision of* S *consists only of tetrahedra, and it is constructed by a sequence of smooth extensions, starting with the point* a_0 *and subsequently adding the points* $a_1, ..., a_N$. *The edges dual to the 2-cells of* S *that intersect* **q** *form the lattice path* $P(A)$ *subsequently going through the points* $a_0, ..., a_N$.

If we wish to count surfaces with singularities, we have fewer point conditions than in the smooth case. This corresponds to leaving out lattice points from the lattice path, or to leaving out steps, i.e., segments, from the lattice path in the case of disconnected lattice paths. See Lemma 7.2.5. The smooth extension algorithm can still be applied in this case, provided we start with the polytope(s) containing the circuit.

7.3 Tropical floor plans

There are many tropical tools, like floor diagrams, for counting curves. In this section, we introduce the concept of tropical floor plans for counting tropical surfaces with multiple nodes as developed in [MMSS22]. We introduce the version of tropical floor plans as generalized by Madeline Brandt and the author in [BG20].

Further, this section recalls the results of [MMS18] on the computation of the complex multiplicities for circuits of type (A), (D) and (E), which are needed to determine the complex lifting multiplicity for tropical surfaces with the corresponding singularities.
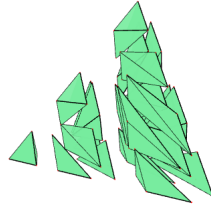
Figure 7.3: The dual subdivision of a floor decomposed smooth tropical cubic surface

This section is closed with a counting example illustrating how tropical floor plans (taking into account the more general circuit occurrences and their multiplicities) can be applied to general surfaces (i.e. surfaces with Newton polytope not $d\Delta_3$).

When the surface has multiple nodes, it is not yet well understood what the dual subdivision of the tropical surface can look like. One possibility is that the nodes are *separated*.

Definition 7.3.1 ([BG20])**.** If two singularities arise from circuits contained in the subdivision as described in Theorem 7.1.6 and the cells dual the circuits intersect at most in a unimodular face, then we say the two nodes are *separated*.

When choosing points in Mikhalkin position and a lattice path through the Newton polytope, we expect to obtain a sliced subdivision corresponding to a floor decomposed surface [BBLdM18].

Definition 7.3.2 ([BM09, FM10])**.** We say a tropical hypersurface is *floor decomposed* if, after a change of coordinates, the dual subdivision of the Newton polytope can be grouped into subdivisions of polytopes of width 1 in x-direction. In other words, a tropical hypersurface is floor decomposed if the subdivision allows a slicing of the Newton polytope into polytopes of width 1 in x-direction (after coordinate change).

Figure 7.3 shows the dual subdivision of a floor decomposed smooth tropical cubic surface.

Remark 7.3.3. It follows from [MMS12, MMSS22] that a one-nodal tropical surface satisfying point conditions in Mikhalkin position is floor decomposed. For multi-nodal surfaces passing through points in Mikhalkin position this is in general still an unsolved problem.

This decomposition of the surface is used in the description of the surface via tropical floor plans. Tropical floor plans are a tool for viewing the surface as a sequence of tropical plane curves. These curves are dual to the 2-dimensional

subdivision, which arise from the intersection of the dual subdivision of the floor decomposed tropical surface with $\{x = i\}$. Thus, the curves hold information about the subdivision and the satisfied point conditions (because the points are contained in 2-cells of the surface which are dual to edges in the dual subdivision). Moreover, they encode nodes of the surface. In joint work with Madeline Brand, we generalized the definition of tropical floor plans in [BG20].

The structures appearing in a curve that could produce a node are called *node germs*.

Definition 7.3.4 ([MMSS22], Definition 5.1)**.** Let C be a plane tropical curve of degree d passing through $\binom{d+2}{2} - 2$ points in general position. A *node germ* of C is one of the following:

1. a vertex dual to a parallelogram,

2. a midpoint of an edge of weight two that is dual to a pair of adjacent triangles of area two each sharing an edge of length two in the dual subdivision of C,

3. a horizontal or diagonal end of weight two,

4. a right or left *string* (see below).

Assume that the triangle at the right (resp. left) lower corner of the Newton polytope of C is part of the subdivision. In the case that none of the points in general position are contained in an end adjacent to the vertex dual the corner triangle, it is possible to prolong the adjacent bounded edge in direction $(1,0)$ (resp. $(-1, -1)$). This produces a family of curves, all of which pass through the points. The union of the two ends is called a *right* (resp. *left*) *string*. This is illustrated in Figure 7.4.

(a) Right string (b) Left string
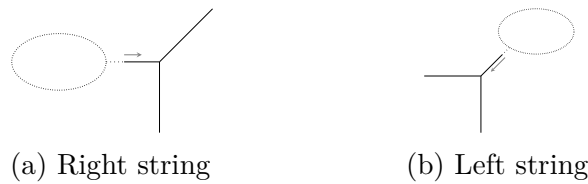
Figure 7.4: Right and left strings

Now we can define tropical floor plans. The following definition is a generalization of the original definition from [MMSS22] taking the results of [BG20] into account. We fix a point configuration $(p_1, ..., p_n)$ of $n = \binom{d+3}{3} - \delta - 1$ points in $\mathbb{K}^3$ and denote $q_i = \text{Trop}(p_i) \in \mathbb{R}^3$. See Remark 7.2.2. Let $Q_i = \Pi_{y,z}(q_i)$ be the projection of q_i along the x-axis.

Definition 7.3.5 ([BG20], generalized from [MMSS22])**.** A *δ-nodal floor plan F of degree d* is a tuple $(C_d, \ldots, C_0)$ of plane tropical curves C_i of degree i together with a choice of indices $d \geq i_{\delta'} > \ldots > i_1 \geq 1$ each assigned a natural number k_j such that $\sum_{j=1}^{\delta'} k_j = \delta$, where $0 < \delta' \leq \delta$, satisfying the following conditions.

1. The curve C_i passes through the following points, where $i_0 = 0$, $i_{\delta+1} = d+1$.

    if $i_\nu > i > i_{\nu-1}$:

    $$Q_{\sum_{k=i+1}^{d} \binom{k+2}{2} - \delta + (\sum_{j:i>i_j} k_j) + 1}, \ldots, Q_{\sum_{k=i}^{d} \binom{k+2}{2} - \delta + (\sum_{j:i>i_j} k_j) - 1},$$

    if $i = i_\nu$:

    $$Q_{\sum_{k=i+1}^{d} \binom{k+2}{2} - \delta + (\sum_{j:i \geq i_j} k_j) + 1}, \ldots, Q_{\sum_{k=i}^{d} \binom{k+2}{2} - \delta + (\sum_{j:i>i_j} k_j) - 1}.$$

2. The plane curve C_{i_j} has k_j node germs for every $j = 1, \ldots, \delta'$.

3. If C_{i_j} contains a left string as a node germ, then its horizontal end aligns with one of the following

    - a horizontal bounded edge of C_{i_j+1},
    - a 3-valent vertex of C_{i+1} not adjacent to a horizontal edge. Here edges are counted with multiplicity.

4. If C_{i_j} contains a right string as a node germ, then its diagonal end aligns with one of the following

    - a diagonal bounded edge of C_{i_j-1},
    - a 3-valent vertex of C_{i_j-1} not adjacent to a diagonal edge. Again, edges are counted with multiplicity.

5. If $i_d = \delta'$, then the node germs of C_d can only be diagonal ends of weight two or a right string.

6. If $i_1 = 1$, then the node germ of C_0 is a left string.

By [MMSS22, Construction 5.8], a unique tropical surface passing through the points **q** can be constructed from the data contained in a tropical floor plan.

Figure 7.5 illustrates some of the cases how a node germ in a tropical curve in the floor plan gives rise to a circuit in the dual subdivision. Example 8.1.8 shows pictures of tropical floor plans for surfaces not dual to a subdivision of $d\Delta_3$.

(a) Left string aligns with vertex not adjacent to horizontal edge: circuit (A)

(b) Left string aligns with horizontal bounded edge: circuit (D)

(c) Right string aligns with diagonal bounded edge: circuit (D)

(d) Vertex dual to a parallelogram: circuit (D)

(e) Diagonal end of weight two: circuit (E)

(f) Horizontal end of weight two: circuit (E)
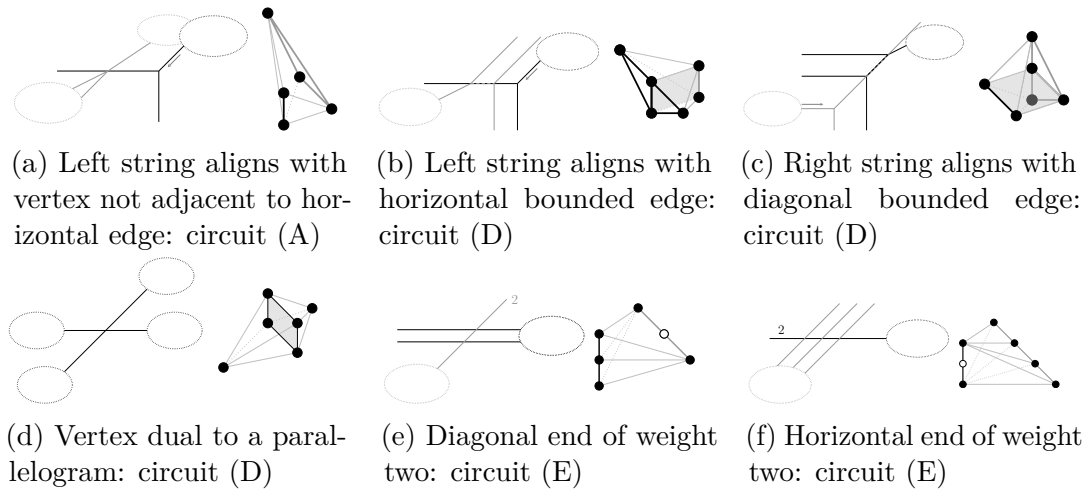
Figure 7.5: Examples how node germs of curves in the tropical floor plan give rise to a circuit (A), (D) or (E) in position as in Theorem 7.1.6 in the dual subdivision.

Remark 7.3.6. This definition of tropical floor plans covers all separated nodes. It follows that a tropical multi-nodal surface passing through points in Mikahlkin position with nodes all separated is floor decomposed.

Further, note that any tropical surface constructed from such a tropical floor plan is floor decomposed. So tropical floor plans only count floor decomposed surfaces.

We now describe how to compute the multiplicity of a floor plan. The multiplicity of a tropical floor plan is the lifting multiplicity (Definition 2.2.12) of the unique tropical surface belonging to this floor plan. In other words, it is the number of lifts of the tropical surface that satisfy the fixed point conditions $\mathbf{p} = \mathrm{Trop}(\mathbf{q})$.

Definition 7.3.7 ([BG20], generalised from [MMSS22, Definition 5.4]). Let $F = (C_d, \ldots, C_0)$ be a δ-nodal floor plan of degree d. Let $C_{i_j}^*$ be a node germ of C_{i_j}, we define the following local complex multiplicity $\mathrm{mult}_{\mathbb{C}}(C_{i_j}^*)$:

1. If $C_{i_j}^*$ is dual to a parallelogram, then $\mathrm{mult}_{\mathbb{C}}(C_{i_j}^*) = 2$.

2. If $C_{i_j}^*$ is the midpoint of an edge of weight two, then $\mathrm{mult}_{\mathbb{C}}(C_{i_j}^*) = 8$.

3. If $C_{i_j}^*$ is a horizontal end of weight two, then $\mathrm{mult}_{\mathbb{C}}(C_{i_j}^*) = 2(i_j + 1)$.

4. If $C_{i_j}^*$ is a diagonal end of weight two, then $\mathrm{mult}_{\mathbb{C}}(C_{i_j}^*) = 2(i_j - 1)$.

5. If $C_{i_j}^*$ is a right string whose diagonal end aligns with a diagonal bounded edge, then $\mathrm{mult}_{\mathbb{C}}(C_{i_j}^*) = 2$.

6. If $C_{i_j}^*$ is a right string whose diagonal end aligns with a vertex not adjacent to a diagonal edge, then $\mathrm{mult}_{\mathbb{C}}(C_{i_j}^*) = 1$.

7. If $C_{i_j}^*$ is a left string whose horizontal end aligns with a horizontal bounded edge, then $\mathrm{mult}_{\mathbb{C}}(C_{i_j}^*) = 2$.

8. If $C_{i_j}^*$ is a left string whose horizontal end aligns with a vertex not adjacent to a horizontal edge, then $\mathrm{mult}_{\mathbb{C}}(C_{i_j}^*) = 1$.

The *complex multiplicity* of a δ-nodal floor plan F is defined as

$$\mathrm{mult}_{\mathbb{C}}(F) = \prod_{j=1}^{\delta'} \prod_{\text{node germs of } C_{i_j}} \mathrm{mult}_{\mathbb{C}}(C_{i_j}^*).$$

The statements under points 7 and 8 in the definition arise from the generalization of the tropical floor plans in [BG20] and are build on the results in [MMSS22].

We are now able to translate the problem of counting tropical surfaces through points to counting floor plans. This leverages the structure imposed by choosing the points to be in Mikhalkin position, since we now count curves (which are well-understood) and the ways they can interact to produce nodes (which is outlined by Definition 7.3.5).

In a joint project with Madeline Brandt, which proceeded the project on which the following chapters of Part II are based, we used this to enumerate binodal cubic surfaces with separated singularities.

Theorem 7.3.8 ([BG20, Theorem 1.3])**.** *There are* 39 *tropical binodal cubic surfaces through* 17 *points in Mikhalkin position containing separated singularities. They lift to* 214 *of the total* 280 *complex binodal cubic surfaces through* 17 *points.*

The multiplicities in Definition 7.3.7 hold of tropical floor decomposed surfaces of degree d. The concept of tropical floor plans can also be used for tropical floor decomposed surfaces that are not of degree d. In these cases, we can obtain different multiplicities.

Remark 7.3.9. All pentatopes appearing in the dual subdivisions of degree d surfaces passing through points in Mikhalkin position have multiplicity 1, see [MMS18, Lemma 5.5]. This is why the node germs that give rise to a pentatope in the subdivision (right and left string aligning with a vertex) are counted with multiplicity one for tropical floor plans of degree d. For more general surfaces, it is possible that pentatopes with higher multiplicity occur. In these cases, the multiplicity has to be determined from the point conditions and the discriminant. This is described in Proposition 7.3.10.

Proposition 7.3.10 ([MMS18, Lemma 3.14 and 4.4])**.** *If the circuit in the dual subdivision of S is of type (A), there exists an affine automorphism $\mathbb{Z}^3 \to \mathbb{Z}^3$ taking the vertices of the pentatope to the position*

$$\mathrm{conv}(\begin{pmatrix} 0 \\ 0 \\ 0 \end{pmatrix}, \begin{pmatrix} 1 \\ 0 \\ 0 \end{pmatrix}, \begin{pmatrix} 0 \\ 1 \\ 0 \end{pmatrix}, \begin{pmatrix} 0 \\ 0 \\ 1 \end{pmatrix}, \begin{pmatrix} 1 \\ p \\ q \end{pmatrix}), \ \textit{with gcd(p,q)} = 1.$$

The discriminantal equation of a polynomial with this support (Definition 7.1.2) can then be written as

$$(-1)^{1+p+q} a_{000}^{p+q} a_{100}^{-1} a_{010}^{-p} a_{001}^{-q} a_{1pq} = 1.$$

If circuit (A) is contained in a subdivision with lattice path

- *Γ_k, then the multiplicity is the absolute value of the exponent of a_{ω_k} in the discriminantal equation.*

- *$\Gamma_{[k,k+1]}$, then the circuit contains*

    - *either ω_k and ω_{k+1} as the last two lattice points (order induced by the path) and the multiplicity is the absolute value of the exponent of $a_{\omega_{k+1}}$ in the discriminantal equation,*

    - *or ω_{k+1} and ω_{k+2} as the last two lattice points (order induced by the path) and the multiplicity is the absolute value of the exponent of $a_{\omega_{k+1}}$ plus the absolute value of the exponent of $a_{\omega_{k+2}}$ from the discriminantal equation.*

In some examples, we will also observe circuits of type (D) and (E) in different positions than they can occur in subdivisions of surfaces of degree d through points in Mikhalkin position. Therefore, the following two propositions will revisit their lattice path multiplicities in the generic case [MMS18]. As we will not come across surfaces with subdivisions containing circuits of type (B) and (C) in this thesis, we will not restate how to compute their multiplicities in general. This can be found in [MMS18, Section 4.4].

Proposition 7.3.11 ([MMS18, Lemma 4.8])**.** *Let S be a tropical singular surface with Newton polytope Ω. Let S satisfy point conditions $\mathbf{q} = \mathrm{Trop}(\mathbf{p})$ in Mikhalkin position and let the dual subdivision to S contain circuit (D).*

Then there are two algebraic surfaces which are lifts of S satisfying the point conditions $\mathbf{p}$ and with a singularity tropicalizing to the midpoint of the edge dual to the circuit, as described in Theorem 7.1.7 (3).

Proposition 7.3.12 ([MMS18, Lemma 4.9]). *Let S be a tropical singular surface with Newton polytope Ω. Let S satisfy point conditions $\mathbf{q} = \mathrm{Trop}(\mathbf{p})$ in Mikhalkin position and let the dual subdivision to S contain circuit (E) with special neighboring points*

- *$\omega_a, \omega_b, \omega_c$ from Theorem 7.1.6 (4a). Let $\rho \subset \mathbb{R}^2$ be the triangle formed by the projections of $\omega_a, \omega_b, \omega_c$ the plane orthogonal to the circuit. Then, there are $2\mathrm{vol}_{\mathbb{Z}}(\rho)$ many algebraic surfaces which are lifts of S, satisfy the point conditions $\mathbf{p}$, and have a singular point tropicalizing to the position described in Theorem 7.1.7 (4).*

- *$\omega_a, \omega_b, \omega_c$ and ω_d from Theorem 7.1.6 (4b). Then there are 8 algebraic surfaces which are lifts of S satisfy the point conditions $\mathbf{p}$, and have a singular point tropicalizing to the position described in Theorem 7.1.7 (4).*

Using the above results for the multiplicity, tropical floor plans can easily be generalized to count surfaces that do not have Newton polytope $d\Delta_3$. This is demonstrated in the following example.

Example 7.3.13. We are interested in the number of binodal surfaces passing through points in Mikhalkin position with Newton polytope Ω as in Figure 7.6.

$$\Omega = \mathrm{conv} \begin{pmatrix} 0 & 0 & 0 & 0 & 1 & 1 & 1 & 1 \\ 0 & 1 & 1 & 2 & 0 & 1 & 1 & 2 \\ 1 & 0 & 1 & 1 & 0 & 0 & 1 & 0 \end{pmatrix}$$
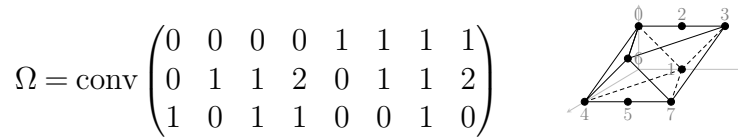
Figure 7.6: Given 5 points in general position and the Newton polytope shown above, how many binodal surfaces with this support pass through the points?

The formula $n = |\Omega \cap \mathbb{Z}^3| - \delta - 1$ from Remark 7.2.2 tells us that we have to fix $8 - 3 = 5$ points p_i in Mikhalkin position. Let $q_i = \mathrm{Trop}(p_i)$ denote the tropical point conditions. After tropicalizing the counting problem we can use tropical floor plans for the counting, taking into account the multiplicities.

Our tropical floor plan will consist of two curves (C_1, C_0), since in x-direction the polytope Ω has width 1. Given some subdivision of Ω the curve C_1 is dual to the subdivision of $\Omega \cap \{x = 0\}$, while C_0 is dual to the subdivision of $\Omega \cap \{x = 1\}$. We make a case distinction by how many points $Q_i = \Pi_{y,z}(q_i)$ are contained in each curve. We first consider only those cases for which the corresponding lattice paths are connected from 0 to 4. In this case one segment of the lattice path has to connect the two facets of Ω at $\{x = 0\}$ and $\{x = 1\}$, we know that in the tropical floor plan the curves C_1 and C_0 pass through 4 points Q_i.

The curve C_1 can pass at most through 3 points of our point configuration. In this case, the curve is completely fixed and smooth, i.e., it does not contain node germs. The curve C_0 has to pass through exactly 1 point of the point configuration and it has to contain two node germs. From the form of the Newton polytope to curve C_0 this can only be a right and a left string, though these look different from Definition 7.3.4, since the curve is not of degree d. To allow alignment, the rightmost diagonal end of the curve contains the last point of the point configuration. Hence, the right string consists of the vertical end and the horizontal bounded edge on which the left string (consisting of the ray of direction $(-1,1)$ and the leftmost vertical end) is connected. For the right string there is only one alignment option that still allows an alignment for the left string. For the left string there are two. The lattice path and the floor plans are depicted in Figure 7.7. For both alignments we observe two pentatopes, i.e., two circuits of type (A), in the subdivision.
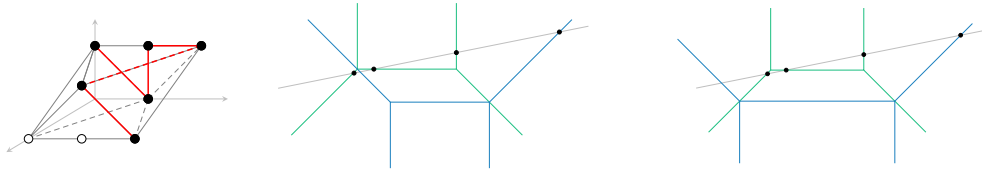
Figure 7.7: This lattice path allows for two alignments. They correspond to different subdivisions of the polytope that both contain two pentatopes.

We count them with their multiplicities as described in Proposition 7.3.10: we investigate the discriminant of the two occurring pentatopes for each of the two floor plans in Figure 7.7. This computation yields that in both cases one pentatope has to be counted with multiplicity 2 and the other with multiplicity 1, so in total we count $2 \cdot 1 + 2 \cdot 1 = 4$ surfaces coming from these floor plans.

If the curve C_1 passes only through 2 points, it has to contain one additional node germ. Let us first consider the case that this is an upwards pointing vertical end of weight 2, i.e., a circuit of type (E). This node germ is not mentioned in Definition 7.3.4 since for surfaces of degree d with Newton polytope $d\Delta_3$ a vertical end of weight 2 would not give rise to a node. However, in this more general case where there exists an end of direction $(-1,1)$ of curve C_0, it does give rise to a singularity.

In this case, the curve C_0 also has to pass through 2 points and contains one node germ. Right or left strings are not possible since curve C_1 does not allow for any alignment that would give rise to a circuit in the subdivision. Hence, curve C_0 also has a downwards pointing vertical end of weight 2, i.e., another circuit of type (E). Since C_0 has an end of direction $(-1,-1)$ this weight 2 end gives rise to a node. The floor plan and the corresponding lattice path are depicted in Figure 7.8.

The floor plan in Figure 7.8 has multiplicity $2 \cdot 2 = 4$ as follows from Proposition 7.3.12.
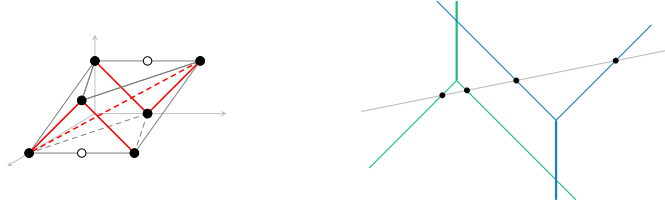
Figure 7.8: There is one lattice path for which the two nodes are coming from intersections of rays with weight two ends.

Another option for curve C_1 to pass through only 2 points of the point configuration, is that we have a right string, i.e., the vertex corresponding to the triangle $\overline{((0,1,0),(0,1,1),(0,2,1))}$ is not fixed by the point conditions. In order to allow an alignment with an edge of C_0 that will give rise to a parallelogram (circuit (C)) in the subdivision, the node germ contained in C_0 has to be a left string, i.e., the the vertex corresponding to the triangle $\overline{((1,0,0),(1,1,0),(1,1,1))}$ is not fixed by the point conditions. This leads to two circuits of type (C) in the subdivision, which
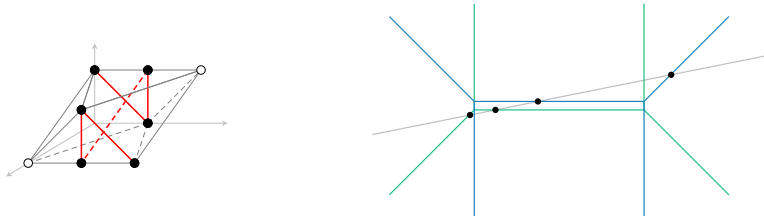
Figure 7.9: This lattice path allows an alignment that corresponds to two bipyramids in the dual subdivision.

each give each rise to a bipyramid in the subdivision By Proposition 7.3.11 we count them with multiplicity 2. So, we obtain $2 \cdot 2 = 4$ surfaces for this floor plan.

The last possibility is for curve C_1 to pass through exactly 1 point of the point configuration. This implies that curve C_0 passes through 3 points and is thus smooth and completely determined by the point conditions. The only possible alignments for the two vertices of C_1 are with the vertical edges of C_0, see Figure 7.10. This gives rise to two parallelograms, i.e., two circuits of type (C), in the subdivision. The multiplicity is computed the same way as before. So, we count $2 \cdot 2 = 4$ surfaces for this floor plan.

Note that the floor plans in Figure 7.9 and 7.10 produce the same alignment of the curves, but they differ in the distribution of the points from the point conditions on the the two curves.
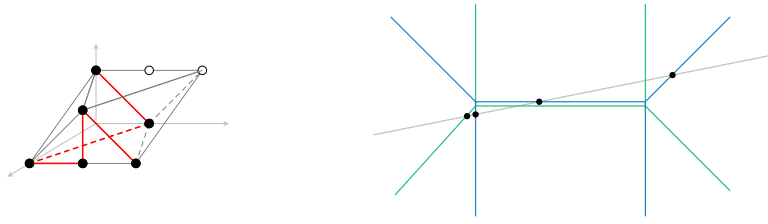
Figure 7.10: This lattice path allows an alignment corresponding to two bipyramids in the dual subdivision. The arising dual subdivision of Ω is the same as induced by the floor plan in Figure 7.9.

In total, we obtain 16 surfaces from the count of the tropical floor plans. This coincides with the degree of the binodal variety of surfaces with Newton polytope Ω, which can be computed using `OSCAR` [osc, Gei22] or `Singular` [DGPS21].

For the definition of the binodal variety, see Definition 9.1.1. Algorithms 5 and 7 present two ways how to compute the binodal variety. The code for the computation in `OSCAR` is available for download at [Gei22] on GitHub, and can be inspected in Appendix B.2.

We can conclude that there are no disconnected paths or connected paths that are not connected from start to end in this case, because the paths connected from 0 to 4 already provided a full count.

This example shows that for some surfaces the tropicalization only contains separated nodes, so that a complete count can be achieved using only the tools of separated nodes.

Remark 7.3.14. Two singularities can tropicalize to points on the tropical surface that are closer together such that the singularities are no longer separated. In this case the tropical floor plans will not recover the full count. This occurs, for example, for binodal tropical cubic surfaces satisfying point conditions in Mikhalkin position, see [BG20, Theorem 1.3]. Unseparated nodes are encoded in the dual subdivision via larger polytope complexes, which have not been classified. See [BG20, Section 5.1]. In Chapter 9, we see how polytopes with 6 lattice points can encode two nodes that are tropically at the same point and coincide with a vertex of the surface.

Chapter 8

Counting with tropical floor plans

This chapter presents two different aspects of tropical floor plans: In Section 8.1 we show how this technique can be extended to count nodal plane curves and prove in Theorem 8.1.7 that the count via this method recovers the Gromov-Witten number.

Section 8.2 investigates the asymptotic count of multi-nodal surfaces via tropical floor plans In Theorem 8.2.6, we prove that tropical floor plans of surfaces as defined in Definition 7.3.5, which only count separated nodes, are not sufficient to recover the asymptotic count of binodal and trinodal surfaces up to two degrees. This motivates the investigation of unseparated nodes and their contribution for the asymptotic count, which is the main topic of Chapters 9 and 10.

This chapter is based on the collaborative preprint [BG21] with Madeline Brandt.

8.1 Floor plans of plane curves

Tropical floor plans for one-nodal plane curves are introduced in [MMSS22, Definition 4.1]. In this section, we generalize this definition to plane curves with δ nodes and prove that with this definition we can recover the Gromov-Witten numbers of plane curves. This section is built on joint work with Madeline Brandt [BG21].

The multicomponent *Gromov-Witten numbers* of plane curves give the number $N_{d,g}$ of plane curves of degree d and genus g passing through $3d-1+g$ points in general position. These numbers belong to the larger family of Gromov-Witten invariants. For this interesting topic, we refer to [Gat03, CH98, Vak08, KM94, Kon95] which is only a small selection of the extensive literature in this area.

We only consider multicomponent Gromov-Witten invariants of plane curves in this section, so we drop the adjective "multicomponent" in the following for shorter notation.

Curves of degree d and genus g passing through $3d-1+g$ points in general position are nodal. This follows from the degree-genus formula.

Theorem 8.1.1 ([Har77], degree-genus formula)**.** *A plane curve of degree d and*

genus g has δ nodes where

$$\delta = \frac{(d-1)(d-2)}{2} - g.$$

The following definition is inspired by [FM10, Definition 3.4] and used similarly in [CJMR21, Section 4.2] and [MMSS22].

Definition 8.1.2. A collection of finitely many points $(q_0, \ldots, q_N)$ in $\mathbb{R}^2$, $q_i = (x_i, y_y)$, is said to be in *horizontally stretched* position, if they satisfy

$$x_0 \ll x_1 \ll \ldots \ll x_N,$$
$$y_0 < y_1 < \ldots < y_N,$$
$$\max_{i \neq j} |y_i - y_j| \in (0, \epsilon), \text{ for } \epsilon \text{ small.}$$

These points are tropically in general position, so it follows from [Mik05, Theorem 1], that there exist lifts in $\mathbb{K}^2$ of the points in this configuration that are algebraically in general position.

Tropical plane curves passing through general points in horizontally stretched position are *floor decomposed*, i.e., all vertical lines appear in the dual subdivision of the Newton polytope [BM09, FM10]. Sometimes such a subdivision is also called *column-wise*.

When we considered tropical floor plans for surfaces in Definition 7.3.5, we noted in Remark 7.3.6 that these only count surfaces that are floor decomposed (Definition 7.3.2). The definition of floor plans for plane curves also uses the property floor decomposed.

When fixing points in Mikhalkin position as in Definition 7.2.1 adapted for $\mathbb{K}^2$, we do not obtain floor decomposed tropical curves [GM07, Remark 3.9]. To count curves via tropical floor plans, we have to fix points in horizontally stretched position because they ensure that the curve is floor decomposed.

For tropical surfaces we have seen in Definition 7.3.5 that a floor plan consists of a tuple of curves. For a tropical curve the floor plan consists of tuples of points, however, in contrast to the surface case, a point can appear with a higher multiplicity. Thus, we need the concept of tropical divisors.

Definition 8.1.3 ([GK08], Definition 1.3)**.** Let X be a tropical plane curve. The *group of divisors* of X is the free abelian group generated by the points of X, i.e., a *divisor* D on X is a linear combination

$$D = \sum_{i=1}^{k} z_i x_i, \text{ where } k \in \mathbb{N} \text{ and the } x_i \in X, z_i \in \mathbb{Z}.$$

The *degree* of D is $\deg(D) = \sum_{i=1}^{k} z_i$. We call divisors on X *tropical divisors.*

We want to use the tropical floor plans for curves to recover the Gromov-Witten numbers, which count degree d curves of genus g passing through $3d - 1 + g$ points in general position. By the degree-genus formula, the correct number of point conditions to achieve the Gromov-Witten numbers is

$$n := 3d - 1 + g = 3d + \frac{(d-1)(d-2)}{2} - \delta - 1 = \binom{d+2}{2} - \delta - 1.$$

Therefore, we fix points $q_1, ..., q_n$ in $\mathbb{R}^2$ in horizontally stretched position. We denote the projection of q_i to its second coordinate by $Q_i := \pi_y(q_i)$.

Now we are ready to give the generalized definition of tropical floor plans for δ-nodal curves of degree d.

Definition 8.1.4. A *tropical floor plan* for a tropical plane curve of degree d with δ nodes consists of a tuple of tropical divisors $(D_d, D_{d-1}, ..., D_1)$ on $\mathbb{R}$ where each D_i is of degree i, together with a choice of indices $d \geq i_{\delta'} > ... > i_1 \geq 1$ each assigned a natural number $k_j \leq i_j$ such that $\sum_{j=1}^{\delta'} k_j = \delta$, where $0 < \delta' \leq \delta$. The divisor D_i passes through the following points, where we set $i_0 = 0, i_{\delta+1} = d + 1$:

$$i_j > i > i_{j-1}: \quad Q_{\binom{d+2}{2} - \binom{i+2}{2} - \delta + \sum_{l=1}^{j-1} k_l + 1}, ..., Q_{\binom{d+2}{2} - \binom{i+1}{2} - \delta + \sum_{l=1}^{j-1} k_l - 1},$$

$$i = i_j: \quad Q_{\binom{d+2}{2} - \binom{i+2}{2} - \delta + \sum_{l=1}^{j} k_l + 1}, ..., Q_{\binom{d+2}{2} - \binom{i+1}{2} - \delta + \sum_{l=1}^{j-1} k_l - 1}.$$

Furthermore, a divisor D_{i_j} may have points of weight w, where $2 \leq w \leq \delta + 1$ if $i_j \notin \{1, d\}$. The sum of the weights of the points is at most $\deg(D_{i_j})$, and the total sum of points with higher weight is at most xδ. If D_{i_j} contains r points of weight ≥ 2, then $k_j - r$ points of weight 1 in D_{i_j} have to align with a point of $D_{i_j - 1}$ or with a point of $D_{i_j + 1}$.

Remark 8.1.5. If i is not in the index tuple, then D_i contains i points and has to meet all of them. If $i = i_j$, then D_i has to meet only $i - k_j$ points. If the last point of D_i is Q_s, then the first point of D_{i-1} is Q_{s+2}, so that there is always exactly one point, Q_{s+1}, between D_i and D_{i-1}.

Similar as for surfaces, a tropical floor plan of plane curves gives rise to a unique tropical plane curve of degree d. This can be shown with the methods from [BBLdM18], also see [MMSS22, Theorem 4.5]. We now only have to define the lifting multiplicity with which the tropical floor plan has to be counted when we want to recover the Gromov-Witten numbers.

Definition 8.1.6. We define the complex multiplicity $\text{mult}_{\mathbb{C}}(F)$ of a floor plan F with r points of weights $w_1, ..., w_r \geq 2$ to be $\text{mult}_{\mathbb{C}}(F) = \prod_{j=1}^{r} w_j^2$.

This generalizes the definition of tropical floor plans and of their multiplicities for one-nodal curves as given in [MMSS22] to multi-nodal curves.

Theorem 8.1.7. *The number of tropical floor plans of degree d with δ nodes counted with complex multiplicity equals the Gromov-Witten number $N_{d,g}$ of curves with genus $g = \frac{(d-1)(d-2)}{2} - \delta$ and degree d passing through $3d-1+g$ general points:*

$$N_{floor}(d,g) := \sum_F mult_{\mathbb{C}}(F) = N_{d,g},$$

where the sum runs over all tropical floor plans F of tropical curves of degree d with δ nodes.

This proof needs the theory of counting plane curves via lattice paths from [Mik05]. A few necessary details are recalled in the proof. For further details we refer to [Mik05, Mar06, GM07].

Proof. The idea behind this proof is to use Mikhalkin's Correspondence Theorem [Mik05, Theorem 1 and 2] which states that the number of λ-increasing lattice paths $N_{\text{path}}(d,g)$ counted with multiplicity equals the Gromov-Witten number $N_{d,g}$,

$$N_{\text{path}}(d,g) = N_{d,g}.$$

To use this result, we will show that $N_{\text{path}}(d,g)$ is the same as the number $N_{\text{floor}}(d,g)$ of tropical floor plans counted with multiplicity.

We first revisit some definitions and facts from curve counting via λ-increasing lattice paths from [Mik05]. In [Mik05, Definition 7.1], a λ-*increasing lattice path* is defined. This is a set of segments of lattice points in 2-dimensional polytopes induced by a partial order of the lattice points given by $\lambda = (1, -\epsilon)$ with $0 < \epsilon \ll 1$ irrational. In Definition 7.2.3 an analogous situation in $\mathbb{R}^3$ was described.

We choose $\lambda := (-1, -\epsilon)$ with $0 < \epsilon \ll 1$ irrational to obtain an easier construction of a tropical floor plan from a lattice path induced subdivision.

For counting tropical curves with λ-increasing lattice paths, the choice of $\lambda = (-1, -\epsilon)$ corresponds to fixing point conditions with growing distances on a line with direction vector $(1, \epsilon)$. These are points in two-dimensional Mikhalkin position, compare Definition 7.2.1 for the three-dimensional case. These point conditions in Mikhalkin position are different from the horizontally stretched points we need to fix for counting with tropical floor plans.

Similar to the smooth extension algorithm for singular surfaces, each point from the point conditions is contained in the relative interior of a different edge of the tropical plane curve. Also, the edges of the tropical curves that contain the points from the point conditions in their relative interior are dual to edges in the dual

subdivision that form the segments of the λ-increasing lattice path. An example of a λ-increasing lattice path is depicted in Figure 8.1a.

Every λ-increasing lattice path is connected from start to end, i.e., it is connected as the union of its line segments, and it starts at $(0,0)$ and ends at $(d,0)$. Moreover, the line segment of the $x = 0$ boundary of the Newton polytope $d\Delta_2$ in the lattice path can only have lattice length 1.

There exists an algorithm in [Mik05, Definition 7.1] on how to obtain subdivisions of $d\Delta_2$ from a λ-increasing lattice path which give tropical nodal curves passing through the points on the line $(1,\epsilon)\mathbb{R}$ by duality. This algorithm mainly consists of going along the lattice path and at each turn (above and below the path) to decide whether to cut the corner to make a triangle or to fold it out to a parallelogram. The subdivision depicted in Figure 8.1a arises in this way.

The *multiplicity of a λ-increasing lattice path* is then defined as the sum over the multiplicity of all subdivisions arising from the path, where a subdivision is given the *multiplicity*

$$\prod_{T \text{ triangle in subdiv.}} (2 \cdot \text{area}(T)). \tag{8.1}$$

The subdivisions arising from λ-increasing lattice paths are not necessarily floor decomposed. However, when we consider tropical floor plans we know the arising tropical curves will have floor decomposed dual subdivisions.

By [GM07, Definition 3.4], we can consider $N_{\text{path}}^{(0),(d)}(d,g)$ instead of $N_{\text{path}}(d,g)$. The number $N_{\text{path}}^{(0),(d)}(d,g)$ counts also via λ-increasing lattice paths, but it counts column-wise subdivisions induced by the λ-increasing lattice path. These floor decomposed subdivisions are counted with the same multiplicity as in Equation (8.1). It is a result of [GM07] that the multiplicity of a λ-increasing lattice path via the algorithm by [Mik05] is the same as the multiplicity of a λ-increasing lattice path via its floor decomposed subdivisions from [GM07]. The number $N_{\text{path}}^{(0),(d)}(d,g)$ does not count every floor decomposed subdivision that contains a λ-increasing lattice path Γ. The conditions are [GM07, Remark 3.9]:

- the subdivision contains all vertical lines above and below Γ,

- in the area above Γ each vertical line segment over the path Γ forms a parallelogram with a line segment to its right (i.e., a vertical line segment with smaller x-coordinate),

- in the area above Γ each triangle in the subdivision "is pointing to the left", i.e., the vertex opposite to its vertical edge lies to the left of this edge,

- in the area below Γ each vertical line segment over the path Γ forms a parallelogram with a line segment to its left, i.e., a vertical line segment with larger x-coordinate, and

- in the area below Γ each triangle in the subdivision "is pointing to the right", i.e., the vertex opposite to its vertical edge lies to the right of this edge.

The aim is now to prove $N_{\text{path}}^{(0),(d)}(d,g) = N_{\text{floor}}(d,g)$. For this purpose we will give a bijection between the floor decomposed subdivisions coming from λ-increasing lattice paths and tropical floor plans and and show that they are counted with the same multiplicities.

We fix a λ-increasing lattice path and a floor decomposed subdivision that arises from this path according to the algorithm.

From the floor decomposed subdivision and its lattice path, we now construct a tropical floor plan as follows: For every vertical line segment of length w in the lattice path contained in the line $x = i$ we allocate one of the points $Q_k(= \pi_y(q_k))$ to the divisor D_{d-i} with weight w. We start with $x = 0$ and Q_0. When passing from $x = i$ to $x = i+1$, we skip one of the Q_k. (Recall that in a tropical floor plan there is always one projected point from the point conditions between two divisors.)

Now we have a d-tuple of tropical divisors. Since for $x = 0$ a λ-increasing lattice path has only line segments of length 1, the divisor D_d satisfies the condition of the tropical floor plan.

For divisors D_i that still have $\deg(D_i) < i$, we obtain the remaining points from the parallelograms in the subdivision: Assume we have D_i with $\deg(D_i) < i$, then there are vertical line segments in the subdivision at $x = d-i$ that are not part of the lattice path. They are part of one or two parallelograms.

For every line segment that lies below the lattice path, we consider the parallelograms they form with line segments in $x = d-(i+1)$ which belong to the lattice path. Their positions tell us with which point of divisor D_{i+1} the corresponding point of D_i has to align with. For the line segments over the lattice path, we proceed analogously with the line segments in $x = d-(i-1)$ and the points of divisor D_{i-1}.

This process is illustrated for an exemplary subdivision of $4\Delta_2$ induced by a λ-increasing lattice path counting 3-nodal curves in Figure 8.1.

Next, we show that the multiplicity of the tropical floor plan constructed from a subdivision arising from a λ-increasing lattice path coincides with the multiplicity of the subdivision.

Recall that the floor decomposed subdivisions arising from λ-increasing lattice paths have multiplicity

$$\prod_{T \text{ triangle in subdiv.}} (2 \cdot \text{area}(T)).$$

Thus, only triangles of area $2w \geq 1$ contribute to the multiplicity of the subdivision. These arise from vertical edges of length $w \geq 2$ inside the subdivision, and each such

(a) A floor decomposed subdivision from a fixed λ-increasing lattice path

(b) The vertical edges corresponding to the divisors marked in color

(c) The tropical floor plan
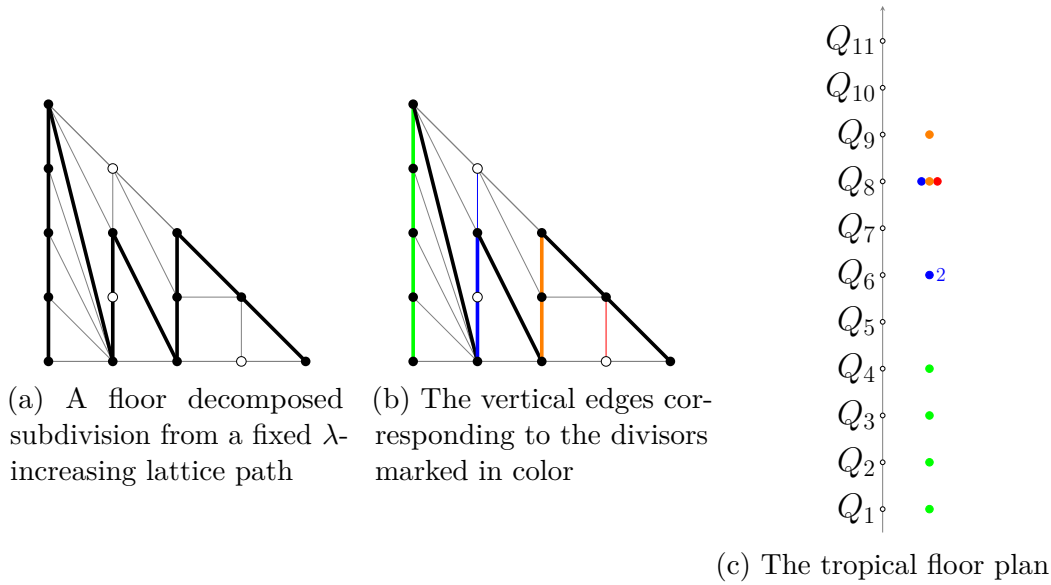
Figure 8.1: Example of how to obtain a tropical floor plan from a floor decomposed subdivision coming from a fixed λ-increasing lattice path.

edge is adjacent to two triangles of area $\frac{w}{2}$. So the multiplicity of the subdivision can also be given as

$$\prod_{\text{vertical edges of length } w_j \geq 2} w_j^2.$$

Vertical edges of length $w \geq 2$ correspond to points of weight w in the tropical divisors of the tropical floor plan. Therefore, the above coincides with the complex multiplicity assigned to the tropical floor plans:

$$\text{mult}(F) = \prod_{i=1}^{d} \prod_{\substack{\text{points in } D_i \\ \text{of weight} w_j}} w_j^2.$$

It remains to demonstrate that every tropical floor plan arises in the way described above. A tropical floor plan $(D_d, \ldots, D_1)$ uniquely defines a tropical curve which is dual to a floor decomposed subdivision consisting of triangles and parallelograms. By reverse engineering the process described above, we obtain from the divisors D_i special vertical line segments in the subdivision that can be uniquely extended to a λ-increasing lattice path of the correct length.

Due to the choice of point conditions in horizontally stretched position, the line segment of the lattice path that connects the last segment of the $x = i$ line with the first segment of the $x = i + 1$ line is of direction $(1, -a)$ with $a \geq 1$. This implies that every vertical line segment over the path forms a parallelogram with a line

segment to its right. All the remaining triangles over the path point to the left. Moreover, under the lattice path we see the symmetric picture (parallelograms formed to the left, triangles pointing to the right). Thus, the subdivision satisfies the conditions of [GM07, Remark 3.9]. Hence, it is one of the floor decomposed subdivisions to the lattice path and therefore in the count.

With [GM07, Section 3] and Mikhalkin's Correspondence Theorem [Mik05, Theorem 1 and 2], it follows that

$$N_{\text{floor}}(d,g) = N_{\text{path}}^{(0),(d)}(d,g) = N_{\text{path}}(d,g) = N_{d,g},$$

where $g = \frac{(d-1)(d-2)}{2} - \delta$ is the genus. $\qquad\qquad\qquad\square$

Example 8.1.8. We now use tropical floor plans to count the 225 binodal plane curves of degree 4 passing through 12 general points [FM10, Figure 1]. We distinguish the cases by the index tuples (i_1,i_2) encoding the position of the nodes in the four floors and their associated numbers (k_1,k_2) that count the number of nodes in the nodal floors. Note that we do not always have i_2 and k_2 since if $k_1 = 2$ there is only one nodal floor in the floor plan.

We compute the case $(i_1,i_2) = (4,3)$ with $(k_1,k_2) = (1,1)$ in detail as an example. The other index choices and their contributions are listed in Table 8.1. For each case, one considers the different types of the nodes that are possible, and if applicable, their possible alignment options. Then, we compute the multiplicities for each case.

Let $(i_1,i_2) = (4,3)$ and $(k_1,k_2) = (1,1)$. In this case the divisor D_4 passes only through the first 3 points from the point conditions.

Since $\deg(D_4) = 4$, there is one "free" point in the divisor, i.e., a point that is not fixed by the point conditions. It has to align with a point in D_3. The divisor D_3 passes only through 2 points from the point conditions and thus either contains a point of weight 2 or a third "free" point that aligns either with a point of D_4 or with a point of D_2.

We make a case distinction by the special point in D_3.

- If D_3 has a point of weight 2, it contains only one point of weight 1 with which the free point of D_4 can align. There are two choices for the point of weight 2 in D_3, thus this situation contributes $2 \cdot 2^2 = 8$ curves to our count.

- If D_3 contains a third "free" point that aligns with a point of

  - D_2. There are 2 options for this alignment. Additionally there are 3 possible alignment options for the "free" point of D_4 with a point of D_3. Counted with multiplicity this adds up to $3 \cdot 2 = 6$ curves.

  - D_4. In this case there are 3 alignment options for the point in D_3 to align with a point of D_4 since we cannot choose the "free" point for this

alignment, as this would contradict the point conditions. There remain 2 alignment possibilities for the point of D_4 to align with a point of D_3. This gives $2 \cdot 3 = 6$ curves.

In total the case $(i_1, i_2) = (4,3)$, $(k_1, k_2) = (1,1)$ contributes $8 + 6 + 6 = 20$ curves to our count. All floor plans with indices $(i_1, i_2) = (4,3)$, $(k_1, k_2) = (1,1)$ can be seen in Figure 8.2. The total count is given in Table 8.1.
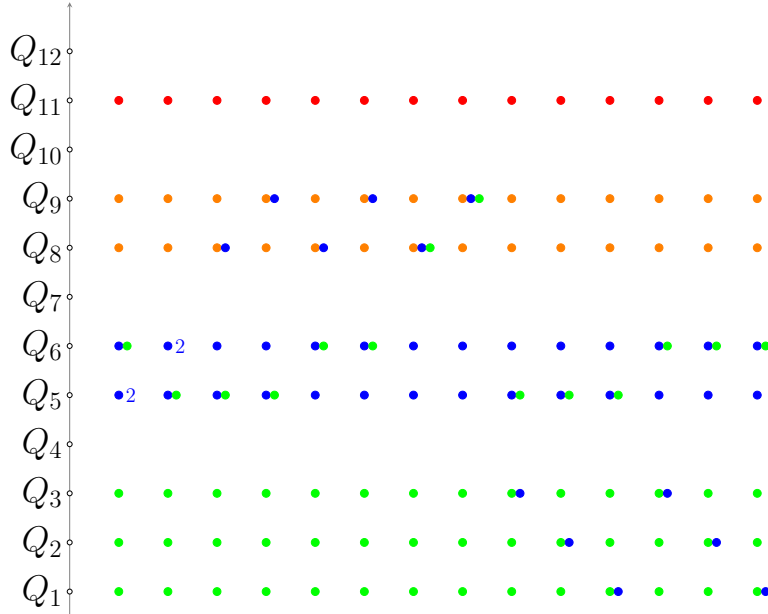
Figure 8.2: Floor plans for plane curves of degree 4 with 2 nodes and index tuple $(i_1, i_2) = (4,3)$.

(i_1, i_2)	$(4,-)$	$(3,-)$	$(2,-)$	**(4,3)**	$(4,2)$	$(4,1)$	$(3,2)$	$(3,1)$	$(2,1)$	sum
(k_1, k_2)	$(2,-)$	$(2,-)$	$(2,-)$	**(1,1)**	$(1,1)$	$(1,1)$	$(1,1)$	$(1,1)$	$(1,1)$	
count	3	48	6	**20**	24	6	84	28	6	225

Table 8.1: A full count of plane curves of degree 2 with 2 nodes passing through general points by tropical floor plans.

8.2 Asymptotic estimation

In this section, we make the step from counting curves, as in the previous section, towards counting surfaces as prepared in Chapter 7. We investigate the use of

tropical floor plans counting surfaces with separated nodes for an asymptotic count of δ-nodal surfaces of degree d. This is joint work with Madeline Brandt [BG21].

The main result is Theorem 8.2.6, which proves that even for counting binodal and trinodal surfaces asymptotically we have to understand how to count nodes that are not separated. They will be called *unseparated*.

The complex surfaces of degree d in $\mathbb{P}^3$ with $\delta < 4(d-4)$ distinct nodes as their only singularities form a family of dimension $\binom{d+3}{3} - 1 - \delta$ [ST99]. As stated by the authors of [MMSS22], it can be shown by procedures in enumerative geometry that the degree of this family for $\delta \geq 1$ fixed and $d \gg \delta$ is described by the following polynomial

$$N_{\delta,\mathbb{C}}^{\mathbb{P}^3}(d) = \frac{4^\delta}{\delta!}(d-1)^{3\delta} + \mathcal{O}(d^{3\delta-3}). \tag{8.2}$$

Only the three terms of highest degree are known. Since this equation holds for $d \gg \delta$, we also call this an *asymptotic count* of δ-nodal surfaces of degree d. Using the original definition of tropical floor plans, [MMSS22, Definition 5.2], for which node germs have to be at least one floor apart, Markwig et al. were able to recover the coefficient of the highest degree term of the polynomial in Equation (8.2).

Theorem 8.2.1 ([MMSS22, Theorem 6.1])**.** *The number $N_{\delta,\mathbb{C}}^{\mathbb{P}^3,floor}(d)$ of δ-nodal floor plans for surfaces of degree d satisfies*

$$N_{\delta,\mathbb{C}}^{\mathbb{P}^3,floor}(d) = \frac{(4d^3)^\delta}{\delta!} + \mathcal{O}(d^{3\delta-1}).$$

From the earlier joint work with Madeline Brandt in [BG20] a generalization of tropical floor plans arose, Definition 7.3.5, which allows node germs to appear closer together as long as they still induce separated nodes (Definition 7.3.1).

A natural question arising from this generalization is whether counting all separated nodes via tropical floor plans allows us to recover the coefficient of the term with second highest degree from the asymptotic count in Equation (8.2). To understand this is a first step towards recovering also terms of lower degree of $N_{\delta,\mathbb{C}}^{\mathbb{P}^3}(d)$, of which only one more is known.

To be able to compare how much closer we get to the asymptotic count when we allow for all separated nodes, we need to have numbers that mirror the different counts.

Notation 8.2.2. Let $S_\delta(d)$ denote the number of δ-nodal floor plans of degree d counted with multiplicity as originally defined in [MMSS22, Definition 5.2]. This means that $S_\delta(d)$ only counts floor plans where each floor C_i contains at most one node germ and where two consecutive singular floors C_{i_j} and $C_{i_{j+1}}$ are separated by at least one smooth floor, i.e, $i_{j+1} > i_j + 1$.

This corresponds to those floor plans from Definition 7.3.5 with $\delta' = \delta$ and $k_j = 1$ for all j, and $i_{j+1} > i_j + 1$. In this case the alignment of a left string with a vertex as described in Definition 7.3.5 is not possible.

In [BG20] we considered floor plans of binodal cubic surfaces where there is no constraint on which floors the node germs may appear. However, some floor plans will produce tropical surfaces in which the nodes are unseparated. For these cases, the dual subdivision, tropical floor plans and multiplicities are unknown, and so we do not know how to count them. To allow for all kinds of separated nodes, we generalized the definition of tropical floor plans (see Definition 7.3.5).

Notation 8.2.3. Let $U_\delta(d)$ denote the number of δ-nodal tropical floor plans of degree d counted with multiplicity as defined in Definitions 7.3.5 and 7.3.7.

We now introduce artificial δ-nodal floor plans. These do not count any true multinodal tropical surfaces, but we use them as a counting tool; they provide an upper bound for $U_\delta(d)$.

Definition 8.2.4. An *artificial δ-nodal floor plan* is a tuple of 1-nodal floor plans $(P_1, \ldots, P_\delta)$ where the node germ of P_i appears in a higher or in the same floor as the node germ of P_{i+1}.

The *multiplicity* of an artificial floor plan is the product of the multiplicities of the P_i.

Let $I_\delta(d)$ denote the number of artificial floor plans counted with multiplicities.

We think of artificial δ-nodal floor plans as simulating how many surfaces there would be if the nodes did not interact with one another at all. It follows from the definitions that $I_1(d) = U_1(d) = S_1(d) = N_{1,\mathbb{C}}^{\mathbb{P}^3}(d)$.

Proposition 8.2.5. *For $d > \delta$ we have the following inequality:*

$$I_\delta(d) \geq U_\delta(d) \geq S_\delta(d).$$

Proof. The floor plans counted by $S_\delta(d)$ are always counted by $U_\delta(d)$ and also by $I_\delta(d)$. The number $U_\delta(d)$ counts the same floor floor plans as $S_\delta(d)$ as well as the floor plans with node germs in adjacent floors or at least two node germs in the same floor such that the node germs give rise to separated nodes. We have to compare the multiplicity of such such a floor plan as counted by $U_\delta(d)$ with the multiplicity an artificial floor plan with nodes in the same positions will be counted with.

If we have strings in adjacent floors or in the same floor and their alignment fits with smooth adjacent floors, then their multiplicities are counted in the same way by $U_\delta(d)$ and $I_\delta(d)$. This does not mean that the adjacent floors have to be
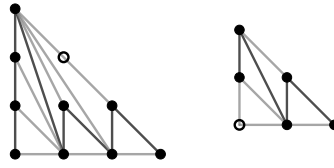
Figure 8.3: The dual subdivisions to the nodal floors in [BG20, Case (7c,9f)]. In the cubic part, the node germ induces a triangle without vertical edges. Without the node germ, there would be two bounded horizontal edges in the cubic floor for the left string in the conic floor to align with.

smooth, it just rules out alignments which are only possible if the adjacent floor is not smooth.

Other alignments arise from strings that align with a vertex, which would not exist if the corresponding floor were smooth. These give a contribution to $U_\delta(d)$ which is smaller than the alignment counted by $I_\delta(d)$. This is due to the fact that an alignment with a vertex is counted only with multiplicity 1, while alignments with bounded edges are counted with multiplicity 2.

For example, in [BG20, Case (7c,9f)] illustrated in Figure 8.3, we have that $U_\delta(d)$ and $I_\delta(d)$ count the same number of alignments, but the alignment of the left string with a vertex not adjacent to a horizontal edge (counted by $U_\delta(d)$) has multiplicity 1, whereas $I_\delta(d)$ counts an alignment with a horizontal bounded edge with multiplicity 2. This horizontal bounded edge is replaced by the vertex dual to the triangle without vertical edges in [BG20, Case (7c,9f)].

Furthermore, smooth adjacent floors offer the maximum number of possible alignments for right strings. If the node germs are weight 2 ends, again smooth adjacent floors offer the highest multiplicity.

As $I_\delta(d)$ counts the situation where every node germ has smooth adjacent floors, $I_\delta(d)$ can count more cases than $U_\delta(d)$, and it counts them with at least the same multiplicity. It follows that $I_\delta(d) \geq U_\delta(d)$. □

We will now show that for small δ, the overcount $I_\delta(d)$ is still too small to produce the second coefficient of $N_{\delta,\mathbb{C}}^{\mathbb{P}^3}(d)$. Therefore, relaxing the notion of a floor plan to allow nodes to be in the same or in adjacent floors is not enough to produce the second order coefficient of the asymptotic count from [MMSS22, Theorem 6.1]. Thus, the unseparated nodes contribute in degree $d^{3\delta-1}$.

Theorem 8.2.6. *For $\delta = 2, 3$, there are at most*

$$I_2(d) = 8d^6 - \frac{168}{5}d^5 + \mathcal{O}(d^4), \qquad I_3(d) = \frac{32}{3}d^9 - \frac{1341}{35}d^8 + \mathcal{O}(d^7),$$

surfaces with separated nodes.

Equivalently, the number of δ-nodal surfaces of degree d passing through points in Mikhalkin position such that their tropicalization has unseparated nodes is at least

$$(\frac{168}{5} - 24)d^5 + \mathcal{O}(d^4) > 0 \ \ for \ \ \delta = 2,$$
$$and \ \ (\frac{1341}{35} - 32)d^8 + \mathcal{O}(d^7) > 0 \ \ for \ \ \delta = 3.$$

Therefore, surfaces with separated nodes are insufficient to asymptotically count binodal and trinodal surfaces up to two degrees.

Proof. We begin by counting the multiplicity of a given artificial floor plan I. Let $(i_1, \ldots, i_\delta)$ be the weakly decreasing sequence which records the floors of the node germs of I.

We now calculate the contribution from the presence of a node germ in floor i_j. This will be a polynomial in i_j. When counting, we will only consider the top two orders in i_j, because these are the only terms that will impact the top two degrees in our asymptotic count. Given a node germ in floor i_j, there are several possibilities for what kind of node germ it is:

1. Parallelogram ($i_j \neq 1, d$). By Proposition 4.6 of [MMSS22], the number of one-nodal curves of degree i_j with a parallelogram is $3i_j^2 - 6i_j + 3$, and the complex multiplicity of such a node germ is 2. This case contributes $6i_j^2 - 12i_j + \mathcal{O}(1)$ to our count.

2. Horizontal end ($1 < i_j < d$). The number of curves of degree d with a weight 2 horizontal end is $i_j - 1$, because there are that many possible locations for a weight 2 horizontal end. The multiplicity is $2(i_j + 1)$ by [MMSS22, Definition 5.4]. This contributes $2i_j^2 + \mathcal{O}(1)$ to our count.

3. Diagonal end($1 < i_j$). Analogous to the the case of the horizontal end, the number of curves of degree d with a weight 2 diagonal end is $i_j - 1$. By [MMSS22, Definition 5.4] the multiplicity for diagonal ends is $2(i_j - 1)$. This contributes $2i_j^2 - 4i_j + \mathcal{O}(1)$ to the count.

4. Right string ($1 < i_j$). There are two alignment options for right strings. A right string can meet a diagonal bounded edge of C_{i_j-1}. There are $i_j - 2$ many diagonal bounded edge of C_{i_j-1}. Each such alignment is counted with multiplicity 2.

   Or, a right string aligns with a vertex not adjacent to a diagonal edge. There are $2(i_j - 3 + i_j - 4 + \ldots + 1) = (i_j - 3)^2 + (i_j - 4) = i_j^2 - 5i_j + \mathcal{O}(1)$ many such vertices. These alignments are counted with multiplicity 1. Thus, we get $2 \cdot (i_j - 2) + i_j^2 - 5i_j + \mathcal{O}(1) = i_j^2 - 3i_j + \mathcal{O}(1)$ surfaces for our count.

5. Left string ($i_j < d$). For a left string there is only one alignment option, since the adjacent floors are smooth: It can align with any horizontal bounded edge of C_{i_j+1}. As C_{i_j+1} is a smooth tropical plane curve of degree $i_j + 1$ satisfying horizontally stretched point conditions, there are $i_j + \ldots + 1 = \frac{1}{2}(i_j^2 + i_j)$ such edges. Each possible alignment is counted with multiplicity 2. This contributes $i_j^2 + i_j$ to the count.

Thus, a node germ in floor i_j for $i_j \neq 1, d$ contributes

$$6i_j^2 - 12i_j + 2i_j^2 + 2i_j^2 - 4i_j + i_j^2 - 3i_j + i_j^2 + i_j + \mathcal{O}(1) = 12i_j^2 - 18i_j + \mathcal{O}(1). \quad (8.3)$$

If $i_j = d$, then it contributes

$$2d^2 - 4d + d^2 - 3d + \mathcal{O}(1) = 3d^2 - 7d + \mathcal{O}(1), \quad (8.4)$$

and if $i_j = 1$, then it contributes

$$1^2 + 1 + \mathcal{O}(1) = \mathcal{O}(1). \quad (8.5)$$

Suppose $\delta = 2$. We sum over all choices of $i_1, i_2 > 1$ to obtain the count. We can discard the case $i_j = 1$, since this will not contribute to the top two terms asymptotically. We have

$$I_2(d) = \sum_{i_1=2}^{d-1} \sum_{i_2=2}^{i_1} \prod_{j=1}^{2} (12i_j^2 - 18i_j) + (3d^2 - 7d)\Big(\sum_{i_2=2}^{d-1} (12i_2^2 - 18i_2)\Big) + (3d^2 - 7d)^2$$

$$= 8d^6 - \frac{168}{5}d^5 + \mathcal{O}(d^4).$$

Suppose $\delta = 3$. We sum over all choices of $i_1, i_2, i_3 > 1$ to obtain the count. We ignore the possibility of a node in the first floor because this will not contribute to the asymptotic count. We have

$$I_3(3) = \sum_{i_1=2}^{d-1} \sum_{i_2=2}^{i_1} \sum_{i_3=2}^{i_2} \prod_{j=1}^{3} (12i_j^2 - 18i_j) + (3d^2 - 7d) \sum_{i_2=2}^{d-1} \sum_{i_3=2}^{i_2} \prod_{j=2}^{3} (12i_2^2 - 18i_2)$$

$$+ (3d^2 - 7d)^2 \sum_{i_3=2}^{d-1} (12i_2^2 - 18i_2) + (3d^2 - 7d)^3$$

$$= \frac{32}{3}d^9 - \frac{1341}{35}d^8 + \mathcal{O}(d^7).$$

$\square$

As immediate consequence from Theorem 8.2.6 and Equation (8.2), we obtain the following corollary.

Corollary 8.2.7. *There are at least $\frac{48}{5}d^5 + \mathcal{O}(d)$ binodal surfaces of degree d with unseparated nodes. There are at least $\frac{221}{35}d^8 + \mathcal{O}(d)$ trinodal surfaces of degree d with unseparated nodes.*

Remark 8.2.8. Note that for $\delta = 4$, our method of proof is inconclusive. This follows from counting artificial floor plans with 4 nodes and comparing the coefficients of the top two degrees with the coefficients of the top two degrees in Equation (8.2) for $\delta = 4$.

To obtain the number of artificial floor plans $I_4(d)$, we proceed as in the proof of Theorem 8.2.6. We sum over all choices of $i_1, i_2, i_3, i_4 > 1$ to obtain the count. As before for $\delta = 2, 3$, we can ignore the cases with $i_j = 1$ as they do not contribute to the top two degrees. Additionally, we allow at most i_1 to possibly equal d, because (as can be seen for $\delta = 2, 3$) having more than one $i_j = d$ does not contribute to the top two degrees. Using the multplicities as determined in Equations (8.3) and (8.4), we obtain:

$$
\begin{aligned}
I_4(d) &= \sum_{i_1=2}^{d-1} \sum_{i_2=2}^{i_1} \sum_{i_3=2}^{i_2} \sum_{i_4=2}^{i_3} \prod_{j=1}^{4} (12i_j^2 - 18i_j) + (3d^2 - 7d) \sum_{i_2=2}^{d-1} \sum_{i_3=2}^{i_2} \sum_{i_4=2}^{i_3} \prod_{j=2}^{4} (12i_2^2 - 18i_2) \\
&= \frac{32}{3}d^{12} - \frac{64}{5}d^{11} + \mathcal{O}(d^{10}).
\end{aligned}
$$

Substituting $\delta = 4$ in Equation (8.2), we get:

$$
\begin{aligned}
N_{4,\mathbb{C}}^{\mathbb{P}^3}(d) &= \frac{4^4}{4!}d^{12} - \frac{3 \cdot 4^4}{4!}d^{11} + \mathcal{O}(d^{10}) \\
&= \frac{32}{3}d^{12} - 32d^{11} + \mathcal{O}(d^{10}).
\end{aligned}
$$

Since $\frac{-64}{5} > -32$, it follows that for 4 nodes this method is inconclusive to determine whether surfaces with unseparated nodes are sufficient to produce the coefficients of the top two degrees of the count.

Chapter 9

Binodal polytopes

We have seen in Theorem 8.2.6 that separated nodes are not sufficient to asymptotically count multi-nodal surfaces up to the second order term. This motivates the investigation of unseparated nodes. This chapter is concerned with the examination of small polytopes that can be the support of a binodal surface.

Section 9.1.1 introduces the (generalized) binodal variety and the algorithms to compute it. In Section 9.1.2, we introduce the notion of binodal polytopes, which are polytopes that are the support of a binodal surface. We determine some first conditions for polytopes to be binodal, for example that they must have at least 6 lattice points (Lemma 9.1.9).

Since we want to improve the counting method of tropical floor plans to include unseparated nodes, and tropical floor plans count floor decomposed surfaces, we start in Section 9.2 with the investigation of lattice polytopes of width 1 with 6 lattice points. We go through the classification from [BS16b] and extract 6 families. Since the families are infinite, we can only verify the claim that they are binodal (Conjecture 9.2.8) for a few representatives fo each family.

Section 9.3 revisits the lattice paths introduced in Section 7.2 and specializes them for the binodal case. Subsection 9.3.2 further explains how to compute the multiplicities of lattice paths.

In Section 9.4, we go through the 6 families of binodal polytopes one by one, determine the valid lattice paths and state conjectures based on computed data for the path multiplicities.

Section 9.5 ends this chapter by a display on how the results determined in the earlier sections can be used to count binodal surfaces.

This chapter is based on joint work with Madeline Brandt [BG21]. The computations are done using [Gei22]. For completeness this code is contained in Appendix B.2.

9.1 Binodal surfaces

To count binodal surfaces passing through general points via tropical geometry, we have to understand the parameter space of binodal surfaces with a fixed support. This is the topic of Section 9.1.1.

In Section 9.1.2 we make first steps towards finding out what kind of polytopes can be the support of a binodal surface.

9.1.1 Binodal variety

We want to count surfaces with two isolated singularities and a fixed dual Newton polytope. Therefore we make the following definition, similar to the discriminant $\mathrm{Sing}(\Omega)$ in Definition 7.1.3:

Definition 9.1.1. Let Ω be a lattice polytope with $\Omega \cap \mathbb{Z}^3 = \{\omega_0, \ldots, \omega_{N+1}\}$. Consider the set of surfaces with support $\Omega \cap \mathbb{Z}^3$ with two distinct nodes as singularities in the torus $(\mathbb{K}^*)^3$:

$$
B_\Omega^{\mathrm{aff}} = \{(a_{\omega_0}, \ldots, a_{\omega_{N+1}}) \in (\mathbb{K}^*)^{N+2} \mid V(f) \text{ with } f = \sum_{i=0}^{N+1} a_{\omega_i} \underline{x}^{\omega_i} \text{ has two}
$$

$$
\text{distinct nodes in } (\mathbb{K}^*)^3\}
$$

$$
= (V(f, \tfrac{\partial f}{\partial x_1}, \tfrac{\partial f}{\partial x_2}, \tfrac{\partial f}{\partial x_3}, q, \tfrac{\partial q}{\partial u_1}, \tfrac{\partial q}{\partial u_2}, \tfrac{\partial q}{\partial u_3}, 1 - t \prod_{i=1}^{3} x_i u_i,) \setminus V(u_1 - x_1, u_2 - x_2, x_3 - u_3))
$$

$$
\cap \mathbb{K}[a_{\omega_0}, \ldots, a_{\omega_{N+1}}],
$$

where $q = \sum_{i=0}^{N+1} a_{\omega_i} \underline{u}^{\omega_i}$. This is an affine variety, which is contained in $\mathrm{Sing}_{\mathrm{aff}}(\Omega)$. As for the discriminant, multiplying all the coordinates a_{ω_i} with a non-zero scalar does not change the support of the surface or the existence of the two singularities. Therefore, we can consider this as a projective variety:

$$
B_\Omega = \{(a_{\omega_0} : \ldots : a_{\omega_{N+1}}) \in \mathbb{P}^{N+1} \mid \text{ all } a_{\omega_i} \neq 0, \text{ and } V(f) \text{ with } f = \sum_{i=0}^{N+1} a_{\omega_i} \underline{x}^{\omega_i}
$$

$$
\text{has two distinct nodes in } (\mathbb{K}^*)^3\}
$$

$$
= (B_\Omega^{\mathrm{aff}} / \sim) \setminus V(a_{\omega_0} \cdots a_{\omega_{N+1}}) \subset \mathrm{Sing}(\Omega).
$$

We call B_Ω the *binodal variety of hypersurfaces of support* $\Omega \cap \mathbb{Z}^3$.

The *tropical binodal variety* is its tropicalization:

$$
\mathrm{Trop}(B_\Omega) \subset \mathbb{R}^{N+2} / (1, \ldots, 1)\mathbb{R}.
$$

Lemma 9.1.2. *The* expected dimension *of the binodal variety is*

$$\dim_{\text{expected}}(B_\Omega) = |\Omega \cap \mathbb{Z}^3| - 3,$$

i.e., we expect it to be of codimension 1 *in the discriminant Sing*(Ω)*.*

By the Structure Theorem for tropical varieties [MS15, Theorem 3.3.5] the dimension of the tropical variety coincides with the dimension of the binodal variety.

Proof. The projective space of all surfaces with support $|\Omega \cap \mathbb{Z}^3|$ has dimension $|\Omega \cap \mathbb{Z}^3| - 1$. We expect the two nodes to be independent, and for each independent node we intersect this space with a codimension-1 space, and thus lose one dimension. However, the surfaces corresponding to points the binodal variety could all contain non-isolated singularities. In this case, the dimension of the binodal variety could be larger. □

Remark 9.1.3. The aim of this chapter and of Chapter 10 is to count binodal surfaces with a given support. For this we will fix $|\Omega \cap \mathbb{Z}^3| - 3$ many points in general position, since the intersection of the binodal variety with the $|\Omega \cap \mathbb{Z}^3| - 3$ linear spaces of dimension 1 given by the generic point conditions will be of dimension 0, so that we will obtain a sensible finite number.

When the binodal variety is not of expected dimension, it either means that the corresponding surfaces can never satisfy our general point conditions, or it means that some singularities are dependent so that the binodal variety is of a too large dimension and our general point conditions do not determine the surface. These cases we want to exclude.

We can compute the binodal variety by using Algorithm 5.

When examining whether a given a lattice polytope is binodal, we want to use computational tools to compute the binodal variety and its properties. The computations in Part II of this thesis are done with `Singular` and `OSCAR`. The functions for `OSCAR` were written by the author during the joint work with Madeline Brandt on [BG21] and edited during the writing of this thesis. The revised functions are available at [Gei22], additionally they are contained in the Appendix B.2. Example 9.1.6 gives a brief demonstration of the functions for computing the (generalized) binodal variety.

To keep the number of variables used in the computation smaller and to avoid an additional variable that needs to be eliminated, we instead compute the generalized binodal variety as defined below, and then check whether the generalized binodal variety has components for which the ideal contains monomials; see Lemma 9.1.5. This is only an auxiliary step. It is also possible to directly compute the binodal

---

Algorithm 5 Computing the binodal variety B_Ω

Input: $M = (m_{i,j}) \in \mathrm{Mat}_{3 \times n}$ filled with the lattice points of Ω
Output: Generators of the ideal I for which $V(I) = B_\Omega$

1: $f = \sum_{j=1}^{n} a_i x_1^{m_{j,1}} x_2^{m_{j,2}} x_3^{m_{j,3}}$

2: $q = \sum_{j=1}^{n} a_i u_1^{m_{j,1}} u_2^{m_{j,2}} u_3^{m_{j,3}}$

3: $J = \langle f, \frac{\partial f}{\partial x_1}, \frac{\partial f}{\partial x_2}, \frac{\partial f}{\partial x_3}, q, \frac{\partial q}{\partial u_1}, \frac{\partial q}{\partial u_2}, \frac{\partial q}{\partial u_3}, 1 - t \prod_{i=1}^{3} x_i u_i, 1 - s \prod_{i=1}^{n} a_i \rangle$

$\quad \triangleright$ *The polynomial $1 - t \prod_{i=1}^{3} x_i u_i$ is used to ensure that the singularities are in the torus*

$\quad \triangleright$ *The polynomial $1 - s \prod_{i=1}^{n} a_i$ is used to ensure that all coefficients of f are non-zero*

4: J_S = saturation of J with respect to $\langle x_1 - u_1, x_2 - u_2, x_3 - u_3 \rangle$ $\triangleright$ *This ensures that the singularities are distinct*

5: J_E = elimination of $s,t,x_1,x_2,x_3,u_1,u_2,u_3$ from J_S

6: G generators of J_E in $\mathbb{Q}[a_1,\ldots,a_n]$

7: **return** $I = \mathrm{Radical}(\langle G \rangle)$

---

variety (see Algorithm 5) but it might take more computational time and/or memory, which is why we introduce the following definition.

Definition 9.1.4. Let Ω be a lattice polytope with $\Omega \cap \mathbb{Z}^3 = \{\omega_0, \ldots, \omega_{N+1}\}$. We define the *generalized binodal variety* of hypersurfaces with support Ω as

$$B_\Omega^{\mathrm{gen}} = \{(a_{\omega_0} : \ldots : a_{\omega_{N+1}}) \in \mathbb{P}^{N+1} | V(f) \text{ with } f = \sum_{i=0}^{N+1} a_{\omega_i} \underline{x}^{\omega_i}$$

$$\text{has two distinct nodes in } (\mathbb{K}^*)^3\}.$$

This is an auxiliary variety for computational reasons as explained above. It is nearly the same as the binodal variety as demonstrated in the following lemma.

Lemma 9.1.5. *Let $B_\Omega^{\mathrm{gen}} = V(I)$ and let $I = J_1 \cap \ldots \cap J_s$ be a primary decomposition of $I \subset \mathbb{K}[a_{\omega_0}, \ldots, a_{\omega_{N+1}}]$. Let $K := \{i : J_i \cap \langle a_{\omega_0} \cdot \ldots \cdot a_{\omega_{N+1}} \rangle = \emptyset\} \subset \{1, \ldots, s\}$. Then*

$$B_\Omega = V(\bigcap_{i \in K} J_i). \tag{9.1}$$

Proof. It follows directly form the definition that $B_\Omega = B_\Omega^{\mathrm{gen}} \setminus V(a_{\omega_0} \cdots a_{\omega_{N+1}})$. Since we choose I to be radical (see Algorithm 6), the J_i are prime ideals. Therefore, $J_i \cap \langle a_{\omega_0} \cdot \ldots \cdot a_{\omega_{N+1}} \rangle = \emptyset$ is equivalent to $\langle a_{\omega_0} \cdot \ldots \cdot a_{\omega_{N+1}} \rangle \subset J_i$. So the claim holds. $\qquad \square$

Algorithm 6 describes the algorithm to determine the generalized binodal variety.

The only difference to Algorithm 5, which describes the binodal variety, is that we dispense with the polynomial $1 - s \prod_{i=1}^{n} a_i$ in the definition of J. Thus, we don't need the variable s anymore, which later had to be eliminated.

Algorithm 6 Computing the generalized binodal variety $B_{\Omega}^{\mathrm{gen}}$

Input: $M = (m_{i,j}) \in \mathrm{Mat}_{3 \times n}$ filled with the lattice points of Ω
Output: Generators of the ideal I for which $V(I) = B_{\Omega}^{\mathrm{gen}}$

1: $f = \sum_{j=1}^{n} a_i x_1^{m_{j,1}} x_2^{m_{j,2}} x_3^{m_{j,3}}$
2: $q = \sum_{j=1}^{n} a_i u^{m_{j,1}} v^{m_{j,2}} w^{m_{j,3}}$
3: $J = \langle f, \frac{\partial f}{\partial x_1}, \frac{\partial f}{\partial x_2}, \frac{\partial f}{\partial x_3}, q, \frac{\partial q}{\partial u_1}, \frac{\partial q}{\partial u_2}, \frac{\partial q}{\partial u_3}, 1 - t \prod_{i=1}^{3} x_i u_i \rangle$
   $\triangleright$ *The polynomial $1 - t \prod_{i=1}^{3} x_i u_i$ is used to ensure that the singularities are in the torus*
4: $J_S =$ saturation of J with respect to $\langle x_1 - u_1, x_2 - u_2, x_3 - u_3 \rangle$ $\triangleright$ *This ensures that the two singularities are distinct*
5: $J_E =$ elimination of $t, x_1, x_2, x_3, u_1, u_2, u_3$ from J_S
6: G generators of J_E in $\mathbb{Q}[a_1, \ldots, a_n]$
7: **return** $I = \mathrm{Radical}(\langle G \rangle)$

We will mostly use Algorithm 7 to compute the binodal variety from the generalized variety. The advantage of this procedure is that we can already deduce from the dimension of the generalized binodal variety whether we have to apply the primary decomposition: Since $B_{\Omega}^{\mathrm{gen}} \supset B_{\Omega}$, we can deduce from $\dim(B_{\Omega}^{\mathrm{gen}}) < \dim_{\mathrm{expected}}(B_{\Omega})$, that the lattice polytope Ω cannot be support of a binodal surface satisfying $|\mathbb{Z}^3 \cap \Omega| - 3$ general point conditions. In this case, we do not need to compute B_{Ω}.

Algorithm 7 Computing the binodal variety B_{Ω} from $B_{\Omega}^{\mathrm{gen}}$

Input: $M = (m_{i,j}) \in \mathrm{Mat}_{3 \times n}$ filled with the lattice points of Ω
Output: ideal I for which $V(I) = B_{\Omega}$

1: J ideal generating $B_{\Omega}^{\mathrm{gen}}$ as computed by Algorithm 6
2: $I = \langle 1 \rangle$
3: Compute primary decomposition $(J_1, \ldots, J_s)$ of J
4: **for** $i \in \{1, \ldots, s\}$ **do**
5:    **if** $J_i \cap \langle a_{\omega_0} \cdot \cdots \cdot a_{\omega_{N+1}} \rangle = \emptyset$ **then**
6:       $I = I \cap J_i$
7:    **end if**
8: **end for**
9: **return** I

Example 9.1.6. We demonstrate the use of the `OSCAR` functions `general_binodal`, `binodal` and `investigate_binodal`, see [Gei22] or Appendix B.2. We first have to include the functions.

```
julia> using Oscar;
julia> include("YOUR/PATH/TO/code_binodals.jl")
```

As an example we consider first the polytope given by the rows of the matrix `M1` as lattice points. The function `general_binodal` computes the generalized binodal variety, while the function `binodal` computes the binodal variety.

```
julia> M1 = matrix(ZZ,6,3,[0,0,0,0,1,0,0,1,1,0,1,2,0,2,0,1,0,0])
[0   0   0]
[0   1   0]
[0   1   1]
[0   1   2]
[0   2   0]
[1   0   0]

julia> general_binodal(M1)
ideal(a6, -64*a1*a4^2*a5 + 16*a2^2*a4^2 - 8*a2*a3^2*a4 + a3^4)

julia> binodal(M1)
ideal(1)
```

We observe that the ideal to the generalized binodal variety of `M1` contains the monomial `a6`. Consequently, the binodal variety of `M1` is empty.

Let us now consider the polytope given by the rows of the matrix `M9` as lattice points. (The numbering of the matrices becomes clear when consulting Table 9.1).

```
julia> M9 = matrix(ZZ,6,3,[0,0,0,0,0,1,0,1,0,0,1,1,1,0,0,1,0,1])
[0   0   0]
[0   0   1]
[0   1   0]
[0   1   1]
[1   0   0]
[1   0   1]

julia> general_binodal(M9)
ideal(-a3*a6 + a4*a5, -a1*a6 + a2*a5, -a1*a4 + a2*a3)

julia> binodal(M9)
ideal(-a3*a6 + a4*a5, -a1*a6 + a2*a5, -a1*a4 + a2*a3)
```

Observe that the generalized binodal variety coincides with the binodal variety. We can now investigate the binodal variety for its dimension and degree. The function `investigate_binodal` prints the results and returns the tuple (dim, deg). The function has two methods: either input the matrix defining the polytope, or the radical ideal defining the binodal variety. We show the example for the polytope.

```
julia> investigate_binodal(M9)
Affine dimension of the generalized variety is 4
The binodal variety is of expected affine dimension.
Degree of the binodal variet is 3
[0 0 0; 0 0 1; 0 1 0; 0 1 1; 1 0 0; 1 0 1] could be a binodal
    polytope.
(4, 3)
```

The notation of binodal polytope is explained in Definition 9.1.8.

9.1.2 Binodal polytopes

This section gives first answers to the question which polytopes we can expect to see as Newton polytopes of binodal surfaces. We demonstrate that a binodal polytope has to have at least 6 lattice points and that prove that for a binodal surface with Newton polytope with exactly 6 lattice points the tropical surface is a fan with both nodes tropicalizing to the unique vertex.

Notation 9.1.7. Let $\Omega \subset \mathbb{R}^3$ be a lattice polytope and let $\omega_0, \ldots, \omega_N$ denote its lattice points. We will abuse notation and instead of $\Omega = \text{conv}\{\omega_0, \ldots, \omega_{N+1}\}$ we will often use the notation

$$\Omega = \begin{pmatrix} m_{1,1} & \cdots & m_{1,N+2} \\ \vdots & \ddots & \vdots \\ m_{3,1} & \cdots & m_{3,N+2} \end{pmatrix} \tag{9.2}$$

where

$$\begin{pmatrix} m_{1,j+1} \\ m_{2,j+1} \\ m_{3,j+1} \end{pmatrix} := \omega_j, \text{ for } j \in \{0, \ldots, N+1\}.$$

Definition 9.1.8. We say that a 3-dimensional lattice polytope Ω is *binodal* if the binodal variety B_Ω is of the expected dimension and if there exists a surface passing through $|\Omega \cap \mathbb{Z}^3| - 3$ points in general position that contains two nodes as its only singularities and has Newton polytope Ω.

If general points in the binodal variety induce surfaces with non-isolated singularities, the binodal variety can still have the expected dimension. Since we want to exclude such a case, we need to add the existence of a binodal variety with support Ω to the definition.

In order to tropically count surfaces of a given degree with at least two nodes we have to count unseparated nodes. To do this, we must first understand the smallest possible Newton polytopes of binodal surfaces.

Lemma 9.1.9. *Let Ω be a 3-dimensional binodal polytope. Then $|\Omega \cap \mathbb{Z}^3| \geq 6$.*

Proof. Suppose Ω were a binodal 3-dimensional lattice polytope with $|\Omega \cap \mathbb{Z}^3| \leq 5$. Then the projective dimension of B_Ω would be ≤ 2. See Definitions 9.1.1 and 9.1.8.

On the other hand, there exists a surface with two isolated singularities that has Newton polytope Ω. By translating this surface in $\mathbb{K}^3$, we obtain a 3-dimensional family of binodal surfaces with Newton polytope Ω. So the dimension of B_Ω is at least 3. This contradicts the number of lattice points of Ω, hence we must have $|\Omega \cap \mathbb{Z}^3| \geq 6$. $\qquad\qquad\square$

For separated nodes, Theorem 7.1.7 stated the position of the tropicalized singularity for each circuit position. Similarly to the case of separated nodes, we want to know where the singularities tropicalize to when we are given a binodal polytope with 6 lattice points.

Proposition 9.1.10. *Let Ω be a binodal polytope with 6 lattice points, and let S be a binodal surface over $\mathbb{C}\{\{t\}\}$ with Newton polytope Ω. Then $trop(S)$ is a fan and both nodes tropicalize to the vertex of the fan.*

Proof. Let B_Ω be the variety of binodal surfaces with Newton polytope Ω. It has projective dimension 3 inside $\mathbb{P}^5$.

Without loss of generality, we may translate the surface S so that one node of S is located at $(1,1,1)$. Let L be the variety of surfaces with Newton polytope Ω and one node at $(1,1,1)$. We denote by $M = (m_{i,j}) \in \mathrm{Mat}_{3\times 6}$ the matrix obtained from the lattice points of Ω as in Notation 9.1.7.

Let $a_0,\ldots,a_5$ be the coordinates on $\mathbb{P}^5$. Let

$$f(x,y,z) = a_0 x^{m_{1,1}} y^{m_{2,1}} z^{m_{3,1}} + \cdots + a_5 x^{a_{1,6}} y^{a_{2,6}} z^{a_{3,6}}$$

be a generic polynomial defining a surface with Newton polytope Ω. Then L is the variety cut out by the linear equations

$$
\begin{aligned}
f(1,1,1) &= a_0 + a_1 + a_2 + a_3 + a_4 + a_5 = 0,\\
\frac{\partial f}{\partial x}(1,1,1) &= a_0 m_{1,1} + a_1 m_{1,2} + a_2 m_{1,3} + a_3 m_{1,4} + a_4 m_{1,5} + a_5 m_{1,6} = 0,\\
\frac{\partial f}{\partial y}(1,1,1) &= a_0 m_{2,1} + a_1 m_{2,2} + a_2 m_{2,3} + a_3 m_{2,4} + a_4 m_{2,5} + a_5 m_{2,6} = 0,\\
\frac{\partial f}{\partial z}(1,1,1) &= a_0 m_{3,1} + a_1 m_{3,2} + a_2 m_{3,3} + a_3 m_{3,4} + a_4 m_{3,5} + a_5 m_{3,6} = 0.
\end{aligned}
$$

It follows that L is the linear space defined by the kernel of the 4×6 matrix

$$M_L := \begin{pmatrix} 1 & 1 & 1 & 1 & 1 & 1 \\ m_{1,1} & m_{1,2} & m_{1,3} & m_{1,4} & m_{1,5} & m_{1,6} \\ m_{2,1} & m_{2,2} & m_{2,3} & m_{2,4} & m_{2,5} & m_{2,6} \\ m_{3,1} & m_{3,2} & m_{3,3} & m_{3,4} & m_{3,5} & m_{3,6} \end{pmatrix} \in \mathrm{Mat}_{4 \times 6}.$$

Since Ω is 3-dimensional, this matrix has rank 4. So $\dim(\ker(M_L)) = 2$, and thus $L = \ker(M_L)$ defines a projective linear space of projective dimension 1.

Consider the discriminant $\mathrm{Sing}(\Omega)$ of hypersurfaces of support $\Omega \cap \mathbb{Z}^3$ (Definition 7.1.3). Then $\mathrm{Sing}(\Omega)$ has codimension 1 in $\mathbb{P}^5$, and $B_\Omega \subset \mathrm{Sing}(\Omega)$ is of codimension 1. Further, the linear space L is contained in the discriminant $L \subset \mathrm{Sing}(\Omega)$. Moreover, the one dimensional linear space L is not contained in B_Ω because there may be surfaces with exactly one node, located at (1,1,1), which are described by points in L and not in B_Ω. It follows that the intersection $B_\Omega \cap L \subset \mathrm{Sing}(\Omega)$ has dimension 0 and consists of finitely many points.

Since B_Ω and L are defined by equations over $\mathbb{C}$, and $\mathbb{C} \subset \mathbb{C}\{\{t\}\}$ is algebraically closed, points in $B_\Omega \cap L$ are defined over $\mathbb{C}$. Each point in $B_\Omega \cap L$ is a complex surface whose nodes are also defined over $\mathbb{C}$. Thus, the tropicalization of surfaces in $B_\Omega \cap L$ are fans with vertex at (0,0,0) and both nodes tropicalizing to (0,0,0). $\square$

Remark 9.1.11. This proposition and its proof hold more generally for δ-nodal polytopes of dimension d with $\delta + d + 1$ lattice points.

Remark 9.1.12. In this thesis we do not investigate polytopes with 7 or more lattice points. Binodal polytopes with 7 lattice points can be properly subdivided inside the subdivision. There are 496 three-dimensional polytopes with 7 lattice points and width greater than 1 [BS18]. The infinite families of polytopes with 7 vertices and width 1 are not classified.

Some subdivisions of polytopes with more than 6 lattice points that might be dual to binodal surface can be found in [BG20, Section 5].

9.2 Polytopes with 6 lattice points of width 1

In this section we analyze polytopes with 6 lattice points and investigate whether they are binodal. This section is based on joint work with Madeline Brandt [BG21].

We use the classifications of three-dimensional polytopes with small numbers of lattice points given by Blanco and Santos [BS16a, BS16b, BS18]. These classifications give the finitely many 3-polytopes with n lattice points for $5 \le n \le 11$ and width greater than 1. For polytopes with width equal to 1, they give a classification of the finitely many infinite families of polytopes with 5 and 6 lattice points.

Because of Lemma 9.1.9 we only consider polytopes with 6 lattice points. We now explain why we restrict to polytopes of width 1.

Remark 9.2.1. When a polytope has width greater than 1, it will not appear in the subdivision of a floor decomposed surface without being further subdivided. However, we do not know that tropical surfaces through points in Mikhalkin position with more than one node are necessarily floor decomposed. See Remark 7.3.3.

As we have seen in Proposition 9.1.10, binodal polytopes with 6 lattice points can only appear in the dual subdivision of a tropical binodal surface if the binodal polytope has the trivial subdivision. Therefore, only the ones with width 1 could appear in a floor decomposed surface.

We use the classification of polytopes with 6 lattice points of width 1 from [BS16b] to search for binodal polytopes.

We only consider polytopes up to integral unimodular affine transformations, also called *IUA-equivalence* [MMS12].

Definition 9.2.2. We consider two polytopes *equivalent* or *IUA-equivalent* if they can be transferred into each other by affine translations and multiplication, of the lattice points with an element of $SL_3(\mathbb{Z})$.

From [BS16b, Tables 5, 6 & 7] that provide a list of the finitely many polytope families with 6 lattice points and of width 1, we have extracted a list of polytope families in Table 9.1 as follows: First, we deleted those polytopes for which an IUA-equivalent polytope appears somewhere else in the Tables 5, 6, and 7 from [BS16b]; see [BS16b, Remark 4.3]. That way, the remaining polytope families contained unique representatives up to IUA-equivalence. To make computations of the binodal variety easier, we have translated each polytope to ensure that all coordinate entries are positive. For consistency with [BG20], we permuted the coordinates by $(x\,z\,y)$ and ordered the lattice points by the partial order induced by $v = (1, \eta, \eta^2)$ with $0 < \eta \ll 1$; see Definition 7.2.3.

We enumerate the resulting polytope families from 1 to 21. They are displayed in Table 9.1.

In [BS16b] polytope family 21 is given with the restriction $ad - bc = \pm 1$. By applying the $SL_3(\mathbb{Z})$ operation that switches the entries in the y and z coordinates, we see that the polytope family satisfies a symmetry condition, and without loss of generality, we can assume that $ad - bc = 1$.

The remainder of this section is concerned with sorting out those polytopes from this list that cannot be binodal.

no.	Figure	Lattice points
1		$\begin{pmatrix} 0 & 0 & 0 & 0 & 0 & 1 \\ 0 & 1 & 1 & 1 & 2 & 0 \\ 0 & 0 & 1 & 2 & 0 & 0 \end{pmatrix}$
2		$\begin{pmatrix} 0 & 0 & 0 & 0 & 0 & 1 \\ 0 & 1 & 1 & 1 & 2 & 0 \\ 1 & 0 & 1 & 2 & 1 & 0 \end{pmatrix}$
3		$\begin{pmatrix} 0 & 0 & 0 & 0 & 0 & 1 \\ 0 & 0 & 0 & 1 & 1 & 0 \\ 0 & 1 & 2 & 0 & 1 & 0 \end{pmatrix}$
4		$\begin{pmatrix} 0 & 0 & 0 & 0 & 0 & 1 \\ 0 & 1 & 1 & 1 & 2 & 0 \\ 0 & 1 & 2 & 3 & 1 & 0 \end{pmatrix}$
5		$\begin{pmatrix} 0 & 0 & 0 & 0 & 0 & 1 \\ 0 & 1 & 1 & 2 & 2 & 0 \\ 0 & 1 & 2 & 1 & 2 & 0 \end{pmatrix}$
6		$\begin{pmatrix} 0 & 0 & 0 & 0 & 1 & 1 \\ 0 & 1 & 1 & 2 & 0 & 1 \\ 0 & 1 & 2 & 1 & 0 & 0 \end{pmatrix}$

no.	Figure	Lattice points
7		$\begin{pmatrix} 0 & 0 & 0 & 0 & 1 & 1 \\ 0 & 1 & 1 & 2 & 0 & 1 \\ 0 & 1 & 2 & 1 & 0 & 1 \end{pmatrix}$
8		$\begin{pmatrix} 0 & 0 & 0 & 0 & 1 & 1 \\ 0 & 1 & 1 & 2 & 0 & a \\ 0 & 1 & 2 & 1 & 0 & b \end{pmatrix}$
		$gcd(a,b) = 1,\ 2b < a,\ 0 < b < a$
		$\begin{pmatrix} 0 & 0 & 0 & 0 & 1 & 1 \\ 0 & 1 & 1 & 2 & 0 & a \\ 0 & 1 & 2 & 1 & 0 & b \end{pmatrix}$
		$gcd(a,b) = 1,\ 2b > a,\ 0 < b < a$
9		$\begin{pmatrix} 0 & 0 & 0 & 0 & 1 & 1 \\ 0 & 0 & 1 & 1 & 0 & 0 \\ 0 & 1 & 0 & 1 & 0 & 1 \end{pmatrix}$
10		$\begin{pmatrix} 0 & 0 & 0 & 0 & 1 & 1 \\ 0 & 0 & 1 & 1 & 0 & a \\ 0 & 1 & 0 & 1 & 0 & b \end{pmatrix}$
		$gcd(a,b) = 1,\ 0 < b < a$
11		$\begin{pmatrix} 0 & 0 & 0 & 0 & 1 & 1 \\ 0 & 1 & 1 & 2 & 0 & 0 \\ 0 & 0 & 1 & 0 & 0 & 1 \end{pmatrix}$

no.	Figure	Lattice points
12		$\begin{pmatrix} 0 & 0 & 0 & 0 & 1 & 1 \\ 0 & 1 & 1 & 2 & 0 & 1 \\ 0 & 0 & 1 & 0 & 0 & 1 \end{pmatrix}$
13		$\begin{pmatrix} 0 & 0 & 0 & 0 & 1 & 1 \\ 0 & 1 & 1 & 2 & 0 & a \\ 0 & 0 & 1 & 0 & 0 & b \end{pmatrix}$ $gcd(a,b) = 1,\ 0 < b < a$
14		$\begin{pmatrix} 0 & 0 & 0 & 0 & 1 & 1 \\ 0 & 1 & 1 & 2 & 0 & b \\ 0 & 0 & 1 & 0 & 0 & a \end{pmatrix}$ $gcd(a,b) = 1,\ 0 < b < a$
15		$\begin{pmatrix} 0 & 0 & 0 & 0 & 1 & 1 \\ 0 & 0 & 0 & 0 & 0 & a \\ 0 & 1 & 2 & 3 & 0 & b \end{pmatrix}$ $gcd(a,b) = 1,\ 0 \le b < a$
16		$\begin{pmatrix} 0 & 0 & 0 & 1 & 1 & 1 \\ 0 & 1 & 2 & 0 & b & 2b \\ 0 & 0 & 0 & 0 & a & 2a \end{pmatrix}$ $gcd(a,b) = 1,\ 0 \le b < a$
17		$\begin{pmatrix} 0 & 0 & 0 & 1 & 1 & 1 \\ 0 & 0 & 1 & 0 & a & 2a \\ 0 & 1 & 0 & 0 & b & 2b \end{pmatrix}$ $gcd(a,b) = 1,\ 0 < b \le a$

189
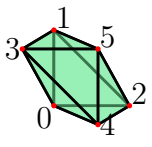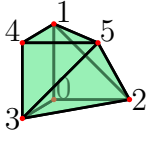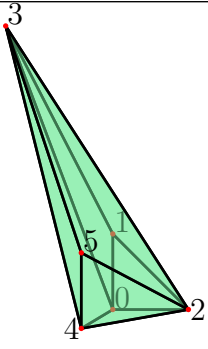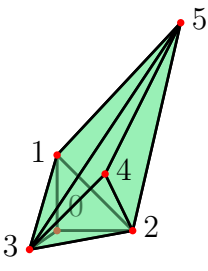
no.	Figure	Lattice points
18		$\begin{pmatrix} 0 & 0 & 0 & 1 & 1 & 1 \\ 0 & 0 & 1 & 0 & 1 & 1 \\ 0 & 1 & 0 & 1 & 0 & 1 \end{pmatrix}$
19		$\begin{pmatrix} 0 & 0 & 0 & 1 & 1 & 1 \\ 0 & 0 & 1 & 0 & 0 & 1 \\ 0 & 1 & 0 & 0 & 1 & 1 \end{pmatrix}$
20		$\begin{pmatrix} 0 & 0 & 0 & 1 & 1 & 1 \\ 1 & 1 & 2 & 0 & 1 & 1 \\ 0 & 1 & 0 & a & 0 & 1 \end{pmatrix}$ $a \geq 3$
21		$\begin{pmatrix} 0 & 0 & 0 & 1 & 1 & 1 \\ 0 & 0 & 1 & 0 & a & c \\ 0 & 1 & 0 & 0 & b & d \end{pmatrix}$ $ad - bc = 1,\ a,b,c,d > 0,\ c+d > a+b,\ c > a$

Table 9.1: The families of polytopes with 6 lattice points of width 1 from the classification in [BS16b]

Proposition 9.2.3. *The polytopes of the families with numbers $1-7$, 11, 12, 18 and 19 in Table 9.1 are not binodal.*

Proof. Each of these families consists of only one polytope. For each we can compute the binodal variety using a computer algebra software like `Singular` or

`OSCAR`. See Algorithms 5 & 6. We used the implementation in `OSCAR` in [Gei22], also contained in Appendix B.2.

For the polytopes of families $1 - 5$ the computations tell us that the binodal variety as defined in Definition 9.1.1 is empty. Example 9.1.6 shows the code snippet for the computation for polytope family 1.

For the polytopes of families 6, 7, 11, 12, 18 and 19 the generalized binodal variety has too small dimension, so the polytopes cannot be binodal. □

Proposition 9.2.4. *The polytopes of the families listed in Table 9.1 with numbers 9, 15, 16, and 17 are not binodal.*

Proof. As the families with numbers 15, 16, and 17 are infinite families, we cannot compute the binodal variety for every polytope of the families since the parameters a and b that parameterize the families end up in the exponents of the variables x, y, z. Instead we eliminate each polytope family by an individual investigation.

The polytope family with number 9 only consists of one polytope, so we can compute the binodal variety and it is of the expected dimension. However, we will prove that a surface with the polytope of family 9 as support and containing at least 2 singularities, contains non-isolated singularities.

Polytope Family 9

Since polytope family 9 consists only of one polytope, we refer to the one element in this family as Polytope 9. We claim that the binodal locus of Polytope 9 consists of surfaces with non-isolated singularities. Using the `OSCAR` code available at [Gei22], we can compute the polynomials generating the binodal variety in the polynomial ring of coefficients $\mathbb{Q}[a_0,\ldots,a_5]$. We obtain the three polynomials

$$g_1 = a_3a_4 - a_2a_5, \quad g_2 = a_1a_4 - a_0a_5, \quad g_3 = a_1a_2 - a_0a_3.$$

Compare with Example 9.1.6, where we computed the binodal variety for Polytope 9 using `OSCAR`.

Let $f = a_0 + a_1z + a_2y + a_3yz + a_4x + a_5xz$ be a polynomial defining a binodal surface. Then we know that the coefficients are zeroes of the three polynomials g_1, g_2, g_3 and the coefficients are all nonzero, so using the above equations, we can write

$$\begin{aligned}
a_3f &= a_0a_3 + a_1a_3z + a_2a_3y + a_3^2yz + a_3a_4x + a_3a_5xz \\
&= a_1a_2 + a_1a_3z + a_2a_3y + a_3^2yz + a_2a_5x + a_3a_5xz \\
&= (a_2 + a_3z)(a_1 + a_3y + a_5x).
\end{aligned}$$

So for any polynomial f with Polytope 9 as Newton polytope such that the surface $V(f)$ contains at least two singularities, the variety $V(f)$ contains non-isolated singularities.

Polytope Family 15

We show that the binodal variety to any polytope of family 15 is empty. Let $f \in \mathbb{K}[a_0,\dots,a_5][x,y,z]$ be a polynomial describing a generic surface with Newton polytope Ω given by a polytope in family 15, so

$$f = a_0 + a_1 z + a_2 z^2 + a_3 z^3 + a_4 x + a_5 x y^a z^b,$$

with $0 \le b < a$ and $\gcd(a,b) = 1$. Its derivatives are given by:

$$\partial f/\partial x = a_4 + a_5 y^a z^b,$$
$$\partial f/\partial y = a a_5 x y^{a-1} z^b,$$
$$\partial f/\partial z = a_1 + 2a_2 z + 3a_3 z^2 + b a_5 x y^a z^{b-1}.$$

Now, consider the projective variety $\mathrm{Sing}(\Omega)$ whose points are given in non-zero coordinates $a_0,\dots,a_5$. The points in $\mathrm{Sing}(\Omega)$ describe singular surfaces with Newton polytope Ω from family 15 that have a singular point in the coordinates x,y,z in the torus $(\mathbb{K}^*)^3$. See Definition 7.1.3. When we substitute the coordinates of the singular point $(\tilde{x},\tilde{y},\tilde{z}) \in (\mathbb{K}^*)^3$ into f and its derivatives, then the four equations are linear in the a_i and they vanish on $\mathrm{Sing}(\Omega)$. In particular we have

$$\partial f/\partial y = a a_5 \tilde{x} \tilde{y}^{a-1} \tilde{z}^b = 0,$$

However, $(\tilde{x},\tilde{y},\tilde{z}) \in (\mathbb{K}^*)^3$, $a > 0$ and the coordinates $a_i \ne 0$. It follows that the discriminant $\mathrm{Sing}(\Omega) \supset B_\Omega$, and thus the binodal variety B_Ω is empty.

Polytope Family 16

Let Ω be a lattice polytope in the family with number 16 from Table 9.1. Let $f \in \mathbb{K}[a_0,\dots,a_5][x,y,z]$ be a polynomial with support Ω. It can be written

$$f = a_0 + a_1 y + a_2 y^2 + x(a_3 + a_4 y^b z^a + a_5 y^{2b} z^{2a}).$$

Its derivatives are given by

$$\partial f/\partial x = a_3 + a_4 y^b z^a + a_5 y^{2b} z^{2a},$$
$$\partial f/\partial y = a_1 + 2a_2 y + b x y^{b-1} z^a (a_4 + 2a_5 y^b z^a),$$

$$\partial f/\partial z = axy^b z^{a-1}(a_4 + 2a_5 y^b z^a).$$

Recall from Definition 7.1.3 the discriminant $\text{Sing}(\Omega)$, whose points (in coordinates $a_0, \ldots, a_5$) describe singular surfaces with Newton polytope Ω that have a singular point (described in coordinates x, y, z) in the torus $(\mathbb{K}^*)^3$. Remember that the binodal variety B_Ω is contained in the discriminant.

By writing $h := a_0 + a_1 y + a_2 y^2$ and $g := a_3 + a_4 y^b z^a + a_5 y^{2b} z^{2a}$ we can rephrase $f = h + xg$. Now, let $(\tilde{x}, \tilde{y}, \tilde{z}) \in (\mathbb{K}^*)^3$ be a singular point of $V(f)$. By $\partial f/\partial x = g$, it follows that $h(\tilde{x}, \tilde{y}, \tilde{z}) = 0$ and $g(\tilde{x}, \tilde{y}, \tilde{z}) = 0$.

Setting $w = y^a z^b$ allows us to rewrite $g = a_3 + a_4 w + a_5 w^2$. Moreover,

$$\partial g/\partial w = a_4 + 2a_5 w = a_4 + 2a_5 y^a z^b.$$

We know that $a > 0$. It follows from $\partial p/\partial z(\tilde{x}, \tilde{y}, \tilde{z}) = 0$ that $a_4 + 2a_5 \tilde{y}^b \tilde{z}^a = 0$, since $\tilde{x}, \tilde{y}, \tilde{z}$ are not zero. So it follows that g as a univariate polynomial in w has a double zero, so $a_4^2 - 4a_3 a_5$ vanishes on $\text{Sing}(\Omega)$. Hence, we can write $g = \gamma(y^a z^b - \epsilon)^2$ for $\gamma, \epsilon \in \mathbb{K}[a_0, \ldots, a_5] \setminus \{0\}$.

Furthermore, we can conclude from $\partial f/\partial y$ and the above that

$$\partial h/\partial y(\tilde{x}, \tilde{y}, \tilde{z}) = a_1 + 2a_2 \tilde{y} = 0,$$

which means that h as a univariate polynomial in y has a double zero. So $a_1 - 4a_0 a_2$ vanishes on $\text{Sing}(\Omega)$, and we can write $h = \beta(y - \alpha)^2$ with $\alpha, \beta \in \mathbb{K}[a_0, \ldots, a_5] \setminus \{0\}$.

Thus, we can rewrite f and its derivatives as

$$
\begin{aligned}
f &= \beta(y - \alpha)^2 + \gamma x(y^a z^b - \epsilon)^2, \\
\partial f/\partial x &= \gamma(y^a z^b - \epsilon)^2, \\
\partial f/\partial y &= 2\beta(y - \alpha) + 2\gamma a x y^{a-1} z^b (y^a z^b - \epsilon), \\
\partial f/\partial z &= 2\gamma b x y^a z^{b-1}(y^a z^b - \epsilon).
\end{aligned}
$$

It follows that all $(\tilde{x}, \tilde{y}, \tilde{z}) \in (\mathbb{K}^*)^3$ satisfying

$$
\begin{aligned}
\tilde{y}^a \tilde{z}^b &= \epsilon, \\
\tilde{y} &= \alpha
\end{aligned}
$$

are singularities of $V(f)$. This is an infinite family of singularities. Therefore, every polytope in family 16 has non-isolated singularities.

Polytope Family 17

Let Ω be a lattice polytope in the family with number 17 from Table 9.1. Let $f \in \mathbb{K}[a_0,\dots,a_5][x,y,z]$ be a polynomial with support Ω. It can be written

$$f = a_0 + a_1 y + a_2 z + x(a_3 + a_4 y^a z^b + a_5 y^{2a} z^{2b}),$$

with $0 < b \leq a$, $\gcd(a,b) = 1$. Its derivatives are given by

$$\partial f / \partial x = a_3 + a_4 y^a z^b + a_5 y^{2a} z^{2b},$$
$$\partial f / \partial y = a_1 + axy^{a-1} z^b (a_4 + 2a_5 y^a z^b),$$
$$\partial f / \partial z = a_2 + bxy^a z^{b-1} (a_4 + 2a_5 y^a z^b).$$

We proceed similarly to the case of polytope family 16. Recall from Definition 7.1.3 the discriminant $\mathrm{Sing}(\Omega)$, whose points (in coordinates $a_0,\dots,a_5$) describe singular surfaces with Newton polytope Ω that have a singular point (described in coordinates x,y,z) in the torus $(\mathbb{K}^*)^3$. Remember that the binodal variety B_Ω is contained in the discriminant.

Setting $h = a_0 + a_1 y + a_2 z$ and $g = a_3 + a_4 y^a z^b + a_5 y^{2a} z^{2b}$ we can write $f = h + xg$. Now, let $(\tilde{x},\tilde{y},\tilde{z}) \in (\mathbb{K}^*)^3$ be a singular point of $V(f)$. By $\partial f / \partial x = g$, it follows that $h(\tilde{x},\tilde{y},\tilde{z}) = 0$ and $g(\tilde{x},\tilde{y},\tilde{z}) = 0$.

We know that the partial derivatives vanish in the singularity $(\tilde{x},\tilde{y},\tilde{z})$. We can thus consider

$$b\tilde{y}\partial f / \partial y(\tilde{x},\tilde{y},\tilde{z}) = a\tilde{z}\partial f / \partial z(\tilde{x},\tilde{y},\tilde{z}),$$
$$\Rightarrow b\tilde{y}(a_1 + a\tilde{x}\tilde{y}^{a-1}\tilde{z}^b(a_4 + 2a_5\tilde{y}^a\tilde{z}^b)) = a\tilde{z}(a_2 + b\tilde{x}\tilde{y}^a\tilde{z}^{b-1}(a_4 + 2a_5\tilde{y}^a\tilde{z}^b)),$$
$$\Rightarrow ba_1\tilde{y} = aa_2\tilde{z},$$
$$\Rightarrow \tilde{y} = \frac{a_2}{a_1}\frac{a}{b}\tilde{z}.$$

We can divide by $b \cdot a_2$ since in $\mathrm{Sing}(\Omega)$ all a_i are non-zero and we know $b > 0$. Substituting this into h, we can solve for z:

$$h(\tilde{x},\tilde{y},\tilde{z}) = a_0 + a_1\tilde{y} + a_2\tilde{z} = 0,$$
$$a_0 + a_1\frac{a_2}{a_1}\frac{a}{b}\tilde{z} + a_2\tilde{z} = 0,$$
$$a_0 + a_2(\frac{a}{b} + 1)\tilde{z} = 0,$$
$$-\frac{a_0}{a_2}\frac{b}{(a+b)} = \tilde{z}.$$

Again we can divide by a_2 and $a+b$ by the same reasons as above. Thus, we have

unique solutions for y and z. It follows that for any singularity $(\tilde{x},\tilde{y},\tilde{z}) \in (\mathbb{K}^*)^3$ of $V(f)$ we have

$$\tilde{z} = -\frac{a_0}{a_2}\frac{b}{(a+b)},$$

$$\tilde{y} = -\frac{a_2}{a_1}\frac{a}{b}\frac{a_0}{a_2}\frac{b}{(a+b)} = \frac{a_0}{a_1}\frac{a}{(a+b)}.$$

With these solutions $\partial f/\partial y(\tilde{x},\tilde{y},\tilde{z}) = 0$ and $\partial f/\partial z(\tilde{x},\tilde{y},\tilde{z}) = 0$ are linear equations in $\tilde{x}$. If $a_4 + 2a_5 y^a z^b \neq 0$, each of these two equations can be solved for $\tilde{x}$. Thus, we see either zero (if the solutions for $\tilde{x}$ do not agree) or exactly one singularity in $V(f)$. Thus, $(a_0 : \ldots : a_5) \notin B_\Omega$. Hence, to allow at least two singularities in $V(f)$ we must have $a_4 + 2a_5 y^a z^b = 0$.

However, with $\partial f/\partial y(\tilde{x},\tilde{y},\tilde{z}) = 0$ and $\partial f/\partial z(\tilde{x},\tilde{y},\tilde{z}) = 0$, this implies $a_1 = a_2 = 0$. So the binodal variety as defined in Definition 9.1.1 is empty. $\qquad\square$

Proposition 9.2.5. *For the following values of the parameters a and b, the polytopes in the families below from Table 9.1 are not binodal.*

Family 10: $a = 1$, $b = 1$ and $a = 2$, $b = 1$.

Family 13: $a = 2$, $b = 1$ and $a = 3$, $b = 1$.

Family 14: $a = 2$, $b = 1$ and $a = 3$, $b = 1$.

Family 20: $a = 3$.

Proof. Similar to the proof of Proposition 9.2.4, we can compute the (generalized) binodal varieties using computer algebra software as `OSCAR` or `Singular`. See Algorithms 5 & 6 and the `OSCAR` code [Gei22] in Appendix B.2. The computations provide the following results: The polytopes with $a = 3$ and $b = 1$ in the polytope families 13 and 14 both give an empty binodal variety, while for the other polytopes in the proposition we obtain that the generalized binodal variety has dimension less than three. $\qquad\square$

The polytope families that remain from the list in Table 9.1 are collected in Figure 9.1.

Notation 9.2.6. We use the notation $\Omega_{a,b}^{(10)}$ to denote a polytope of family number 10 with parameters a and b and analogously for the other polytope families.

Remark 9.2.7. In the list of remaining polytopes, it is possible that some still have the property that their binodal locus contains only surfaces with non-isolated singularities. Since we deal with infinite families of polytopes we cannot make a

No. 8
$$\begin{pmatrix} 0 & 0 & 0 & 0 & 1 & 1 \\ 0 & 1 & 1 & 2 & 0 & a \\ 0 & 1 & 2 & 1 & 0 & b \end{pmatrix}$$
$gcd(a,b) = 1,$
$2b \neq a,\ 0 < b < a$

No. 10
$$\begin{pmatrix} 0 & 0 & 0 & 0 & 1 & 1 \\ 0 & 0 & 1 & 1 & 0 & a \\ 0 & 1 & 0 & 1 & 0 & b \end{pmatrix}$$
$gcd(a,b) = 1,$
$0 < b \leq a,\ a \geq 3$

No. 13
$$\begin{pmatrix} 0 & 0 & 0 & 0 & 1 & 1 \\ 0 & 1 & 1 & 2 & 0 & a \\ 0 & 0 & 1 & 0 & 0 & b \end{pmatrix}$$
$gcd(a,b) = 1,\ 0 < b < a,$
$a + b \geq 5$

No. 14
$$\begin{pmatrix} 0 & 0 & 0 & 0 & 1 & 1 \\ 0 & 1 & 1 & 2 & 0 & b \\ 0 & 0 & 1 & 0 & 0 & a \end{pmatrix}$$
$gcd(a,b) = 1,\ 0 < b < a,$
$a + b \geq 5$

No. 20
$$\begin{pmatrix} 0 & 0 & 0 & 1 & 1 & 1 \\ 1 & 1 & 2 & 0 & 1 & 1 \\ 0 & 1 & 0 & a & 0 & 1 \end{pmatrix}$$
$a > 3$

No. 21
$$\begin{pmatrix} 0 & 0 & 0 & 1 & 1 & 1 \\ 0 & 0 & 1 & 0 & a & c \\ 0 & 1 & 0 & 0 & b & d \end{pmatrix}$$
$ad - bc = 1,\ a,b,c,d > 0,$
$c + d > a + b,\ c > a$

Figure 9.1: The polytopes with 6 lattice points of width 1 that after Propositions 9.2.3, 9.2.4 and 9.2.5 remain from the list in Table 9.1 as possibly binodal.

general statement on whether the polytopes are all binodal. However, there is a way to check for non-isolated singularities for a single polytope Ω for which we can compute the binodal ideal in the a_i with $i = 0, \ldots, 6$, as follows: Intersecting the ideal with 4 generic conditions for 4 arbitrarily chosen a_i should give a 0-dimensional ideal. If it does not, the conditions and a_i were not generic enough. We then solve for the remaining two a_i and obtain a generic point in our binodal variety B_Ω. When we compute the singular locus of the algebraic surface corresponding to that point, and this locus is of dimension zero, then the surface has only isolated singularities.

This procedure is described in Algorithm 8 and partially implemented in two functions for `OSCAR` in [Gei22]; see Appendix B.2. The first function `find_generic_point` computes the intersection of the binodal ideal with a choice of generic conditions for a election of 4 coefficients a_i and computes the dimension of the intersection. The step of solving for the remaining two variables in the case of dimension zero is not implemented in `OSCAR`, but left to the user. For the solved system, the second function `singular_locus` computes the dimension of the singular locus of the corresponding surface.

Conjecture 9.2.8. *The polytopes as in Figure 9.1 are binodal.*

This conjecture is verified for polytopes with small coordinates of each family by applying Algorithm 8. The verified polytopes and coefficient vectors for which the verification was run are collected in Table 9.2.

We illustrate the computations using the code from [Gei22] in `OSCAR` by showing them for $\Omega_{3,1}^{(8)}$. First, we find a generic point in the binodal variety $B_{\Omega_{3,1}^{(8)}}$.

Algorithm 8 Checking for isolated singularities

Input: $M = (m_{i,j}) \in \text{Mat}_{3 \times n}$ filled with the lattice points of Ω, a set s of $n-2$ indices and $n-2$ arbitrary values v_i for each $i \in s$

Output: Whether the surface defined by M and v contains isolated or non-isolated singularities

 1: Compute binodal ideal I via Algorithm 5 or Algorithm 7
 2: **if** $\dim(I) = n-2$ **then**
 3:     **for each** Generator g of I **do**
 4:         $h_g = g|_{a_i = v_i \forall i \in s}$
 5:     **end for**
 6:     $J = \langle h_g | g \text{ generator of } I \rangle$ the ideal in $\mathbb{K}[a_{i_0}, a_{j_0}]$ where $\{i_0, j_0\} = \{1, \dots, n\} \setminus s$
 7:     **if** $\dim(J) = 0$ **then**
 8:         solve for a solution (v_{i_0}, v_{j_0}) for (a_{i_0}, a_{j_0})
 9:         $p = \sum_{j=1}^n v_i x^{m_{j,1}} y^{m_{j,2}} z^{m_{j,3}}$
10:         $J_S = \langle p, \partial p / \partial x, \partial p / \partial y, \partial p / \partial z \rangle$
11:         **if** $\dim(J_S) = 0$ **then**
12:             The polytope Ω is binodal
13:         **else**
14:             Either the chosen conditions were not generic enough or Ω is not binodal.
15:         **end if**
16:     **end if**
17: **end if**

```
julia> A = matrix(ZZ,6,3,[0,0,0,0,1,1,0,1,2,0,2,1,1,0,0,1,3,1]);
julia> p = [1,1//2,1//3,1//5];
julia> find_generic_point(A,[2,5],p)
ideal(9*e1 + 8*e2, 128*e2^3 - 225)
```

We compute a generic point in the binodal variety by solving for `e1` and `e2` by hand. The solutions are not rational, so we need to define a field extension.

```
julia> Qt, t = QQ["t"];
julia> K, a = NumberField(t^3-225//128,"a")
(Number field over Rational Field with defining polynomial t^3 -
   225//128, a)
```

Now, we compute the singular locus of the polynomial with coefficient vector `v`. We need to specify the field `K` in the function `singular_locus`. If the coefficient vector is rational, this last input entry to the function has to be omitted.

```
julia> v = [1,-8//9*a,1//2,1//3,a,1//5]; #the coefficient vector
julia> singular_locus(A,v,K)
(ideal(1//5*x1*x2^3*x3 + a*x1 + 1//3*x2^2*x3 + 1//2*x2*x3^2 -
   8//9*a*x2*x3 + 1, 1//5*x2^3*x3 + a, 3//5*x1*x2^2*x3 + 2//3*x2*
```

```
x3 + 1//2*x3^2 - 8//9*a*x3, 1//5*x1*x2^3 + 1//3*x2^2 + x2*x3 -
8//9*a*x2), 0)
```

The singular locus is of dimension zero, so the surface does not contain non-isolated singularities and $\Omega_{3,1}^{(8)}$ is binodal.

polytope	coefficient vector
$\Omega_{3,1}^{(8)}$	$(1, -\frac{8}{9}\sqrt[3]{\frac{225}{128}}, \frac{1}{2}, \frac{1}{3}, \sqrt[3]{\frac{225}{128}}, \frac{1}{5})$
$\Omega_{3,2}^{(8)}$	$(1, \frac{-48}{25}, \frac{746496}{390625}, \frac{1}{2}, \frac{1}{3}, \frac{1}{5})$
$\Omega_{3,1}^{(10)}$	$(1, -\frac{3}{40}, \frac{1}{2}, \frac{3}{10}, \frac{1}{3}, \frac{1}{5})$
$\Omega_{3,2}^{(10)}$	$(1, \frac{1}{2}, \frac{32}{75}, \frac{1}{3}, \frac{-27}{8}, \frac{1}{5})$
$\Omega_{3,2}^{(13)}$	$(1, \frac{48}{125}, \frac{1}{2}, \frac{2304}{78125}, \frac{1}{3}, \frac{1}{5})$
$\Omega_{3,2}^{(14)}$	$(1, \frac{625}{6912}\sqrt{\frac{63700992}{76125}}, \frac{1}{2}, \sqrt{\frac{63700992}{76125}}, \frac{1}{3}, \frac{1}{5})$
$\Omega_{4}^{(20)}$	$(1, \frac{1}{2}, \frac{1}{3}, \frac{3}{160}, \frac{-2}{5}, \frac{1}{5})$
$\Omega_{5}^{(20)}$	$(1, \frac{1}{2}, \frac{1}{3}, \frac{1}{640000}(-\frac{264465}{100} + \sqrt{\frac{55^2 - 400 \cdot 16}{40000}}), -\frac{55}{200} + \sqrt{\frac{55^2 - 400 \cdot 16}{40000}}, \frac{1}{5})$
$\Omega_{1,1,2,3}^{(21)}$	$(1, \frac{1}{2}, \frac{1}{3}, \frac{8192}{46875}, \frac{256}{1125}, \frac{1}{5})$
$\Omega_{2,1,3,2}^{(21)}$	$(1, \frac{1}{2}, \frac{1}{3}, \frac{78732}{15625}, \frac{81}{50}, \frac{1}{5})$

Table 9.2: Polytopes and coefficient vectors for which Conjecture 9.2.8 is verified.

9.3 Lattice paths for binodal polytopes with 6 vertices of width 1

In this chapter we first introduce notation for lattice paths that induce binodal surfaces satisfying point conditions and how to check whether the lattice path is valid (Section 9.3.1). Then in Section 9.3.2 we show how to compute the path multiplicities and briefly demonstrate how to use the `OSCAR` functions ([Gei22], Appendix B.2) written for this purpose.

9.3.1 Lattice paths

Lattice paths are a key ingredient to tropical surface counting. In this section we consider binodal surfaces and deduce properties of their possible lattice paths and introduce notation for the following sections.

Lemma 9.3.1. *Let Ω be a binodal polytope with 6 lattice points and S a tropical surface with Newton polytope Ω. Assuming that S passes through points in Mikhalkin position, the induced lattice path on Ω passes along the edges of the polytope.*

Proof. By Proposition 9.1.10, the dual subdivision to a binodal tropical surface whose Newton polytope is a binodal polytope with 6 lattice points is always the trivial subdivision. $\square$

Lemma 9.3.2. *Let Ω be a binodal lattice polytope of width 1 with 6 lattice points, and let S be the tropical surface dual to the trivial subdivision of Ω.*
 Let $\mathbf{p} = (p_1,\ldots,p_{N-1})$ be a point configuration in $\mathbb{K}^3$ in Mikhalkin position where the $q_i = \mathrm{Trop}(p_i)$ are distributed with growing distances along a line L of direction $(1,\eta,\eta^2)$ with $0 < \eta \ll 1$. The direction vector $v = (1,\eta,\eta^2)$ induces an order on the lattice points of a polytope $\Omega : \omega_0,\ldots,\omega_{N+1}$.
 Then the line L has to pass through the 3-dimensional regions of $\mathbb{R}^3 \setminus S$ that are dual to ω_0 and ω_{N+1}.

Proof. By [MMS18, Lemma 3.2], the line L on which the points in Mikhalkin position are distributed has to pass through the 3-dimensional regions defined by the tropical surface via $\mathbb{R}^3 \setminus S$ in the order given by the partial order induced on their dual vertices by the direction vector of L.

The ordering of the lattice points induced by v is given by $\omega_i < \omega_j$ if and only if $\langle \omega_j - \omega_i, v \rangle > 0$, see Definition 7.2.3. The ordering of the vertices stands for the order in which the line through the point configuration passes through the cells dual to the vertices. For a smooth surface, the line L has to pass through all $N+2$ regions into which the surface divides $\mathbb{R}^3$. Due to the direction vector of the line on which the points are distributed, the line always has to start in the region of $\mathbb{R}^3$ dual to the first vertex ω_0 and it always has to end in the region dual to ω_{N+1}, even when the surface is no longer smooth. $\square$

We introduce notation similar to Lemma 7.2.5 for lattice paths that induce binodal surfaces. Let L denote the line with direction vector $(1,\eta,\eta^2)$ on which the point conditions are distributed. Recall, that in Lemma 7.2.5 we distinguished lattice paths depending on how many intersection points L has with the tropical surface S, or equivalently, how many 3-dimensional regions $\mathbb{R}^3 \setminus S$ are intersected by L. When we now consider lattice paths that count binodal singularities, there are more options. They are all described in the following Lemma.

Lemma 9.3.3 ([MMS18, Lemma 3.2])**.** *We fix a point configuration* **p** *in Mikhalkin position. Let S be a binodal tropical surface passing through* $\mathbf{q} = \mathrm{Trop}(\mathbf{p})$. *Let L denote the line on which the q_i are distributed with growing distances.*

1. *If the line L passes through N of the 3-dimensional regions of $\mathbb{R}^3 \setminus S$, the lattice path $P(S,\mathbf{q})$ satisfies*

   (i) $P(S,\mathbf{q}) = P(A)$, *where* $A = \Omega \cap \mathbb{Z}^3 \setminus \{\omega_k, \omega_l\}$ *for some* $1 \le k < l \le N$. *In this case the lattice path is connected. We denote such a path by* $\Gamma_{k,l}$.

2. *If the line L passes through $N+1$ of the 3-dimensional regions of $\mathbb{R}^3 \setminus S$, the lattice path $P(S,\mathbf{q})$ satisfies exactly one of the following conditions:*

   (ii) $P(S,\mathbf{q}) = P(A)$, *where* $A = \Omega \cap \mathbb{Z}^3 \setminus \{\omega_0, \omega_l\}$ *for some* $1 \le l \le N$. *In this case the lattice path is connected from 1 to $N+1$ if $l > 1$ resp from 2 to $N+1$ if $l = 1$, and we call this path* $\Gamma_{k,l}$.

   (iii) $P(S,\mathbf{q}) = P(A)$, *where* $A = \Omega \cap \mathbb{Z}^3 \setminus \{\omega_l, \omega_{N+1}\}$ *for some* $1 \le l \le N$. *In this case the lattice path is connected from 0 to N if $l < N$ resp from 0 to $N-1$ if $l = N$, and we call this path* $\Gamma_{k,l}$.

   (iv) $P(S,\mathbf{q}) = P(A') \cup P(A'')$, *where A is partitioned in the two sets* $A' = \{\omega_0, \ldots, \omega_k\} \setminus \{\omega_l\}$, *and* $A'' = \{\omega_{k+1}, \ldots, \omega_{N+1}\}$ *for some* $1 \le k \le N-1$ *and $l < k$. In this case the lattice path is disconnected and we call this path* $\Gamma_{l,[k,k+1]}$.

   (v) $P(S,\mathbf{q}) = P(A') \cup P(A'')$, *where A is partitioned in* $A' = \{\omega_0, \ldots, \omega_k\}$, *and* $A'' = \{\omega_{k+1}, \ldots, \omega_{N+1}\} \setminus \{\omega_l\}$ *for some* $1 \le k \le N-1$ *and $k+1 < l$. In this case the lattice path is disconnected and we call this path* $\Gamma_{[k,k+1],l}$.

   (vi) $P(S,\mathbf{q}) = P(A') \cup P(A'')$, *where A is partitioned in* $A' = \{\omega_0, \ldots, \omega_k\}$, *and* $A'' = \{\omega_{k+2}, \ldots, \omega_{N+1}\}$ *for some* $1 \le k \le N-1$. *In this case the lattice path is disconnected and we call this path* $\Gamma_{[k,k+2],k+1}$.

3. *If the line L passes through $N+2$ of the 3-dimensional regions of $\mathbb{R}^3 \setminus S$, the lattice path $P(S,\mathbf{q})$ satisfies exactly one of the following conditions:*

   (vii) $P(S,\mathbf{q}) = P(A)$, *where* $A = \Omega \cap \mathbb{Z}^3 \setminus \{\omega_0, \omega_{N+1}\}$. *In this case the lattice path is connected from 1 to N, and we call this path* $\Gamma_{0,N+1}$.

   (viii) $P(S,\mathbf{q}) = P(A)$, *where* $A = \Omega \cap \mathbb{Z}^3 \setminus \{\omega_0, \omega_1\}$ *resp.* $A = \Omega \cap \mathbb{Z}^3 \setminus \{\omega_N, \omega_{N+1}\}$. *In this case the lattice path is connected from 2 to $N+1$ resp. 0 to $N-1$, and we call this path* $\Gamma_{0,1}$ *resp.* $\Gamma_{N,N+1}$.

   (ix) $P(S,\mathbf{q}) = P(A') \cup P(A'')$, *where A is partitioned in the two sets* $A' = \{\omega_1, \ldots, \omega_k\}$, *and* $A'' = \{\omega_{k+1}, \ldots, \omega_{N+1}\}$ *for some* $1 < k \le N-1$. *In this case the lattice path is disconnected and we call this path* $\Gamma_{0,[k,k+1]}$.

(x) $P(S,\mathbf{q}) = P(A') \cup P(A'')$, *where A is partitioned in the two sets $A' = \{\omega_0,\dots,\omega_k\}$, and $A'' = \{\omega_{k+1},\dots,\omega_N\}$ for some $1 \le k < N-1$. In this case the lattice path is disconnected and we call this path $\Gamma_{[k,k+1],N+1}$.*

(xi) $P(S,\mathbf{q}) = P(A') \cup P(A'') \cup P(A''')$, *where A is partitioned in the three sets $A' = \{\omega_0,\dots,\omega_k\}$, $A'' = \{\omega_{k+1},\dots,\omega_l\}$, and $A''' = \{\omega_{l+1},\dots,\omega_{N+1}\}$. for some $1 \le k$, $k+1 < l < N$. In this case the lattice path is disconnected and we call this path $\Gamma_{[k,k+1],[l,l+1]}$.*

(xii) $P(S,\mathbf{q}) = P(A') \cup P(A'')$, *where A is partitioned in $A' = \{\omega_0,\dots,\omega_k\}$, and $A'' = \{\omega_{k+2},\dots,\omega_{N+1}\}$ for some $1 \le k < N-1$. In this case the lattice path is disconnected and we call this path $\Gamma_{[k,k+2]}$.*

When constructing possible lattice paths, please note that the start and end points of gaps in the lattice path have to be vertices of the dual subdivision of the Newton polytope. Lattice points that are not vertices of the subdivision can always only appear as skipped points, as they do not define a 3-dimensional region of $\mathbb{R}^3 \setminus S$.

Proof. A lattice path that induces a binodal surface has to contain at least N lattice points, and L therefore intersects at least N of the 3-dimensional regions of $\mathbb{R}^3 \setminus S$. By Lemma 9.3.2, we know that L always has to pass through the 3-dimensional regions dual the vertices ω_0 and ω_{N+1}.

We distinguish three cases: If L intersects exactly N of the 3-dimensional regions of $\mathbb{R}^3 \setminus S$, then there are exactly $N-1$ points where L intersects S. These are the q_i and the $N-1$ distinct 2-cells of S containing the q_i form the lattice path $P(S,\mathbf{q})$. Since L is of direction $v = (1,\eta,\eta^2)$ and we have a partial order on the lattice points given by v, the induced lattice path is connected.

If L intersects $N+1$ of the 3-dimensional regions of $\mathbb{R}^3 \setminus S$, then there are exactly N points where L intersects S. Thus, we have one additional intersection point to the q_i. The shape of the path $P(S,\mathbf{q})$ is determined by the position of the additional intersection point t. This point t is contained in the relative interior of a 2-cell of S which corresponds to an edge in the dual subdivision of the Newton polytope Ω of S. Lets call the lattice points forming this edge ω_{t_1} and ω_{t_2}. If $\omega_{t_1} \succ \omega_i$ for all ω_i in the lattice path, then $\omega_{t_1} = \omega_0$ and $t_2 \in \{1,2\}$ and the induced lattice path is connected from t_2 to $N+1$. The case $\omega_{t_2} \prec \omega_i$ for all ω_i in the lattice path is analogous.

If the line segment formed by ω_{t_1} and ω_{t_2} is in the middle of the lattice path, we are in case (iv), (v) or (vi) depending on which connected half of the lattice path skips the lattice point ω_l. If $\omega_l \prec \omega_{t_1}$ we are in case (iv), if $\omega_{t_2} \prec \omega_l$ we are in case (vi) and if $\omega_{t_1} \prec \omega_l \prec \omega_{t_2}$ we are in case (v).

If L intersects $N+2$ of the 3-dimensional regions of $\mathbb{R}^3 \setminus S$, then there are exactly $N+1$ points where L intersects S. Thus, we have two additional intersection points

of L with S to the q_i. The shape of the path $P(S,\mathbf{q})$ is determined by the position of the two additional intersection points. The cases (vii) to (xii) distinguish the different options: If the additional intersection points of L with S are both before q_0 or after q_{N-1}, we are in the cases (vii) or $(viii)$. If exactly one of the additional points corresponds to a gap in the lattice path, we are in the cases (ix) or (x). Otherwise, both additional intersections correspond to line segments that interrupt the lattice path and we are in the cases (xi) or (xii). $\qquad\square$

We will not observe option (3) in Lemma 9.3.3 for any of the polytopes investigated in this thesis.

We will use the following condensed, extracted information of Lemma 9.3.3 to exclude certain lattice paths in the following sections.

Remark 9.3.4. For a lattice path connected from 0 to $N+1$ the line L intersects N regions of $\mathbb{R}^3 \setminus S$. If either ω_0 or ω_{N+1} are not part of the lattice path, the line L has to intersect at least $N+1$ regions of $\mathbb{R}^3 \setminus S$. If both are not contained, it has to intersect all $N+2$ regions of $\mathbb{R}^3 \setminus S$.

For each gap in the lattice path the line L intersects one additional region of $\mathbb{R}^3 \setminus S$: For a lattice path with one gap, L intersects $N+1$ regions; for a lattice path with two gaps, L intersects all $N+2$ regions.

We compute a list of possible lattice paths for each polytope family. We note, that for each polytope family in Table 9.1 the edge-vertex combinatorics remains constant across different choices of parameters, except for polytope family 8, where there are two cases, depending on whether $2b > a$ or $2b < a$. This is significant, because the possible lattice paths only depend on the ordering of the vertices and the existence of edges between the vertices.

Definition 9.3.5. We call a lattice path $P(A)$ with $A \subset \Omega \cap \mathbb{Z}^3$ a *valid binodal lattice path on* Ω, if it arises from a tropical binodal surface S with Newton polytope Ω satisfying $|\Omega \cap \mathbb{Z}^3| - 3$ point conditions in Mikhalkin position.

The following remark describes how we can check whether a given lattice path is valid.

Remark 9.3.6. The idea is to check whether the lattice points forming the lattice path define a set of 3-dimensional regions of $\mathbb{R}^3 \setminus S$ that L can pass through in the order induced by the partial order on the lattice points. Here, L is the line of direction $(1,\eta,\eta^2)$ on which the q_i from the point conditions are distributed.

Since the polytopes in the 6 binodal families in Figure 9.1 all have 6 lattice points, we know that we are in the case of the trivial subdivision by Proposition 9.1.10. Example 2.2.20 described for this case how to compute the 3-dimensional regions of $\mathbb{R}^3 \setminus S$ which are pointed cones. Without loss of generality we can assume that the line L passes through $(0,0,0)$ and that the unique vertex of S is in (x,y,z).

When we have computed the rays spanning the cones, the lattice path tells us with which facets of the cones (i.e. 2-dimensional cells of S) the line $L = (1,\eta,\eta^2)\mathbb{R}$ intersects and in which order. By fixing the points q_i as $(0,0,0)$ and positive multiplies of $(1,\eta,\eta^2)$ with growing distances on L, we obtain a set of linear equations in (x,y,z) and the parameters of the 2-dimensional cells. If this linear system can be solved such that the parameters of the 2-dimensional cells are all positive (only then we see an intersection of L with the relative interior of the 2-cell), and the independence of the distances of the q_i and the direction vector is not violated (this ensures the generality of our point conditions), then the lattice path is valid as in Definition 9.3.5.

Sometimes we can already exclude certain lattice paths by looking at the 3-dimensional regions of $\mathbb{R}^3 \setminus S$ and, for example, observing that a line of the given direction could never pass through two of the regions but only through one of them. These observations are helpful, as they limit the possible paths as described in Lemma 9.3.3, since they are determined by the number of 3-dimensional regions of $\mathbb{R}^3 \setminus S$ the line L crosses.

9.3.2 Multiplicity of lattice paths

This section explains how we can compute the multiplicity of a lattice path for a given binodal polytope Ω. The theory is described by Algorithms 9 and 10. For the computational execution we use the `OSCAR` code [Gei22], which we will demonstrate with short code snippets in this section. The functions are also contained in Appendix B.2.

Determining the multiplicity of a lattice path is a crucial step towards counting surfaces. A path multiplicity is the lifting multiplicity of the tropical surface passing through the points in Mikhalkin position that induce the lattice path. The path multiplicities of all valid lattice paths should therefore always add up to the degree of the binodal variety of the polytope.

We can compute the multiplicity of a lattice path for a binodal polytope as follows. We make a distinction between connected and disconnected lattice paths. In this context it is not important if the lattice path is connected from 0 to $N+1$ or from l to k. We will not discuss the multiplicity of lattice paths of type (3) from Lemma 9.3.3. Most of the following can be adapted for paths of type (3) with at most one gap. For two gaps, or one gap of length 2, there is a modified technique which we do not discuss here as it will not appear for any of the polytopes investigated in this thesis.

Connected lattice paths

For a connected lattice path $\Gamma_{k,l}$ leaving out the two lattice points ω_k and ω_l, we substitute the remaining parameters in the binodal variety (i.e., all a_{ω_i} for which $i \neq k,l$) by generic values. Similar to the computation of the binodal variety, we have to eliminate all those components of the resulting variety that contain monomials. This can be done by computing the primary decomposition and checking the primary components. We keep only those components that do not contain monomials. Computing the degree of this variety gives the multiplicity of the lattice path. The values for the parameters have not been chosen generically enough if the dimension of the variety in a_{ω_k} and a_{ω_l} is not zero.

This procedure is the same for all connected lattice paths, the ones described by Lemma 9.3.3 in (1) and (2). It is summarized in Algorithm 9.

Algorithm 9 Multiplicity of a connected lattice path

Input: $M = (m_{i,j}) \in \mathrm{Mat}_{3 \times (N+2)}$ filled with the lattice points of Ω, a set $s = \{0, \ldots, N+1\} \setminus \{k,l\}$ of N indices and N arbitrary values v_i for each $i \in s$

Output: Multiplicity of lattice path $\Gamma_{k,l}$

 1: Compute binodal ideal I via Algorithm 5 or Algorithm 7
 2: **if** $\dim_{proj}(I) = N - 1$ **then**
 3:     **for each** Generator g of I **do**
 4:         $h_g = g|_{a_{\omega_i} = v_i \forall i \in s}$
 5:     **end for**
 6:     $J = \langle h_g | g \text{ generator of } I \rangle$ the ideal in $\mathbb{K}[a_{\omega_k}, a_{\omega_l}]$ where $\{k,l\} = \{1, \ldots, n\} \setminus s$
 7:     **if** $\dim_{aff}(J) = 0$ **then**
 8:         $I_P = \langle 1 \rangle$
 9:         Compute primary decomposition $(J_1, \ldots, J_s)$ of J
10:         **for** $i \in \{1, \ldots, s\}$ **do**
11:             **if** $J_i \cap \langle a_{\omega_k} \cdot a_{\omega_l} \rangle = \emptyset$ **then**
12:                 $I_P = I_P \cap J_i$
13:             **end if**
14:         **end for**
15:         **return** path multiplicity $\deg(I_P)$.
16:     **end if**
17: **end if**

Example 9.3.7. We briefly demonstrate the use of the `OSCAR` function `path_mult` for connected paths. As an example we use the polytope $\Omega_{3,2}^{(8)}$ and the lattice path $\Gamma_{1,4}(\Omega_{3,1}^{(8)})$, see Figure 9.4

The function `path_mult` can be applied either directly to the binodal polytope Ω or to the radical ideal generating the binodal variety B_Ω. We demonstrate its

use for the polytope. We provide the polytope by its lattice points in a matrix `A`. To apply it to the ideal I, the user inserts the ideal instead of the matrix into the function. The other entries have to stay the same.

Additionally, we have to provide a vector `v` filled with the general values that substitute the coefficients corresponding to those lattice points that are part of the path.

```
julia> A = matrix(ZZ,6,3,[0,0,0,0,1,1,0,1,2,0,2,1,1,0,0,1,3,1])
[0   0   0]
[0   1   1]
[0   1   2]
[0   2   1]
[1   0   0]
[1   3   1]
julia> v = [1,1//2,1//3,1//5];
```

We need to specify the lattice points that are left out of the path. Note that `OSCAR` starts counting at 1, while we start with 0 when enumerating the lattice points. So for path $\Gamma_{1,4}(\Omega_{3,1}^{(8)})$ the left out lattice points, starting to count at 1, are `2` and `3`.

```
julia> p = [2,3];
julia> path_mult(A, p, [true,true], v)
Affine dimension is 0
Path multiplicity is 1
(ideal(25*e2 - 2, 3*e1 + 2), 1)
```

The third entry to the function `[true,true]` states that the two lattice points given by `p` are indeed left out points and not points of gap of a disconnected path.

We see that $\mathrm{mult}(\Gamma_{1,4}(\Omega_{3,1}^{(8)})) = 1$, as also stated in Table 9.3.

Disconnected lattice paths

In this thesis we will not observe a polytope for which a lattice path can have two gaps or a gap of length 2 as described in Lemma 9.3.3 (3). Therefore, we restrict to the disconnected paths as described in Lemma 9.3.3 (2).

For a disconnected lattice path the procedure is similar. If ω_l is the lattice point left out of the lattice path, and the segment $[\omega_{k_1}, \omega_{k_2}]$ is the one filling the gap in the disconnected lattice path, and the path up to $a_{\omega_{k_1}}$ is connected, then we proceed with the parameters up to $a_{\omega_{k_1}}$ as described before. The parameters a_{ω_l} and $a_{\omega_{k_2}}$ do not get assigned a value, but stay variable. However, all the following parameters, i.e., a_{ω_j} with $j > k_2$, will be substituted by generic linear equations in $a_{\omega_{k_2}}$, such that the quotient $a_{\omega_j}/a_{\omega_{k_2}}$ is constant. The degree of the new variety gives the multiplicity of the disconnected lattice path. The values and linear equations are generic enough if the variety is of dimension 0.

Analogous to the computation of the multiplicity of the connected lattice paths, we have to eliminate all those components of the resulting variety that contain

monomials. For this we compute the primary decomposition and check the primary components. We keep only those components that do not contain monomials. This procedure works for all types of disconnected paths with one gap of length 1 as described in Lemma 9.3.3 (2). It is illustrated in Algorithm 10.

Note that in the case of the disconnected paths we have either $k_2 = k_1 + 1$ with $l > k_2$ or $l < k_1$, or $k_2 = k_1 + 2$ and $l = k_1 + 1$.

Algorithm 10 Multiplicity of a disconnected lattice path

Input: $M = (m_{i,j}) \in \mathrm{Mat}_{3 \times (N+2)}$ filled with the lattice points of Ω, the index $k \in \{0, \ldots N+1\}$ of the left out point, a segment $[k_1, k_2]$ that stands for the gap and N arbitrary values v_i

Output: Multiplicity of a disconnected lattice path

1: Compute binodal ideal I via Algorithm 5 or Algorithm 7
2: **if** $\dim_{proj}(I) = N - 1$ **then**
3: **for each** Generator g of I **do**
4:   $h_g = g|_{a_{\omega_i} = v_i \forall i \in s', a_{\omega_j} = a_{\omega_{k_2}} \cdot v_i \forall j \in s''}$ where $s' = \{0, \ldots, k_1\} \setminus \{l\}$ and $s'' = \{k_2 + 1, \ldots, N + 1\} \setminus \{l, \}$
5: **end for**
6: $J = \langle h_g | g \text{ generator of } I \rangle$ the ideal in $\mathbb{K}[a_{\omega_{k_2}}, a_{\omega_l}]$
7: **if** $\dim_{aff}(J) = 0$ **then**
8:   $I_P = \langle 1 \rangle$
9:   Compute primary decomposition $(J_1, \ldots, J_s)$ of J
10:   **for** $i \in \{1, \ldots, s\}$ **do**
11:    **if** $J_i \cap \langle a_{\omega_{k_2}} \cdot a_{\omega_l} \rangle = \emptyset$ **then**
12:     $I_P = I_P \cap J_i$
13:    **end if**
14:   **end for**
15:   **return** path multiplicity $\deg(I_P)$.
16: **end if**
17: **end if**

Example 9.3.8. We briefly demonstrate the use of the `OSCAR` function `path_mult` for disconnected paths. As an example we use the polytope $\Omega^{(21)}_{1,1,2,3}$ and the lattice path $\Gamma_{1,[3,4]}(\Omega^{(21)}_{1,1,2,3})$, see Figure 9.15.

As before for the connected paths, we only demonstrate the function when it is applied directly to the polytope. We provide the polytope by its lattice points in a matrix `B`. We can use the same vector `v` filled with the general values that we used in Example 9.3.7 for the connected case.

```
julia> B = matrix(ZZ,6,3,[0,0,0,0,0,1,0,1,0,1,0,0,1,1,1,1,2,3])
```

```
[0   0   0]
[0   0   1]
[0   1   0]
[1   0   0]
[1   1   1]
[1   2   3]
```

We need to specify the lattice point that is left out of the path and the lattice point that ends the gap. To indicate which is which, we use the boolean vector, which for the connected case was `[true,true]`.

For the path $\Gamma_{1,[3,4]}(\Omega^{(21)}_{1,1,2,3})$, the left out point ω_1 comes first, so the boolean vector `b` has a first entry `true`, while the vector with the special lattice points `p` has `p[1]=2` (recall that `OSCAR` starts counting at 1). The gap of the path is between the lattice points ω_3 and ω_4. The function needs as input only the endpoint of the gap, so `p[2]=5`. That this is indeed the endpoint of a gap is indicated by setting `b[2]=false`.

```julia
julia> p = [2,5];
julia> b = [true, false];
julia> path_mult(B, p, b, v)
Affine dimension is 0
Path multiplicity is 2
(ideal(125*e1 - 96*e2, 1944*e2^2 - 125), 2)
```

As stated in Table 9.8, we see that $\mathrm{mult}(\Gamma_{1,[3,4]}(\Omega^{(21)}_{1,1,2,3})) = 2$.

Remark 9.3.9. We note that the above constructions work even for invalid paths, i.e., lattice paths that do not come from the a tropical surface satisfying point conditions in Mikhalkin position. Hence, a non-zero multiplicity resulting from these computations does not imply that the lattice path contributes to the total count.

To check the validity of a lattice path, we refer to Remark 9.3.6.

9.4 Counting binodal polytopes of width 1 with 6 lattice points

We have determined the 6 families of binodal polytopes with 6 lattice points of width 1 and we have collected information on the lattice paths and their multiplicities in the previous sections. In this section we are ready to present the main results of this chapter: We ascertain the valid lattice paths for each of the 6 families of binodal polytopes, compute their multiplicities and the degree of the binodal varieties for small values and pose general conjectures on the multiplicities of the lattice paths and the degrees of the binodal varieties in dependence of the parameters of the family.

We consider each family separately in its own subsection. The procedure will be similar for all 6 cases: First, we exclude specific cases for the lattice paths according to Lemma 9.3.3. Then we go through all remaining possible lattice paths and determine which of these are valid. Finally, we present the conjecture based on the computed data of lattice path multiplicities and degrees of binodal varieties. Each conjecture is accompanied by a table presenting the cases for which the conjecture could be verified using `OSCAR`, and on which the conjecture is based.

Remark 9.4.1. Please note that the validity of a lattice path depends highly on the ordering induced on the lattice points of the polytope by the point conditions on the surface. When we have points in Mikhalkin position we have fixed the tropical points on a line of direction $(1,\eta,\eta^2)$ with growing distances (Definition 7.2.1).

This is important to keep in mind when we consider a different IUA-representative of a binodal polytope family, or, in other words, when we consider a polytope of one of the binodal families that has been transformed by affine translation and actions of $SL_3(\mathbb{Z})$. If we can determine the transformation and apply it to the direction vector $(1,\eta,\eta^2)$ of the line with the tropical point conditions and count with these new point conditions, we obtain the same lattice paths and multiplicities as before. If that is for some reason not possible, for example because the polytope is part of a larger subdivision and we want to keep the original point conditions, as will be the case in Chapter 10, we have to recompute the valid lattice paths and their point conditions.

From now on, we assume that the points our surfaces pass through are in Mikhalkin position.

9.4.1 Polytope family 8

$$\Omega_{a,b}^{(8)} = \begin{pmatrix} 0 & 0 & 0 & 0 & 1 & 1 \\ 0 & 1 & 1 & 2 & 0 & a \\ 0 & 1 & 2 & 1 & 0 & b \end{pmatrix}$$
$$gcd(a,b) = 1,\ 2b \neq a,\ 0 < b < a$$

$\Omega_{a,b}^{(8),<}$ where $2b < a$ $\Omega_{a,b}^{(8),>}$ where $2b > a$
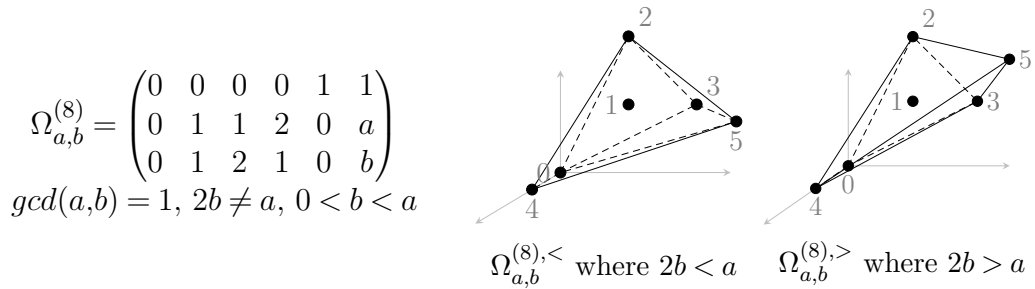
Figure 9.2: Polytope family 8

Recall, that for each polytope family in Table 9.1 the edge-vertex combinatorics remains constant across different choices of parameters, except for polytope family 8, where there are two cases, depending on whether $2b > a$ or $2b < a$. This is

significant, because the possible lattice paths only depend on the ordering of the vertices and on the existence of edges between the vertices. See Figure 9.2 to see the two different polytope types. We observe that for $2b < a$ there is an edge from ω_0 to ω_5, while for $2b > a$ we see instead an edge from ω_3 to ω_4.

We now investigate the possible lattice paths for this polytope family. Wherever necessary we distinguish between the two subfamilies of family 8 by using the following notation:

$\Omega_{a,b}^{(8),<}$ stands for a polytope of family 8 where $2b < a$.

$\Omega_{a,b}^{(8),>}$ stands for a polytope of family 8 where $2b > a$.

We write $\Omega_{a,b}^{(8)}$ if it is not necessary to make a difference between the two subtypes.

Lemma 9.4.2. *For all polytopes of family 8 with lattice points as in Figure 9.1, only lattice paths connected from 0 to 5 are possible.*

Recall that the lattice paths are induced by point conditions in Mikhalkin position (Definition 7.2.1).

Proof. Let $\Omega_{a,b}^{(8)}$ be a polytope of family 8. Without loss of generality, we can assume that the surface S dual to the polytope has a unique vertex at $(0,0,0)$. The direction vector of the line L on which the points of the point condition lie is $(1,\eta,\eta^2)$ with $0 < \eta \ll 1$.

In the following, we use the notation $\cdot^\vee$ as introduced in Corollary 2.1.15 to denote the dual object under the duality connection between the Newton polytope and the tropical surface.

There can only exist disconnected lattice paths for $\Omega_{a,b}^{(8)}$ if the line L, on which the points from the point conditions are distributed, intersects with the tropical surface S more than 3 times; see Lemma 9.3.3. Label the lattice points of the polytope with ω_0, ω_1, ω_2, ω_3, ω_4 and ω_5. The lattice point ω_1 is then never a vertex of the polytope. Therefore, a tropical surface with support $\Omega_{a,b}^{(8)}$ divides $\mathbb{R}^3$ into only five 3-dimensional regions. For a path not connected from 0 to 5, the line L must pass through all five regions. In the proof of Proposition 9.4.3, the rays generating the regions are computed (compare Remark 9.3.6 and Example 2.2.20). We observe that if the line L passes through $\omega_0^\vee$, $\omega_2^\vee$, $\omega_3^\vee$, the remaining ray of L is contained in the $\{z > 0, y > 0\}$ quadrant of $\mathbb{R}^3$. However, for each polytope of family 8, $\omega_4^\vee \cap \{z > 0, y > 0\} = \emptyset$ (compare with the proof of Proposition 9.4.3). Thus, L cannot pass through all five 3-dimensional regions $\mathbb{R}^3 \setminus S$. □

Proposition 9.4.3. *The lattice paths depicted in Figures 9.4 resp. 9.5 are the only possible lattice paths for the polytopes in family 8 with $2b < a$ resp. $2b > a$.*
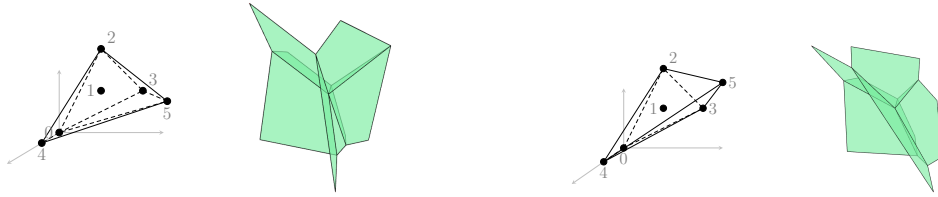
(a) Exemplary polytope and dual hypersurface for family number 8 with $2b < a$.

(b) Exemplary polytope and dual hypersurface for family number 8 with $2b > a$.

Figure 9.3: The two types of polytope family 8 with exemplary polytope and its dual hypersurface for $a = 3$ and $b = 1$ resp. $b = 2$.

Proof. By Lemma 9.3.1 we know that the lattice path has to run along the edges. Further, we know that the lattice path has to be connected from 0 to 5, as this follows from Lemma 9.4.2, and that $\omega_1 = (0,1,1)$ can never be part of the path. Since the $\Omega_{a,b}^{(8),<}$ and $\Omega_{a,b}^{(8),>}$ have different edges, we need to distinguish the two subtypes in the remainder of this proof.

For $\Omega_{a,b}^{(8),<}$ the previous arguments limit the possible cases to all lattice paths depicted in Figure 9.4. For $\Omega_{a,b}^{(8),>}$ the previous arguments limit the possible cases to all lattice paths depicted in Figure 9.5.

It remains to check for both subtypes whether all the lattice paths are valid. We do this using the methods described in Remark 9.3.6:

We examine each possible lattice path through the vertices of the two subtypes of the polytope family and check whether it is possible for a line to pass through the corresponding regions and through points in Mikhalkin position. This is done by choosing general points $(0,0,0)$, $(1,\eta,\eta^2)$, $(\lambda,\lambda\eta,\lambda\eta^2)$, $0 < \eta \ll 1 \ll \lambda$ and letting (x,y,z) be the vertex of the tropical surface. This gives rise to 9 equations, one for each coordinate of each point, asserting that the point is contained in the claimed cell of the tropical surface. These equations are given in 6 variables corresponding to the coefficients on the rays and the 3 variables x,y,z. Solving these equations either results in a solution or a contradiction.

Recall, that we use the notation $\cdot^\vee$ to indicate dual objects under the duality between the subdivision of the Newton polytope (which in our case is trivial) and the tropical surface S and the 3-dimensional regions of $\mathbb{R}^3 \setminus S$. In particular, for a vertex V of the polytope $V^\vee$ denotes the 3-dimensional region of $\mathbb{R}^3 \setminus S$ dual to V.

For a polytope $\Omega_{a,b}^{(8)}$ we know that its lattice points are given by $\omega_0 = (0,0,0)$, $\omega_1 = (0,1,1)$, $\omega_2 = (0,1,2)$, $\omega_3 = (0,2,1)$, $\omega_4 = (1,0,0)$, and $\omega_5 = (1,a,b)$. The rays defining the dual regions are different depending on $2b > a$ or $2b < a$ because they depend on the edges of the polytope.

(a) $\Gamma_{1,4}(\Omega_{a,b}^{(8),<})$ (b) $\Gamma_{1,3}(\Omega_{a,b}^{(8),<})$
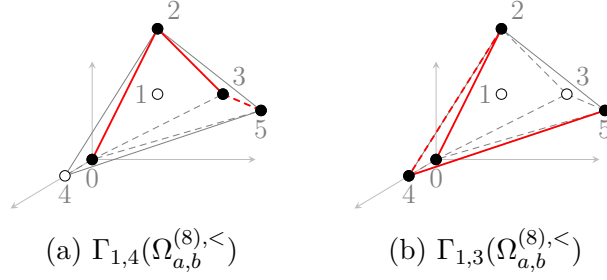
Figure 9.4: Lattice paths for polytopes $\Omega_{a,b}^{(8),<}$ of family 8 where $2b < a$

In the following, let S denote the tropical surface dual to $\Omega_{a,b}^{(8)}$ passing through 3 points $\mathbf{p} = (p_1, p_2, p_3)$ in Mikhalkin position and let L denote the line on which the points $\mathbf{q} = \mathrm{Trop}(\mathbf{p})$ are distributed.

We first consider $\Omega_{a,b}^{(8),<}$, that means $2b < a$. In this case we have the following five 3-dimensional regions of $\mathbb{R}^3 \setminus S$:

$\omega_0^\vee$ is defined by $(-1,0,0),(0,-2,1),(2b-a,1,-2),(0,b,-a)$;
$\omega_2^\vee$ is defined by $(-1,0,0),(0,-2,1),(3-(a+b),1,1),(2a-b,-b,a)$;
$\omega_3^\vee$ is defined by $(-1,0,0),(2b-a,1,-2),(3-(a+b),1,1)$;
$\omega_4^\vee$ is defined by $(0,-2,1),(0,b,-a),(2a-b,-b,a)$;
$\omega_5^\vee$ is defined by $(2b-a,1,-2),(0,b,-a),(3-(a+b),1,1),(2a-b,-b,a)$.

Now we consider the two paths depicted in Figure 9.4 separately.

The path $\Gamma_{1,4}(\Omega_{a,b}^{(8),<})$ passes through the 2-dimensional cells of S given by $(\overline{\omega_0\omega_2})^\vee$, $(\overline{\omega_2\omega_3})^\vee$ and $(\overline{\omega_3\omega_5})^\vee$. This gives us the following set of equations:

$$\begin{pmatrix} 0 \\ 0 \\ 0 \end{pmatrix} = \begin{pmatrix} x \\ y \\ z \end{pmatrix} + \alpha_1 \begin{pmatrix} -1 \\ 0 \\ 0 \end{pmatrix} + \alpha_2 \begin{pmatrix} 0 \\ -2 \\ 1 \end{pmatrix}, \ \alpha_1, \alpha_2 > 0,$$

$$\begin{pmatrix} 1 \\ \eta \\ \eta^2 \end{pmatrix} = \begin{pmatrix} x \\ y \\ z \end{pmatrix} + \beta_1 \begin{pmatrix} -1 \\ 0 \\ 0 \end{pmatrix} + \beta_2 \begin{pmatrix} 3-(a+b) \\ 1 \\ 1 \end{pmatrix}, \ \beta_1, \beta_2 > 0,$$

$$\begin{pmatrix} \lambda \\ \lambda\eta \\ \lambda\eta^2 \end{pmatrix} = \begin{pmatrix} x \\ y \\ z \end{pmatrix} + \gamma_1 \begin{pmatrix} 3-(a+b) \\ 1 \\ 1 \end{pmatrix} + \gamma_2 \begin{pmatrix} 2b-a \\ 1 \\ -2 \end{pmatrix}, \ \gamma_1, \gamma_2 > 0.$$

This system has the solutions

$$x = \alpha_1 = \lambda + \gamma_1(a+b-3) + \gamma_2(a-2b) > 0,$$

$$y = 2\alpha_2 = \frac{2}{3}(\eta - \eta^2) > 0,$$

$$z = \frac{1}{3}(\eta^2 - \eta),$$

$$\beta_1 = x - 1 + (3 - (a+b))\beta_2 > 0,$$

$$\beta_2 = \eta - \frac{2}{3}(\eta - \eta^2) > 0,$$

$$\gamma_1 = \lambda\eta - (\lambda + 1)\frac{1}{3}(\eta - \eta^2) > 0,$$

$$\gamma_2 = \frac{\lambda - 1}{3}(\eta - \eta^2) > 0.$$

We know $\alpha_1 = x > 0$ since $\gamma_1, \gamma_2 > 0$, $a > 2b$ and $a + b > 3$. $\beta_1 > 0$ since $\gamma_1 > \beta_2$.

It follows that the path $\Gamma_{1,4}(\Omega_{a,b}^{(8),<})$ is valid.

The path $\Gamma_{1,3}(\Omega_{a,b}^{(8),<})$ passes through the 2-dimensional cells of S given by $(\overline{\omega_0\omega_2})^\vee$, $(\overline{\omega_2\omega_4})^\vee$ and $(\overline{\omega_4\omega_5})^\vee$. This gives us the following set of equations:

$$\begin{pmatrix} 0 \\ 0 \\ 0 \end{pmatrix} = \begin{pmatrix} x \\ y \\ z \end{pmatrix} + \alpha_1 \begin{pmatrix} -1 \\ 0 \\ 0 \end{pmatrix} + \alpha_2 \begin{pmatrix} 0 \\ -2 \\ 1 \end{pmatrix}, \ \alpha_1, \alpha_2 > 0,$$

$$\begin{pmatrix} 1 \\ \eta \\ \eta^2 \end{pmatrix} = \begin{pmatrix} x \\ y \\ z \end{pmatrix} + \beta_1 \begin{pmatrix} 0 \\ -2 \\ 1 \end{pmatrix} + \beta_2 \begin{pmatrix} 2a - b \\ -b \\ a \end{pmatrix}, \ \beta_1, \beta_2 > 0,$$

$$\begin{pmatrix} \lambda \\ \lambda\eta \\ \lambda\eta^2 \end{pmatrix} = \begin{pmatrix} x \\ y \\ z \end{pmatrix} + \gamma_1 \begin{pmatrix} 2a - b \\ -b \\ a \end{pmatrix} + \gamma_2 \begin{pmatrix} 0 \\ b \\ -a \end{pmatrix}, \ \gamma_1, \gamma_2 > 0.$$

This system of equations has the solution

$$x = \alpha_1 = 1 - \eta - 2\eta^2 > 0,$$

$$y = 2\alpha_2 = \lambda\eta + \frac{b\lambda}{2a - b}(\eta + 2\eta^2) > 0,$$

$$z = -\alpha_2 = -\frac{1}{2}\lambda\eta - \frac{b\lambda}{2(2a - b)}(\eta + 2\eta^2),$$

$$\beta_1 = \frac{\lambda\eta}{2} + \eta^2 + \frac{\lambda b - 2a}{2(2a - b)}(\eta + 2\eta^2) > 0,$$

$$\beta_2 = \frac{1}{2a - b}(\eta + 2\eta^2) > 0,$$

$$\gamma_1 = \frac{1}{2a - b}(\lambda - 1 + \eta + 2\eta^2) > 0,$$

$$\gamma_2 = \frac{\lambda - 1}{2a - b}(1 - \eta - 2\eta^2) > 0.$$

Thus, the path $\Gamma_{1,3}(\Omega_{a,b}^{(8),<})$ is valid.

Now we can consider the second subtype $\Omega_{a,b}^{(8),>}$, that means the cases where $2b > a$. In this case we have the following five 3-dimensional regions of $\mathbb{R}^3 \setminus S$:

$\omega_0^\vee$ is defined by $(-1,0,0),(0,-2,1),(0,1,-2)$;
$\omega_2^\vee$ is defined by $(-1,0,0),(0,-2,1),(3-(a+b),1,1),(2a-b,-b,a)$;
$\omega_3^\vee$ is defined by $(-1,0,0),(0,1,-2),(3-(a+b),1,1),(2b-a,b,-a)$;
$\omega_4^\vee$ is defined by $(0,-2,1),(0,1,-2),(2a-b,-b,a),(2b-a,b,-a)$;
$\omega_5^\vee$ is defined by $(2a-b,-b,a),(3-(a+b),1,1),(2b-a,b,-a)$.

As before we consider the three possible paths depicted in Figure 9.5 separately.

(a) $\Gamma_{1,4}(\Omega_{a,b}^{(8),>})$ (b) $\Gamma_{1,3}(\Omega_{a,b}^{(8),>})$ (c) $\Gamma_{1,2}(\Omega_{a,b}^{(8),>})$
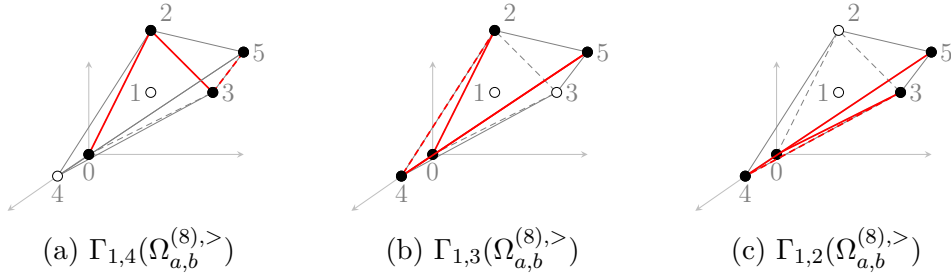
Figure 9.5: Lattice paths for polytopes $\Omega_{a,b}^{(8),>}$ of family 8 where $2b > a$

The path $\Gamma_{1,4}(\Omega_{a,b}^{(8),>})$ passes through the 2-dimensional cells of S given by $(\overline{\omega_0 \omega_2})^\vee$, $(\overline{\omega_2 \omega_3})^\vee$ and $(\overline{\omega_3 \omega_5})^\vee$. This gives us the following set of equations:

$$\begin{pmatrix} 0 \\ 0 \\ 0 \end{pmatrix} = \begin{pmatrix} x \\ y \\ z \end{pmatrix} + \alpha_1 \begin{pmatrix} -1 \\ 0 \\ 0 \end{pmatrix} + \alpha_2 \begin{pmatrix} 0 \\ -2 \\ 1 \end{pmatrix}, \ \alpha_1, \alpha_2 > 0,$$

$$\begin{pmatrix} 1 \\ \eta \\ \eta^2 \end{pmatrix} = \begin{pmatrix} x \\ y \\ z \end{pmatrix} + \beta_1 \begin{pmatrix} -1 \\ 0 \\ 0 \end{pmatrix} + \beta_2 \begin{pmatrix} 3-(a+b) \\ 1 \\ 1 \end{pmatrix}, \ \beta_1, \beta_2 > 0,$$

$$\begin{pmatrix} \lambda \\ \lambda\eta \\ \lambda\eta^2 \end{pmatrix} = \begin{pmatrix} x \\ y \\ z \end{pmatrix} + \gamma_1 \begin{pmatrix} 3-(a+b) \\ 1 \\ 1 \end{pmatrix} + \gamma_2 \begin{pmatrix} 2b-a \\ b \\ -a \end{pmatrix}, \ \gamma_1, \gamma_2 > 0.$$

This system of equations has the solution

$$x = \alpha_1 = \lambda + (a+b-3)\gamma_1 - (2b-a)\gamma_2 > 0,$$

$$y = 2\alpha_2 = \eta - \frac{1}{3}(\eta + 2\eta^2) > 0,$$

$$z = -\alpha_2 = \eta^2 - \frac{1}{3}(\eta + 2\eta^2),$$

$$\beta_1 = x - 1 + \beta_2(3 - (a+b)) > 0,$$

$$\beta_2 = \frac{1}{3}(\eta + 2\eta^2) > 0,$$

$$\gamma_1 = (\lambda - 1)(\eta - \frac{b}{a+b}(\eta - \eta^2)) + \frac{\eta + 2\eta^2}{3} > 0,$$

$$\gamma_2 = \frac{1}{a+b}(\lambda - 1)(\eta - \eta^2) > 0.$$

We have $\alpha_1 > 0$ since $\lambda > \gamma_2$, and $\beta_1 > 0$ holds since $\gamma_1 - \beta_2 > 0$. Thus, the path $\Gamma_{1,4}(\Omega_{a,b}^{(8),>})$ is valid.

The path $\Gamma_{1,3}(\Omega_{a,b}^{(8),>})$ passes through the 2-dimensional cells of S given by $(\overline{\omega_0 \omega_2})^\vee$, $(\overline{\omega_2 \omega_4})^\vee$ and $(\overline{\omega_4 \omega_5})^\vee$. This gives us the following set of equations:

$$\begin{pmatrix} 0 \\ 0 \\ 0 \end{pmatrix} = \begin{pmatrix} x \\ y \\ z \end{pmatrix} + \alpha_1 \begin{pmatrix} -1 \\ 0 \\ 0 \end{pmatrix} + \alpha_2 \begin{pmatrix} 0 \\ -2 \\ 1 \end{pmatrix}, \; \alpha_1, \alpha_2 > 0,$$

$$\begin{pmatrix} 1 \\ \eta \\ \eta^2 \end{pmatrix} = \begin{pmatrix} x \\ y \\ z \end{pmatrix} + \beta_1 \begin{pmatrix} 0 \\ -2 \\ 1 \end{pmatrix} + \beta_2 \begin{pmatrix} 2a-b \\ -b \\ a \end{pmatrix}, \; \beta_1, \beta_2 > 0,$$

$$\begin{pmatrix} \lambda \\ \lambda\eta \\ \lambda\eta^2 \end{pmatrix} = \begin{pmatrix} x \\ y \\ z \end{pmatrix} + \gamma_1 \begin{pmatrix} 2a-b \\ -b \\ a \end{pmatrix} + \gamma_2 \begin{pmatrix} 2b-a \\ b \\ -a \end{pmatrix}, \; \gamma_1, \gamma_2 > 0.$$

This system has the set of solutions

$$x = \alpha_1 = 1 - \eta - 2\eta^2 > 0,$$

$$y = 2\alpha_2 = \lambda\eta + \frac{b}{2a-b}(\lambda\eta + 2\lambda\eta^2),$$

$$z = -\alpha_2 = \lambda\eta^2 - \frac{a}{2a-b}(\lambda\eta + 2\lambda\eta^2) > 0,$$

$$\beta_1 = \frac{\lambda - 1}{2a-b}(a\eta + b\eta^2) > 0,$$

$$\beta_2 = \frac{1}{2a-b}(\eta+2\eta^2) > 0,$$

$$\gamma_1 = \frac{1}{2a-b}(\lambda\eta+2\lambda\eta^2) + \frac{1}{a+b}(\lambda-1)(1-\eta-2\eta^2) > 0,$$

$$\gamma_2 = \frac{\lambda-1}{a+b}(1-\eta-2\eta^2) > 0.$$

We have $\beta_1 > 0$ because $a > (a-b)\eta$. It follows that the path $\Gamma_{1,3}(\Omega_{a,b}^{(8),>})$ is valid.

Finally, we consider the path $\Gamma_{1,2}(\Omega_{a,b}^{(8),>})$. It passes through the 2-dimensional cells of S given by $(\overline{\omega_0\omega_3})^\vee$, $(\overline{\omega_3\omega_4})^\vee$ and $(\overline{\omega_4\omega_5})^\vee$. We get the following equations:

$$\begin{pmatrix} 0 \\ 0 \\ 0 \end{pmatrix} = \begin{pmatrix} x \\ y \\ z \end{pmatrix} + \alpha_1 \begin{pmatrix} -1 \\ 0 \\ 0 \end{pmatrix} + \alpha_2 \begin{pmatrix} 0 \\ 1 \\ -2 \end{pmatrix}, \quad \alpha_1,\alpha_2 > 0,$$

$$\begin{pmatrix} 1 \\ \eta \\ \eta^2 \end{pmatrix} = \begin{pmatrix} x \\ y \\ z \end{pmatrix} + \beta_1 \begin{pmatrix} 0 \\ 1 \\ -2 \end{pmatrix} + \beta_2 \begin{pmatrix} 2b-a \\ b \\ -a \end{pmatrix}, \quad \beta_1,\beta_2 > 0,$$

$$\begin{pmatrix} \lambda \\ \lambda\eta \\ \lambda\eta^2 \end{pmatrix} = \begin{pmatrix} x \\ y \\ z \end{pmatrix} + \gamma_1 \begin{pmatrix} 2a-b \\ -b \\ a \end{pmatrix} + \gamma_2 \begin{pmatrix} 2b-a \\ b \\ -a \end{pmatrix}, \quad \gamma_1,\gamma_2 > 0.$$

This system has the set of solutions

$$x = \alpha_1 = 1 - 2\eta - \eta^2 > 0,$$

$$y = -\alpha_2 = \lambda\eta - \frac{b}{2b-a}(2\lambda\eta+\lambda\eta^2),$$

$$z = 2\alpha_2 = \lambda\eta^2 + \frac{a}{2b-a}(2\lambda\eta+\lambda\eta^2) > 0,$$

$$\beta_1 = \frac{a}{2b-a}(\lambda-1)\eta + \frac{b}{2b-a}(\lambda-1)\eta^2 > 0,$$

$$\beta_2 = \frac{1}{2b-a}(2\eta+\eta^2) > 0,$$

$$\gamma_1 = \frac{1}{a+b}(\lambda-1)(1-2\eta-\eta^2) > 0,$$

$$\gamma_2 = \frac{1}{2b-a}(2\lambda\eta+\lambda\eta^2) + \frac{1}{a+b}(\lambda-1)(1-2\eta-\eta^2) > 0.$$

It follows that the path $\Gamma_{1,2}(\Omega_{a,b}^{(8),>})$ is valid. $\qquad\qquad\square$

Recall that for $\gcd(a,b) = 1$ and $2b > a$ it follows that $\gcd(a,a-b) = 1$ and $2(a-b) < a$. Thus, $\Omega_{a,b}^{(8),>}$ and $\Omega_{a,a-b}^{(8),<}$ are both polytopes of family 8. The following

conjecture postulates their connection.

Conjecture 9.4.4. *The degree of the binodal variety for a polytope in family* 8 *with parameters* a *and* b *satisfying* $2b > a$ *is equal to the degree of the binodal variety for the polytope in family* 8 *with parameters* a *and* $a - b$:

$$\deg(B_{\Omega_{a,b}^{(8),>}}) = \deg(B_{\Omega_{a,a-b}^{(8),<}}).$$

Furthermore, we have the following conjecture for the connection of the lattice path multiplicities between $\Omega_{a,b}^{(8),>}$ *and* $\Omega_{a,a-b}^{(8),<}$:

$$mult(\Gamma_{1,4}(\Omega_{a,a-b}^{(8),<})) = mult(\Gamma_{1,4}(\Omega_{a,b}^{(8),>})),$$
$$mult(\Gamma_{1,3}(\Omega_{a,a-b}^{(8),<})) = mult(\Gamma_{1,3}(\Omega_{a,b}^{(8),>})) + mult(\Gamma_{1,2}(\Omega_{a,b}^{(8),>})),$$
$$mult(\Gamma_{1,3}(\Omega_{a,b}^{(8),>})) = \frac{1}{2}(mult(\Gamma_{1,3}(\Omega_{a,a-b}^{(8),<})) + mult(\Gamma_{1,4}(\Omega_{a,a-b}^{(8),<}))),$$
$$mult(\Gamma_{1,2}(\Omega_{a,b}^{(8),>})) = mult(\Gamma_{1,3}(\Omega_{a,b}^{(8),>})) - mult(\Gamma_{1,4}(\Omega_{a,b}^{(8),>})).$$

This conjecture is verified up to $b < a \leq 7$ by the computations as described in Section 9.3.2 executed with the `OSCAR` code in [Gei22], which can also be found in Appendix B.2. The results of this computation are collected in Table 9.3. Remark 9.4.5 explains how to read the table.

$b \setminus a$	3	4	5	6	7
1	8	20	24	56	80
	3+5	6+14	6+18	12+44	15+65
2	8	x	33	x	60
	3+(4+1)		9+24		12+48
3	x	20	33	x	70
		6+(10+4)	9+(21+3)		15+55
4	x	x	24	x	70
			6+(12+6)		15+(50+5)
5	x	x	x	56	60
				12+(28+16)	12+(36+12)
6	x	x	x	x	80
					15+(40+25)

Table 9.3: The degree of the binodal variety and the multiplicities of the lattice paths for polytopes in family number 8. These were computed using [Gei22]. The presentation is explained in Remark 9.4.5.

Remark 9.4.5. We explain briefly how the data supporting Conjecture 9.4.4 is displayed in Table 9.3. The table displays the computed results for both subtypes of family number 8: The computed data for $\Omega_{a,b}^{(8),<}$ can be found in the white cells, the gray cells belong to $\Omega_{a,b}^{(8),>}$. To highlight the the border between the cases where $2b < a$ and $2b > a$ the cells with $2b = a$ are colored half in gray. The cells corresponding to parameters (a,b) for which $a \leq b$ are not colored at all to keep the table uncluttered.

Each cell contains the degree of the binodal variety $\deg(B_{\Omega_{a,b}^{(8)}}$ in its first line. The second line shows the path multiplicities. They are presented as sums, to demonstrate that they sum up to the degree of the binodal variety. The order of the lattice path multiplicities in the sum is as follows:

- For $\Omega_{a,b}^{(8),<}$: $\mathrm{mult}(\Gamma_{1,4}(\Omega_{a,b}^{(8),<})) + \mathrm{mult}_{(}(\Gamma)_{1,3}(\Omega_{a,b}^{(8),<}))$.

- For $\Omega_{a,b}^{(8),>}$: $\mathrm{mult}(\Gamma_{1,4}(\Omega_{a,b}^{(8),>})) + \mathrm{mult}_{(}(\Gamma)_{1,3}(\Omega_{a,b}^{(8),>})) + \mathrm{mult}_{(}(\Gamma)_{1,2}(\Omega_{a,b}^{(8),>}))$.

9.4.2 Polytope family 10

$$\Omega_{a,b}^{(10)} = \begin{pmatrix} 0 & 0 & 0 & 0 & 1 & 1 \\ 0 & 0 & 1 & 1 & 0 & a \\ 0 & 1 & 0 & 1 & 0 & b \end{pmatrix}$$
$$gcd(a,b) = 1, \ 0 < b \leq a, \ a \geq 3$$
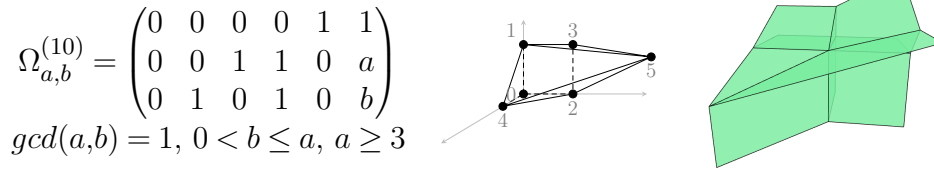
Figure 9.6: Polytope family 10

We investigate possible lattice paths for the polytope family number 10 and their multiplicities.

Lemma 9.4.6. *For all polytopes* $\Omega_{a,b}^{(10)}$ *of family* 10 *with lattice points as in Figure 9.1, only lattice paths connected from* 0 *to* 5 *are possible.*

Proof. We proceed similarly to the proof of Lemma 9.4.2. Let S be the surface dual to $\Omega_{a,b}^{(10)}$. We translate S such that the vertex is at $(0,0,0)$. The direction vector of the line L on which the points of the point condition lie is $(1,\eta,\eta^2)$ with $0 < \eta \ll 1$.

Recall the notation $\cdot^\vee$ for the dual object under the duality connection between the Newton polytope and the tropical surface (Corollary 2.1.15).

$$\text{(a) } \Gamma_{2,4}(\Omega_{a,b}^{(10)}) \qquad \text{(b) } \Gamma_{2,3}(\Omega_{a,b}^{(10)}) \qquad \text{(c) } \Gamma_{1,4}(\Omega_{a,b}^{(10)}) \qquad \text{(d) } \Gamma_{1,3}(\Omega_{a,b}^{(10)})$$
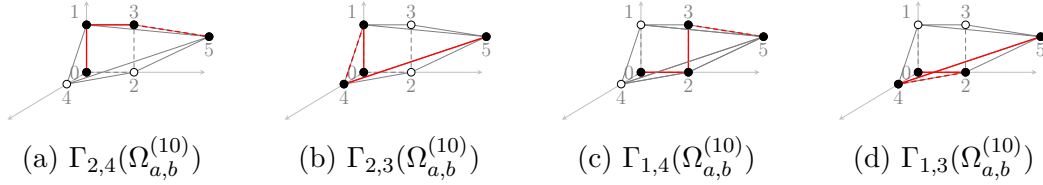
Figure 9.7: Valid lattice paths for polytopes of family 10

For a lattice path which is not connected from 0 to 5, the line L on which the points **q** from the point conditions are distributed intersects with the tropical surface more than 3 times, e.g. if the line passes through more than four of the 3-dimensional regions of $\mathbb{R}^3 \setminus S$.

The vertices of $\Omega_{a,b}^{(10)}$ are $\omega_0 = (0,0,0)$, $\omega_1 = (0,0,1)$, $\omega_2 = (0,1,0)$, $\omega_3 = (0,1,1)$, $\omega_4 = (1,0,0)$, $\omega_5 = (1,a,b)$. In dependence of a,b we can determine the rays defining the six regions into which the surface subdivides $\mathbb{R}^3$. We know that

$\omega_0^\vee$ is defined by $(-1,0,0),(0,-1,0),(0,0,-1)$;
$\omega_1^\vee$ is defined by $(-1,0,0),(0,0,1),(0,-1,0),(a,-b,a)$;
$\omega_2^\vee$ is defined by $(-1,0,0),(0,0,-1),(-a+1,1,0),(b,b,-a)$;
$\omega_3^\vee$ is defined by $(-1,0,0),(0,0,1),(-a+1,1,0)$;
$\omega_4^\vee$ is defined by $(0,-1,0),(0,0,-1),(b,b,-a),(a,-b,a)$;
$\omega_5^\vee$ is defined by $(0,0,1),(-a+1,1,0),(b,b,-a)(a,-b,a)$.

Since we know that $a,b > 0$, we can make containment statements for the 3-cells dual to the vertices with respect to the quadrants of $\mathbb{R}^3$: We have $\omega_1^\vee \subset \{y < 0, z > 0\}$ and $\omega_2^\vee \subset \{y > 0, z < 0\}$, so we know that L can only pass through one of them. Moreover, $\omega_3^\vee \subset \{y > 0, z > 0\}$ and $\omega_4^\vee \cap \{y > 0\} \subset \{z < 0\}$ while $\omega_4^\vee \cap \{z > 0\} \subset \{y < 0\}$, so again L can only pass through one of these regions. It follows that L can pass at most through four of the six 3-dimensional regions defined by the tropical surface. Hence, the claim follows with Lemma 9.3.3. $\qquad \square$

Remark 9.4.7. Under IUA-transformations, polytopes of family 10 can be brought into a position where the lattice points are distributed 3+3 between two floors. We will see this position in Section 10.1.1. As the argument in the proof of Lemma 9.4.6 depends on the exact position of the vertices under transformation, this case has to be checked independently. However, an analysis using the same tools as above shows that there are still no disconnected lattice paths possible.

Proposition 9.4.8. *The lattice paths depicted in Figures 9.7 are the only possible lattice paths for the polytopes in family* 10 *in the IUA-representation as in Figure 9.6.*

Proof. From Lemma 9.4.6 we know that any possible lattice path has to be connected from 0 to 5, and by Lemma 9.3.1 we know that the lattice path has to run along the edges of the polytope. This limits the possibilities to the four cases in Figure 9.7. Similarly to the proof of Proposition 9.4.3, we check the validity of the lattice paths by using the technique from Remark 9.3.6. In the following let S denote the tropical surface dual to $\Omega_{a,b}^{(10)}$ passing through points in Mikhalkin position. Let L denote the line on which the points $\mathbf{q} = \text{Trop}(\mathbf{p})$ are distributed. To this purpose we choose the points $q_1 = (0,0,0)$, $q_2 = (1,\eta,\eta^2)$, $q_3 = (\lambda, \lambda\eta, \lambda\eta^2)$ with $0 < \eta \ll 1 \ll \lambda$ and let (x,y,z) be the vertex of the tropical surface.

For polytopes $\Omega_{a,b}^{(10)}$ we know that its lattice points are given by $\omega_0 = (0,0,0)$, $\omega_1 = (0,0,1)$, $\omega_2 = (0,1,0)$, $\omega_3 = (0,1,1)$, $\omega_4 = (1,0,0)$, and $\omega_5 = (1,a,b)$. Recall the regions of $\mathbb{R}^3 \setminus S$ from the proof of Lemma 9.4.6.

We have to set up the linear systems for each path in Figure 9.7 and prove that they have a solution. The path $\Gamma_{2,4}(\Omega_{a,b}^{(10)})$ passes through the 2-dimensional cells of S given by $(\overline{\omega_0\omega_1})^\vee$, $(\overline{\omega_1\omega_3})^\vee$ and $(\overline{\omega_3\omega_5})^\vee$. We obtain the following system of linear equations:

$$\begin{pmatrix} 0 \\ 0 \\ 0 \end{pmatrix} = \begin{pmatrix} x \\ y \\ z \end{pmatrix} + \alpha_1 \begin{pmatrix} -1 \\ 0 \\ 0 \end{pmatrix} + \alpha_2 \begin{pmatrix} 0 \\ -1 \\ 0 \end{pmatrix}, \quad \alpha_1, \alpha_2 > 0,$$

$$\begin{pmatrix} 1 \\ \eta \\ \eta^2 \end{pmatrix} = \begin{pmatrix} x \\ y \\ z \end{pmatrix} + \beta_1 \begin{pmatrix} -1 \\ 0 \\ 0 \end{pmatrix} + \beta_2 \begin{pmatrix} 0 \\ 0 \\ 1 \end{pmatrix}, \quad \beta_1, \beta_2 > 0,$$

$$\begin{pmatrix} \lambda \\ \lambda\eta \\ \lambda\eta^2 \end{pmatrix} = \begin{pmatrix} x \\ y \\ z \end{pmatrix} + \gamma_1 \begin{pmatrix} 0 \\ 0 \\ 1 \end{pmatrix} + \gamma_2 \begin{pmatrix} -a+1 \\ 1 \\ 0 \end{pmatrix}, \quad \gamma_1, \gamma_2 > 0.$$

This system has the solution:

$$x = \alpha_1 = \lambda + (a-1)(\lambda-1)\eta > 1 > 0,$$
$$y = \alpha_2 = \eta > 0,$$
$$z = 0,$$
$$\beta_1 = \alpha_1 - 1 > 0,$$
$$\beta_2 = \eta^2 > 0,$$
$$\gamma_1 = \lambda\eta^2 > 0,$$
$$\gamma_2 = (\lambda-1)\eta > 0,$$

which satisfies all the conditions. Therefore the path $\Gamma_{2,4}(\Omega_{a,b}^{(10)})$ is valid.

The path $\Gamma_{2,3}(\Omega_{a,b}^{(10)})$ passes through the 2-dimensional cells of S given by $(\overline{\omega_0\omega_1})^\vee$, $(\overline{\omega_1\omega_4})^\vee$ and $(\overline{\omega_4\omega_5})^\vee$. We obtain the following system of linear equations:

$$\begin{pmatrix} 0 \\ 0 \\ 0 \end{pmatrix} = \begin{pmatrix} x \\ y \\ z \end{pmatrix} + \alpha_1 \begin{pmatrix} -1 \\ 0 \\ 0 \end{pmatrix} + \alpha_2 \begin{pmatrix} 0 \\ -1 \\ 0 \end{pmatrix}, \ \alpha_1, \alpha_2 > 0,$$

$$\begin{pmatrix} 1 \\ \eta \\ \eta^2 \end{pmatrix} = \begin{pmatrix} x \\ y \\ z \end{pmatrix} + \beta_1 \begin{pmatrix} 0 \\ -1 \\ 0 \end{pmatrix} + \beta_2 \begin{pmatrix} a \\ -b \\ a \end{pmatrix}, \ \beta_1, \beta_2 > 0,$$

$$\begin{pmatrix} \lambda \\ \lambda\eta \\ \lambda\eta^2 \end{pmatrix} = \begin{pmatrix} x \\ y \\ z \end{pmatrix} + \gamma_1 \begin{pmatrix} b \\ b \\ -a \end{pmatrix} + \gamma_2 \begin{pmatrix} a \\ -b \\ a \end{pmatrix}, \ \gamma_1, \gamma_2 > 0.$$

This system has the solution:

$$x = \alpha_1 = 1 - \eta^2 > 0,$$

$$y = \alpha_2 = \lambda\eta(1 + \frac{b}{a}\eta) > 0,$$

$$z = 0,$$

$$\beta_1 = \lambda\eta(1 + \frac{b}{a}\eta) - \eta - \frac{b}{a}\eta^2 > 0,$$

$$\beta_2 = \frac{\eta^2}{a} > 0,$$

$$\gamma_1 = \frac{1}{b}(\lambda - 1 + \eta^2 - \gamma_2 a) > 0,$$

$$\gamma_2 = \frac{b}{a+b}(\frac{1}{b}(\lambda - 1) + \frac{1}{a}(\lambda + \frac{a}{b})\eta^2) > 0.$$

Therefore, the path $\Gamma_{2,3}(\Omega_{a,b}^{(10)})$ is valid.

The path $\Gamma_{1,4}(\Omega_{a,b}^{(10)})$ passes through the 2-dimensional cells of S given by $(\overline{\omega_0\omega_2})^\vee$, $(\overline{\omega_2\omega_3})^\vee$ and $(\overline{\omega_3\omega_5})^\vee$. We obtain the following system of linear equations:

$$\begin{pmatrix} 0 \\ 0 \\ 0 \end{pmatrix} = \begin{pmatrix} x \\ y \\ z \end{pmatrix} + \alpha_1 \begin{pmatrix} -1 \\ 0 \\ 0 \end{pmatrix} + \alpha_2 \begin{pmatrix} 0 \\ 0 \\ -1 \end{pmatrix}, \ \alpha_1, \alpha_2 > 0,$$

$$\begin{pmatrix} 1 \\ \eta \\ \eta^2 \end{pmatrix} = \begin{pmatrix} x \\ y \\ z \end{pmatrix} + \beta_1 \begin{pmatrix} -1 \\ 0 \\ 0 \end{pmatrix} + \beta_2 \begin{pmatrix} -a+1 \\ 1 \\ 0 \end{pmatrix}, \ \beta_1, \beta_2 > 0,$$

$$\begin{pmatrix} \lambda \\ \lambda\eta \\ \lambda\eta^2 \end{pmatrix} = \begin{pmatrix} x \\ y \\ z \end{pmatrix} + \gamma_1 \begin{pmatrix} 0 \\ 0 \\ 1 \end{pmatrix} + \gamma_2 \begin{pmatrix} -a+1 \\ 1 \\ 0 \end{pmatrix}, \ \gamma_1, \gamma_2 > 0.$$

This system has the solution:

$$\begin{aligned} x &= \alpha_1 = \lambda + (a-1)\lambda\eta > 0, \\ y &= 0, \\ z &= \alpha_2 = \eta^2 > 0, \\ \beta_1 &= \lambda - 1 + (a-1)(\lambda-1)\eta > 0, \\ \beta_2 &= \eta > 0, \\ \gamma_1 &= (\lambda - 1)\eta^2 > 0, \\ \gamma_2 &= \lambda\eta > 0. \end{aligned}$$

Therefore, the path $\Gamma_{1,4}(\Omega_{a,b}^{(10)})$ is valid.

The path $\Gamma_{1,3}(\Omega_{a,b}^{(10)})$ passes through the 2-dimensional cells of S given by $(\overline{\omega_0\omega_2})^\vee$, $(\overline{\omega_2\omega_4})^\vee$ and $(\overline{\omega_4\omega_5})^\vee$. We obtain the following system of linear equations:

$$\begin{pmatrix} 0 \\ 0 \\ 0 \end{pmatrix} = \begin{pmatrix} x \\ y \\ z \end{pmatrix} + \alpha_1 \begin{pmatrix} -1 \\ 0 \\ 0 \end{pmatrix} + \alpha_2 \begin{pmatrix} 0 \\ 0 \\ -1 \end{pmatrix}, \ \alpha_1, \alpha_2 > 0,$$

$$\begin{pmatrix} 1 \\ \eta \\ \eta^2 \end{pmatrix} = \begin{pmatrix} x \\ y \\ z \end{pmatrix} + \beta_1 \begin{pmatrix} 0 \\ 0 \\ -1 \end{pmatrix} + \beta_2 \begin{pmatrix} b \\ b \\ -a \end{pmatrix}, \ \beta_1, \beta_2 > 0,$$

$$\begin{pmatrix} \lambda \\ \lambda\eta \\ \lambda\eta^2 \end{pmatrix} = \begin{pmatrix} x \\ y \\ z \end{pmatrix} + \gamma_1 \begin{pmatrix} b \\ b \\ -a \end{pmatrix} + \gamma_2 \begin{pmatrix} a \\ -b \\ a \end{pmatrix}, \ \gamma_1, \gamma_2 > 0.$$

This system has the solution:

$$\begin{aligned} x &= \alpha_1 = 1 - \eta > 0, \\ y &= 0, \\ z &= \alpha_2 = \frac{a}{b}\lambda\eta + \lambda\eta^2 > 0, \\ \beta_1 &= \frac{a}{b}(\lambda-1)\eta + (\lambda-1)\eta^2 > 0, \\ \beta_2 &= \frac{\eta}{b} > 0, \\ \gamma_1 &= \frac{\lambda\eta + \gamma_2 b}{b} > 0, \end{aligned}$$

$$\gamma_2 = \frac{\lambda(1-\eta)+\eta-1}{a+b} > 0.$$

Therefore, the path $\Gamma_{1,3}(\Omega_{a,b}^{(10)})$ is valid. $\qquad\square$

Now that we know that all lattice paths in Figure 9.7 are valid, we can compute the path multiplicities by using `OSCAR` (see Section 9.3.2 and [Gei22]). From the results depicted in Table 9.4 we worked out the following conjecture.

Conjecture 9.4.9. *For polytopes $\Omega_{a,b}^{(10)}$ of family number 10 as in Figure 9.6 where $gcd(a,b)=1$, $0 < b \le a$ and $a \ge 3$, we have the following conjecture about the degree of the binodal variety and the path multiplicities:*

$$deg(B_{\Omega_{a,b}^{(10)}}) = (a-2)(a+b+2),$$

$$mult(\Gamma_{2,4}(\Omega_{a,b}^{(10)})) = a-2,$$

$$mult(\Gamma_{2,3}(\Omega_{a,b}^{(10)})) = a(a-2),$$

$$mult(\Gamma_{1,4}(\Omega_{a,b}^{(10)})) = a-2,$$

$$mult(\Gamma_{1,3}(\Omega_{a,b}^{(10)})) = b(a-2).$$

This conjecture is verified up to $a \le 7$ and $b \le 4$ by using the `OSCAR` code [Gei22] as in Appendix B.2. The values for these cases are depicted in Table 9.4. Remark 9.4.10 explains the presentation of the data in the table.

$b \setminus a$	3	4	5	6	7
1	6	14	24	36	50
	1+3+1+1	2+8+2+2	3+15+3+3	4+24+4+4	5+35+5+5
2	7	x	27	x	55
	1+3+1+2		3+15+3+6		5+35+5+10
3	x	18	30	x	60
		2+8+2+6	3+15+3+9		5+35+5+15
4	x	x	33	x	65
			3+15+3+12		5+35+5+20
5	x	x	x	52	-
				4+24+4+20	

Table 9.4: Verified path multiplicities and degree of binodal variety for polytope family number 10 as computed using [Gei22] in `OSCAR`. The case $a=7$, $b=5$ did not terminate. See Remark 9.4.10 for more explanations on the data.

Remark 9.4.10. The data supporting Conjecture 9.4.9 displayed in Table 9.4 can be read as follows: The first line in each cell states the degree of the binodal variety $\deg(B_{\Omega_{a,b}^{(10)}})$. The second line in each cell shows how the path multiplicities partition the binodal degree. The order of the summands is as follows:

$$\text{mult}(\Gamma_{2,4}(\Omega_{a,b}^{(10)})) + \text{mult}(\Gamma_{2,3}(\Omega_{a,b}^{(10)})) + \text{mult}(\Gamma_{1,4}(\Omega_{a,b}^{(10)})) + \text{mult}(\Gamma_{1,3}(\Omega_{a,b}^{(10)})).$$

9.4.3 Polytope family 13

$$\Omega_{a,b}^{(13)} = \begin{pmatrix} 0 & 0 & 0 & 0 & 1 & 1 \\ 0 & 1 & 1 & 2 & 0 & a \\ 0 & 0 & 1 & 0 & 0 & b \end{pmatrix}$$

$$gcd(a,b) = 1, \ 0 < b < a, \ a+b \geq 5$$
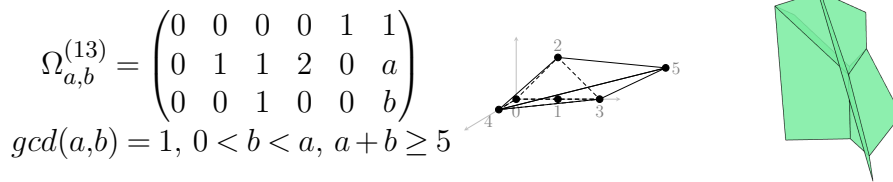
Figure 9.8: Polytope family 13

We investigate possible lattice paths for the polytope family number 13 and their multiplicities.

Lemma 9.4.11. *For all polytopes of family* 13 *with lattice points as in Figure 9.1, only lattice paths connected from* 0 *to* 5 *are possible.*

Proof. The proof runs along the same lines as for polytope family 8. Let $\Omega_{a,b}^{(13)}$ be a polytope of family 13. Without loss of generality we can assume that the surface S dual to the polytope has a unique vertex at $(0,0,0)$. The direction vector of the line L on which the points of the point condition lie is $(1,\eta,\eta^2)$ with $0 < \eta \ll 1$.

There can only exist disconnected lattice paths for $\Omega_{a,b}^{(13)}$ if the line L, on which the points from the point conditions are distributed, intersects with the tropical surface S more than 3 times; see Lemma 9.3.3. Label the lattice points of the polytope with ω_0, ω_1, ω_2, ω_3, ω_4 and ω_5 in the order as induced by $v = (1,\eta,\eta^2)$ (Definition 7.2.3). We know by Proposition 9.1.10 that in order to be dual to a binodal surface $\Omega_{a,b}^{(13)}$ has the trivial subdivision, so the lattice point ω_1 is never a vertex of the subdivision. Therefore, a tropical surface with support $\Omega_{a,b}^{(13)}$ divides $\mathbb{R}^3$ into only five 3-dimensional regions. For a path not connected from 0 to 5, the line L must pass through all five regions. We refer to the proof of Proposition 9.4.12 for the rays generating these regions.

Considering these we observe that if the line L passes through $\omega_0^\vee$, $\omega_2^\vee$ and $\omega_3^\vee$, the remaining ray of L is contained in the $\{z > 0, y > 0\}$ quadrant of $\mathbb{R}^3$.

For each polytope of family 13 we have

$$\omega_4^\vee = \left\{ \mu_1 \begin{pmatrix} 0 \\ 0 \\ -1 \end{pmatrix} + \mu_2 \begin{pmatrix} 0 \\ -1 \\ 1 \end{pmatrix} + \mu_3 \begin{pmatrix} a-b \\ -b \\ a \end{pmatrix} + \mu_4 \begin{pmatrix} 2b \\ b \\ -a \end{pmatrix} \,\middle|\, \mu_i > 0 \,\forall i \in \{1,2,3,4\} \right\}.$$

Assume μ_1, μ_2, μ_3, $\mu_4 > 0$ determine a point in $\omega_4^\vee \cap \{z > 0, y > 0\}$. It follows:

$$-\mu_2 - b\mu_3 + b\mu_4 > 0,$$
$$-\mu_1 + \mu_2 + a\mu_3 - a\mu4 > 0,$$

which implies the following two inequalities

$$b\mu_4 > \mu_2 + b\mu_3,$$
$$\mu_2 + a\mu_3 > \mu_1 + a\mu_4 > \mu_1 + \frac{a}{b}\mu_2 + a\mu_3.$$

This in its turn implies $\mu_2 > \mu_1 + \frac{a}{b}\mu_2$, which contradicts $\mu_1, \mu_2 > 0$ since $\frac{a}{b} > 1$.

So $\omega_4^\vee \cap \{z > 0, y > 0\} = \emptyset$. Thus, L cannot pass through all five 3-dimensional regions $\mathbb{R}^3 \setminus S$. $\qquad\square$

Proposition 9.4.12. *The lattice paths depicted in Figure 9.9 are the only possible lattice paths for the polytopes in family* 13 *with vertices as in Figure 9.8.*

(a) $\Gamma_{1,3}(\Omega_{a,b}^{(13)})$ (b) $\Gamma_{1,4}(\Omega_{a,b}^{(13)})$ (c) $\Gamma_{1,2}(\Omega_{a,b}^{(13)})$
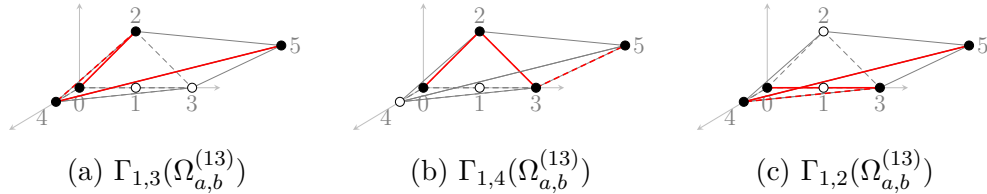
Figure 9.9: Valid lattice paths for polytopes of family number 13

Proof. The paths depicted in Figure 9.9 are all the possible lattice paths that run along edges (Lemma 9.3.1), are connected from 0 to 5 and leave out ω_1 (Lemma 9.4.11). Analogous to the proofs of Propositions 9.4.3 and 9.4.8 we prove that the paths are valid by setting up the linear equation systems and computing their solutions.

In the following let $\Omega_{a,b}^{(13)}$ be a binodal polytope of family 13 and S the tropical surface dual to the trivial subdivision of $\Omega_{a,b}^{(13)}$.

For polytopes of family 13 we know that $\omega_0 = (0,0,0)$, $\omega_1 = (0,1,0)$, $\omega_2 = (0,1,1)$, $\omega_3 = (0,2,0)$, $\omega_4 = (1,0,0)$, $\omega_5 = (1,a,b)$. The 3-dimensional regions of $\mathbb{R}^3 \setminus S$ with

vertex of the surface at (0,0,0) are given by the dual regions of the vertices:

$\omega_0^\vee$ is defined by $(-1,0,0),(0,0,-1),(0,-1,1)$;

$\omega_2^\vee$ is defined by $(-1,0,0),(0,-1,1),(a-b,-b,a),(2-(a+b),1,1)$;

$\omega_3^\vee$ is defined by $(-1,0,0),(0,0,-1),(2b,b,-a),(2-(a+b),1,1)$;

$\omega_4^\vee$ is defined by $(0,0,-1),(0,-1,1),(a-b,-b,a),(2b,b,-a)$;

$\omega_5^\vee$ is defined by $(2b,b,-a),(2-(a+b),1,1),(a-b,-b,a)$.

Assume S passes through points in Mikhalkin position. We fix these points as $(0,0,0)$, $(1,\eta,\eta^2)$, $(\lambda,\lambda\eta,\lambda\eta^2)$, where $\lambda \gg 1 \gg \eta > 0$. Let L denote the line on which these points are distributed. For the above regions, this means that we have to add the vertex (x,y,z) of S to translate the cones to their correct position.

Now we check that the paths in Figure 9.9 are valid.

The path $\Gamma_{1,4}(\Omega_{a,b}^{(13)})$ passes through the 2-dimensional cells of S given by $(\overline{\omega_0\omega_2})^\vee$, $(\overline{\omega_2\omega_3})^\vee$ and $(\overline{\omega_3\omega_5})^\vee$. This gives us the following set of equations:

$$\begin{pmatrix} 0 \\ 0 \\ 0 \end{pmatrix} = \begin{pmatrix} x \\ y \\ z \end{pmatrix} + \alpha_1 \begin{pmatrix} -1 \\ 0 \\ 0 \end{pmatrix} + \alpha_2 \begin{pmatrix} 0 \\ -1 \\ 1 \end{pmatrix}, \; \alpha_1,\alpha_2 > 0,$$

$$\begin{pmatrix} 1 \\ \eta \\ \eta^2 \end{pmatrix} = \begin{pmatrix} x \\ y \\ z \end{pmatrix} + \beta_1 \begin{pmatrix} -1 \\ 0 \\ 0 \end{pmatrix} + \beta_2 \begin{pmatrix} 2-(a+b) \\ 1 \\ 1 \end{pmatrix}, \; \beta_1,\beta_2 > 0,$$

$$\begin{pmatrix} \lambda \\ \lambda\eta \\ \lambda\eta^2 \end{pmatrix} = \begin{pmatrix} x \\ y \\ z \end{pmatrix} + \gamma_1 \begin{pmatrix} 2-(a+b) \\ 1 \\ 1 \end{pmatrix} + \gamma_2 \begin{pmatrix} 2b \\ b \\ -a \end{pmatrix}, \; \gamma_1,\gamma_2 > 0.$$

This system has the solutions

$$x = \alpha_1 = \lambda + (a+b-2)\lambda\eta + \frac{\eta-\eta^2}{2}(2-(a+b)-2(\lambda-1)b) > 0,$$

$$y = \alpha_2 = \frac{\eta-\eta^2}{2} > 0,$$

$$z = -y,$$

$$\beta_1 = x - 1 + (2-(a+b))\beta_2 > 0,$$

$$\beta_2 = \frac{\eta+\eta^2}{2} > 0,$$

$$\gamma_1 = \lambda\eta - \frac{\eta-\eta^2}{2} - \frac{b}{a+b}(\lambda-1)(\eta-\eta^2) > 0,$$

$$\gamma_2 = \frac{1}{a+b}(\lambda-1)(\eta-\eta^2) > 0.$$

To see that $\beta_1 > 0$, we substitute the values for x and β_2 and observe that negative summands only appear for terms with η or η^2. Since $\lambda \gg 1 \gg \eta > 0$, it follows that $\beta_1 > 0$. It follows that the path $\Gamma_{1,4}(\Omega_{a,b}^{(13)})$ is valid.

The path $\Gamma_{1,3}(\Omega_{a,b}^{(13)})$ passes through the 2-dimensional cells of S given by $(\overline{\omega_0\omega_2})^\vee$, $(\overline{\omega_2\omega_4})^\vee$ and $(\overline{\omega_4\omega_5})^\vee$. This gives us the following set of equations:

$$\begin{pmatrix}0\\0\\0\end{pmatrix} = \begin{pmatrix}x\\y\\z\end{pmatrix} + \alpha_1\begin{pmatrix}-1\\0\\0\end{pmatrix} + \alpha_2\begin{pmatrix}0\\-1\\1\end{pmatrix}, \ \alpha_1,\alpha_2 > 0,$$

$$\begin{pmatrix}1\\\eta\\\eta^2\end{pmatrix} = \begin{pmatrix}x\\y\\z\end{pmatrix} + \beta_1\begin{pmatrix}0\\-1\\1\end{pmatrix} + \beta_2\begin{pmatrix}a-b\\-b\\a\end{pmatrix}, \ \beta_1,\beta_2 > 0,$$

$$\begin{pmatrix}\lambda\\\lambda\eta\\\lambda\eta^2\end{pmatrix} = \begin{pmatrix}x\\y\\z\end{pmatrix} + \gamma_1\begin{pmatrix}2b\\b\\-a\end{pmatrix} + \gamma_2\begin{pmatrix}a-b\\-b\\a\end{pmatrix}, \ \gamma_1,\gamma_2 > 0.$$

This system has the solutions

$$x = \alpha_1 = 1 - \eta - \eta^2 > 0,$$
$$y = \alpha_2 = \lambda\eta + \frac{b}{a-b}(\lambda\eta+\lambda\eta^2) > 0,$$
$$z = \lambda\eta^2 - \frac{a}{a-b}(\lambda\eta+\lambda\eta^2),$$
$$\beta_1 = (\lambda-1)(\eta+\frac{b}{a-b}(\eta+\eta^2)) > 0,$$
$$\beta_2 = \frac{1}{a-b}(\eta+\eta^2) > 0,$$
$$\gamma_1 = \frac{1}{a+b}(\lambda-1)(1-\eta-\eta^2) > 0,$$
$$\gamma_2 = \frac{1}{a-b}(\lambda\eta+\lambda\eta^2) + \frac{1}{a+b}(\lambda-1)(1-\eta-\eta^2) > 0.$$

It follows that the path $\Gamma_{1,3}(\Omega_{a,b}^{(13)})$ is valid.

The path $\Gamma_{1,2}(\Omega_{a,b}^{(13)})$ passes through the 2-dimensional cells of S given by $(\overline{\omega_0\omega_3})^\vee$,

$(\overline{\omega_3\omega_4})^\vee$ and $(\overline{\omega_4\omega_5})^\vee$. This gives us the following set of equations:

$$\begin{pmatrix} 0 \\ 0 \\ 0 \end{pmatrix} = \begin{pmatrix} x \\ y \\ z \end{pmatrix} + \alpha_1 \begin{pmatrix} -1 \\ 0 \\ 0 \end{pmatrix} + \alpha_2 \begin{pmatrix} 0 \\ 0 \\ -1 \end{pmatrix}, \ \alpha_1, \alpha_2 > 0,$$

$$\begin{pmatrix} 1 \\ \eta \\ \eta^2 \end{pmatrix} = \begin{pmatrix} x \\ y \\ z \end{pmatrix} + \beta_1 \begin{pmatrix} 0 \\ 0 \\ -1 \end{pmatrix} + \beta_2 \begin{pmatrix} 2b \\ b \\ -a \end{pmatrix}, \ \beta_1, \beta_2 > 0,$$

$$\begin{pmatrix} \lambda \\ \lambda\eta \\ \lambda\eta^2 \end{pmatrix} = \begin{pmatrix} x \\ y \\ z \end{pmatrix} + \gamma_1 \begin{pmatrix} 2b \\ b \\ -a \end{pmatrix} + \gamma_2 \begin{pmatrix} a-b \\ -b \\ a \end{pmatrix}, \ \gamma_1, \gamma_2 > 0.$$

This system has the solutions

$$x = \alpha_1 = 1 - 2\eta > 0,$$
$$y = 0,$$
$$z = \alpha_2 = \lambda\eta(\frac{a}{b} + \eta) > 0,$$
$$\beta_1 = \frac{a}{b}(\lambda - 1)\eta + (\lambda - 1)\eta^2 > 0,$$
$$\beta_2 = \frac{1}{b}\eta > 0,$$
$$\gamma_1 = \frac{1}{b}\lambda\eta + \frac{1}{a+b}(\lambda - 1)(1 - 2\eta) > 0,$$
$$\gamma_2 = \frac{1}{a+b}(\lambda - 1)(1 - 2\eta) > 0.$$

It follows that the path $\Gamma_{1,2}(\Omega_{a,b}^{(13)})$ is valid. □

We can now compute the multiplicities of the valid lattice paths for binodal polytopes of family 13. We do this in the same way as for the other polytope families: We use the `OSCAR` functions which are based on Algorithms 9 and 10 from Section 9.3.2. The functions are displayed in Appendix B.2 and are available on GitHub[1], see [Gei22].

Conjecture 9.4.13. *For polytopes $\Omega_{a,b}^{(13)}$ of family number 13 as in Figure 9.8 where $gcd(a,b) = 1$, $0 < b < a$ and $a + b \geq 5$, we have the following conjecture about the degree of the binodal variety and the path multiplicities.*

---

[1]`https://github.com/AlheydisGeiger/Code-Binodal-Surfaces`

If a and b have different parities, we conjecture

$$deg(B_{\Omega_{a,b}^{(13)}}) = \frac{1}{2}(a^2 - a + b^2 - b) + ab - 3,$$

$$mult(\Gamma_{1,4}(\Omega_{a,b}^{(13)})) = a + b - 3,$$

$$mult(\Gamma_{1,3}(\Omega_{a,b}^{(13)})) = \frac{1}{2}(a^2 - 3a - b^2 + 3b),$$

$$mult(\Gamma_{1,2}(\Omega_{a,b}^{(13)})) = b(a + b - 3).$$

If a and b are both odd, we conjecture

$$deg(B_{\Omega_{a,b}^{(13)}}) = \frac{1}{2}(a^2 - 2a + b^2 - 2b) + ab - 4,$$

$$mult(\Gamma_{1,4}(\Omega_{a,b}^{(13)})) = a + b - 4,$$

$$mult(\Gamma_{1,3}(\Omega_{a,b}^{(13)})) = \frac{1}{2}(a^2 - 4a - b^2 + 4b),$$

$$mult(\Gamma_{1,2}(\Omega_{a,b}^{(13)})) = b(a + b - 4).$$

This conjecture is verified up to $a \leq 9$ and $b \leq 8$ by using the `OSCAR` code [Gei22], also displayed in Appendix B.2.

Remark 9.4.14. The data supporting Conjecture 9.4.13 displayed in Table 9.5 can be read as follows: The first line in each cell states the degree of the binodal variety $\deg(B_{\Omega_{a,b}^{(13)}})$. The second line in each cell shows how the path multiplicities partition the binodal degree. The order of the summands is as follows:

$$\mathrm{mult}(\Gamma_{1,4}(\Omega_{a,b}^{(13)})) + \mathrm{mult}(\Gamma_{1,3}(\Omega_{a,b}^{(13)})) + \mathrm{mult}(\Gamma_{1,2}(\Omega_{a,b}^{(13)})).$$

$b \backslash a$	3	4	5	6	7	8	9
1	x	7 2+3+2	8 2+4+2	18 4+10+4	20 4+12+4	33 6+21+6	36 6+24+6
2	7 2+1+4	x	18 4+6+8	x	33 6+15+12	x	52 8+28+16
3	x	18 4+2+12	20 4+4+12	x	36 6+12+18	52 8+20+24	x
4	x	x	33 6+3+24	x	52 8+12+32	x	75 10+25+40
5	x	x	x	52 8+4+40	56 8+8+40	75 10+15+50	80 10+20+50
6	x	x	x	x	75 10+5+60	x	x
7	x	x	x	x	x	102 12+6+84	108 12+12+84
8	x	x	x	x	x	x	133 14+7+112

Table 9.5: Verified path multiplicities and degree of binodal variety for polytope family number 13 as computed using [Gei22] in OSCAR. See Remark 9.4.14 for more details on the data.

9.4.4 Polytope family 14

$$\Omega_{a,b}^{(14)} = \begin{pmatrix} 0 & 0 & 0 & 0 & 1 & 1 \\ 0 & 1 & 1 & 2 & 0 & b \\ 0 & 0 & 1 & 0 & 0 & a \end{pmatrix}$$

$$gcd(a,b) = 1,\ 0 < b < a,\ a+b \geq 5$$
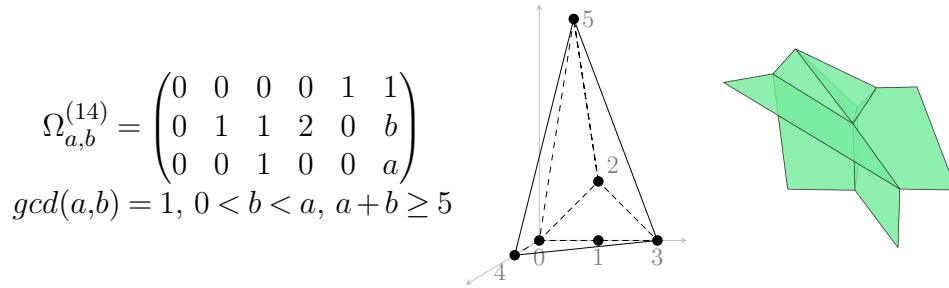
Figure 9.10: Polytope family 14

We investigate possible lattice paths for the polytope family number 14 and their multiplicities.

Lemma 9.4.15. *For all polytopes of family* 14 *with lattice points as in Figure 9.1, only lattice paths connected from* 0 *to* 5 *are possible.*

In the following, we use the notation $\cdot^\vee$ as introduced in Corollary 2.1.15 to denote the dual object under the duality connection between the Newton polytope and the tropical surface.

Proof. The proof runs along the same lines as for polytope family 8. Let $\Omega_{a,b}^{(14)}$ be a polytope of family 14. Without loss of generality we can assume that the surface S dual to the polytope has a unique vertex at $(0,0,0)$. The direction vector of the line L on which the points of the point condition lie is $(1,\eta,\eta^2)$ with $0 < \eta \ll 1$.

There can only exist disconnected lattice paths for $\Omega_{a,b}^{(14)}$ if the line L, on which the points from the point conditions are distributed, intersects with the tropical surface S more than 3 times; see Lemma 9.3.3. Label the lattice points of the polytope with ω_0, ω_1, ω_2, ω_3, ω_4 and ω_5 in the order as induced by $v = (1,\eta,\eta^2)$ (Definition 7.2.3). We know by Proposition 9.1.10 that in order to be dual to a binodal surface $\Omega_{a,b}^{(14)}$ has the trivial subdivision, so the lattice point ω_1 is never a vertex of the subdivision. Therefore, a tropical surface with support $\Omega_{a,b}^{(14)}$ divides $\mathbb{R}^3$ into only five 3-dimensional regions. For a path not connected from 0 to 5, the line L must pass through all five regions. We refer to the proof of Proposition 9.4.16 for the rays generating these regions.

Considering these we observe that if the line L passes through $\omega_0^\vee$, $\omega_2^\vee$ and $\omega_3^\vee$, the remaining ray of L is contained in the $\{z > 0, y > 0\}$ quadrant of $\mathbb{R}^3$.

However, for each polytope of family 14 we have

$$
\omega_4^\vee = \left\{ \mu_1 \begin{pmatrix} 0 \\ 0 \\ -1 \end{pmatrix} + \mu_2 \begin{pmatrix} 0 \\ -a \\ b \end{pmatrix} + \mu_3 \begin{pmatrix} 2a \\ a \\ -b \end{pmatrix} \mid \mu_i > 0 \forall i \in \{1,2,3\} \right\}.
$$

Assume μ_1, μ_2, $\mu_3 > 0$ determine a point in $\omega_4^\vee \cap \{z > 0, y > 0\}$. It follows:

$$
-a\mu_2 + a\mu_3 > 0,
$$
$$
-\mu_1 + b\mu_2 - b\mu_3 > 0.
$$

The first inequality implies $\mu_3 > \mu_2$, which in combination with the second inequality leads to $\mu_1 < 0$.

So $\omega_4^\vee \cap \{z > 0, y > 0\} = \emptyset$. Thus, L cannot pass through all five 3-dimensional regions $\mathbb{R}^3 \setminus S$. □

Proposition 9.4.16. *The lattice paths depicted in Figure 9.11 are the only possible lattice paths for the polytopes in family 14 with vertices as in Figure 9.10.*

Proof. The proof is analogous to the proof of Proposition 9.4.12. The paths depicted in Figure 9.11 are all the possible lattice paths that run along edges (Lemma 9.3.1), are connected from 0 to 5 and leave out ω_1 (Lemma 9.4.15). Analogous to the proofs of Propositions 9.4.3, 9.4.8 and 9.4.12, we prove that the paths are valid by setting up the linear equation systems and computing their solutions.

In the following let S denote the tropical surface dual to $\Omega_{a,b}^{(14)}$ passing through points **q** in Mikhalkin position. Let L denote the line on which the points $q_1 = (0,0,0)$, $q_2 = (1,\eta,\eta^2)$ and $q_3 = (\lambda,\lambda\eta,\lambda\eta^2)$ are distributed.

For polytope $\Omega_{a,b}^{(14)}$ we know that $\omega_0 = (0,0,0)$, $\omega_1 = (0,1,0)$, $\omega_2 = (0,1,1)$, $\omega_3 = (0,2,0)$, $\omega_4 = (1,0,0)$, $\omega_5 = (1,b,a)$.

The 3-dimensional regions of $\mathbb{R}^3 \setminus S$ with vertex of the surface at $(0,0,0)$ are given by the dual regions to the vertices (Remark 9.3.6):

$\omega_0^\vee$ is defined by $(-1,0,0),(0,0,-1),(0,-a,b),(b-a,-1,1)$;
$\omega_2^\vee$ is defined by $(-1,0,0),(b-a,-1,1),(b-a,1,1)$;
$\omega_3^\vee$ is defined by $(-1,0,0),(0,0,-1),(2a,a,-b),(b-a,1,1)$;
$\omega_4^\vee$ is defined by $(0,0,-1),(0,-a,b),(2a,a,-b)$;
$\omega_5^\vee$ is defined by $(b-a,-1,1),(2a,a,-b),(b-a,1,1),(0,-a,b)$.

Assume S passes through points in Mikhalkin position. We fix these points as $(0,0,0)$, $(1,\eta,\eta^2)$, $(\lambda,\lambda\eta,\lambda\eta^2)$, where $\lambda \gg 1 \gg \eta > 0$. Let L denote the line on which these points are distributed. For the above regions this means, that we have to add the vertex (x,y,z) of S to translate the cones to their correct position.

(a) $\Gamma_{1,4}(\Omega_{a,b}^{(14)})$ (b) $\Gamma_{1,2}(\Omega_{a,b}^{(14)})$
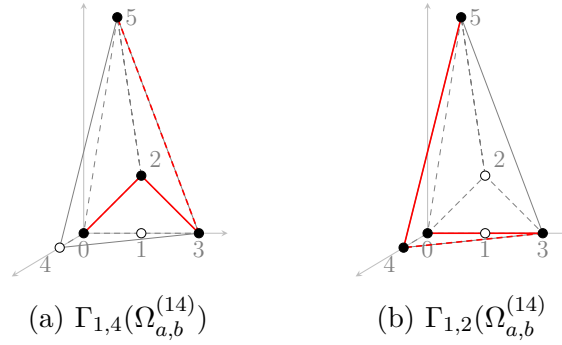
Figure 9.11: Valid lattice paths for polytopes of family 14

Now we check that the paths in Figure 9.9 are valid.

The path $\Gamma_{1,4}(\Omega_{a,b}^{(14)})$ passes through the 2-dimensional cells of S given by $(\overline{\omega_0\omega_2})^\vee$, $(\overline{\omega_2\omega_3})^\vee$ and $(\overline{\omega_3\omega_5})^\vee$. This gives us the following set of equations:

$$\begin{pmatrix} 0 \\ 0 \\ 0 \end{pmatrix} = \begin{pmatrix} x \\ y \\ z \end{pmatrix} + \alpha_1 \begin{pmatrix} -1 \\ 0 \\ 0 \end{pmatrix} + \alpha_2 \begin{pmatrix} b-a \\ -1 \\ 1 \end{pmatrix}, \ \alpha_1, \alpha_2 > 0,$$

$$\begin{pmatrix} 1 \\ \eta \\ \eta^2 \end{pmatrix} = \begin{pmatrix} x \\ y \\ z \end{pmatrix} + \beta_1 \begin{pmatrix} -1 \\ 0 \\ 0 \end{pmatrix} + \beta_2 \begin{pmatrix} b-a \\ 1 \\ 1 \end{pmatrix}, \ \beta_1, \beta_2 > 0,$$

$$\begin{pmatrix} \lambda \\ \lambda\eta \\ \lambda\eta^2 \end{pmatrix} = \begin{pmatrix} x \\ y \\ z \end{pmatrix} + \gamma_1 \begin{pmatrix} b-a \\ 1 \\ 1 \end{pmatrix} + \gamma_2 \begin{pmatrix} 2a \\ a \\ -b \end{pmatrix}, \ \gamma_1, \gamma_2 > 0.$$

This system has the solutions

$$x = \lambda + \frac{1}{a+b}((a-b)b\lambda + \frac{(a-b)^2}{2} - 2a(\lambda-1))\eta$$
$$+ \frac{1}{a+b}((a-b)a\lambda - \frac{(a-b)^2}{2} + 2a(\lambda-1))\eta^2,$$
$$y = \alpha_2 = \frac{\eta - \eta^2}{2} > 0,$$
$$z = \frac{-\eta + \eta^2}{2},$$
$$\alpha_1 = \lambda + \frac{1}{a+b}((a-b)b(\lambda-1) - 2a(\lambda-1))\eta$$
$$+ \frac{1}{a+b}((a-b)(a\lambda+b) + 2a(\lambda-1))\eta^2 > 0,$$

$$\beta_1 = \lambda - 1 + \frac{1}{a+b}((a-b)b(\lambda-1) - 2a(\lambda-1))\eta$$
$$+ \frac{1}{a+b}((a-b)a(\lambda-1) + 2a(\lambda-1))\eta^2 > 0,$$
$$\beta_2 = \frac{\eta + \eta^2}{2} > 0,$$
$$\gamma_1 = (\frac{b}{a+b}\lambda + \frac{a-b}{2(a+b)})\eta + (\frac{a}{a+b}\lambda + \frac{b-a}{2(a+b)})\eta^2 > 0,$$
$$\gamma_2 = \frac{1}{a+b}(\lambda-1)(\eta-\eta^2) > 0.$$

It follows that the path $\Gamma_{1,4}(\Omega_{a,b}^{(14)})$ is valid.

The path $\Gamma_{1,2}(\Omega_{a,b}^{(14)})$ passes through the 2-dimensional cells of S given by $(\overline{\omega_0\omega_3})^\vee$, $(\overline{\omega_3\omega_4})^\vee$ and $(\overline{\omega_4\omega_5})^\vee$. This gives us the following set of equations:

$$\begin{pmatrix} 0 \\ 0 \\ 0 \end{pmatrix} = \begin{pmatrix} x \\ y \\ z \end{pmatrix} + \alpha_1 \begin{pmatrix} -1 \\ 0 \\ 0 \end{pmatrix} + \alpha_2 \begin{pmatrix} 0 \\ 0 \\ -1 \end{pmatrix}, \ \alpha_1, \alpha_2 > 0,$$

$$\begin{pmatrix} 1 \\ \eta \\ \eta^2 \end{pmatrix} = \begin{pmatrix} x \\ y \\ z \end{pmatrix} + \beta_1 \begin{pmatrix} 0 \\ 0 \\ -1 \end{pmatrix} + \beta_2 \begin{pmatrix} 2a \\ a \\ -b \end{pmatrix}, \ \beta_1, \beta_2 > 0,$$

$$\begin{pmatrix} \lambda \\ \lambda\eta \\ \lambda\eta^2 \end{pmatrix} = \begin{pmatrix} x \\ y \\ z \end{pmatrix} + \gamma_1 \begin{pmatrix} 2a \\ a \\ -b \end{pmatrix} + \gamma_2 \begin{pmatrix} 0 \\ -a \\ b \end{pmatrix}, \ \gamma_1, \gamma_2 > 0.$$

This system has the solutions

$$x = \alpha_1 = 1 - 2\eta > 0,$$
$$y = 0,$$
$$z = \alpha_2 = \lambda\eta^2 + \frac{b}{a}\lambda\eta > 0,$$
$$\beta_1 = (\lambda-1)(\eta^2 + \frac{b}{a}\eta) > 0,$$
$$\beta_2 = \frac{\eta}{a} > 0,$$
$$\gamma_1 = \frac{1}{2a}(\lambda - 1 + 2\eta) > 0,$$
$$\gamma_2 = \frac{1}{2a}(\lambda-1) + \frac{1}{a}(1-\lambda)\eta > 0.$$

We can follow the positivity of the parameters by $\lambda \gg 1 \gg \eta > 0$ and $a > b > 0$. It

follows that the path $\Gamma_{1,2}(\Omega_{a,b}^{(14)})$ is valid. $\qquad\qquad\qquad\qquad\qquad\qquad$ □

$b \setminus a$	3	4	5	6	7	8	9
1	x	10	12	28	32	54	60
		2+8	2+10	4+24	2+28	6+48	6+54
2	8	x	24	x	48	x	80
	2+6		4+20		6+42		8+72
3	x	20	24	x	48	72	x
		4+16	4+20		6+42	8+64	
4	x	x	36	x	64	x	100
			6+30		8+56		10+90
5	x	x	x	56	64	90	100
				8+48	8+56	10+80	10+90
6	x	x	x	x	80	x	x
					10+70		
7	x	x	x	x	x	108	120
						12+96	12+108

Table 9.6: Verified path multiplicities and degree of binodal variety for polytope family number 14 as computed using [Gei22] in `OSCAR`. See Remark 9.4.18 on how to read the table.

Knowing all the valid lattice paths for binodal polytopes of family 14, we can compute their multiplicities, similarly as for the other polytope families. We use the `OSCAR` functions based on Algorithms 9 and 10 from Section 9.3.2. The functions are displayed in Appendix B.2 and are available on GitHub[2], see [Gei22].

Conjecture 9.4.17. *For polytopes $\Omega_{a,b}^{(14)}$ of family number 14 as in Figure 9.10 where $gcd(a,b) = 1$, $0 < b < a$ and $a+b \geq 5$, we have the following conjecture about the degree of the binodal variety and the path multiplicities.*

If a and b have different parities, we conjecture

$$deg(B_{\Omega_{a,b}^{(14)}}) = (a+1)(a+b-3),$$

$$mult(\Gamma_{1,4}(\Omega_{a,b}^{(14)})) = a+b-3,$$

$$mult(\Gamma_{1,2}(\Omega_{a,b}^{(14)})) = a(a+b-3).$$

---

[2]`https://github.com/AlheydisGeiger/Code-Binodal-Surfaces`

If a and b are both odd, we conjecture

$$deg(B_{\Omega_{a,b}^{(14)}}) = (a+1)(a+b-4),$$

$$mult(\Gamma_{1,4}(\Omega_{a,b}^{(14)})) = a+b-4,$$

$$mult(\Gamma_{1,2}(\Omega_{a,b}^{(14)})) = a(a+b-4).$$

This conjecture is verified up to $a \leq 9$ and $b \leq 7$ by using the `OSCAR` code [Gei22], as displayed in Appendix B.2; see Table 9.6.

Remark 9.4.18. The data supporting Conjecture 9.4.17 displayed in Table 9.6 can be read as follows: The first line in each cell states the degree of the binodal variety $deg(B_{\Omega_{a,b}^{(14)}})$. The second line in each cell shows how the path multiplicities partition the binodal degree. The order of the summands is as follows:

$$\text{mult}(\Gamma_{1,4}(\Omega_{a,b}^{(14)})) + \text{mult}(\Gamma_{1,2}(\Omega_{a,b}^{(14)})).$$

9.4.5 Polytope family 20

$$\Omega_a^{(20)} = \begin{pmatrix} 0 & 0 & 0 & 1 & 1 & 1 \\ 1 & 1 & 2 & 0 & 1 & 1 \\ 0 & 1 & 0 & a & 0 & 1 \end{pmatrix}$$
$$a > 3$$
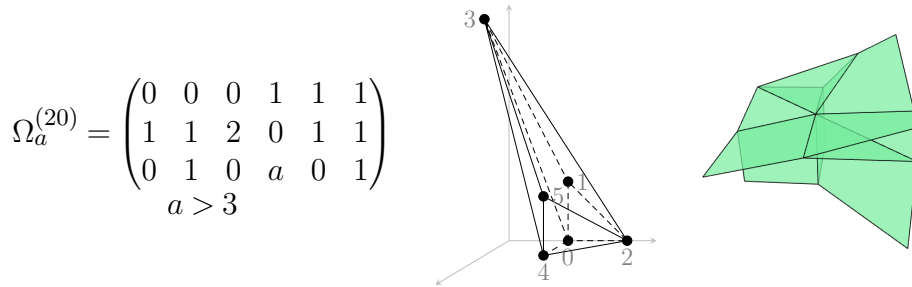
Figure 9.12: Polytope family 20

We investigate possible lattice paths for the polytope family number 20 and their multiplicities.

Lemma 9.4.19. *For a tropical surface S dual to a binodal polytope $\Omega_a^{(20)}$ of family* 20 *passing through points in Mikhalkin position, the line L on which the points are distributed can pass through at most* 5 *of the 3-dimensional regions of $\mathbb{R}^3 \setminus S$.*

This implies that lattice paths as in Lemma 9.3.3 (3) cannot appear.

Proof. We have to prove that the line L, on which the points from the point condition are distributed, cannot pass through all the regions of $\mathbb{R}^3 \setminus S$. We can

compute the regions of $\mathbb{R}^3 \setminus S$ as described in Remark 9.3.6. Let ω_i denote the lattice points of $\Omega_a^{(20)}$ and assume the vertex of S is in $(0,0,0)$.

A polytope of family 20 has the vertices $\omega_0 = (0,1,0)$, $\omega_1 = (0,1,1)$, $\omega_2 = (0,2,0)$, $\omega_3 = (1,0,a)$, $\omega_4 = (1,1,0)$, $\omega_5 = (1,1,1)$. We can compute the cones $\omega_1^\vee$ and $\omega_4^\vee$ using Remark 9.3.6. The generating rays are displayed in the proof of Proposition 9.4.20.

We observe that $\omega_1^\vee \subset \{z > 0\}$ and $\omega_4^\vee \subset \{z < 0\}$. Thus, it immediately follows that if our line L passes through $\omega_1^\vee$ it cannot pass through $\omega_4^\vee$ afterwards. $\qquad\square$

Next, we identify all valid lattice paths for binodal polytopes of family 20.

Proposition 9.4.20. *For the polytopes of family 20 with lattice points as in Figure 9.12, we can only have the lattice paths shown in Figure 9.13.*

(a) $\Gamma_{3,4}(\Omega_a^{(20)})$ (b) $\Gamma_{2,4}(\Omega_a^{(20)})$ (c) $\Gamma_{1,3}(\Omega_a^{(20)})$ (d) $\Gamma_{1,2}(\Omega_a^{(20)})$ (e) $\Gamma_{0,4}(\Omega_a^{(20)})$
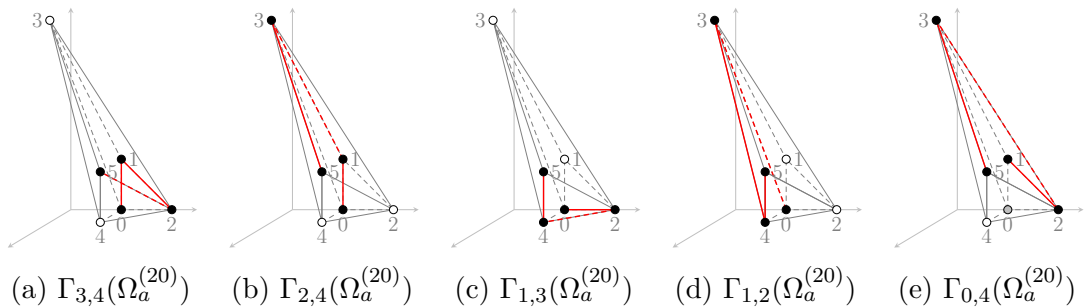
Figure 9.13: Valid lattice paths for polytopes of family number 20. The vertex ω_0 in the path $\Gamma_{0,4}(\Omega_a^{(20)})$ is colored in gray, since the line on which the points are distributed passes through its dual region.

Proof. Let S be a tropical surface dual to the trivial subdivision of a binodal polytope $\Omega_a^{(20)}$ of family number 20. We examine each possible lattice path through the vertices of the two polytopes and check whether it is possible for a line to pass through the corresponding regions and through points in Mikhalkin position. This is done by choosing general points $(0,0,0)$, $(1,\eta,\eta^2)$, $(\lambda, \lambda\eta, \lambda\eta^2)$, $0 < \eta \ll 1 \ll \lambda$ and letting (x,y,z) be the vertex of the tropical surface. This gives rise to 9 equations, one for each coordinate of each point, asserting that the point is contained in the claimed cell of the tropical surface. This system of equations has 6 variables corresponding to the coefficients on the rays and the 3 coordinate points x,y,z of the vertex of S. Solving these equations either results in a solution or a contradiction.

For polytopes $\Omega_a^{(20)}$ of family 20, we have the vertices $\omega_0 = (0,1,0)$, $\omega_1 = (0,1,1)$, $\omega_2 = (0,2,0)$, $\omega_3 = (1,0,a)$, $\omega_4 = (1,1,0)$, $\omega_5 = (1,1,1)$. The 3-dimensional regions defined by the tropical surface dual to this kind of polytope with vertex of the

surface at (0,0,0) are given by the dual regions to the vertices:

$\omega_0^\vee$ defined by $(-1,0,0), (0,0,-1), (-1,-1,0), (0,-a,-1)$;

$\omega_1^\vee$ defined by $(-1,0,0), (-1,-1,0), (-a,1,1)$;

$\omega_2^\vee$ defined by $(-1,0,0), (0,0,-1), (a-2,a-1,1), (-a,1,1), (1,1,0)$;

$\omega_3^\vee$ defined by $(1,0,0), (-1,-1,0), (0,-a,-1), (-a,1,1), (a-2,a-1,1)$;

$\omega_4^\vee$ defined by $(1,0,0), (0,0,-1), (0,-a,-1), (1,1,0)$;

$\omega_5^\vee$ defined by $(1,1,0), (1,0,0), (a-2,a-1,1)$.

We know from Lemma 9.4.19 that a lattice path for $\Omega_a^{(20)}$ has to come from a line L containing the points in Mikhalkin position that intersects at most 5 of the 3-dimensional regions of $\mathbb{R}^3 \setminus S$. Further, we recall from Lemma 9.3.1 that the lattice path has to run along edges of the polytope. By taking into account that we know from the proof of Lemma 9.4.19 that ω_1 and ω_4 are never part of a lattice path together, we therefore obtain the following list of possible lattice paths which we have to check for validity:

1. $\Gamma_{[1,2],4}(\Omega_a^{(20)})$,

2. $\Gamma_{[2,3],4}(\Omega_a^{(20)})$,

3. $\Gamma_{0,4}(\Omega_a^{(20)})$,

4. $\Gamma_{4,5}(\Omega_a^{(20)})$,

5. $\Gamma_{3,4}(\Omega_a^{(20)})$,

6. $\Gamma_{2,4}(\Omega_a^{(20)})$,

7. $\Gamma_{1,4}(\Omega_a^{(20)})$,

8. $\Gamma_{1,3}(\Omega_a^{(20)})$,

9. $\Gamma_{1,2}(\Omega_a^{(20)})$.

This list excludes the paths $\Gamma_{1,[3,4]}(\Omega_a^{(20)})$, $\Gamma_{1,5}(\Omega_a^{(20)})$ for the following reason: If L passes through $\omega_0^\vee, \omega_2^\vee$ and $\omega_3^\vee$, then we know that L passes in $\omega_3^\vee$ through $\omega_3^\vee \cap \{y > 0\} \subset \{z > 0\}$, since $\omega_2^\vee \subset \{y > 0\}$. Then the line L cannot pass through $\omega_4^\vee \subset \{z < 0\}$.

We first consider the paths (1)-(4) for which the line L intersects with the tropical surface more than 3 times, i.e., if the line passes through more than four of the

3-dimensional regions into which the tropical surface subdivides $\mathbb{R}^3$. Then, we go through the remaining connected paths one at a time.

Recall that $\lambda \gg 1 \gg \eta > 0$, that these two parameters have to be independent of each other, and that λ cannot have an upper bound while η is not allowed a lower bound in order to ensure the genericity of the point conditions.

1. For $\Gamma_{[1,2],4}(\Omega_a^{(20)})$ the points q_i are contained in the cells $(\overline{\omega_0 \omega_1})^\vee$, $(\overline{\omega_2 \omega_3})^\vee$, $(\overline{\omega_3 \omega_5})^\vee$ of the surface. We obtain the following system of 9 equations in 9 unknowns:

$$
\begin{pmatrix} 0 \\ 0 \\ 0 \end{pmatrix} = \begin{pmatrix} x \\ y \\ z \end{pmatrix} + \alpha_1 \begin{pmatrix} -1 \\ 0 \\ 0 \end{pmatrix} + \alpha_2 \begin{pmatrix} -1 \\ -1 \\ 0 \end{pmatrix}, \ \alpha_1, \alpha_2 > 0,
$$

$$
\begin{pmatrix} 1 \\ \eta \\ \eta^2 \end{pmatrix} = \begin{pmatrix} x \\ y \\ z \end{pmatrix} + \beta_1 \begin{pmatrix} 2-a \\ 1 \\ 1 \end{pmatrix} + \beta_2 \begin{pmatrix} a-2 \\ a-1 \\ 1 \end{pmatrix}, \ \beta_1, \beta_2 > 0,
$$

$$
\begin{pmatrix} \lambda \\ \lambda\eta \\ \lambda\eta^2 \end{pmatrix} = \begin{pmatrix} x \\ y \\ z \end{pmatrix} + \gamma_1 \begin{pmatrix} a-2 \\ a-1 \\ 1 \end{pmatrix} + \gamma_2 \begin{pmatrix} 1 \\ 0 \\ 0 \end{pmatrix}, \ \gamma_1, \gamma_2 > 0.
$$

We solve from the first condition that $z = 0$, and therefore $\gamma_1 = \lambda\eta^2$. Then, the third condition yields $y = \lambda\eta(1 - (a-1)\eta)$. Applying $z = 0$ to the second equation, we obtain $\beta_1 = \eta^2 - \beta_2$ and consequently $\beta_2 = \frac{\eta}{a-2}(1 - \lambda(1 - \eta(a-1)) - \eta)$. But β_2 has to be positive. This implies

$$
\lambda < \frac{1-\eta}{1-\eta(a-1)}.
$$

However, to ensure the genericity of our points, there cannot be an upper boundary to the value of λ.

2. For $\Gamma_{[2,3],4}(\Omega_a^{(20)})$ the points q_i are contained in the cells $(\overline{\omega_0 \omega_1})^\vee$, $(\overline{\omega_1 \omega_2})^\vee$, $(\overline{\omega_3 \omega_5})^\vee$ of the surface. We obtain the following system of equations:

$$
\begin{pmatrix} 0 \\ 0 \\ 0 \end{pmatrix} = \begin{pmatrix} x \\ y \\ z \end{pmatrix} + \alpha_1 \begin{pmatrix} -1 \\ 0 \\ 0 \end{pmatrix} + \alpha_2 \begin{pmatrix} -1 \\ -1 \\ 0 \end{pmatrix}, \ \alpha_1, \alpha_2 > 0,
$$

$$
\begin{pmatrix} 1 \\ \eta \\ \eta^2 \end{pmatrix} = \begin{pmatrix} x \\ y \\ z \end{pmatrix} + \beta_1 \begin{pmatrix} -1 \\ 0 \\ 0 \end{pmatrix} + \beta_2 \begin{pmatrix} 2-a \\ 1 \\ 1 \end{pmatrix}, \ \beta_1, \beta_2 > 0,
$$

$$\begin{pmatrix} \lambda \\ \lambda\eta \\ \lambda\eta^2 \end{pmatrix} = \begin{pmatrix} x \\ y \\ z \end{pmatrix} + \gamma_1 \begin{pmatrix} a-2 \\ a-1 \\ 1 \end{pmatrix} + \gamma_2 \begin{pmatrix} 1 \\ 0 \\ 0 \end{pmatrix}, \ \gamma_1, \gamma_2 > 0.$$

Similar as before, we conclude $z = 0$ and $\beta_2 = \eta^2$. It follows $y = \eta - \eta^2$. Applying the two solutions for y and z to the third equation of vectors, we obtain two solutions for γ_1, which coincide if $\lambda = \frac{1-\eta}{1+\eta(1-a)}$ where a is the parameter from the polytope, η is from the direction vector $(1,\eta,\eta^2)$, with $\eta < \frac{1}{a}$ and $\lambda > a+1$ is the distance for the third marked point. This implies a condition on the exact value of λ which contradicts the general choice of our points.

3. For $\Gamma_{0,4}(\Omega_a^{(20)})$ the points q_i are contained in the cells $(\overline{\omega_1\omega_2})^\vee$, $(\overline{\omega_2\omega_3})^\vee$, $(\overline{\omega_3\omega_5})^\vee$ of the surface. We obtain the following system of equations:

$$\begin{pmatrix} 0 \\ 0 \\ 0 \end{pmatrix} = \begin{pmatrix} x \\ y \\ z \end{pmatrix} + \alpha_1 \begin{pmatrix} -1 \\ 0 \\ 0 \end{pmatrix} + \alpha_2 \begin{pmatrix} 2-a \\ 1 \\ 1 \end{pmatrix}, \ \text{with } \alpha_1, \alpha_2 > 0,$$

$$\begin{pmatrix} 1 \\ \eta \\ \eta^2 \end{pmatrix} = \begin{pmatrix} x \\ y \\ z \end{pmatrix} + \beta_1 \begin{pmatrix} 2-a \\ 1 \\ 1 \end{pmatrix} + \beta_2 \begin{pmatrix} a-2 \\ a-1 \\ 1 \end{pmatrix}, \ \text{with } \beta_1, \beta_2 > 0,$$

$$\begin{pmatrix} \lambda \\ \lambda\eta \\ \lambda\eta^2 \end{pmatrix} = \begin{pmatrix} x \\ y \\ z \end{pmatrix} + \gamma_1 \begin{pmatrix} a-2 \\ a-1 \\ 1 \end{pmatrix} + \gamma_2 \begin{pmatrix} 1 \\ 0 \\ 0 \end{pmatrix}, \ \text{with } \gamma_1, \gamma_2 > 0.$$

This system has the solutions:

$$x = 1 + (\lambda - 2)(\eta - \eta^2) - (a-2)(\lambda - 1)\eta^2,$$

$$y = \lambda(\eta^2 - \frac{\eta - \eta^2}{a-2}),$$

$$z = \lambda(\eta^2 - \frac{\eta - \eta^2}{a-2}),$$

$$\alpha_1 = 1 - 2\eta + a\eta^2 > 0,$$

$$\alpha_2 = \lambda(\frac{\eta - \eta^2}{a-2} - \eta^2) > 0,$$

$$\beta_1 = (\lambda - 1)(\frac{\eta - \eta^2}{a-2} - \eta^2) > 0,$$

$$\beta_2 = \frac{\eta - \eta^2}{a-2} > 0,$$

$$\gamma_1 = \lambda \frac{\eta - \eta^2}{a - 2} > 0,$$

$$\gamma_2 = (\lambda - 1)(1 - 2\eta + a\eta^2) > 0.$$

To show that $\alpha_1 > 0$ we use $a - 2 \geq 1$ and $(a+2)\eta < 1$. Solving the equations does not produce contradictions, so the path $\Gamma_{0,4}(\Omega_a^{(20)})$ is valid.

4. For $\Gamma_{4,5}(\Omega_a^{(20)})$ the points q_i are contained in the cells $(\overline{\omega_0\omega_1})^\vee$, $(\overline{\omega_1\omega_2})^\vee$, $(\overline{\omega_2\omega_3})^\vee$ of the surface. We obtain the following system of equations:

$$\begin{pmatrix} 0 \\ 0 \\ 0 \end{pmatrix} = \begin{pmatrix} x \\ y \\ z \end{pmatrix} + \alpha_1 \begin{pmatrix} -1 \\ 0 \\ 0 \end{pmatrix} + \alpha_2 \begin{pmatrix} -1 \\ -1 \\ 0 \end{pmatrix}, \text{ with } \alpha_1, \alpha_2 > 0,$$

$$\begin{pmatrix} 1 \\ \eta \\ \eta^2 \end{pmatrix} = \begin{pmatrix} x \\ y \\ z \end{pmatrix} + \beta_1 \begin{pmatrix} -1 \\ 0 \\ 0 \end{pmatrix} + \beta_2 \begin{pmatrix} 2-a \\ 1 \\ 1 \end{pmatrix}, \text{ with } \beta_1, \beta_2 > 0,$$

$$\begin{pmatrix} \lambda \\ \lambda\eta \\ \lambda\eta^2 \end{pmatrix} = \begin{pmatrix} x \\ y \\ z \end{pmatrix} + \gamma_1 \begin{pmatrix} 2-a \\ 1 \\ 1 \end{pmatrix} + \gamma_2 \begin{pmatrix} a-2 \\ a-1 \\ 1 \end{pmatrix}, \text{ with } \gamma_1, \gamma_2 > 0.$$

This gives the following solution for γ_1:

$$\gamma_1 = \lambda\eta^2 - \frac{(\eta - \eta^2)(\lambda - 1)}{a - 2}.$$

Then, $\gamma_1 > 0$ if and only if $\lambda + 1 < a$. This contradicts the genericity conditions of our points.

5. For $\Gamma_{3,4}(\Omega_a^{(20)})$ the points q_i are contained in the cells $(\overline{\omega_0\omega_1})^\vee$, $(\overline{\omega_1\omega_2})^\vee$, $(\overline{\omega_2\omega_5})^\vee$ of the surface. We obtain the following system of equations:

$$\begin{pmatrix} 0 \\ 0 \\ 0 \end{pmatrix} = \begin{pmatrix} x \\ y \\ z \end{pmatrix} + \alpha_1 \begin{pmatrix} -1 \\ 0 \\ 0 \end{pmatrix} + \alpha_2 \begin{pmatrix} -1 \\ -1 \\ 0 \end{pmatrix}, \text{ with } \alpha_1, \alpha_2 > 0,$$

$$\begin{pmatrix} 1 \\ \eta \\ \eta^2 \end{pmatrix} = \begin{pmatrix} x \\ y \\ z \end{pmatrix} + \beta_1 \begin{pmatrix} -1 \\ 0 \\ 0 \end{pmatrix} + \beta_2 \begin{pmatrix} 2-a \\ 1 \\ 1 \end{pmatrix}, \text{ with } \beta_1, \beta_2 > 0,$$

$$\begin{pmatrix} \lambda \\ \lambda\eta \\ \lambda\eta^2 \end{pmatrix} = \begin{pmatrix} x \\ y \\ z \end{pmatrix} + \gamma_1 \begin{pmatrix} a-2 \\ a-1 \\ 1 \end{pmatrix} + \gamma_2 \begin{pmatrix} 1 \\ 1 \\ 0 \end{pmatrix}, \text{ with } \gamma_1, \gamma_2 > 0.$$

This system has the solutions:

$$
\begin{aligned}
x &= \lambda - (\lambda - 1)\eta + (\lambda - 1)\eta^2, \\
y &= \eta - \eta^2, \\
z &= 0, \\
\alpha_1 &= \lambda(1 - \eta + \eta^2) > 0, \\
\alpha_2 &= \eta - \eta^2 > 0, \\
\beta_1 &= (\lambda - 1)(1 - \eta + \eta^2) + (2 - a)\eta^2 > 0, \\
\beta_2 &= \eta^2 > 0, \\
\gamma_1 &= \lambda \eta^2 > 0, \\
\gamma_2 &= (\lambda - 1)\eta + \eta^2(1 - a\lambda + \lambda) > 0.
\end{aligned}
$$

As this solutions satisfy all the constrains, the path $\Gamma_{3,4}(\Omega_a^{(20)})$ is valid.

6. For $\Gamma_{2,4}(\Omega_a^{(20)})$ the points q_i are contained in the cells $(\overline{\omega_0\omega_1})^\vee$, $(\overline{\omega_1\omega_3})^\vee$, $(\overline{\omega_3\omega_5})^\vee$ of the surface. We obtain the following system of equations:

$$
\begin{pmatrix} 0 \\ 0 \\ 0 \end{pmatrix} = \begin{pmatrix} x \\ y \\ z \end{pmatrix} + \alpha_1 \begin{pmatrix} -1 \\ 0 \\ 0 \end{pmatrix} + \alpha_2 \begin{pmatrix} -1 \\ -1 \\ 0 \end{pmatrix}, \text{ with } \alpha_1, \alpha_2 > 0,
$$

$$
\begin{pmatrix} 1 \\ \eta \\ \eta^2 \end{pmatrix} = \begin{pmatrix} x \\ y \\ z \end{pmatrix} + \beta_1 \begin{pmatrix} -1 \\ -1 \\ 0 \end{pmatrix} + \beta_2 \begin{pmatrix} 2 - a \\ 1 \\ 1 \end{pmatrix}, \text{ with } \beta_1, \beta_2 > 0,
$$

$$
\begin{pmatrix} \lambda \\ \lambda\eta \\ \lambda\eta^2 \end{pmatrix} = \begin{pmatrix} x \\ y \\ z \end{pmatrix} + \gamma_1 \begin{pmatrix} a - 2 \\ a - 1 \\ 1 \end{pmatrix} + \gamma_2 \begin{pmatrix} 1 \\ 0 \\ 0 \end{pmatrix}, \text{ with } \gamma_1, \gamma_2 > 0.
$$

This system has the solutions

$$
\begin{aligned}
x &= 1 + (\lambda - 1)\eta + (\lambda - 1)(1 - a)\eta^2, \\
y &= \lambda\eta(1 - (a - 1)\eta), \\
z &= 0, \\
\alpha_1 &= 1 - \eta + \eta^2(a - 1) > 0, \\
\alpha_2 &= \lambda\eta(1 - (a - 1)\eta) > 0, \\
\beta_1 &= (\lambda - 1)\eta + (1 - a\lambda + \lambda)\eta^2 > 0, \\
\beta_2 &= \eta^2 > 0, \\
\gamma_1 &= \lambda\eta^2 > 0,
\end{aligned}
$$

$$\gamma_2 = (\lambda - 1)(1 - \eta + \eta^2) - (a - 2)\eta^2 > 0.$$

It follows that the path $\Gamma_{2,4}(\Omega_a^{(20)})$ is valid.

7. For $\Gamma_{1,4}(\Omega_a^{(20)})$ the points q_i are contained in the cells $(\overline{\omega_0 \omega_2})^\vee$, $(\overline{\omega_2 \omega_3})^\vee$, $(\overline{\omega_3 \omega_5})^\vee$ of the surface. We obtain the following system of equations:

$$\begin{pmatrix} 0 \\ 0 \\ 0 \end{pmatrix} = \begin{pmatrix} x \\ y \\ z \end{pmatrix} + \alpha_1 \begin{pmatrix} -1 \\ 0 \\ 0 \end{pmatrix} + \alpha_2 \begin{pmatrix} 0 \\ 0 \\ -1 \end{pmatrix}, \ \alpha_1, \alpha_2 > 0,$$

$$\begin{pmatrix} 1 \\ \eta \\ \eta^2 \end{pmatrix} = \begin{pmatrix} x \\ y \\ z \end{pmatrix} + \beta_1 \begin{pmatrix} 2-a \\ 1 \\ 1 \end{pmatrix} + \beta_2 \begin{pmatrix} a-2 \\ a-1 \\ 1 \end{pmatrix}, \ \beta_1, \beta_2 > 0,$$

$$\begin{pmatrix} \lambda \\ \lambda\eta \\ \lambda\eta^2 \end{pmatrix} = \begin{pmatrix} x \\ y \\ z \end{pmatrix} + \gamma_1 \begin{pmatrix} a-2 \\ a-1 \\ 1 \end{pmatrix} + \gamma_2 \begin{pmatrix} 1 \\ 0 \\ 0 \end{pmatrix}, \ \gamma_1, \gamma_2 > 0.$$

The first equation implies that $y = 0$ and $x, z > 0$. The last equation however implies that $z = \lambda\eta(\eta - \frac{1}{a-1})$. Since $\eta < \frac{1}{a} < \frac{1}{a-1}$, it follows that $z < 0$, a contradiction. So, this path is not valid.

8. For $\Gamma_{1,3}(\Omega_a^{(20)})$ the points q_i are contained in the cells $(\overline{\omega_0 \omega_2})^\vee$, $(\overline{\omega_2 \omega_4})^\vee$, $(\overline{\omega_4 \omega_5})^\vee$ of the surface. We obtain the following system of equations:

$$\begin{pmatrix} 0 \\ 0 \\ 0 \end{pmatrix} = \begin{pmatrix} x \\ y \\ z \end{pmatrix} + \alpha_1 \begin{pmatrix} -1 \\ 0 \\ 0 \end{pmatrix} + \alpha_2 \begin{pmatrix} 0 \\ 0 \\ -1 \end{pmatrix}, \ \text{with } \alpha_1, \alpha_2 > 0,$$

$$\begin{pmatrix} 1 \\ \eta \\ \eta^2 \end{pmatrix} = \begin{pmatrix} x \\ y \\ z \end{pmatrix} + \beta_1 \begin{pmatrix} 0 \\ 0 \\ -1 \end{pmatrix} + \beta_2 \begin{pmatrix} 1 \\ 1 \\ 0 \end{pmatrix}, \ \text{with } \beta_1, \beta_2 > 0,$$

$$\begin{pmatrix} \lambda \\ \lambda\eta \\ \lambda\eta^2 \end{pmatrix} = \begin{pmatrix} x \\ y \\ z \end{pmatrix} + \gamma_1 \begin{pmatrix} 1 \\ 1 \\ 0 \end{pmatrix} + \gamma_2 \begin{pmatrix} 1 \\ 0 \\ 0 \end{pmatrix}, \ \text{with } \gamma_1, \gamma_2 > 0.$$

We obtain the following solutions:

$$x = 1 - \eta,$$
$$y = 0,$$
$$z = \lambda\eta^2,$$
$$\alpha_1 = 1 - \eta > 0,$$

$$\alpha_2 = \lambda\eta^2 > 0,$$
$$\beta_1 = (\lambda - 1)\eta^2 > 0,$$
$$\beta_2 = \eta > 0,$$
$$\gamma_1 = \lambda\eta > 0,$$
$$\gamma_2 = (\lambda - 1)(1 - \eta) > 0.$$

There are no contradictions, so the path $\Gamma_{1,3}(\Omega_a^{(20)})$ is valid.

9. For $\Gamma_{1,2}(\Omega_a^{(20)})$ the points q_i are contained in the cells $(\overline{\omega_0\omega_3})^\vee$, $(\overline{\omega_3\omega_4})^\vee$, $(\overline{\omega_4\omega_5})^\vee$ of the surface. We obtain the following system of 9 equations in 9 unknowns:

$$\begin{pmatrix} 0 \\ 0 \\ 0 \end{pmatrix} = \begin{pmatrix} x \\ y \\ z \end{pmatrix} + \alpha_1 \begin{pmatrix} -1 \\ -1 \\ 0 \end{pmatrix} + \alpha_2 \begin{pmatrix} 0 \\ -a \\ -1 \end{pmatrix}, \ \alpha_1, \alpha_2 > 0,$$

$$\begin{pmatrix} 1 \\ \eta \\ \eta^2 \end{pmatrix} = \begin{pmatrix} x \\ y \\ z \end{pmatrix} + \beta_1 \begin{pmatrix} 1 \\ 0 \\ 0 \end{pmatrix} + \beta_2 \begin{pmatrix} 0 \\ -a \\ -1 \end{pmatrix}, \ \beta_1, \beta_2 > 0,$$

$$\begin{pmatrix} \lambda \\ \lambda\eta \\ \lambda\eta^2 \end{pmatrix} = \begin{pmatrix} x \\ y \\ z \end{pmatrix} + \gamma_1 \begin{pmatrix} 1 \\ 0 \\ 0 \end{pmatrix} + \gamma_2 \begin{pmatrix} 1 \\ 1 \\ 0 \end{pmatrix}, \ \gamma_1, \gamma_2 > 0.$$

This system has the following solutions:

$$x = \alpha_1 = \eta - a\eta^2 > 0,$$
$$y = \eta + a(\lambda - 1)\eta^2,$$
$$z = \alpha_2 = \lambda\eta^2 > 0,$$
$$\alpha_2 = \lambda\eta^2 > 0,$$
$$\beta_1 = 1 - \eta + a\eta^2 > 0,$$
$$\beta_2 = (\lambda - 1)\eta^2 > 0,$$
$$\gamma_1 = \lambda(1 - \eta + a\eta^2) > 0,$$
$$\gamma_2 = (\lambda - 1)(\eta - a\eta^2) > 0.$$

As there are no contradictions against positivity of the ray parameters or genericity of the points, the path $\Gamma_{1,2}(\Omega_a^{(20)})$ is valid.

$\square$

Now that we know all valid lattice paths for a polytope $\Omega_a^{(20)}$, we can determine

their multiplicities using the `OSCAR` functions [Gei22]. The computed values are arranged in Table 9.7

lattice path	$a = 4$	$a = 5$	$a = 6$	$a = 7$
$\Gamma_{3,4}(\Omega_a^{(20)})$	1	2	3	4
$\Gamma_{2,4}(\Omega_a^{(20)})$	1	2	3	4
$\Gamma_{1,3}(\Omega_a^{(20)})$	1	2	3	4
$\Gamma_{1,2}(\Omega_a^{(20)})$	1	2	3	4
$\Gamma_{0,4}(\Omega_a^{(20)})$	2	6	12	20
$\deg(B_{(\Omega_a^{(20)})})$	6	14	24	36

Table 9.7: Verified path multiplicities and degree of binodal variety for polytope family number 20 as computed using `OSCAR`.

Conjecture 9.4.21. *For binodal polytopes $\Omega_a^{(20)}$ of family number* 20 *as in Figure 9.12 where $a \geq 4$, we have the following conjecture about the degree of the binodal variety and the path multiplicities.*

$$\deg(B_{\Omega_a^{(20)}}) = (a+2)(a-3),$$
$$mult(\Gamma_{3,4}(\Omega_a^{(20)})) = a - 3,$$
$$mult(\Gamma_{2,4}(\Omega_a^{(20)})) = a - 3,$$
$$mult(\Gamma_{1,3}(\Omega_a^{(20)})) = a - 3,$$
$$mult(\Gamma_{1,2}(\Omega_a^{(20)})) = a - 3,$$
$$mult(\Gamma_{0,4}(\Omega_a^{(20)})) = (a-2)(a-3).$$

This conjecture is verified up to $a \leq 7$.

9.4.6 Polytope family 21

We investigate possible lattice paths for the polytope family number 21 and their multiplicities.

Lemma 9.4.22. *For a tropical surface S dual to a binodal polytope $\Omega_{a,b,c,d}^{(21)}$ of family* 21 *passing through points in Mikhalkin position, the line L on which the points are distributed can pass through at most five of the 3-dimensional regions of $\mathbb{R}^3 \setminus S$.*

This implies that lattice paths as in Lemma 9.3.3 (3) cannot appear.

$$\Omega_{a,b}^{(21)} = \begin{pmatrix} 0 & 0 & 0 & 1 & 1 & 1 \\ 0 & 0 & 1 & 0 & a & c \\ 0 & 1 & 0 & 0 & b & d \end{pmatrix}$$
$$ad - bc = 1,\ a,b,c,d > 0,$$
$$c + d > a + b,\ c > a$$
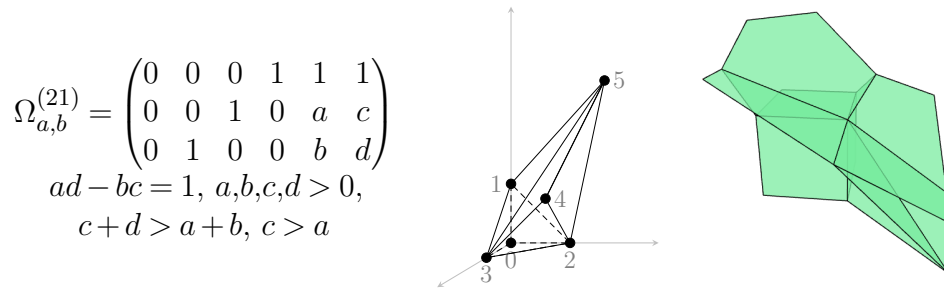
Figure 9.14: Polytope family 21

Proof. The proof is similar to the proof of Lemma 9.4.19.

We have to show that the line L, on which the points from the point condition are distributed, cannot pass through all the regions of $\mathbb{R}^3 \setminus S$. For this we compute the regions of $\mathbb{R}^3 \setminus S$ as described in Remark 9.3.6. Let ω_i denote the lattice points of $\Omega_{a,b,c,d}^{(21)}$ and assume the vertex of S is in $(0,0,0)$.

We have the vertices $\omega_0 = (0,0,0)$, $\omega_1 = (0,0,1)$, $\omega_2 = (0,1,0)$, $\omega_3 = (1,0,0)$, $\omega_4 = (1,a,b)$, $\omega_5 = (1,c,d)$, where $ad - bc = 1$, $c + d > a + b$, $c > a$ and a, b, c, $d > 0$.

We can compute the cones $\omega_1^\vee$ and $\omega_4^\vee$ using Remark 9.3.6. The generating rays are displayed in the proof of Proposition 9.4.23.

We observe that $\omega_1^\vee \subset \{z > 0\}$ and $\omega_4^\vee \subset \{z < 0\}$. Thus, it immediately follows that if our line L passes through $\omega_1^\vee$ it cannot pass through $\omega_4^\vee$ afterwards. Therefore, the claim holds. $\qquad\square$

Proposition 9.4.23. *For the polytopes of family* 21 *with lattice points as in Figure 9.14 we can only have the lattice paths shown in Figure 9.15.*

(a) $\Gamma_{3,4}(\Omega_{a,b,c,d}^{(21)})$ (b) $\Gamma_{2,4}(\Omega_{a,b,c,d}^{(21)})$ (c) $\Gamma_{0,1}(\Omega_{a,b,c,d}^{(21)})$ (d) $\Gamma_{1,5}(\Omega_{a,b,c,d}^{(21)})$ (e) $\Gamma_{1,[3,4]}(\Omega_{a,b,c,d}^{(21)})$
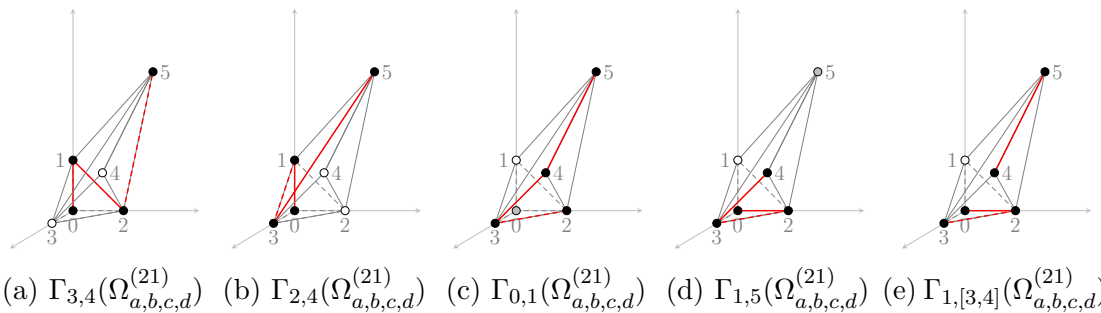
Figure 9.15: Valid lattice paths for polytopes of family 21. The vertices ω_0 in the path $\Gamma_{0,1}(\Omega_{a,b,c,d}^{(21)})$ and ω_5 in the path $\Gamma_{1,5}(\Omega_{a,b,c,d}^{(21)})$ are colored in gray, since the line on which the points are distributed passes through their dual region.

Proof. This proof works the same way as the proof of Proposition 9.4.20.

Let S denote the tropical surface dual to a polytope of family 21. We start by making a list of all possible lattice paths and check whether it is possible for a line to pass through the corresponding regions and through points in Mikhalkin position.

For this we choose general points $q_1 = (0,0,0)$, $q_2 = (1,\eta,\eta^2)$, $q_3 = (\lambda,\lambda\eta,\lambda\eta^2)$, with $0 < \eta \ll 1 \ll \lambda$ and let (x,y,z) be the vertex of the tropical surface S. For each lattice path this gives rise to 9 equations, one for each coordinate of each point ensuring that the point is contained in the claimed cell of the tropical surface. We have 6 variables corresponding to the coefficients on the rays and the 3 variables x, y, z of the vertex of S. Solving these equations either results in a solution or a contradiction.

Recall, that we use the notation $\cdot^{\vee}$ to indicate dual objects under the duality between the subdivision of the Newton polytope (which in our case is trivial) and the tropical surface S and the 3-dimensional regions of $\mathbb{R}^3 \setminus S$. In particular, for a vertex V of the polytope $V^{\vee}$ denotes the 3-dimensional region of $\mathbb{R}^3 \setminus S$ dual to V.

Polytopes of family 21 have the vertices $\omega_0 = (0,0,0)$, $\omega_1 = (0,0,1)$, $\omega_2 = (0,1,0)$, $\omega_3 = (1,0,0)$, $\omega_4 = (1,a,b)$, $\omega_5 = (1,c,d)$, where $ad - bc = 1$, $c + d > a + b$, $c > a$ and $a, b, c, d > 0$. Thus, we obtain the following regions of $\mathbb{R}^3 \setminus S$:

$\omega_0^{\vee}$ is defined by $(-1,0,0),(0,-1,0),(0,0,-1)$;

$\omega_1^{\vee}$ is defined by $(-1,0,0),(0,-1,0),(1-(d+c),1,1),(c,-d,c)$;

$\omega_2^{\vee}$ is defined by $(-1,0,0),(0,0,-1),(d-b-1,d-b,a-c),(1-(d+c),1,1),(b,b,-a)$;

$\omega_3^{\vee}$ is defined by $(0,-1,0),(0,0,-1),(1,0,0),(b,b,-a),(c,-d,c)$;

$\omega_4^{\vee}$ is defined by $(1,0,0),(b,b,-a),(d-b-1,d-b,a-c)$;

$\omega_5^{\vee}$ is defined by $(c,-d,c),(1-(d+c),1,1),(1,0,0),(d-b-1,d-b,a-c)$.

We recall from Lemma 9.3.1 that the lattice path has to run along edges of the polytope. Moreover, we know from Lemma 9.4.22 that a lattice path for $\Omega_{a,b,c,d}^{(21)}$ has to come from a line L containing the points in Mikhalkin position that intersects at most 5 of the 3-dimensional regions of $\mathbb{R}^3 \setminus S$.

We know from the proof of Lemma 9.4.22 that ω_1 and ω_4 are never part of a lattice path together. Further, as $\omega_1^{\vee} \subset \{z > 0\}$, $\omega_2^{\vee} \subset \{y > 0\}$, and $\omega_3^{\vee} \cap \{z > 0, y > 0\} = \emptyset$, it is not possible for L to pass through $\omega_1^{\vee}$, $\omega_2^{\vee}$ and $\omega_3^{\vee}$. It follows that if a lattice path is not connected from 0 to 5 (i.e., L intersects 5 of the 3-dimensional regions of $\mathbb{R}^3 \setminus S$), it has to contain ω_4 and has to skip ω_1.

We therefore obtain the following list of possible lattice paths which we have to check for validity:

1. $\Gamma_{1,[2,3]}(\Omega_{a,b,c,d}^{(21)})$,

2. $\Gamma_{1,[3,4]}(\Omega_{a,b,c,d}^{(21)})$,

3. $\Gamma_{0,1}(\Omega_{a,b,c,d}^{(21)})$,

4. $\Gamma_{1,5}(\Omega_{a,b,c,d}^{(21)})$,

5. $\Gamma_{3,4}(\Omega_{a,b,c,d}^{(21)})$,

6. $\Gamma_{2,4}(\Omega_{a,b,c,d}^{(21)})$,

7. $\Gamma_{1,3}(\Omega_{a,b,c,d}^{(21)})$,

8. $\Gamma_{1,2}(\Omega_{a,b,c,d}^{(21)})$.

This list excludes the path $\Gamma_{1,4}(\Omega_{a,b,c,d}^{(21)})$ for the following reason: Since $\omega_0^\vee \subset \{x < 0, y < 0, z < 0\}$, $\omega_2^\vee \subset \{y > 0\}$ and $\omega_3^\vee \subset \{x > 0\}$, it follows that L passes through $\omega_3^\vee \cap \{x > 0, y > 0\}$. To pass from $\omega_3^\vee$ directly to $\omega_5^\vee$, L has to pass through $\mathbb{R}_{>0} \cdot (1,0,0) + \mathbb{R}_{>0} \cdot (c, -d,c) \subset \{y < 0\}$. This is impossible since the direction of L is $(1,\eta,\eta^2)$ with $1 \gg \eta > 0$.

As in the proof of Proposition 9.4.20 we go through the list of possible lattice paths, set up the system of equations from the point conditions for each and check if it is solvable under the given constraints.

1. For $\Gamma_{1,[2,3]}(\Omega_{a,b,c,d}^{(21)})$ the points q_i are contained in the 2-cells $(\overline{\omega_0 \omega_2})^\vee$, $(\overline{\omega_3 \omega_4})^\vee$ and $(\overline{\omega_4 \omega_5})^\vee$. We obtain the following system of equations:

$$\begin{pmatrix} 0 \\ 0 \\ 0 \end{pmatrix} = \begin{pmatrix} x \\ y \\ z \end{pmatrix} + \alpha_1 \begin{pmatrix} -1 \\ 0 \\ 0 \end{pmatrix} + \alpha_2 \begin{pmatrix} 0 \\ 0 \\ -1 \end{pmatrix} \text{ with } \alpha_1, \alpha_2 > 0,$$

$$\begin{pmatrix} 1 \\ \eta \\ \eta^2 \end{pmatrix} = \begin{pmatrix} x \\ y \\ z \end{pmatrix} + \beta_1 \begin{pmatrix} 1 \\ 0 \\ 0 \end{pmatrix} + \beta_2 \begin{pmatrix} b \\ b \\ -a \end{pmatrix} \text{ with } \beta_1, \beta_2 > 0,$$

$$\begin{pmatrix} \lambda \\ \lambda\eta \\ \lambda\eta^2 \end{pmatrix} = \begin{pmatrix} x \\ y \\ z \end{pmatrix} + \gamma_1 \begin{pmatrix} 1 \\ 0 \\ 0 \end{pmatrix} + \gamma_2 \begin{pmatrix} d - b - 1 \\ d - b \\ a - c \end{pmatrix} \text{ with } \gamma_1, \gamma_2 > 0.$$

The first two conditions lead to $y = 0$ and $z = \eta^2 + \frac{a \cdot \eta}{b}$. Inserting this into the last condition we can solve for $\gamma_2 = \frac{\lambda\eta}{d-b}$ and obtain another equation for z:

$$z = \lambda\left(\eta^2 + \frac{c - a}{d - b}\eta\right) \implies \eta^2 + \frac{a \cdot \eta}{b} = \lambda\left(\eta^2 + \frac{c - a}{d - b}\eta\right)$$

$$\Rightarrow 0 = (\lambda - 1)\eta^2 + (\lambda\frac{c-a}{d-b} - \frac{a}{b})\eta.$$

Since for the parameter condition $ad - bc = 1$ and $d + c > a + b$, it follows that $d - b > 0$ so we do not divide by zero. For the genericity of our point conditions, it is important that η and λ can be chosen independently of each other. This is not satisfied by the above equation for all a, b, c, d. Thus, this path is not valid for any polytope in family 21.

2. For $\Gamma_{1,[3,4]}(\Omega_{a,b,c,d}^{(21)})$ the points q_i are contained in the 2-cells $(\overline{\omega_0\omega_2})^\vee$, $(\overline{\omega_2\omega_3})^\vee$ and $(\overline{\omega_4\omega_5})^\vee$. We obtain the following system of equations:

$$\begin{pmatrix} 0 \\ 0 \\ 0 \end{pmatrix} = \begin{pmatrix} x \\ y \\ z \end{pmatrix} + \alpha_1 \begin{pmatrix} -1 \\ 0 \\ 0 \end{pmatrix} + \alpha_2 \begin{pmatrix} 0 \\ 0 \\ -1 \end{pmatrix} \quad \text{with } \alpha_1, \alpha_2 > 0,$$

$$\begin{pmatrix} 1 \\ \eta \\ \eta^2 \end{pmatrix} = \begin{pmatrix} x \\ y \\ z \end{pmatrix} + \beta_1 \begin{pmatrix} 0 \\ 0 \\ -1 \end{pmatrix} + \beta_2 \begin{pmatrix} b \\ b \\ -a \end{pmatrix} \quad \text{with } \beta_1, \beta_2 > 0,$$

$$\begin{pmatrix} \lambda \\ \lambda\eta \\ \lambda\eta^2 \end{pmatrix} = \begin{pmatrix} x \\ y \\ z \end{pmatrix} + \gamma_1 \begin{pmatrix} 1 \\ 0 \\ 0 \end{pmatrix} + \gamma_2 \begin{pmatrix} d-b-1 \\ d-b \\ a-c \end{pmatrix} \quad \text{with } \gamma_1, \gamma_2 > 0.$$

We can compute the following solutions:

$$x = \alpha_1 = 1 - \eta > 0,$$
$$y = 0,$$
$$z = \alpha_2 = \lambda(\frac{c-a}{d-b}\eta + \eta^2) > 0,$$
$$\beta_1 = \lambda(\frac{c-a}{d-b}\eta + \eta^2) - \eta^2 - \frac{a}{b}\eta > 0,$$
$$\beta_2 = \frac{1}{b}\eta > 0,$$
$$\gamma_1 = \lambda - 1 + \eta + (-1 + \frac{1}{d-b})\lambda\eta > 0,$$
$$\gamma_2 = \frac{1}{d-b}\lambda\eta > 0.$$

We can see $\beta_1 > 0$ since $c > a$, $d > b$, $\lambda \gg 1$ so $b(\lambda - 1)(c - a) > 1$. Solving for all variables does not lead to a contradiction, so the path is valid.

3. For $\Gamma_{0,1}(\Omega_{a,b,c,d}^{(21)})$ the points q_i are contained in the 2-cells $(\overline{\omega_2\omega_3})^\vee$, $(\overline{\omega_3\omega_4})^\vee$

and $(\overline{\omega_4\omega_5})^\vee$. We obtain the following system of equations:

$$\begin{pmatrix} 0 \\ 0 \\ 0 \end{pmatrix} = \begin{pmatrix} x \\ y \\ z \end{pmatrix} + \alpha_1 \begin{pmatrix} 0 \\ 0 \\ -1 \end{pmatrix} + \alpha_2 \begin{pmatrix} b \\ b \\ -a \end{pmatrix} \quad \text{with } \alpha_1,\alpha_2 > 0,$$

$$\begin{pmatrix} 1 \\ \eta \\ \eta^2 \end{pmatrix} = \begin{pmatrix} x \\ y \\ z \end{pmatrix} + \beta_1 \begin{pmatrix} b \\ b \\ -a \end{pmatrix} + \beta_2 \begin{pmatrix} 1 \\ 0 \\ 0 \end{pmatrix} \quad \text{with } \beta_1,\beta_2 > 0,$$

$$\begin{pmatrix} \lambda \\ \lambda\eta \\ \lambda\eta^2 \end{pmatrix} = \begin{pmatrix} x \\ y \\ z \end{pmatrix} + \gamma_1 \begin{pmatrix} 1 \\ 0 \\ 0 \end{pmatrix} + \gamma_2 \begin{pmatrix} d-b-1 \\ d-b \\ a-c \end{pmatrix} \quad \text{with } \gamma_1,\gamma_2 > 0.$$

Using $ad - bc * 1$, we can solve this system of equations as follows:

$$x = (1 - b(c-a)(\lambda-1))\eta + (1-\lambda)b(d-b)\eta^2,$$
$$y = (1 - b(c-a)(\lambda-1))\eta + (1-\lambda)b(d-b)\eta^2,$$
$$z = a(c-a)(\lambda-1)\eta + (a(d-b)\lambda - b(c-a))\eta^2,$$
$$\alpha_1 = \frac{a}{b}\eta + \eta^2 > 0,$$
$$\alpha_2 = ((c-a)(\lambda-1) - \frac{1}{b})\eta + (\lambda-1)(d-b)\eta^2 > 0,$$
$$\beta_1 = (\lambda-1)((c-a)\eta + (d-b)\eta^2) > 0,$$
$$\beta_2 = 1 - \eta > 0,$$
$$\gamma_1 = \lambda + (\lambda(a-1) - a)\eta + (\lambda-1)b\eta^2 > 0,$$
$$\gamma_2 = (\lambda-1)(a\eta + b\eta^2) > 0.$$

We see that $\alpha_2 > 0$ because $\lambda \gg 1 \gg \eta > 0$, so $\lambda - 1 > \frac{1}{b\eta(d-b)}$. When fixing the point conditions we choose η first. After fixing η we are not allowed to have upper bounds for λ. This lower bound for λ in dependence of η does not contradict our genericity conditions. So the path $\Gamma_{0,1}(\Omega^{(21)}_{a,b,c,d})$ is valid.

4. For $\Gamma_{1,5}(\Omega^{(21)}_{a,b,c,d})$ the points q_i are contained in the 2-cells $(\overline{\omega_0\omega_2})^\vee$, $(\overline{\omega_2\omega_3})^\vee$ and $(\overline{\omega_3\omega_4})^\vee$. We obtain the following system of equations:

$$\begin{pmatrix} 0 \\ 0 \\ 0 \end{pmatrix} = \begin{pmatrix} x \\ y \\ z \end{pmatrix} + \alpha_1 \begin{pmatrix} -1 \\ 0 \\ 0 \end{pmatrix} + \alpha_2 \begin{pmatrix} 0 \\ 0 \\ -1 \end{pmatrix} \quad \text{with } \alpha_1,\alpha_2 > 0,$$

$$
\begin{pmatrix} 1 \\ \eta \\ \eta^2 \end{pmatrix} = \begin{pmatrix} x \\ y \\ z \end{pmatrix} + \beta_1 \begin{pmatrix} 0 \\ 0 \\ -1 \end{pmatrix} + \beta_2 \begin{pmatrix} b \\ b \\ -a \end{pmatrix} \quad \text{with } \beta_1, \beta_2 > 0,
$$

$$
\begin{pmatrix} \lambda \\ \lambda\eta \\ \lambda\eta^2 \end{pmatrix} = \begin{pmatrix} x \\ y \\ z \end{pmatrix} + \gamma_1 \begin{pmatrix} 1 \\ 0 \\ 0 \end{pmatrix} + \gamma_2 \begin{pmatrix} b \\ b \\ -a \end{pmatrix} \quad \text{with } \gamma_1, \gamma_2 > 0.
$$

We obtain the following solutions:

$$
\begin{aligned}
x &= 1 - \eta, \\
y &= 0, \\
z &= \lambda(\frac{a}{b}\eta + \eta^2), \\
\alpha_1 &= 1 - \eta > 0, \\
\alpha_2 &= \lambda(\frac{a}{b}\eta + \eta^2) > 0, \\
\beta_1 &= (\lambda - 1)(\eta^2 + \frac{a}{b}\eta) > 0, \\
\beta_2 &= \frac{1}{b}\eta > 0, \\
\gamma_1 &= (\lambda - 1)(1 - \eta) > 0, \\
\gamma_2 &= \frac{1}{b}\lambda\eta > 0.
\end{aligned}
$$

It follows that the path $\Gamma_{1,5}(\Omega^{(21)}_{a,b,c,d})$ is valid.

5. For $\Gamma_{3,4}(\Omega^{(21)}_{a,b,c,d})$ the points q_i are contained in the 2-cells $(\overline{\omega_0\omega_1})^\vee$, $(\overline{\omega_1\omega_2})^\vee$ and $(\overline{\omega_2\omega_5})^\vee$. We obtain the following system of equations:

$$
\begin{pmatrix} 0 \\ 0 \\ 0 \end{pmatrix} = \begin{pmatrix} x \\ y \\ z \end{pmatrix} + \alpha_1 \begin{pmatrix} -1 \\ 0 \\ 0 \end{pmatrix} + \alpha_2 \begin{pmatrix} 0 \\ -1 \\ 0 \end{pmatrix} \quad \text{with } \alpha_1, \alpha_2 > 0,
$$

$$
\begin{pmatrix} 1 \\ \eta \\ \eta^2 \end{pmatrix} = \begin{pmatrix} x \\ y \\ z \end{pmatrix} + \beta_1 \begin{pmatrix} -1 \\ 0 \\ 0 \end{pmatrix} + \beta_2 \begin{pmatrix} 1 - (d+c) \\ 1 \\ 1 \end{pmatrix} \quad \text{with } \beta_1, \beta_2 > 0,
$$

$$
\begin{pmatrix} \lambda \\ \lambda\eta \\ \lambda\eta^2 \end{pmatrix} = \begin{pmatrix} x \\ y \\ z \end{pmatrix} + \gamma_1 \begin{pmatrix} d - b - 1 \\ d - b \\ a - c \end{pmatrix} + \gamma_2 \begin{pmatrix} 1 - (d+c) \\ 1 \\ 1 \end{pmatrix} \quad \text{with } \gamma_1, \gamma_2 > 0.
$$

This system of equation is solvable as follows:

$$
\begin{aligned}
x &= \alpha_1 = \lambda - \gamma_1(d-b-1) + \gamma_2(d+c-1) > 0, \\
y &= \alpha_2 = \eta - \eta^2 > 0, \\
z &= 0, \\
\beta_1 &= x - 1 + \eta^2(1 - (d+c)) > 0, \\
\beta_2 &= \eta^2 > 0, \\
\gamma_1 &= \frac{(\lambda - 1)(\eta - \eta^2)}{d + c - (b + a)} > 0, \\
\gamma_2 &= \frac{(d-b)\lambda\eta^2 + (c-a)((\lambda-1)\eta + \eta^2)}{d + c - (b + a)} > 0.
\end{aligned}
$$

Since $(d+c) - (a+b) > 0$, we do not divide by zero and the denominator is positive. To see that $\alpha_1 > 0$, we observe that $\frac{d-b-1}{d+c-(b+a)} < 1$ so

$$
\lambda - \gamma_1(d-b-1) > 0.
$$

For $\beta_1 > 0$, we note

$$
\begin{aligned}
\beta_1 &= x - 1 + \eta^2(1 - (d+c)) \\
&= \lambda - 1 - \gamma_1(d-b-1) + (\gamma_2 - \eta^2)(d+c-1).
\end{aligned}
$$

With the same argument as $\alpha_1 > 0$, we conclude $\lambda - 1 - \gamma_1(d-b-1) > 0$. Moreover,

$$
\gamma_2 - \eta^2 = \frac{(\lambda-1)(d-b)\eta^2 + (c-a)(\lambda-1)\eta}{d + c - (b + a)} > 0.
$$

Thus, all parameters are positive as required and there are no dependencies for λ and η. Therefore, the path $\Gamma_{3,4}(\Omega^{(21)}_{a,b,c,d})$ is valid.

6. For $\Gamma_{2,4}(\Omega^{(21)}_{a,b,c,d})$ the points q_i are contained in the 2-cells $(\overline{\omega_0\omega_1})^\vee$, $(\overline{\omega_1\omega_3})^\vee$ and $(\overline{\omega_3\omega_5})^\vee$. We obtain the following system of equations:

$$
\begin{pmatrix} 0 \\ 0 \\ 0 \end{pmatrix} = \begin{pmatrix} x \\ y \\ z \end{pmatrix} + \alpha_1 \begin{pmatrix} -1 \\ 0 \\ 0 \end{pmatrix} + \alpha_2 \begin{pmatrix} 0 \\ -1 \\ 0 \end{pmatrix} \quad \text{with } \alpha_1, \alpha_2 > 0,
$$

$$
\begin{pmatrix} 1 \\ \eta \\ \eta^2 \end{pmatrix} = \begin{pmatrix} x \\ y \\ z \end{pmatrix} + \beta_1 \begin{pmatrix} 0 \\ -1 \\ 0 \end{pmatrix} + \beta_2 \begin{pmatrix} c \\ -d \\ c \end{pmatrix} \quad \text{with } \beta_1, \beta_2 > 0,
$$

$$\begin{pmatrix} \lambda \\ \lambda\eta \\ \lambda\eta^2 \end{pmatrix} = \begin{pmatrix} x \\ y \\ z \end{pmatrix} + \gamma_1 \begin{pmatrix} c \\ -d \\ c \end{pmatrix} + \gamma_2 \begin{pmatrix} 1 \\ 0 \\ 0 \end{pmatrix} \quad \text{with } \gamma_1, \gamma_2 > 0.$$

This system of equation is solvable as follows:

$$x = 1 - \eta^2,$$
$$y = \lambda(\eta + \frac{d}{c}\eta^2),$$
$$z = 0,$$
$$\alpha_1 = 1 - \eta^2 > 0,$$
$$\alpha_2 = \lambda(\eta + \frac{d}{c}\eta^2) > 0,$$
$$\beta_1 = (\lambda - 1)(\eta + \frac{d}{c}\eta^2) > 0,$$
$$\beta_2 = \frac{\eta^2}{c} > 0,$$
$$\gamma_1 = \frac{\lambda}{c}\eta^2 > 0,$$
$$\gamma_2 = (\lambda - 1)(1 - \eta^2) > 0.$$

We do not divide by zero as $c > 0$. So the path $\Gamma_{2,4}(\Omega_{a,b,c,d}^{(21)})$ is valid.

7. For $\Gamma_{1,3}(\Omega_{a,b,c,d}^{(21)})$ the points q_i are contained in the 2-cells $(\overline{\omega_0\omega_2})^\vee$, $(\overline{\omega_2\omega_4})^\vee$ and $(\overline{\omega_4\omega_5})^\vee$. We obtain the following system of equations:

$$\begin{pmatrix} 0 \\ 0 \\ 0 \end{pmatrix} = \begin{pmatrix} x \\ y \\ z \end{pmatrix} + \alpha_1 \begin{pmatrix} -1 \\ 0 \\ 0 \end{pmatrix} + \alpha_2 \begin{pmatrix} 0 \\ 0 \\ -1 \end{pmatrix} \quad \text{with } \alpha_1, \alpha_2 > 0,$$

$$\begin{pmatrix} 1 \\ \eta \\ \eta^2 \end{pmatrix} = \begin{pmatrix} x \\ y \\ z \end{pmatrix} + \beta_1 \begin{pmatrix} b \\ b \\ -a \end{pmatrix} + \beta_2 \begin{pmatrix} d-b-1 \\ d-b \\ a-c \end{pmatrix} \quad \text{with } \beta_1, \beta_2 > 0,$$

$$\begin{pmatrix} \lambda \\ \lambda\eta \\ \lambda\eta^2 \end{pmatrix} = \begin{pmatrix} x \\ y \\ z \end{pmatrix} + \gamma_1 \begin{pmatrix} 1 \\ 0 \\ 0 \end{pmatrix} + \gamma_2 \begin{pmatrix} d-b-1 \\ d-b \\ a-c \end{pmatrix} \quad \text{with } \gamma_1, \gamma_2 > 0.$$

Solving for β_2, shows that $\beta_2 > 0$ if and only if $\frac{a}{b} + \eta > \lambda(\frac{c-a}{d-b} + \eta)$. For any choice of a, b, c, d parameters of the polytope family 21, this implies an upper bound for the value of λ which contradicts the generality of our chosen points. So, the path $\Gamma_{1,3}(\Omega_{a,b,c,d}^{(21)})$ is not valid.

8. For $\Gamma_{1,2}(\Omega_{a,b,c,d}^{(21)})$ the points q_i are contained in the 2-cells $(\overline{\omega_0\omega_3})^\vee$, $(\overline{\omega_3\omega_4})^\vee$ and $(\overline{\omega_4\omega_5})^\vee$. We obtain the following system of equations:

$$\begin{pmatrix} 0 \\ 0 \\ 0 \end{pmatrix} = \begin{pmatrix} x \\ y \\ z \end{pmatrix} + \alpha_1 \begin{pmatrix} 0 \\ -1 \\ 0 \end{pmatrix} + \alpha_2 \begin{pmatrix} 0 \\ 0 \\ -1 \end{pmatrix} \quad \text{with } \alpha_1, \alpha_2 > 0,$$

$$\begin{pmatrix} 1 \\ \eta \\ \eta^2 \end{pmatrix} = \begin{pmatrix} x \\ y \\ z \end{pmatrix} + \beta_1 \begin{pmatrix} 1 \\ 0 \\ 0 \end{pmatrix} + \beta_2 \begin{pmatrix} b \\ b \\ -a \end{pmatrix} \quad \text{with } \beta_1, \beta_2 > 0,$$

$$\begin{pmatrix} \lambda \\ \lambda\eta \\ \lambda\eta^2 \end{pmatrix} = \begin{pmatrix} x \\ y \\ z \end{pmatrix} + \gamma_1 \begin{pmatrix} 1 \\ 0 \\ 0 \end{pmatrix} + \gamma_2 \begin{pmatrix} d-b-1 \\ d-b \\ a-c \end{pmatrix} \quad \text{with } \gamma_1, \gamma_2 > 0.$$

By using only the $y,z-$equations of the second and third condition we can solve for β_2, γ_2, y, z:

$$y = \lambda\eta - (\lambda - 1)(d - b)(a\eta + b\eta^2),$$
$$z = \lambda\eta^2 + (\lambda - 1)(c - a)(a\eta + b\eta^2),$$
$$\beta_2 = \frac{1}{a}(\lambda - 1)(\eta^2 + (c - a)(a\eta + b\eta^2)) = \frac{1}{b}(\lambda - 1)(-\eta + (d - b)(a\eta + b\eta^2)),$$
$$\gamma_2 = (\lambda - 1)(a\eta + b\eta^2).$$

Since $\alpha_1 = y$ we have to check whether $y > 0$. However, since $d > b$, we have

$$y > 0 \iff \lambda < \frac{(b-d)(a+b\eta)}{1 + (b-d)(a+b\eta)}.$$

This contradicts the generality of our point conditions. The path $\Gamma_{1,2}(\Omega_{a,b,c,d}^{(21)})$ is not valid.

We conclude that only the lattice paths depicted in Figure 9.15 are valid for binodal polytopes of family 21. $\qquad\square$

We can now determine the multiplicities of the valid lattice paths using the `OSCAR` functions from [Gei22]. The computed values are displayed in Table 9.8.

Conjecture 9.4.24. *For binodal polytopes $\Omega_{a,b,c,d}^{(21)}$ of family number 21 as in Figure 9.14 where $ad - bc = 1$, $c + d > a + b$, $c > a$, $a, b, c, d > 0$ we have the following conjecture about the degree of the binodal variety and the path multiplicities.*

$$\deg(B_{\Omega_{a,b,c,d}^{(21)}}) = (d + c + 2)(d + c - 4),$$

$$mult(\Gamma_{3,4}(\Omega_{a,b,c,d}^{(21)})) = c + d - 4,$$

$$mult(\Gamma_{2,4}(\Omega_{a,b,c,d}^{(21)})) = c(c + d - 4),$$

$$mult(\Gamma_{0,1}(\Omega_{a,b,c,d}^{(21)})) = c + d - 4,$$

$$mult(\Gamma_{1,5}(\Omega_{a,b,c,d}^{(21)})) = b(c + d - 4),$$

$$mult(\Gamma_{1,[3,4]}(\Omega_{a,b,c,d}^{(21)})) = (d - b)(c + d - 4).$$

This conjecture is verified for the values in Table 9.8.

(a,b,c,d)	$\Gamma_{3,4}$	$\Gamma_{2,3}$	$\Gamma_{0,1}$	$\Gamma_{1,5}$	$\Gamma_{1,[3,4]}$	$\deg(B_{\Omega_{a,b,c,d}^{(21)}})$
(1,1,2,3)	1	2	1	1	2	7
(2,1,3,2)	1	3	1	1	1	7
(1,1,3,4)	3	9	3	3	9	27
(3,2,4,3)	3	12	3	6	3	27
(1,1,4,5)	5	20	5	5	20	55
(1,2,2,5)	3	6	3	6	9	27
(2,1,5,3)	4	20	4	4	8	40
(2,3,3,5)	4	12	4	12	8	40
(3,1,5,2)	3	15	3	3	3	27
(4,3,5,4)	5	25	5	15	5	55

Table 9.8: Verified path multiplicities and degree of binodal variety for polytope family number 21 as computed using [Gei22] in `OSCAR`. In order to keep the table slim we shorten the notation of the lattice path by leaving out the polytope.

9.5 Example for counting binodal surfaces

In this section, we show by means of one example, which is small enough to allow a computational verification, how the binodal polytopes, their lattice paths and the associated multiplicities as determined in Chapter 9 can be used to obtain a count of binodal surfaces that could not have been recovered using only the techniques from Chapter 7.

There are two ways how to find all tropical binodal surfaces with a given support passing through points in Mikhalkin position together with their lifting multiplicities. The first is to consider the tropicalization of the binodal variety, which is a subfan of the secondary fan of the Newton polytope. Each cone in the tropicalized binodal variety gives rise to a subdivision of the Newton polytope for which we can check

for valid lattice paths and compute their multiplicities. This approach however is only feasible for small examples.

The second way is to start with the lattice paths. To better see what happens with respect to the point conditions induced by the path, and thus to easier find valid lattice paths, we consider tropical floor plans. This is the way that will be demonstrated in this section.

In our example we work with tropical floor plans as introduced Chapter 7, Definition 7.3.5 and adapt this definition to the binodal case. Formally, tropical floor plans for binodal surfaces of degree d will be introduced in Chapter 10, Definition 10.2.1.

Notation 9.5.1. Let P be a Newton polytope with a floor decomposed subdivision $\mathcal{S}$. We assume that P is contained in the positive orthant of $\mathbb{R}^3$.

Let $d := \max\{\omega_x \,|\, (\omega_x, \omega_y, \omega_z)$ is a lattice point of $P\}$. The intersection of $\mathcal{S}$ with the plane $\{x = i\}$ for each $i \in \{0, ..., d\}$ such that this intersection is not empty gives 2-dimensional subdivisions $\mathcal{S}_i$ of $P \cap \{x = i\}$.

In this section, we will speak of a *tropical floor plan* of a tropical surface dual to $\mathcal{S}$ when we consider the constellation of the tropical curves C_{d-i} dual to the $\mathcal{S}_i$.

The positions of the curves C_{d-i} are fixed by the lattice path and the dual subdivision of P in the following way: We say two curves are neighbors if they are dual to neighboring slices of the subdivision $\mathcal{S}_i$ and $\mathcal{S}_{i+1}$. Any alignment or intersection of neighboring curves corresponds to a 3-dimensional polytope in the subdivision. This polytope is spanned by the edges in the subdivision dual to the aligning or intersection edges of the curves. As an example, think of the pentatope or the bipyramids as illustrated in Figure 7.5 in Section 7.3.

Further, we recall that each segment in the lattice path stands for a 2-cell of the dual tropical surface S that contains a point from the point conditions in its relative interior. Each edge of a tropical curve C_{d-i} in the tropical floor plan corresponds to an edge of the subdivision. If this edge is part of the lattice path, the associated edge in the curve contains the projection of the point to the last two coordinates $Q_i = \Pi_{y,z}(q_i)$.

When we fix points in Mikhalkin position (Definition 7.2.1), these points, through which the curves of the floor plan pass, are distributed with growing distances along a line of direction $(1, \eta)$.

The point conditions need to determine the positions of the curves C_{d-i} up to possible alignments, which give rise to the two nodes in the tropical surface; compare Definition 7.3.4 of node germs for separated nodes. When counting, we have to identify those alignments of the curves in the tropical floor plan that give rise to a binodal polytope in the subdivision and thus hide two unseparated nodes.

Remark 9.5.2. In this example we will not present the computations to check the validity of the lattice paths. When working with tropical floor plans, the fact that

the curves of the floor plan pass through the projections of the points gives a strong indication that the lattice path can be valid. However, it does not imply it; so a check via the linear systems of equations as shown in Section 9.4 is necessary to obtain a full proof.

Remark 9.5.3. When counting binodal surfaces with a Newton polytope of more than 6 lattice points, it does no longer hold that lattice paths have to run along edges of the polytope. Instead a lattice path has to run along edges of the subdivision of the Newton polytope to which the surface passing through the point conditions is dual.

Consider the polytope P given by the following lattice points

$$\begin{pmatrix} 0 & 0 & 0 & 0 & 1 & 1 & 1 \\ 0 & 0 & 1 & 1 & 0 & 1 & 3 \\ 0 & 1 & 0 & 1 & 0 & 0 & 1 \end{pmatrix}.$$

Let ω_i denote the lattice points of P in the order as given above. Note that this is the order induced by $v = (1, \eta, \eta^2)$. We observe that this polytope can be obtained by taking the convex hull of the lattice points of $\Omega_{3,1}^{(10)}$ and the lattice point $(1,1,0)$.

The binodal variety of P can be computed via `OSCAR` using [Gei22]. It has degree 12.

```
julia> P = matrix(ZZ,7,3,
    [0,0,0,0,0,1,0,1,0,0,1,1,1,0,0,1,1,0,1,3,1]);
julia> I = binodal(P);
julia> investigate_binodal(I);
Affine dimension of the binodal variety is 5
The binodal variety is of expected affine dimension.
Degree of the binodal variet is 12
(5, 12)
```

This computation does not need much memory, but takes a few days to terminate.

We fix $|P \cap \mathbb{Z}^3| - 3 = 4$ points $\mathbf{p} = (p_0, \dots, p_3)$ in Mikhalkin position. As usual let $q_i = \mathrm{Trop}(p_i)$. We denote by $Q_i = \Pi_{y,z}(q_i)$ the projection of the tropical point conditions to the last two coordinates.

We observe that the polytope P has width 1, so any subdivision will be floor decomposed. Furthermore, this tells us that any floor plan will consist of two curves: One dual to the subdivision $\mathcal{S}_0$ of

$$\begin{pmatrix} 0 & 0 & 1 & 1 \\ 0 & 1 & 0 & 1 \end{pmatrix},$$

and one dual to the subdivision $\mathcal{S}_1$ of

$$\begin{pmatrix} 0 & 1 & 3 \\ 0 & 0 & 1 \end{pmatrix}.$$

There are three possibilities for $\mathcal{S}_0$. These induce three options for the dual curve C_1, which are depicted in Figures 9.16a, 9.16b and 9.16c. As the polytope $P \cap \{x = 1\}$ is a unimodular triangle, there is only the trivial subdivision possible. The dual tropical curve C_0 is depicted in Figure 9.16d.

(a) First op-
tion for C_1

(b) Second
option for C_1

(c) Third op-
tion for C_1

(d) C_0
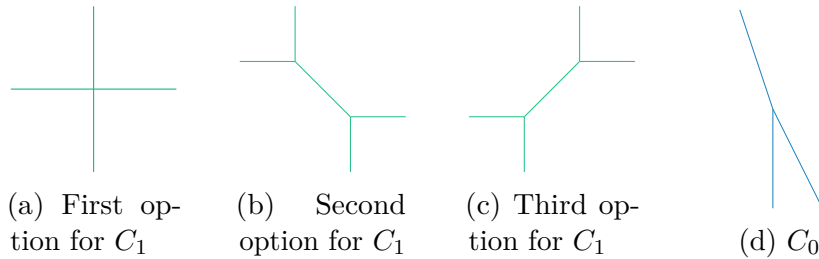
Figure 9.16: There are three possibilities for $\mathcal{S}_0$: the trivial subdivision induces Figure 9.16a, the subdivision given by the diagonal from (0,0) to (1,1) induces the curve in Figure 9.16b, and the subdivision given by the diagonal from (1,0) to (0,1) induces the curve in Figure 9.16c. For the subdivision $\mathcal{S}_1$ only the trivial subdivision of the triangle is possible. The dual curve is shown in Figure 9.16d.

To find all valid lattice paths we go through the different options for C_1. In each case we consider different distributions of the points Q_i on the two curves:

1. C_1 passes through Q_0, Q_1, Q_2, and C_0 passes through Q_3;

2. C_1 passes through Q_0, Q_1, and C_0 passes through Q_2, Q_3;

3. C_1 passes through Q_0, Q_1, Q_2, and C_0 passes through no point;

4. C_1 passes through Q_0, Q_1, and C_0 passes through Q_3;

5. C_1 passes through Q_0, and C_0 passes through Q_2, Q_3.

Curve C_1 as in Figure 9.16a

If $\mathcal{S}_0$ is the trivial subdivision of the square we see curve C_1 as in Figure 9.16a. In this case C_1 can only pass through at most 2 points. We therefore only have to consider the cases 2, 4 and 5.

Figure 9.17: For these two distributions of the point conditions with C_0 as in Figure 9.16a, the tropical floor plan cannot be binodal.

(9.16a, 2): Point distribution $2+2$

Assume that C_1 passes through Q_0 and Q_1 and that C_0 passes through Q_2 and Q_3; see case (2). In this case both curves are completely determined and they intersect in 3 points. The dual subdivision contains 3 tetrahedra and one pyramid over the square. See Figure 9.17. Therefore, the subdivision contains neither a binodal polytope, nor two circuits that could give rise to 2 separated nodes.

(9.16a, 4): Point distribution $2+1$

If C_1 passes through Q_0 and Q_1, the curve C_1 is completely determined by the point conditions and by the argument above we know that C_0 has to pass only through Q_3. This means that C_0 is not fixed by the point conditions. Therefore, we need an alignment to determine the floor plan. There are three possible positions of the point Q_3 in C_0: one for each ray of C_0.

If Q_3 is contained the vertical ray of C_0, there does not exist a possible alignment to fix the curve.

If Q_3 is contained in the ray with direction $(-1,3)$, the only possible alignment that determines the curve is to fix the vertex of C_0 on the horizontal ray of C_1. See Figure 9.18a. This intersection gives rise to a pentatope in the subdivision. The ray with direction $(-1,3)$ intersects the vertical ray of C_1. This leads to a tetrahedron in the subdivision of P. The vertex of C_1 gives a pyramid over the square. This subdivision does not lead to a binodal surface, since additionally to the node at the vertex dual to the pentatope we do not see another circuit that would induce a second separated node.

If Q_3 is contained the ray of C_0 with direction $(1,-2)$, the only possible way to fix the curve is to align the vertex of C_0 with the horizontal ray of C_1. See Figure 9.18b. This also aligns the vertical rays of C_0 and C_1 and therefore leads to a polytope in the subdivision that is IUA-equivalent to the polytope of family 9. As proven in Lemma 9.2.4 this polytope is not binodal.

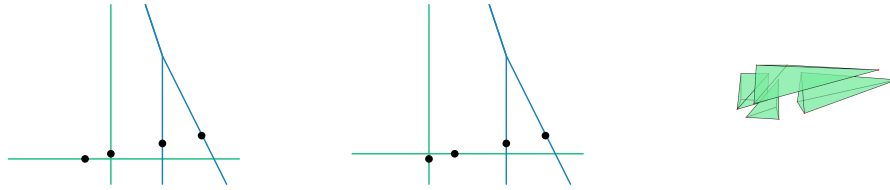(a)   (b)
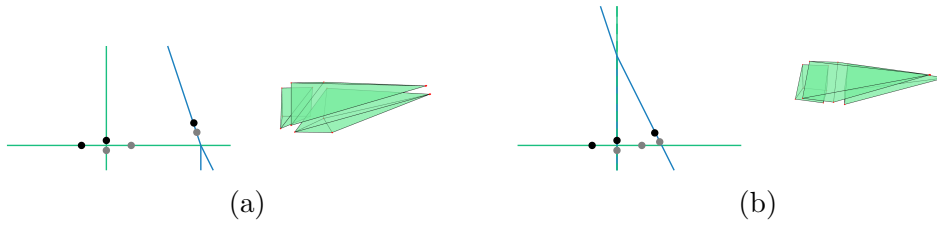
Figure 9.18: For these four distributions of the point conditions with C_0 as in Figure 9.16a, the tropical floor plan cannot be binodal.

$(9.16a, 5)$: Point distribution $1 + 2$

In this last case, C_1 passes through Q_0, and C_0 passes through Q_2 and Q_3. This means that C_0 is fixed by the point conditions. We can conclude from the fact that the Q_i are distributed on a line of direction $(1, \eta)$ with $1 \gg \eta > 0$ that Q_2 and Q_3 are contained in the two downwards pointing rays of C_0, and that Q_0 is contained in the vertical ray of C_1.

The horizontal ray of C_1 is the part of the floor plan that is not fixed. There are two possible alignments: with the vertex of C_0 or with the intersection of the ray with direction $(-1, 3)$ of C_0 with the vertical ray of C_1. The first alignment gives rise to a pentatope in the subdivision. Apart from the point conditions, this is the same alignment as in Figure 9.18a, and similarly as before we see that this case does not lead to a binodal surface.

The second alignment leads to a polytope with 6 lattice points in the subdivision, which is equal to $\Omega_{3,1}^{(10)}$. This is formed by the convex hull of ω_0, ω_1, ω_2, ω_3, ω_4 and ω_6. The tropical floor plan together with the corresponding lattice path and tropical surface is shown in Figure 9.19.

Figure 9.19: Tropical floor plan for $(9.16a, 5)$ with lattice path, dual subdivision and tropical surface. In the subdivision the binodal polytope is colored red.

The lattice path depicted in Figure 9.19, corresponds to the lattice path $\Gamma_{1,3}(\Omega_{3,1}^{(10)})$ as studied in Section 9.4.2. We know from Table 9.4 that this lattice path has multiplicity 1. So the tropical floor plan Figure 9.19 contributes one surface to our count.
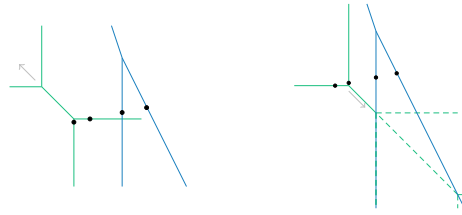
Figure 9.20: When the point conditions are distributed $2+2$ with C_0 as in Figure 9.16b, the tropical floor plan cannot be fixed.

Curve C_1 as in Figure 9.16b

The next case to consider is that curve C_1 is of the form as in Figure 9.16b. First we note that in this case the curve C_1 can pass through at most 2 points, because the points are distributed along a line of direction $(1, \eta)$, $1 \gg \eta > 0$.

$(9.16\text{b}, 2)$: Point distribution $2+2$

In this case C_0 is completely fixed by the point conditions. For C_1 there are two choices on how the curve can pass through two points, each determines the position of one of the two vertices of C_1. For the first of these choices, Figure 9.20 depicts the two possible alignments of the second vertex of C_1 with C_0. They both do not lead to either a binodal polytope in the subdivision nor to two unseparated nodes.

For the second choice, the lower vertex of C_1 is determined by the point conditions, while the vertex with larger y-coordinate is not fixed. We can therefore pull this vertex along the direction $(-1, 1)$ without ever meeting C_0. This means that the curves cannot be determined. So they do not lead to a tropical floor plan of a binodal surface.

$(9.16\text{b}, 4)$: Point distribution $2+1$

As for the case discussed above, there are two ways how C_1 can pass through 2 of the points. With the same argument as before, we exclude the case that the point conditions fix the lower vertex of C_1; see left picture in Figure 9.20. For C_0 we have three rays each of which can contain Q_3. We obtain the three options depicted in Figure 9.21.

In the floor plan depicted in Figure 9.21a, the alignment of the two undetermined vertices of C_1 and C_0 gives rise to a polytope in the subdivision that is IUA-equivalent to $\Omega_{2,1}^{(10)}$ which is not binodal by Proposition 9.2.5.

We see that in Figure 9.21b no alignment fixing the vertex of C_0 is possible. So the curves are not fixed and we do not obtain a valid floor plan.

(a)   (b)   (c)
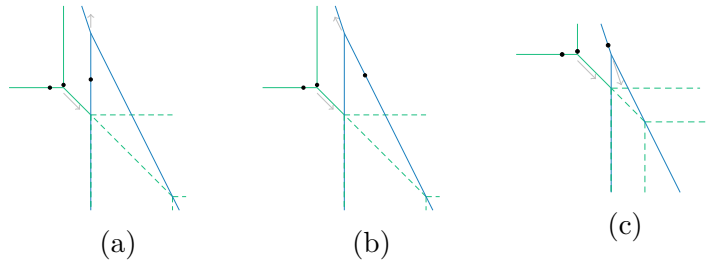
Figure 9.21: When the point conditions are distributed $2 + 1$ with C_0 as in Figure 9.16b, the tropical floor plan cannot be fixed.

However, the floor plan in Figure 9.21c induces a subdivision containing two bipyramids and one pentatope. We get a tropical surface with two separated nodes.
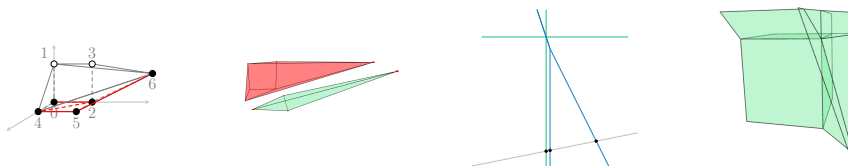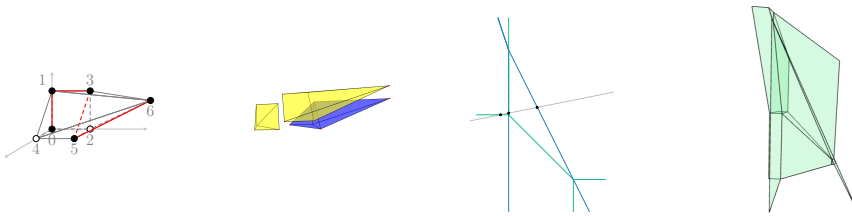

Figure 9.22: Tropical floor plan for $(9.16b, 4)$ with lattice path, dual subdivision and tropical surface. In the subdivision the two pyramids are colored yellow and the pentatope is colored blue.

We recall from Proposition 7.3.11 that we have to count the node given by the bipyramids with multiplicity 2. To obtain the multiplicity of the pentatope we use Proposition 7.3.10: via an affine automorphism of $\mathbb{Z}^3$ we can bring it into the position as in Proposition 7.3.10:

$$\begin{pmatrix} 0 & 0 & 0 & 1 & 1 \\ 0 & 1 & 1 & 1 & 3 \\ 0 & 0 & 1 & 0 & 1 \end{pmatrix} \rightsquigarrow \begin{pmatrix} 0 & 0 & 0 & 1 & 1 \\ 0 & 1 & 0 & 0 & 1 \\ 0 & 0 & 1 & 0 & 1 \end{pmatrix},$$

and then compute its discriminant

$$4a_{(0,1,0)}a_{(0,0,1)}a_{(1,0,0)} + a_{(0,0,0)}^2 a_{(1,1,1)} = 0. \tag{9.3}$$

We see that lattice point $(0,1,0)$ is the one left out of the path, so we get multiplicity $\deg_{a_{(0,1,0)}}(4a_{(0,1,0)}a_{(0,0,1)}a_{(1,0,0)} + a_{(0,0,0)}^2 a_{(1,1,1)}) = 1$. Hence, we have to count this tropical floor plan with multiplicity $2 \cdot 1 = 2$, and we obtain 2 more surfaces to our count.

Figure 9.23: For these four distributions of the point conditions and with C_0 as in Figure 9.16b, the tropical floor plan cannot be fixed.

(9.16b,5): Point distribution $1+2$

If C_1 contains only Q_0, then C_0 has to pass through Q_2 and Q_3, and it is therefore determined. There are five edges in C_1 that could contain Q_0. For the bounded edge and the rays of directions $(0,1)$, $(1,0)$ and $(0,-1)$ we see that the vertex of C_1 with larger y-coordinate can not be fixed by any alignment with C_0. This is illustrated in Figure 9.23. So only the case with Q_0 contained in the ray of direction $(-1,0)$ remains. We need to fix both vertices of C_1 by alignments with C_0 that give rise to two singularities. There is only one choice, which is depicted in Figure 9.24.
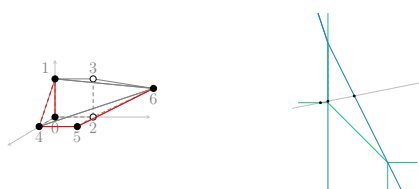
Figure 9.24: Tropical floor plan for (9.16b,5) with lattice path. The dual subdivision and tropical surface are the same as in Figure 9.22.

We observe that this looks like the tropical floor plan in Figure 9.22. The difference is which of the two curves contains the second point and which is aligned. This difference is not visible in the floor plan, but in the lattice path.

For the multiplicity, we get a factor 2 from the alignment of the vertical rays. To obtain the multiplicity of the pentatope, which is dual to the alignment of the second vertex of C_1 with C_0, we use that we know the discriminant, see Equation (9.3). It is again lattice point $(0,1,0)$ that is left out of the path, so we get a factor 1. Hence, we have to count this tropical floor plan with multiplicity $2 \cdot 1 = 2$, and we obtain 2 more surfaces to our count.
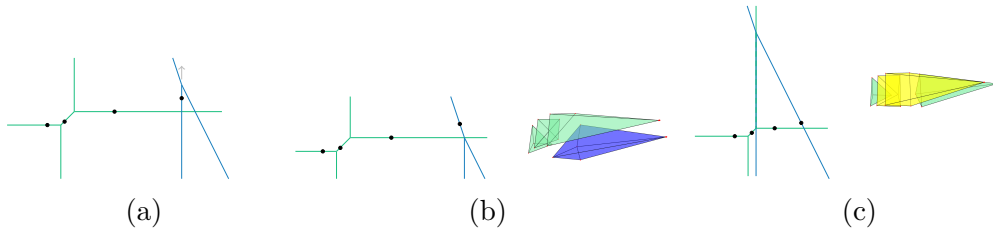
Figure 9.25: For these three distributions of the point conditions with C_0 as in Figure 9.16c, the tropical floor plan is either not determined (Figure 9.25a) or not binodal (Figures 9.25b and 9.25c).

Curve C_1 as in Figure 9.16c

The last case is to consider C_1 as in Figure 9.16c. We first exclude the cases that all four points are visible in the floor plan.

(9.16c,1): Point distribution $3+1$

Assume that C_1 passes through Q_0, Q_1 and Q_2, and C_0 passes through Q_3. In this case the curve C_1 is completely determined by the point conditions. For C_0 there are three possibilities which of the rays contains Q_3.

If Q_3 is contained in the ray with direction $(0,-1)$ the curve cannot be fixed by any alignment with C_1; see Figure 9.25a.

If Q_3 is contained in the ray with direction $(-1,3)$, the only possible alignment with C_1 to fix the curve is to align the vertex of C_0 with the ray of C_1 in direction $(1,0)$. See Figure 9.25b. This floor plan induces a subdivision of P that contains of a pentatope, but no other circuit. This does not give rise to a binodal surface.

If Q_3 is contained in the ray with direction $(1,-2)$, the only possible alignment of C_0 with C_1 is to align the vertex of C_0 with the ray of direction $(0,1)$ in C_1. See Figure 9.25c. This floor plan induces a subdivision of P that contains two pyramids over a parallelogram, but contains no other circuit. This does not give rise to a binodal surface.

(9.16c,2): Point distribution $2+2$

In this case C_0 is completely determined by the point conditions. For C_1 there are five possible options how the two points can be contained in the curve.

For the first four of these options, which are depicted in Figure 9.26, the curve C_0 cannot be fixed by alignments with C_0. For the last option, there are two possible alignments as depicted in Figure 9.27. However, both of these do not give rise to a binodal surface as the dual subdivision neither contains two circuits inducing separated nodes, nor a binodal polytope.
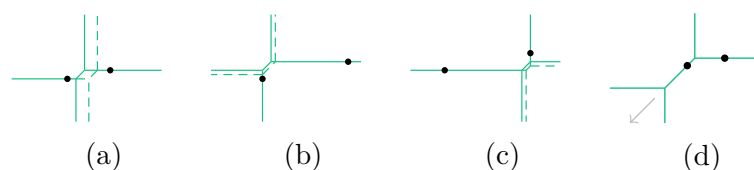
Figure 9.26: When C_1 is as in Figure 9.16c and passes through 2 points, the curve cannot be fixed in the tropical floor plan by the depicted four point distributions.
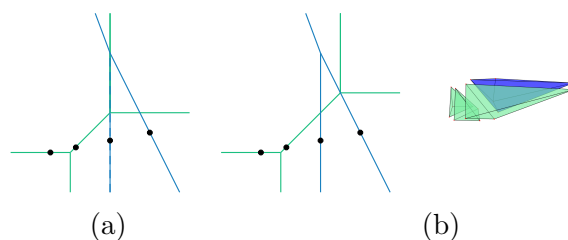
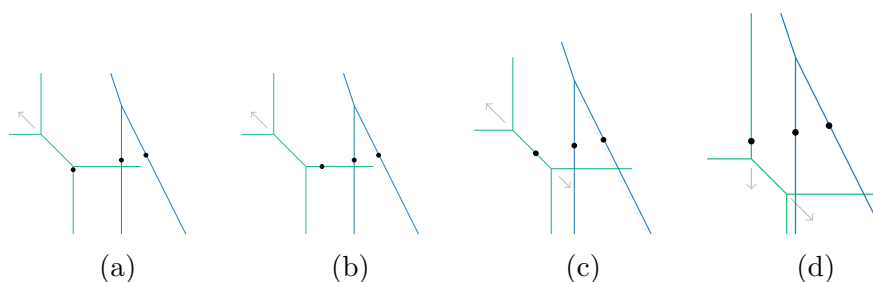

Figure 9.27: For the two distributions of the point conditions with C_0 as in Figure 9.16c, the tropical floor plan is not binodal. The dual subdivision for the tropical floor plan in Figure 9.27a is the same as in Figure 9.25c

(9.16c,3): Point distribution $3+0$

In this case the curve C_1 is determined by the point conditions. In order to determine the position of the curve C_0 in the plane, we have to fix the vertex of C_0 by some alignment. There are two options: the two vertices of C_1. These floor plans arise from the same lattice path, but give rise to different tropical floor plans and different binodal polytopes in the subdivision. The alignment with the vertex of C_1 with larger y-coordinate is depicted in Figure 9.28.

The induced subdivision consists of one tetrahedron and one polytope with 6
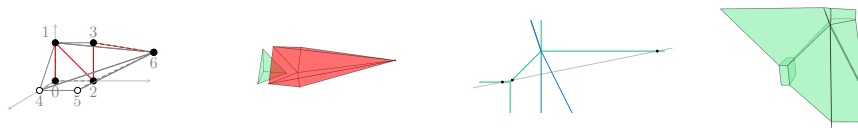
Figure 9.28: Tropical floor plan for $(9.16c, 3)$ of the first choice of alignment, with lattice path, dual subdivision and tropical surface. In the subdivision, the binodal polytope is colored in red.

lattice points, which is IUA-equivalent to a polytope of family 20 with $a = 4$:

$$\begin{pmatrix} 0 & 0 & 0 & 1 \\ 0 & 0 & 1 & 0 \\ 0 & 1 & 0 & 0 \end{pmatrix} \text{ and } \begin{pmatrix} 0 & 0 & 0 & 1 & 1 & 1 \\ 0 & 1 & 1 & 0 & 1 & 3 \\ 1 & 0 & 1 & 0 & 0 & 1 \end{pmatrix}.$$

We can compute the path multiplicity for this case by using [Gei22] in `OSCAR`.

```
julia> A1 = matrix(ZZ,6,3,[0,0,1,0,1,0,0,1,1,1,0,0,1,1,0,1,3,1]);
julia> path_mult(A1,[4,5],[true,true],[1,1//2,1//3,1//5]);
Affine dimension is 0
Path multiplicity is 1
```

The alignment with the vertex of C_1 with larger y-coordinate is depicted in Figure 9.29.
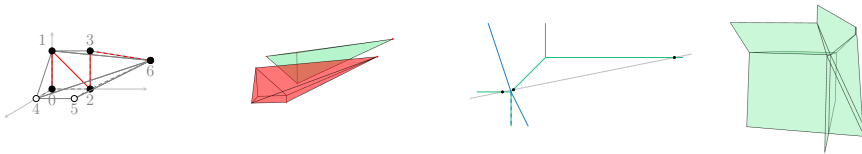
Figure 9.29: Tropical floor plan for (9.16c,3) of the second choice of alignment with lattice path, dual subdivision and tropical surface. In the subdivision, the binodal polytope is colored in red.

The induced subdivision consists of one tetrahedron and one polytope with 6 lattice points, which is IUA-equivalent to a polytope of family 10 with $a = 3$, $b = 1$:

$$\begin{pmatrix} 0 & 0 & 0 & 1 \\ 0 & 1 & 1 & 3 \\ 1 & 0 & 1 & 1 \end{pmatrix} \text{ and } \begin{pmatrix} 0 & 0 & 0 & 1 & 1 & 1 \\ 0 & 0 & 1 & 0 & 1 & 3 \\ 0 & 1 & 0 & 0 & 0 & 1 \end{pmatrix}.$$

We can compute the path multiplicity for this case by using [Gei22] in `OSCAR`.

```
julia> A2 = matrix(ZZ,6,3,[0,0,0,0,0,1,0,1,0,1,0,0,1,1,0,1,3,1]);
julia> path_mult(A2,[4,5],[true,true],[1,1//2,1//3,1//5]);
Affine dimension is 0
Path multiplicity is 1
```

Therefore, we obtain two more surfaces to our count from these two cases.

(9.16c, 4): Point distribution $2 + 1$

As in the case with the distribution of the point conditions $2 + 2$ between the two curves, we have five options how C_1 can pass through Q_0 and Q_1. With the same arguments we can exclude the four cases shown in Figure 9.26. Thus, the only way
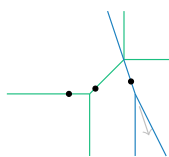
Figure 9.30: For this distribution of the point conditions and with C_0 as in Figure 9.16c, the tropical floor plan cannot be fixed.

(a)   (b)
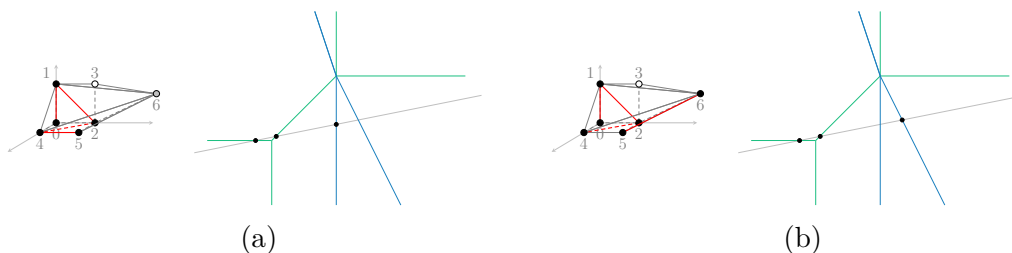
Figure 9.31: Tropical floor plan for $(9.16c, 4)$ with lattice path. The dual subdivision and tropical surface are the same as in Figure 9.28.

that can lead to a valid tropical floor plan is that Q_0 is contained in the horizontal ray with direction $(-1,0)$ and Q_1 is contained in the bounded edge.

We know that there are three possibilities for C_0 to contain Q_3. If Q_3 is contained in the ray with direction $(-1,3)$ we cannot determine the position of the vertex of C_0 along that ray by any alignment with C_1, see Figure 9.30.

The other two options are depicted in Figures 9.31a and 9.31b. Both tropical floor plans induce the same subdivision, which coincides with the subdivision given induced by the tropical floor plan in Figure 9.28.

From this case we know that the subdivision contains a binodal polytope IUA-equivalent to $\Omega_4^{(20)}$. We can compute the multiplicities of the two lattice paths by using [Gei22] in OSCAR.

```
julia> A1 = matrix(ZZ,6,3,[0,0,1,0,1,0,0,1,1,1,0,0,1,1,0,1,3,1]);
julia> path_mult(A1,[3,6],[true,true],[1,1//2,1//3,1//5]); #Path
    in Figure 9.31 (a)
Affine dimension is 0
Path multiplicity is 1
julia> path_mult(A1,[3,5],[true,false],[1,1//2,1//3,1//5]); #Path
    in Figure 9.31 (b)
Affine dimension is 0
Path multiplicity is 3
```

Summing both cases, we obtain 4 more surfaces to our count.
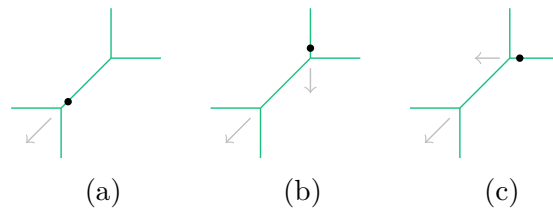
Figure 9.32: When C_1 is as in Figure 9.16b and passes through 1 point, the curve cannot be fixed in the tropical floor plan by the depicted three positions of the point condition.
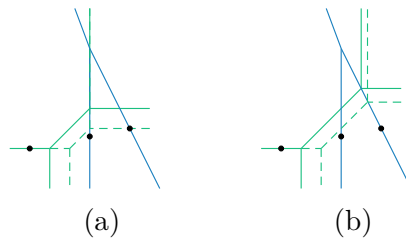

Figure 9.33: None of the two possible alignments determine the tropical floor plan.

(9.16c,5): Point distribution $1+2$

By this distribution of the point conditions, the curve C_0 is determined. For C_1 there are five possibilities how the point Q_0 can be contained in the relative interior of one of its edges. They are depicted in Figure 9.32. We see that the first four options in Figure 9.32 do not make it possible to fix the curve C_0 in the floor plan.

The last option leads to the floor plan shown in Figure 9.34.
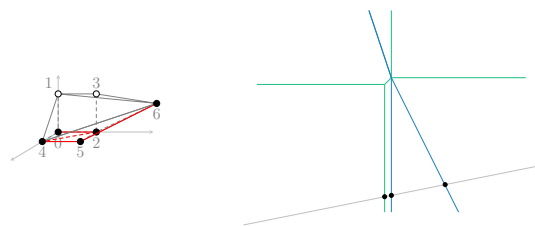
Figure 9.34: Tropical floor plan for (9.16c,5) with lattice path. The dual subdivision and tropical surface are the same as in Figure 9.28

This floor plan leads to the same subdivision as the tropical floor plans in Figures 9.28, 9.31a and 9.31b, which contains a binodal polytope IUA-equivalent to $\Omega_4^{(20)}$. We can compute the path multiplicity for this case by using `OSCAR`.

```julia
julia> A1 = matrix(ZZ,6,3,[0,0,1,0,1,0,0,1,1,1,0,0,1,1,0,1,3,1]);
```

```
julia> path_mult(A1,[1,3],[true,true],[1,1//2,1//3,1//5]); #Path
    in Figure 9.34
Affine dimension is 0
Path multiplicity is 1
```

The count:

One can verify using the techniques as described in Remark 9.3.6 that all these lattice paths are indeed valid.

To obtain the total count we sum together all the multiplicities of the tropical floor plans and obtain

$$\sum_{F \text{ floor plan}} \text{mult}_{\mathbb{C}}(F) = (1) + (2+2) + (1+1+3+1+1) = 12 = \deg(B_P).$$

Remark 9.5.4. When we tropicalize the binodal variety of P, we observe that it has a lineality space of dimension 4 and consists of 4 rays. These four rays give rise to four different subdivisions of P. These are exactly the four subdivisions that can be constructed from the tropical floor plans.

However, in general it is not know that the subdivisions to binodal surfaces are contained in the maximal dimensional cones of the tropicalized binodal variety.

Chapter 10

Counting binodal surfaces

We now turn to the question of counting binodal degree d surfaces. In order to improve on the tropical count of binodal degree d surfaces via tropical floor plans, we have to understand how we can use the results on binodal polytopes of Chapter 9 in this situation.

That means we need to understand which binodal polytopes with 6 lattice points and width 1 can be contained in the dual subdivision of a degree d surface passing through points in Mikhalkin position. We have to determine all the possible lattice paths for these cases and discover their multiplicities. This is done in Section 10.1. The results are collected in Theorem 10.1.6 and Conjecture 10.2.2.

Building on this conjecture, Section 10.2 poses that binodal polytopes with 6 lattice points contribute $\frac{1}{4}d^4$ to the asymptotic count of binodal surfaces (Conjecture 10.2.5). Moreover, we extend the definition of tropical floor plans for surfaces of degree d to count surfaces for which the tropicalization of the two singularities is a vertex of the tropical surface dual to a binodal polytope with 6 lattice points and width 1 (Definition 10.2.1). This generalization is an important step towards achieving a definition of tropical floor plans that will provide the full number $N^{\mathbb{P}^3}_{\delta,\mathbb{C}}(d)$.

This chapter is based on joint work with Madeline Brandt [BG21].

10.1 Binodal polytopes in degree d surfaces

Recall from Conjecture 9.2.8, that there are six families of binodal polytopes. In this section, we investigate which of these contribute to the count of binodal floor decomposed degree d surfaces. For those that contribute, we find all valid lattice paths and their multiplicities. For the multiplicities we proceed as in Chapter 9: we compute the multiplicities for small values, and pose a conjecture building on this data.

To decide whether a binodal polytope can appear in a dual subdivision of a floor decomposed tropical surface passing through points in Mikahlkin position, we use the concept of tropical floor plans as defined in Definition 7.3.5. However, we have

to adapt and extend the definition to fit the binodal cases. Accordingly, before we start investigating the binodal polytopes, we need some definitions and notations.

This section is based on joint work with Madeline Brandt [BG21].

The formal definition of tropical floor plans for surfaces of degree d can be found in Section 10.2 as this definition builds on the results of this section.

Remember that we assume our binodal tropical surface to pass through points in Mikhalkin position. The tropical points $(q_1, \ldots, q_N)$ are distributed with growing distances along a line of direction $(1, \eta, \eta^2)$ where $1 \gg \eta > 0$. This induces an order on the lattice points of $d\Delta_3$, Definition 7.2.3.

The problem of finding a way to fit a polytope of width 1 into a subdivision $\mathcal{S}$ of $d\Delta_3$ arising from a lattice path induced by the above partial order can be viewed as a problem on tropical floor plans: The tropical floor plan is the constellation of tropical plane curves C_{d-i} dual to the subdivisions $\mathcal{S}_i = \mathcal{S} \cap \{x = i\}$, where a curve C passes through the projected points $\Pi_{y,z}(q_i) =: Q_i$ if and only if the edge of the curve C containing Q_i in its relative interior corresponds to the 2-cells of the tropical surface S that contains q_i. Polytopes in $\mathcal{S}$ correspond to vertices of these curves or intersection points. See also Section 9.5 for an explanation on this topic.

If we leave out lattice points from the lattice path, the curves in the tropical floor plan gain degrees of freedom. To fix the curves, we need to align them. And to obtain singular surfaces, these alignments need to give rise to polytopes in the subdivision which hold nodes. Definition 7.3.5 contains all alignments that give rise to separated nodes. Recall Figure 7.5 for an illustration how node germs induce circuits in the subdivision.

In the following investigation of how to fit binodal polytopes into subdivision of $d\Delta_3$ dual to a binodal tropical surface through Mikhalkin points, we also need to check what kind of alignments are possible in the tropical floor plan to give rise to such a binodal polytope. This is not only necessary to later extend the definition of tropical floor plans to these cases, but more importantly it helps to see whether the arising tropical surface will pass through the fixed point conditions and therefore be a valid choice.

Notation 10.1.1. The *i-th floor* of a tropical floor plan, is the tropical plane curve C_{d-i}. We use *i-th floor subdivision* to mean the dual subdivision $\mathcal{S}_i$ of the plane curve C_{d-i}.

When we speak of *alignments* between floors we mean the alignments of the tropical plane curves to fix the degrees of freedom as explained above. This is equivalent to choosing edges in the floors of $d\Delta_3$ to form polytopes which are not determined by the lattice path. We will also sometimes call this an alignment.

We recover an observation from [BG20, Section 5.1] that we can now phrase as a definition, and that gives us new option for alignments between floors that might give rise to binodal polytopes.
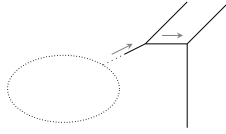
Figure 10.1: A double right string

Definition 10.1.2. We fix points in Mikhalkin position. If none of the points pass through an end adjacent to the lower right vertex of the Newton polytope and none of the points passes through the horizontal bounded edge adjacent to this end, then we can both prolong the edge in direction (2,1) and the edge in direction (1,0). This produces a family of curves that all pass through the chosen points in Mikhalkin position. The union of the two ends together with the unfixed horizontal edge is called a *double right string*. This is illustrated in Figure 10.1.

Remark 10.1.3. In accordance with the naming of the right and left strings from [MMSS22] (Definition 7.3.4) we call it a double *right* string, even though we will not look at the left analogue. This is because a "left double string" would have two degrees of freedom in the directions $(-1, -1)$ and $(-1, -2)$, for which the slopes are too steep to allow any curve fixing alignments.

Now we start investigating which polytopes of the 6 families of binodal polytopes determined in Chapter 9 can occur in the dual subdivision of a binodal floor decomposed surface of degree d passing through points in Mikhalkin position. We need the concept of IUA-equivalence of lattice polytopes as described in Definition 9.2.2. The first results shows that we can exclude three families entirely.

Proposition 10.1.4. *Let S be a floor decomposed binodal surface of degree d passing through points in Mikhalkin position. Then the dual subdivision to S cannot contain polytopes which are IUA-equivalent to polytopes of families 8, 14 or 21.*

Proof. We know $|d\Delta_3 \cap \mathbb{Z}^3| = \binom{d+3}{3}$. Therefore, S passes through $\binom{d+3}{3} - 3$ points in Mikhalkin position. Recall that the tropical points are distributed with growing distances along a line of direction $(1, \eta, \eta^2)$ where $1 \gg \eta > 0$ and that this induces a partial order on the lattice points of $d\Delta_3$ which the lattice path needs to follow. We consider the three polytope families separately.

Family 8

Any polytope that is IUA-equivalent to a polytope of family 8 has a triangular facet that contains one interior lattice point. A lattice path inducing a subdivision of $d\Delta_3$ that contains a triangle with an interior point in a floor subdivision must skip at least 3 lattice points. This comes from the partial order on the lattice points of $d\Delta_3$.

Thus, S satisfies at most $\binom{d+3}{3} - 4$ of the point conditions.

Family 14

A polytope of family 14 has width 1 and since we assume the tropical surface S to be floor decomposed, we can assume that any IUA-equivalent polytope $\tilde{\Omega}$ contained in the dual subdivision $\mathcal{S}$ satisfies that $\tilde{\Omega} \cap \{x = i\}$ is a triangle with one edge of length 2 and that $\tilde{\Omega} \cap \{x = i \pm 1\}$ is the opposite edge.

We assume that $\tilde{\Omega} \cap \{x = 0\}$ is the triangle with the edge of length 2, and that the opposite edge is $\tilde{\Omega} \cap \{x = 1\}$. The case that $\tilde{\Omega} \cap \{x = 1\}$ is the triangle with the edge of length 2, and that the opposite edge is $\tilde{\Omega} \cap \{x = 0\}$ works analogous. The contradictions we see below arise in a similar way for this second case.

We make a case distinction by the direction of the edge of length two. Due to the points in Mikhalkin position, the edge can only be either vertical, horizontal or diagonal. An edge of length two in the subdivision of a different direction would require leaving out more than 2 lattice points from the lattice path to fit the edge into one floor subdivision and a the same time to enable an alignment between the floor and a neighboring floor which corresponds to the polytope in the subdivision.

As $\tilde{\Omega}$ has a triangle in the 0-th floor subdivision and an edge in the 1st floor subdivision, we need an alignment between the two floors in the tropical floor plan. Additionally, we have to leave out at least one lattice point to obtain the edge of length 2, so we have only two options: Either the triangle with the edge of length 2 is missing another lattice point from the path, or we can use only tools from the one-nodal case, i.e., right and left string, to achieve the alignment.

If the edge of length 2 is horizontal, it has to be contained in $d\Delta_3 \cap \{z = 0\}$. That means that the curve in the associated floor has a vertical end of weight 2. We can apply IUA-equivalences to bring $\Omega_{a,b}^{(14)}$ in this position:

$$\begin{pmatrix} 0 & 0 & 0 & 0 & 1 & 1 \\ y-2 & y-1 & y-1 & y & 0 & b \\ 0 & 0 & 1 & 0 & a & 0 \end{pmatrix}.$$

In the floor subdivision $\mathcal{S}_1$ the edge of the polytope has direction (b,a) with $0 < b < a$ with $gcd(a,b) = 1$. This only fits between two columns if $b = 1$.

$$\tilde{\Omega} = \begin{pmatrix} 0 & 0 & 0 & 0 & 1 & 1 \\ y-2 & y-1 & y-1 & y & 0 & 1 \\ 0 & 0 & 1 & 0 & a & 0 \end{pmatrix}.$$

This polytope can be contained in $d\Delta_3$ with $a+1 \leq d$ and it does not immediately contradict our point conditions, since we can draw a lattice path leaving out the point $(0,y-1,0)$. If $y = d$, it is possible to draw a lattice path that leaves out $(0,d-1,0)$ and $(0,d,0)$.

In both cases, the vertex of the curve from which the vertical end of weight two starts, will be below the line on which the points from the point conditions are distributed. That means that if the triangle has three points in the lattice path, an alignment can only be possible via a left string. However, considering the IUA-representative of the polytope above, we see that this is not possible for $1 = b < a$.

If the triangle only has two points in the lattice path, it must be in the position $y = d$. In this case, the left out points in the path lead to a $Y-$formed string whose vertex needs to be aligned with the edge dual to $\mathcal{S}_1 \cap \tilde{\Omega}$. The only vertex that is free to move to achieve the alignment is the vertex of the $Y-$formed string. This vertex lies below the line on which the points Q_i from the point conditions are distributed. However, the edge dual to $\mathcal{S}_1 \cap \tilde{\Omega}$, with which the vertex has to align, is relatively close to that line but with y-coordinate much larger. This makes an alignment impossible.

If the edge of length 2 in $\tilde{\Omega}$ is diagonal, it has to be dual to a diagonal end of weight 2 in the tropical floor plan. The triangle containing this edge in the dual subdivision contains either a vertical or a horizontal edge. If the triangle contains a vertical edge, the midpoint of the edge of length two has to be the only lattice point from the triangle that is left out of the lattice path. It follows that the vertex in the floor plan dual to the triangle is fixed, and lies above the line on which the points from the point conditions are distributed. This implies that an alignment between the two floors is only possible via a left string in the neighboring curve C_{d-1}. However, that end of the left string, which would align with the vertex, is the horizontal end. Such an alignment leads to a polytope IUA-equivalent to a polytope of family 12 in the dual subdivision, and by Proposition 9.2.4 we know that this is not binodal.

It follows that the triangle needs to be the right tip of $d\Delta_3$ because this is the only way to get a horizontal edge for the triangle. In this position the second lattice point of the triangle cannot be part of the lattice path. We apply IUA-equivalences to bring $\Omega_{a,b}^{(14)}$ in this position:

$$
\tilde{\Omega} = \begin{pmatrix} 0 & 0 & 0 & 0 & 1 & 1 \\ d-2 & d-1 & d-1 & d & 0 & b \\ 2 & 0 & 1 & 0 & a+b & 0 \end{pmatrix}.
$$

The point conditions enforce $b = 1$, because the lattice path restricted to $\mathcal{S}_1$ is smooth and therefore this floor subdivision is column-wise. Since we have already determined that the lattice path needs to leave out two points in the triangle, we can move the vertex in C_d dual to the triangle in (2,1)-direction. This vertex is above the line on which the points from the point conditions are distributed.

Therefore, it can never be aligned with any bounded edge in C_{d-1} that corresponds to the edge $\tilde{\Omega} \cap \{x = 1\}$ for $b = 1$, $a \geq 4$.

If the edge of length 2 is vertical, it is dual to a horizontal edge of weight 2 in the floor plan. This edge can be bounded or unbounded depending on whether the edge is in the boundary of $d\Delta_3$. Applying IUA-equivalence we obtain two representatives, which fit into the subdivision:

$$\begin{pmatrix} 0 & 0 & 0 & 0 & 1 & 1 \\ 0 & 0 & 0 & 1 & 0 & a \\ z-2 & z-1 & z & 0 & az-(a+b) & 0 \end{pmatrix} \text{ or } \begin{pmatrix} 0 & 0 & 0 & 0 & 1 & 1 \\ 0 & 1 & 1 & 1 & 0 & a \\ z & 0 & 1 & 2 & b+a(d-1) & 0 \end{pmatrix},$$

where $z \leq d$. For both choices for $\tilde{\Omega}$ we see that $\tilde{\Omega} \cap \{x = 1\}$ cannot be made to fit between two columns. However, an alignment of the vertex dual to the triangle and the edge dual to $\tilde{\Omega} \cap \{x = 1\}$ that fits together with the lattice path is only possible if $\tilde{\Omega} \cap \{x = 1\}$ has width 1. So this case is not possible.

Family 21

Polytopes of family 21 have no parallel edges. The existence of parallel edges is not influenced by IUA-equivalences. Therefore, any polytope that is IUA-equivalent to a polytope of family 21 has no pair of parallel edges.

With just two lattice points that can be left out, it is impossible to fit two triangles into adjacent floor subdivisions such that they have no parallel edges, and such that the point conditions allow an alignment of their dual vertices in the floor plan. As long as all floor subdivisions are column-wise, this follows directly.

Leaving out only two lattice points from the lattice path in $d\Delta_3$, we cannot fit a triangle in a floor subdivision such that it does not have either a vertical or a diagonal edge. In the adjacent floor subdivision the alignment needs to be done with a string or double string, depending on how many lattice points we can still leave out. However, the triangle dual to the vertex that aligns in a (double) string always has a diagonal and a vertical edge. Thus, even if the point conditions allow an alignment, we always have parallel edges, so the emerging polytope will not belong to family 21. □

Remark 10.1.5. For multi-nodal tropical surfaces with more than two nodes passing through points in Mikhalkin position the above arguments do not necessarily apply. It is therefore possible that polytopes IUA-equivalent to polytopes of the families 8, 14 or 21 appear in subdivisions dual to such surfaces.

To keep notation short, we say a polytope *belongs to family m* or *is of family m* if it is IUA-equivalent to a polytope of family number m as in Table 9.1.

In the following sections we deal with each of the remaining three binodal polytope families one by one. We summarize the results in the following theorem:

Theorem 10.1.6. *Of the binodal polytopes with* 6 *lattice points of width* 1 *only polytopes belonging to the families with numbers* 10, 13 *and* 20 *can appear in the dual subdivision of a floor decomposed binodal surface of degree d through n points in Mikhalkin position. They can only appear if* $d > 4$.

Proof. This follows from Propositions 10.1.7, 10.1.10 and 10.1.13. □

For each polytope family we first determine the options how we can use IUA-equivalences to get the polytope in a dual subdivision of a floor decomposed tropical binodal surface passing through points in Mikhalkin position. Then, we find the possible lattice paths, prove that they are valid and compute their multiplicities using `OSCAR`. From this data we pose a general conjecture for each path.

10.1.1 Polytope family 10

Proposition 10.1.7. *Let S be a floor decomposed tropical binodal surface of degree d passing through points in Mikhalkin position. Then, the dual subdivision $\mathcal{S}$ to S can only contain a polytope of family 10 if $d \geq 5$.*
We distinguish three different positions, which are shown in Table 10.1.

Proof. Let Ω be a binodal polytope of polytope family 10. The IUA-representative of Ω in Figure 9.6 in Chapter 9 satisfies that its intersection with $\{x = 1\}$ is a sloped edge from the point (1,0,0) to the point (1,a,b), where $a \geq b > 0$.

We know that when a floor decomposed binodal surface S passes through points in Mikhalkin position there are only few possibilities for the floor subdivisions to be not column-wise. Considering these options we deduce that $b = 1$ for any IUA-equivalence of Ω to appear in a floor decomposed surface.

We use the facets of Ω to make a case distinction to cover all options: the unique facet of Ω that is a parallelogram is either contained in a floor subdivision or between two floor subdivisions.

If the parallelogram is contained between two floor subdivisions, it arises from the alignment of two vertices of the two corresponding plane curves. In order to induce a parallelogram the two aligning vertices must have an outgoing edge of the same direction. Moreover, when investigating the combinatorics of Ω, we observe that the two triangles in the two floor subdivisions of Ω have only one pair of parallel edges. This is the pair that forms the parallelogram. We argue that these two edges have to be vertical. The two triangles in the floor subdivisions of $d\Delta_3$ that belong to Ω are of minimal lattice volume. Assume the triangles both do not have a vertical edge. We can only obtain such triangles in the subdivision induced

on $d\Delta_3$ by the points in Mikhalkin position if the lattice path leaves out a point on the diagonal boundary. But then, we do not have enough degrees of freedom left to obtain an alignment in the tropical floor plan that leads to the binodal polytope of family 10. Hence, the edges forming the parallelogram have to be vertical.

We can align two vertices of adjacent floors either by fixing one vertex and leaving the other vertex two degrees of freedom, or by leaving one degree of freedom to both vertices. Since the alignment of a left and right string does yield a polytope of family 9, which is not binodal, we know that at least one of the two triangles does not correspond to a right or left string. But a vertex in a floor that does not correspond to a left or right string and that is not determined by the point conditions can have only a limited area of movement because the surrounding vertices of the curve are fixed by the point conditions. Thus, the alignment of the two vertices corresponding to the triangles of Ω is not possible.

Leaving two degrees of freedom to one vertex such that it can be moved to align with the other vertex is only possible when we have a double right string. Applying IUA-equivalences we can move Ω into such a position in $d\Delta_3$:

$$\begin{pmatrix} 0 & 0 & 0 & 1 & 1 & 1 \\ d-1 & d-1 & d & y & y & y+1 \\ 0 & 1 & 0 & a & a+1 & 0 \end{pmatrix},$$

where we assume without loss of generality that the polytope is contained between the 0th and the 1st floor, and y is a parameter for the column in the higher floor. The generic version of the IUA-representative can be found in Table 10.1. Figure 10.2 shows this for $a = 3$, $y = 0$ and $d = 5$.

A polytope of family 10 with $b = 1$ is only binodal if $a \geq 3$, so we conclude $d \geq 5$.

We denote this position of Ω by $\tilde{\Omega}_I^{(10)}$ and the polytope by $\tilde{\Omega}_I^{(10)}(a,d,f,y)$, where f stands for the degree of the floor containing the double right string.
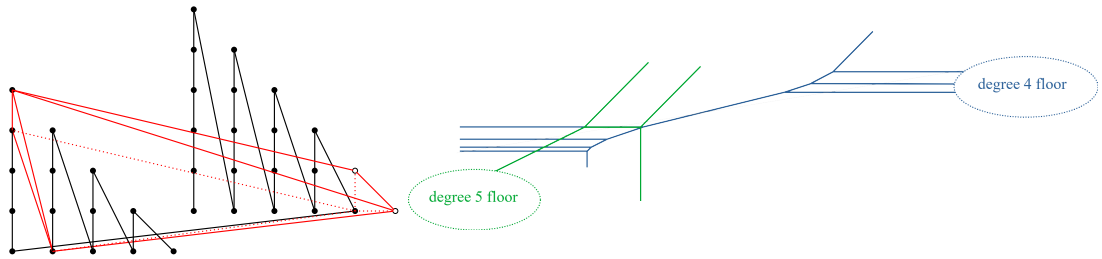
Figure 10.2: Polytope of family 10 in $5\Delta_3$ in position $\tilde{\Omega}_I^{(10)}$

If the parallelogram is contained in one of the floor subdivisions, it comes from the alignment of an edge of an adjacent floor with the 4-valent vertex dual to the parallelogram.

The parallelogram arises from a left out lattice point and the folding out of a corner. This means that we have one more lattice point that we can leave out to make the alignment possible. An additional left out point in the parallelogram does not give enough freedom to the vertex to move the relatively far way towards the next floor. It follows that the alignment has to happen via a left or right string. Hence, the edge in $\Omega \cap \{x = 1\}$ needs to be transformed to either the diagonal edge of the right string or the vertical edge of the left string.

If $\Omega \cap \{x = 1\}$ is the vertical edge of the left string, the parallelogram cannot have vertical edges, since this would be a polytope of family 9. Thus, due to the point conditions, the parallelogram must have either a pair of horizontal or a pair of diagonal edges. We obtain the following two IUA-representatives under these conditions:

$$\begin{pmatrix} 0 & 0 & 0 & 0 & 1 & 1 \\ 0 & 1 & a & a+1 & 0 & 0 \\ 1 & 1 & 0 & 0 & 0 & 1 \end{pmatrix} \text{ or } \begin{pmatrix} 0 & 0 & 0 & 0 & 1 & 1 \\ 0 & 1 & a & a+1 & 0 & 0 \\ 2+a & a+1 & 1 & 0 & 0 & 1 \end{pmatrix}.$$

In both cases the parallelogram is in a position that cannot be contained in the subdivision with our choice of point conditions since $a \geq 3$.

It follows that the alignment must be due to a right string. Because of the point conditions and the fact that the edges of the parallelogram cannot be parallel to the edge dual to the diagonal end of the right string, it follows that the parallelogram has a pair of vertical parallel edges. Such a parallelogram appears from the folding out of an edge when a lattice point at the top or bottom of a column is left out. Applying IUA-equivalences we obtain the two positions:

$$\begin{pmatrix} 0 & 0 & 1 & 1 & 1 & 1 \\ d-1 & d & y & y & y+1 & y+1 \\ 1 & 0 & d-2 & d-1 & d-a-3 & d-a-2 \end{pmatrix},$$

$$\text{and } \begin{pmatrix} 0 & 0 & 1 & 1 & 1 & 1 \\ d-1 & d & y & y & y+1 & y+1 \\ 1 & 0 & a+1 & a+2 & 0 & 1 \end{pmatrix},$$

where $y \in \mathbb{N}_0$ is a parameter for the column that contains the parallelogram. Here we assume that the poltope Ω is contained between the 0th and the 1st floor. The generic representatives can be found in Table 10.1. We denote the first of these positions $\tilde{\Omega}_{II}^{(10)}$ and the second $\tilde{\Omega}_{III}^{(10)}$, and add the parameters (a,d,f,y) if we want to speak of a specific polytope in this position. Figure 10.3 shows position $\tilde{\Omega}_{II}^{(10)}$ for $a = 3$, $y = 0$, $f = 5$ and $d = 6$. In this case the positions $\tilde{\Omega}_{II}^{(10)}$ and $\tilde{\Omega}_{III}^{(10)}$ coincide. The difference is given by the lattice path: For $\tilde{\Omega}_{III}^{(10)}$ the lattice path would follow

the upper part of the parallelogram instead of the lower part, passing through $(1,0,5)$ and leaving out $(1,1,0)$. Since the polytopes from family 10 with $b = 1$ are only binodal for $a \geq 3$, it follows that $d \geq 6$. $\qquad\qquad\qquad\qquad\square$
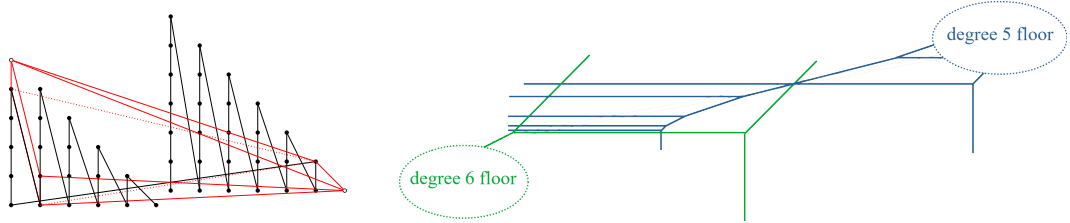
Figure 10.3: Polytope of family 10 in $6\Delta_3$ in position $\tilde{\Omega}_{II}^{(10)}$

$\tilde{\Omega}_{\mathbf{I}}^{\mathbf{(10)}}(\mathbf{a,d,f,y})$					
$d-(f+1)$	$d-(f+1)$	$d-(f+1)$	$d-f$	$d-f$	$d-f$
f	f	$f+1$	y	y	$y+1$
0	1	0	a	$a+1$	0
Example: $\tilde{\Omega}_{I}^{(10)}(3,5,4,0)$ in Figure 10.2					
$\tilde{\Omega}_{\mathbf{II}}^{\mathbf{(10)}}(\mathbf{a,d,f,y})$					
$d-(f+1)$	$d-(f+1)$	$d-f$	$d-f$	$d-f$	$d-f$
f	$f+1$	y	y	$y+1$	$y+1$
1	0	$f-y-1$	$f-y$	$f-y-a-2$	$f-y-a-1$
Example: $\tilde{\Omega}_{II}^{(10)}(3,6,4,0)$ in Figure 10.2					
$\tilde{\Omega}_{\mathbf{III}}^{\mathbf{(10)}}(\mathbf{a,d,f,y})$					
$d-(f+1)$	$d-(f+1)$	$d-f$	$d-f$	$d-f$	$d-f$
f	$f+1$	y	y	$y+1$	$y+1$
1	0	$a+1$	$a+2$	0	1
Example: $\tilde{\Omega}_{III}^{(10)}(3,6,4,0)$ in Figure 10.2					

Table 10.1: The three types of possible positions for a polytope belonging to family 10 to appear in the dual subdivision of a binodal surface of degree d through points in Mikhalkin position. The parameters have the following meaning: f is the degree of the floor containing the main part of the polytope, y is the value that can be obtained in the y-coordinate and a is the parameter of the polytope family.

We have already seen possible lattice paths for the three positions in the proof of Proposition 10.1.7. It is enough to show that these lattice paths are locally

valid, i.e., we only have to consider the binodal polytope without the remaining subdivision of $d\Delta_3$.

Proposition 10.1.8. *For each of the three positions of a polytope belonging to family* 10 *in Table 10.1 there is one valid lattice path that agrees with the lattice path for $d\Delta_3$:*

$$\Gamma_{1,2}(\tilde{\Omega}_I^{(10)}), \ \Gamma_{1,3}(\tilde{\Omega}_{II}^{(10)}), \ \Gamma_{1,4}(\tilde{\Omega}_{III}^{(10)}).$$

Note that there are polytopes that can be at the same time in position $\tilde{\Omega}_{II}^{(10)}$ and $\tilde{\Omega}_{III}^{(10)}$; see Figure 10.3.

Proof. We know these three lattice paths from the proof of Proposition 10.1.7, where we have seen that these are the only possible paths agreeing with the point conditions in Mikhalkin position for a floor decomposed binodal tropical surface. I remains to show that they are valid lattice paths.

We use IUA-equivalences that preserve the order of the lattice points to obtain representatives of the three polytopes that are minimal with respect to the lattice points, but still in the positive orthant of $\mathbb{R}^3$. This polytope does depend on a but it will no longer depend on d, f and y. We thus consider

$$\tilde{\Omega}_I^{(10)}(a) = \begin{pmatrix} 0 & 0 & 0 & 1 & 1 & 1 \\ 0 & 0 & 1 & 0 & 0 & 1 \\ 0 & 1 & 0 & a & a+1 & 0 \end{pmatrix}.$$

For this polytope we can apply the same methods as in Proposition 9.4.8. Let ω_i denote the lattice points of $\tilde{\Omega}_I^{(10)}(a)$ in the order as given above. The path $\Gamma_{1,2}(\tilde{\Omega}_I^{(10)}(a))$ passes through the 2-dimensional cells of S given by $(\overline{\omega_0\omega_3})^\vee$, $(\overline{\omega_3\omega_4})^\vee$ and $(\overline{\omega_4\omega_5})^\vee$. We can compute the rays spanning these cones as described in Remark 9.3.6. We obtain the following system of linear equations:

$$\begin{pmatrix} 0 \\ 0 \\ 0 \end{pmatrix} = \begin{pmatrix} x \\ y \\ z \end{pmatrix} + \alpha_1 \begin{pmatrix} 0 \\ -1 \\ 0 \end{pmatrix} + \alpha_2 \begin{pmatrix} 0 \\ -a \\ -1 \end{pmatrix}, \ \alpha_1, \alpha_2 > 0,$$

$$\begin{pmatrix} 1 \\ \eta \\ \eta^2 \end{pmatrix} = \begin{pmatrix} x \\ y \\ z \end{pmatrix} + \beta_1 \begin{pmatrix} 0 \\ -1 \\ 0 \end{pmatrix} + \beta_2 \begin{pmatrix} 1 \\ 0 \\ 0 \end{pmatrix}, \ \beta_1, \beta_2 > 0,$$

$$\begin{pmatrix} \lambda \\ \lambda\eta \\ \lambda\eta^2 \end{pmatrix} = \begin{pmatrix} x \\ y \\ z \end{pmatrix} + \gamma_1 \begin{pmatrix} 1 \\ 0 \\ 0 \end{pmatrix} + \gamma_2 \begin{pmatrix} 0 \\ a+1 \\ 1 \end{pmatrix}, \ \gamma_1, \gamma_2 > 0.$$

This system has the solution:

$$x = 0,$$
$$y = \lambda\eta - (a+1)(\lambda-1)\eta^2,$$
$$z = \alpha_2 = \eta^2 > 0,$$
$$\alpha_1 = \lambda\eta - (a+1)(\lambda-1)\eta^2 - a\eta^2 > 0,$$
$$\beta_1 = (\lambda-1)(\eta - (a+1)\eta^2) > 0,$$
$$\beta_2 = 1 > 0,$$
$$\gamma_1 = \lambda > 0,$$
$$\gamma_2 = (\lambda-1)\eta^2 > 0.$$

which satisfies all the conditions, provided $\frac{1}{a+1} > \eta$. So, the path $\Gamma_{1,2}(\tilde{\Omega}_I^{(10)}(a))$ is valid.

For position the IUA-equivalence gives us the following representative:

$$\tilde{\Omega}_{II}^{(10)}(a) = \begin{pmatrix} 0 & 0 & 1 & 1 & 1 & 1 \\ 0 & 1 & 0 & 0 & 1 & 1 \\ 1 & 0 & a+1 & a+2 & 0 & 1 \end{pmatrix}.$$

We denote by ω_i the lattice points of $\tilde{\Omega}_{II}^{(10)}(a)$ in the order as given above. We can apply the same methods as in Proposition 9.4.8.

The path $\Gamma_{1,3}(\tilde{\Omega}_{II}^{(10)}(a))$ passes through the 2-dimensional cells of S given by $(\overline{\omega_0\omega_2})^\vee$, $(\overline{\omega_2\omega_4})^\vee$ and $(\overline{\omega_4\omega_5})^\vee$. We can compute the rays spanning these cones as described in Remark 9.3.6 and obtain the following system of linear equations:

$$\begin{pmatrix} 0 \\ 0 \\ 0 \end{pmatrix} = \begin{pmatrix} x \\ y \\ z \end{pmatrix} + \alpha_1 \begin{pmatrix} 0 \\ -1 \\ 0 \end{pmatrix} + \alpha_2 \begin{pmatrix} 0 \\ -(a+1) \\ -1 \end{pmatrix}, \ \alpha_1,\alpha_2 > 0,$$

$$\begin{pmatrix} 1 \\ \eta \\ \eta^2 \end{pmatrix} = \begin{pmatrix} x \\ y \\ z \end{pmatrix} + \beta_1 \begin{pmatrix} a \\ -(a+1) \\ -1 \end{pmatrix} + \beta_2 \begin{pmatrix} 1 \\ 0 \\ 0 \end{pmatrix}, \ \beta_1,\beta_2 > 0,$$

$$\begin{pmatrix} \lambda \\ \lambda\eta \\ \lambda\eta^2 \end{pmatrix} = \begin{pmatrix} x \\ y \\ z \end{pmatrix} + \gamma_1 \begin{pmatrix} 1 \\ 0 \\ 0 \end{pmatrix} + \gamma_2 \begin{pmatrix} 0 \\ 1 \\ 0 \end{pmatrix}, \ \gamma_1,\gamma_2 > 0.$$

This system has the solution:

$$x = 0,$$

$$y = \eta + (a+1)(\lambda - 1)\eta^2,$$
$$z = \alpha_2 = \lambda\eta^2 > 0,$$
$$\alpha_1 = \eta - (a+1)\eta^2 > 0,$$
$$\beta_1 = (\lambda - 1)\eta^2 > 0,$$
$$\beta_2 = 1 - a(\lambda - 1)\eta^2 > 0,$$
$$\gamma_1 = \lambda > 0,$$
$$\gamma_2 = (\lambda - 1)(\eta - (a+1)\eta^2) > 0.$$

which satisfies all the conditions, provided $\frac{1}{a+1} > \eta$. Therefore, the path $\Gamma_{1,3}(\tilde{\Omega}_{II}^{(10)}(a))$ is valid.

Under the IUA-equivalence that moves the polytopes to their minimal positive representative, we have $\tilde{\Omega}_{II}^{(10)}(a) = \tilde{\Omega}_{III}^{(10)}(a)$.

The path $\Gamma_{1,4}(\tilde{\Omega}_{III}^{(10)}(a))$ passes through the 2-dimensional cells of S given by $(\overline{\omega_0\omega_2})^\vee$, $(\overline{\omega_2\omega_3})^\vee$ and $(\overline{\omega_3\omega_5})^\vee$. We obtain the following system of linear equations:

$$\begin{pmatrix} 0 \\ 0 \\ 0 \end{pmatrix} = \begin{pmatrix} x \\ y \\ z \end{pmatrix} + \alpha_1 \begin{pmatrix} 0 \\ -1 \\ 0 \end{pmatrix} + \alpha_2 \begin{pmatrix} a \\ -(a+1) \\ -1 \end{pmatrix}, \ \alpha_1, \alpha_2 > 0,$$

$$\begin{pmatrix} 1 \\ \eta \\ \eta^2 \end{pmatrix} = \begin{pmatrix} x \\ y \\ z \end{pmatrix} + \beta_1 \begin{pmatrix} 0 \\ -1 \\ 0 \end{pmatrix} + \beta_2 \begin{pmatrix} 1 \\ 0 \\ 0 \end{pmatrix}, \ \beta_1, \beta_2 > 0,$$

$$\begin{pmatrix} \lambda \\ \lambda\eta \\ \lambda\eta^2 \end{pmatrix} = \begin{pmatrix} x \\ y \\ z \end{pmatrix} + \gamma_1 \begin{pmatrix} 1 \\ 0 \\ 0 \end{pmatrix} + \gamma_2 \begin{pmatrix} -1 \\ a+1 \\ 1 \end{pmatrix}, \ \gamma_1, \gamma_2 > 0.$$

This system has the solution:

$$x = -a\eta^2,$$
$$y = \lambda\eta - (a+1)(\lambda - 1)\eta^2,$$
$$z = \alpha_2 = \eta^2 > 0,$$
$$\alpha_1 = \lambda(\eta - (a+1)\eta^2) > 0,$$
$$\beta_1 = (\lambda - 1)(\eta - (a+1)\eta^2) > 0,$$
$$\beta_2 = 1 + a\eta^2 > 0,$$
$$\gamma_1 = \lambda + (a + \lambda - 1)\eta^2 > 0,$$
$$\gamma_2 = (\lambda - 1)\eta^2 > 0,$$

which satisfies all the conditions, provided $\frac{1}{a+1} > \eta$. So, the path $\Gamma_{1,4}(\tilde{\Omega}_{III}^{(10)}(a))$ is valid. $\qquad\qquad\qquad\qquad\qquad\qquad\qquad\qquad\qquad\qquad\qquad\qquad\square$

As the changes from $\tilde{\Omega}_I^{(10)}(a)$ to $\tilde{\Omega}_I^{(10)}(a,d,f,y)$ did not change the order of the lattice points with respect to the induced partial order, nor the polytope of family 10 that the polytope is equivalent to, the lattice path and its multiplicities are preserved. The same holds for $\tilde{\Omega}_{II}^{(10)}(a,d,f,y)$ and $\tilde{\Omega}_{III}^{(10)}(a,d,f,y)$. Therefore, the lattice paths as determined in Proposition 10.1.8 can be used to compute the multiplicities of the three positions of a polytope of family 10 in $d\Delta_3$.

Conjecture 10.1.9. *The multiplicity of the lattice paths depends only on a and is given by*

$$mult(\Gamma_{1,2}(\tilde{\Omega}_I^{(10)}(a))) = mult(\Gamma_{1,2}(\tilde{\Omega}_{II}^{(10)}(a))) = mult(\Gamma_{1,2}(\tilde{\Omega}_{III}^{(10)}(a))) = a - 2.$$

This conjecture is verified for $3 \leq a \leq 7$ by using [Gei22] in `OSCAR`. The computed values are collected in Table 10.2.

lattice path	$a = 3$	$a = 4$	$a = 5$	$a = 6$	$a = 7$
$\Gamma_{1,2}(\tilde{\Omega}_I^{(10)}(a))$	1	2	3	4	5
$\Gamma_{1,3}(\tilde{\Omega}_{II}^{(10)}(a))$	1	2	3	4	5
$\Gamma_{1,4}(\tilde{\Omega}_{III}^{(10)}(a))$	1	2	3	4	5

Table 10.2: Verified multiplicities for polytope 10 in $d\Delta_3$

10.1.2 Polytope family 13

Proposition 10.1.10. *Let S be a floor decomposed tropical binodal surface of degree d passing through points in Mikhalkin position. Then, the dual subdivision $\mathcal{S}$ to S can only contain a polytope of family 13 if $d \geq 7$.*

In this case the edge of length 2 of the polytope has to be a vertical edge of the subdivision. We distinguish two positions which are shown in Table 10.3.

Proof. Let Ω be a polytope belonging to family 13. Then Ω has a unique edge of length 2. The procedure is similar to the proof of Proposition 10.1.4: We make a case distinction by the direction of the edge of length 2. With the same argument as for the polytope family 14 in the proof of Proposition 10.1.4, we conclude that the edge of length 2 can only be either vertical, horizontal or diagonal due to the point conditions in Mikhalkin position.

If the edge of length 2 is horizontal, it has to be contained in the boundary of $d\Delta_3$, so in the tropical floor plan it is dual to a vertical weight 2 end. In this

case the edge opposite the triangle in Ω is of direction $(0,a,b)$ with $0 < b < a$ with $gcd(a,b) = 1$. This never fits between two columns in a floor subdivision. Since we know that the middle lattice point of the edge of length two can never be part of the lattice path we can only leave out one more lattice point from the path. This does not give us any options to fit an edge of the above mentioned direction into a floor subdivision in agreement with the lattice path.

If the edge of length 2 is diagonal, it has to be dual to a diagonal end of weight 2 in the tropical floor plan. The triangle containing this edge in the dual subdivision contains either a vertical or a horizontal end. If the triangle contains a vertical edge, the midpoint of the edge of length two is the only lattice point from the triangle left out of the lattice path. It follows that the vertex in the floor plan from which the diagonal end of weight 2 starts is fixed. Moreover, the vertex lies in the tropical floor plan above the line on which the points from the point conditions are distributed. Similarly to the arguments for polytope family 14 in the proof of Proposition 10.1.4, we obtain a polytope of family 12 instead, so this case is not possible.

It remains to consider the case where the triangle contains a horizontal edge. This is only possible if the triangle with the edge of length 2 is positioned at the right tip of $d\Delta_3$. We apply IUA-equivalences to bring Ω in this position:

$$\begin{pmatrix} 0 & 0 & 0 & 0 & 1 & 1 \\ d-2 & d-1 & d-1 & d & 0 & a \\ 2 & 0 & 1 & 0 & a+b & 0 \end{pmatrix},$$

where we assume that Ω is contained between the 0th and the 1st floor. Due to the point conditions, the edge of Ω that would be in $\mathcal{S}_1$ does not agree with the lattice path: We can only leave out one lattice point in the path restricted to $\mathcal{S}_1$, this does not allow for an edge of direction $(a, -a - b)$ with $a + b \geq 5$, $a > b > 0$. So this case is not possible.

If the edge of length 2 is vertical, it is dual to a horizontal edge of weight 2 in the tropical floor plan. This edge can be bounded or unbounded depending on whether the edge is in the boundary of $d\Delta_3$. Considering the polytope Ω belonging to family 13, we observe that the edge opposite to the triangle with the edge of length 2 can only be contained between two columns if $b = 1$. If that edge is not contained between two columns in the floor subdivision, the edge stands in conflict with the lattice path unless we leave out more than two lattice points in total from the path. That would contradict the number of point conditions. So we know $b = 1$.

We first exclude the case that the lattice path passes only through two of the vertices of the triangle containing the edge of length 2. In this case the edge of length 2 has to be the boundary of $d\Delta_3$. Since it is a vertical edge, this means it has y-coordinate zero. It follows that the edge either has z coordinates $0, 1, 2$ (we

say it is at the bottom) or the maximal values possible in the corresponding floor subdivision (we say it is at the top).

If it is at the top, the vertex dual to the triangle is above the line containing the points from the conditions in the tropical floor plan. Moreover, we can only move the vertex along the direction of the edge dual to the bottom edge of the triangle and the movement is restricted due to the surrounding point conditions. This does not allow enough freedom to align the vertex with an edge of an adjacent floor.

If the edge of length two is at the bottom, the vertex dual to the triangle is below the line containing the points from the conditions. Moreover, we can only move the vertex in the tropical floor plan along the direction $(-2, -1)$. Since the slope of the line containing the points from the point conditions is very small and the points are distributed with growing distances it is not possible to align the vertex with an edge of the adjacent floors.

It follows that the lattice path contains all three vertices of the triangle containing the edge of length 2. This means that an alignment is only possible via a right or left string. For a left string the end aligning with the triangle has the same direction as the weight 2 edge. This leads to a polytope from family 11, which is not binodal (Proposition 9.2.3). So the alignment happens via a right string.

With this alignment, the relative positions of 4 vertices are fixed, and after applying IUA-equivalence we obtain two representatives for the containment of Ω in $d\Delta_3$:

$$\begin{pmatrix} 1 & 1 & 1 & 1 & 0 & 0 \\ 1 & 0 & 0 & 0 & d-1 & d \\ 0 & a & a+1 & a+2 & 1 & 0 \end{pmatrix}$$

$$\text{and} \begin{pmatrix} 1 & 1 & 1 & 1 & 0 & 0 \\ 0 & 1 & 1 & 1 & d-1 & d \\ d-1 & d-a-3 & d-a-2 & d-a-1 & 1 & 0 \end{pmatrix},$$

where a is the parameter of the polytope family. We denote the first of these positions $\tilde{\Omega}_I^{(13)}$ and the second $\tilde{\Omega}_{II}^{(13)}$, and add the parameters (a,d,f,y) if we want to speak of a specific polytope in this position. Figure 10.4 shows both positions for the parameters $a = 4$, $y = 0$, $f = 6$ and $d = 7$.

The positions in the two matrices above are exemplary: We assume Ω to be contained between the 0th and 1st floor and that the triangle with the edge of length two is contained in the highest column of the floor subdivision. The same can be achieved for different floor subdivisions and different columns, as long as the minimum of the absolute values of the slopes of the non-vertical edges of the triangle of volume 2 is at least 4. This is because for $b = 1$, polytopes of family 13 are only binodal for $4 \leq a$. The generic representatives can be found in Table 10.3. For both positions, we conclude that $d \geq 7$. □

(a) Polytope of family 13 in $7\Delta_3$ in position $\tilde{\Omega}_I^{(13)}$

(b) Polytope of family 13 in $7\Delta_3$ in position $\tilde{\Omega}_{II}^{(13)}$
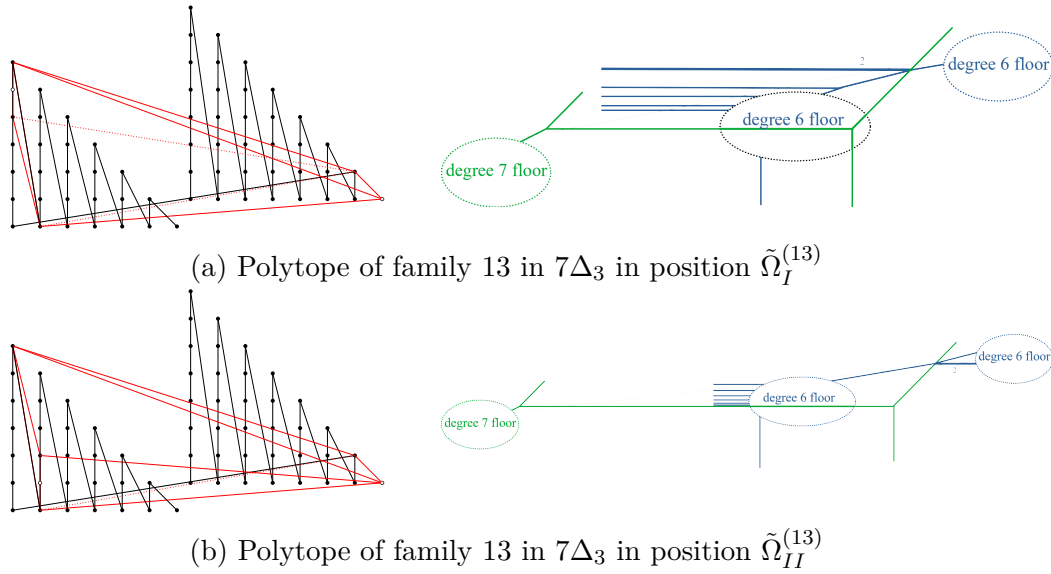
Figure 10.4: The two positions for Polytope 13 contained in $7\Delta_3$

In the proof of Proposition 10.1.10, we have seen possible lattice paths for the two positions. As for polytopes of family 10 in Section 10.1.1 it is enough to show that these lattice paths are locally valid. Consequently, we only have to consider the binodal polytope without the remaining subdivision of $d\Delta_3$.

Proposition 10.1.11. *For each of the two positions of a polytope belonging to family* 13 *in Table 10.3 there is one valid lattice path that agrees with the lattice path for $d\Delta_3$:*

$$\Gamma_{1,3}(\tilde{\Omega}_I^{(13)}), \Gamma_{1,4}(\tilde{\Omega}_{II}^{(13)}).$$

Proof. We know the two lattice paths from the proof of Proposition 10.1.10, where we have seen that these are the only possible paths agreeing with the point conditions in Mikhalkin position for a floor decomposed binodal tropical surface. I remains to show that they are valid lattice paths.

We use IUA-equivalences that preserve the order of the lattice points to obtain representatives of the two polytopes contained in the positive orthant of $\mathbb{R}^3$ and minimal with respect to the lattice points. This polytopes depend on a but they will no longer depend on d, f and y. We start with

$$\tilde{\Omega}_I^{(13)}(a) = \begin{pmatrix} 0 & 0 & 1 & 1 & 1 & 1 \\ 0 & 1 & 0 & 0 & 0 & 1 \\ 1 & 0 & a & a+1 & a+2 & 0 \end{pmatrix}.$$

For this polytope we can apply the same methods as in Proposition 9.4.12. We

$\tilde{\Omega}_{\mathbf{I}}^{(\mathbf{13})}(\mathbf{a,d,f,y})$					
$d-(f+1)$	$d-(f+1)$	$d-f$	$d-f$	$d-f$	$d-f$
f	$f+1$	y	y	y	$y+1$
1	0	a	$a+1$	$a+2$	0

Example: $\tilde{\Omega}_{I}^{(13)}(3,7,6,0)$ in Figure 10.4a

$\tilde{\Omega}_{\mathbf{II}}^{(\mathbf{13})}(\mathbf{a,d,f,y})$					
$d-(f+1)$	$d-(f+1)$	$d-f$	$d-f$	$d-f$	$d-f$
f	$f+1$	y	$y+1$	$y+1$	$y+1$
1	0	$f-y$	$f-y-a-2$	$f-y-a-1$	$f-y-a$

Example: $\tilde{\Omega}_{II}^{(13)}(3,7,6,0)$ in Figure 10.4b

Table 10.3: The two types of possible positions for a polytope belonging to family 13 to appear in the dual subdivision of a binodal surface of degree d through points in Mikhalkin position. The parameters have the following meaning: f is the degree of the floor containing the main part of the polytope, y is the value that can be obtained in the y-coordinate and a is the parameter of the polytope family.

denote by ω_i the lattice points of $\tilde{\Omega}_I^{(13)}(a)$ in the order as given above.

The path $\Gamma_{1,3}(\tilde{\Omega}_I^{(13)})$ passes through the 2-dimensional cells of S given by $(\overline{\omega_0\omega_2})^\vee$, $(\overline{\omega_2\omega_4})^\vee$ and $(\overline{\omega_4\omega_5})^\vee$. We compute the directions of the rays spanning the cones associated to the facets and obtain the following system of linear equations from the point conditions:

$$\begin{pmatrix} 0 \\ 0 \\ 0 \end{pmatrix} = \begin{pmatrix} x \\ y \\ z \end{pmatrix} + \alpha_1 \begin{pmatrix} 0 \\ -1 \\ 0 \end{pmatrix} + \alpha_2 \begin{pmatrix} a-1 \\ -a \\ -1 \end{pmatrix}, \ \alpha_1, \alpha_2 > 0,$$

$$\begin{pmatrix} 1 \\ \eta \\ \eta^2 \end{pmatrix} = \begin{pmatrix} x \\ y \\ z \end{pmatrix} + \beta_1 \begin{pmatrix} 0 \\ -1 \\ 0 \end{pmatrix} + \beta_2 \begin{pmatrix} 1 \\ 0 \\ 0 \end{pmatrix}, \ \beta_1, \beta_2 > 0,$$

$$\begin{pmatrix} \lambda \\ \lambda\eta \\ \lambda\eta^2 \end{pmatrix} = \begin{pmatrix} x \\ y \\ z \end{pmatrix} + \gamma_1 \begin{pmatrix} 1 \\ 0 \\ 0 \end{pmatrix} + \gamma_2 \begin{pmatrix} 0 \\ a+2 \\ 1 \end{pmatrix}, \ \gamma_1, \gamma_2 > 0.$$

This system has the solution:

$$x = (1-a)\eta^2,$$
$$y = \lambda\eta - (a+2)(\lambda-1)\eta^2,$$

$$z = \alpha_2 = \eta^2 > 0,$$
$$\alpha_1 = \lambda\eta - (a+2)\lambda\eta^2 + 2\eta^2 > 0,$$
$$\beta_1 = (\lambda - 1)(\eta - (a+2)\eta^2) > 0,$$
$$\beta_2 = 1 + (a-1)\eta^2 > 0,$$
$$\gamma_1 = \lambda + (a-1)\eta^2 > 0,$$
$$\gamma_2 = (\lambda - 1)\eta^2 > 0,$$

which satisfies all the conditions, provided $\frac{1}{a+2} > \eta$. This can be satisfied without violating the genericity of our point conditions because $1 \gg \eta > 0$. Therefore, the path $\Gamma_{1,3}(\tilde{\Omega}_I^{(13)})$ is valid.

For the second position we obtain the IUA-representative

$$\tilde{\Omega}_{II}^{(13)}(a) = \begin{pmatrix} 0 & 0 & 1 & 1 & 1 & 1 \\ 0 & 1 & 0 & 1 & 1 & 1 \\ 1 & 0 & a-2 & 0 & 1 & 2 \end{pmatrix}.$$

The path $\Gamma_{1,4}(\tilde{\Omega}_{II}^{(13)})$ passes through the 2-dimensional cells of S given by $(\overline{\omega_0\omega_2})^\vee$, $(\overline{\omega_2\omega_3})^\vee$ and $(\overline{\omega_3\omega_5})^\vee$. We compute the directions of the rays spanning the cones associated to the facets and obtain the following system of linear equations:

$$\begin{pmatrix} 0 \\ 0 \\ 0 \end{pmatrix} = \begin{pmatrix} x \\ y \\ z \end{pmatrix} + \alpha_1 \begin{pmatrix} 3-a \\ 1 \\ 1 \end{pmatrix} + \alpha_2 \begin{pmatrix} a-3 \\ 2-a \\ -1 \end{pmatrix}, \ \alpha_1, \alpha_2 > 0,$$

$$\begin{pmatrix} 1 \\ \eta \\ \eta^2 \end{pmatrix} = \begin{pmatrix} x \\ y \\ z \end{pmatrix} + \beta_1 \begin{pmatrix} a-3 \\ 2-a \\ -1 \end{pmatrix} + \beta_2 \begin{pmatrix} 1 \\ 0 \\ 0 \end{pmatrix}, \ \beta_1, \beta_2 > 0,$$

$$\begin{pmatrix} \lambda \\ \lambda\eta \\ \lambda\eta^2 \end{pmatrix} = \begin{pmatrix} x \\ y \\ z \end{pmatrix} + \gamma_1 \begin{pmatrix} 0 \\ 1 \\ 0 \end{pmatrix} + \gamma_2 \begin{pmatrix} 1 \\ 0 \\ 0 \end{pmatrix}, \ \gamma_1, \gamma_2 > 0.$$

This system has the solution:

$$x = -(a-3)\lambda\eta^2,$$
$$y = \eta + (a-2)(\lambda - 1)\eta^2,$$
$$z = \lambda\eta^2 > 0,$$
$$\alpha_1 = \frac{1}{a-3}(\eta - (a-2)\eta^2) > 0,$$
$$\alpha_2 = \frac{1}{a-3}(\eta - (a-2)\eta^2) + \lambda\eta^2 > 0,$$

$$\beta_1 = (\lambda - 1)\eta^2 > 0,$$
$$\beta_2 = 1 + (a - 3)\eta^2 > 0,$$
$$\gamma_1 = (\lambda - 1)(\eta - (a - 2)\eta^2) > 0,$$
$$\gamma_2 = \lambda(1 + (a - 3)\eta^2) > 0.$$

which satisfies all the conditions, provided $\frac{1}{a-2} > \eta$. As $1 \gg \eta > 0$ this can be satisfied without violating the genericity of our point conditions. Thus, the path $\Gamma_{1,4}(\tilde{\Omega}_{II}^{(13)})$ is valid. $\qquad\square$

Analogously to Section 10.1.1 we see that the changes from $\tilde{\Omega}_I^{(13)}(a,d,f,y)$ to $\tilde{\Omega}_I^{(13)}(a)$ did not change the order of the lattice points with respect to the induced partial order, nor did it change the polytope of family 13 that the polytope is equivalent to. The same holds for $\tilde{\Omega}_{II}^{(13)}(a,d,f,y)$. Hence, the lattice path and its multiplicities are preserved, and the lattice paths as determined in Proposition 10.1.11 can be used to compute the multiplicities of the positions of a polytope of family 13 in $d\Delta_3$.

Conjecture 10.1.12. *The multiplicity of the lattice paths depends only on a and is given by*

$$mult(\Gamma_{1,3}(\tilde{\Omega}_I^{(13)}(a))) = mult(\Gamma_{1,4}(\tilde{\Omega}_{II}^{(13)}(a))) = \begin{cases} a - 2 & \textit{if } a \textit{ even,} \\ a - 3 & \textit{if } a \textit{ odd.} \end{cases}$$

This conjecture is verified for $4 \le a \le 10$ by using [Gei22] in `OSCAR`; see Table 10.4.

Lattice path	$a = 4$	$a = 5$	$a = 6$	$a = 7$	$a = 8$	$a = 9$	$a = 10$
$\Gamma_{1,3}(\tilde{\Omega}_I^{(13)}(a))$	2	2	4	4	6	6	8
$\Gamma_{1,4}(\tilde{\Omega}_{II}^{(13)}(a))$	2	2	4	4	6	6	8

Table 10.4: Verified multiplicities for polytope 13 in $d\Delta_3$

10.1.3 Polytope family 20

Proposition 10.1.13. *Let S be a floor decomposed tropical binodal surface of degree d passing through points in Mikhalkin position. Then, the dual subdivision $\mathcal{S}$ to S can only contain a polytope of family 20 if $d \ge 5$.*

In this case there is one type of position for the polytope; see Table 10.5.

Proof. Let Ω be a binodal polytope of family 20, then only one pair of the edges of Ω is parallel. Assume these two parallel edges were in the same floor subdivision of

$d\Delta_3$. From the combinatorics of polytopes of family 20 we know that the other two lattice points of Ω are distributed on the two adjacent floor subdivisions. Thus, Ω would have width 2 in the x-direction and S would no longer be floor decomposed.

Accordingly, we know that the two parallel edges of Ω are in adjacent floor subdivisions in $\mathcal{S}$.

Since Ω has only triangular facets, the polytope corresponds to the alignment of two vertices of adjacent floors in the tropical floor plan. Analogous to the case of the parallelogram between the floors for polytopes of family 10 in Proposition 10.1.7, we argue that the two parallel edges of Ω have to be vertical.

We can align two vertices of adjacent floors either by fixing one vertex entirely while the other has two degrees of freedom, or by leaving one degree of freedom to each vertex such that both can be moved to enable the alignment.

If we leave out one lattice point in each of the two triangles spanning Ω, each of the corresponding vertices will have one degree of freedom in the tropical floor plan. However, at least one of the vertices will only have a limited area for movement, since the surrounding vertices are fixed by the point conditions. This is only not true for left and right strings, but an alignment of a left with a right string does not induce a polytope of family 20.

The other approach, fixing one vertex and giving the other two degrees of freedom, leads to a double right string. The position of Ω is therefore fixed to give one representative for the containment in $d\Delta_3$ by applying IUA-equivalences:

$$
\begin{pmatrix}
0 & 0 & 0 & 1 & 1 & 1 \\
d-1 & d-1 & d & y & y+1 & y+1 \\
0 & 1 & 0 & d-y-1 & d-a-1 & d-a
\end{pmatrix},
$$

where a is the parameter of the polytope family and y is the parameter the position of the second triangle in the y-coordinate. Here we assume that Ω is contained between the 0th and 1st floor subdivision in $\mathcal{S}$. The generic representative can be found in Table 10.5. For consistence with the notation in Sections 10.1.1 and 10.1.2, we denote this position $\tilde{\Omega}^{(20)}$ and use $\tilde{\Omega}^{(20)}(a,d,f,y)$ when we mean a particular polytope. Figure 10.5 depicts this containment and the dual floor plan alignment for $a=4$, $d=5$, $f=5$ and $y=0$.

Since polytopes of family 20 are only binodal for $a \geq 4$, it follows that $d \geq 5$. $\quad\square$

Remark 10.1.14. Note that $\tilde{\Omega}^{(20)}(a,2,1,0)$ under the $SL_2(\mathbb{Z})$ transformation $(1,0,0) \mapsto (1,0,a-1)$, is equal to $\Omega_a^{(20)}$ as in Figure 9.12 in Chapter 9. This transformation does not change the order of the lattice points as induced by $(1,\eta,\eta^2)$. Therefore, we can use the results from Section 9.4.5 from Chapter 9, instead of having to recompute as in Sections 10.1.1 and 10.1.2.
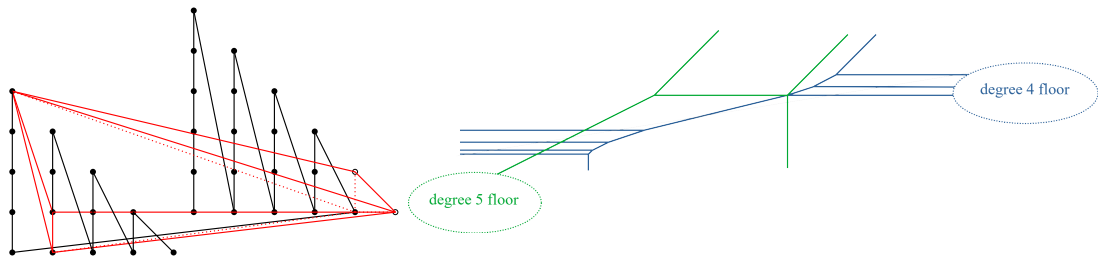
Figure 10.5: Polytope of family 20 in $5\Delta_3$ in position $\tilde{\Omega}^{(20)}$

Proposition 10.1.15. *There is one valid lattice path that agrees with the lattice path for $d\Delta_3$ for the one position $\tilde{\Omega}^{(20)}$ of a polytope belonging to family 20:*

$$\Gamma_{1,2}(\tilde{\Omega}^{(20)}).$$

Proof. This follows from the proof of Proposition 10.1.13, Remark 10.1.14 and Proposition 9.4.20. □

Conjecture 10.1.16. *The multiplicity of the lattice path $\Gamma_{1,2}(\tilde{\Omega}^{(20)}(a))$ depends only on a and is given by*

$$mult(\Gamma_{1,2}(\tilde{\Omega}^{(20)}(a))) = a - 3.$$

This conjecture is verified for $4 \leq a \leq 7$ by using [Gei22] in `OSCAR`; see Table 9.7.

Polytope	Lattice points	Path	Mult.
$\tilde{\Omega}_I^{(10)}$ $a \geq 3,$ $d \geq 5$	$\begin{pmatrix} d-(f+1) & d-(f+1) & d-(f+1) & d-f & d-f & d-f \\ f & f & f+1 & y & y & y+1 \\ 0 & 1 & 0 & a & a+1 & 0 \end{pmatrix}$	$\Gamma_{1,2}$	$a-2$
$\tilde{\Omega}_{II}^{(10)}$ $a \geq 3,$ $d \geq 6$	$\begin{pmatrix} d-(f+1) & d-(f+1) & d-f & d-f & d-f & d-f \\ f & f+1 & y & y & y+1 & y+1 \\ 1 & 0 & f-y-1 & f-y & f-y-a-2 & f-y-a-1 \end{pmatrix}$	$\Gamma_{1,3}$	$a-2$
$\tilde{\Omega}_{III}^{(10)}$ $a \geq 3,$ $d \geq 6$	$\begin{pmatrix} d-(f+1) & d-(f+1) & d-f & d-f & d-f & d-f \\ f & f+1 & y & y & y+1 & y+1 \\ 1 & 0 & a+1 & a+2 & 0 & 1 \end{pmatrix}$	$\Gamma_{1,4}$	$a-2$
$\tilde{\Omega}_I^{(13)}$ $a \geq 4,$ $d \geq 7$	$\begin{pmatrix} d-(f+1) & d-(f+1) & d-f & d-f & d-f & d-f \\ f & f+1 & y & y & y+1 & y+1 \\ 1 & 0 & a & a+1 & a+2 & 0 \end{pmatrix}$	$\Gamma_{1,3}$	$\begin{cases} a-2 & \text{if } a \text{ even} \\ a-3 & \text{if } a \text{ odd} \end{cases}$
$\tilde{\Omega}_{II}^{(13)}$ $a \geq 4,$ $d \geq 7$	$\begin{pmatrix} d-(f+1) & d-(f+1) & d-f & d-f & d-f & d-f \\ f & f+1 & y & y & y+1 & y+1 \\ 1 & 0 & f-y & f-y-a-2 & f-y-a-1 & f-y-a \end{pmatrix}$	$\Gamma_{1,4}$	$\begin{cases} a-2 & \text{if } a \text{ even} \\ a-3 & \text{if } a \text{ odd} \end{cases}$
$\tilde{\Omega}^{(20)}$ $a \geq 4,$ $d \geq 5$	$\begin{pmatrix} d-(f+1) & d-(f+1) & d-f & d-f & d-f & d-f \\ f & f & f+1 & y & y+1 & y+1 \\ 0 & 1 & 0 & f-y & f-y-a & f-y-a+1 \end{pmatrix}$	$\Gamma_{1,2}$	$a-3$

Table 10.5: The multiplicities of the binodal polytopes appearing in degree d surfaces through points in Mikhalkin position. The parameters are to be read like this: f is the degree of the floor containing the main part of the polytope, y is the value that can be obtained in the y-coordinate and a is the parameter of the polytope family.

291

10.2 Counting binodal polytopes in degree d surfaces

In this section we apply the results of the previous sections to counting binodal surfaces of degree d.

In Definition 10.2.1, we formally extend tropical floor plans to the cases of binodal polytopes with 6 lattice points and width 1 as determined in Section 9.4. This step is important as a foundation for future research in counting tropical surfaces via tropical floor plans.

Then, building on the conjectured multiplicities from Section 9.4, we state a conjecture on the contribution of the binodal polytopes to the asymptotic count of binodal degree d surfaces $N_{2,\mathbb{C}}^{\mathbb{P}^3}(d)$, asserting that they add to the third highest term.

This section is based on joint work with Madeline Brandt [BG21].

We adapt some of the definitions from [MMSS22] to define floor plans that enumerate tropical surfaces with a binodal polytope in their dual subdivision. First, we note some differences from the original definitions.

We will count a double right string as two node germs to assure that two node germs in the tropical floor plan correspond to two nodes in the associated surface.

Unlike the original definition of node germs by [MMSS22], we let a bounded edge of length two be a node germ, instead of just its midpoint. We do this because for polytopes from family 13, the edge of weight 2 in the tropical floor plan contributes to the two nodes via one of its vertices, not via its midpoint.

Definition 10.2.1 (Generalized from [MMSS22, BG20]). Let Q_i be the projection of q_i along the x-axis. A *δ-nodal floor plan F of degree d* is a tuple $(C_d, \ldots, C_1)$ of plane tropical curves C_i of degree i together with a choice of indices $d \geq i_{\delta'} > \ldots > i_1 \geq 1$ each assigned a natural number k_j such that $\sum_{j=1}^{\delta'} k_j = \delta$, where $0 < \delta' \leq \delta$, satisfying:

1. The curve C_i passes through the following points, where $i_0 = 0, i_{\delta+1} = d+1$.

   if $i_\nu > i > i_{\nu-1}$:

   $$Q_{\sum_{k=i+1}^d \binom{k+2}{2} - \delta + (\sum_{j:i>i_j} k_j) + 1}, \cdots, Q_{\sum_{k=i}^d \binom{k+2}{2} - \delta + (\sum_{j:i>i_j} k_j) - 1},$$

   if $i = i_\nu$:

   $$Q_{\sum_{k=i+1}^d \binom{k+2}{2} - \delta + (\sum_{j:i \geq i_j} k_j) + 1}, \cdots, Q_{\sum_{k=i}^d \binom{k+2}{2} - \delta + (\sum_{j:i>i_j} k_j) - 1}.$$

2. The plane curves C_{i_j} has k_j node germs for each $j = 1, \ldots, \delta'$, where the double right string counts for two.

3. If C_{i_j} contains a left string as a node germ, then its horizontal end aligns either with a horizontal bounded edge of C_{i_j+1} or with a 3-valent (where edges are counted with multiplicity) vertex of C_{i+1} not adjacent to a horizontal edge.

4. If C_{i_j} contains a right string as a node germ, then its diagonal end aligns either

   - with a diagonal bounded edge of C_{i_j-1},

   - with a 3-valent (where edges are counted with multiplicity) vertex of C_{i_j-1} which is not adjacent to a diagonal edge,

   - with a vertex dual to a parallelogram which has two vertical edges and two edges of slope of absolute value at least 4, or

   - with a vertex dual to a triangle which consists of one vertical edge of length two and two edges with slope of absolute value at least 4.

5. If C_{i_j} contains a double right string, then the vertex adjacent to the diagonal and vertical end of the double right string aligns with a vertex dual to a triangle that is formed of a vertical edge and two edges with slope of absolute value at least 3.

6. If $i_d = \delta'$, then the node germs of C_d can only be diagonal ends of weight two, a right string, or a double right string.

7. If $i_1 = 1$, then the node germ of C_1 is a left string.

Now we have to decide with which complex lifting multiplicity we have to count a tropical floor plan that allows for binodal polytopes in the dual subdivision. We first summarize the results on the multiplicities of lattice paths for subdivisions of $d\Delta_3$ containing a binodal polytope with 6 lattice points of width 1 from Section 9.4 in the following conjecture:

Conjecture 10.2.2. *Let S be a floor decomposed, tropical binodal surface of degree d passing through points in Mikhalkin position such that the dual subdivision contains one of the binodal polytopes*

$$\tilde{\Omega}_I^{(10)}(a),\ \tilde{\Omega}_{II}^{(10)}(a),\ \tilde{\Omega}_{III}^{(10)}(a),\ \tilde{\Omega}_I^{(13)}(a),\ \tilde{\Omega}_{II}^{(13)}(a),\ \tilde{\Omega}^{(20)}(a),$$

and only unimodular simplices everywhere else.
Then the complex lifting multiplicity of S is given by

$$mult_{\mathbb{C}}(S) = \begin{cases} a-3 & \text{for } \tilde{\Omega}^{(20)}(a),\ \text{and for } \tilde{\Omega}_I^{(13)}(a), \tilde{\Omega}_{II}^{(13)}(a)\ \text{if } a\ \text{odd,} \\ a-2 & \text{else.} \end{cases}$$

Conjecture 10.2.2 is verified for polytopes belonging to family 13 when $4 \leq a \leq 9$, for polytopes belonging to family 20 when $a \leq 7$, and for polytopes belonging to family 10 when $3 \leq a \leq 7$; see Tables 10.1, 10.3 and 9.7.

To generalize the definition of the multiplicity of a floor plan, we distinguish between node germs appearing in separated mode and unseparated mode.

Definition 10.2.3. A node germ appears in *separated mode* if the corresponding singularity is separated. Otherwise, we say the node germ appears in *unseparated mode*.

By definition a double right string is always in unseparated mode. All other node germs in unseparated mode are accompanied by a second node germ in unseparated mode with which it interacts, e.g. by alignment. These node germs in unseparated mode with be always given as a pair.

The definition of separated or unseparated modes of node germs allows us to distinguish between node germs giving rise to binodal polytopes in the dual subdivision (unseparated mode) and node germs giving rise to the polytope complexes described in connection with the circuits in Section 7.1 (separated mode).

The following definition is based on Conjecture 10.2.2.

Definition 10.2.4 (Generalized from Definition 5.4, [MMSS22])**.** Let F be a δ-nodal floor plan of degree d. Let $C_{i_j}^*$ be a node germ of C_{i_j} in separated mode. Then we define the following local complex multiplicity $\text{mult}_{\mathbb{C}}(C_{i_j}^*)$:

1. If $C_{i_j}^*$ is dual to a parallelogram, then $\text{mult}_{\mathbb{C}}(C_{i_j}^*) = 2$.

2. If $C_{i_j}^*$ is the midpoint of an edge of weight two, then $\text{mult}_{\mathbb{C}}(C_{i_j}^*) = 8$.

3. If $C_{i_j}^*$ is a horizontal end of weight two, then $\text{mult}_{\mathbb{C}}(C_{i_j}^*) = 2(i_j + 1)$.

4. If $C_{i_j}^*$ is a diagonal end of weight two, then $\text{mult}_{\mathbb{C}}(C_{i_j}^*) = 2(i_j - 1)$.

5. If $C_{i_j}^*$ is a left string whose horizontal end aligns with a horizontal bounded edge, then $\text{mult}_{\mathbb{C}}(C_{i_j}^*) = 2$.

6. If $C_{i_j}^*$ is a left string whose horizontal end aligns with a vertex not adjacent to a horizontal edge, then $\text{mult}_{\mathbb{C}}(C_{i_j}^*) = 1$.

7. If $C_{i_j}^*$ is a right string whose diagonal end aligns with a diagonal bounded edge, then $\text{mult}_{\mathbb{C}}(C_{i_j}^*) = 2$.

8. If $C_{i_j}^*$ is a right string whose diagonal end aligns with a vertex not adjacent to a diagonal edge, then $\text{mult}_{\mathbb{C}}(C_{i_j}^*) = 1$.

If $(C_{i_j}^*, C_{i_j-1}^*)$ is a pair of node germs in unseparated mode, where $C_{i_j-1}^*$ is the node germ in C_{i_j-1} associated to $C_{i_j}^*$, or $C_{i_j}^*$ is a double right string, we assign the following local multiplicities:

9. If $C_{i_j}^*$ is a double right string that aligns with a vertex dual to a triangle that is formed of a vertical edge and two edges with slope $|a| \geq 3$ with the vertical edge on the left side of the triangle, it has multiplicity $|a| - 2$. Otherwise it has multiplicity $|a| - 3$.

10. If $(C_{i_j}^*, C_{i_j-1}^*)$ consists of a right string and an edge of weight 2 dual to the vertical edge of length two of a triangle for which the minimum of the absolute value of the slope of the other two edges is $|a| \geq 4$, the pair has multiplicity $|a| - 2$ if $|a|$ is even, and $|a| - 3$ if $|a|$ is odd.

11. If $(C_{i_j}^*, C_{i_j-1}^*)$ consists of a right string and a parallelogram which has two vertical edges and two edges of slope $|a| \geq 4$, the pair has multiplicity $|a| - 2$.

The multiplicity of a δ-nodal floor plan F is

$$\text{mult}_{\mathbb{C}}(F) = \prod_{j=1}^{\delta'} \prod_{\substack{\text{node germs in} \\ \text{separated mode of } C_{i_j}}} \text{mult}_{\mathbb{C}}(C_{i_j}^*)$$
$$\cdot \prod_{\substack{\text{double right strings of } C_{i_j}^*}} \text{mult}_{\mathbb{C}}(C_{i_j}^*)$$
$$\cdot \prod_{\substack{\text{node germs in unseparated} \\ \text{mode of } (C_{i_j}, C_{i_j-1})}} \text{mult}_{\mathbb{C}}((C_{i_j}^*, C_{i_j-1}^*)).$$

We can use these multiplicities to compute the contribution of tropical surfaces with binodal polytopes in their dual subdivision to the count of binodal surfaces of degree d.

Conjecture 10.2.5. *Assuming Conjecture 10.2.2 is true, it follows that tropical degree d surfaces with a binodal polytope with 6 vertices and width 1 in the dual subdivision contribute $\frac{1}{4}d^4 + \mathcal{O}(d^3)$ surfaces to $N_{2,\mathbb{C}}^{\mathbb{P}^3}(d)$, which is the count of binodal degree d surfaces.*

So, binodal polytope with 6 vertices and width 1 contribute to the third highest term of the polynomial $N_{2,\mathbb{C}}^{\mathbb{P}^3}(d)$.

Proof. By Theorem 10.1.6 we know that the only polytopes that can contribute are IUA-equivalent to binodal polytopes of the families 10, 13 and 20. Let $n = \binom{d+3}{3} - 3$ be the number of points in Mikhalkin position the tropical binodal surface has to pass through.

There were three different positions, each with one valid lattice path, on how to include a polytope belonging to family number 10 in a subdivision $\mathcal{S}$ of $d\Delta_3$ induced by point conditions in Mikhalkin position: $\tilde{\Omega}_I^{(10)}$, $\tilde{\Omega}_{II}^{(10)}$, and $\tilde{\Omega}_{III}^{(10)}$. We consider them separately.

First, we consider position $\tilde{\Omega}_I^{(10)}$, in which the parallelogram of the polytope of family 10 is contained between two floor subdivisions. This arises from an alignment as in Definition 10.2.1 (5).

Let f denote the degree of the $(d-f)$th floor. We consider the general representative of $\tilde{\Omega}_I^{(10)}(a,d,f,y)$ in Table 10.5, and observe that to enumerate all it inclusions in $\mathcal{S}$ we need to find all the ways how the triangle spanned by the vertices $(d-f,y,a)$, $(d-f,y,a+1)$, $(d-f,y+1,0)$ can be contained in $\mathcal{S}$. Then we have to count them all with the multiplicity of their lattice path to gain their contribution to the count.

To give rise to a polytope of family 10, the triangle can only occur in floor subdivisions dual to a curve of degree $f = \deg(F)$ with $4 \leq f < d$. For such a floor subdivision, there are $f-3$ many columns that can accommodate the triangle. In each of these columns, we have to fit in the triangle spanned by $(d-f,y,a)$, $(d-f,y,a+1)$, $(d-f,y+1,0)$ while ensuring $a \geq 3$. There are $f-y-3$ many options. We count each option with multiplicity $a-2$. This yields a total contribution of

$$\sum_{f=4}^{d-1}\sum_{y=0}^{f-4}\sum_{a=3}^{f-y-1}(a-2) = \frac{d^4}{24} - \frac{5d^3}{12} + \frac{35d^2}{24} - \frac{25d}{12} + 1.$$

In both the positions $\tilde{\Omega}_{II}^{(10)}$ and $\tilde{\Omega}_{III}^{(10)}$ the parallelogram is contained in a floor subdivision of $\mathcal{S}$. Further, these two options are symmetric, and the corresponding paths give the same multiplicity. So, we only enumerate the possibilities of $\tilde{\Omega}_{II}^{(10)}(a,d,f,y)$ to be contained in $\mathcal{S}$.

Let again f denote the degree of the $(d-f)$th floor. We have to find all the ways how the parallelogram spanned by $(d-f,y,f-y-1)$, $(d-f,y,f-y)$, $(d-f,y+1,f-y-a-3)$, $(d-f,y+1,f-y-a-2)$ can be contained in a floor subdivision of $d\Delta_3$ and count them with multiplicity. We know from Proposition 10.1.7 that it can only be contained in floor subdivisions with dual curve of degree $5 \leq f < d$. Such a floor subdivision contains $f-4$ many columns that can accommodate the parallelogram.

For each of these columns there are $f-y-3$ many ways to fit the parallelogram into it while ensuring $a \geq 3$. We count each option with multiplicity $a-2$. This

yields a total contribution of

$$\sum_{f=5}^{d-1}\sum_{y=1}^{f-4}\sum_{a=3}^{f-y-1}(a-2) = \frac{d^4}{24} - \frac{7d^3}{12} + \frac{71d^2}{24} - \frac{77d}{12} + 5.$$

Counting this contribution twice (once for position $\tilde{\Omega}_{II}^{(10)}$ and once for $\tilde{\Omega}_{III}^{(10)}$) and adding the contribution for position $\tilde{\Omega}_{I}^{(10)}$ we get a total contribution of

$$\frac{d^4}{8} - \frac{19d^3}{12} + \frac{59d^2}{8} - \frac{179d}{12} + 11$$

from the tropical floor plans with an alignment corresponding to a polytopes of family 10.

For polytopes of family 13, Proposition 10.1.10 determined two different ways of including the polytope in a subdivision $\mathcal{S}$ of $d\Delta_3$ arising from point conditions in Mikhalkin position: $\tilde{\Omega}_{I}^{(13)}$ and $\tilde{\Omega}_{II}^{(13)}$. For each there is one valid lattice path by Proposition 10.1.11. However, the two cases are symmetric and they both give the same lattice path multiplicity, so we only need to count the contribution of $\tilde{\Omega}_{I}^{(13)}$.

We have to find all the ways how the triangle spanned by the lattice points $(d-f,y,a)$, $(d-f,y,a+2)$, $(d-f,y+1,0)$ an be contained in $\mathcal{S}$, and count them with multiplicity. As for polytopes of family 10, we let f denote the degree of the curve in the $(d-f)$th floor. By Proposition 10.1.10 we know that any floor subdivision containing the triangle with $a \geq 4$ has to correspond to a floor of degree $6 \leq f < d$. Such a floor subdivision has $f-5$ many columns that can accommodate the triangle such that $a \geq 4$. For any such column there are $f-y-2$ many ways to fit the triangle in while ensuring $a \geq 4$. We count each option with its multiplicity: $a-2$ if a is even, and $a-3$ if a is odd. In the sum we use $a=2k$ resp. $a=2k+1$, and see that in both cases the multiplicity can be computed by $2k-2$. Thus, we obtain the following sum as the contribution of polytopes in position $\tilde{\Omega}_{I}^{(13)}$:

$$2 \cdot \sum_{f=6}^{d-1}\sum_{y=1}^{f-5}\sum_{k=2}^{\lfloor\frac{f-y-1}{2}\rfloor}(2k-2) = \begin{cases} \frac{1}{24}d^4 - \frac{7}{12}d^3 + \frac{17}{6}d^2 - \frac{17}{3}d + 4 & \text{if } d \text{ even,} \\ \frac{1}{24}d^4 - \frac{1}{2}d^3 + \frac{25}{12}d^2 - \frac{7}{2}d - \frac{17}{8} & \text{if } d \text{ odd.} \end{cases}$$

So both positions, $\tilde{\Omega}_{I}^{(13)}$ and $\tilde{\Omega}_{II}^{(13)}$, contribute via their lattice path multiplicities the following number to our count:

$$\frac{1}{12}d^4 - \frac{7}{6}d^3 + \frac{17}{3}d^2 - \frac{34}{3}d + 8 \qquad \text{if } d \text{ even,}$$
$$\frac{1}{12}d^4 - d^3 + \frac{25}{6}d^2 - 7d - \frac{17}{4} \qquad \text{if } d \text{ odd.}$$

By Propositions 10.1.13 and 10.1.15 we know that for a polytope belonging to family 20 there is only one position, $\tilde{\Omega}^{(20)}$, with only one valid lattice path in a subdivision $\mathcal{S}$ of $d\Delta_3$ induced by n points in Mikhalkin position.

To find all ways how this position can be attained in $d\Delta_3$, we have to enumerate all the ways how the triangle $(d-f,y,f-y)$, $(d-f,y+1,f-y-a)$, $(d-f,y+1,f-y-a+1)$ can be contained in $\mathcal{S}$, where f is the degree of the $(d-f)$th floor. The parameter a has to satisfy $a \geq 4$, otherwise the polytope is not binodal (Proposition 9.2.5). It follows from Proposition 10.1.13 that $4 \leq f < d$. A floor subdivision corresponding to a floor of degree $4 \leq f < d$ has $f-3$ many columns that can accommodate the triangle such that $a \geq 4$. For any such arbitrary column, we have to fit in $(d-f,y,f-y)$, $(d-f,y+1,z)$, $(d-deg(F),y+1,f-y-a+1)$ ensuring $a \geq 4$. This yields $f-y-3$ many options. We count each option with multiplicity $a-3$. This yields the following contribution of polytopes in position $\tilde{\Omega}^{(20)}$ to the count:

$$\sum_{f=4}^{d-1}\sum_{y=0}^{f-4}\sum_{a=4}^{f-y}(a-3) = \frac{d^4}{24} - \frac{5d^3}{12} + \frac{35d^2}{24} - \frac{25d}{12} + 1.$$

It follows that for $d > 6$ binodal polytopes contribute

$$\frac{1}{4}d^4 - \frac{19}{6}d^3 + \frac{29}{2}d^2 - \frac{85}{3}d + 20 \qquad \text{if } d \text{ even,}$$

$$\frac{1}{4}d^4 - 3d^3 + 13d^2 - 24d - \frac{31}{4} \qquad \text{if } d \text{ odd.}$$

to the count of binodal degree d surfaces. $\qquad\qquad\square$

Appendix A

Polytopes with 6 lattice points of width 2 and 3

The lattice polytopes with 6 lattice points of width 2 and 3 have been classified in [BS16b]. In this section, we record all these polytopes together with dimension and degree of the associated generalized binodal variety for those cases, where the computations terminated. We order the polytopes in different tables, depending on the results of the computations. The polytopes are transposed so that all coordinates are positive and permuted by $(x\,y\,z)$. They are numbered according to the numbering in [BS16b][1].

no.	vertices	(dim, deg) of the generalized binodal variety
2	$\begin{pmatrix} 1 & 1 & 2 & 1 & 1 & 0 \\ 0 & 1 & 1 & 1 & 2 & 2 \\ 0 & 1 & 1 & 2 & 1 & 5 \end{pmatrix}$	$\dim = 3,\ \deg = 9$
3	$\begin{pmatrix} 1 & 1 & 2 & 1 & 0 & 1 \\ 0 & 1 & 1 & 1 & 1 & 2 \\ 0 & 1 & 1 & 2 & 4 & 1 \end{pmatrix}$	$\dim = 3,\ \deg = 24$
4	$\begin{pmatrix} 1 & 1 & 2 & 1 & 1 & 0 \\ 0 & 1 & 1 & 1 & 2 & 2 \\ 0 & 1 & 1 & 2 & 1 & 6 \end{pmatrix}$	$\dim = 3,\ \deg = 44$
5	$\begin{pmatrix} 1 & 1 & 2 & 1 & 1 & 0 \\ 0 & 1 & 1 & 1 & 2 & 2 \\ 0 & 1 & 1 & 2 & 1 & 7 \end{pmatrix}$	$\dim = 3,\ \deg = 65$
12	$\begin{pmatrix} 5 & 0 & 0 & 1 & 0 & 0 \\ 0 & 1 & 2 & 2 & 2 & 3 \\ 0 & 0 & 1 & 1 & 2 & 1 \end{pmatrix}$	$\dim = 3,\ \deg = 45$
13	$\begin{pmatrix} 7 & 0 & 0 & 1 & 0 & 0 \\ 0 & 1 & 2 & 2 & 2 & 3 \\ 0 & 0 & 1 & 1 & 2 & 1 \end{pmatrix}$	$\dim = 3,\ \deg = 91$

---

[1]`https://personales.unican.es/santosf/3polytopes/Size_6_latticepoints.txt`

no.	vertices	(dim, deg) of the generalized binodal variety
14	$\begin{pmatrix} 0 & 2 & 3 & 2 & 3 & 2 \\ 0 & 2 & 2 & 3 & 3 & 4 \\ 0 & 1 & 1 & 1 & 2 & 1 \end{pmatrix}$	dim = 3, deg = 14
15	$\begin{pmatrix} 0 & 1 & 2 & 1 & 2 & 1 \\ 0 & 1 & 1 & 2 & 2 & 3 \\ 0 & 1 & 1 & 1 & 3 & 1 \end{pmatrix}$	dim = 3, deg = 27
16	$\begin{pmatrix} 0 & 1 & 2 & 3 & 2 & 3 \\ 0 & 1 & 2 & 2 & 3 & 3 \\ 0 & 1 & 2 & 2 & 2 & 4 \end{pmatrix}$	dim = 3, deg = 20
17	$\begin{pmatrix} 0 & 1 & 2 & 1 & 2 & 1 \\ 0 & 1 & 1 & 2 & 2 & 3 \\ 0 & 2 & 2 & 2 & 5 & 2 \end{pmatrix}$	dim = 3, deg = 65
18	$\begin{pmatrix} 0 & 1 & 2 & 3 & 2 & 3 \\ 0 & 1 & 2 & 2 & 3 & 3 \\ 0 & 2 & 4 & 4 & 4 & 7 \end{pmatrix}$	dim = 3, deg = 44
19	$\begin{pmatrix} 0 & 1 & 2 & 3 & 2 & 3 \\ 0 & 1 & 2 & 2 & 3 & 4 \\ 0 & 2 & 4 & 4 & 4 & 9 \end{pmatrix}$	dim = 3, deg = 119
24	$\begin{pmatrix} 0 & 2 & 3 & 4 & 3 & 4 \\ 0 & 1 & 2 & 2 & 3 & 3 \\ 0 & 2 & 4 & 4 & 4 & 7 \end{pmatrix}$	dim = 3, deg = 14
29	$\begin{pmatrix} 0 & 1 & 2 & 1 & 2 & 3 \\ 0 & 1 & 1 & 2 & 2 & 4 \\ 0 & 1 & 1 & 1 & 3 & 8 \end{pmatrix}$	dim = 3, deg = 136
38	$\begin{pmatrix} 1 & 1 & 2 & 1 & 1 & 0 \\ 0 & 1 & 1 & 1 & 2 & 2 \\ 0 & 1 & 1 & 2 & 1 & 3 \end{pmatrix}$	dim = 3, deg = 7
39	$\begin{pmatrix} 1 & 1 & 2 & 1 & 1 & 0 \\ 0 & 1 & 1 & 1 & 2 & 2 \\ 0 & 1 & 1 & 2 & 1 & 4 \end{pmatrix}$	dim = 3, deg = 16
40	$\begin{pmatrix} 1 & 1 & 2 & 0 & 1 & 1 \\ 0 & 1 & 1 & 1 & 1 & 2 \\ 0 & 1 & 1 & 2 & 2 & 1 \end{pmatrix}$	dim = 3, deg = 6
42	$\begin{pmatrix} 1 & 0 & 1 & 2 & 1 & 1 \\ 0 & 1 & 1 & 1 & 1 & 2 \\ 0 & 1 & 1 & 1 & 2 & 1 \end{pmatrix}$	dim = 3, deg = 6
43	$\begin{pmatrix} 3 & 3 & 4 & 3 & 3 & 0 \\ 0 & 1 & 1 & 1 & 2 & 2 \\ 0 & 1 & 1 & 2 & 1 & 3 \end{pmatrix}$	dim = 3, deg = 36

no.	vertices	(dim, deg) of the generalized binodal variety
44	$\begin{pmatrix} 3 & 3 & 4 & 3 & 3 & 0 \\ 0 & 1 & 1 & 1 & 2 & 2 \\ 0 & 1 & 1 & 2 & 1 & 6 \end{pmatrix}$	dim = 3, deg = 84
46	$\begin{pmatrix} 0 & 0 & 0 & 0 & 1 & 3 \\ 0 & 1 & 1 & 2 & 2 & 2 \\ 0 & 1 & 2 & 1 & 2 & 3 \end{pmatrix}$	dim = 3, deg = 10
47	$\begin{pmatrix} 1 & 2 & 1 & 1 & 1 & 0 \\ 0 & 0 & 0 & 1 & 1 & 3 \\ 0 & 0 & 1 & 0 & 1 & 4 \end{pmatrix}$	dim = 3, deg = 7
48	$\begin{pmatrix} 1 & 2 & 1 & 1 & 1 & 0 \\ 0 & 0 & 0 & 1 & 1 & 4 \\ 0 & 0 & 1 & 0 & 1 & 5 \end{pmatrix}$	dim = 3, deg = 18
50	$\begin{pmatrix} 5 & 0 & 1 & 0 & 0 & 0 \\ 0 & 2 & 2 & 2 & 3 & 3 \\ 0 & 1 & 1 & 2 & 1 & 2 \end{pmatrix}$	dim = 3, deg = 14
52	$\begin{pmatrix} 0 & 1 & 1 & 2 & 1 & 2 \\ 0 & 0 & 1 & 1 & 2 & 2 \\ 0 & 1 & 1 & 1 & 1 & 3 \end{pmatrix}$	dim = 3, deg = 8
53	$\begin{pmatrix} 0 & 1 & 2 & 1 & 2 & 2 \\ 0 & 1 & 1 & 2 & 2 & 2 \\ 0 & 1 & 1 & 1 & 2 & 3 \end{pmatrix}$	dim = 3, deg = 6
54	$\begin{pmatrix} 0 & 1 & 1 & 2 & 1 & 2 \\ 0 & 0 & 1 & 1 & 2 & 2 \\ 0 & 2 & 2 & 2 & 2 & 5 \end{pmatrix}$	dim = 3, deg = 24
55	$\begin{pmatrix} 0 & 1 & 2 & 1 & 2 & 2 \\ 0 & 1 & 1 & 2 & 2 & 2 \\ 0 & 2 & 2 & 2 & 4 & 5 \end{pmatrix}$	dim = 3, deg = 16
56	$\begin{pmatrix} 0 & 1 & 2 & 1 & 2 & 2 \\ 0 & 1 & 1 & 2 & 2 & 3 \\ 0 & 2 & 2 & 2 & 4 & 7 \end{pmatrix}$	dim = 3, deg = 48
57	$\begin{pmatrix} 0 & 2 & 3 & 2 & 3 & 5 \\ 0 & 2 & 2 & 3 & 3 & 6 \\ 0 & 1 & 1 & 1 & 2 & 2 \end{pmatrix}$	dim = 3, deg = 20
58	$\begin{pmatrix} 0 & 2 & 3 & 2 & 3 & 5 \\ 0 & 2 & 2 & 3 & 3 & 8 \\ 0 & 1 & 1 & 1 & 2 & 2 \end{pmatrix}$	dim = 3, deg = 70
59	$\begin{pmatrix} 0 & 1 & 2 & 1 & 1 & 2 \\ 0 & 1 & 1 & 2 & 2 & 2 \\ 0 & 1 & 1 & 0 & 1 & 3 \end{pmatrix}$	dim = 3, deg = 18

no.	vertices	(dim, deg) of the generalized binodal variety
60	$\begin{pmatrix} 0 & 1 & 2 & 1 & 2 & 1 \\ 0 & 1 & 1 & 2 & 2 & 4 \\ 0 & 1 & 1 & 1 & 3 & 2 \end{pmatrix}$	dim = 3, deg = 48
62	$\begin{pmatrix} 0 & 3 & 4 & 5 & 4 & 5 \\ 0 & 2 & 3 & 3 & 4 & 4 \\ 0 & 4 & 5 & 5 & 5 & 7 \end{pmatrix}$	dim = 3, deg = 56
65	$\begin{pmatrix} 0 & 1 & 2 & 1 & 2 & 2 \\ 0 & 1 & 1 & 2 & 2 & 3 \\ 0 & 2 & 2 & 2 & 5 & 7 \end{pmatrix}$	dim = 3, deg = 65
68	$\begin{pmatrix} 0 & 1 & 2 & 3 & 2 & 3 \\ 0 & 2 & 3 & 3 & 4 & 4 \\ 0 & 3 & 5 & 5 & 5 & 8 \end{pmatrix}$	dim = 3, deg = 75
69	$\begin{pmatrix} 0 & 2 & 3 & 4 & 3 & 4 \\ 0 & 3 & 4 & 4 & 5 & 5 \\ 0 & 5 & 7 & 7 & 7 & 10 \end{pmatrix}$	dim = 3, deg = 126
74	$\begin{pmatrix} 0 & 1 & 2 & 1 & 1 & 2 \\ 0 & 1 & 1 & 2 & 2 & 3 \\ 0 & 1 & 1 & 0 & 1 & 6 \end{pmatrix}$	dim = 3, deg = 180

Table A.1: Polytopes with 6 lattice points and width 2 or 3 that could be binodal.

For the following polytopes the ideal generating the general binodal variety contains monomials. Therefore, the binodal varieties is empty and the polytopes cannot be binodal.

no.	vertices	(dim, deg) of the generalized binodal variety
1	$\begin{pmatrix} 0 & 0 & 0 & 0 & 0 & 2 \\ 0 & 1 & 1 & 1 & 2 & 2 \\ 0 & 0 & 1 & 2 & 0 & 1 \end{pmatrix}$	dim = 3, deg = 4, contains monomials
6	$\begin{pmatrix} 1 & 1 & 2 & 1 & 0 & 1 \\ 0 & 1 & 1 & 1 & 1 & 2 \\ 0 & 1 & 1 & 2 & 3 & 1 \end{pmatrix}$	dim = 3, deg = 3, contains monomials
9	$\begin{pmatrix} 0 & 2 & 0 & 1 & 0 & 0 \\ 0 & 0 & 1 & 1 & 1 & 2 \\ 0 & 1 & 1 & 1 & 2 & 1 \end{pmatrix}$	dim = 2, deg = 3, contains monomials
10	$\begin{pmatrix} 0 & 0 & 1 & 2 & 0 & 0 \\ 0 & 1 & 1 & 1 & 1 & 2 \\ 0 & 1 & 1 & 1 & 2 & 1 \end{pmatrix}$	dim = 2, deg = 3, contains monomials

no.	vertices	(dim, deg) of the generalized binodal variety
20	$\begin{pmatrix} 0 & 2 & 3 & 2 & 3 & 4 \\ 0 & 2 & 2 & 3 & 3 & 6 \\ 0 & 1 & 1 & 1 & 2 & 2 \end{pmatrix}$	dim = 1, deg = 2, contains monomials
21	$\begin{pmatrix} 0 & 1 & 2 & 0 & 1 & 2 \\ 0 & 1 & 1 & 2 & 2 & 2 \\ 1 & 2 & 2 & 0 & 2 & 4 \end{pmatrix}$	dim = 1, deg = 2, contains monomials
22	$\begin{pmatrix} 0 & 2 & 3 & 4 & 3 & 4 \\ 0 & 2 & 3 & 3 & 4 & 4 \\ 0 & 3 & 4 & 4 & 4 & 6 \end{pmatrix}$	dim = 3, deg = 5, contains monomials
23	$\begin{pmatrix} 0 & 1 & 2 & 1 & 2 & 2 \\ 0 & 1 & 1 & 2 & 2 & 3 \\ 0 & 2 & 2 & 2 & 5 & 8 \end{pmatrix}$	dim = 3, deg = 7, contains monomials
37	$\begin{pmatrix} 0 & 0 & 0 & 0 & 2 & 0 \\ 0 & 1 & 1 & 1 & 2 & 2 \\ 1 & 0 & 1 & 2 & 0 & 1 \end{pmatrix}$	dim = 3, deg = 4, contains monomials
41	$\begin{pmatrix} 1 & 1 & 2 & 1 & 1 & 0 \\ 0 & 1 & 1 & 1 & 2 & 2 \\ 0 & 1 & 1 & 2 & 1 & 2 \end{pmatrix}$	dim = 2, deg = 8, contains monomials
49	$\begin{pmatrix} 5 & 0 & 1 & 0 & 0 & 0 \\ 0 & 2 & 2 & 2 & 3 & 3 \\ 0 & 1 & 1 & 2 & 1 & 2 \end{pmatrix}$	dim = 2, deg = 2, contains monomials
51	$\begin{pmatrix} 0 & 2 & 2 & 3 & 2 & 3 \\ 0 & 1 & 2 & 2 & 3 & 3 \\ 0 & 1 & 1 & 1 & 1 & 2 \end{pmatrix}$	dim = 3, deg = 3, contains monomials

Table A.2: For these polytopes with 6 lattice points and width 2 or 3 the binodal variety is empty.

For the following polytopes the question of binodality is undecided, because the generalized binodal variety is a hypersurface. One would have to compute the binodal variety, to see if the binodal variety is of the expected dimension.

no.	vertices	(dim, deg) of the generalized binodal variety
8	$\begin{pmatrix} 3 & 0 & 3 & 3 & 3 & 6 \\ 0 & 0 & 1 & 1 & 2 & 2 \\ 0 & 2 & 1 & 2 & 1 & 3 \end{pmatrix}$	dim = 4, deg = 12
11	$\begin{pmatrix} 0 & 0 & 0 & 0 & 3 & 6 \\ 0 & 1 & 1 & 2 & 2 & 3 \\ 0 & 1 & 2 & 1 & 3 & 5 \end{pmatrix}$	dim = 4, deg = 6

no.	vertices	(dim, deg) of the generalized binodal variety
45	$\begin{pmatrix} 0 & 3 & 3 & 3 & 3 & 6 \\ 0 & 0 & 1 & 1 & 2 & 2 \\ 0 & 1 & 2 & 3 & 2 & 4 \end{pmatrix}$	dim $= 4$, deg $= 6$

Table A.3: For these polytopes the generalized binodal variety is a hypersurface. The question of binodality is undecided.

For the remaining polytopes the computations did not terminate. We include them for completeness.

no.	vertices
7	$\begin{pmatrix} 3 & 3 & 4 & 3 & 3 & 0 \\ 0 & 1 & 1 & 1 & 2 & 2 \\ 0 & 1 & 1 & 2 & 1 & 9 \end{pmatrix}$
25	$\begin{pmatrix} 0 & 11 & 13 & 14 & 13 & 14 \\ 0 & 10 & 12 & 12 & 13 & 13 \\ 0 & 6 & 7 & 7 & 7 & 8 \end{pmatrix}$
26	$\begin{pmatrix} 0 & 15 & 17 & 18 & 17 & 18 \\ 0 & 13 & 15 & 15 & 16 & 16 \\ 0 & 7 & 8 & 8 & 8 & 9 \end{pmatrix}$
27	$\begin{pmatrix} 0 & 7 & 8 & 9 & 8 & 9 \\ 0 & 6 & 7 & 7 & 8 & 8 \\ 0 & 8 & 9 & 9 & 9 & 11 \end{pmatrix}$
28	$\begin{pmatrix} 0 & 9 & 10 & 11 & 10 & 11 \\ 0 & 7 & 8 & 8 & 9 & 9 \\ 0 & 8 & 9 & 9 & 9 & 11 \end{pmatrix}$
30	$\begin{pmatrix} 0 & 1 & 2 & 1 & 2 & 6 \\ 0 & 1 & 1 & 2 & 2 & 5 \\ 0 & 1 & 1 & 1 & 3 & 12 \end{pmatrix}$
31	$\begin{pmatrix} 0 & 4 & 5 & 6 & 5 & 6 \\ 0 & 3 & 4 & 4 & 5 & 5 \\ 0 & 5 & 7 & 7 & 7 & 10 \end{pmatrix}$
32	$\begin{pmatrix} 0 & 5 & 6 & 7 & 6 & 7 \\ 0 & 6 & 7 & 7 & 8 & 8 \\ 0 & 9 & 11 & 11 & 11 & 14 \end{pmatrix}$
33	$\begin{pmatrix} 0 & 1 & 2 & 1 & 2 & 0 \\ 0 & 1 & 1 & 2 & 2 & 3 \\ 0 & 2 & 2 & 2 & 5 & 1 \end{pmatrix}$

no.	vertices
34	$\begin{pmatrix} 0 & 1 & 2 & 1 & 2 & 4 \\ 0 & 1 & 1 & 2 & 2 & 5 \\ 0 & 2 & 2 & 2 & 5 & 15 \end{pmatrix}$
35	$\begin{pmatrix} 0 & 3 & 4 & 5 & 4 & 5 \\ 0 & 4 & 5 & 5 & 6 & 7 \\ 0 & 7 & 9 & 9 & 9 & 14 \end{pmatrix}$
36	$\begin{pmatrix} 0 & 1 & 2 & 1 & 2 & 3 \\ 0 & 1 & 1 & 2 & 3 & 5 \\ 0 & 2 & 2 & 2 & 7 & 13 \end{pmatrix}$
61	$\begin{pmatrix} 1 & 2 & 3 & 0 & 2 & 3 \\ 0 & 1 & 1 & 2 & 2 & 2 \\ 2 & 3 & 3 & 0 & 3 & 5 \end{pmatrix}$
63	$\begin{pmatrix} 0 & 5 & 6 & 7 & 6 & 7 \\ 0 & 4 & 5 & 5 & 6 & 6 \\ 0 & 6 & 7 & 7 & 7 & 9 \end{pmatrix}$
64	$\begin{pmatrix} 0 & 1 & 2 & 1 & 2 & 1 \\ 0 & 1 & 1 & 2 & 2 & 3 \\ 0 & 2 & 2 & 2 & 5 & 3 \end{pmatrix}$
66	$\begin{pmatrix} 0 & 1 & 2 & 1 & 2 & 2 \\ 0 & 1 & 1 & 2 & 2 & 3 \\ 0 & 2 & 2 & 2 & 5 & 9 \end{pmatrix}$
67	$\begin{pmatrix} 0 & 0 & 1 & 2 & 1 & 2 \\ 0 & 1 & 2 & 2 & 3 & 3 \\ 1 & 0 & 2 & 2 & 2 & 5 \end{pmatrix}$
70	$\begin{pmatrix} 0 & 2 & 3 & 4 & 3 & 4 \\ 0 & 3 & 4 & 4 & 5 & 5 \\ 0 & 3 & 5 & 5 & 5 & 8 \end{pmatrix}$
71	$\begin{pmatrix} 0 & 0 & 1 & 2 & 1 & 2 \\ 0 & 0 & 1 & 1 & 2 & 3 \\ 0 & 1 & 2 & 2 & 2 & 7 \end{pmatrix}$
72	$\begin{pmatrix} 0 & 1 & 2 & 3 & 2 & 3 \\ 0 & 1 & 2 & 2 & 3 & 4 \\ 0 & 1 & 3 & 3 & 3 & 8 \end{pmatrix}$
73	$\begin{pmatrix} 0 & 1 & 2 & 3 & 2 & 3 \\ 0 & 2 & 3 & 3 & 4 & 5 \\ 0 & 3 & 5 & 5 & 5 & 10 \end{pmatrix}$
75	$\begin{pmatrix} 2 & 0 & 1 & 2 & 1 & 2 \\ 0 & 0 & 1 & 1 & 2 & 3 \\ 0 & 1 & 2 & 2 & 2 & 7 \end{pmatrix}$

no.	vertices
76	$\begin{pmatrix} 0 & 1 & 2 & 3 & 2 & 3 \\ 0 & 1 & 2 & 2 & 3 & 4 \\ 0 & 2 & 3 & 3 & 3 & 8 \end{pmatrix}$

Table A.4: For these polytopes with 6 lattice points and width 2 or 3 the computation did not terminate.

Appendix B

Software code and functions

For completeness, this section contains code and functions used to obtain the computational results of this thesis.

B.1 `polymake` extension `TropicalQuarticCurves`

The main functions in the `polymake` extension `TropicalQuarticCurves` [GP] can be downloaded from the `polymake` wiki. Because of the length of the code of the extension, this section of the Appendix contains the code that is not bundled in the extension, and that was used to achieve the results in Sections 5.2 and 6.2.

B.1.1 Code for proof of Theorem 5.2.2

We first present the function to check whether a given vector of signs satisfies a given real lifting condition.

```
use application "polytope";
$Verbose::files=0;
# The function checks whether a given signvector satisfies a given
    set of lifting conditions.
# The condition is given as the product of those entries of the
  sign vector $vector, for which the indices are elements of the
  entry of $signset, is positive.
# This has to hold for both entries of $signset
# If the signset contains a -1 it means that the product (after
  taking -1 out) has to be negative to satisfy the condition.
# The boolean output states whether the conditions are satisfied.
# INPUT: Vector<Set<Int>> with 2 entries and Vector<Int>
  containing only +/- 1 of length 15
# OUTPUT: boolean
sub validate_signs {
    my $signset = $_[0];
    my $vector = $_[1];
    my $cond1 = new Bool(true);
    my $cond2 = new Bool(true);
```

```
my $product = new Int(1);
if ($signset->[0]->size != 0) {
    if (contains($signset->[0], -1)) {
        my $set = $signset->[0] - new Set<Int>(-1);
        my $subvector = $vector->slice($set);
        my $size = $subvector->dim();
        for my $i (0..$size-1) {
            $product = $product*$subvector->[$i];
        }
        $product = -1*$product;
        $cond1 = ($product == 1);
    }
    else {
        my $subvector = $vector->slice($signset->[0]);
        my $size = $subvector->dim();
        for my $i (0..$size-1) {
            $product = $product*$subvector->[$i];
        }
        $cond1 = ($product == 1);
    }
}
if ($cond1 == true) {
    $product = new Int(1);
    if ($signset->[1]->size != 0) {
        if (contains($signset->[1], -1)) {
            my $set = $signset->[1] - new Set<Int>(-1);
            my $subvector = $vector->slice($set);
            my $size = $subvector->dim();
            for my $i (0..$size-1) {
                $product = $product*$subvector->[$i];
            }
            $product = -1*$product;
            $cond2 = ($product == 1);
        }
        else {
            my $subvector = $vector->slice($signset->[1]);
            my $size = $subvector->dim();
            for my $i (0..$size-1) {
                $product = $product*$subvector->[$i];
            }
            $cond2 = ($product == 1);
        }
    }
}
my $output = $cond1 && $cond2;
return $output;
}
```

The lifting of tropical bitangents over $\mathbb{R}$ depends on the signs of the coefficients

of the real quartic curve. To compute all possible numbers of lifts to real bitangents of a tropical smooth quartic curve, we need to check all possible signs of the 15 coefficients. Without loss of generality, we can assume that the first coefficient is positive. The following function computes the 2^{14} vectors with entries $\{\pm 1\}$ of length 15 starting with 1. The list is printed into the file `signs.txt`.

```perl
use application "polytope";
$Verbose::files=0;

open (my $output, ">", "signs.txt") or die "Can't␣open␣:␣$!";

sub compute_signs {
   my $S = new Set<Int>([0,1,2,3,4,5,6,7,8,9,10,11,12,13]);
   for my $k (0..14) {
      my $subsets = all_subsets_of_k($S, $k);
      foreach my $sset (@$subsets) {
         my $V = new Vector<Int>([1,1,1,1,1,1,1,1,1,1,1,1,1,1]);
         my $W = new Vector<Int>(15);
         foreach my $s (@$sset) {
            $V->[$s] = -1;
            $W->[0] = 1;
            for my $i (1..14) {
               $W->[$i] = $V->[$i-1];
            }
         }
         print $output "[".join(",", @{$W})."]\n";
      }
   }
}
```

Using the following subroutine we can compute the number of real bitangents for a given combinatorial type of the tropical quartic and a given vector of signs. Running this function over all S_3-representatives of smooth tropical quartics and all $\{\pm 1\}^{15}$ proves Theorem 5.2.2.

```perl
# INPUT: DualSubdivisionOfCQuartics and Vector<Int> with 15
#    entries +/-1
# OUTPUT: Integer
sub give_pluecker {
   my $trn = new DualSubdivisionOfQuartic($_[0]);
   if ($trn->IS_GENERIC != true) {
      print "Triangulation␣is␣not␣generic.","\n";
   }
   else {
      my $signvector = $_[1];
      my $conditions = $trn->ALL_SIGN_CONDITIONS;
      my $output = 0;
      for my $i (0..6) {
         my $signconditions = $conditions->row($i);
```

```
                if (validate_signs($signconditions,$signvector)==true) {
                    $output = $output+4;
                }
            }
            return $output;
        }
}
```

For a given combinatorial type of the tropical quartic curve, we can compute all possible numbers of real bitangents (in the code called Plücker numbers) together with an exemplary sign vector for this number of real lifts.

```
# Function to compute all possible numbers of real bitangents
    together with an exemplary sign vector for a given
    DualSubdivisionOfQuartic.
# The output is a Set<Int> and  Array<Set<Vector<Int>>> consisting
    of 4 entries. Each entry consists of one of the 4 numbers 4,
    8, 16, 28 of real lifts, and, if applicable, an associated
    signvector.
# INPUT: DualSubdivisionOfQuartic
# OUTPUT: (Set<Int>, Array<Set<Vector<Int>>>)
sub give_signvectors {
    my $trn = $_[0];
    my @output = ();
    if ($trn->IS_GENERIC != true) {
        @output = (new Set<Int>(), new Array<Set<Vector<Int>>>());
        print "Triangulation␣is␣not␣generic.","\n";
    }
    else {
        my $cond = $trn->ALL_SIGN_CONDITIONS;
        my $PlueckerNums = new Set<Int>();
        my $SignsNumbers = new Array<Set<Vector<Int>>>(new Set<
            Vector<Int>>(new Vector<Int>([4])), new Set<Vector<Int>>(
            new Vector<Int>([8])), new Set<Vector<Int>>(new Vector<
            Int>([16])), new Set<Vector<Int>>(new Vector<Int>([28]))
            );
        my $check = new Set<Int>();
        open (my $input, "<", "signs.txt") or die "Can't␣open␣:␣$!";
        while (<$input>) {
            my $signs = new Vector<Int>(eval $_);
            my $number = give_pluecker($trn,$signs);
            $PlueckerNums->collect(new Int($number));
            if (contains($check,$number)==0){
                $SignsNumbers->[$check->size]->collect($signs);
            }
            $check->collect($number);
        }
        close $input;
        @output = ($PlueckerNums,$SignsNumbers);
    }
```

```
        return @output;
}
```

B.1.2 Code for the analyses in Chapter 6

The following code computes the distribution of orbit sizes for Theorem 6.2.1 using
the data of [BJMS15] directly.

```
use application "polytope";
$Verbose::files=0;

open (my $input, "<",  "/YOUR/PATH/TO/TropicalModuliData/
   Computations/g3/preprocessing/g3TriangulationsData/
   g3FineRegularAffine.txt");
my $i=0;
my $S3 = new group::PermutationAction(GENERATORS=>
   [[0,2,1,5,4,3,9,8,7,6,14,13,12,11,10],
   [10,6,11,3,7,12,1,4,8,13,0,2,5,9,14]]);
my $sizes = new Vector<Int>([0,0,0,0,0,0]);
while (<$input>) {
   my $trn = new Set<Set<Int>>(eval $_);
   my $A = new Set<Set<Set<Int>>>(group::orbit<group::on_elements
      >($S3->ALL_GROUP_ELEMENTS,$trn));
   my $orbsize = $A->size();
   $sizes->[$orbsize-1] = $sizes->[$orbsize-1] +1;
   ++$i;
   print $i."\n";
}
print $sizes;
close $input;
```

The following code computes that every smooth tropical quartic curve is combi-
natorially determined by its deformation classes, Theorem 6.2.5.

```
# We go through the list of representatives. For each
   representative we collect the set of triangles, that is
   determined by its deformation classes.
# To avoid the problem, that there might be different S3-
   equivalent options for completing the unimodular triangulation,
# we add all elements of the orbits of the set of triangles fixed
   by the deformation classes.
# We collect all these sets, there are 7422 sets of this type.
# A there are 7422 regular unimodular triangulations in total, we
   can conclude, that the deformation classes combinatorially
   determine the quartic curve.

application "fan";
$polydb = polyDB();
$set = new Set<Set<Set<Int>>>();
```

```
$collection = $polydb->get_collection("Tropical.QuarticCurves");
$cur=$collection->find({});
$k = 0;
while ($cur->has_next()) {
   my $p = $cur->next();
   my $triangles = new Set<Set<Int>>();
   for my $i (0..6) {
      my $size = $p->ALL_DEFORMATION_MOTIFS->[$i]->TRIANGLES->size
         ;
      for my $j (0..$size-1){
         $triangles ->collect($p->ALL_DEFORMATION_MOTIFS->[$i]->
            TRIANGLES->[$j]);
      }
   }
   for my $o (0..5) {
      $helptriangles = group::action<group::on_elements>($p->
         ACTION->ALL_GROUP_ELEMENTS->[$o],$triangles);
      $set->collect($helptriangles);
   }
   print $k,"\n";
   print $set->size,"\n";
   $k = $k+1;
}
print $set->size == 7422;
```

Using the following code, we can obtain the identifiers of the cones with constant bitangent shapes and count them. This code was used to prove Proposition 6.3.2.

```
application "fan";
$polydb = polyDB();
$collection = $polydb->get_collection("Tropical.QuarticCurves");
open (my $output, ">", "ConstantShapeCones.txt") or die "Can't␣
   open␣:␣$!";
for my $i (1..1278) {
   my $cur=$collection->find({_id=>"$i"});
   my $p= $cur->next();
   my $motifs = $p->ALL_DEFORMATION_MOTIFS;
   my $j = 0;
   for my $k (0..6) {
      my $hyp = $motifs->[$k]->HYPERPLANES;
      if ($hyp->rows==0) {
         $j = $j+1;
      }
   }
   if ($j==7) {
      print $output $i."\n";
   }
   $i = $i+1;
}
```

The 128 secondary cones with constant bitangent shapes, Proposition 6.3.2, numbering according to the database identifyers:

12	385	935
18	412	936
27	459	937
32	475	939
39	477	957
52	484	958
60	497	968
70	504	972
77	543	989
82	546	992
83	547	993
92	549	994
98	572	997
99	573	1000
100	574	1001
101	620	1018
121	629	1019
129	631	1046
139	652	1047
141	653	1049
152	654	1055
156	660	1110
158	661	1147
168	664	1155
170	668	1156
176	702	1157
177	720	1159
186	749	1160
195	752	1179
209	753	1185
257	754	1186
264	755	1199
265	756	1209
272	767	1240
280	768	1251
303	769	1256
304	770	1267
313	849	1274
326	893	1275
334	914	1278
344	915	
359	916	
360	925	
384	933	

B.2 Functions in `OSCAR` for binodal polytopes

Here the functions written by the author for the joint project [BG21] with Madeline Brandt are contained. The code can also be downloaded [Gei22]. The code was written in `OSCAR` [osc] version 0.8.2. The first section, Section B.2.1 contains the main functions used for the investigations in Chapters 9 and 10. In Section B.2.2, the helper functions are contained for completeness.

Disclaimer: The computations do not terminate for larger input values on a standard computer.

B.2.1 Main functions

This section consists of the functions to investigate binodal varieties for a fixed support of the surfaces given by a (small) lattice polytope. These functions use certain helper functions enclosed in Section B.2.2. They have to be loaded first in `OSCAR`. In the downloadable version available at [Gei22], this is already done by the script.

This function computes the generalized binodal variety (Definition 9.1.4) by using Algorithm 6.

```
#INPUT: matrix(ZZ,n,3,[...])
#OUTPUT: returns the radical ideal generating the generalized
   binodal variety
function general_binodal(A::MatElem)
   n = nrows(A)
   R, c =  PolynomialRing(QQ,vcat(["c$i" for i in 1:n+7]))
   x = c[n+1]
   y = c[n+2]
   z = c[n+3]
   u = c[n+4]
   v = c[n+5]
   w = c[n+6]
   t = c[n+7]
#(x,y,z) stand for the position of the first node, (u,v,w) for the
    position of the second node
#t is an additional variable to make sure that the nodes are
   contained in the torus
   Id = identity_matrix(ZZ,n)
   M = hcat(Id,A)
   M = hcat(M, zero_matrix(ZZ,n,4)) #add coefficients for u,v,w,t
   h = MPolyBuildCtx(R)
   for i in 1:n
      push_term!(h,1,Vector{Int64}([M[i,j] for j in 1:ncols(M)]))
   end
   p= finish(h)
   q = evaluate(p,[x,y,z],[u,v,w])
```

```
   I = ideal(R,[p,q,derivative(p,x),derivative(p,y),derivative(p,z
      ),derivative(q,u),derivative(q,v),derivative(q,w),1-t*x*y*z*
      u*v*w])
   Sat = saturation(I, ideal(R,[x-u,y-v,z-w]))
   K = eliminate(Sat,[t,x,y,z,u,v,w])
   J = gens(K)
   RR, a = PolynomialRing(QQ, ["a$i" for i in 1:n])
   V = Vector{fmpq_mpoly}(undef,length(J))
   for i in 1:length(J)
      V[i] = evaluate(J[i],vcat(a,[zero(RR) for i in 1:7]))
   end
   II = ideal(RR,V)
   Radical = radical(II)
   return Radical
end
```

The next function computes the binodal variety (Definition 9.1.1) following Algorithm 7. It uses the function `general_binodal` above. This function has two methods: it can be applied either to an integer matrix filled with the lattice points of the polytope, or to the ideal generating the generalized binodal variety. If the affine dimension of the generalized binodal variety is less than $n-2$, where n is the number of variables, the function returns an error.

```
#INPUT: matrix(ZZ,n,3,[...])
#OUTPUT: returns the radical ideal generating the binodal variety
function binodal(A::MatElem)
   n = nrows(A)
   Var = general_binodal(A);
   RR = base_ring(Var)
   monomes = RR(Rational{BigInt}[1],[fill(1,6)])# this is the
      monomial a[1]*...*a[n]
   Mon = ideal(RR, monomes)
   dimension = dim(Var)
   @assert dimension >= n-2 "Generalized binodal variety is of too
      small dimension."
   Bin = helper_component_check(Var)
   return Bin
end

#INPUT: ideal of type MPolyIdeal{fmpq_mpoly}
#OUTPUT: returns the radical ideal generating the binodal variety
function binodal(I::MPolyIdeal{fmpq_mpoly})
RR = base_ring(I)
n = nvars(RR);
monomes = RR(Rational{BigInt}[1],[fill(1,n)])# this is the
   monomial a[1]*...*a[n]
Mon = ideal(RR, monomes)
dimension = dim(I)
@assert dimension >= n-2 "Generalized binodal variety is of too
```

```
    small dimension."
Bin = helper_component_check(I)
return Bin
end
```

Given a radical ideal this function computes the degree of the associated variety.

```
#INPUT: ideal of type MPolyIdeal{fmpq_mpoly}
#OUTPUT: the degree of the given ideal (an integer)
function compute_degree(Path::MPolyIdeal{fmpq_mpoly})
    Gens = gens(Path)
    k = nvars(base_ring(Path))
    Genshom = Vector(undef, length(Gens))
    for i in 1:length(Gens)
        Genshom[i] = homogenization(Gens[i],"z",k+1)
    end
    RRhom = parent(Genshom[1]) # This is RR, homogenous with
        additional variable e3 and weights [1, 1,..., 1]
    IIhom = ideal(RRhom, RRhom.(Genshom))
    Q, _ = quo(RRhom, IIhom)
    deg = degree(quo(RRhom, IIhom)[1]) #this is the degree of the
        hyperplane section of the binodal variety in the left out
        points
    return deg
end
```

The next function investigates the properties of the binodal variety. It returns the affine dimension and the degree. If the binodal variety is empty or not of expected dimension, the function prints the corresponding message. This function has again two methods: it can be used on the ideal generating the binodal variety, or directly on the matrix filed with the lattice points of the polytope.

Note that the main time of the computations is taken up by computing the binodal variety. Therefore, it might be advisable to compute the binodal variety only once, save it, and apply the first method of the investigative function.

```
#INPUT: matrix(ZZ,n,3,[...])
#OUTPUT: Pair (dimension, degree)
function investigate_binodal(I::MPolyIdeal{fmpq_mpoly})
    deg = compute_degree(I)
    dimension = dim(I)
    n = nvars(base_ring(I))
    println("Affine dimension of the binodal variety is ",
        dimension)
    if isone(I)
        println("Binodal variety is empty")
        elseif dimension==n-2
        println("The binodal variety is of expected affine dimension
            .")
        println("Degree of the binodal variet is ", deg)
```

```
   else
      println("The binodal variety is not of expected affine
         dimension.")
   end
   return dimension, deg
end

#INPUT: matrix(ZZ,n,3,[...])
#OUTPUT: Pair (dimension, degree)
function investigate_binodal(A::MatElem)
   I = binodal(A)
   deg = compute_degree(I)
   dimension = dim(I)
   n = nvars(base_ring(I))
   println("Affine dimension of the generalized variety is ",
      dimension)
   if isone(I)
      println("Binodal variety is empty")
   elseif dimension==n-2
      println("The binodal variety is of expected affine dimension
         .")
      println("Degree of the binodal variet is ", deg)
      println(A, " could be a binodal polytope.")
   else
      println("The binodal variety is not of expected affine
         dimension.")
   end
   return dimension, deg
end
```

The next function computes the intersection of the binodal variety for a 3-polytope given as a matrix filled with the lattice points, with 4 linear spaces of codimension 1 given by substituting all variables with the values given in `v`, apart from those two with indices specified in `p`. In the code this is called *path ideal*, because the degree of this ideal is the multiplicity of the connected lattice path given by skipping the two lattice points with indices specified in `p` (Lemma 9.3.3, (*i*), (*ii*) and (*iii*)). The function follows Algorithm 9, only that it returns the ideal, not the degree.

This function has again two methods, similar to `binodal` or `investigate_binodal`.

```
#INPUT: The n lattice points of the polytope as matrix, the
   positions of the two left out lattice points as a Vector, a
   generic point Vector of length n-2
#OUTPUT: the Path ideal
function con_mult(A::MatElem, p::Vector{Int}, v::Vector)
   @assert p[1]!= p[2] "Left out points must me different"
   @assert length(p)==2 "This function is only meant for lattice
      paths with 2 left out points."
```

```
    @assert p[1] < p[2] "Left out points must be ordered from small
        to large."
    I = binodal(A)
    J = gens(I);
    n = nrows(A)
    o = helper_find_indices(n,p)
    V = Vector{fmpq_mpoly}(undef,length(J))# we fill this vector
        according to the left out point conditions p[1] and p[2]
        with the values from v
    for i in 1:length(J)
        V[i] = evaluate(J[i],[o[i] for i in 1:(n-2)], [v[i] for i in
            1:(n-2)])
    end
    RRR, e = PolynomialRing(QQ,["e$i" for i in 1:2])
    w = helper_switch_ring(n,p,[true,true],v,RRR)
    m = length(J)
    V2 = helper_finish_switch_ring(n,m,w,V)
    II = ideal(RRR,V2) # this is the ideal of the intersection of
        the binodal variety with the hyperplanes given by v
    Radical = radical(II)
    Path = helper_component_check(Radical)
    return Path
end

# INPUT: the binodal variety, the positions of the two left out
    lattice points as a Vector, a generic point Vector of length n
    -2
# OUTPUT: the Path ideal
function con_mult(I::MPolyIdeal{fmpq_mpoly}, p::Vector{Int}, v::
    Vector)
    @assert p[1]!= p[2] "Left out points must me different"
    @assert length(p)==2 "This function is only meant for lattice
        paths with 2 left out points."
    @assert p[1] < p[2] "Left out points must be ordered from small
        to large."
    J = gens(I);
    n = nvars(base_ring(I))
    o = helper_find_indices(n,p)
    V = Vector{fmpq_mpoly}(undef,length(J))# we fill this vector
        according to the left out point conditions p[1] and p[2]
        with the values from v
    for i in 1:length(J)
        V[i] = evaluate(J[i],[o[i] for i in 1:(n-2)], [v[i] for i in
            1:(n-2)])
    end
    RRR, e = PolynomialRing(QQ,["e$i" for i in 1:2])
    w = helper_switch_ring(n,p,[true,true],v,RRR)
    m = length(J)
    V2 = helper_finish_switch_ring(n,m,w,V)
```

```
    II = ideal(RRR,V2) # this is the ideal of the intersection of
        the binodal variety with the hyperplanes given by v
    Radical = radical(II)
    Path = helper_component_check(Radical)
    return Path
end
```

The function below computes the multiplicity of a lattice path following Algorithms 9 and 10. The polytope is as always given by a matrix filled with the lattice points. We indicate the lattice path by two vectors: The first vector `p` contains the indices of the lattice points that are left out of the path resp. are the end point of a gap of the path. The second vector `b` contains boolean values, where `true` indicates that the lattice point in the corresponding position in `p` is a skipped point. Consequently, `false` indicates that the lattice point in the corresponding position in `p` is the end point of a gap in the path.

Example: `b[1] = true` means, that the point at position `p[1]` is a skipped point, not part of a gap. For the moment, `p` and `b` are only allowed exactly 2 entries. It should be possible to expand the function if needed for further research.

Analogous to `con_mult`, this function has two methods.

Note that `p` needs to be filled according to size, i.e., the smallest value first, the largest at the end.

```
# INPUT: The n lattice points of the polytope as matrix, the
    positions of the two left out lattice points as a Vector, the
    types of the indicated lattice points as a boolean vector, a
    generic point Vector of length n-2
# OUTPUT: prints the lattice path multiplicity if the points in v
    are generic enough.
function path_mult(A::MatElem, p::Vector{Int}, b::Vector{Bool}, v
    ::Vector)
    n = nrows(A)
    @assert p[1]!= p[2] "Left out points must me different"
    @assert length(p) ==2 "This function is only meant for lattice
        paths with 2 left out points."
    @assert length(p) ==length(b)  "$p and $b need to have the same
         length"
    @assert length(v)== n-length(p) "Number of point conditions in
        $v is wrong."
    @assert p[1] < p[2] "Left out points must be ordered from small
         to large."
    @assert b[1] || b[2] "This function is only meant for lattice
        paths with at most one gap."
    @assert (!(p[1] == 1 || p[1] == 2) || !b[1] || b[2] || p[2]>=4)
         "Invalid Path given."
    @assert (b[1] || !(p[1]<3||p[1]==n-1)) "Invalid Path given."
    I = binodal(A)
    J = gens(I)
```

```
    if b[1] && b[2] #case of the connected paths (no gap in the
       path)
       Path = con_mult(A,p,v)
    else #disconnected multiplicty
       if b[1] && !b[2] #first left out point, then gap
          o = helper_find_indices(p[2],p)
          V = Vector{fmpq_mpoly}(undef,length(J))
          for i in 1:length(J)
             V[i] = evaluate(J[i],[o[i] for i in 1:(p[2]-2)], [v[i]
                for i in 1:(p[2]-2)])
          end
          println(V)
          RRR, e = PolynomialRing(QQ,["e$i" for i in 1:2])
          w = helper_switch_ring(n,p,b,v,RRR)
          V2 = helper_finish_switch_ring(n,length(J),w,V)
       elseif !b[1] && b[2] # here the gap appears first
          o = helper_find_indices(p[1],p)
          V = Vector{fmpq_mpoly}(undef,length(J))
          for i in 1:length(J)
             V[i] = evaluate(J[i],[o[i] for i in 1:(p[1]-1)], [v[i]
                for i in 1:(p[1]-1)])
          end
          RRR, e = PolynomialRing(QQ,["e$i" for i in 1:2])
          w = helper_switch_ring(n,p,b,v,RRR)
          V2 = helper_finish_switch_ring(n,length(J),w,V)
       end
       II = ideal(RRR,V2)
       Radical = radical(II)
       Path = helper_component_check(Radical)
    end
    deg = compute_degree(Path)
    if isone(Path)
       println("Path variety is empty")
    else
       dimension = dim(Path)
       println("Affine dimension is ", dimension)
       if dimension == 0
          println("Path multiplicity is ", deg)
       else
          error("Given point conditions were not generic enough or
             the polytope is not binodal.")
       end
    end
    return Path, deg
end

#INPUT: The binodal variety, the positions of the two left out
   lattice points as a Vector, a generic point Vector of length n
   -2
```

```
#OUTPUT: prints the lattice path multiplicity if the points in v
    are generic enough.
function path_mult(I::MPolyIdeal{fmpq_mpoly}, p::Vector{Int}, b::
    Vector{Bool}, v::Vector)
  n = nvars(base_ring(I))
  @assert p[1]!= p[2] "Left out points must me different"
  @assert length(p)==2 "This function is only meant for lattice
      paths with 2 left out points."
  @assert length(p)==length(b) "$p and $b need to have the same
      length"
  @assert length(v)== n-length(p) "Number of point conditions in
      $v is wrong."
  @assert p[1] < p[2] "Left out points must be ordered from small
       to large."
  @assert b[1] || b[2] "This function is only meant for lattice
      paths with at most one gap."
  @assert (!(p[1] == 1 || p[1] == 2) || !b[1] || b[2] || p[2]>=4)
       "Invalid Path given."
  @assert (b[1] || !(p[1]<3||p[1]==n-1)) "Invalid Path given."
  J = gens(I)
  if b[1] && b[2] #case of the connected paths (no gap in the
      path)
    Path = con_mult(I,p,v)
  else #disconnected multiplicty
    if b[1] && !b[2] #first left out point, then gap
      o = helper_find_indices(p[2],p)
      V = Vector{fmpq_mpoly}(undef,length(J))
      for i in 1:length(J)
        V[i] = evaluate(J[i],[o[i] for i in 1:(p[2]-2)], [v[i]
            for i in 1:(p[2]-2)])
      end
      println(V)
      RRR, e = PolynomialRing(QQ,["e$i" for i in 1:2])
      w = helper_switch_ring(n,p,b,v,RRR)
      V2 = helper_finish_switch_ring(n,length(J),w,V)
    elseif !b[1] && b[2] # here the gap appears first
      o = helper_find_indices(p[1],p)
      V = Vector{fmpq_mpoly}(undef,length(J))
      for i in 1:length(J)
        V[i] = evaluate(J[i],[o[i] for i in 1:(p[1]-1)], [v[i]
            for i in 1:(p[1]-1)])
      end
      RRR, e = PolynomialRing(QQ,["e$i" for i in 1:2])
      w = helper_switch_ring(n,p,b,v,RRR)
      V2 = helper_finish_switch_ring(n,length(J),w,V)
    end
    II = ideal(RRR,V2)
    Radical = radical(II)
    Path = helper_component_check(Radical)
```

```
      end
   deg = compute_degree(Path)
   if isone(Path)
      println("Path variety is empty")
   else
      dimension = dim(Path)
      println("Affine dimension is ", dimension)
      if dimension == 0
         println("Path multiplicity is ", deg)
      else
         error("Given point conditions were not generic enough or
            the polytope is not binodal.")
      end
   end
   return Path, deg
end
```

Now, we present the functions used for the verification of binodal polytopes (Conjecture 9.2.8). The procedure is Algorithm 8. The first step is to find a generic point in the binodal variety. For this we use the function `find_generic_point`, which is just a more intuitive name for the function `con_mult`. See the explanation above for that function.

```
# INPUT: The n lattice points of the polytope as matrix, the
   positions of the two left out lattice points as a Vector, a
   generic point Vector of length n-2
# OUTPUT: the Path ideal
function find_generic_point(A::MatElem, p::Vector{Int}, v::Vector)
   Path = con_mult(A,p,v);
   return Path
end
```

This function returns an ideal that induces a zero dimensional variety. We can solve for a point in this variety. In general, this is not easy. When we have a solution, we can compute the singular locus of the surface generated by the coordinates of point in the variety as coefficients.

If the coefficients are not rational, we need to define a field extension. Usually this is a simple number field. Therefore, the function has again two methods, which can be used depending on whether the field extension is needed.

```
#INPUT: the monomials given as matrix(ZZ,n,3,[...]) and the
   ocefficients given as Vector{Rational{Int64}}
#OUTPUT: Pair (the ideal of the singular locus, its dimension)
function singular_locus(A::MatElem,v::Vector{Rational{Int64}})
   R, x =  PolynomialRing(QQ,["x$i" for i in 1:3])
   n = nrows(A)
   h = MPolyBuildCtx(R)
   for i in 1:n
```

```
            push_term !(h,v[i],Vector{Int64}([A[i,j] for j in 1:ncols(A)
                ]))
        end
        p= finish(h)
        I = ideal(R,[p,derivative(p,x[1]),derivative(p,x[2]),derivative
            (p,x[3])])
        return I, dim(I)
    end


#Works for a simple NumberField K
#INPUT: the monomials given as matrix(ZZ,n,3,[...]), the
    ocefficients given as Vector{Rational{Int64}} and the field
    extension given as AnticNumberField
#OUTPUT: Pair (the ideal of the singular locus, its dimension)
function singular_locus(A::MatElem,v::Vector{Any},K::
    AnticNumberField )
R, x =  PolynomialRing(K,["x$i" for i in 1:3])
n = nrows(A)
h = MPolyBuildCtx(R)
for i in 1:n
push_term !(h,v[i]*one(K),Vector{Int64}([A[i,j] for j in 1:ncols(A)
    ]))
end
p= finish(h)
I = ideal(R,[p,derivative(p,x[1]),derivative(p,x[2]),derivative(p,
    x[3])])
return I, dim(I)
end
```

B.2.2 Helper functions

This section contains the helper functions for the functions computing the multiplicities of lattice paths, as contained in Section B.2.1, together with a brief description of the functions.

This following function fills a vector with the indices of the variables which have to be substituted by fixed values.

```
#INPUT: integer n giving the number of the coefficients that have
    to be substituted, vector p stating the indices  of the
    coefficients that are not to be substituted
#OUTPUT: Vector{Int64}
function helper_find_indices(n::Int,p::Vector{Int})
    o = Vector{Int64}() #this is auxiliary vector to help us fill
        the point conditions in the vector V
    s = p[1]
    t = p[2]
    for i in 1:n
```

```
        if i<s && i<t
            append!(o,i)
        elseif s<i && i<t
            append!(o,i)
        elseif i<s && t<i
            append!(o,i)
        elseif s<i && t<i
            append!(o,i)
        end
    end
    return o
end
```

The following is the first helper function to switch from the polynomial ring with `n` variables $a_{\omega_0}, \ldots, a_{\omega_{N+1}}$ to the polynomial ring in 2 variables. The function is used in the computation of multiplicities of lattice paths. It computes the vector `w`, which is used to substitute the remaining variables and move the ideal into the polynomial ring with 2 variables, so that we can compute the degree of the path ideal. Depending on connected (if `(b[1]&&b[2])==true`) or disconnected paths (if `(b[1] &&!b[2])||(!b[1]&&b[2])==true`), the vector `w` gets filled differently. This is explained in detail in Section 9.3.2. See Algorithms 9 and 10. The vector `w` is filled with zeros at those coordinates which do not depend on the new two variables, because these entries are substituted before by the general rational entries of the input vector `v` in `path_mult`.

```
#INPUT: Integer n, Vector p, Vector of bools b, PolynomialRing RRR
#OUTPUT: Vector w filled with zero(RRR) for all indices not in p
    and with monomials in e[1], e[2] for the entries of p
function helper_switch_ring(n::Int,p::Vector{Int},b::Vector{Bool},
    v::Vector,RRR::FmpqMPolyRing)
    w = Vector(undef,n)
    RRR, e = PolynomialRing(base_ring(RRR),symbols(RRR))
    if b[1] && b[2]
        for i in 1:n
            if i!=p[1] && i!=p[2]
                w[i] = zero(RRR)
            elseif (p[1]==i && p[1]<p[2]) || (p[2]==i && p[2]<p[1])
                w[i] = e[1]
            elseif (p[1]==i && p[2]<p[1]) || (p[2]==i && p[1]<p[2])
                w[i] = e[2]
            end
        end
    elseif b[1] && !b[2]
        for i in 1:n
            if i<p[1] || p[1]<i<p[2]
                w[i] = zero(RRR)
            elseif i == p[1]
                w[i] = e[1]
```

```
            elseif i == p[2]
                w[i] = e[2]
            else
                w[i] = v[i-2]*e[2]
            end
        end
    elseif !b[1] && b[2]
        for i in 1:n
            if i<p[1]
                w[i] = zero(RRR)
            elseif i == p[1]
                w[i] = e[1]
            elseif i == p[2]
                w[i] = e[1]*e[2]
            elseif p[1]<i<p[2]
                w[i] = v[i-1]*e[1]
            else
                w[i] = v[i-2]*e[1]
            end
        end
    end
    return w
end
```

Next is the second helper function to switch from the Polynomial ring with `n` variables $a_{\omega_0}, \ldots, a_{\omega_{N+1}}$ to the polynomial ring in 2 variables. This is needed for the computation of the Path multiplicities. The function substitutes the variables in the `m` generating polynomial of the binodal variety, according to the vector `w` defined by the function above.

```
#INPUT:  Integer n for the number of inital variables, Integer m
    for the number of polynomials that have to be substituted,
    vector w that contains the polynomials in the new variables e
    [1], e[2] that have to be substituted in the indices
    complementary to those found by using helper_find_indices,
    vector V consisting of the m polynomials in which the entries
    with indices found by helper_find_indices are already
    substituted by fixed values
#OUTPUT: Vector V2 that consists for each variable of the original
     ring of fixed values or monomials in e[1],e[2]
function helper_finish_switch_ring(n::Int,m::Int,w::Vector,V::
    Vector)
    V2 = Vector(undef,m)
    for i in 1:m
        V2[i] = evaluate(V[i],[w[i] for i in 1:n])
    end
    return V2
end
```

The following function takes an ideal, computes its primary decomposition and checks for each primary component whether the associated prime ideal contains monomials. The function returns the radical ideal consisting of the intersection of all those prime ideals that do not contain monomials. This function is used for the computation of the binodal variety in `binodal`, and for the path varieties in `con_mult` and `path_mult`.

```
#INPUT: ideal I of type MPolyIdeal{fmpq_mpoly}
#OUTPUT: the maximal radical ideal in I such that no primary
    component contains monomials
function helper_component_check(I::MPolyIdeal{fmpq_mpoly})
    RRR = base_ring(I)
    k = nvars(RRR)
    monomes = RRR(Rational{BigInt}[1],[fill(1,k)]) #e[1]*e[2]
    Mon = ideal(RRR, monomes)
    L = primary_decomposition(I)
    II = ideal(RRR, one(RRR))
    l = length(L)
    for i in 1:l
        if !issubset(Mon,L[i][2])
            II = intersect(II,L[i][2])
        end
    end
    return II
end
```

Bibliography

[ACP15]   Dan Abramovich, Lucia Caporaso, and Sam Payne. The tropicalization of the moduli space of curves. *Ann. Sci. Éc. Norm. Supér. (4)*, 48(4):765–809, 2015.

[AHK18]   Karim Adiprasito, June Huh, and Eric Katz. Hodge theory for combinatorial geometries. *Ann. of Math. (2)*, 188(2):381–452, 2018.

[Arn99]   V. I. Arnold. Symplectization, complexification and mathematical trinities. In *The Arnoldfest (Toronto, ON, 1997)*, volume 24 of *Fields Inst. Commun.*, pages 23–37. Amer. Math. Soc., Providence, RI, 1999.

[BBLdM18]   Benoît Bertrand, Erwan Brugallé, and Lucía López de Medrano. Planar tropical cubic curves of any genus, and higher dimensional generalisations. *Enseign. Math.*, 64(3-4):415–457, 2018.

[Ber71]   George M. Bergman. The logarithmic limit-set of an algebraic variety. *Trans. Amer. Math. Soc.*, 157:459–469, 1971.

[BG84]   Robert Bieri and J. R. J. Groves. The geometry of the set of characters induced by valuations. *J. Reine Angew. Math.*, 347:168–195, 1984.

[BG20]   Madeline Brandt and Alheydis Geiger. A tropical count of binodal cubic surfaces. *Matematiche (Catania)*, 75(2):627–649, 2020.

[BG21]   Madeline Brandt and Alheydis Geiger. Towards tropically counting binodal surfaces. `arXiv:2112.10626`, submitted to La Matematica, 2021.

[BJMS15]   Sarah Brodsky, Michael Joswig, Ralph Morrison, and Bernd Sturmfels. Moduli of tropical plane curves. *Res. Math. Sci.*, 2:Art. 4, 31, 2015.

[BK12]   Tristram Bogart and Eric Katz. Obstructions to lifting tropical curves in surfaces in 3-space. *SIAM J. Discrete Math.*, 26(3):1050–1067, 2012.

[BK19]   Elizabeth Baldwin and Paul Klemperer. Understanding preferences: "demand types", and the existence of equilibrium with indivisibilities. *Econometrica*, 87(3):867–932, 2019.

[BLM⁺16] Matthew Baker, Yoav Len, Ralph Morrison, Nathan Pflueger, and Qingchun Ren. Bitangents of tropical plane quartic curves. *Math. Z.*, 282(3-4):1017–1031, 2016.

[BM07] Erwan Brugallé and Grigory Mikhalkin. Enumeration of curves via floor diagrams. *C. R. Math. Acad. Sci. Paris*, 345(6):329–334, 2007.

[BM09] Erwan Brugallé and Grigory Mikhalkin. Floor decompositions of tropical curves: the planar case. In *Proceedings of Gökova Geometry-Topology Conference 2008*, pages 64–90. Gökova Geometry/Topology Conference (GGT), Gökova, 2009.

[BPR06] Saugata Basu, Richard Pollack, and Marie-Françoise Roy. *Algorithms in real algebraic geometry*, volume 10 of *Algorithms and Computation in Mathematics*. Springer-Verlag, Berlin, second edition, 2006.

[BS15] Erwan Brugallé and Kris Shaw. Obstructions to approximating tropical curves in surfaces via intersection theory. *Canad. J. Math.*, 67(3):527–572, 2015.

[BS16a] Mónica Blanco and Francisco Santos. Lattice 3-polytopes with few lattice points. *SIAM J. Discrete Math.*, 30(2):669–686, 2016.

[BS16b] Mónica Blanco and Francisco Santos. Lattice 3-polytopes with six lattice points. *SIAM J. Discrete Math.*, 30(2):687–717, 2016.

[BS18] Mónica Blanco and Francisco Santos. Enumeration of lattice 3-polytopes by their number of lattice points. *Discrete Comput. Geom.*, 60(3):756–800, 2018.

[Cay49] Arthur Cayley. On the triple tangent planes of surfaces of the third order. *Cambridge and Dublin Math. J.*, 4:118–138, 1849.

[CC99] Luca Chiantini and Ciro Ciliberto. On the Severi varieties of surfaces in $\mathbb{P}^3$. *J. Algebraic Geom.*, 8(1):67–83, 1999.

[CGP21] Melody Chan, Søren Galatius, and Sam Payne. Tropical curves, graph complexes, and top weight cohomology of $\mathcal{M}_g$. *J. Amer. Math. Soc.*, 34(2):565–594, 2021.

[CH98] Lucia Caporaso and Joe Harris. Counting plane curves of any genus. *Invent. Math.*, 131(2):345–392, 1998.

[CJ17]   Melody Chan and Pakawut Jiradilok. Theta characteristics of tropical K_4-curves. In *Combinatorial algebraic geometry*, volume 80 of *Fields Inst. Commun.*, pages 65–86. Fields Inst. Res. Math. Sci., Toronto, ON, 2017.

[CJMR21] Renzo Cavalieri, Paul Johnson, Hannah Markwig, and Dhruv Ranganathan. Counting curves on Hirzebruch surfaces: tropical geometry and the Fock space. *Math. Proc. Cambridge Philos. Soc.*, 171(1):165–205, 2021.

[CM21]   Maria Angelica Cueto and Hannah Markwig. Combinatorics and real lifts of bitangents to tropical quartic curves. `arXiv:2004.10891v2`, to appear in Discrete and Computational Geometry, 2021.

[CS03]   Lucia Caporaso and Edoardo Sernesi. Recovering plane curves from their bitangents. *J. Algebraic Geom.*, 12(2):225–244, 2003.

[DGPS21] Wolfram Decker, Gert-Martin Greuel, Gerhard Pfister, and Hans Schönemann. `Singular` 4-2-1 — A computer algebra system for polynomial computations. `http://www.singular.uni-kl.de`, 2021.

[FG22]   Claudia Fevola and Christiane Görgen. The mathematical research-data repository MathRepo. *Computeralgebra-Rundbrief*, 70:16–20, 2022.

[FM10]   Sergey Fomin and Grigory Mikhalkin. Labeled floor diagrams for plane curves. *J. Eur. Math. Soc. (JEMS)*, 12(6):1453–1496, 2010.

[Gat03] A. Gathmann, 2003. Habilitation Thesis, TU Kaiserslautern.

[Gei20] Alheydis Geiger. On realizability of lines on tropical cubic surfaces and the Brundu-Logar normal form. *Matematiche (Catania)*, 75(2):651–671, 2020.

[Gei22] Alheydis Geiger. Github, functions in `OSCAR` for binodal polytopes, 2022. `https://github.com/AlheydisGeiger/Code-Binodal-Surfaces`.

[GJ00]   Ewgenij Gawrilow and Michael Joswig. `polymake`: a framework for analyzing convex polytopes. In *Polytopes—combinatorics and computation (Oberwolfach, 1997)*, volume 29 of *DMV Sem.*, pages 43–73. Birkhäuser, Basel, 2000.

[GK08]   Andreas Gathmann and Michael Kerber. A Riemann-Roch theorem in tropical geometry. *Math. Z.*, 259(1):217–230, 2008.

[GKZ94] I. M. Gel'fand, M. M. Kapranov, and A. V. Zelevinsky. *Discriminants, resultants, and multidimensional determinants.* Mathematics: Theory & Applications. Birkhäuser Boston, Inc., Boston, MA, 1994.

[GM07] Andreas Gathmann and Hannah Markwig. The Caporaso-Harris formula and plane relative Gromov-Witten invariants in tropical geometry. *Math. Ann.*, 338(4):845–868, 2007.

[GP] Alheydis Geiger and Marta Panizzut. `polymake` extension `TropicalQuarticCurves`. `https://polymake.org/doku.php/extensions/tropicalquarticcurves`.

[GP21a] Alheydis Geiger and Marta Panizzut. Computing tropical bitangents of smooth quartics in `polymake`. `arXiv:2112.04447`, submitted to Journal of Symbolic Computation special issue for „MEGA 2022 Effective Methods in Algebraic Geometry", 2021.

[GP21b] Alheydis Geiger and Marta Panizzut. A tropical count of real bitangents to plane quartic curves. `arXiv:2112.04433`, submitted to The Electronic Journal of Combinatorics, 2021.

[GS] Daniel R. Grayson and Michael E. Stillman. Macaulay2, a software system for research in algebraic geometry. Available at `http://www.math.uiuc.edu/Macaulay2/`.

[GS18] Yaniv Ganor and Eugenii Shustin. Enumeration of plane unicuspidal curves of any genus via tropical geometry. `arXiv:1807.11443`, 2018.

[Ham14] Simon Hampe. `a-tint`: a polymake extension for algorithmic tropical intersection theory. *European J. Combin.*, 36:579–607, 2014.

[Har77] Robin Hartshorne. *Algebraic geometry.* Graduate Texts in Mathematics, No. 52. Springer-Verlag, New York-Heidelberg, 1977.

[IKS03] Ilia Itenberg, Viatcheslav Kharlamov, and Eugenii Shustin. Welschinger invariant and enumeration of real rational curves. *Int. Math. Res. Not.*, (49):2639–2653, 2003.

[Jen] Anders N. Jensen. Gfan, a software system for Gröbner fans and tropical varieties. Available at `http://home.imf.au.dk/jensen/software/gfan/gfan.html`.

[JJK18] Charles Jordan, Michael Joswig, and Lars Kastner. Parallel enumeration of triangulations. *Electron. J. Combin.*, 25(3):Paper 3.6, 27, 2018.

[JJK20] Michael Joswig, Charles Jordan, and Lars Kastner. `mptopcom` (2018-2020)：open source software for the parallel enumeration of triangulations. Preprint, 2020.

[JPS] Michael Joswig, Marta Panizzut, and Bernd Sturmfels. `polymake` extension `TropicalCubics`. `https://polymake.org/doku.php/extensions/tropicalcubics`.

[JPS20] Michael Joswig, Marta Panizzut, and Bernd Sturmfels. The Schläfli fan. *Discrete Comput. Geom.*, 64(2):355–381, 2020.

[KM94] M. Kontsevich and Yu. Manin. Gromov-Witten classes, quantum cohomology, and enumerative geometry. *Comm. Math. Phys.*, 164(3):525–562, 1994.

[KM97] Vassili N. Kolokoltsov and Victor P. Maslov. *Idempotent analysis and its applications*, volume 401 of *Mathematics and its Applications*. Kluwer Academic Publishers Group, Dordrecht, 1997. Translation of ıt Idempotent analysis and its application in optimal control (Russian), "Nauka" Moscow, 1994 [MR1375021 (97d:49031)], Translated by V. E. Nazaikinskii, With an appendix by Pierre Del Moral.

[Kon95] Maxim Kontsevich. Enumeration of rational curves via torus actions. In *The moduli space of curves (Texel Island, 1994)*, volume 129 of *Progr. Math.*, pages 335–368. Birkhäuser Boston, Boston, MA, 1995.

[KP20] Lars Kastner and Marta Panizzut. Hyperplane arrangements in `polymake`. In *Mathematical software—ICMS 2020*, volume 12097 of *Lecture Notes in Comput. Sci.*, pages 232–240. Springer, Cham, [2020] ©2020.

[Kra98] V. A. Krasnov. On the theta characteristics of a real algebraic curve. *Mat. Zametki*, 64(3):403–406, 1998.

[KRSNS18] Avinash Kulkarni, Yue Ren, Mahsa Sayyary Namin, and Bernd Sturmfels. Real space sextics and their tritangents. In *ISSAC'18—Proceedings of the 2018 ACM International Symposium on Symbolic and Algebraic Computation*, pages 247–254. ACM, New York, 2018.

[KRZB16] Eric Katz, Joseph Rabinoff, and David Zureick-Brown. Uniform bounds for the number of rational points on curves of small Mordell-Weil rank. *Duke Math. J.*, 165(16):3189–3240, 2016.

[LL18]   Heejong Lee and Yoav Len. Bitangents of non-smooth tropical quartics. *Port. Math.*, 75(1):67–78, 2018.

[LM20]   Yoav Len and Hannah Markwig. Lifting tropical bitangents. *J. Symbolic Comput.*, 96:122–152, 2020.

[LV21]   Hannah Larson and Isabel Vogt. An enriched count of the bitangents to a smooth plane quartic curve. *Res. Math. Sci.*, 8(2):Paper No. 26, 21, 2021.

[MaR]   Mardi: Mathematical research data initiative. `https://www.mardi4nfdi.org/`.

[Mar06] Hannah Markwig, 2006. PhD thesis. Technische Universität Kaiserslautern.

[MCT21] Petros Maragos, Vasileios Charisopoulos, and Manos Theodosis. Tropical geometry and machine learning. *Proceedings of the IEEE*, PP:1–28, 04 2021.

[Mik05] Grigory Mikhalkin. Enumerative tropical algebraic geometry in $\mathbb{R}^2$. *J. Amer. Math. Soc.*, 18(2):313–377, 2005.

[MMS12] Hannah Markwig, Thomas Markwig, and Eugenii Shustin. Tropical surface singularities. *Discrete Comput. Geom.*, 48(4):879–914, 2012.

[MMS18] Hannah Markwig, Thomas Markwig, and Eugenii Shustin. Enumeration of complex and real surfaces via tropical geometry. *Adv. Geom.*, 18(1):69–100, 2018.

[MMSS22] Hannah Markwig, Thomas Markwig, Kris Shaw, and Eugenii Shustin. Tropical floor plans and enumeration of complex and real multi-nodal surfaces. *J. Algebraic Geom.*, 31(2):261–301, 2022.

[MS15]   Diane Maclagan and Bernd Sturmfels. *Introduction to tropical geometry*, volume 161 of *Graduate Studies in Mathematics*. American Mathematical Society, Providence, RI, 2015.

[MSP22] Hannah Markwig, Kris Shaw, and Sam Payne. Bitangents to plane quartics via tropical geometry: $\mathbb{A}^1$-enumeration, rationality, and avoidance loci. `arXiv:2207.01305`, 2022.

[osc]   `OSCAR` Computer Algebra Research System. `https://oscar.computeralgebra.de/`.

[Paf17]   Andreas Paffenholz. `polyDB`: a database for polytopes and related objects. In *Algorithmic and experimental methods in algebra, geometry, and number theory*, pages 533–547. Springer, Cham, 2017.

[Plü34]   Julius Plücker. Solution d'une question fondamentale concernant la théorie générale des courbes. *J. Reine Angew. Math.*, 12:105–108, 1834.

[Plü39]   Julius Plücker. *Theorie der algebraischen Curven: gegründet auf eine neue Behandlungsweise der analytischen Geometrie.* Bonn: Adolph Marcus., 1839.

[PV22]   Marta Panizzut and Magnus Dehli Vigeland. Tropical lines on cubic surfaces. *SIAM J. Discrete Math.*, 36(1):383–410, 2022.

[Ram02]   Jörg Rambau. Topcom: Triangulations of point configurations and oriented matroids. In *Proceedings of the International Congress of Mathematical Software*, 2002. available online[1].

[RGST05] Jürgen Richter-Gebert, Bernd Sturmfels, and Thorsten Theobald. First steps in tropical geometry. In *Idempotent mathematics and mathematical physics*, volume 377 of *Contemp. Math.*, pages 289–317. Amer. Math. Soc., Providence, RI, 2005.

[RSS14]   Qingchun Ren, Steven V. Sam, and Bernd Sturmfels. Tropicalization of classical moduli spaces. *Math. Comput. Sci.*, 8(2):119–145, 2014.

[Sal49]   George Salmon. On the triple tangent planes to a surface of the third order. *Cambridge and Dublin Math. J.*, 4:252–260, 1849.

[Seg42]   Beniamino Segre. *The Non-singular Cubic Surfaces.* Oxford University Press, Oxford, 1942.

[Sim88]   Imre Simon. Recognizable sets with multiplicities in the tropical semiring. In *Mathematical foundations of computer science, 1988 (Carlsbad, 1988)*, volume 324 of *Lecture Notes in Comput. Sci.*, pages 107–120. Springer, Berlin, 1988.

[Sin22]   Uriel Sinichkin. Enumeration of algebraic and tropical singular hypersurfaces. *Transactions of the American Mathematical Society*, 09 2022.

---

[1]http://www.zib.de/PaperWeb/abstracts/ZR-02-17

[ST99]   Eugenii Shustin and Ilya Tyomkin. Versal deformation of algebraic hypersurfaces with isolated singularities. *Math. Ann.*, 313(2):297–314, 1999.

[ST08]   Bernd Sturmfels and Jenia Tevelev. Elimination theory for tropical varieties. *Math. Res. Lett.*, 15(3):543–562, 2008.

[Tho06] Rekha R. Thomas. *Lectures in geometric combinatorics*, volume 33 of *Student Mathematical Library*. American Mathematical Society, Providence, RI; Institute for Advanced Study (IAS), Princeton, NJ, 2006. IAS/Park City Mathematical Subseries.

[TY19]   Ngoc Mai Tran and Josephine Yu. Product-mix auctions and tropical geometry. *Math. Oper. Res.*, 44(4):1396–1411, 2019.

[Vak08] Ravi Vakil. The moduli space of curves and Gromov-Witten theory. In *Enumerative invariants in algebraic geometry and string theory*, volume 1947 of *Lecture Notes in Math.*, pages 143–198. Springer, Berlin, 2008.

[Vig10] Magnus Dehli Vigeland. Smooth tropical surfaces with infinitely many tropical lines. *Ark. Mat.*, 48(1):177–206, 2010.

[Vir84] O. Ya. Viro. Gluing of plane real algebraic curves and constructions of curves of degrees 6 and 7. In *Topology (Leningrad, 1982)*, volume 1060 of *Lecture Notes in Math.*, pages 187–200. Springer, Berlin, 1984.

[Zeu73] Hieronymus Georg Zeuthen. Sur les diférentes formes des curbes planes du quatrième ordre. *Math. Ann.*, 7:408–432, 1873.

[ZNL18] Liwen Zhang, Gregory Naitzat, and Lek-Heng Lim. Tropical geometry of deep neural networks. In *International Conference on Machine Learning*, pages 5824–5832. PMLR, 2018.